CIVIL ENGINEERING

C. Ionescu, F. Paulet-Crainiceanu, R. Scinteie, A. Nicuta

editors

EDITURA SOCIETATII ACADEMICE "MATEI - TEIU BOTEZ"

Iasi, 2007

Civil Engineering

C. Ionescu, F. Păuleț-Crăiniceanu, R. Scînteie, A. Nicuță
Editors

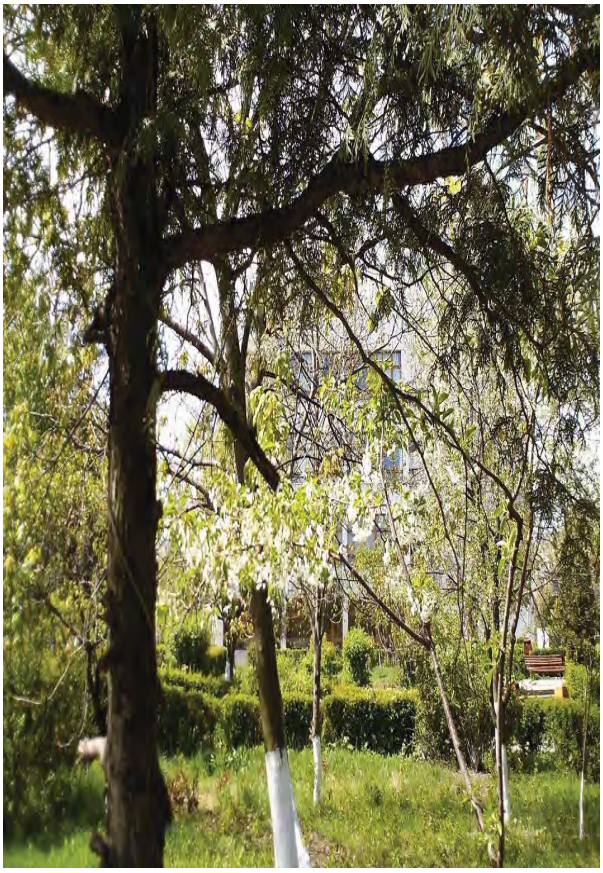

EDITURA SOCIETĂȚII ACADEMICE "MATEI-TEIU BOTEZ"
Iași, 2007

Proceedings of the Fifth International Symposium

"Computational Civil Engineering 2007"

Iaşi, România, May 25, 2007

C. Ionescu, F. Păuleț-Crăiniceanu, R. Scînteie, A. Nicuță
Editors

Descrierea CIP a Bibliotecii Naționale a României

Civil engineering / ed.: C. Ionescu, F. Păuleț-Crăiniceanu, R. Scînteie, A. Nicuță. - Iaşi : Editura Societății Academice "Matei - Teiu Botez", 2007
Bibliogr.
ISBN 978-973-8955-14-1

I. Ionescu, Constantin (ed.)
II. Păuleț-Crăiniceanu, Fideliu (ed.)
III. Scînteie, Rodian (ed.)
IV. Nicuță, Ana (ed.)

624

Computerized processing: F. Păuleț-Crăiniceanu, R. Scînteie

Table of Contents

Civil Engineering, a domain based on computation

Fideliu Păuleț-Crăiniceanu[1], Rodian Scînteie[2], Constantin Ionescu[1] and Alina Mihaela Nicuță[1]
[1] *"Gh. Asachi" Technical University of Iași, România*
[2] *Department, University, City, Zip code, Country*

Summary

In Civil Engineering, the computation is at the base of almost all activity. An international symposium as Computational Civil Engineering 2007*, [1], is a good opportunity to present researches, technical and scientific work in the field and represents a show on the importance computers and computations play in this domain.*

This paper tries to withdraw the main ideas, approaches and achievements reflected in the proceedings of the above mentioned symposium.

A nice tradition regarding computation in Civil Engineering is already established. The diversity of work together with the diversity of countries, universities and other institutions implied in Computational Civil Engineering symposiums lead to the conclusion that the field is strong and needed.

KEYWORDS: Civil Engineering, computers, research, education, computation in engineering and science.

1. INTRODUCTION

In Civil Engineering, as in other engineering fields, information processing is vital. This processing must be done quickly and reliable.

As computational means are progressing exponentially, the engineering is also progressing. Civil Engineering is now in the middle of this progress. It could be stated that computational means and instrumentation are ahead of their full use in Civil Engineering.

Every year since 2003 in Iasi, Romania, the international symposium Computational Civil Engineering is held. The proceedings of the symposiums show that the computational/instrumental "revolution" is underway.

During the Computational Civil Engineering 2007 symposium complex applications were presented [1]. The general evolution (compared to the previous

years) is obvious. The mixture between civil engineers and computer/automation engineers (sometimes in the same person) is becoming essential, though the inertia (specific to construction domain) is still powerful.

This paper is doing a review of the achievements/problems specified by the authors participating at the above mentioned symposium.

2. COMPUTER-BASED CIVIL ENGINEERING

Tomas Apeltauer and a team from Brno University of Technology [2] present their results of the research on traffic behavior. Traffic jams become a challenge all over the world and huge losses in terms of time and resources are caused by this phenomenon. In order to mitigate the effects one must understand the intimate processes and overall behavior. It is therefore necessary to use most advanced tools available. For the simulation a program was created using Java programming language, due to its easy accessibility, simplicity and portability on internet. Each vehicle is represented by an object with its own parameters and the whole system of vehicles is represented by the so called binded list. In such way it is possible to dynamically change number of vehicles in the system. The paper presents the nonlinear effect in traffic simulation. The analysis uses real data collected with different methods like aerial photography and inductive loops. The traffic was studied at both microscopic and macroscopic using cellular automata and analog models. Authors work also with the concept of chaos in traffic flow analysis.

The influence of deformation at a heritage building support on stability of groined masonry arch is studied by Kaspars Bondars and Aleksandrs Korjakins with applications at Riga Cathedral [3]. The settlements monitoring of cathedral's supports and numerical modeling to define settlement inequality were used as initial information to compare computer modeled deformed structure shape with existing cracked masonry structure. Geodesic monitoring by optical tools and mechanical tensometers have been used for determination of a crack expansion.

Wind, solar radiation and temperature loading give no big influence on computational results but can be important. Two-step computational method highlights deformed shape influence on thrust line position in cross section of arch shell. For further study a long term monitoring program was set since 2005 using SOFO optical tensometer tool.

Jacek Boroń [4] is interested in solving structural and management problems with tools offered by MS Excel® Solver. Spreadsheet programs are very popular software and many engineers are using them. The article is offering a model about using their resources to solve technical and managerial issues. This tool is able to solve small-scale linear programming (LP), smooth nonlinear programming (NLP),

and mixed integer programming (MIP) problems. Examples are drafted both from structural design and economic calculation.

Calculation and analysis of the position of underground structures in discontinuous rock mass are presented by Jiří Boštík in his articles [5]. Three typical alternatives were considered: the underground structure in rock mass with one-sided dip of discontinuities, the underground structure situated in synclinal bend and the underground structure situated in anticlinal bend. Mathematical models were used for the analysis by Finite Element Method using Plaxis software. Mathematical models were planar – plane strain. Maximum vertical displacement is calculated for each case.

Adam Dósa and Valentin-Vasile Ungureanu present in their paper [6] a discrete model which was developed for the buckling analysis of continuous welded rail subjected to temperature load. The model is based on a nonlinear analysis in total lagrangean formulation. The structure consists of beam elements and lateral, longitudinal and torsional spring elements. The source of nonlinearity is due to the geometric nonlinearity of the rail high axial forces and also to the nonlinearity of material type for the lateral and longitudinal resistance of the ballast and the torsional resistance of the fasteners. The track model is encoded into a special purpose program which allows a parametric study of the influence of vehicle loading, the stiffness properties of the structure and of the geometric imperfections on the track stability. Both theoretical and practical experiments data are presented.

In his article Petre Ene [7] deals with the effects of soil-structure interactions in damper structures. The classical approach is to investigating the seismic behavior of structures with seismic dampers by neglecting the effects of foundation-structure interaction. The paper presents a rigorous time-domain procedure to address the interaction effects of structures equipped with fluid viscous dampers and foundations with an unbounded medium. Quantitative results show that, during earthquakes, there are significant differences between a system with and without radiation damping. For greater accuracy, radiation damping should be properly taken into account. More-over, the efficiency of fluid viscous dampers in reducing seismic disturbance of a structure is very dependent on the flexibility of the foundation.

A new approach on fiber reinforced concrete is presented in the study Gherman et al. [8]. Numerical modeling is applied, using a finite element method (FEM) program, to study the behavior of linear structural elements, made from steel fiber reinforced concrete (SFRC). The results stress out the favorable influence of the fibers on the bearing capacity and especially on the ductility of the loaded members. Lack of design standards and practice codes on this material is bringing this field of study under researchers' consideration. The results are largely illustrated with tables and pictures, outputs from the analysis software.

A new look on finite element templates is presented by Wojciech Gilewski [9]. Beams, plates and shells are widely considered in engineering applications. However the corresponding discretization procedures are not yet sufficiently reliable. The formulation aims to satisfy several conditions: ellipticity, consistency and the inf-sup condition. A template, an algebraic form of element matrices, which contains free parameters is generated. Setting the parameters to specific values produces element instances. Two templates are analyzed: Bernoulli and Timoshenko beam. The number of free parameters is discussed by a general method.

The article of Mihail Iancovici and Georgiana Ionică [10] presents an evaluation of the inelastic demand of structures subjected to multiple ground motions. The paper investigates the effect of repeated Vrancea strong ground motions on the behavior factors and the related parameters that accounts for cyclic structural deterioration due to inelastic response. A large number of integrated analyses, nonlinear response analyses and energy balance-based analyses were carried out and estimates were made on the behavior factors for inelastic SDOF systems controlled by flexure with stiffness degradation. It is shown that multiple ground motion of Vrancea type for Bucharest, may lead to an important increase of force and drift demand of structures that usually is not taken into account by the present seismic design codes.

Roxana-Adina Irimia and Alina Nicoleta Vlăsceanu present in their paper [11] a view on the use of databases-business support for the civil engineering. The actual development trend regarding the Databases Management Systems must focus on: using intensively the integration of the Information Systems; obtaining open applications; ensuring interoperability and communication for the Information Systems; focusing on the global performances; Databases Management Systems must become platforms for the databases. Spatial databases (which have resulted by combining the technology of data bases with geographical systems and assisted design) and the multimedia databases (which store and process classical data-text and graphics and also multimedia data-images, audio and video) are strongly recommended for civil engineering use.

Nicolae Boți et al. [12] present foundation solutions for a marketing center in Cluj. In order to accommodate the site conditions three foundation solutions has been discussed: open caissons, embedded 0.3m into the good foundation soil; drilled short piles or precast driven piles inserted into the good foundation soil at lest 15d; foundation beam networks onto an improved soil by a granular material cushion. Based on the analysis performed on the foundation solutions, the foundation system is recommended to consist of flexible continuous footing for the external shear walls and a foundation beam network of the columns inside, all performed on a compacted ballast cushion.

The expert analysis and assessment of the offshore structures is the subject of the paper of Ludovic G. Kopenetz and Ferdinand-Zsongor Gobesz [13]. The structural expertise must cover, beside the vastness of interfering random variables, all-important aspects in order to avoid the pollution of the pelagic environment. Load evaluation, structural analysis aspects and problems concerning fatigue test are presented.

Petr Kotek and Filip Jordán [14] are interested by scenario and impact of global warming in building energy performance simulation. This paper is focused in impact of different outside temperature and sun radiation during the year and mainly in point of view: "what if in future". The climate is lunatic every year and we can see and feel that the temperature is slowly rising all over the world. Nowadays the question of global warming is more and more discussed. Two case studies were chosen for different scenarios of climate change First and second cases are one real administration building in Czech Republic, Prague. One is performed without thermal insulation on the wall construction and second with and their appropriate sensitivity in point of view of climate change is shown.

Lungu Irina, Nicolae Boți and Anghel Stanciu [15] analyze the possibility to predict settlement of a pile group based on design charts. The article starts from the strong intention to modify the actual capacity based design to a settlement based design when foundation systems on piles are concerned. Two main issues are treated: settlement prediction of a pile group based on the single pile behavior; and combination of boundary element with finite element approach.

Design charts proved to be useful tools to set comparative values at work in order to select the foundation elements in the best combination to face even the most pessimistic hypothesis of soil-foundation interaction. A successful and economic design is reached only when the interaction effects are taken into account.

The importance of controlling subsystem in information systems for building industry is illustrated in the article of Peter Mesároš and František Mesároš [16]. The paper presents the necessity, possibility, assumptions and advantages of implementation of the controlling subsystem. In this context authors advise to institutionalize the position of the controller who, on the basis of his knowledge and practical experience, could analyze the detected deviations between the plan and reality. This could assure the uninterrupted operation of information flows, i.e. providing objective information for decision-making on the basis of real processes taking place in the construction.

Roman Musil is interested in the analysis of water consumption in residential building areas [17]. Water supply is essential for residential areas. Water need must be assessed and predict. Using monitoring systems and computation tools the author is evaluating the daily water need, but also minimal and maximal hourly consumption. Results are used for better planning of the water supply and better use of accumulate reservoirs and automatic pumping stations.

Computational instruments are not only used for industrial purpose but also as teaching tools. Irina Radinschi and Brindusa Ciobanu [18] are using Mathematica 5.1 to improving civil engineering physics teaching-learning process. Some examples for studying physical concepts and phenomena and for plotting a general class of physics phenomena are presented. The software provides a good environment for computation, a high-level programming language, text, graphics, and animation. Further, embedded tools allow carrying out length calculations and evaluating the components of some tensor and pseudo-tensor quantities.

Radinschi Irina, Brindusa Ciobanu and Mircea Daniel Frunza [19] are presenting the possibility to study Physics with Maple 9.5. The paper sketches how computer algebra systems like Maple 9.5 can be used to helping the students connecting physical concepts and phenomena with powerful mathematical formalisms and graphical representations. The experience in this area demonstrated that computational physics, together with traditional theoretical and experimental physics, is a reliable tool which helps students to explore a wide variety of phenomena and give them a deeper understanding of these topics. Static charts and animation might be used to demonstrate physical behavior like wave propagation or kinetic and potential energy. The main goal is to allow students the ability to learn physics, to perform length calculations, to make graphical representations and introduce animations, and also to solve practical problems.

Irina Radinschi and Brindusa Ciobanu [20] uncover a strong connection between the computational methods and study of physics. Platforms as Mathematica and Maple have advantages as flexibility and speed, and more advanced graphical facilities. Further, the computational methods allow a rapid learning of physics and they can successfully replace the traditional methods.

Radinschi Irina and Brindusa Ciobanu [21] develop a computer algebra system for energy-momentum localization. Maple 9.5 with the GrTensorII package is used to perform complex calculations. Procedures are used for evaluating the energy and momentum components of the Einstein, Landau-Lifshitz and Møller energy-momentum complexes. Some of the results are presented, and the metric under consideration describes a magnetic stringy solution. GrTensorII yields the energy and momentum components which are involved in the expression for energy and momentum densities. The expressions for energy in the Einstein, Landau-Lifshitz and Møller prescriptions are plotted.

The state of stresses in RC beams with installation holes located in compressed zone is studied by Przemysław Siwiec and Sebastian Toś [22]. The paper presents the influence of locating holes in the compressed area of the reinforced concrete beam. In order to research the actual behavior of the elements a numerical model based on Finite Element Method was created. Two independent analyses were performed in which linear and nonlinear constitutive relations for concrete and for steel have been used. The results acquired have been compared and discussed. The

nonlinear computer model proved to be highly reliable for the analyses of cracked RC elements.

Computer graphics become efficient tools in understanding the design of wooden trusses. Andrei Slonovschi, Ion Antonescu, and Liviu Prună [23] use 3D models to design study and verify wood structures. Use of computer graphical communication and of CADD programs (like AutoCAD) together with classical graphical disciplines (Descriptive Geometry, Technical Drawing) is essential in forming and developing of spatial vision and the ability of reading triple orthographic projection drawings, tools useful for future design and execution engineers.

The paper of Jaroslav Smutny and Lubos Pazdera [24] analyze the dynamic parameters of rail fastening. For evaluation of response signals obtained by rail fastening analysis a new method using time and frequency related transformations has been developed. In the paper the laboratory measurements and dynamic parameter analyses of flexible fastening of Vossloh SKL14 type were described. Short Time Fourier Transformation and Rihaczek Transformation were used for time-localization of the occurrence of frequency elements of stationary and non-stationary signals. The method can be used for designing new rail fastening systems and their parts.

Smutny Jaroslav and Lubos Pazdera present the use time frequency transformations in testing structural elements. The paper [25] deals with the non-destructive testing of structural elements by means of the acoustic response using the jointed time and frequency transforms: short time Fourier and wavelet transforms. These methods make possible to localize the beginning and the end of frequency components contained in the measured signal and they enable to perfectly analyze the spectrum of the non-stationary noise. This way, this mathematical procedure enables to distinguish a good specimen from a defective one.

Based on the measurement and analyses made, it is possible to state that the experiment checked the possibilities of using the given methodology for the detection of structural defects of the measured products and materials from the homogeneity and the cracks formation points of view.

Reinforced soil represents an alternative solution to consolidate earth massifs and perform retaining structures included in the present transportation infrastructure. Anghel Stanciu, Oana Colț and Irina Lungu [26], based on the computer program Cartage, present a method to design of reinforced soil works. The computer program can evaluate the stress within the reinforcement, the displacement of the soil massive, and the safety coefficients at anchorage as well, based on the stability analysis of the massive in case of cylindrical failure surfaces going through the toe of the reinforced soil structure. The method may significantly decrease the design time.

Voiculescu Dragos and Daniela Preda developed computer software for pipe section column sizing. The paper [27] presents the Excel program which has three main parts: the first one is the data input, where the proposed size of the column is set; the second one is the load section, where the maximum loads are input from the structural analysis program, such as SAP or ETABS; the third part gives the results of the structural checks on the proposed section

In [28], Anghel is presenting an implementation of Newton's algorithm (tangent method) in solving nonlinear equations. A C++ program is shown together with an example. Conditions of availability and discussions on the method are extensively treated.

Libuše Beckerová, Gergely Bölckei and Jiří Brožovský observe [29] that the use of the brick chipping from brick factories could be very useful in composition of concrete. This solution is a way to recycle a part of the waste and to have a more environment friendly construction industry. The finely ground brick body shows pozzuolana activity and, tehrefore, it can replace in part even the cement part in the concrete. As a consequence, the price of concrete could be lowered. The authors are showing an analysis of the chemical composition of the compounds in the brick body. Also, experiments are presented in details (compositions, parameters, methods). Conclusions show very good behavior of the concrete characteristics (compression strength, bending strength, depth of the pressure water ingress, dynamic modulus of elasticity).

The method of inequalities method is proposed by Amariei and Mihai [30] for minimum weight building design. Ways and hypotheses to compute optimization of the weight for structures is firstly analyzed. Then the proposed inequalities method is presented. Static equilibrium equations, plastic yielding conditions and the weight function are discussed. An extended numerical example is probing the method.

Ciobanu, Silisteanu and Radinschi [31] are presenting a project focussed on fundamental properties of short-lived radionuclides from decay and from in-beam studies. A first goal is shown to be the formulation of a reaction theory for cluster decay in which the clustering and reaction amplitudes will be represented by means of resonance formulas. A brief outlook of the experimental results and theoretical ideas which define the field is presented together with quantities estimations for the resonance decay widths and relative intensities. A direct numerical integration using step-by-step methods on computer is envisioned.

In their paper, "Experimental and numerical analysis of compressed concrete elements confined with FRP composites", [32], Gabriel Oprisan, Nicolae Taranu and Vlad Munteanu show a method proposed for increasing the strength and ductility of concrete subjected to compressive loading. A detailed testing methodology and an experimental program are developed. Compositions used for fiber reinforced polymer (FRP) resin together with the properties of glass/carbon

fibers are shown. Experimental stages were noticed. Finite element models for the specimen used in experiments were analyzed. Experimental and analytical results have shown very good agreement, proofing the chosen solutions.

Coefficients for Rayleigh models of damping are investigated by Florin Ţepeş Onea in [33]. Damping coefficients are obtained as a linear combination between the mass and stiffness matrices, using a Cauchy sequence. The approach leads to solving the problem of the influence of superior modes of vibration on the energy dissipation in the backlash of a dam. FEM 2D and 3D models were used. Analyzing the results it was observed that, for two modes of vibration, the effect of the mass matrix increase and the effect of stiffness matrix decrease in the same direction with the increase of the second frequency taken into account.

In [34], the authors, Magda Brosteanu and Teodor Brosteanu, refer to the non-destructive testing devices in assessing of old masonry buildings. They focus on flat-jacks technique to determine the state of stress in masonry. Also, they are performing health monitoring using IR thermal-graphic method. The obtained data is used for strengthening structural design of masonry members and thermal renovation design. Photos on instrumentation and buildings are presented.

The same authors write a paper titled, “IT Approach in Heat Transmission Visualizing through Opaque Walls”, [35]. Heat flow image and density, surface temperature distribution, isothermal lines are the problem solved through computational processing of infrared (IR) photographs. Mathematical models are presented and analyzed. Applications using Finite Element Methods for determination of the thermal resistance for different typical wa;; structures are shown. The effectiveness of the IT means is underlined.

A “Comparative Study on the Results of Analytical and Experimental Analysis of a Steel Taintor (Radial) Gate” is performed by Prodescu and Bîtcă in [36]. They intended to test the stress and strain state of a hydraulic gate undertaking a pressure of 20m of water. For this, a 1:4 scale model was built. Also the model was described and analyzed through FEM. The comparison between the two cases has shown good accuracy. Therefore, the models were validated and the required adjustments for design of the original (to be build) gate were withdrawn.

Jiří Brožovský, Alois Materna and Ivan Kološ are contributing to the solving of the non-linear constitutive modelling of masonry structures in 2D, [37]. They apply different laws for bricks and mortar. In the case of mortar, the 2D failure criteria is the Kupfer's criteria. The Bazant's crack-band model is employed for avoiding the use of re-refining the FEM mesh. For bricks, an approach similar to non-local material models is proposed. It guarantees that crack is detected. However, the authors stress that the brick model must be improved. A FEM model of a small wall and the corresponding numerical analysis is shown and discussed. Results were the expected ones.

An extended experimental and numerical work is done in [38]. David Horak, Martin Zlamal, and Petr Danek propose newly developed FRP reinforcements and see their effects under various loads (static and dynamic). The reinforcement is used on longitudinal and (in some cases) on transversal direction in concrete beams. Also, application of FRP for masonry strengthening was in the views of the authors. Data experimentally obtained was used in improving the analytical model for the reinforced structures (FE software based on fracture mechanics of quasi-brittle materials). All results are very encouraging and the paper shows a high quality experimental and analytical achievement.

Josef Fink and Lubomir Ondris propose new shear connectors for composite girders that are subject to patenting at the Technical University of Vienna, Institute of Steel Constructions. The authors are analyzing the new connectors in experimental work as in FEM models. Experiences with ABAQUS push-out test simulation are largely described. Importance of parameters in FEM analysis (mesh, precision, procedure, careful visual check of graphical results etc) is commented. Validation of numerical FEM model parameters was achieved and future connectors' experiments could be, therefor, optimized.

"Structural Expertise of Steel Cables" is the title of a paper [40] presented by Ludovic G. Kopenetz and Ferdinand-Zsongor Gobesz. Taking into account the importance of cable structures, an exhaustive consideration of the main parts an expertise should be composed from is outlined. In situ and laboratory tests together with analytical work for determination of fatigue or corrosion are reviewed. The authors discuss the main topics to be observed in an expertise: steel quality and brands, type of bearing with cables, the effects of loads (wind, self-weight, thermal loads, dynamic loads, etc). A diagram of the site's investigation method based on digital cameras (currently under patenting) is proposed for cables. Typical patterns of wire rope degradation and failure are also shown. A computer program (using FEM) is developed in order to help in cable analysis.

In order to have a better building management, Mária Kozlovská and Michal Danko are proposing a "Computer aided building diary" [41]. They have developed a database application that covers all the legal and technical problems involved in building management. The structure of the application in graphical format is shown. Main screens are also presented and discussed. Advantages for building management of this new tool are revealed.

Ioan Moga and Ligia Moga are concerned about the introduction of the legislation in "determination of the heat flows, of the solar and luminous characteristics of the glazing and of the devices for the solar protection" [42]. They develop a computer program called "SOLAR". Considerations on: glazing system and the solar protection devices; solar and optical characteristics of the glazing; and heat transfer are elaborated. Then a validation of the computer program is performed according to the European (and national) standards.

"Effect of moulding humidity on the properties of dry pressed ceramic tiles" is the focus of the paper [43] presented by Radomir Sokolar. Use of fly ashes in ceramic (green or fired) products is in the views of the study. Taking into account a large interval of moisture for the pressing granulate, and for the two types of ceramic bodies, the properties of the products were experimentally determined. Also capillarity of fired bodied in dependence on pressing moisture of pressing granulate is presented. Tables and graphics illustrate the parametrical studies.

In his paper, [44], Jerzy Szołomicki is applying a damage model for analysis of masonry structures. The model is based on the finite elements method to simulate the ultimate response and the mode of failure. It takes into account the nonlinear analysis of masonry structures (effect of stiffness degradation and the problem of the finite element mesh). After the mathematical concept (of damage accumulation functions) is developed the author is defining the function of the damage criterion. Also global damage indices are developed. They provide accurate data on the state of any component of a damaged structure and the importance to the entire structure.

"A new form of the Active Moments Method" is proposed by Constantin Ionescu in [45]. Based on the work of former famous Romanian Professors Anton Sesan, Nicolae Orlovschi and Gh. Em. Filipescu, the author is improving the method by generalizing it. Equilibrium equations are written together with a description of the Active Moment Method. Then the proposed improvements are theoretically demonstrated.

In [46], Elena Carmen Teleman, Elena Axinte are dealing with priorities in insuring curtain walling's safety design. The authors are showing the influence of climate change on Romanian wind action for buildings. Because of new high speed winds, the effects on the glass-covered buildings rise questions on safety. Design criteria, studies on safety (accuracy in the determination of realistic values of wind pressure action; consideration of wind-induced vibrations in design of light envelopes) and laboratory studies of buildings aerodynamics are the main parts of the paper.

Grzegorz Dmochowski, Przemysław Siwiec and Piotr Berkowski, [47], are performing a "FEM 3D analysis of RC frame foundations of rotary cement kiln". Firstly, a description of the damaged foundations for cement tubular oven are presented. Those foundations have been designed using 2D methods. Authors show the way they have been taken into account the damage to the concrete and steel (passive or active). They also present the high temperature load conditions. For the FEM model osoparametric 3-D finite elements with eight nodes have been used. Results of the analysis revealed that the allowable stress was exceeded in some points and/or because of initial in-plane design damages/cracks are explained. Measures to strengthen the structure are proposed.

Using 'Femme' (a open computer program that simulates the environment and developed by NIOO-Netherlands Institute of Ecology) L. De Doncker, P. Troch, R. Verhoeven, K. Buis, and P. Meire, are researching the way to integrate into that software the flood routing [48]. The complexity for the description and propagation of waves in rivers is solved through different wave models (based on the kinematic, parabolic and Saint-venant equations). As an immediate application, the case of river Aa in Belgium is studied. The importance of the research on environment and prediction of floods is underlined.

In order to explain observed failure and prevent eventual future failures, Przemysław Siwiec and Sebastian Toś are conducting a "Simulation of cooling tower collapse on the basis of non-linear concrete model and FEM analysis", [49]. They firstly describe the sequence of the collapse of the cooling tower. The collapse (from 1987) occurred in a calm day and without any previous signs, therefore practically unexplained. A computer FEM detailed model (geometry and materials' properties) is shown and material and geometric non-linear analyses under various loads are carried out. The computer simulations lead to the explanation: because of strong winds that occurred only few days before the collapse together with material degradation were the cause of that failure phenomenon.

Irene Daprà and Giambattista Scarpi study the "Unsteady axial Poiseuille flow of a Bingham fluid in an annulus", [50]. They propose a new model based on the error function to regularize the constitutive equation for Bingham fluid (as bentonite, montmorillonite, slurries), fluids which present a yield stress. Steady and unsteady flow (start-up flow, cessation of flow, pulsatile flow) laws are presented. Numerical analyses were conducted and solution has been carried out via an implicit finite difference method.

The problem of lime efflorescence on concrete is a hard task and studied from long time ago. A paper on "Formation of lime efflorescence on concrete and concrete products", [51], is presented by Tomáš Fojtík and Jiří Brožovský. Firstly a description of the conditions the phenomenon occurs is performed. Then primary and secondary lime efflorescence notions are explained. The 15 conditions that could lead to efflorescence occurring and the mechanism involved are shown. Measure that can be taken for avoiding and measures to remove the efflorescence are also presented. Various experiments for combating the lime efflorescence were underwent and detailed by the authors.

Monica Gheorghiu and Mirela Chelcea are showing how "The use of computer means in representation of the ruled surfaces", [52], is very useful in teaching Descriptive Geometry to university students. Very difficult to imagine 3D representations become easy to produce and easy to understand. The use of animations also helps the teaching process. Examples of paraboloids, conoids,

cylindroids, helicoidal surfaces and hyperboloids illustrate the teaching/learning proposed procedure.

Horațiu Mociran and Eugen Panțel are concerned about the problem of limiting earthquakes' effects on structures, [53]. They propose a numerical study on seismic performance of three different structural systems: simple framed structure, base isolation and viscous damped structure. The loads are three scaled artificial earthquakes of Vrancea type that matches on P100-1/2006 code response spectrum. Base shear, interstory drift, floor accelerations and some performance indexes show that viscously damped frame was best performing.

The topic of [54] is the "Identification Methods of the Nonlinear Systems Subjected to Seismic Actions". The two authors, Doina Stefan and Violeta-Elena Chitan, present an extended overview on the development of stochastic methods in the field of identification. Techniques for linearization of stochastic equation of motion are firstly explained for single degree of freedom systems and then for multi-degree of freedom systems. The case of the non-linear oscillator model is also treated.

3. CONCLUSIONS

The Computational Civil Engineering symposiums held every year since 2003 in Iasi, Romania, show that civil engineers are united through their need for computation and also by the need to exchange their findings.

The progress in Civil Engineering is strongly connected to the implementation of advanced computational means and to the fast spread of the knowledge to the education/research/production sites.

Computational Civil Engineering symposiums series are becoming, no doubt, a vector of progress especially in the Eastern part of Europe with nice perspectives for growing.

References

1. Ionescu, C., Păuleț-Crăiniceanu, F., Scinteie, R., Nicuta, A. (editors), *Civil Engineering,* Proceedings of the International Symposium "Computational Civil Engineering 2007", Editura Societății Academice "Matei-Teiu Botez", Iaşi, 2007, ISBN 978-973-8955-14.
2. Apeltauer Tomas, Petr Holcner, Martin Kysely and Jiri Macur: Non-linear effects in traffic simulations, *idem*, pp.25-38;
3. Bondars Kaspars, Aleksandrs Korjakins: Influence of deformation at a heritage building support on stability of groined masonry arch, *idem*, pp.39-54;
4. Boroń Jacek: Application of MS Excel® Solver in Solving Structural and Management Problems, *idem*, pp.55-65;
5. Boštík Jiří: Underground structure in discontinuous rock mass, *idem*, pp.66-74;

6. Dósa Adam, Valentin-Vasile Ungureanu: Discrete model for the stability of continuous welded rail, *idem*, pp.75-84;
7. Ene Petre: Soil-Structure Interaction Effects of Damped Structures, *idem*, pp.85-94;
8. Gherman Liviu, Petru Mihai, Nicolae Florea, Constantin Gavriloaia, Ioan Paul Vodă: Numerical Modeling of Fiber Reinforced Concrete (FRC). Fiber orientation angle α = 00, fiber length lf = 50mm, *idem*, pp.95-102;
9. Gilewski Wojciech: A new look into finite element templates, *idem*, pp.103-112;
10. Iancovici Mihail, Georgiana Ionică: Evaluation of the inelastic demand of structures subjected to multiple ground motions, *idem*, pp.113-123;
11. Irimia Roxana-Adina, Vlăsceanu Alina Nicoleta: Databases-business support for the Civil Engineering, *idem*, pp.124-133;
12. Boți Nicolae, Irina Lungu, Ioan Boți: Foundation solutions for a marketing center in Cluj, *idem*, pp.134-139;
13. Kopenetz Ludovic G., Ferdinand-Zsongor Gobesz: The Expertise of Offshore Structures, *idem*, pp.140-147;
14. Kotek Petr, Jordán Filip: Scenario and impact of global warming in building energy performance simulation, *idem*, pp.148-158;
15. Lungu Irina, Nicolae Boți, Anghel Stanciu: Settlement prediction of a pile group based on design charts, *idem*, pp.159-164;
16. Mesároš Peter, František Mesároš: The importance of controlling subsystem in information systems for building industry, *idem*, pp.165-171;
17. Musil Roman: Analysis of Water Consumption in Residential Building, *idem*, pp.172-179;
18. Radinschi Irina, Brindusa Ciobanu: Improving Civil Engineering Physics Teaching-Learning with Mathematica 5.1, *idem*, pp.180-190;
19. Radinschi Irina, Brindusa Ciobanu, Mircea Daniel Frunza: Physics with Maple 9.5, *idem*, pp.191-200;
20. Radinschi Irina, Brindusa Ciobanu: Physics Studies – Computational Methods, a Strong Connection, *idem*, pp.201-210;
21. Radinschi Irina, Brindusa Ciobanu: Computer Algebra System for Energy-Momentum Localization, *idem*, pp.211-219;
22. Siwiec Przemysław, Sebastian Toś: The state of stresses in RC beams with installation holes located in compressed zone, *idem*, pp.220-230;
23. Slonovschi Andrei, Ion Antonescu, Liviu Prună: Computer Graphical Communication an Efficient Tool for Understanding the Design of Wooden Trusses, *idem*, pp.231-245;
24. Smutny Jaroslav, Lubos Pazdera: Analysis of dynamic parameters of rail fastening by Rihaczek transformation, *idem*, pp.246-255;
25. Smutny Jaroslav, Lubos Pazdera: The use of time frequency transformations in testing structural elements, *idem*, pp.256-268;
26. Stanciu Anghel, Oana Colț, Irina Lungu: Design of reinforced soil works – Textomur structures – based on the computer program Cartage, *idem*, pp.269-276;
27. Voiculescu Dragos, Daniela Preda: Computer program for Pipe Section Column Sizing, *idem*, pp.277-281;
28. Cornelia Victoria Anghel: Computational method and application using Newton Algorithm, *idem*, pp.282-286.
29. Libuše Beckerová, Gergely Bölckei and Jiří Brožovský: Partial substitution of Cement in Concrete by Finely Ground Brick Body, *idem*, pp.287-294.
30. Constantin Amariei, Iulian Gabriel Mihai: Minimum weight buildings design using inequalities method, *idem*, pp.295-306.
31. Brindusa Ciobanu, Ion Silisteanu, Irina Radinschi: Scientific Perspectives for Future Research Work in Fundamental Properties of Short-Lived Radionuclides from Decay and from in-Beam Studies, *idem*, pp.307-315.
32. Gabriel Oprisan, Nicolae Taranu, Vlad Munteanu: Experimental and numerical analysis of compressed concrete elements confined with FRP composites, *idem*, pp.316-325.

"Computational Civil Engineering 2007", International Symposium
Iaşi, România, May 25, 2007

Non-linear effects in traffic simulations

Tomas Apeltauer, Petr Holcner, Martin Kysely and Jiri Macur
Faculty of Civil Engineering, Brno University of Technology, Brno, CZ-602 00, Czech Republic

Summary

Growing requirements on transport of passengers and goods have a principle impact on life and economy. It is not need not intricately needed to search accurate formulation of economic consequences, on the contrary would be enough to quote, for example, United States Secretary of Transportation Norman Mineta, according to which local drivers lose in traffic jams almost 4 billions hours and 2 billions gallons of fuel each year. Upward trend is perceptible especially on highways, where some out of traffic jams affects two-thirds drivers every day, which is double compared to situation twenty years ago.

In Los Angeles at that time transportation problem lasted 4.5 hours every day, about two decade later in the same town transport breaks down for 7 hours every day. It is evident it is not always possible extend capacity carriage according to their users needs and is necessary to search alternative manners. One of these is transition to description of traffic flow via nonlinear dynamics, which explains the behavior of very complicated systems.

If we explain properties of the traffic flow, we can try to describe emergency of traffic jams and search manners, how those situation precede at least in part.

KEYWORDS: non-linear dynamics; traffic flow; congestions; traffic modeling; simulations

1. TRAFFIC CHAOS AS A TECHNICAL TERM

Nonlinear dynamics as a tool for understanding chaos emergency already gets through wide spectra branch. Presently it is perceptible that we cannot apply the clean deterministic look even on very simple system, whereas the meaning of nonlinear system features grows with their complexity. One of such dynamic systems is the traffic flow. A group of German physicists headed by Dirk Helbing, Boris Kerner and Michael Schreckenberg published in top class magazines like *Physical Review Letters, Journal of Physics* and *Nature* results of computer simulations of the vehicle movement. They noticed following interesting matter: while using equations for a gas molecule movement, supplemented by some specific characteristics of the human driver (among others the effort to avoid

collision), they discovered special effects which truly copies real characteristics of traffic. For example in places of bottlenecks traffic started compression, whereas this perturbation expands as a density wave against the direction of traffic flow. It is the exact analogy of known retardation and accumulation out in fronts before bottlenecks – as soon as vehicles near bottleneck slow down, other vehicles will slow down too, which causes the wave of "stop-and-go" spreading upstream.

At all the biggest surprise was the following result: the traffic jam can emerge in certain circumstances spontaneously, without bottlenecks, traffic accident or other at first sight obvious causes. Traffic flow is able to flow freely, and nevertheless suddenly will change to the slowly ridden flow. Under certain condition the "negligible" fluctuation in the vehicle velocity or headway can lead to the system collapse, which last for long hours after primary impulse.

In spite of it is relatively cheerless inquest, it is absolutely in agreement with results of mathematical models of many physical and biological systems. All these studied systems have the common emergency of phenomenon known from popular literature as the "chaos". Simply: in every complex system with many parts which influences each other a weak fluctuations can lead to big consequences. But we cannot predict the emergency of such turnover. Scientists these phenomena describe like non-linear – seemingly unimportant change in one characteristic might have unreasonably extensive incidence on entire system. Non-linear characteristics were detected in weather, biological systems or chemistry. And during recent decades it is also mentioned in transport.

2. REAL TRAFFIC DYNAMICS OBSERVING

Every correct physical theory requires agreement with experimental data. Good theory had to reproduce known system behavior as also predict its future. It will be shown further that selection of the right method for data collection on road is a very idyllic business with comparison to the construction of the right theory.

2.1. Measuring of the traffic variables

Probably the oldest and at the same time most complicated technology of traffic detection is *aerial photography*, by the help of whose we can obtain total view of the situation on tracked section. If we need to obtain concrete traffic variable such as traffic flow velocity, we have to use digital picture analysis. Problems of visual analysis generally belongs to the most complicated tasks, it is very time consuming and not balanced with corresponding result accuracy. Its usage in current traffic research is therefore rather border. But some advantage aerial photograph has further: emergency of traffic jam and its progress is apparent at the first sight.

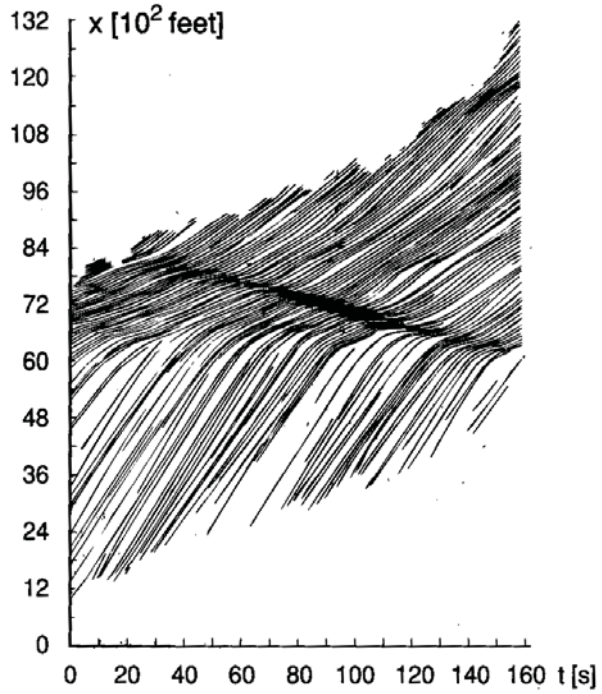

Figure 1. The traffic jam behavior, derived from aerial photography [17].

The second way can be taken with *floating vehicle*, which works as a movable detector. But the biggest data sets are now collected by detectors placed on concrete fixed place on the motorway. Most widespread is the *induction loop* placed closely below the road surface. Incoming vehicle turns its inductance and creates a weak signal.

From a simple induction loop we can obtain especially information about vehicles that passed tracked place during definite time, which matches the definition of *traffic intensity*. Today double induction loops ale placed in the most cases, which make possible to measure in addition vehicle lengths and its velocity. Combination of these values finally makes it possible to determine *traffic density* like second crucial traffic variable. Correlation between traffic intensity and its density is a very basic tool in the traffic research.

2.2. Measurement with induction loops

We can obtain a good notion about possibilities of detection via induction loops from A5-Nord highway nearby German Frankfurt.

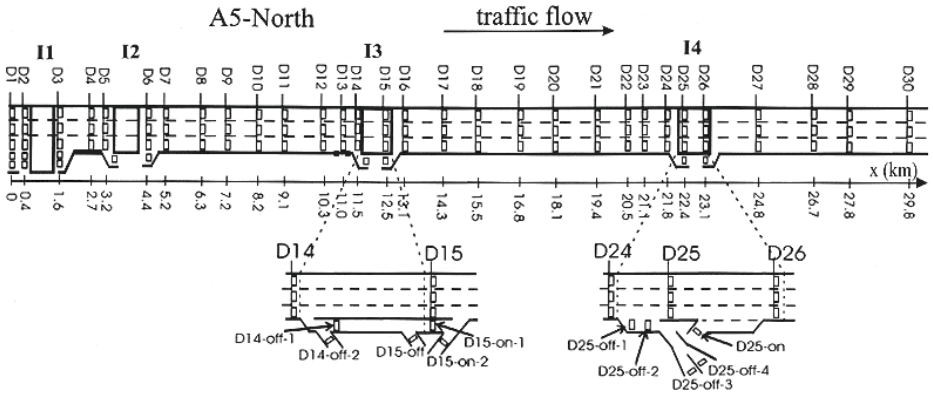

Figure 2. Location of induction loops on the part of A5-Nord highway [5].

Described section of highway has on the whole four intersections which join it on next communications. On that section there are deployed about thirty double induction loops with labels from D1 to D30. Each set of loops includes three detectors for every lane, special cases are slip and trunk roads.

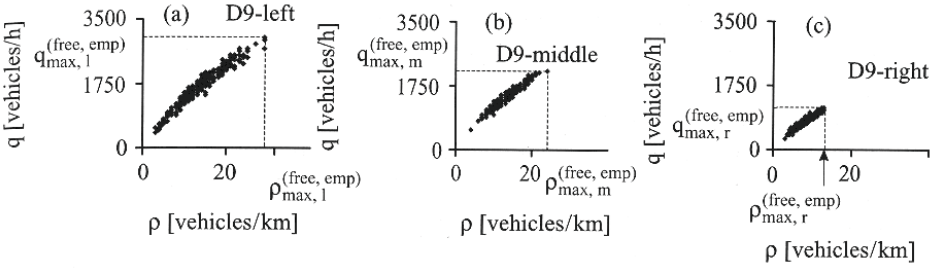

Figure 3. Data collected on A5-Nord highway. We can see one minute averages of traffic densities and intensities from lanes on the place od detector D6. Measurement was on 9th October 1992 between 7.00 – 12.00 [5].

We can see results on selected detectors on fig. 3. Three graphs a) to c) shows the dependence of traffic flow intensity on traffic density for every of the three lanes. How we will see further, in all cases this values correspond to *free traffic flow* and at first sight there are perceptible expressive differences in maximal measured values. Here we have to remark that the on German motorways there is a big asymmetry in vehicle types among lanes. Trucks here usually do not move in the left lane, only use the right one in some cases the middle one for overtaking.

2.3. Free flow and congestions

As mentioned above, there are three basic variables which characterize traffic flow in specific time and place: *traffic density* (number of vehicles in one kilometer), *velocity* (in most cases km.h^{-1}) and *traffic intensity* (number of vehicles which passed specific point in some period of time, one hour generally). It holds in steady traffic flow the traffic intensity is a product of its velocity and density. Unfortunately both these variables are not mutually independent and that is why it is necessary to determine its correlation.

We can start from obvious and empirically tested facts: maximal velocity in traffic flow corresponds to the density near zero, when each one vehicle in not influenced by another one. Then we denote that case as *free traffic flow*. From this we can define *congestion* as a state supplemental to the free flow, which contains some other traffic situations. One of these states is the critical value of density, when the speed of traffic flow drops to zero and the flow moves via small jumps or it stops definitely (headways are too small for safe and useful constant speed). We can see that between the free flow and this critical value the velocity must go down (usually supposed monotonously and continuously). Determination of this dependency is very basic and also very complicated task during investigation of traffic flow.

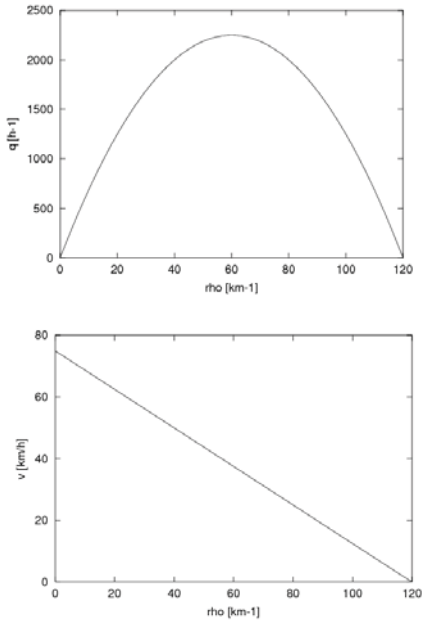

Figure 4. Basic and very simple traffic model according to Greenshields, which comes from strictly linear velocity-density dependency. Maximal traffic intensity is reached in middle velocity for this model.

2.3. Fundamental diagrams

The basic instrument for description of steady flow and its global properties is the fundamental diagram. Its most common type describes dependency of the traffic intensity on the traffic density. In is not obvious from diagram itself that the key correlation between density and velocity is uncertain and efforts to determine it precisely were not successful yet. Nevertheless we can some derive some basic characteristic also from empirically gained average values of traffic quantities. We can use for demonstration data from A5-Nord again (fig. 5).

Contrary from previous entry are now showed all measured values which clearly apportioned into two independent groups. Left part graph appertain to already discussed free flow, the right pat to congestions. The waveform corresponds to reality, when the traffic intensity is able to growth almost linear as far as to the certain critical value. Then be enough so ever minor perturbation to switch free stream into congestion. Traffic density nevertheless doesn't need to necessarily growth and may even temporarily tail off. We can see again the phenomenon of sudden emergency of traffic jams at the same time key feature of complicated systems.

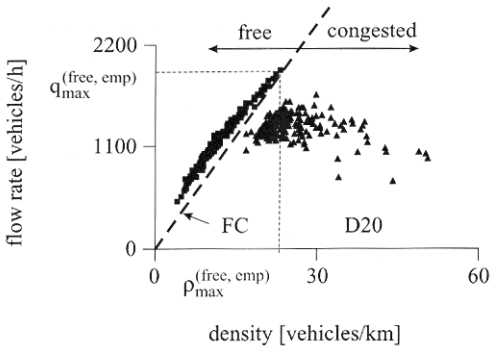

Figure 5. Fundamental diagram of traffic flow, gained from one minute averages traffic density and intensity. Data was collected on A5-Nord on 23. March 2001 between 9.00 - 15.00 via detector D20, it is an average from all three lanes [5].

3. TRAFFIC FLOW SIMULATIONS

It is possible to see dynamic properties of traffic also through the numerical simulation. We have to create a model, which truly describes vehicle behavior and at the same time won't contain unbearable quantity of parameters. As well it is necessary to choose a good simulation method which generates results in a good time. We will present methods at first.

Till this time plentifully used access are *cellular automata*. Its principle is in dividing the motorway to the finite count of blocks and each block in each computation step contains or does not contain just one vehicle. That is why are cellular automata extreme discreet and then only crudest approximation of the real situation which is balanced by high simulation speed and low hardware exigencies.

Analog models as an opposite access have slow entrance only in last years. In contrast to cellular automata it works with vehicles, which are equipped with moving equations. Evolution of this model looks as moving of bubbles in narrow pipe for example. The model behavior is more realistic but also much more time-consuming for computational time.

Cellular automata were used for investigation of traffic flow at the beginning of wider focus to this problem. The main reason was relatively low level of computers and quite good results of this model. Especially the first reason is not actual in last years.

Together with choosing of good method we have to find a good model. This situation is much more transparent, because two main groups of models have difference in the basic principle.

We can consider the traffic flow as a complicated system with separated vehicles. Each vehicle is defined by its features and the main one is dependency between acceleration and the situation around the vehicle. Some used algorithms try to Describe observed properties of a real traffic flow (dynamics, physiological and psychological ability of a driver). These models are known as *microscopic*.

Macroscopic access assume with traffic flow as a continuum defined by the common presumptions. These can be derived by inference from border conditions, measured values in real flow may be based on analogies with physical phenomena, for example from fluxion liquids or gas.

It is often used the third combine approach, when the characteristics macroscopic features are derived from integration of microscopic transport models and presumptions about fluctuations.

The main advantage of the macroscopic access is the ability to describe evolution of traffic flow by one or more differential equations. Is however debatable, if is this presumption of possibilities this unification lawful – analytical complication and venture of this access appears to be also heavy cost behind aesthetics of classical theory.

Users of microscopic models on the other hand can get round of the danger of complicated equations. But it is not all, they early snarl up on crossroad of necessary numeral definition of this model pivotal parameters. About the uncertainty generally witnesses for example historical survey of 23 models defined by "safe distance from previous vehicles in dependency of its speed" and

"responsing time" [1]. Response time is between 0 – 2 s, its arithmetic mean is 0.78 s. The maximal value of traffic intensity is 1050 – 4800 vehicles per hour, with the realistic average 2050 vehicles per hour. The vehicle speed, at which is achieved full intensity, is between 10.6 – 55.2 kmh^{-1}, in some cases even growth to infinity (virtually it is necessary to consider about technical or legislative limit). The average (without infinite values) is 29.0 $km.h^{-1}$. Arithmetic mean itself do not give any help – rather only underscore frustrating motley of models, from which only little is unusable and unfortunately till this time any model is not implicitly good. Perhaps that is just it at projection and scheduling communication meanwhile dominates experiential access, which does not consider behavior inside traffic flow.

3.1. Car following models

Vehicle-following models, exactly Car Following Models (CFM) are investigated nearly for a half century. Determination of the dependency of vehicle acceleration on traffic conditions is in this case fundamental – in the simplest case just on the condition of the previous vehicle (the vehicle driving before). In spite of the fact that this task may appear at the first sight trivial, we did not manage to find a generally respected model which would reflect the reality and would be at the same time sufficiently compact, transparent and especially reasoned until today.

Thus certain general demands were accepted which would meet this proposal without the apparent internal connection of the model with reality. Among these "outer" demands belong especially:

- Non-collision character of simulations performed in the whole spectrum of possible parameters and initial conditions.
- Physically reasonable values of the vehicle velocities and accelerations in course of simulation.
- Asymmetrical character of the model – acceleration different from deceleration (usually a stronger deceleration is admissible, e.g. in case of a threatening collision).
- Emergency of global conditions corresponding to the real observation – non linear character of the model (waves "stop and go", spontaneous emergency of congestions in case of above critical densities, hysteresis of traffic flow intensity in case of above critical and under critical density etc.).

One of the most often studied models in last time, which partly satisfies the requirements mentioned above, is the so called Intelligent Driver Model (IDM) which was used for experiments of simulation. This model may be considered to be an interpolation of two members for acceleration and deceleration with different shapes in both parts.

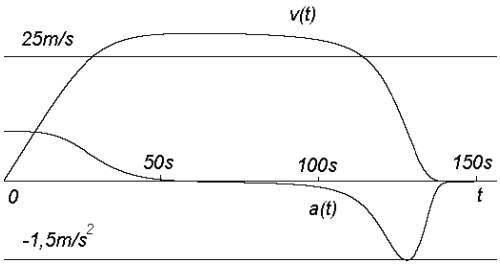

Figure 6. Vehicle velocity and acceleration according to IDM model. Start and stop before an obstacle at the distance 3000 m were used. This kind of test is a good indicator of the model relevance.

Before the simulation we can check for example the first outer demand via the simple experiment, when we test the ability of vehicle to stop ahead the block (fig. 6).

3.2. Model simulations

For the simulation itself we have created a program environment in Java programming language due its easy accessibility, simplicity and portability in internet. Each vehicle is represented by an object with its own parameters and the whole system of vehicles is represented by the so called binded list. In such way it is possible to dynamically change number of vehicles in the system.

For a traffic flow simulation it is advantageous to use the cyclic border conditions which are commonly used for a systems of interacting particles – in this case it means to put vehicles on a circular road with sufficiently large radius. In our case we have chosen the radius 1 km, the total road length is more than 6 km and so we can suppose the system behavior is not rather deformed by correlation between the first and the last vehicle.

3.2.1. System visualization

Direct system animation, when a movement of each vehicle is animated by an object on the circular road, is suitable just for program tuning – it does not bring a good idea about actions in the flow and more over it decelerates the calculation. The representation of time dependent development of density field is more interesting. We unwrap the road in abscissa, where we record each vehicle position by one point. After the selected time interval we similarly indicate a further line of the density field. After sufficiently long interval there arises a model giving a good idea about the development of a vehicle density on the whole road (fig. 7).

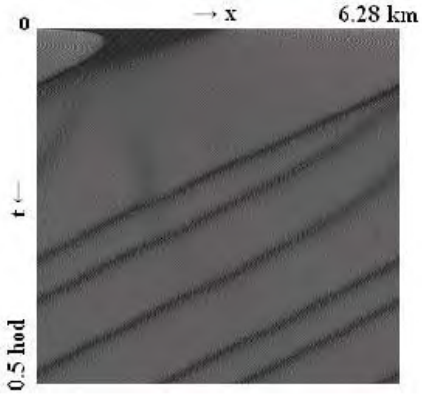

Figure 7. Development of vehicle density. In the beginning vehicles do not move and are homogeneously dislocated in the first half of the road length.

In the mentioned visualization of the density field development there is the distinct quick fixation to the stable state with three synchronized congestions moving upstream. The system moves to stable state with arbitrary initial vehicle distribution. Total number of vehicles in the system is 200.

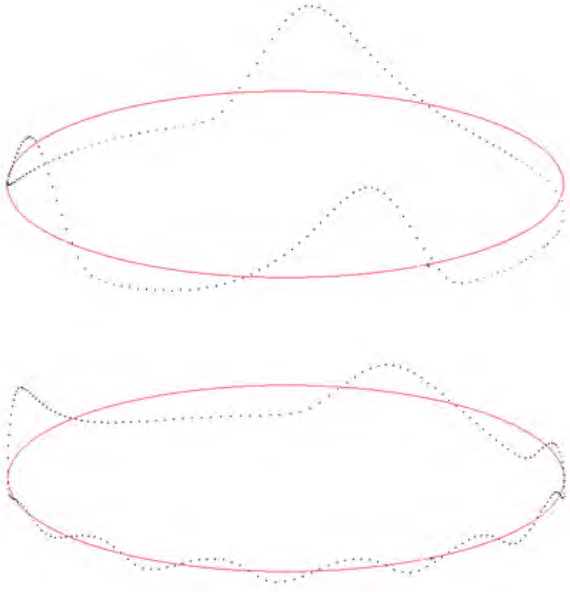

Figure 8. Screen shot from the animation of density distribution in stabilized condition. Full ellipse represents the average density level, which remains constant. The first picture shows the system state after one hour of simulated time, the second one shows the system after seven hours.

Another type of visualization of system development could be the local density animation (fig. 8). The calculation speed evidently suffers from the animation; however it gives a good idea about mutual interaction of density fluctuations during the stabilization of system and their motion in stabilized condition, which is always upstream.

We can make an interesting conclusion from the simulation: In spite of the fact that congestions in a flow can be unevenly distributed, they have the same form and size which is obviously an expression of vehicles with identical properties.

3.2.2. Obtained results

The main question could be the shape of fundamental diagram. In simulations we used mean values of traffic density and intensity gained from all vehicles on whole road. The final shape of fundamental diagram is too “smooth” and does not show real transient processes in the traffic flow (fig. 9).

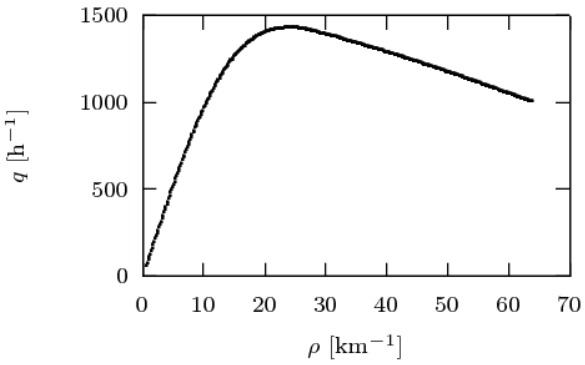

Figure 9. Dependency of simulated traffic intensity on average traffic density.

But we do not have so complex data during the real physical measuring. That is why the real fundamental diagram has so different shape. The main difference in not only in clear reasons: physical measuring do not work with stable traffic flow and vehicles do not have the identical properties. The basic reason is finite time interval, when we measure traffic intensity and density. With the sufficiently long time interval we can obtain similar results in modified simulation experiments, which reflect physical measuring.

It is possible to choose reference point on the simulated road. Each vehicle in each step tests, if it crossed over this point. In positive case the global counter increments with one. By this way we can simply “measure” the traffic intensity in

the selected point for the selected time interval (corresponding number of computational steps).

The same trivial situation is during measuring of corresponding traffic density. This quantity is in real situation derived from measured vehicle speeds and time gaps. Each simulated vehicle has the value of distance from previous vehicle for computing of acceleration.

This value is then possible to use for calculation corresponding local mean density for a period of measuring interval. Then we have to collect to the other counter headways of vehicles, which goes through the reference point.

It is obvious that for traffic densities, when we have stable traffic flow without congestions, we will obtain same values for fundamental diagram as in averaging in the whole system. Totally different situation occurs when we have traffic flow with congestions. Then some few measurements will not give same values, but set of different values on discreet levels of traffic intensities. Dividing into groups is caused by counting only integer over of the vehicle on the bounds of time interval. By this way we will get fundamental diagram which looks more realistic despite of same vehicle properties and stable flow (fig. 10).

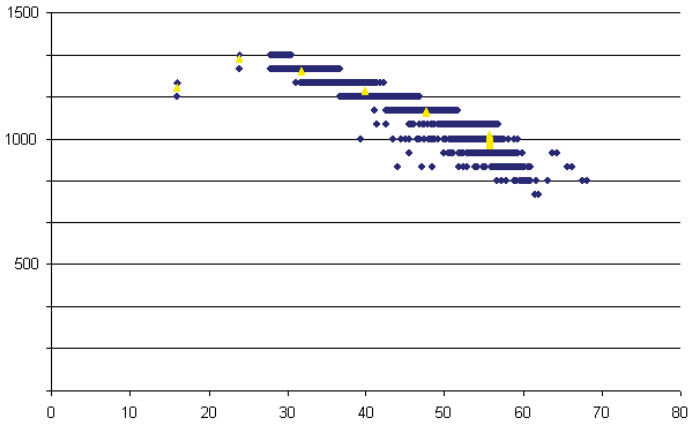

Figure 10. During profile measuring the fundamental diagram looks more realistic as the method of its construction.

From the figure it is apparent that in linear part of diagram is profile measuring concurrent with measuring on the whole system. With emergency of congestions data “blurred” and distances of these levels depends on the period of measuring. We can anticipate that for sufficiently long measuring interval the measured values will converge to values of the whole system.

3.2.3. Non-linear phenomena

The basic simulation experiment was performed on a system with a maximum number of 400 vehicles, i.e. with density of 63.7 vehicles/km. The flow stabilization was indicated by a stabilization of root-mean-square deviation of distances from an average value. The stabilization was considered as a difference between individual cycles (the passage of reference vehicle through the start) smaller than 10^{-5}. After each stabilization one vehicle was removed from the system while maintaining the existing states of other vehicles. The gap thus generated was quickly filled, though the existing imbalance was sufficient for the system to jump over into near state with various numbers of congestions. For comparison there an experiment was performed – after each change of the vehicle number, a new initial situation was set (vehicles homogenously distributed along the road without move).

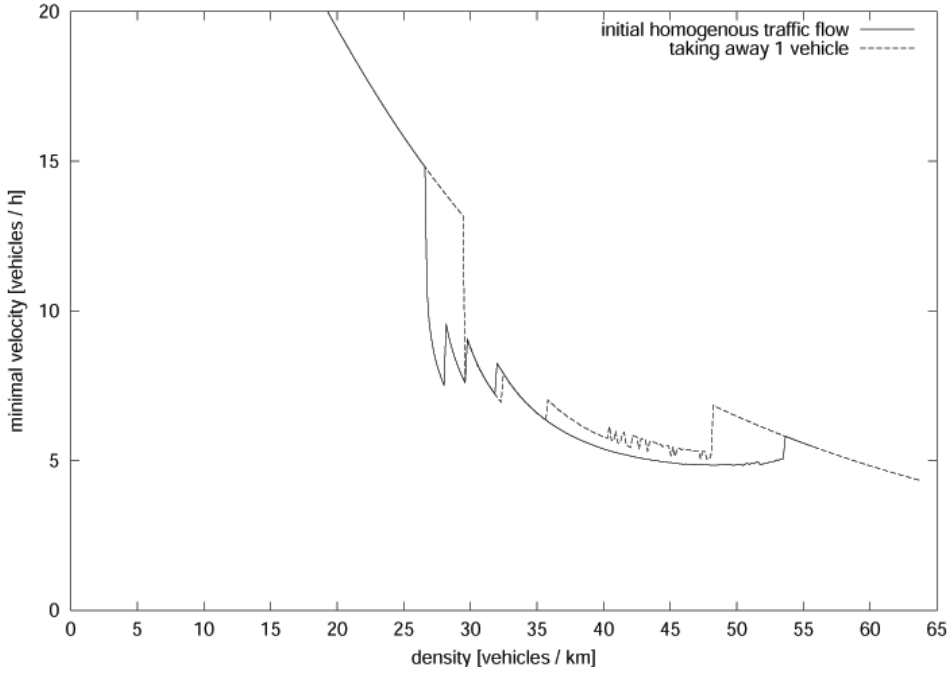

Figure 11. Comparison of dependency of velocities congestion on average density at various strategies of setting initial conditions. Bold line corresponds to the setting of the homogenous traffic flow, thin line to the taking away of the vehicle from the flow without any change of other vehicles states.

From fig. 11 we can see that the disturbance created by taking away the vehicle will be sufficient for the system to overlap into the congestion sooner than it is created by rounding up errors and discretization. In another words in the interval 48

– 53 vehicles/km at least two stable situations exist side by side – homogeneous distribution of vehicles and balanced congestions, while the final situation depends on the initial conditions. At densities about 45 vehicles per km there are stable situations with various numbers of congestions. During the stabilization from a homogeneous initial situation the system converges alternatively to five or six congestions distributed along the road; with a strategy of taking away vehicles the system stays in a stable state of four congestions. For a lower density the state with six congestions become unstable and extinguishes. A detailed investigation of stable areas of this model is difficult with regard to the fact that space of initial conditions is created among others by the density function.

Together with the state overlapping, occurrence of higher number of stable situations is a typical property of non-linearities.

4. CONCLUSIONS

The outlined microscopic models of traffic flow are only part of a wide spectrum of further models being used. Many of them are not sufficiently theoretically described because they are parts of commercial products, and therefore subject to commercial confidence.

At present a coexistence of models is admitted with some of them describing traffic flow better at higher densities and others at lower densities or other modes. Traffic engineers still wait for a model which would not contain large number of parameters with the necessity of calibration and which would at the same time characterize various traffic modes. Nevertheless it is possible to make a series of interesting conclusions even from the existing models which may be verified in practice – this is what we tried to do in this paper.

References

1. Bernard, M., Notes Notes on the Design Concepts for Transport Infrastructure: Past and Future, *4th Swiss Transport Research Conference*, Monte Verita, Ascona, 2004.
2. Transportation Research Board, **Highway Capacity Manual 2000**, *National Academy of Sciences*, USA, 2000.
3. Lighthill, M. J., Whitham G. B., *Proceedings of the Royal Society* A 229, 1955
4. Helbing, D., Hennecke, A., Shvetsov, V., Treiber, M., Micro- and Macrosimulation of Freeway Traffic, *Physical Review Letters* **82**, 2000
5. Kerner, B. S., *The Physics of Traffic*, Springer, New York, 2004
6. Schreckenberg, M., Schadschneider, A., Cellular automaton models and traffic flow, *Journal of Physics A: Mathematical and General* 26 **L679-L683**, 1993
7. Schreckenberg, M., Schadschneider, A., Car-oriented mean-field theory for traffic flow models, *Journal of Physics A: Mathematical and General* 30 **L69-L75**, 1997
8. Helbing, D., Traffic and Related self-driven many particle systems, *Reviews of Modern Physics* 73 **1067-1141**, 2001

"Computational Civil Engineering 2007", International Symposium
Iaşi, România, May 25, 2007

Influence of deformation at a heritage building support on stability of groined masonry arch

Kaspars Bondars[1], Aleksandrs Korjakins[1]
1Faculty of Building and Civil Engineering, Riga Technical University, Riga, Kalku str. 1 LV-1658, Latvia

Summary

Masonry arch stability criteria definition has been developed by numerical modeling of cracked arch shell structure of Riga cathedral. Settlement of supports induced strains in masonry arch shells which lead to stress redistribution and crack forming in masonry shell structures is serious problem for heritage buildings. Deformation criteria should be developed for safety exploitation of heritage masonry structures. The main task of the present research is - developing deformation criteria for evaluating of masonry shell construction stress-strain state. Three-dimensional scanning of arch structure by means of Leica 3D laser scanners were used to determine geometric model of masonry arch shell. Previously accomplished monitoring data was used and a new monitoring program was developed to define unequal settlements of supports. The settlements monitoring of Riga cathedral supports and numerical modeling to define settlement inequality were used as initial information to compare computer modeled deformed structure shape with existing cracked masonry structure. Geodesic monitoring by optical tools and mechanical tensometers have been used for determination of a crack expansion since 2005. Twenty one Optical Fiber Sensors of SOFO type are used now to measure deformations to establish safe exploitation limits. Multilevel analysis of masonry shell has been fulfilled by finite element software and applied for developing safe exploitation criteria.

KEYWORDS: structural masonry, masonry fracture, groined arch, heritage building safety, numerical modeling.

1. INTRODUCTION

Since past masonry structures were built by time-honored method of trial and error. The one of the first written rules and building code was "de Architectura" in ten volumes written by Marcus Vitruvius Pollio, roman architect approximately at 1st century. Medieval time masonry unions use time approved methods of masonry structure cross sections, shell geometry, proportions and forms. Masonry code in medieval Europe was distributed by Christianity influence as sacral building forms, proportions and architectural styles. An objective of investigation is deformed

structure of Riga cathedral in Latvia capital city shown in figure 1. 13th century built masonry Gothic arch shells which are built from solid clay bricks are one of the first masonry shell covered structures in Latvia.

Figure 1. North front of Riga Cathedral

Cross arch and star arch shell where commonly used as type of heritage building shell. Long building process and changes in finale view of cathedral was usual by-effect in building process centuries ago. Riga cathedral had long erection process with stops and design changes. Few steps of erection and enlargement by changing city demands took place also. Fire took place in 1547 when tower and nearest roof parts were lost. A cross and star type masonry arches were partly rebuilt after Swedish / Russian war in 16th century. Medieval European Hansa union cities were usually located near river deltas. The supporting piles and subsoil situation therefore in Riga cathedral are survived today and found in not satisfied conditions. Weak subsoil under building foundations is common situation in Old Riga city. For lot of buildings wooden piled foundations are used to transfer loads to dense sandy layer through loose sand located under footings. Wooden pile life time practically is not limited under ground water minimum level but pile condition after eight centuries of building life time were found in unconditional situation. Seismic risk in Latvia region is low but support deformations proceeds in most of Old Riga piled supported buildings.

Structural weakness or overloading, dynamic vibrations, settlement, and in-plane and out-of-plane deformations can cause failure of masonry structures. To prevent the accidental situation in heritage buildings safety criteria must be specified determining deformation limit between masonry arch shell interacting parts. Surveillance des Ouvrages par Fibres (SOFO) optical fiber sensors will be mounted on arch shell cracks for deformation monitoring. Cathedral arch internal surface laser scanning were made by tools of three-dimensional 3D Leica laser scanner for geometrical description of structure. Whole building thee-dimensional model is available at modern software computing. The plastic analyze approach is

developed to define safety exploitation of deformed structure. Proposed methodology on existing heritage buildings reduce necessary time for first approximation of deformed structure. Numerical modeling of masonry structures by modern computing tools demand additional material parameters such as elasticity, stiffness, compression, tensile and shear resistance of stone material and lime mortar, friction angle and cracking energy. Cracked masonry shell part interaction also must be specified by friction because of safe exploitation possibility after crack forming. Thrust line in non-cracked arks show center of compression force in cross section and for medieval buildings almost is located on center of cross section predicted by geometric proportions carefully improved in mason unions. Based on "middle third rule" later computing method also is in safe exploitation zone. Uncracked masonry arch shells can be easily computed using modern GEM software's and plastic material approach. After support deformations and crack forming in shell structures thrust line change position in cross section and internal forces relocates significantly. Therefore the main task of present research is safety exploitation criteria definition for deformed masonry arch shell of Riga cathedral.

2. MASONRY COMPUTING EVOLUTION

The main problems in the structural analysis of historic buildings are following:

1. Lack of data about geometric dimensions,
2. Material properties of the inner parts those are not visible exteriorly of the structural members that are huge in cross-sectional dimensions,
3. Difficulties in identifying the characteristics of construction materials,
4. Excessive cost of detailed laboratory analyses,
5. Variety of the data due to construction techniques and natural material utilization,
6. Altering material properties even along the same structural member due to long-lasting construction process,
7. Uncertainties in construction process and steps,
8. Indefiniteness of general stability and strength continuity due to the existing damage on the structure,
9. Inability in the application of modern construction materials, structural analysis and loading conditions.

However modern computing technique mainly based on FEM software gives possibility to detail analyze of heritage buildings. The historical review is necessary to understand the computing evolution and background of modern computing technologies.

2.1. Geometrical approach

Time honored geometry of arch structures was approved by geometric methods till 17th century. Arch and cross arch is a statically indeterminate structure therefore the first calculation methods were developed to simplify design methodology. In 17th century Hook's ca. 1670 proposed hanging flexible line thrust line definition method was brilliant idea for very first arch geometry approach. Adequately weight distributed hanged line give ideal tension line which in inverse form gives ideal compression line or trench line as brilliant solution of statically indeterminate structure. That type of solution is useful for vertically loaded arch structure but doesn't include horizontal loading. In Riga cathedral three arch horizontal interacting forms the horizontal loading eliminate this methodology usage for that type of buildings. Developed by Moseley (1833) "new Theorem in Statics" where the Principle of Least Pressure was proposed describes structures widely. Later Moseley (1843) specialized this approach to arches. Methodology, proposed by Villarceau (1853) reduces the statically indeterminate level of arch by inserting the three hinges to statically determinate system, was mostly useful analytic method till development of elastic analysis method. Towards the end of the 17th century, the studies of Galileo on strength analysis brought the medieval structural theory to the end. In those times, the scientific deal was mainly in the analysis of string- resembling the arch form- under vertical forces. In 1826, Navier put forward that the buildings should stand by means of calculations of the stresses on its structural members rather than the application of some geometric rules.

2.2. Elastic analysis

In end of 19th century elastic analysis was developed. In fact, until ca. 1880, engineers divided arches into "elastic", made of wood or wrought iron, and "rigid", made of masonry. Poncelet (1852) was conscious of the problem and in his historical review of arch theory suggested to apply the elastic theory to masonry arches in order to obtain a unique solution. Already in the 1860=s some elastic analysis of masonry arches were made. Winlker (1879) make a discussion of elastic material approach to masonry structure. However, he added a discussion on the "Störungen" that can affect the position of the line of thrust. Their main origins were: the deformation of the centering during construction, the yield of the buttresses under the thrust and the effect of changes of temperature. All these perturbations would produce some cracking of the arch and Winkler was well aware this would affect notably the position of the line of thrust, which could be very different from the calculated. Winlker suggested that some means of controlling the position of the line of thrust by inserting internal hinges during construction. Castigliano (1879) applied his theory of elastic systems also for masonry bridges. Elasticity theory gives admissible results till elasticity limit of material. In heritage building supporting structures compressive stress level is not

high and elastic material behavior is applicable. In early stage of elastic analysis develop for masonry structures engineers showed a certain resistance because of material anisotropic and irregularity. Elastic material approach in masonry shell systems uncertain results is giving therefore computing approach development seams necessary. The historical development review of first computational methods was done by Heyman [1,2].

2.3. Kinematic approach and arch collapse mechanism

Hinge forming by loading, thermal variations or geometric changes is most of arch collapse reasons. Material plasticity in hinges in self-weight loaded masonry shell system is main reason of safety limit exceeding initiated by support deformation. Support deformation forms the hinges in arch masonry structure as interaction contact by sliding surface. Safe exploitation criteria therefore must be defined. The kinematic or 'mechanism' method was first introduced by Heyman [3]. Heyman assumptions for arch safety analyze method were infinite compressive strength and friction resistance and zero tensile strength. He pointed out that plastic limit analysis can apply well to the case of masonry gravity structures, such as piers and arch bridges. In his book, for the single span arch, Heyman assumed the arch will collapse when four hinges form. Furthermore, he assumed that the arch has infinite compressive strength and sliding failures cannot occur. The hinges can alternately form at the intrados or extrados of the arch, and at failure, the thrust line must pass through the hinges. Therefore, it is possible to determine the magnitude of the applied load which will cause the arch to collapse. By Heyman, [4,5] the kinematic approach takes into account a collapse mechanism activated by an adequate number of plastic hinges. As main criteria of safe exploitation definition was Heyman proposed methodology. When the thrust line in a cross section is adjacent to the ring of the arch, a hinge is opened in that point. According to the upper bound theorem from the theory of plasticity, the maximum load corresponding to some collapse mechanism is greater or equal to the maximum load corresponding to the real collapse mechanism. This theorem implies that when the thrust line is adjacent to the ring of the arch in four points then the arch is not safe. Friction is high enough between stones and sliding failure cannot occur. The masonry has an infinite compressive strength. More complicate collapse mechanism has been considered for twin-span models by Hughes [6]. The pioneer in using modern computational methods to determine the collapse load of block structures was Livesley [7], who attempted to solve the problem as a linear programming problem using the lower bound formulation of limit analysis. In his paper Livesley showed that the adoption of associative friction leads to an incorrect collapse mechanism. More importantly it may also give an overestimate of the true collapse load. When using linear programming to solve limit analysis problems, flow will always occur normal to the specified surface (i.e. according to the so-called ‘normality rule’).

3. MASONRY MATERIAL APPROACH

In present research are proposed two step computational approaches. A complete and detailed review of micro and macro material approach may be found in Lourenco [8] for mechanical aspects at both scales. As first stage of presented computational methodology is deformed structure modeling by elastic macro modeling approach to understand whole building situation and decrease computing amount. In second stage of analysis deformed structure situation must be investigated defining cracked masonry part interaction. Therefore micro modeling material approach is most convenient.

3.1. Macro modeling approach

Homogenizations of material included in most of building codes give simplify rules for material property description and usage in calculations. In previously done research other heritage brick building was investigated to find masonry material elasticity properties and work out material definitions according Latvian building code. The homogenization of material means generalization of stone and mortar properties for elastic material property definition adopted for computational usage in elastic stage. Hooke law defined in 1676 long lasting linear elastic material approach was used for analytic calculations. As main parameter for elastic material approach elastic modulus was defined. Elasticity dependence from brick and masonry class defined from cube resistances of brick and mortar material shown in figure 2. Not cracked cross groined arch loading capacity computational analyze for 1912 year built building using defined lower elasticity modulus in previously done investigations earlier.

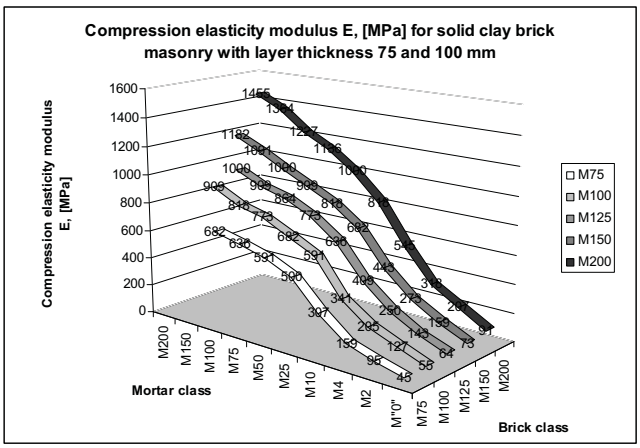

Figure 2. Latvian building code methodology defined mean elasticity modulus for elastic masonry approach

To understand the heritage masonry there are 3 point brick bending tests done. Shown in figure 3 bending test results highlight main problem of heritage masonry material definition – load bearing resistance result dispersion induced by home manufacturing process variability.

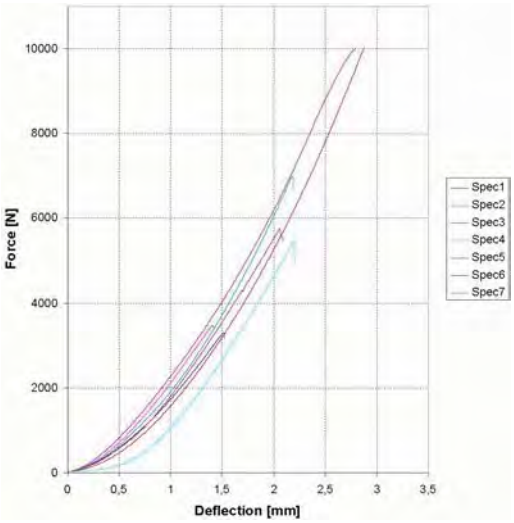

Figure 3. Three point brick bending test results

3 point bending test shows different tensile resistance by crash force. Test also shows equal elasticity for all specimens and brittle material approach of stone material. Structural analysis in elastic stage using FEM linear masonry approach is not acceptable for close to compression resistance calculations. In that cause plasticity theory must be used. Not only brick manufacturing significantly affect whole masonry material properties but also various stone material usage, block size and form variations, mortar component variations and joint thickness variations. Our aim is to give possibility to understand and analyze masonry arch, in fact, any combination of them, i.e., a masonry building. The 3D surface scanning with 20mm precision is so detailed that the internal structure can be described easily. Behind plaster layers forming the regular forms and levels of masonry wall surface a most irregular internal structure is found. Homogeneity, isotropy, uniform mechanical properties, etc., all the common assumptions of modern conventional structural analysis cannot be made in this case without violence to the most basic common sense. Taken from Riga Technical University building material laboratory test report Nr 65-2000, masonry compression resistance, 3 point bending test given tensile resistance was used for definition of masonry property. Used in computational software material behavior is approximate by material property variations but can give very close deformed stage structural understanding. Used in FEM software Staad Pro material properties are described as: Prime modulus of

elasticity (E_0 = 3600 MPa), average modulus of elasticity (E_{mean} = 818 MPa), Yong's modulus (G = 1200 MPa), poisson's ratio (0.2), thermal linear expansion coefficient (α_t = 0.000005 1/degree), density (ρ = 18 kN/m3), brick compression resistance (R_1 = 4.5 MPa), mortar compression resistance (R_2 = 2.5 MPa), masonry compression resistance (R = 1.1 MPa), masonry centric tensile resistance (R_t = 0.05 MPa), masonry shear resistance for head joint (R_{sq} = 0.11 MPa), masonry tensile resistance in bending for head joint (R_{tb}=0.08 MPa), resistance to main tensile stresses (R_{tw} = 0.08 MPa), coefficient of creep effect (v = 2.2).

$$\tau_{red} \le R_{sq} + 0.8 * \mu * \sigma_0 \tag{1}$$

Defined in equation 1 by Latvian building code methodology limiting tangential stresses, where μ = 0.7 friction coefficient by joint mortar; σ_0 – compression stresses average value from lightest loading with reduction coefficient 0.9. Tangential limiting value in second stage of calculation is defined as crack forming value for shear forces in macro modeling material approach. Macro modeling approach is simplifying material description and may normally be used in analytic FEM structural computing by Rikards [9]. The macro modeling of masonry as a composite is latest developed material approach by Rots [10]. Lourenço and Rots [11] macro-modeling technique, specifically formulated for the analysis of masonry constructions, is based on lumping all inelastic phenomena to the joints by means of a composite interface model. This model, stemming from plasticity, comprehends three different failure mechanisms, namely, a straight tension cut-off for mode I failure, the Coulomb friction model for mode II failure as well as an elliptical cap for compression and combined shear-compression failure. As in the previous case, Lourenço and Rots model requires the values of the initial axial and shear stiffnesses K_N and K_T as input data.

3.2. Micro modeling approach

Micro modeling of masonry material is precise stone material interaction description possibility but also significantly increase computing time and amount. In early stage of micro modeling dry joint approach was used. In latest developments the block and the mortar in the joints are represented by continuum models, whilst the interface unit-mortar is represented by discontinuous elements. The Young model, the Poisson coefficient and the inelastic properties of the units and the mortar are taken into account. Micro modeling is widely investigated and described by Lourenco and Rots [12] and find mortar material and stone material plasticity, load bearing tensile and compression resistances depending from joint position, friction angle a.c. Micro modeling material approach must be used in second step of computational investigation to analyze support settlement deformed structure situation. For those purposes additional masonry material properties must by involved.

4. MONITORING DATA COLLECTION

After World War Two Riga cathedral was closed as church and reorganized to concert hall. Soviet government put serious amount of funding to uplift and repair the structure, installed new ventilation, heating and fire safety systems. Latest funding in those systems renovation, crack monitoring and geological survey make a possibility to install long term monitoring system and make the present research.

4.1. Cracked arch photo fixation

Since 1959 cracks has been survived in Riga cathedral. Photo fixation made by heritage building protection institutions show lack of cracks in masonry shells. This is useful information to understand the new crack forming and prolongation of existing in long term monitoring.

4.2. Arch masonry building sequence and layer orientation fixation

From 1960 to 1961 each arch has been sketched and described by J. Stukmanis. In very careful way each brick and block sizes, form, orientation and position in masonry structure. Shown in figure 4 arch orientation, rib positions, brick sizes and forms were fixed in his work. Also description of damages and cracks for each arch was written totally on 68 pages and 30 sketches done. Collected in State Cultural Monument Archive materials about structure investigations and reconstruction process give we better understanding of existing situation.

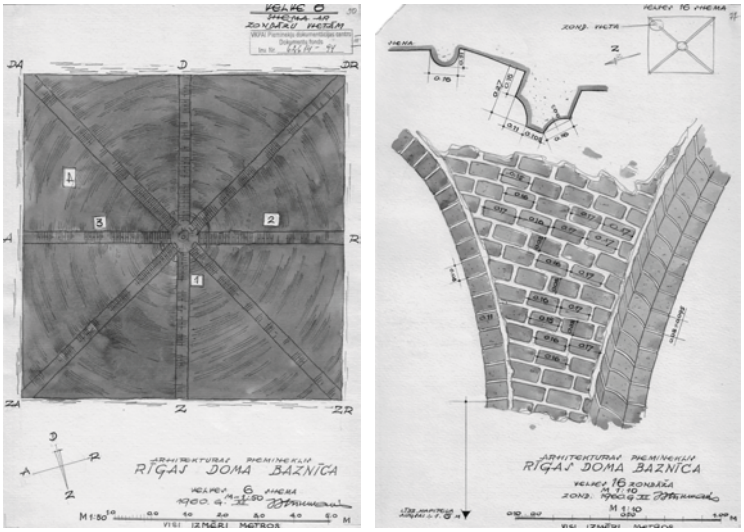

Figure 4. Careful fixation of all cross arch shells was done by J. Stukmanis

Fixation of damages after World War Two is very useful information in nowadays to understand changes since that time. Crack prolongation, widening and new cracking fixation of masonry structure therefore can be done by present crack monitoring. After crack fixation plastering of arch surface was accomplished and cracks hided.

4.3. Cathedral scanning by 3D Leica laser scanners

Building scanning gives the possibility of virtual three dimensional presentations in tourist web sites. This very detailed scanning by three dimensional Leica laser scanner give precise geometric surface defining for computational analyze of structure. Made by Kalinka and Reiniks, specialists from geodesic company Merko laser scanning in 2006 used for FEM computational analyze. Precision of 20mm on internal surfaces and less detailed for outside is today used for structures. Increase out coming virtual model precision theoretically gives whole structure computing possibility. Future development of computational hardware will provide us with powerful method of masonry structure analyze.

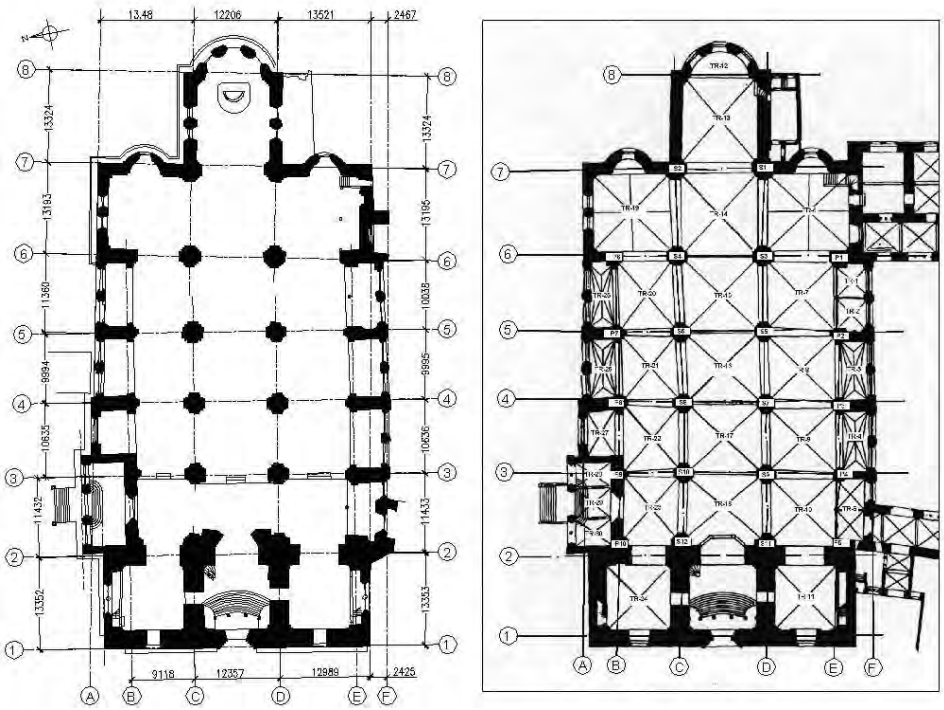

Figure 5. From full 3D model made plan and arch marking in plan made by Stukmanis

Figure 5 shows building plan section of model highlights geometrical uniformity of structure in comparing with Slavietis, Seglins and Drugis in 1959 made hand tool measurements. Scanned Gothic arch geometry also is preferable in comparing with Erdmanis 1963 proportionality findings shown in figure 6. Proportion findings are simplifying method of geometric approach to use the hand calculations of thrust line. Geometrical inequalities lead to serious difference between existing situation and real situation in cross section.

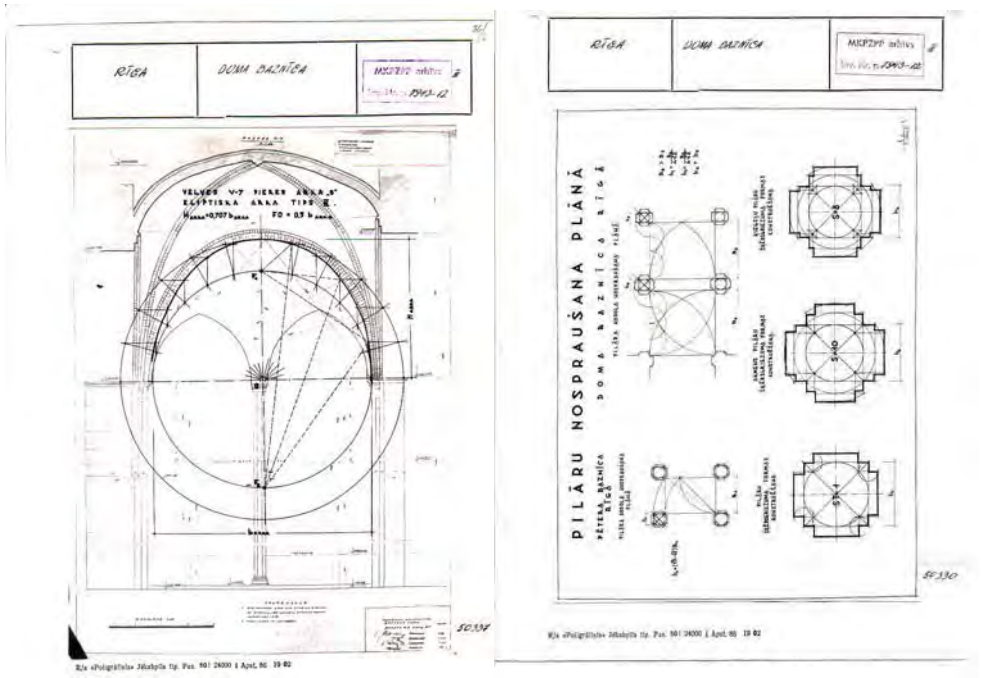

Figure 6. Proportionality findings by Erdmanis in 1963

By means of modern computational FEM software there is a possibility to analyze the whole building. We find the laser scanning as very fast geometric modeling for FEM software.

4.4. Microclimate monitoring

Staff managed microclimate monitoring for internal temperature and humidity was performed from January 2002 to June 2004. Temperature oscillation gives significant influence on masonry deformations and crack movement. In developed now SOFO type based monitoring temperature external and internal measure is included.

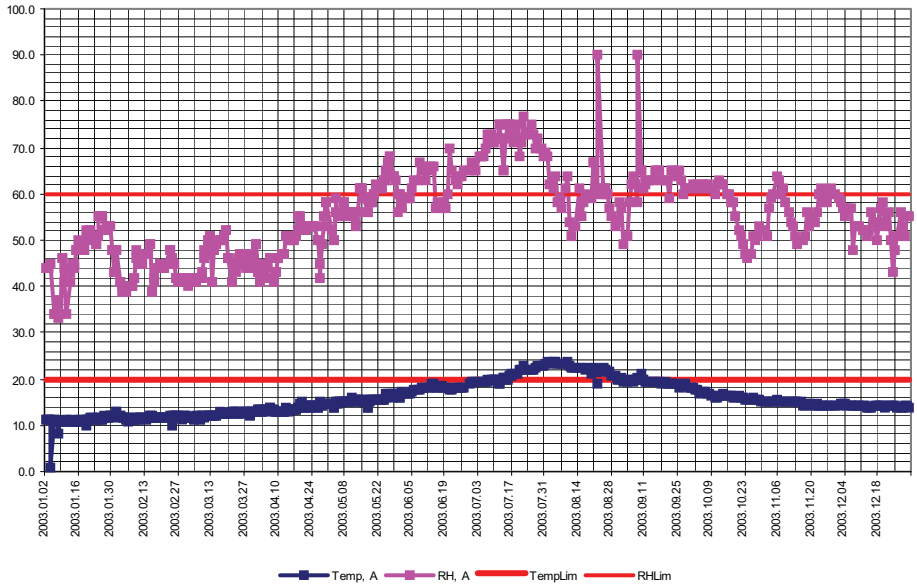

Figure 7. 2003 year internal temperature and humidity monitoring by staff

At figure 7 shown staff made monitoring for temperature and humidity for year 2003. Line Temp,A shows temperature variation during 2003 year period. RH,A line shows humidity variations along 2003 year period. Temp,Lim and RH,Lim lines show lower limiting values favorable to fungous forming. Temperature initiated deformations simulated by computer modeling show significant influence on crack forming, prolongation and movements. Cyclic temperature loading in eight hundred years of cathedral life time affect not only internal comfort but also stress situation in cross arch system seriously changing thrust line position. Solar radiation effect on cathedral external surface can be defined as load on FEM elements also.

4.5. Support condition survey

Support condition and subsoil situation survey in last two years made by CM GIB Geotechnical Company presented by Celmins and Markvarts show weak soil layer presence under footings. Started in 2005 geotechnical survey is more detailed than in former Soviet period ever done. Cross section of piled supported column footing is shown in figure 8. Marked as 7’’’D low density sand layer around the wooden pile footing is main Riga cathedral part unequal deformation reason.

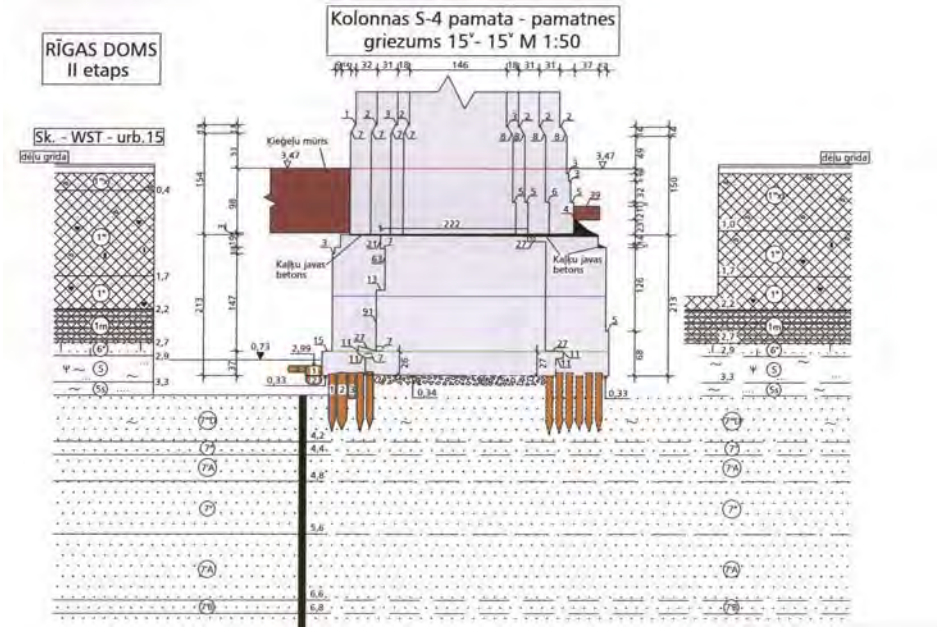

Figure 8 Column footing section in building middle span

Also an unsuited condition wooden piling was found. Support deformations along time counted as main reason of crack forming in masonry arch shell system. This is object of present research to fix the safe exploitation limits. Extreme support deformation of masonry shell system change force lines and part interacting stresses in shell section. Cracking changed thrust line position in cross section is safe situation definition criteria. Present deformed situation and LBS Konsultants make support deformation simulation by Plaxis in 2005 show approximate unequal support deformations in 16 cm by various parts of cathedral. Future support deformations predict crack prolongation, plastic hinge forming and unequal support deformation possibility.

To understand ground water flow and level changes Riga Department ordered ground water control monitoring from Balt-Ost-Geo Company. The ground water table monitoring during 2006 showed approximately 0.4m wooden pile coverage and less. In situation when wooden pile caps are not covered with ground water table wood structure degradation is possible. Solutions must be found to prevent air exposure possibility.

4.6. SOFO deformation monitoring system development

Surveillance des Ouvrages par Fibres (SOFO) optical fiber sensors monitoring system received from Smartec and would be mounted in few following months to

change mechanical tensometer crack monitoring to a long term. Optical sensor mounting cracks to provide masonry part movement in five years is decided to control safe exploitation. According with mechanical tensometer monitoring reports presented from 2005 crack oscillation varies 1-2mm every year depending on season. The main reason of optical tensometer usage is computational control of measurement data, long lasting life period and minimized side factor's influence on measurement's quality.

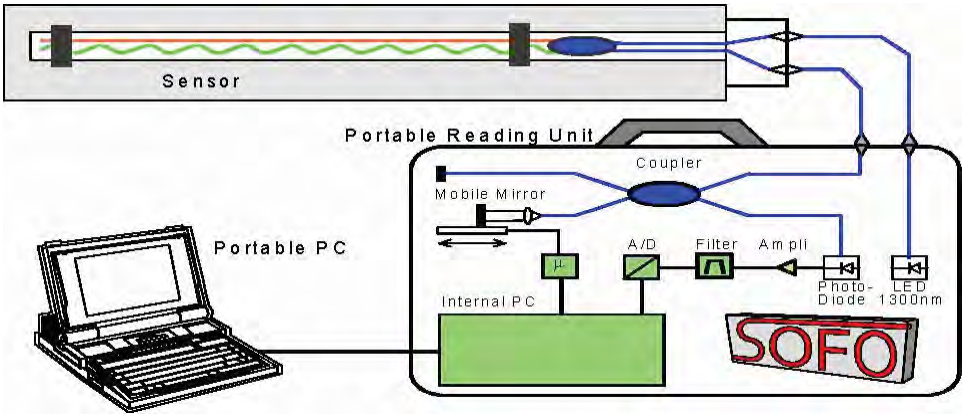

Figure 9 SOFO principles of optic tensometer

The SOFO measuring system gives precision of 0.02mm therefore defining high level of monitoring. Used as reading unit Smartec Bee allows control of 24 optical sensor units and communicates with registration PC trough telephone line. Additional thermo sensors for external and internal temperature control are included in measured program. Internal memory of reading unit gives possibility of data downloading by reasonable schedule. Battery support of reading unit gives possibility of non-stop monitoring. Support deformation caused crack widening is the way of safe criteria exploitation definition.

5. STABILITY CALCULATION AND SAFETY CRITERIA DEFINITION

As discussed before critical thrush line position must be found on deformed structure of masonry arch shell structure. Laser three dimensional scanning geometrical models were used to define geometric forms of Gothic arch system. The latest FEM software usage in heritage building masonry calculations in two stages is developed. In first stage shown in figure 10 linear elastic material

approach is used. Support deformation loading is applied by Staad Pro software. In second stage of analyze deformed structure shape and plastic material approach is used to define stability by thrust line position in section.

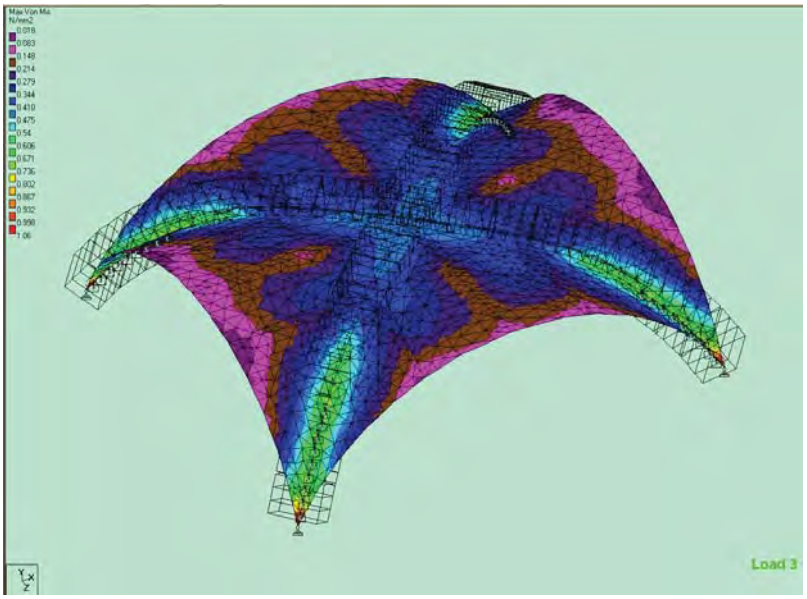

Figure 10 First stages analyzed with Staad Pro elastic material approach using

The second stage of deformed structure includes the fixed and measured by monitoring support settlements, cracked part interaction and subsoil elasticity. Plaxis computing tool is developed for taking into account masonry plasticity and stiffness. Each arch part is stabile and safe till thrust line locate in curved shell cross section. Defined by Heyman four hinge forming as safety criteria is also used to find the support deformation limits by numerical computing.

6. CONCLUSIONS

The present research is a small part of huge monitoring and investigation amount done in Riga cathedral. All previously collected investigations data and calculations increase the cathedral structure detailed understanding. Our view about masonry material computing technologies and possible material assumptions received from available papers are used to prepare FEM model and computational strategy choice. Laser scanning based surface geometric data transfer to FEM computational software significantly reduce modeling time. Improving laser scanned precision and computational devices will give the powerful tool for

structural analyze of heritage buildings. Detailed investigations of material properties, exploitation conditions and deformed situation must be taken into account. None methodology describing masonry material is possible to include the side effects of building process. It is necessary to point out the side effect of building process: significant dispersion of material properties; geometric and material variations; shell structure deformed conditions and various material interactions. Wind, solar radiation and temperature loading give no big influence on computational results but can be important. Two step computational method highlight deformed shape influence on thrust line position in cross section of arch shell. The monitoring improvement by long term SOFO optical tensometer tool is the way for detailed structure investigation and safe exploitation system establish of Riga cathedral. Methodology developed with curved arch surfaces laser scanning in reason to use data as geometrical model for FEM computing software is our aim of future improvement.

Acknowledgements

Thanks to Riga cathedral staff for huge amount of former Soviet time investigation and monitoring data, which is included in this paper. Involved investigator's permit give us big acknowledge to understand the cathedral building. Thanks to the Riga cathedral representatives understanding in the latest technology usage on arch long term monitoring advantage. Thanks a lot for complex monitoring development and funding in heritage building to keep it in good health.

References

1. Heyman J., The Stone Skeleton: Structural Engineering of Masonry Architecture, Cambridge University Press, Cambridge, 1990 pp 45.
2. Heyman J., The science of structural engineering, Imperial College Press, 1999.
3. Heyman, J. The equilibrium of shell structures. Oxford: Clarendon Press. 1997
4. Heyman, J., "The masonry arch", Ellis Horwood Limited, UK. 1982.
5. Heyman J., 'The safety of masonry arches', Int. Journ. Mech. Sci., 11 (4), 1969, pp. 363-385.
6. Hughes, T.G., Analysis and assessment of twin-span masonry arch bridges, Proc. Instn. Civ. Engrs., 110, 1995, 373-382.
7. Livesley, R. K. Limit analysis of structures formed from rigid blocks. Int. Journ. for Num. Meth. in Eng. 12, 1978, p. 1853-1871.
8. Lourenço, P. B. Computational Strategies for Masonry Structures. PhD thesis, Delft University of Technology, 1996
9. Rikards, R., and Cate A., Finite element method, Riga Technical University, Riga, pp 78, 2002
10. Rots, J.G. - Numerical simulation of cracking in structural masonry, Heron, 36(2), 1991, p. 49-63.
11. Lourenço, P.B., de Borst, R., Rots, J.G., A plane stress softening plasticity model for orthotropic materials, Int. J. Numer. Meth. Engng., 40, 1997, p. 4033-4057
12. Lourenço, P.B., Rots, J.G., A multi-surface interface model for the analysis of masonry structures, J. Engrg. Mech., ASCE, 123(7), 1997, p. 660-668

"Computational Civil Engineering 2007", International Symposium
Iaşi, România, May 25, 2007

Application of MS Excel® Solver in Solving Structural and Management Problems

Jacek Boroń
Building Engineering Institute, Wroclaw University of Technology, Wroclaw, 50-377, Poland

Summary

Solvers, or optimizers, we call software tools that help us as users to find the best way to allocate scarce resources. The resources may be everything in limited supply. The "best" or optimal solution may mean maximizing profits, minimizing costs, or achieving the best possible quality. An almost infinite variety of problems can be tackled this way, but here are some typical examples: finance and investment, manufacturing, distribution and networks.

To use the solver you have to build a model that specifies: decision variables, constraints and objective. The Solver will find values for the decision variables that satisfy the constraints while optimizing (maximizing or minimizing) the objective. Spreadsheets such as Microsoft® (MS) Excel provide a convenient way to build such a model.

Anyone who has used a spreadsheet is already familiar with the process: Cells on a worksheet can hold numbers, labels, or formulas that calculate new values, such as the objective of an optimization. Constraints are simply limits (specified with <=, = or >= relations) on formula cells. And the decision variables are simply input cells containing numbers. Whether the Solver can find a globally optimal solution, a locally optimal solution, or a good solution depends on the nature of the mathematical relationship between the variables and the objective function and constraints (and the solution algorithm used)[1].

In this paper it will be shown how we can use the Excel-Solver (the product developed by Frontline Systems, Inc. for MS Excel) to find the best (optimal) solutions in some structural problems, as well tasks connected with management of an enterprise. The illustrative examples will be these, which I always use for my didactics at Building Engineering Institute. Numerical results for two of sample problems demonstrate how versatile (multipurpose) and useful tool was used.

KEYWORDS: excel-solver, modeling, optimizers, structural optimization problems, managing optimization problems

1. INTRODUCTION

The Solver being part of Microsoft Excel (developed by Frontline Systems for Microsoft) is one of the widely used optimization tools. It is able to solve small-scale linear programming (LP), smooth nonlinear programming (NLP), and mixed integer programming (MIP) problems. An upgraded Premium Solver Platform (PSP) is a tool that extends functionality and speed of the MSE Solver to handle industrial-scale problems of over tens of thousands variables and constraints. PSP is also challenging global optimization problems using multi-start or clustering methods and non-smooth problems using methods based on genetic and evolutionary algorithms (or tabu search).

Table 1. The Characteristic of the Enhanced Excel Solvers [1].

MICROSOFT EXCEL SOLVER

	Excel Built-In Solver	Premium Solver	Premium Solver Plus	Premium Solver Platform
NLP variables/ constraints	200/100 + bounds	400/200 + bounds	400/200 + bounds	1000/1000 + bounds
LP variables/ constraints	200/ unlimited	800/unlimited	800/unlimited	2000/unlimited to 16,000/unlimited
Setup performance	1x	1–50x	1–50x	1–50x
NLP performance	1x	1x	1.5x	2–10x
LP performance	1x	2–3x	2–3x	Large scale
MIP performance	1x	5–10x	25–50x	25–50x
Selection of optimizers	Fixed set	Fixed set	Fixed set	Multiple choices, field-installable
LP/QP methods	Simplex w/bounds	Enhanced simplex w/bounds	Enhanced simplex, dual, quadratic	Sparse simplex, LU, Markowitz
MIP methods	B&B	Enhanced B&B	Enhanced B&B, P&P, dual, simplex	Enhanced B&B, P&P, dual, simplex
NLP methods	GRG2	GRG2	Enhanced GRG2	LSGRG, SQP, etc.
Reports	Standard: Answer, Limits, Sensitivity	Standard + Linearity, Feasibility	Standard + Linearity, Feasibility	Standard + Linearity, Feasibility

Remark for the Table 1: For integer problems B&B refers to branch and bound and P&P refers to preprocessing and probing. For nonlinear problems "GRG" refers to the generalized reduced gradient method and "SQP" refers to sequential quadratic programming.

2. USING SPREADSHEETS

2.1. Spreadsheets vs. Individual Programming

Spreadsheets such as Microsoft Excel provide a convenient way to build such a model. Anyone who has used a spreadsheet is already familiar with the process:

Cells on a worksheet can hold numbers, labels, or formulas that calculate new values (such as the objective of an optimization).

Constraints are simply limits (specified with <=, = or >= relations) on formula cells.

The decision variables are simply input cells containing numbers. Frontline's Premium Solver products provide powerful tools for solving, or optimizing, such model.

Another way to build an optimization model is to write code in a programming language such as Visual Basic or C/C++. Instead of spreadsheet cells, variables or arrays in the program hold the decision variables and calculate the constraints and objective.

2.2. How do we define a model?

Every optimization model consists of:

-decision (design) variables and parameters,

-objective function,

-constraints.

2.2.1. Decision variables

They usually measure the amounts of resources, such as money, to be allocated to some purpose, or the level of some activity, such as the number of products to be manufactured, the number of pounds or gallons of a chemical to be blended, etc. In engineering problems decision variables are dimension of the structures or cross-sections.

2.2.2. Objective function

After defining the decision variables, the next step is to define the objective, which is normally some function that depends on the variables. We'd be finished at this point, if the model did not require any constraints (but in engineering problems it is rather impossible). For example, in a curve-fitting application, the objective is to minimize the sum of squared differences between each actual data value, or observation, and the corresponding predicted value. This sum has a minimum value of zero, which occurs only when the actual and predicted values are all identical. If we asked a solver to minimize this objective function, we would not need any constraints.

In most models, however, constraints play a key role in determining what values can be assumed by the decision variables, and what sort of objective value can be attained.

2.2.3. Constraints

Constraints reflect real-world limits on production capacity, market demand, available funds, and so on. To define a constraint, you first compute a value based on the decision variables. Then you place a limit (<=, = or >=) on this computed value.

General Constraints. For example, if A1:A5 contains the percentage of funds to be invested in each of 5 stocks, you might use B1 to calculate =SUM(A1:A5), and then define a constraint B1 = 1 to say that the percentages allocated must sum up to 100%.

Bounds on Variables. Of course, you can also place a limit directly on a decision variable, such as A1 <= 100. Upper and lower bounds on the variables are efficiently handled by most optimizers and are very useful in many problems.

Policy Constraints. Some constraints are determined by policies that you or your organization may set. For example, in an investment portfolio optimization, you might have a limit on the maximum percentage of funds to be invested in any one stock, or one industry group.

Physical Constraints. Many constraints are determined by the physical nature of the problem. For example, if your decision variables measure the number of products of different types that you plan to manufacture, producing a negative number of products would make no sense. This type of non-negativity constraint is very common. Although it may be obvious to you, constraints such as A1 >= 0 must be stated explicitly, because the solver has no other way to know that negative values are disallowed.

As another example of a physically determined constraint, suppose you are modeling product shipments in and out of a warehouse over time. You'll probably

need a balance constraint, which specifies that, in each time period, the beginning inventory plus the products received minus the products shipped out equals the ending inventory (and hence the beginning inventory for the next period).

Integer Constraints. Advanced optimization software also allows you to specify constraints that require decision variables to assume only integer (whole number) values at the solution. If you are scheduling a fleet of trucks, for example, a solution that called for a fraction of a truck to travel a certain route would not be useful. Integer constraints normally can be applied only to decision variables, not to quantities calculated from them. A particularly useful type of integer constraint specifies that a variable must have an integer value with a lower bound of 0, and upper bound of 1. This forces the variable to be either 0 or 1 (nothing in between) at the final solution. Hence, it can be used to model "yes/no" decisions. For example, you might use a 0-1 or binary integer variable to represent a decision on whether to lease a new machine. Your model might then calculate a fixed lease cost per month, but also a lower cost per item processed with the machine, if it is used. A solver can help determine whether leasing the machine will yield higher or lower profits.

2.2.4. Interpreting solutions

A solution (set of values for the decision variables) for which all of the constraints in the Solver model are satisfied is called a **feasible solution**. Most solution algorithms first try to find a feasible solution, and then try to improve it by finding another feasible solution that increases the value of the objective function (when maximizing, or decreases it when minimizing). An **optimal solution** is a feasible solution where the objective function reaches a maximum (or minimum) value.

A **globally optimal solution** is one where there are no other feasible solutions with better objective function values. A **locally optimal** solution is one where there are no other feasible solutions "in the vicinity" with better objective function values (we can picture this as a point at the top of a "peak" or at the bottom of a "valley" which may be formed by the objective function and/or the constraints). The Solver is designed to find optimal solutions (ideally the global optimum) but this is not always possible. In many cases, though, we may be happy to find a **good solution** (one that is better than the solution we are using now). Whether the Solver can find a globally optimal solution, a locally optimal solution, or a good solution depends on the nature of the mathematical relationship between the variables and the objective function and constraints (and the solution algorithm used).

2.2.5. What makes a model hard to solve?

Solver models can be easy or hard to solve. "Hard" models may require a great deal of CPU time and random-access memory (RAM) to solve (if they can be solved at

all). The good news is that, with today's very fast PCs and advanced optimization software from Frontline Systems, a very broad range of models can be solved.

Three major factors interact to determine how difficult it will be to find an optimal solution to a solver model:

-the **mathematical relationships** between the objective and constraints, and the decision variables

-the **size of the model** (number of decision variables and constraints) and its sparsity

-the **use of integer variables** - memory and solution time may rise exponentially as you add more integer variables

2.3. Using the Solver dialogs

Assuming that we have the standard Excel Solver or a Premium Solver product installed, the next step is to create a worksheet where the formulas for the objective function and the constraints are calculated. In the worksheet below, we have reserved cells C15, D15, E15 and F15 to hold our decision variables x_1, x_2, x_3 and x_4: amount of advertisments through TV, radio, direct mail and newspapers.

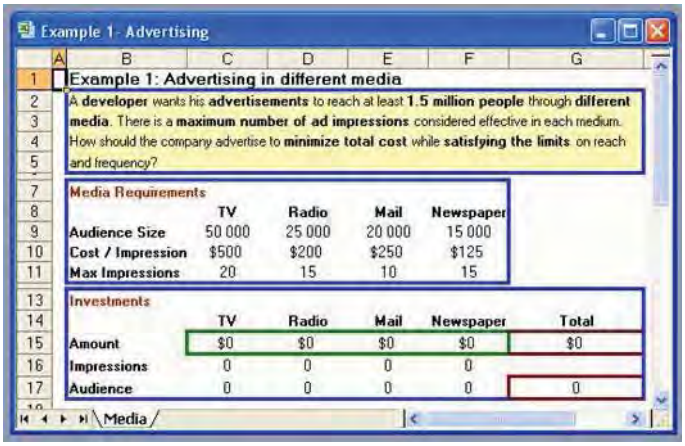

Fig.1. Example 1: Advertising

To add the constraints, we click on the Add button, select cells C16:F16 in the Cell Reference edit box (the left hand side), and select cells C11:F11 in the Constraint edit box (the right hand side); the default relation <= is OK (Fig.2.)

Fig.2. Adding the constraints in the edit box (polish version of MS Office)

We choose the Add button again (either from the dialog above, or from the main Solver Parameters dialog) to define the non-negativity constraint on the decision variables.

When we've completely entered the problem, the Solver Parameters dialog looks like this (Fig.3.) This dialog appears for the Standard Solver Platform.

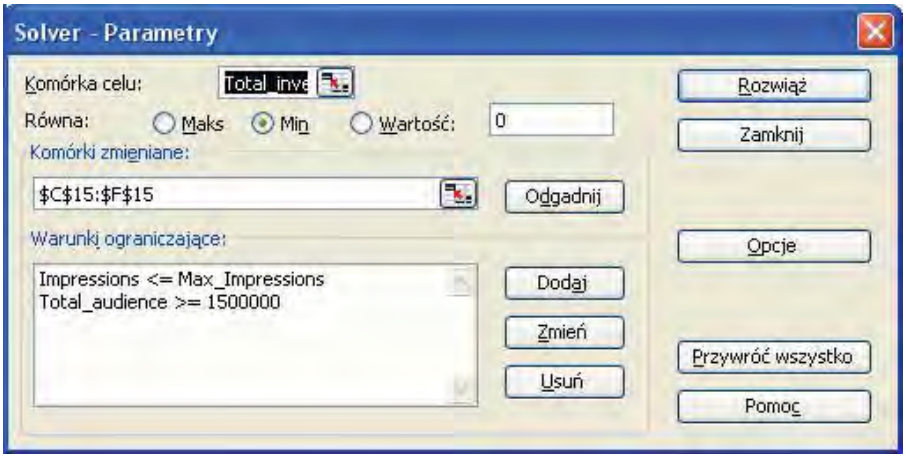

Fig.3. The Solver Parameters Dialog Box (polish version of MS Office)

2.4. Finding and using the solution

To find the solution, we should click on the Solve button. After a moment, the Solver returns the optimal solution: $9000 in cell C15, $3000 in D15, $0 in E15 and $1875 in cell F15. This means that we should advertise 18 times in TV, 15 times in radio and newspaper, to make a total, minimal cost $13875 (shown at cell G15). We shouldn't invest in ads through direct mail. The message "Solver found a solution" appears in the Solver Results dialog, as shown here (Fig.4.). We now click on "Answer" in the Reports list box to produce an Answer Report, and click OK to keep the optimal solution values in cells C15:F15.

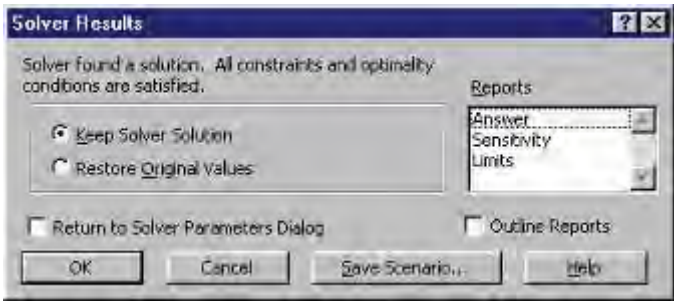

Fig.4. Solver results dialog box

After a moment, the Solver creates another worksheet containing an Answer Report, like the one below, and inserts it to the left of the problem worksheet in the Excel workbook. (Fig.5.)

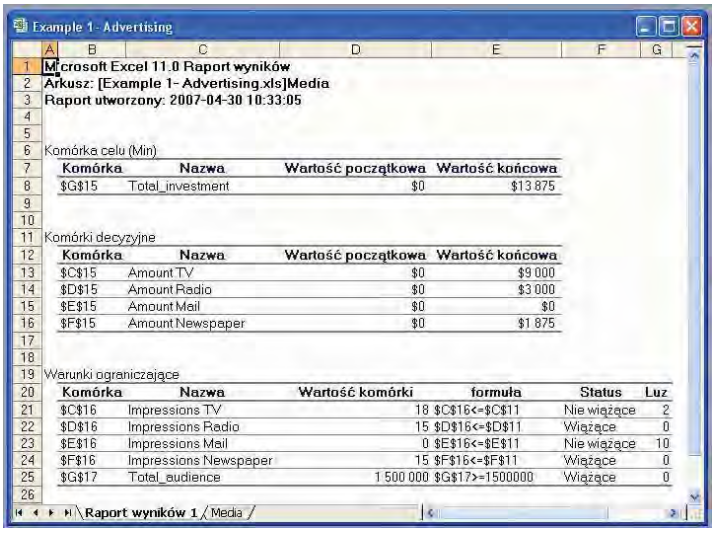

Fig.5. Answer report worksheet

3. ILLUSTRATIVE EXAMPLES

3.1. Design (structural) problem – optimization of the welded cross-section

Our target is to optimize a double-T, bisymmetric cross-section of a welded, steel beam, connected with a stiff plate made of armed concrete (Fig.6.). We allow only

one loading condition: bending moment M. We consider 4 design variables t, h, b and g. Objective function F_c going to be minimized:

$$\mathbf{F_c = (0{,}125 \cdot R_e + s) \cdot (h \cdot t + 2 \cdot b \cdot g)} \quad (1)$$

The worksheet prepared to solve the problem is presented below (Fig. 6.).

STEEL BEAM OPTIMIZATION

Input data:

M = 5000 kNm *(bending moment)*

l_0 = 4,000 m. *(beam span)*

steel class: **St3S**

Strenght constraints (simple bending, by Polish Standard PN-90/B-03200)

$M <= M_R * \phi_L$, where $M_R = \alpha_p * W_z * f_d$,

therefore $W_z >= M_z/(\alpha_p * \phi_L * f_d)$ = **0,022148**

Considering conection of our beam with stiff plate gives: $\phi_L = 1$ and $\alpha_p = 1{,}05$.

Design (geometric) constraints:

t >= 0,008

0< h <= 0,85

g > 0

6*g<= b <= 20*g ◄prevents stretching out of the belts during welding

	SOLVER				
cost	***F_c =***	***1663,082***	***61688,97***		
design	b =	0,387	*1,000*	*starting*	
variables	g =	0,850	*1,000*	*values*	
	h =	0,064	*1,000*	◄	
	t =	0,008	*0,100*		

R_e =	**2,35E+05**	2,25E+05	2,15E+05	kPa	◄*plasticity border*
J(b,g,h,t) =	0,011	m^4			
W_z(b,g,h,t) =	0,022	m^3			

s =	0,7				
f_d =	**215**	205	195	MPa	◄*strenght of the steel*
α_p =	1,05				

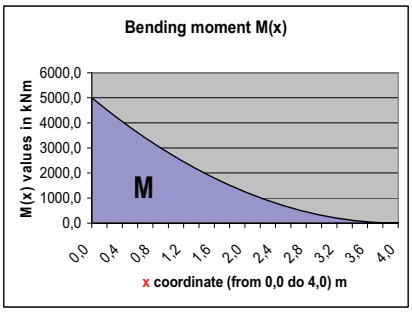

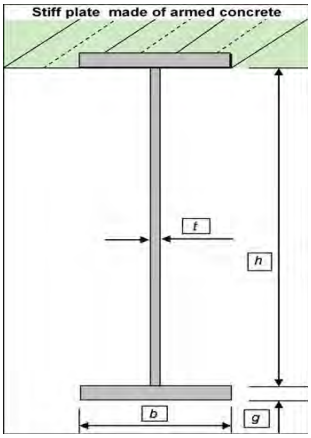

Fig.6. Optimization of the welded steel beam cross-section (4 design variables)

3.2. Management of an enterprise problem - purchasing & transportation

Problem. A concrete manufacturer has 4 different plants that all require a certain amount of cement. There are 5 different companies (cement factories) where the cement can be bought. Where should the concrete manufacturer buy the cement and how much should it buy, to minimize its' cost and shipping?

Solution. The variables are the amounts of cement to be bought from each company for each plant. On worksheet Purchasing & Transportation Model these are given the name Amounts_of_cement_to_buy: cells C15:G18 (see Fig.7.). The constraints are simple and straightforward:

$$\textbf{Amounts\_to\_buy (C15:G18) >= 0 via the Assume Non-Negative option} \quad (2)$$

$$\textbf{Total\_amounts\_to\_buy (H15:H18) >= Demand (I15:I18)} \quad (3)$$

$$\textbf{Total\_sold(C19:G19) <= Supply(C20:G20)} \quad (4)$$

The objective is to minimize the cost. This is defined as Total_cost on the worksheet (cell H24).

Purchasing & Transportation Model

	A	B	C	D	E	F	G	H	I
1		Purchasing & Transportation Model (concrete manufacturing)							
3			Company 1	Company 2	Company 3	Company 4	Company 5		
4		Cement prices (per ton)	$100	$118	$114	$110	$108		
5									
6		Cost of shipping from companies to plants (per ton)							
7			Company 1	Company 2	Company 3	Company 4	Company 5		
8		Plant 1	$8	$4	$5	$4	$3		
9		Plant 2	$7	$6	$3	$2	$4		
10		Plant 3	$7	$3	$7	$5	$2		
11		Plant 4	$8	$2	$5	$6	$7		
13		Amounts of cement to buy (tons)							
14			Company 1	Company 2	Company 3	Company 4	Company 5	Total	Demand
15		Plant 1	180	0	140	0	100	420	420
16		Plant 2	0	0	60	300	0	360	360
17		Plant 3	0	0	0	0	400	400	400
18		Plant 4	170	205	0	0	0	375	375
19		Total	350	205	200	300	500		
20		Available supply	350	250	200	300	500		
22		Cost of cement	$35 000	$24 190	$22 800	$33 000	$54 000	$168 990	
23		Cost of shipping	$2 800	$410	$880	$600	$1 100	$5 790	
24							Total cost	$174 780	

Raport wyników 1 | Purchase

Fig.7. Purchasing & Transportation Model (concrete manufacturing)

Even though this model is very simple, it is one of the most used models in the industry. It routinely saves many companies thousands or even millions a year.

4. CONCLUSIONS

The optimizer developed by Frontline Systems, Inc. under simple name "Solver" is multipurpose and friendly-in-use tool also for engineering and management problems. Therefore I decided to include it successfully in my didactic program beginning from the third semester at Faculty of Civil Engineering.

However in real world optimization problems can be both simple and "cheap" or complicated and "expensive", so the types of mathematical relationships in a model (for example, linear or nonlinear, and especially convex or non-convex) determine how hard it is to solve, and the confidence we can have that the solution is truly optimal.

These relationships also have a direct bearing on the maximum size of models that can be realistically solved. A few advanced solvers can break down a problem into linear, smooth nonlinear and non-smooth parts and apply the most appropriate method to each part, but in general, we should try to keep the mathematical relationships in a model as simple (i.e. close to linear) as possible [2].

References

1. Fylstra, D. et al., *Design and Use of the Microsoft Excel Solver,* Copyright 1998, Institute for Operation Research and the Management Sciences, 0092-2102/98/2805/0029.
2. Nenov, I., Fylstra, D., *Interval Methods for Accelerated Global Search in the Microsoft Excel Solver,* Reliable Computing 9: 143-159, 2003, Copyright 2003, Kluver Academic Publishers.

"Computational Civil Engineering 2007", International Symposium
Iaşi, România, May 25, 2007

Underground structure in discontinuous rock mass

Jiří Boštík
Institute of Geotechnics, Brno University of Technology, Brno, 602 00, Czech republic

Summary

The results of parametric analysis on influence of discontinuities orientation on the response of rock mass during driving an underground structure in the direction of discontinuity planes are presented in the contribution. Three typical alternatives were considered: the underground structure in rock mass with one-sided dip of discontinuities, the underground structure situated in synclinal bend and the underground structure situated in anticlinal bend. In all three cases, the variability of discontinuities dip angle in the range of 0 - 90 ^{o} was considered.

Mathematical models were used for the analysis by Finite Element Method using software Plaxis. Mathematical models were planar – plane strain. Rock Jointed model was used to simulate mechanical behaviour of the rock environment. The underground structure is driven in full -face with no lining.

All the analysed alternatives are compared to one another considering the vertical displacement at the top of the underground structure and maximum vertical surface displacement. From the results presented, it can be concluded that from the point of view of vertical displacement at the top of the underground structure, situating the underground structure in the axis of the synclinal bend, if the dip of discontinuities is not very steep, is the least favourable. On the other hand, taking into account the maximum vertical surface displacement, situating the underground structure, in relation to the discontinuities orientation, seems to be of no importance.

KEYWORDS: underground structure, discontinuities, mathematical simulation.

1. INTRODUCTION

The rock environment, in which the underground structures are build and which is an inseparable part of them, is usually weakened by several discontinuities. These discontinuities are created either during the rock formation itself (e.g. stratification of sedimentary rocks) or in rock which have already been formed (e.g. joints, fault planes).

In case of sedimentary rocks, the stratification, which is developed by lithological changes of deposited material, is the most significant structural property.

Occurrence of the discontinuities in rock mass described above has an impact to its behaviour during driving of underground structures. For instance, in [1] the authors presented that in case of the stratified rocks their placing, thickness and dip of the layers and strength of the rock need to be considered. The angle between tunnel axis and layers direction, which are generally of a various aslope, contorted or folded, is a very important feature as well.

Driving of a tunnel in the direction of layers [1] is less convenient, especially when the rock is non-homogenous. The tunnel can be subjected to one-sided pressures when the layers are skewed (Fig. 1a). When the tunnel is situated in the axis of anticline (Fig. 1c), the dip of layers need to be taken into account. Such a situating the tunnel is very inconvenient in case the layers are steeply skewed as the crown of the tunnel was loaded by full weight of the loose layers. Situating the tunnel in synclinal bend (Fig. 1b) is also considered to be very inconvenient – the rock would pressure on the tunnel from either side and huge water inflow would occur if permeable layers were presented. Situating the tunnel path in the direction of the vertical or steeply skewed layers is very unsuitable due to large weight of overburden affecting the crown of the tunnel.

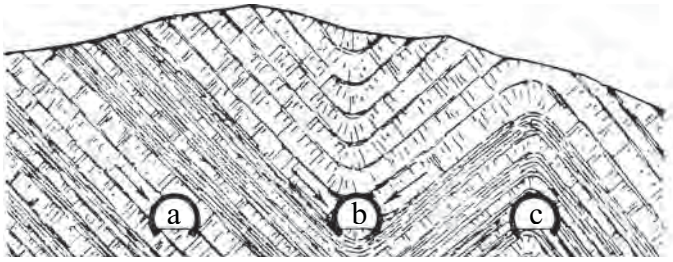

Figure 1. Situating tunnel in stratified rock in the direction of the layers [1]

2. PARAMETRIC STUDY

In order to analyse an influence of discontinuity planes orientation on the response of rock mass during driving an underground structure, the following model example was considered. This was solved by Finite Element Method using software Plaxis [2].

2.1. Geometric arrangement

A linear underground structure (collector) of horse-shoe shape, 3.3 m wide, 4.05 m high and sectional area of 12.2 m^2 (Fig. 2) is considered. Top of the underground structure is 13.2 m under the horizontal surface, i.e. in depth that equals four times width of the underground structure.

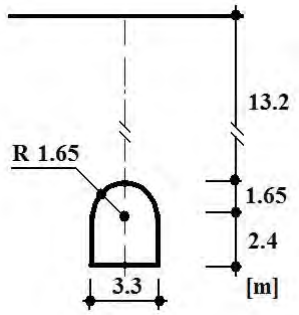

Figure 2. Schematic arrangement of underground structure

2.2. Geology conditions

Rock environment is created by one kind of stratified rock. It is assumed, that single layers are of the same width (D), which is relatively small as compared to transverse dimensions of the underground structure (B), as schematically illustrated in Fig. 3. Further, it is supposed the discontinuities are not filled.

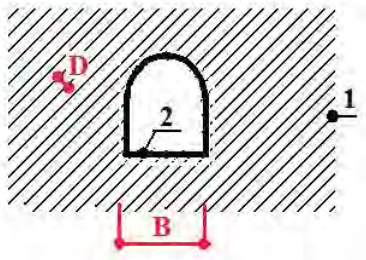

Figure 3. Discontinuities – 1, Underground structure – 2

Mechanical behaviour of rock environment in the mathematic model is approximated by the Jointed Rock model. This model is an anisotropic elastic perfectly – plastic model, especially meant to simulate the behaviour of stratified and jointed rock layers and its more detailed description can be found in [2].

Within the analysis, one set of discontinuities (stratification) is used and elastic behaviour of rock environment is fully isotropic, i.e.

$$E_2 = E_1 \quad \text{and} \quad \nu_2 = \nu_1 , \tag{1}$$

$$G_2 = \frac{1}{2} E_1 (1 + \nu_1) , \tag{2}$$

where E_1, ν_1 stand for Young's modulus and Poisson's ratio of the rock as a continuum respectively, E_2, ν_2, G_2 stand for Young's modulus, Poisson's ratio and Shear modulus in the discontinuity plane direction respectively.

In the discontinuity plane direction it is assumed that shear stresses are limited according to Coulomb's criterion. Parameters of strength in the direction of stratification are as follows: cohesion (c), friction angle (φ), dilatancy angle (ψ), tensile strength (T - Strength).

Throughout the calculation, the material parameters from Table 1 were used.

Table 1. Material parameters used

γ [kN/m3]	E_1 [kPa]	ν_1 [-]	E_2 [kPa]	ν_2 [-]
23.7	$6x10^4$	0.33	$6x10^4$	0.33
G_2 [kPa]	c [kPa]	φ [°]	ψ [°]	T-Strength [kPa]
$2.3x10^4$	20	24	0	0

Three basic alternatives according to Fig. 4 are solved. In the first one (J), one-sided dip of discontinuities is considered. In the second one (S), the underground structure is driven in the symmetrical synclinal bend. In the last one (A) the underground structure is situated in symmetrical anticlinal bend. In all the three cases above, the various orientation of the discontinuities, determined by dip angle α_1, is involved. Value of α_1 is chosen from the range of 15 - 75 ° with 15 ° step.

2.3. Technology

From the point of view of driving method, driving of the underground structure in full - face with no use of lining is considered.

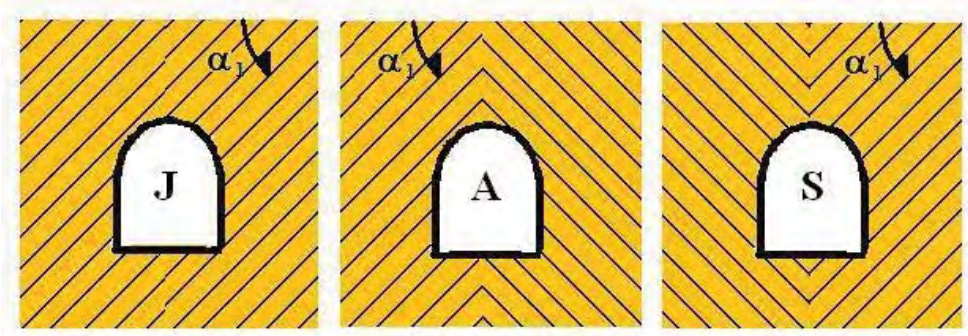

Figure 4. Considered alternatives: J – one-sided dip of discontinuities, A – symmetrical anticlinal bend, S – symmetrical synclinal bend

2.4. Mathematical model

The planar mathematical model (plane strain) is formed by Finite Element Method using the software Plaxis [2]. The analysed area is of a rectangle shape of the size of 35 x 27.7 m. The mesh with 1 336 elements, 2 753 nodes and 4 008 stress points (Fig. 5) was created by discretisation using six-node triangular element.

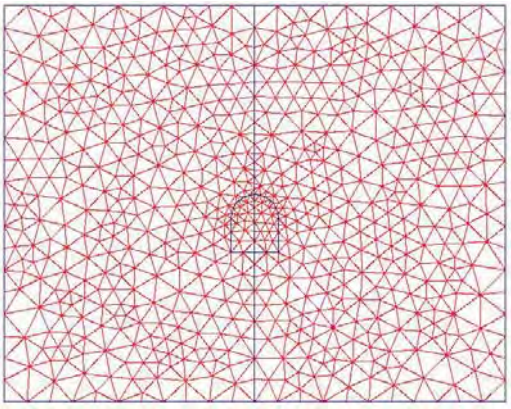

Figure 5. Finite element discretisation

The top boundary of the mathematical model representing the surface is freely sliding, while the other model boundaries are tied with standard boundary conditions: the vertical boundaries restricted on slide in horizontal plane, the bottom boundary restricted on slide in both horizontal and vertical directions.

Solving the mathematical models was performed in the two calculation phases illustrated in Fig. 6:

1. Calculating the primary state of stress caused, in this case, only by self-weight of rock mass γ. Value of horizontal and vertical effective stresses ratio (coefficient of lateral earth pressure) K_0 was 0.593.
2. Carrying out the excavation of the underground structure.

For all the three alternatives – J, S and A, five models with different discontinuities orientation (see section 2.2) were created. Furthermore, cases where set of the discontinuities is horizontally and vertically oriented were solved as well. In total, seventeen models were created.

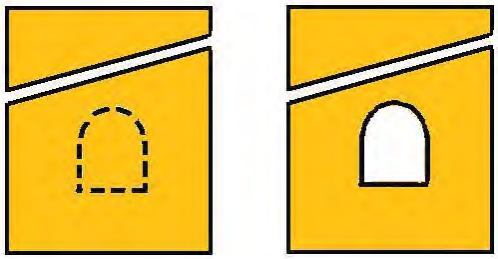

Figure 6. Calculation phases

3. RESULTS

Vertical displacement at the top of the underground structure (named as a point I further in the text) and maximum vertical surface displacement were selected in order to compare the results of the solved alternatives and their variations. Relation between these values and discontinuities orientation (dip angle) for the analysed cases are graphically illustrated in Fig. 7 and Fig. 8. In these diagrams, the vertical displacement between calculated values for the specific discontinuities orientation are approximated by bisector.

Case J

In the case J (one-sided dip of discontinuities), the maximum vertical displacement at the top of the underground structure was found for dip angle 45^o and equals 24.0 mm. If the dip angle increases or decreases the value of vertical displacement at the top of the underground structure decreases. The lowest value (19.5 mm) of the vertical displacement in the point I was verified for the case of horizontally oriented discontinuities ($\alpha_1 = 0^o$). This value practically corresponds to the value obtained in the case of vertically oriented discontinuities ($\alpha_1 = 90^o$).

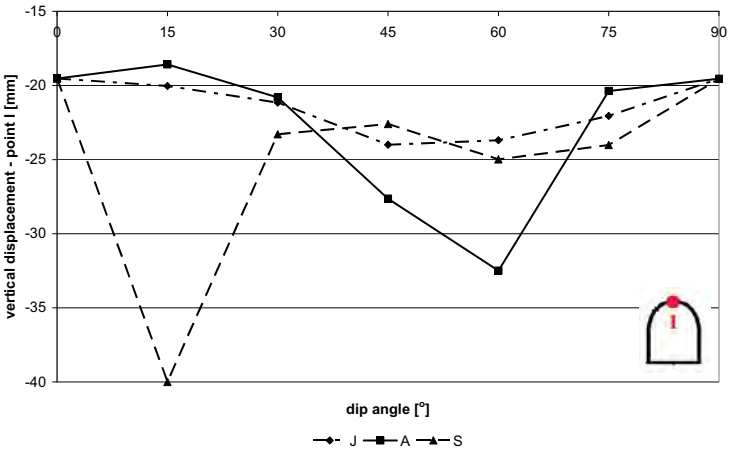

Figure 7. Vertical displacement at the top of the underground structure

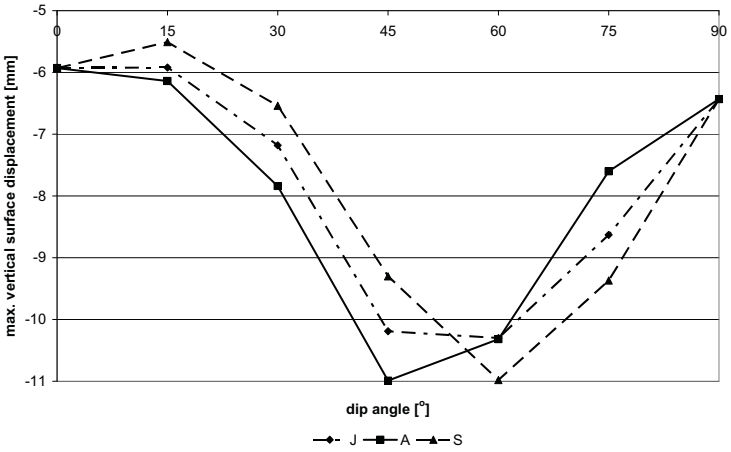

Figure 8. Maximum vertical surface displacement

Similar relation can also be found for maximum value of the vertical surface displacement. The highest value of 10.3 mm is achieved for $\alpha_1 = 60^o$ (almost the same as 10.2 mm for $\alpha_1 = 45^o$). Minimum value of the vertical surface displacement of 5.9 mm was verified for $\alpha_1 = 0^o$ and in fact corresponds to the value of 6.4 mm calculated for $\alpha_1 = 90^o$.

Case A

In the case A, the maximum vertical displacement at the top of the underground structure was found for dip angle 60^o and equals 32.5 mm. The dependency on α_1

is of almost the same as in the case J except the displacements are bigger and the maximum value is found for steeper discontinuities dip as presented above. Variations with α_1 = 15, 30 and 75° when the calculated displacements are slightly smaller; more specifically 1.4, 0.3 and 1.6 mm respectively, are an exception.

Maximum vertical surface displacement reaches the biggest value of 11 mm for α_1 = 45°. For α_1 = 60°, maximum vertical surface displacement of 10.3 mm is the same as in the case J. Nevertheless, this does not apply to vertical displacement of a point at the top of the underground structure, which is for α_1 = 60° significantly bigger than in the case J. The difference equals 8.8 mm, which is approximately 37 %.

Case S

In the case of situating the underground structure in synclinal bend for all alternatives considered, the maximum vertical displacement at top of the structure (40.0 mm) is achieved for α_1 = 15°. Concurently, for dip angle from the range of 30° – 75°, vertical displacement of the point I does not significantly vary, similarly to the case J.

The maximum vertical surface displacement (11.0 mm) was found for α_1 = 60° as in the case J. The change in relation to the discontinuities orientation is basically of simillar nature as in the earlier cases.

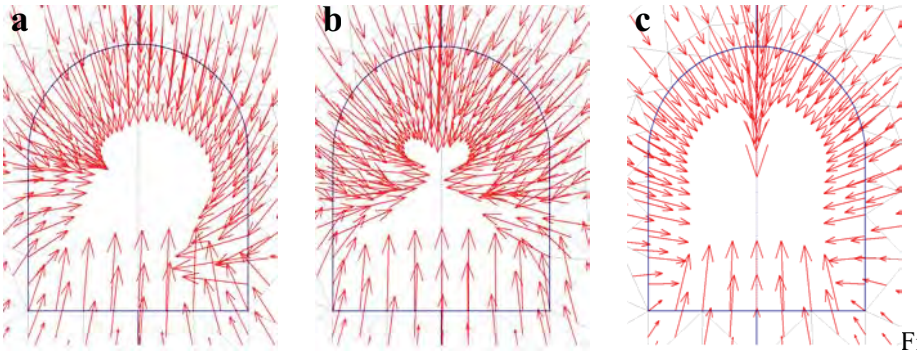

Figure 9. Total displacements around the underground structure: a – case J (α_1 = 45°), b – case A (α_1 = 60°), c – case S (α_1 = 15°)

A field of displacements in the very vicinity of shape of the underground structure is illustrated by arrows in Fig. 9. Only those alternatives of analysed cases, where the biggest vertical displacement at the top of the underground structure was calculated, are presented. Here, the deformation of the underground structure shape for one-sided dip of discontinuities is asymmetric and the biggest displacement is approximately localised in the area of vault support in the direction transverse to the direction of discontinuities (Fig. 9a). In the case A, the biggest displacements

occur at the top of the underground structure and at the sides of the underground structure closely below its vault support (Fig. 9b). In the case S, the biggest displacement was found at the top of the underground structure (Fig. 9c).

4. CONCLUSION

From the results of the parametric study, it can be concluded that from the point of view of vertical deformation at the top of the top heading, driving of the underground structure in the axis of synclinal bend, if the dip of discontinuities is not very steep ($\alpha_1 = 15^o$), is the least favourable. Further, for the case of situating the underground structure in the axis of anticlinal bend, the calculated maximum vertical displacement at the top of the underground structure is 19 % less than in the previous case. From this perspective, the most favourable is driving of the underground structure in case of one-sided askew aslope layers, where maximum value of vertical displacement of the top of the top heading is 60 % of the value obtained for the underground structure in synclinal bend.

From the perspective of the maximum vertical surface displacement, situating the underground structure, in relation to the discontinuities orientation, seems to be of no importance. This observed quantity is practically of the same value for all the cases analysed.

It also results from the analysis, that maximum values of vertical displacement of the top of the underground structure and vertical surface displacement are not reached for the same discontinuities orientation, which is significant especially in the case of synclinal bend.

Along to the all above it needs to be considered, that the alternatives were analysed only for certain selected values of dip angle α_1 in the presented analysis. Therefore, the maximum values of the monitored displacements and corresponding values of dip angle do not have to be the values of absolute maximum for the case itself.

Acknowledgements

The contribution was processed within the grant project GA ČR 103/07/P323 and the research project of MSM0021630519.

References

1. Záruba, Q., Mencl, V., *Engineering geology*, Publisher ČSAV, Prague, 1954. (in Czech)
2. Plaxis 2D – Version 8, Edited by R. B. J. Brinkgreve, A.A. Balkema Publishers, 2002.

"Computational Civil Engineering 2007", International Symposium
Iaşi, România, May 25, 2007

Discrete model for the stability of continuous welded rail

Adam Dósa, Valentin-Vasile Ungureanu
Department of civil engineering, "TRANSILVANIA" UNIVERSITY, Braşov, Romania

Summary

In this paper a discrete model is developed for the buckling analysis of continuous welded rail subjected to temperature load. The model is based on a nonlinear analysis in total lagrangean formulation. The structure consists of beam elements and lateral, longitudinal and torsional spring elements. The source of nonlinearity is due to the geometric nonlinearity of the rail high axial forces and also to the nonlinearity of material type for the lateral and longitudinal resistance of the ballast and the torsional resistance of the fasteners. The use of a displacement control algorithm leads the analysis beyond the critical point and permits a more realistic computation of the structural safety. The track model is encoded into a special purpose program which allows a parametric study of the influence of vehicle loading, the stiffness properties of the structure and of the geometric imperfections on the track stability.

The validity of the present model is verified through a series of comparative analyses with other author's results.

KEYWORDS: Continuous welded rail, Non-linear stability analysis, Temperature loading, Structural safety.

1. INTRODUCTION

The first computational models of the buckling of the continuous welded rail (CWR) were developed at the beginning of the 1930 years. These models can take into account the main parameters which control the stability of CWR like the horizontal and vertical stiffness of the rail, the longitudinal and transversal resistance of the rail, the torsional resistance of the fasteners, the stresses induced by the vehicle and temperature loading, the geometry and the misalignment of the rail. In the SCFJ model presented in this paper the structure consists of beam elements and lateral, longitudinal and torsional spring elements. The beam elements are modeling the rail and have geometric nonlinear characteristics due to high compressive thermal stresses. The spring elements are describing the material nonlinear behavior of the ballast and the fasteners.

2. DEVELOPMENT OF THE TRACK MODEL

2.1. The longitudinal ballast behavior

In the SCFJ model the longitudinal resistance of the ballast is introduced by spring elements having the, linear or bilinear displacement-force curves given in figure 1. In the case of vehicle loading, the bilinear curve is corrected [6] by the equation (1) taking into account the vertical force Q on each sleeper.

$$U_v^c = U_v + Q \cdot tan\phi_L \quad , \quad U_v^c \geq \frac{2}{3} U_v \tag{1}$$

In the above equation U_v is the reference value of the longitudinal resistance (without vehicle loading), U_v^c is the corrected value of this resistance and ϕ_L is the angle of the longitudinal friction between the sleeper and the ballast.

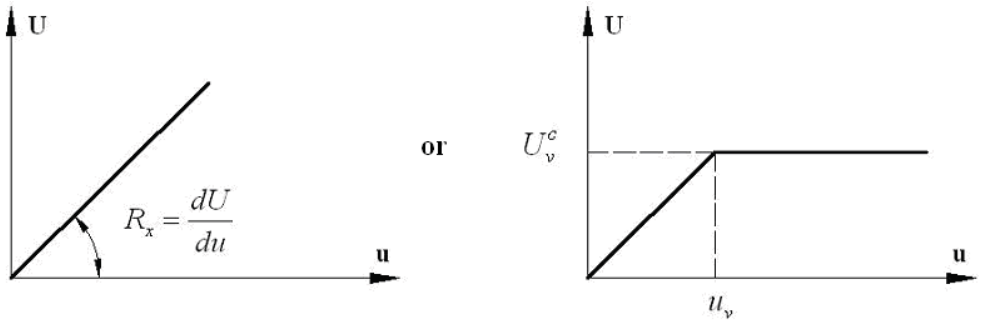

Figure 1. Longitudinal resistance versus longitudinal displacement of the ballast

2.2. The transversal ballast behavior

The transversal resistance of the ballast is introduced by spring elements having the displacement-force curves given in figure 2. In both cases the elasto-plastic model includes softening. This kind of ballast behavior has been measured for consolidated ballast. In the case of vehicle loading, the bilinear curve is corrected [6] by the equation (1) taking into account the vertical force Q on each sleeper using equations (2), (3) or (4).

$$V_v^c = V_v + Q \cdot tan\phi_T \quad , \quad V_v^c \geq \frac{2}{3} V_v \tag{2}$$

$$V_r^c = V_r \cdot V_v^c / V_v \tag{3}$$

$$\text{for } tipV=1 : V = V_r^c + (V_v^c - V_r^c)\cdot 2^{-2\frac{v-v_v}{v_r-v_v}} \quad (\text{if } v > v_v) \tag{4}$$

In the above ecuations V_v is the reference value of the peak transversal resistance (without vehicle loading), V_v^c is the corrected value of this resistance, ϕ_T is the angle of the transversal friction between the sleeper and the ballast, V_r is the reference value of the rezidual transversal resistance (without vehicle loading), and V_r^c is the corrected value of this resistance. In the case of exponential softening the difference $V_v^c - V_r^c$ is half at the middle of $v_v^c - v_r^c$ interval.

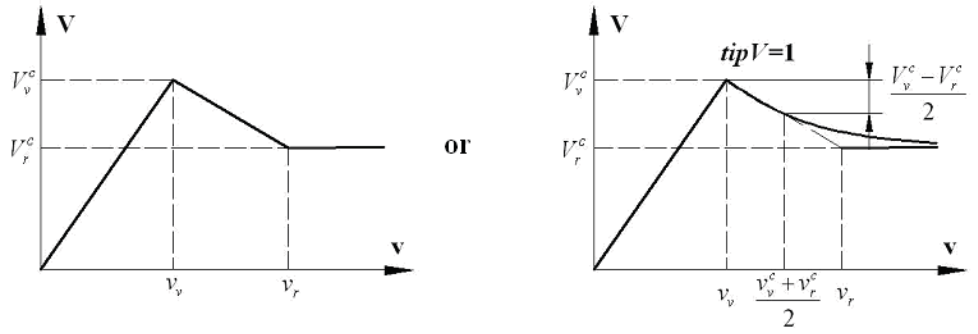

Figure 2. Transversal resistance versus transversal displacement of the ballast

2.3. The torsional stiffness of the fasteners

The resistance of the fasteners is introduced by torsional springs having the linear or tri-linear behavior shown in figure 3. In the case of loaded rail this behavior also can be corrected taking into account the vertical force acting on each sleeper.

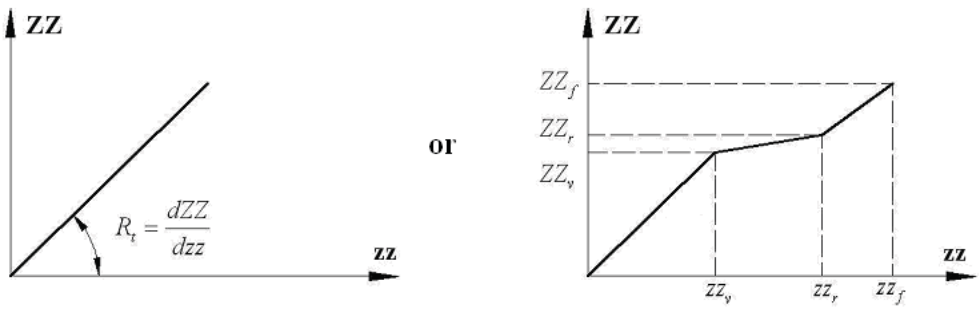

Figure 3. The torsional stiffness of the fasteners

2.4. The geometrical and physical characteristics of the rail

The rail is modeled by beam elements having area of the cross section A, second order moment about the vertical and horizontal axes I_z and I_y respectively. The Young modulus and the thermal expansion coefficient of the material are E and respectively α. In the model the misalignment of the rail can be described by two types of curves: a complete or a half cosine wave having the total length λ and the amplitude δ (figure 6). The length of the model is an input of the program. At the end of the model special infinite boundary elements are introduced -equivalent with the theoretical infinite rail [6]. This elements lead to the reduction of the length of the model and hence the computational effort. Further reduction can be obtained by using the symmetric half structure.

3. THE NUMERICAL ALGORITHM

Since in a simplified manner, the horizontal and vertical behavior are considered decoupled, the numerical algorithm has two phases.

3.1. The computational model for vertical loadings

This model is linear elastic consisting of a beam on elastic springs. The nodes of the structure are considered at the sleepers. Each node has two degrees of freedom: the vertical translation w and the rotation θ_y. The system of equations of equilibrium is:

$$\mathbf{Ka} = \mathbf{F}\,. \tag{5}$$

where:

K is the stiffness matrix of the structure and results by assembling the stiffness matrices **k** of the beams and the vertical stiffness of the fasteners.

a is the displacement vector of the nodes of the structure.

F is the vector of forces at the nodes of the structure, which (in this case) results by assembling the vectors $\mathbf{f}_0$ of the forces on the beams.

The stiffness matrix $\mathbf{k}_{(4x4)}$ of a beam is given by the equation:

$$\mathbf{k} = \mathbf{B}^T \mathbf{k}^d \mathbf{B}\,. \tag{6}$$

Here $\mathbf{B}_{(2\ x\ 4)}$ is a transformation vector, which links the vector of displacements of the beam and the reduced vector of displacements of the beam. The reduced vector of displacements does not contain the rigid body displacements.

$$\mathbf{a}_{el}^{d} = \begin{Bmatrix} \theta_{yi}^{d} \\ \theta_{yi+1}^{d} \end{Bmatrix} = \mathbf{B} \cdot \mathbf{a}_{el} = \begin{bmatrix} 1/L & 1 & -1/L & 0 \\ 1/L & 0 & -1/L & 1 \end{bmatrix} \begin{pmatrix} w_i & \theta_{yi} & w_{i+1} & \theta_{yi+1} \end{pmatrix}^T \tag{7}$$

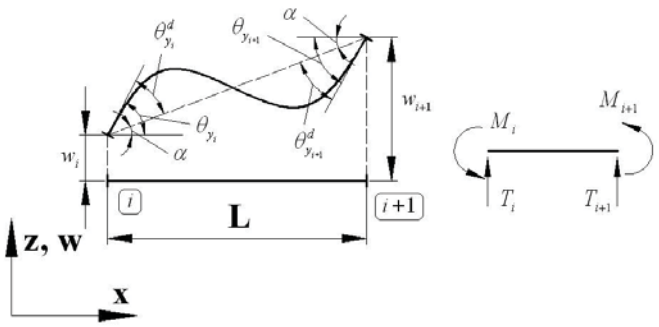

Figure 4. The displacements of the beam in the vertical plane

$\mathbf{k}^{d}_{(2\,x\,2)}$ is the reduced stiffness matrix of the beam.

$$\mathbf{k}^{d} = \frac{EI_y}{L} \begin{bmatrix} 4 & 2 \\ 2 & 4 \end{bmatrix} \tag{8}$$

If the beam is loaded, the vector $\mathbf{f}_0$ of equivalent forces in the nodes is given by equations (9).

$$\begin{aligned} M_i^0 &= P \cdot b^2 a / L^2 \qquad & T_i^0 &= (P \cdot b + M_i + M_{i+1})/L \\ M_{i+1}^0 &= -P \cdot a^2 b / L^2 \qquad & T_{i+1}^0 &= (P \cdot a - M_i - M_{i+1})/L \\ \mathbf{f}_0 &= (T_i^0 \;\; M_i^0 \;\; T_{i+1}^0 \;\; M_{i+1}^0)^T \end{aligned} \tag{9}$$

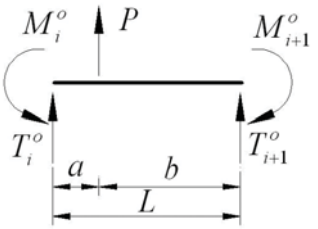

Figure 5. Equivalent nodal forces of the beam

The stiffness matrices and the load vectors of the beams are assembled by the relation (10).

$$\mathbf{K}_{ind,ind} = \mathbf{K}_{ind,ind} + \mathbf{k}, \quad \mathbf{F}_{ind} = \mathbf{F}_{ind} + \mathbf{f}_0 \,. \tag{10}$$

Here *ind* is the vector of the indices of the displacements of the current beam.

The stiffness of the sleepers is assembled with the help of the equation (11).

$$\mathbf{K}_{jnd,jnd} = \mathbf{K}_{jnd,jnd} + R_z L \tag{11}$$

In the above equation *jnd* is the set of indices of vertical displacements of the nodes *jnd*=1, 3, ..., 2*nnd*-1. The constraints of the structure are introduced by setting to zero the displacements of the supports. The free displacements of the nodes result by solving the system of linear equations:

$$\mathbf{a}_{id} = (\mathbf{K}_{id,id})^{-1}\mathbf{F}_{id}\,. \tag{12}$$

In equation (12) *id* is the set of the free displacements of the structure.

Using the vertical displacements, the vertical force on each sleeper can be computed by the equation (13)

$$Q = -wR_z L + G_{sleeper}\,. \tag{13}$$

The transversal, longitudinal and torsional resistances are corrected taking into account the forces Q on each sleeper using equations (1) to (4).

3.2. The computational model in the horizontal plane

The model is a straight or curved beam on elastic supports with misalignments (figure 6). The nodes of the structure are considered at the sleepers. At each node are introduced longitudinal, transversal and rotational spring elements which are modeling the sleepers. The infinite boundary elements at the ends of the model have equivalent characteristics (Young modulus and thermal expansion coefficient) in order to replace the theoretical infinite rail [6]. The loading of the model is an increase of the temperature in the rail. The characteristics of the beams and of the springs correspond to the two rails of the track panel. A node has three degrees of freedom: two linear displacements in the horizontal plane, u and v and the rotation θ_z around the vertical axis. In the analysis of the structure the goal is to obtain the displacement-temperature curve. The problem is solved by a displacement control based incremental process. The behavior of the system is determined as a sequence of increments of state parameters (forces and displacements). In the current increment j characterized by the small control displacement δv_{cj}, the nonlinear behavior of the system can be approximated by a linear relation between the successive increments of the state parameters:

$$\mathbf{a}_{j+1} = \mathbf{a}_j + \delta\mathbf{a}_j, \quad \delta\mathbf{F}_j = \mathbf{K}_j\delta\mathbf{a}_j\,. \tag{14}$$

In the above equation $\mathbf{a}_j$ is the displacement vector in the current configuration, $\delta\mathbf{a}_j$ is the increment of the displacements, $\delta\mathbf{F}_j$ is the incremental load vector and $\mathbf{K}_j$ is the incremental (tangent) stiffness matrix of the structure.

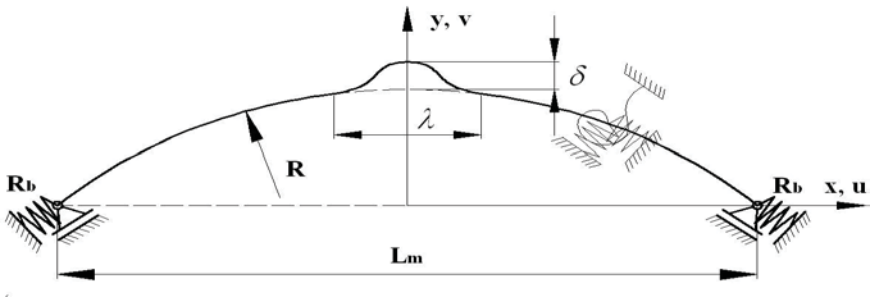

Figure 6. The model for horizontal displacements

By using equations (14), the following incremental scheme results:

$$\delta\mathbf{a}_j = (\mathbf{K}_j)^{-1}\delta\mathbf{F}_j, \quad \mathbf{a}_{j+1} = \mathbf{a}_j + \delta\mathbf{a}_j . \tag{15}$$

In this paper an improved scheme is used, known as Heun's or midpoint rule:

$$\begin{aligned} &\mathbf{a}_{j+1/2} = \mathbf{a}_j + 1/2(\mathbf{K}_j)^{-1}\delta\mathbf{F}_j, \\ &\mathbf{K}_{j+1/2} = \mathbf{K}(\mathbf{a}_{j+1/2}), \\ &\delta\mathbf{F}_{j+1/2} = \delta\mathbf{F}(\mathbf{a}_{j+1/2}), \\ &\mathbf{a}_{j+1} = \mathbf{a}_j + 1/2(\mathbf{K}_{j+1/2})^{-1}\delta\mathbf{F}_{j+1/2}. \end{aligned} \tag{16}$$

The incremental load vector $\delta\mathbf{F}_j$ is not computed. The incremental displacement $\delta\mathbf{a}_j$ is the result of a yet unknown increment of the temperature produced by a known increment δv_{cj} of the control displacement. For simplicity, in the next equations indices j of the current configuration are dropped. The displacement control consists of loading the system with displacement increments δv_c in a specific node. As a rule in this paper: the control displacement is taken as the maximum transversal displacement of the node on the symmetry axe of the structure. The phases of the computation are the following:

- It is adopted a base system with the control displacement fixed at zero.
- This base system is loaded with two load cases:

i) Load 1 is a temperature increase $\delta T = 1$, which produces displacements $\delta\mathbf{a}^{(1)}$ at the free nodes and reaction $R^{(1)}$ in the artificial support.

ii) Load 2 is a displacement δv_c of the artificial support, which produces displacements $\delta\mathbf{a}^{(2)}$ at the free nodes and reaction $R^{(2)}$ in the artificial support.

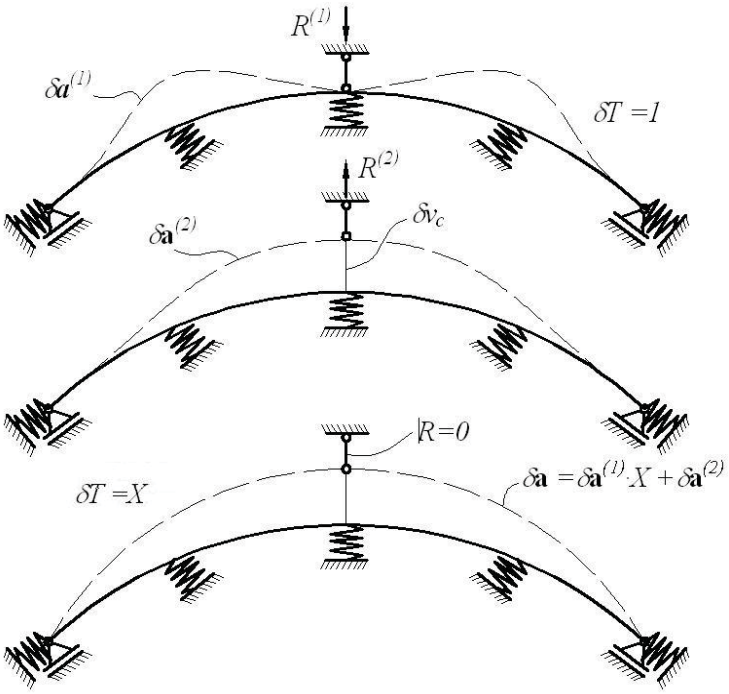

Figure 7. The determination of the temperature and displacement increments

The base system and the initial system are identical if the total reaction in the artificial support is zero. $R= R^{(1)}\delta T + R^{(2)}=0$. This equation yields the unknown variation δT of temperature and the incremental displacements $\delta\mathbf{a}$ of the free nodes.

$$\delta T = -R^{(2)} / R^{(1)}, \tag{17}$$

$$\delta\mathbf{a} = \delta\mathbf{a}^{(1)} \cdot \delta T + \delta\mathbf{a}^{(2)}. \tag{18}$$

The tangent stiffness matrix $\mathbf{K}_j$ in the j increment depends on the parameters of the system in the current step and results by assembling the stiffness matrices $\mathbf{k}_{t(6\,x\,6)}$ of the beams and of the springs which model the sleepers.

$$\mathbf{k}_t = EA / L \cdot \mathbf{r}^T\mathbf{r} + \mathbf{B}^T(\mathbf{k}^d + \mathbf{k}_G^d)\mathbf{B} + N_j / L \cdot \mathbf{z}^T\mathbf{z}. \tag{19}$$

In this equation $\mathbf{r}$=*(-cosβ -sinβ 0 cosβ sinβ 0),*
$\boldsymbol{z}$*=(sinβ -cosβ 0 -sinβ cosβ 0),*

$$\mathbf{B} = \begin{bmatrix} 0 & 0 & 1 & 0 & 0 & 0 \\ 0 & 0 & 0 & 0 & 0 & 1 \end{bmatrix} - \frac{1}{L}\begin{bmatrix} \mathbf{z} \\ \mathbf{z} \end{bmatrix}, \quad \mathbf{k}^d = \frac{EI_z}{L}\begin{bmatrix} 4 & 2 \\ 2 & 4 \end{bmatrix}, \quad \mathbf{k}_G^d = \frac{N_j L}{30}\begin{bmatrix} 4 & -1 \\ -1 & 4 \end{bmatrix},$$

and N_j is the axial force in the beam in the j-th incremental step: $N_j=EA\ \Delta L_j/ L_j$, $\Delta L_j = L_j - L_0$, $L_0 = \sqrt{(\mathbf{x}_{i+1}^0 - \mathbf{x}_i^0)^2}$, $L_j = \sqrt{(\mathbf{x}_{i+1}^j - \mathbf{x}_i^j)^2}$.

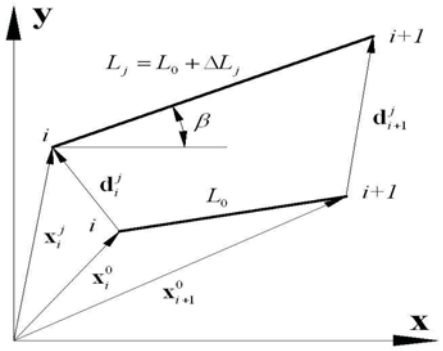

Figure 8. The axial deformation of the beam

Matrices $\mathbf{k}^d$ and $\mathbf{k}_G^d$ are the material and geometric stiffness matrices respectively. They are expressed with the reduced set of displacements which produce deformations and they are not containing the rigid body displacements of the beam. This reduced form of the stiffness matrices needs less computational effort and speeds up significantly the computation. Equation (19) introduces the non-linear effect of the axial force N_j. The complete tangent stiffness matrix in the updated lagrangean formulation used here has two more terms corresponding to the variation of the length of the beam in bending and to the effect of the shear force [1], [2], [3], [4], [5]. Since in the current cases the structure is divided in a sufficient number of beams, the errors are very small, when neglecting these two terms. In a study using the complete tangent stiffness matrix and equation (19) the differences between the resulting limit temperatures were only at the fifth digit.

4. NUMERICAL EXPERIMENTS

The validity of the present model is verified through a series of comparative analyses with other author's results. The numerical example presented here corresponds with one given in [1]. The track length is L=24.359/2 m corresponding to 21 sleepers on the symmetric half of the structure. The curvature radius is R=400 m. The horizontal misalignment is characterized by a half wave cosine with a length λ=9.144 m and an amplitude δ=0.0381 m. The rails have the characteristics of two AREA 136 rails. The vertical stiffness of the ballast elements is R_z=68900 kN/m per meter of track. The longitudinal stiffness is R_x=1378 kN/m per meter of track. The torsional stiffness of the fasteners is 111.250 kNm/rad per meter of

track. Laterally the ballast is modeled by the tri-linear constitutive behavior given in figure 2. The reference values of the lateral peak resistance and residual resistance are V_v=17.508 and V_r=9.630 kN per meter of track. These values are corrected with the vertical forces resulting from the vehicle loading. The lateral displacement at the peak value is v_v=0.00635 m and at the limit value is v_r=0.0381 m. The model is vertically loaded by a vehicle with two bogies represented by four vertical loads of 293 kN each. The centre spacing between the bogies is 12.85 m. The spacing between the axles in a bogie is 1.78 m. The centre of the misalignment is located in the middle between the bogies. The track is loaded by a temperature increase from zero to a maximal value corresponding to the buckling of the rail. The lateral displacement of the middle node versus the resulting temperature increase is shown in figure 9.

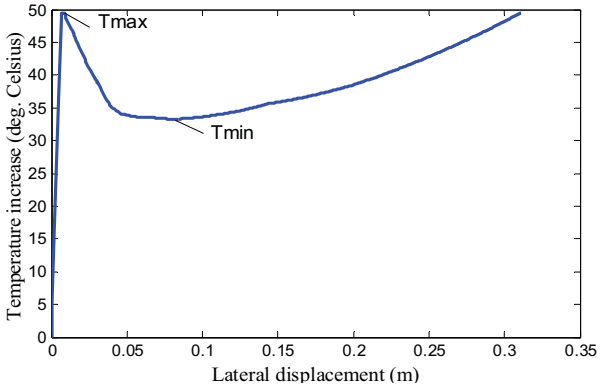

Figure 9. Lateral displacement versus temperature increase

The curve in the figure 9 is characterized by two points: T_{max} - the maximum increase of temperature for which the buckling certainly starts, and T_{min} - the minimum increase of temperature which occurs in the post-buckling domain. The values computed by the SCFJ model - T_{max}=49.5 ^{0}C and T_{min}=33.3 ^{0}C - are in a good agreement with those given in [1].

References

1. Bănuţ, V. *Calculul neliniar al structurilor*, Editura tehnică, Bucureşti, 1981.
2. Crisfield, M.A. *Non-linear Finite Element Analysis of Solids and Structures*, Wiley, 1991.
3. Dósa,A., Litră E. Elemente de bară încovoiată cu precizie îmbunătățită pentru calculul neliniar şi de stabilitate , *Revista Construcțiilor*, 2006.
4. Dósa,A., Popa L. High order beam elements for the stability and non-linear analysis of frame structures, "*Computational Civil Engineering 2006*", Iaşi, România.
5. Felippa C.A., *Nonlinear Finite Element Methods*, www.colorado.edu/engineering/CAS/courses.d/NFEM.d.
6. Van, M.A., Stability of Continuous Welded Rail Track, Delft University Press, 1997.

"Computational Civil Engineering 2007", International Symposium
Iaşi, Romania, May 25, 2007

Soil-Structure Interaction Effects of Damped Structures

Petre Ene
Technical University of Construction, Bucharest, Romania

Summary

In the past, much effort has been devoted to investigating the seismic behavior of structures with seismic dampers by neglecting the effects of foundation-structure interaction. In order to ensure the safety of structures, it is necessary to apprehend the interactive behavior of damped structures and unbounded foundations under intense earthquake ground motions. This paper presents a rigorous time-domain procedure to address the interaction effects of structures equipped with fluid viscous dampers and foundations with an unbounded medium. Quantitative results show that, during earthquakes, there are significant differences between a system with and without radiation damping. For greater accuracy, radiation damping should be properly taken into account. More-over, the efficiency of fluid viscous dampers in reducing seismic disturbance of a structure is very dependent on the flexibility of the foundation.

1. INTRODUCTION

Seismic dampers have been recently used to enhance seismic performance for some tall buildings in California (Pong, 1999). For example, an eight story concrete building located on the campus of the California State University at Los Angeles was retrofitted by adding viscous dampers (Elhassan et al., 1996). An eleven story steel building, the new national headquarters for the Money Store located in Sacramento, California, was one of the first buildings in the United States that use seismic dampers to limit story drift during earthquakes (Miyamoto and Scholl, 1998). However, many structural analyses and designs ignore the behavior of soil-structure interaction due to the complexity and uncertainty of modeling techniques. In the last twenty years, some advances have been made in this area. Most notable is the development of procedures based on boundary-integral or boundary-element methods for unbounded media. Nonetheless, a major need still exists for alternative approaches, particularly for procedures that could be implemented within the context of finite-element analyses. These procedures would be more familiar to structural analyses, and would allow greater flexibility in terms of the geometrical and material characterization of the unbounded medium.

In this paper, a new time-domain procedure, based on the finite element method, the semi-analytical solution and the infinitesimal finite-element cell method, is

presented to address the interactive behavior of structures equipped with fluid viscous dampers and foundation with an unbounded region (Fig.1a). To yield more accurate results, a time domain procedure has been developed to simulate the radiation features of an infinite domain.

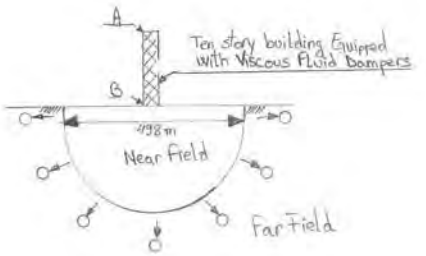

Fig. 1a Ten-Story Building Equipped with Fluid Viscous Dampers and Foundation

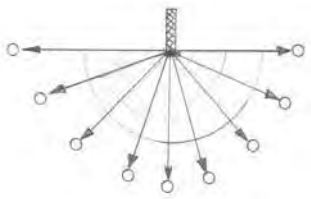

Fig. 1b Finite Element Mesh for Building Equipped with Fluid Viscous Damper and Foundation

2. TIME-DOMAIN SUBSTRUCTURE METHOD

The substructure method is adopted for the study. The entire system is divided into three substructures including the building, foundation and fluid dampers. Furthermore, the soil medium is also divided into two regions: the near and the far field of the soil. The far field of the soil extends to infinity.

Equations of Motion of Building and Near Field of Foundation

As shown in Figs. 1a and 1b, the structure, fluid damper and the near field of the soil can be descretized by the finite element method. The equation of motion of the structure and the near field of the foundation is given as:

$$M\ddot{U}(t) + C\dot{U}(t) + KU(t) = -MB\ddot{u}_g(t) + Q(t) \tag{1}$$

M, C, K = symmetrical mass, damping, and stiffness matrices, respectively, for the building and the near field of the foundation;

$U(t), \dot{U}(t), \ddot{U}(t)$ = vectors of nodal displacements, velocities, and accelerations relative to the ground, respectively;

$\ddot{u}_g(t)$ = ground motion;

B = displacement transformation matrix;

And Q (t) = vector of dynamic forces resulting from the far field of the foundation.

Analytical Model for Fluid Viscous Damper

The fluid damper exhibits viscoelastic fluid behavior over a large frequency. The simplest model to simulate the mechanical behavior of the fluid viscous damper is the Maxwell model (Bird et al., 1987) given as:

$$P(t) + \lambda \dot{P}(t) = C_0 \dot{U}(t) \qquad (2)$$

Where "t" is the relaxation time, C_0 is the damping constant at zero frequency, P (t) is the force acting on the fluid damper, $U(t)$ is the damper position velocity.

Another finite element formulation model for fluid dampers was adopted in this study (Pong et al., 1994). Using the virtual work principle, the equivalent modal forces F (t) can be obtained as:

$$F(t) = B^T P(t) = \frac{C_0}{1+\frac{\lambda}{\Delta t}} B^T B \dot{U}(t) + \frac{\lambda}{\Delta t}\frac{1}{1+\frac{\lambda}{\Delta t}} B^T P_{n-1}(t) =$$
$$= C_f \dot{U}(t) + \frac{\lambda}{\Delta t}\frac{1}{1+\frac{\lambda}{\Delta t}} B^T P_{n-1}(t) \qquad (3)$$

Where the matrix C_f is the added damping result from fluid dampers:

$$C_f = \frac{C_0}{1+\frac{\lambda}{\Delta t}} B^T B \qquad (4)$$

System Equations for Far Field of Foundation

As shown in Fig. 1a, the foundation medium is divided into two regions: the near and far fields of the foundation. The far field of the foundation extends to infinity. Adopting the similarity theorem, as shown in Fig. 2, Song and Wolf developed the consistent infinitesimal finite-element cell method accounting for the radiation damping for the unbounded medium in the time domain (Song and Wolf, 1995; 1996).

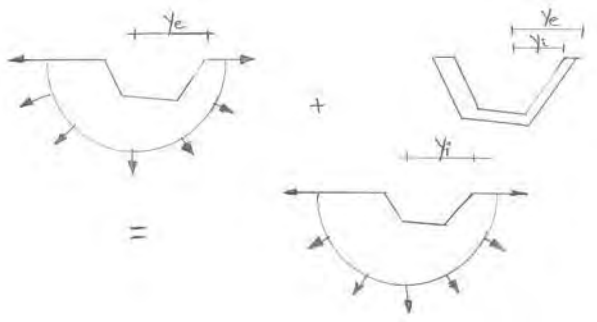

Fig.2 Fundamental Concept of Consistent infinitesimal Finite-Element Cell Method

The governing equation of the far field of foundation can be expressed as:

$$I(t) = \int_0^t M^{\infty}(t-\tau)\ddot{U}(\tau)d\tau \qquad (5)$$

Where $I(t)$ the interaction is force at the interface of the near and far fields of the unbounded medium and $M^{n}(t)$ is the acceleration unit-impulse response matrix in the time domain. The relation of the vector of dynamic forces from the far field $I(t)$ to those acting on the near field $Q(t)$ is given as:

$$Q(t) = -I(t) \qquad (6)$$

As shown in Fig.3, owing to similarity, the coordinates of the nodes on the exterior boundary can be expressed by those of the nodes on the interior boundary and the dimensionless cell width

$$y_4 = (1+w)y_1, y_5 = (1+w)y_2, y_6 = (1+w)y_3 \qquad (7)$$

$$z_4 = (1+w)z_1, z_5 = (1+w)z_2, z_6 = (1+w)z_3 \qquad (8)$$

The nodes on the interior boundary are identified by subscripts 1, 2, 3 and the nodes on the exterior boundary are identified by subscripts 4, 5, 6, respectively. The cell width w can be expressed as $w = (r_e - r_i)/r_i$ and

$$Y_e = (1+w)Y_i \qquad (9)$$

$$Z_e = (1+w)Z_i \qquad (10)$$

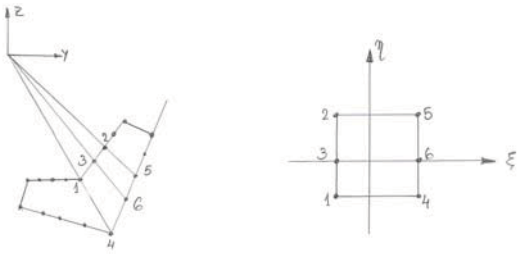

Fig.3 Two-dimensional Finite-element Cell and Parent Element on Descretized Interface

Note that the subscript i and e portray the interior boundary and the exterior boundary, respectively. Y_e and Z_e denote the coordinates of the nodes on the exterior boundary. Y_i and Z_i indicate the coordinates of the nodes on the interior boundary. The shape function matrix of the finite-element is:

$$\bar{N} = [N_i \quad N_e] \tag{11}$$

$$N_j = \frac{1}{2}(1 - \xi_j \xi)N, \ (j = i, e) \tag{12}$$

Where $\xi_e = 1$ and $\xi_i = -1$, N = the shape function vector in the η direction. Therefore, the stiffness matrix of the finite element equals:

$$K_{jl} = \int_S B_i^T D B_j dS = \iint_{-1}^{+1} B_i^T D B_j |\tilde{J}| d\xi d\eta, \ (j = i, e; l = i, e) \tag{13}$$

The Jacobean matrix of a particular element equals:

$$\tilde{J} = \begin{bmatrix} \frac{\omega}{2} & 0 \\ 0 & 1 + \frac{\omega}{2}(1 + \xi) \end{bmatrix} J \tag{14}$$

$$\text{Where } J = \begin{bmatrix} NY_e & NZ_e \\ N_{j\eta} Y_i & N_{j\eta} Z_i \end{bmatrix} \tag{15}$$

The determinant of the Jacobean matrix is given as:

$$|\tilde{J}| = \frac{\omega}{2}\left(1 + \frac{\omega}{2}(1 + \xi)\right)|J| \tag{16}$$

$$\text{where } J^{-1} \text{ is denoted as } J^{-1} = \begin{bmatrix} j_{11} & j_{12} \\ j_{21} & j_{22} \end{bmatrix} \tag{17}$$

The strain-nodal displacement matrix is

$$B = [B_i \quad B_e] \tag{18}$$

$$B_{jk} = \frac{\xi_j}{\omega} B_k{}^1 + \frac{1+\xi_j\xi}{2\left(1+\frac{\omega}{2}(1+\xi)\right)} B_k{}^2, \ (j = i, e; k = 1,2,\dots) \tag{19}$$

$$\text{And } B_k{}^1 = \begin{bmatrix} j_{11} & 0 \\ 0 & j_{21} \\ j_{21} & j_{11} \end{bmatrix} N_k \tag{20}$$

$$B_k{}^2 = \begin{bmatrix} j_{12} & 0 \\ 0 & j_{22} \\ j_{22} & j_{12} \end{bmatrix} N_k, \ (k = 1,2,\dots) \tag{21}$$

N_k = *the shape functions at nodal point k. The final form of the consistent infinitesimal finite-element cell equation in the time domain is given as:*

$$\int_0^1 [m^n(t-\tau)][m^n(\tau)]d\tau + e^1 \int_0^1 \int_0^1 [m^n(\tau')]d\tau' d\tau + e^1 \int_0^1 \int_0^1 [m^n(\tau')]d\tau' d\tau (e^1)^\tau + \int_0^1 [m^n(t-\tau)]d\tau -$$

$$\frac{t^3}{6} e^2 II(t) - t m^n II(t) - 0 \tag{22}$$

$$\text{Where} \quad m^n(t) = (V^{-1})^T M^n(\tau) V^{-1} \tag{23}$$

$$E^0 = V^T V \tag{24}$$

$$e^1 = (V^{-1})^T E^1 V^{-1} - \frac{3}{2} I \tag{25}$$

$$e^2 = (V^{-1})^T [(E^2 - E^1 (E^0)^{-1} (E^1)^T] V^{-1} \tag{26}$$

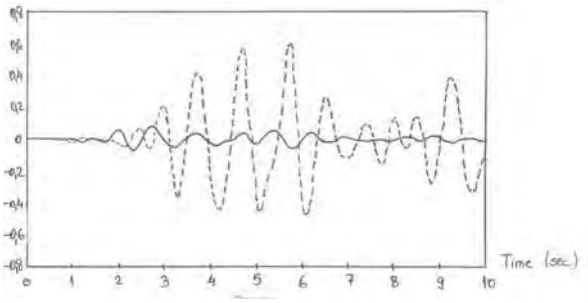

Fig.4a Comparison of Relative Displacements between Points A and B while Elastic Modulus of Near Field is $10^7 KN/m^2$ and Elastic Modulus of Near Field is $10^8 KN/m^2$

$$m^o = (V^{-1})^T M^0 V^{-1} \quad (27)$$

$$M^0 = \int_{-1}^{+1} \rho N^2 N |J| d\eta \quad (28)$$

ρ = *mass density. After determining* $m^\eta(t)$ *from eq. (22), the acceleration unit-impulse response matrix may be written as:*

$$M^\eta(t) = V^T m^\eta(\tau) V \quad (29)$$

The entire history of time is divided into n equal intervalsΔt. It is assumed that matrix $m^\eta(t)$ and the acceleration is piece-wise constant over each time step:

$$\ddot{U}(\tau) = \frac{1}{2}\{\ddot{U}[(n-1)\Delta t] + \ddot{U}[(n\Delta t)]\}, \quad (n \quad 1\Delta t \leq \tau \leq n\Delta t) \quad (30)$$

With the aid of eq. (30), $I(t)$ of eq. (5) can be expressed as:

$$I(t) = \int_0^1 [M^\eta(t-\tau)]\ddot{U}(\tau)\, d\tau - \int_0^1 [M^\eta(\tau)]\ddot{U}(t-\tau)\, d\tau -$$

$$-\frac{\Delta t}{2}\sum_{n=0}^{N} M^\eta\left[\left(n-\frac{1}{2}\right)\Delta t\right]\{\ddot{U}[(N-n+1)\Delta t] + \ddot{U}[(N-n)\Delta t]\} +$$

$$+\frac{\Delta t}{2}M^\eta\left(\frac{\Delta t}{2}\right)\{\ddot{U}[(N-1)\Delta t]\} + \frac{\Delta t}{2}M^\eta\left(\frac{\Delta t}{2}\right)[\ddot{U}(N-1)\Delta t] = \bar{M}\ddot{U}(N\Delta t) + \bar{F} \quad (31)$$

Where $\bar{M} = \frac{\Delta t}{2}M^\eta\left(\frac{\Delta t}{2}\right)$ (32)

$$\bar{F} = \frac{\Delta t}{2}\sum_{n=0}^{N} M^\eta\left[\left(n-\frac{1}{2}\right)\Delta t\right]\{\ddot{U}[(N-n+1)\Delta t] + \ddot{U}[(N-n)\Delta t]\} +$$
$$\frac{\Delta t}{2}M^\eta\left(\frac{\Delta t}{2}\right)\{\ddot{U}[(N-1)\Delta t]\} \quad (33)$$

Time-Domain Finite Element Method for Structure Equipped with Fluid Viscous Dampers and Unbounded Media

Substituting eq. (6) and eq. (31) into eq. (1) results in

$$(M+\bar{M})\ddot{U}(t) + C\dot{U}(t) + KU(t) = -MB\ddot{u}_g(t) - \bar{F}(t) \quad (34)$$

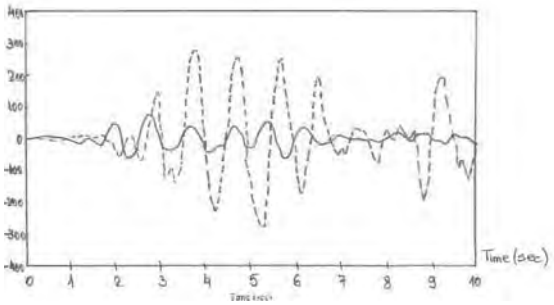

Fig.4b Comparison of Shear Forces at Point B while Elastic Modulus of Far Field is $10^7 KN/m^2$ and Elastic Modulus of Near Field is $10^8 KN/m^2$

$\bar{M}$ is an added-load matrix representing the previous time effect. Applying the new mark method to eq.(34), at the Nth time step, we have

$$\hat{K}U^N = \hat{R}^N \qquad (35)$$

Where $\hat{K} = k + a_0(M + \bar{M}) + a_1 C$ (36)

$$\hat{R}^N = -MB\ddot{u}_g(t) + (M + \bar{M})(a_0 U^{N-1} + a_2 \dot{U}^{N-1} + a_3 \ddot{U}^{N-1}) +$$

$$+C\left(a_1 U^{N-1} + a_4 \dot{U}^{N-1} + a_5 \ddot{U}^{N-1}\right) - \bar{F} \qquad (37)$$

Where $a_0 = \frac{1}{\alpha \Delta t^2}$; $a_1 = \frac{\delta}{\alpha \Delta t}$; $a_2 = \frac{1}{\alpha \Delta t}$; $a_3 = \frac{1}{2\alpha} - 1$; $a_4 = \frac{\delta}{\alpha} - 1$; $\delta \geq 0{,}50$;

$\alpha \geq 0{,}25(0{,}5 + \delta)$.

Application

A ten story steel building frame was used for this application. The building span width is 9,20m. The typical story height is 3,70m, except the first story height is 4,60m. Point A is designated at the roof, while Point B is designated at the base. The material used for the building has Poisson‘s ratio and elastic modulus equal to 0,3 and 200 GPa, respectively. The weight for each floor is 4460,60N/m. The radius of the near field of the soil below the building is around the 249m. The Poisson’s ratio of the stratum is 0,30 and the weight density is 1,80KN/m^3.

It was assumed that the floor were in their own plane. The damping constant C_0 of fluid viscous damper is 525,59KNs/m and the whole system was subjected to 1940 El Centro earthquake ground motion. Fig. 4a shows the shear force responses at point B when the building equipped with fluid viscous dampers during earthquakes. In these figures, the bold-solid line is the seismic response of the building on rigid foundation (without soil) and the dotted line is the response of the

building on the flexible foundation with radiation damping during earthquakes. With reference to Fig. 4a and 4b, they indicate that the seismic responses of the building have remarkable differences on different foundations.

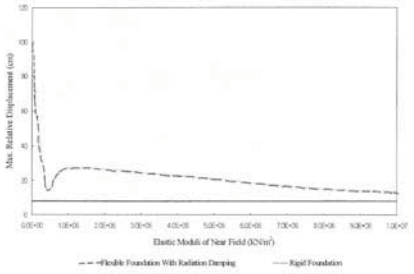

Fig. 5a Comparison of Max. Relative Displacements between Points A and B while Elastic Modulus of Far Field is $10^7 KN/m^2$ *and Different Modulus of Near Field are Applied*

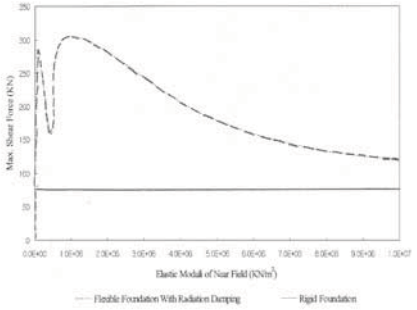

Fig. 5a Comparison of Max. Shear Forces at Point B while Elastic Modulus of Far Field is $10^7 KN/m^2$ *and Different Modulus of Near Field are Applied*

When the elastic modules of the near field of foundation are different, the comparison of the maximum relative displacement responses at points A and B of the building equipped with fluid viscous dampers on the unbounded soil are shown in Fig. 5a. In addition, Fig. 5b shows the comparisons of the maximum shear force responses at point B when the building equipped with fluid viscous dampers on the unbounded soil. These two figures show that significant differences exist between the responses of the building on different foundations during earthquakes. They also show that the whole system becomes more flexible due to the interaction effects of the foundation and the effectiveness of the fluid viscous damper in reducing seismic responses of the building is considerably downgraded.

Conclusions

Seismic dampers have been recognized as an effective tool in improving seismic resistance for both new and existing buildings. Recently, they have been used extensively to achieve enhanced structural performance for the seismic rehabilitation of tall buildings in California. Nevertheless, soil-structure interaction is a very complicated behavior and it requires time-consuming effort in structural analyses and designs. To ensure the safety of a structure, it necessitates considering the interaction behavior of the damped structure under intense ground motions. It is prudent to consider the effects of radiation damping and the flexibility of the soil media when designing tall buildings with seismic dampers since taller buildings tend to be much more flexible than shorter buildings.

This study demonstrates differences between a damped structure with and without consideration of the soil media. The structural behavior of a building can be quite different if the soil-structure interaction is ignored. Quantitative results show that remarkable differences exist in the seismic behavior of the system with and without a flexible foundation. The role of radiation damping becomes extremely important during an earthquake when supplemental damping is added to the structure. Therefore, the design of a tall structure with supplemental damping in an earthquake one area should consider the effects of soil-structure interaction to ensure optimal seismic performance.

References

1. Elhassan, R.M., Arminak, A., 1996 – Design and Analysis of a Seismic Retrofit of a Tall Concrete Building using Supplemental Viscous Dampers;
2. Miyamoto, H.K., Scholl, R., 1998 – Modern Steel Construction;
3. Pong, W.S., 1999 – Performance - Based Design Procedures for Buildings with supplemental Dampers;
4. Pong, W.S., Tsai, C.S., 1994 – Seismic Study of Building Frames with added Energy-absorbing Devices;
5. Song, C., Wolf, J.P., 1995 – Consistent Infinitesimal Finite-Element Cell Method: Out of Plane Motion;
6. Song, C., Wolf, J.P., 1996 – Consistent Infinitesimal Finite-Element Cell Method: Three-Dimensional Vector Wave Equation.

"Computational Civil Engineering 2007", International Symposium
Iaşi, România, May 25, 2007

Numerical Modeling of Fiber Reinforced Concrete (FRC). Fiber orientation angle $\alpha = 0^0$, fiber length $l_f = 50$mm

Liviu Gherman[1], Petru Mihai[2], Nicolae Florea[3], Constantin Gavriloaia[4], and Ioan Paul Vodă[5]

[1]*Faculty of Civil Engineering, BMTO, Tehnical University "Gh. Asachi", Iasi, Romania*
[2]*Faculty of Civil Engineering, BMTO,Tehnical University "Gh. Asachi", Iasi, Romania*
[3]*Faculty of Civil Engineering, BMTO, Tehnical University "Gh. Asachi", Iasi, Romania*
[4]*Faculty of Civil Engineering, BMTO, Tehnical University "Gh. Asachi", Iasi, Romania*
[5]*Faculty of Civil Engineering, BMTO, Tehnical University "Gh. Asachi", Iasi, Romania*

Summary

The paper presents a new approach on FRC study, which has similar characteristics to a multi-phase composite material. Numerical modeling is applied, using a finite element method (FEM) program, to study the behavior of linear structural elements, made from steel fiber reinforced concrete (SFRC).

The results stress out the favorable influence of the fibers on the bearing capacity and especially on the ductility of the loaded members. Lack of design standards and practice codes on this material is bringing this field of study under researchers' consideration.

KEYWORDS: numerical modeling, steel fiber reinforced concrete, influence of the steel fibers.

1. INTRODUCTION

Enhancement of SFRC properties is more evident for hardened concrete than for fresh concrete. It is influenced by the fiber characteristics: length and geometry, reinforcement percentage, orientation and adherence to the concrete matrix.

For this new type of material, the workability is decreasing, the concrete having low to very low plasticity. If a high reinforced percentage is used, or fibers having length higher than the critical one, the workability decreases dramatically, the fibers having the tendency to bundle. This shortcoming can be overcome with supplementary execution costs.

Studying the influence of the fibers on the concrete behavior, as well as the wide possibilities for using this material makes it necessary that it is studied using numerical modeling.

2. NUMERICAL MODELING USING FEM

2.1. Used Finite Element Types

Any loaded body with a given shape must be analyzed, in order to establish the proper finite elements to be used for meshing. Usually, the choice of the finite element is determined by the geometry of the body and by the number of independent spatial coordinates necessary to describe the system. Some types of finite elements, one-dimensional or bi-dimensional, are presented in Figures 1, 2.

When the geometry, properties and other parameters of the material (stresses, displacements, pressure, temperature) can be described using only one spatial coordinate, the one-dimensional finite element can be used (Figure 1). Even though this element has a transversal cross-section, it can be idealized as a line.

In some cases, the cross-sectional area of this element may vary along its length.

Figure 1 – One-dimensional finite element

When the geometry and details of the studied problem can be expressed function of two independent spatial coordinates, bi-dimensional finite elements are used (Figure 2), the basic type having triangular shape.

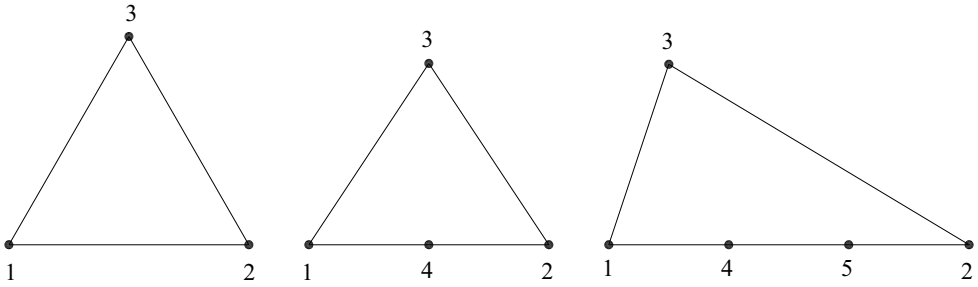

Figura 2 – Bi-dimensional triangular finite element

2.2. Finite Element Analysis Steps

Most of the finite element analysis steps are performed successfully by the FEM program, so their succession is highly simplified:

- The preparatory stage, consisting in the precise meshing of the element, using a CAD program, after which it was exported to a FEM program.
- Definition of the physical and mechanical characteristics of the materials, and of the plain stress analysis manner in the nonlinear domain.
- Analysis and interpretation of the results.

2.2.1. The meshing was performed in two variants.

The corresponding free body diagrams are also presented (Figure 3, 4).

a.) plain concrete beam, where triangular finite elements were used,

b.) SFRC beam, where triangular elements were used for the concrete and one-dimensional finite elements were used for the steel fibers. The fiber orientation angle was considered $\alpha = 0^0$.

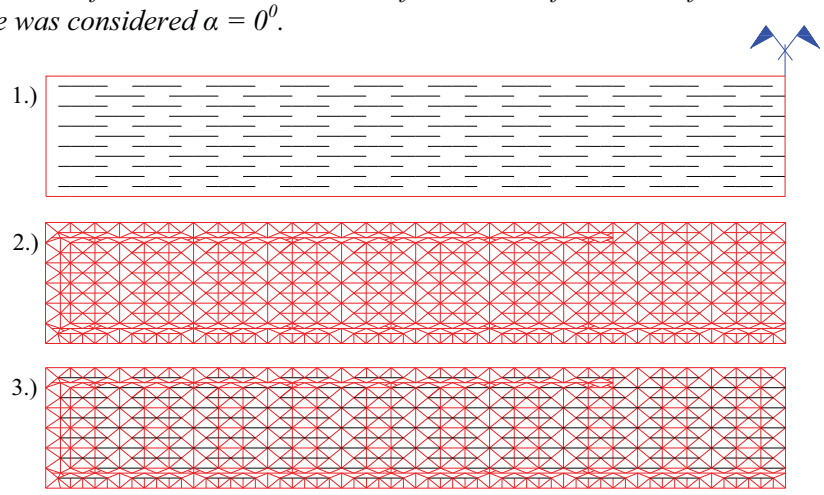

Figure 3 – Meshing

3.1 – fiber orientation angle $\alpha = 0^0$, 3.2 – plain concrete beam, 3.3 – SFRC beam

2.2.2. Definition of the physical and mechanical characteristics of the materials and of the plain stress analysis manner in the nonlinear domain

The studied model has the cross-sectional area A = 108cm^2 (12x9cm) and the length 150cm, being simply supported. The distance between the supports is 120cm. It is acted by two concentrated forces, 40cm apart from each other and from the supports, so that on the middle third the bending moment is constant (Figure 4). The concrete class is C20/25, with Young modulus E = 3000N/mm^2.

The disperse fibers (the fiber orientation angle being considered $\alpha=0^0$), have the diameter Φ =1,05mm, the cross-sectional area A$\approx$1mm^2, Young modulus E = 210000N/mm^2, tensile strength R_{ti} = 200N/mm^2, and length $l_f = 50mm$.

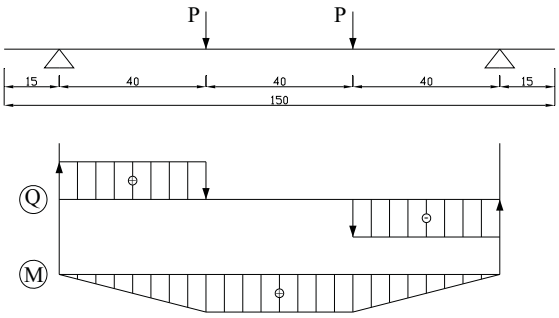

Figure 4 – Free body diagram of the beam

2.2.3. Analysis and interpretation of the results.

After applying the loading steps, there were obtained the load-displacements curves presented in Figures 5.1 and 5.2, and the stress maps corresponding to the loading steps (Figures 6 and 7).

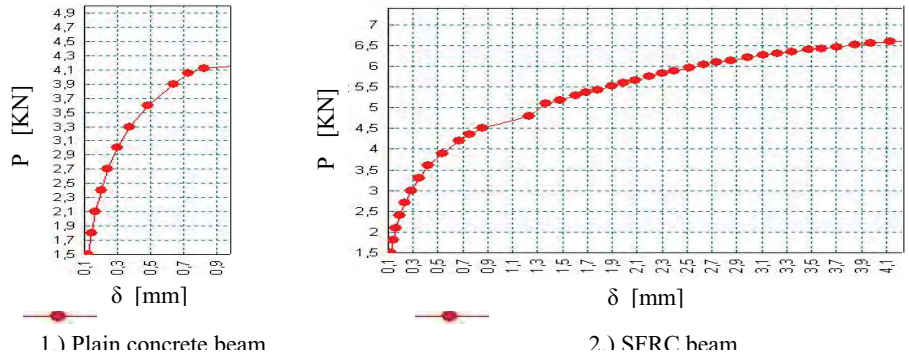

1.) Plain concrete beam 2.) SFRC beam

Figure 5 – Load-displacement curve (P-δ) for:
5.1. – the plain concrete beam, 5.2. – the SFRC beam

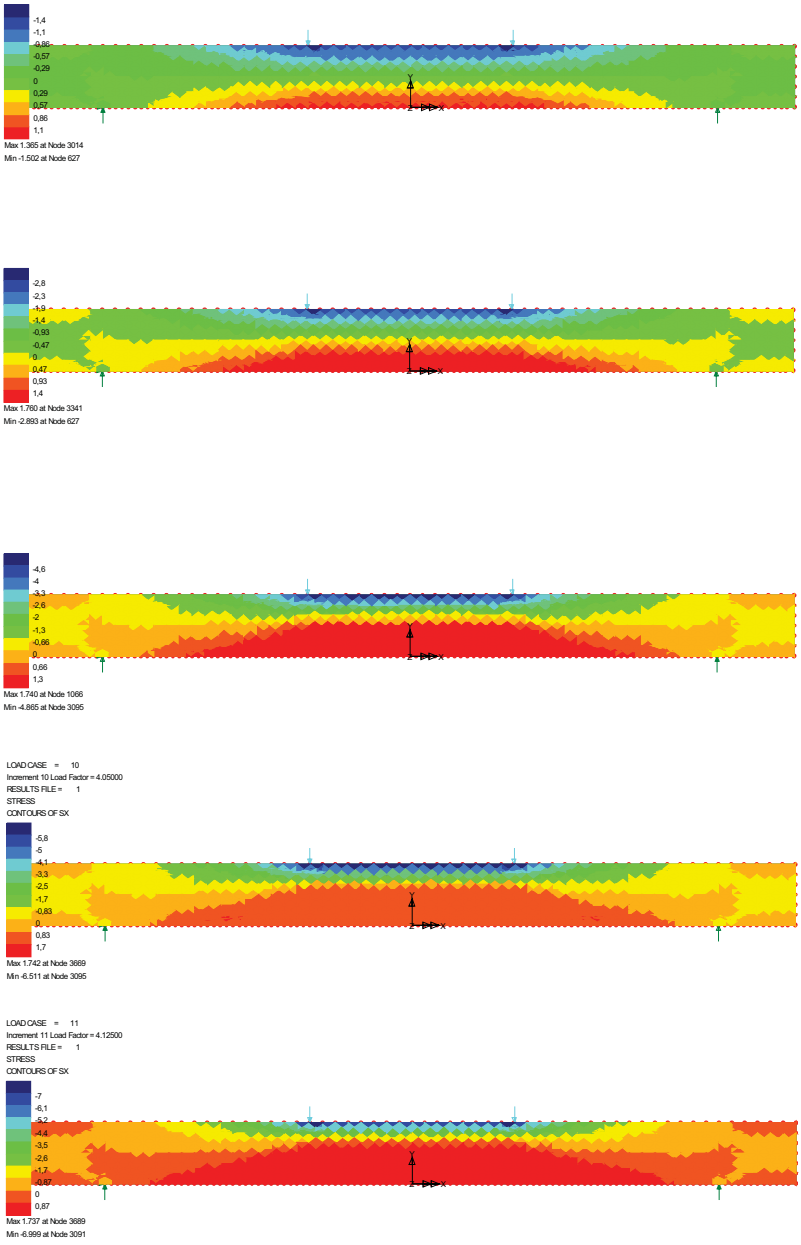

Figure 7 – Stresses maps for the plain concrete beam.

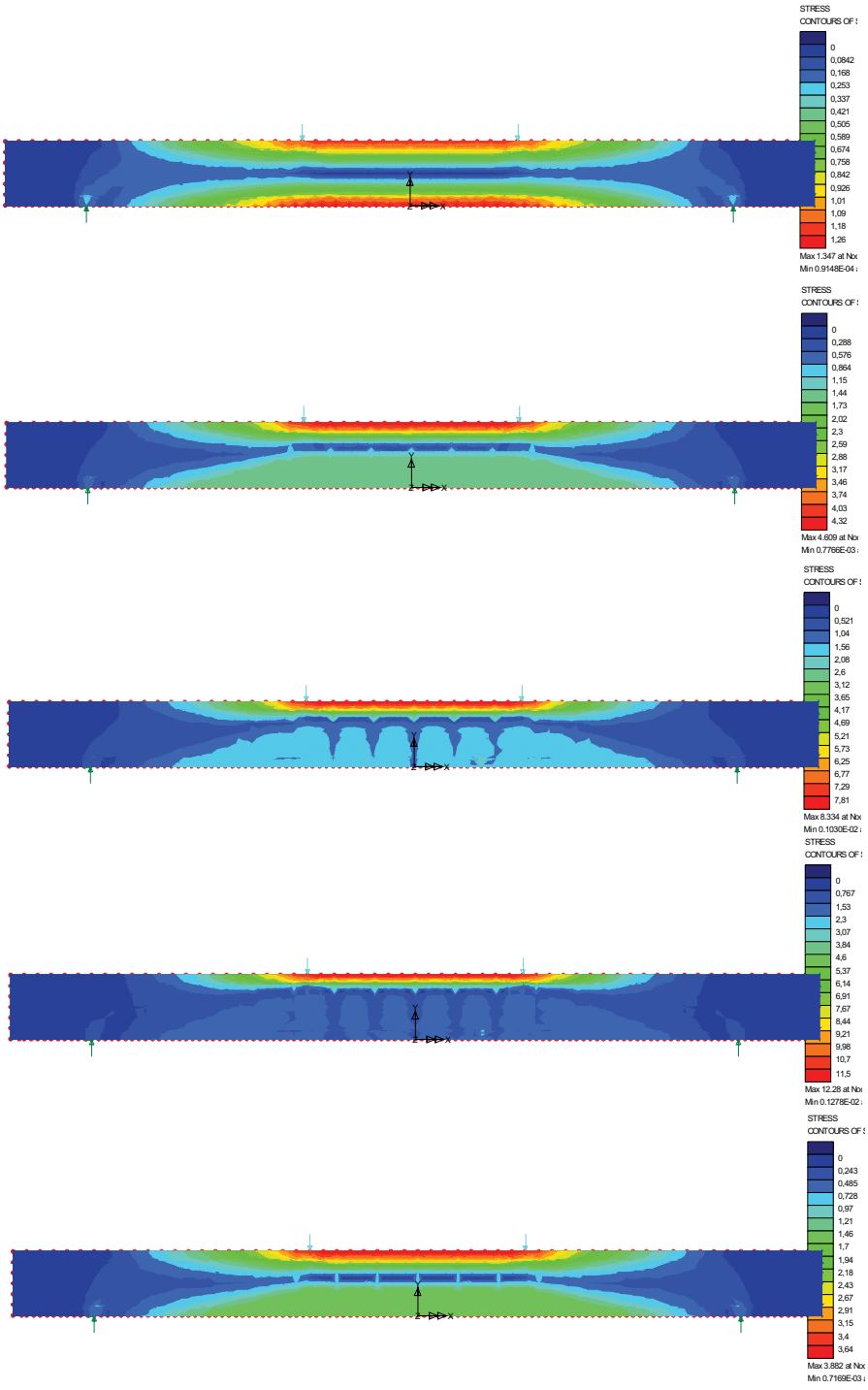

Figure 8 – Stresses maps for the SFRC beam

There are presented the load values for each loading steps and the corresponding displacements, for the plain concrete beam (Table 1) and for the SFRC beam, respectively (Table 2). The displacement decrease, for each loading step, for the SFRC beam compared to the plain concrete one, is presented in Table 1, column 3. Notes and comments on the behavior of the SFRC beam under loading are presented in Table 3.

Table 1

Loading step	Load magnitude [KN]	Displacement [mm]	Displacements decrease for the SFRC beam, compared to the plain concrete beam [mm]	Comments
0	1	2	3	4
1	1,5	0,119	0,002	
2	1,8	0,143	0,003	
3	2,1	0,169	0,004	
4	2,4	0,2	0,005	
5	2,7	0,241	0,008	
6	3	0,296	0,014	
7	3,3	0,369	0,024	
8	3,6	0,483	0,062	
9	3,9	0,639	0,105	
10	4,05	0,729	0,056	
11	4,125	0,825	0,074	Beam failure

Table 2

Loading step	Load magnitude [KN]	Displacement [mm]	Comments
0	1	2	3
1	1,5	0,117	
2	1,8	0,14	
3	2,1	0,165	
4	2,4	0,195	
5	2,7	0,233	
6	3	0,282	
7	3,3	0,345	
8	3,6	0,42	
9	3,9	0,534	
10	4,2	0,673	
11	**4,35**	**0,751**	The first fissure occurs
12	**4,5**	**0,86**	The fissure opens
13	**4,8**	**1,231**	In-between steps 12 and 13, the fibers take over the tensile stresses
14	**5,1**	1,371	In-between steps 14 and 38, the concrete and the fibers work together to take over the tensile stresses
15	5,175	**1,48**	
16	5,3	1,6	
38	6,598	4,127	

Table 3

	Bearing capacity increase for the SFRC beam, compared to the plain concrete beam	Displacements of the SFRC beam, compared to the plain concrete beam
Bearing capacity increase until the first fissure occurs	5,45% (4,35 compared to 4,125)	The displacement of the SFRC beam is 9.1% lower (0,751 compared to 0,825)
Bearing capacity increase until concrete failure	16,36% (4,8 compared to 4,125)	The displacement of the SFRC beam is 67,02% higher (1,231 compared to 0,825)
Bearing capacity increase until fibers yielding	23,64% (5,1 compared to 4,125)	The displacement of the SFRC beam is 166,18% higher (1,371 compared to 0,825)
Bearing capacity increase until fibers failure	62,25% (6,598 compared to 4,125)	The displacement of the SFRC beam is 500,24% higher (4,127 compared to 0,825)

3. CONCLUSIONS

Compared to the plain concrete, the SFRC behavior, on elastic and elasto-plastic domains, is characterized by:

1. elastic domain – an increase of the bearing capacity:

- until the first fissure, of 5.45%, and the displacement is 9.1% lower;
- until the concrete failure, of 16.36%, and the deformation is 67.02 higher, leading to the increase of the area under the force-displacement curve.

2. plastic domain - an increase of the bearing capacity:

- until the fibers yielding, of 23.64%, and the displacement is 166.18% higher;
- until the fibers strain hardening and failure, of 23.64%, and the deformation is 500.24 higher.

References

1. Chiaia, B., Fantilli, A.P., Valini, P., Kalamaras, G. – Fiber reinforced concrete for massive structures the case of craviale tunnel, FIB, Italy, Napoli, 2006.

2. Falkner, H. and Henke, V. Steel fibre reinforced concrete, from research to standards. Concrete Structures – Annual Technical Journal of the Hungarian Group of fib, 2005; 6: 39-46. Proceedings of the 2nd Congress Session 2 June 5-8, 2006 – Naples, Italy Design and construction

3. Rilem TC 162-TDF, $\sigma - \varepsilon$ design method – final recommendation. Materials and structures, 36, 560-567, 2003,

4. Barla, G., Barpi, F., Bertolino, C. and Chiaia, B. A note on the design of fibre-reinforced shotcrete linings for underground support. Computational Modeling of Concrete Structures EURO-C 2003, Eds. Bicanic, N., de Borst, R., Mang, H. and Meschke, G., A.A. Balkema Publishers, Lisse, 2003: 627-634.

5. Balaguru, P.N. and Shah, S.P. Fiber - Reinforced Cement Composites. McGraw-Hill Inc, New York, 1992.

6. Cuteanu, E., Marinov, R., - Metoda elementelor finite în proiectarea structurilor, Ed. Facla, Timişoara, 1980.

"Computational Civil Engineering 2007", International Symposium

Iaşi, România, May 25, 2007

A new look into finite element templates.

Wojciech Gilewski[1]

[1]*Institute of Structural Mechanics, Warsaw University of Technology, Warsaw, Poland*

Summary

The present paper is dedicated to evaluation and new method of construction the finite element templates. A template is an algebraic form of element matrices, which contains free parameters. Setting the parameters to specific values produces element instances. Two templates are analyzed: Bernoulli and Timoshenko beam. The number of free parameters is discussed by a general method.

KEYWORDS: finite element template, consistency, ellipticity

1. INTRODUCTION

Beams, plates and shells are widely considered in engineering applications. However the corresponding discretization procedures are not yet sufficiently reliable. It is difficult to obtain an element that is optimal. In a formulation we should aim to satisfy: ellipticity, consistency and the inf-sup condition.

Ellipticity ensures that the finite element model is solvable and physically means there are no spurious zero energy modes. This condition can easily be verified by studying the zero eigenvalues and corresponding eigenvectors of the stiffness matrix of a single unsupported finite element. *Consistency* is related to the convergence. The finite element solution must converge to the solution of a mathematical problem the element size h is close to zero. The bilinear forms used in the finite element discretization must approach the exact bilinear forms of the mathematical model as h approaches zero. The *inf-sup* condition ensures optimal convergence in bending-dominated problems and is not a subject of this paper.

One of the interesting concepts are finite element templates proposed by Felippa [1,2]. The objective of this paper is to evaluate finite element templates, proposed by Felippa, with the use of the energy-difference criterion (to check if the template is consistent) and the spectral analysis (to check if the template is elliptical). Two beam templates are discussed: for Bernoulli theory and for Timoshenko theory. A new, general method for development of finite element templates is proposed.

2. TEMPLATES

A finite element template is an algebraic form for element matrices, which contains free parameters (Felippa [1,2]). Setting those parameters to specific values produces element instances. The set of free parameters is called the template *signature.* Borrowing the terminology from biogenetics, the signature may be viewed as an "element DNA" that uniquely characterizes it as an individual entity. Elements derived by different techniques thet share the same signature are called *clones.* The template should fulfill the following conditions:

- consistency (the individual element test is passed),
- stability (correct rank and nonnegativity conditions),
- parametrization (free parameters)
- invariance (the element is observer invariant).

The element stiffness matrix derived through the template approach is based on the fundamental decomposition

$$\mathbf{K} = \mathbf{K}_b(\alpha_i) + \mathbf{K}_h(\beta_j),$$

where $\mathbf{K}_b$ and $\mathbf{K}_h$ are the basis and higher-order stiffness matrices respectively.

α_i, β_j are free parameters. These two matrices play different and complementary roles. The basic stiffness $\mathbf{K}_b$ takes care of consistency and element-type-mixing. The higher order stiffness $\mathbf{K}_h$ is a stabilization term that provides the correct rank and may be adjusted for accuracy.

3. BERNOULLI BEAM TEMPLATE

Let us consider a finite element template for Bernoulli beam [1] of two-noded element of the length L with natural d.o.f. $\mathbf{q}_e = \{w_i, \phi_i, w_k, \phi_k\}$.

$$\mathbf{K}^{\substack{Template\\Bernoulli}} = \mathbf{K_b} + \mathbf{K_h} = \frac{EJ}{L}\begin{bmatrix} 0 & 0 & 0 & 0 \\ 0 & 1 & 0 & -1 \\ 0 & 0 & 0 & 0 \\ 0 & -1 & 0 & 1 \end{bmatrix} + \beta\frac{EJ}{L^3}\begin{bmatrix} 4 & 2L & -4 & 2L \\ 2L & L^2 & -2L & L^2 \\ -4 & -2L & 4 & -2L \\ 2L & L^2 & -2L & L^2 \end{bmatrix}$$

For $\beta = 3$ the well known beam element with Herimite's polynomial shape functions. The template depends on one free parameter β. The energy-difference procedure (described in details in [3,5], and used for evaluation of beam and plate finite elements in [4,5]) can be used to check if the template satisfies the consistency condition.

The strain energy density of a beam is expected to be:

$$2\widetilde{E}_s = EJ\left(\frac{d^2w}{dx^2}\right)^2.$$

The equivalent density of element strain energy is a quadratic form

$$2\widetilde{E}_s^{ES-Template} = \frac{1}{L}\mathbf{q}_e^T \mathbf{K}_{Bernoulli}^{Template}\mathbf{q}_e.$$

The nodal displacements can be expressed by average displacements and its derivatives in the midpoint of the element with the use of Taylor series expansion

$$w_i = w(x) - \frac{\Delta w}{\Delta x}(x)\frac{L}{2} + \frac{1}{2}\frac{\Delta^2 w}{(\Delta x)^2}(x)\left(\frac{L}{2}\right)^2 - \frac{1}{6}\frac{\Delta^3 w}{(\Delta x)^3}(x)\left(\frac{L}{2}\right)^3 + ...,$$

$$w_k = w(x) + \frac{\Delta w}{\Delta x}(x)\frac{L}{2} + \frac{1}{2}\frac{\Delta^2 w}{(\Delta x)^2}(x)\left(\frac{L}{2}\right)^2 + \frac{1}{6}\frac{\Delta^3 w}{(\Delta x)^3}(x)\left(\frac{L}{2}\right)^3 + ...,$$

$$\phi_i = \frac{\Delta w}{\Delta x}(x) - \frac{\Delta^2 w}{(\Delta x)^2}(x)\frac{L}{2} + \frac{1}{2}\frac{\Delta^3 w}{(\Delta x)^3}(x)\left(\frac{L}{2}\right)^2 - \frac{1}{6}\frac{\Delta^4 w}{(\Delta x)^4}(x)\left(\frac{L}{2}\right)^4 + ...,$$

$$\phi_k = \frac{\Delta w}{\Delta x}(x) - \frac{\Delta^2 w}{(\Delta x)^2}(x)\frac{L}{2} + \frac{1}{2}\frac{\Delta^3 w}{(\Delta x)^3}(x)\left(\frac{L}{2}\right)^2 - \frac{1}{6}\frac{\Delta^4 w}{(\Delta x)^4}(x)\left(\frac{L}{2}\right)^4 + ...$$

After collecting the expressions with respect to L we have

$$2\widetilde{E}_s^{ES-Template} = EJ\left(\frac{\Delta^2 w}{\Delta x^2}\right)^2 + L^2 EJ\left[\frac{\beta}{36}\left(\frac{\Delta^3 w}{(\Delta x)^3}\right)^2 + \frac{1}{12}\frac{\Delta^2 w}{\Delta x^2}\frac{\Delta^4 w}{\Delta x^4}\right] + 0(L^4).$$

In the limit case $L \to 0$ the following relation is valid

$$\lim_{L\to 0}\widetilde{E}_s^{ES-Template} = \widetilde{E}_s.$$

This is a proof that the element template satisfies the consistency requirement for any β. The basis stiffness matrix $\mathbf{K}_b$ is responsible for the first term of the strain energy. Formally the β parameter is free from zero to infinity.

The element template should also elliptical. To check this condition it is necessary to calculate the eigenvalues and eigenvectors of the template. Two zero eigenvalues related to rigid body motions are expected. The two other eigenvalues are to be positive and related to the deformed element. The results are the following

$$\lambda_1 = 0,\ \ \lambda_2 = 0,\ \ \lambda_3 = 2\frac{EJ}{L},\ \ \lambda_4 = 10\beta\frac{EJ}{L},$$

$$\mathbf{w}_1 = \{-L,\ 1,\ 0,\ 1\ \},$$
$$\mathbf{w}_2 = \{\ 1,\ 0,\ 1,\ 0\ \},$$
$$\mathbf{w}_3 = \{\ 0,\ -1,\ 0,\ 1\ \},$$
$$\mathbf{w}_1 = \{\ 2L,\ 1,\ -2L,\ 1\ \}.$$

It is seen that the element is elliptical if $\beta > 0$. If $\beta \to 0$ the fourth eigenvalue tends to be zero with the eigenvector that describes deformed element.

Since the development of the element template is rather complicated, a couple of questions arises after reading the texts of Felippa [1,2]:

How many free parameters exist in the template ?

Are the free parameters exist in both matrices (basis and higher order) ? etc.

Let us examine some more general matrices to answer the questions.

$$\mathbf{K}^{\substack{Extended\\Bernoulli}} = \frac{EJ}{L}\begin{bmatrix} 0 & 0 & 0 & 0 \\ 0 & a_{22} & 0 & -a_{24} \\ 0 & 0 & 0 & 0 \\ 0 & -a_{24} & 0 & a_{44} \end{bmatrix} + \frac{EJ}{L^3}\begin{bmatrix} 4b_{11} & 2Lb_{12} & -4b_{13} & 2Lb_{14} \\ 2Lb_{12} & L^2b_{22} & -2Lb_{23} & L^2b_{24} \\ -4b_{13} & -2Lb_{23} & 4b_{33} & -2Lb_{34} \\ 2Lb_{14} & L^2b_{24} & -2Lb_{34} & L^2b_{144} \end{bmatrix}$$

The basis matrix is responsible for the first term of the strain energy, so it depends only on rotations. There are 3 formally independent parameters in this matrix. The second matrix formally depends on 10 parameters. Following the procedure described above one can receive the following strain energy density of the element:

$$
\begin{aligned}
2\widetilde{E}_s^{ES-Extended} &= \frac{4}{L^4} EJ\left(b_{11} - 2b_{13} + b_{33}\right)w^2 + \\
&+ \frac{4}{L^3} EJ\left(-b_{11} + b_{12} + b_{14} - b_{23} + b_{33} - b_{34}\right)w\frac{\Delta w}{\Delta x} + \\
&+ \frac{1}{L^2} EJ\left(b_{11} - 2b_{12} + 2b_{13} - 2b_{14} + b_{22} - 2b_{23} + 2b_{24} + b_{33} - 2b_{34} + b_{44}\right)\left(\frac{\Delta w}{\Delta x}\right)^2 + \\
&+ \frac{1}{L^2} EJ\left(b_{11} - 2b_{12} - 2b_{13} + 2b_{14} + 2b_{23} + b_{33} - 2b_{34}\right)w\frac{\Delta^2 w}{\Delta x^2} + \\
&+ \frac{1}{L^2} EJ\left(a_{22} - 2a_{24} + a_{44}\right)\left(\frac{\Delta w}{\Delta x}\right)^2 + \\
&+ \frac{1}{2L} EJ\left(-b_{11} + 3b_{12} - b_{14} - 2b_{22} + b_{23} + b_{33} - 3b_{34} + 2b_{44}\right)\frac{\Delta w}{\Delta x}\frac{\Delta^2 w}{\Delta x^2} + \\
&+ \frac{1}{2L} EJ\left(-b_{11} + 3b_{12} + 3b_{14} - 3b_{23} + b_{33} - 3b_{34}\right)w\frac{\Delta^3 w}{\Delta x^3} + \\
&+ \frac{1}{L} EJ\left(-a_{22} + a_{44}\right)\frac{\Delta w}{\Delta x}\frac{\Delta^2 w}{\Delta x^2} + \\
&+ \frac{EJ}{12}\left(b_{11} - 4b_{12} + 2b_{13} - 4b_{14} + 3b_{22} - 4b_{23} + 6b_{24} + b_{33} - 4b_{34} + 3b_{44}\right)\frac{\Delta w}{\Delta x}\frac{\Delta^3 w}{\Delta x^3} + \\
&+ \frac{EJ}{12}\left(-b_{12} + b_{23} + b_{14} - b_{34}\right)w\frac{\Delta^4 w}{\Delta x^4} + \\
&+ \frac{EJ}{16}\left(b_{11} - 4b_{12} - 2b_{13} + 4b_{14} + 4b_{22} + 4b_{23} - 8b_{24} + b_{33} - 4b_{34} + 4b_{44}\right)\left(\frac{\Delta^2 w}{\Delta x^2}\right)^2 + \\
&+ 0(L)
\end{aligned}
$$

To fulfill the consistency condition the following equations are to be satisfied:

$$
\begin{bmatrix} 1 & -2 & 1 \\ -1 & 0 & 1 \\ 1 & 2 & 1 \end{bmatrix}\begin{bmatrix} a_{22} \\ a_{24} \\ a_{44} \end{bmatrix} = \begin{bmatrix} 0 \\ 0 \\ 4 \end{bmatrix}.
$$

$$\begin{bmatrix} 1 & 0 & 0 & -2 & 0 & 1 & 0 & 0 & 0 \\ -1 & 1 & 0 & 0 & -1 & 1 & 1 & 2 & -1 \\ 1 & -2 & 1 & 2 & -2 & 1 & -2 & 0 & -2 \\ 1 & -2 & 0 & -2 & 2 & 1 & 2 & 0 & -2 \\ -1 & 3 & -2 & 0 & 1 & 1 & -1 & 0 & -3 \\ -1 & 3 & 0 & 0 & -3 & 1 & 3 & 0 & -3 \\ 1 & -4 & 3 & 2 & -4 & 1 & -4 & 6 & -4 \\ 0 & -1 & 0 & 0 & 1 & 0 & 1 & 0 & -1 \\ 1 & -4 & 4 & -2 & 4 & 1 & 4 & -8 & -4 \end{bmatrix} \begin{bmatrix} b_{11} \\ b_{12} \\ b_{22} \\ b_{13} \\ b_{23} \\ b_{33} \\ b_{14} \\ b_{24} \\ b_{34} \end{bmatrix} = \begin{bmatrix} 0 \\ 0 \\ -1 \\ 0 \\ -2 \\ 0 \\ -3 \\ 0 \\ -4 \end{bmatrix} b_{44}$$

There are 3 equations for 3 parameters "*a*". We have

$$a_{22} = a_{24} = a_{44} = 1.$$

It is seen that the basis matrix of Bernoulli beam template is independent on the free parameters.

There are 9 equations for 10 parameters "*b*". Thus

$$b_{44} = \beta,\ b_{11} = b_{12} = b_{22} = b_{13} = b_{23} = b_{33} = b_{14} = b_{24} = b_{34} = b_{44} = \beta.$$

3. TIMOSHENKO BEAM TEMPLATE

Let us consider a two-noded element of the length L with natural d.o.f. $\mathbf{q}_e = \{w_i, \phi_i, w_k, \phi_k\}$. Timoshenko beam template proposed by Felippa [2] is more complex than for Bernoulli beam and depends on 3 parameters:

$$\mathbf{K}^{\substack{Template \\ Bernoulli}} = \mathbf{K}_{\mathbf{b}} + \mathbf{K}_{\mathbf{h}} =$$

$$= \frac{\alpha EJ}{L} \begin{bmatrix} 0 & 0 & 0 & 0 \\ 0 & 1 & 0 & -1 \\ 0 & 0 & 0 & 0 \\ 0 & -1 & 0 & 1 \end{bmatrix} + 3\beta \frac{EJ}{L^3} \begin{bmatrix} 4 & 2L & -4 & 2L \\ 2L & \psi L^2 & -2L & \psi L^2 \\ -4 & -2L & 4 & -2L \\ 2L & \psi L^2 & -2L & \psi L^2 \end{bmatrix}.$$

Following a similar procedure like for the Bernoulli beam we have:

- Density of strain energy

$$2\widetilde{E}_s = EJ\left(\frac{d\phi}{dx}\right)^2 + H\left(\phi - \frac{dw}{dx}\right)^2$$

- Nodal parameters

$$w_i = w(x) - \frac{\Delta w}{\Delta x}(x)\frac{L}{2} + \frac{1}{2}\frac{\Delta^2 w}{(\Delta x)^2}(x)\left(\frac{L}{2}\right)^2 - \frac{1}{6}\frac{\Delta^3 w}{(\Delta x)^3}(x)\left(\frac{L}{2}\right)^3 + ...,$$

$$w_k = w(x) + \frac{\Delta w}{\Delta x}(x)\frac{L}{2} + \frac{1}{2}\frac{\Delta^2 w}{(\Delta x)^2}(x)\left(\frac{L}{2}\right)^2 + \frac{1}{6}\frac{\Delta^3 w}{(\Delta x)^3}(x)\left(\frac{L}{2}\right)^3 + ...,$$

$$\phi_i = \phi(x) - \frac{\Delta \phi}{\Delta x}(x)\frac{L}{2} + \frac{1}{2}\frac{\Delta^2 \phi}{(\Delta x)^2}(x)\left(\frac{L}{2}\right)^2 - \frac{1}{6}\frac{\Delta^3 \phi}{(\Delta x)^3}(x)\left(\frac{L}{2}\right)^4 + ...,$$

$$\phi_k = \phi(x) + \frac{\Delta \phi}{\Delta x}(x)\frac{L}{2} + \frac{1}{2}\frac{\Delta^2 \phi}{(\Delta x)^2}(x)\left(\frac{L}{2}\right)^2 + \frac{1}{6}\frac{\Delta^3 \phi}{(\Delta x)^3}(x)\left(\frac{L}{2}\right)^4 + ...$$

- Density of the template strain energy

$$2\widetilde{E}_s^{Template} = \alpha EJ\left(\frac{\Delta\phi}{\Delta x}\right)^2 + \frac{12\beta EJ}{L^2}\left(\phi - \frac{\Delta w}{\Delta x}\right)^2 +$$
$$+ \beta EJ 3\frac{\Delta^2\phi}{\Delta x^2}\left(\psi\phi - \frac{\Delta w}{\Delta x}\right) - \beta EJ 3\frac{\Delta^3 w}{\Delta x_3}\left(\phi - \frac{\Delta w}{\Delta x}\right) + 0(L^2)$$

To fulfill the condition of consistency it is necessary to take $\alpha = 1$ and β in the following form

$$\beta = \frac{HL^2}{12EJ}(1 + ...)$$

with any ψ.

Let us propose more general form of the stiffness decomposition:

$$\mathbf{K}^{\substack{Extended\\Bernoulli}} = \frac{EJ}{L}\begin{bmatrix} 0 & 0 & 0 & 0 \\ 0 & a_{22} & 0 & -a_{24} \\ 0 & 0 & 0 & 0 \\ 0 & -a_{24} & 0 & a_{44} \end{bmatrix} + \frac{H}{L}\begin{bmatrix} 4b_{11} & 2Lb_{12} & -4b_{13} & 2Lb_{14} \\ 2Lb_{12} & L^2 b_{22} & -2Lb_{23} & L^2 b_{24} \\ -4b_{13} & -2Lb_{23} & 4b_{33} & -2Lb_{34} \\ 2Lb_{14} & L^2 b_{24} & -2Lb_{34} & L^2 b_{144} \end{bmatrix}$$

- Density of the extended template strain energy

$$\begin{aligned} 2\widetilde{E}_s^{Extended} &= EJ\left(a_{22} - 2a_{24} + a_{44}\right)\frac{\phi^2}{L^2} + EJ\left(-a_{22} + a_{44}\right)\frac{\phi}{L}\frac{\Delta\phi}{\Delta x} + \\ &+ \frac{EJ}{4}\left(a_{22} + 2a_{24} + a_{44}\right)\left(\frac{\Delta\phi}{\Delta x}\right)^2 + H\left(b_{11} - 6b_{13} + 3b_{33}\right)\frac{w^2}{L^2} + \\ &+ H\left(3b_{12} - 3b_{23} + 3b_{14} - 3b_{34}\right)\frac{\phi w}{L} + H\left(-b_{11} + 3b_{33}\right)\frac{w}{L}\frac{\Delta w}{\Delta x} + \\ &+ \frac{H}{4}\left(3b_{22} + 6b_{24} + 3b_{44}\right)\phi^2 + H\left(-3b_{12} + 3b_{23} + 3b_{14} - 3b_{34}\right)w\frac{\Delta\phi}{\Delta x} + \\ &+ \frac{H}{2}\left(-3b_{12} - 3b_{23} - 3b_{14} - 3b_{34}\right)\phi\frac{\Delta w}{\Delta x} + \frac{H}{4}\left(b_{11} + 6b_{13} + 3b_{33}\right) + 0(L) \end{aligned}$$

To fulfill the consistency requirement 3 equations for 3 coefficients “a” and 7 equations for 10 coefficients “b” are to be satisfied:

$$\begin{bmatrix} 1 & -2 & 1 \\ -1 & 0 & 1 \\ 1 & 2 & 1 \end{bmatrix}\begin{bmatrix} a_{22} \\ a_{24} \\ a_{44} \end{bmatrix} = \begin{bmatrix} 0 \\ 0 \\ 4 \end{bmatrix}$$

This matrix equation is equivalent to the conditions received for the Bernoulli beam template in the previous chapter.

$$\begin{bmatrix} 1 & 0 & 0 & -6 & 0 & 3 & 0 \\ 0 & 3 & 0 & 0 & -3 & 0 & 3 \\ -1 & 0 & 0 & 0 & 0 & 3 & 0 \\ 0 & 0 & 3 & 0 & 0 & 0 & 0 \\ 0 & -3 & 0 & 0 & 3 & 0 & 3 \\ 0 & -3 & 0 & 0 & -3 & 0 & -3 \\ 1 & 0 & 0 & 6 & 0 & 3 & 0 \end{bmatrix} \begin{bmatrix} b_{11} \\ b_{12} \\ b_{22} \\ b_{13} \\ b_{23} \\ b_{33} \\ b_{34} \end{bmatrix} = \begin{bmatrix} 0 & 0 & 0 \\ 0 & 3 & 0 \\ 0 & 0 & 0 \\ -6 & 0 & -3 \\ 0 & 3 & 0 \\ 0 & 3 & 0 \\ 0 & 0 & 0 \end{bmatrix} \begin{bmatrix} b_{24} \\ b_{34} \\ b_{44} \end{bmatrix} + \begin{bmatrix} 0 \\ 0 \\ 0 \\ 4 \\ 0 \\ 2 \\ 4 \end{bmatrix}$$

One can receive $a_{22} = a_{24} = a_{44} = 1$.

There are 3 independent constants in the group "b". If we put $b_{24} = C_1$, $b_{34} = C_2$, $b_{44} = C_3$ the other coefficients are the following:

$$b_{11} = 1, \quad b_{12} = -\frac{1}{3}(1 + C_2), \quad b_{22} = \frac{1}{3}(4 - 6C_1 - 3C_3),$$
$$b_{13} = \frac{1}{3}, \quad b_{23} = -\frac{1}{3}(1 + C_2), \quad b_{33} = \frac{1}{3}, \quad b_{34} = C_2.$$

The derivation above is a proof that there are 3 independent coefficients in the Timoshenko beam template.

4. CONCLUSIONS

The finite element templates, proposed by Felippa [1,2], are algebraic forms that contains some free parameters. The finite element templates for Bernoulli beam and Timoshenko beam are examined in the paper, from the point of view of the consistency condition. A new way of template construction is proposed. It is confirmed that there is 1 free parameter for Bernoulli beam template and 3 free parameters for Timoshenko beam template. The new method of creation the template can be extended for 2D and 3D problems.

References

1. Felippa C.A., A template tutorial I: panels, families, clones, winners and losers. Report No. CU-CAS-03-03, University of Colorado, 2003
2. Felippa C.A., The amusing history of shear flexible beam elements. Report No. CU-CAS-05-01, University of Colorado, 2005
3. Gilewski W., Correctness of plate bending finite element with physical shape functions, *Finite Element News*, 3, 1993, pp.29-34
4. Gilewski W., Evaluation of finite elements. *16th Int.Conf. on Computer Methods in Mechanics CMM-2005,* Garstecki A., Mochancki B., Szczygiol N. Eds., Częstochowa 2005
5. Gilewski W., *On the Criteria for Evaluation of Finite Elements – From Timoshenko Beam to Hencky-Bolle Plate* (in Polish), OW Politechniki Warszawskiej, Warsaw 2005

"Computational Civil Engineering 2007", International Symposium
Iaşi, România, May 25, 2007

Evaluation of the inelastic demand of structures subjected to multiple ground motions

Mihail Iancovici[1,2], Georgiana Ionică[1]
[1]*Department of Mechanics, Statics and Dynamics of Structures, Technical University of Civil Engineering (UTCB), Bucharest, 020396, Romania*
[2] *National Center for Seismic Risk Reduction (NCSRR), Bucharest, 021652, Romania*

Summary

In the current seismic design format, the key issue in establishing realistic seismic loads is the behavior factor. It accounts for all the dissipative mechanisms that a structural system may develop under a strong ground motion, however not clearly enough stated yet. It corresponds to the performance level associated to the ultimate limit state (i.e. life safety), related to a 100 years mean return interval of earthquake ground motion with a prescribed peak acceleration of ground.

The paper investigates the effect of repeated Vrancea strong ground motions on the behavior factors and the related parameters that accounts for cyclic structural deterioration due to inelastic response. A large number of integrated analyses, nonlinear response analyses and energy balance-based analyses were carried out and estimates were made on the behavior factors for inelastic SDOF systems controlled by flexure with stiffness degradation. The correlation between behavior factors and damage level are investigated, using the Bozorgnia and Bertero (2001), improved damage index. It is shown that multiple ground motion of Vrancea type for Bucharest, may lead to an important increase of force and drift demand of structures that usually is not taken into account.

KEYWORDS: multiple earthquake ground motions, behavior factor, hysteretic energy, damage index, artificial accelerogram

1. INTRODUCTION

Romanian territory and neighboring countries are repeatedly exposed to medium to high intensity earthquake ground motions generated from the same source, located in Vrancea region. Bucharest is one of the most exposed cities to damage to buildings and human losses as well. It is therefore obviously needed to explore the effects of repeated Vrancea strong ground motion and the related implications that may improve the seismic design of new buildings and the evaluation procedures of the existing ones. In the current Romanian seismic design format, based on strength principles, the key issue in establishing realistic seismic loads that account for the actual inelastic response, is the force reduction factor/behavior factor, namely q. Basically it accounts for all the dissipative mechanisms that a structural system may develop under a strong ground motion, however not clearly enough stated yet. It is recognized however that the complexity of inelastic behavior phenomena cannot be reproduced through a single parameter that is intended to fully describe the actual structural response. q factor is primarily related to the structural inelastic response (ductility and cumulative effects of repeated cycles of inelastic deformations) and contains some of the ground motions properties.

In most of the seismic design codes and Romanian as well, q factor primarily addresses to the selected structural type and includes the effect of inelastic behavior and the over-strength effect. It does not directly account for the influence of strong motion duration nor for the hysteretic behavior of the structural elements. It corresponds to the ultimate limit state performance level (i.e. life safety), related to a 100 years mean return interval of a prescribed peak ground acceleration (PGA).

For repeated earthquake ground motions however, there is no clear evidence on how this important factor might be interpreted and used in analyses.

The purpose of the paper is to study the effect of repeated strong ground motions of Vrancea type, on the behavior factors of buildings located in Bucharest; we study the variability of q factor and related parameters on structural vibration period and ductility, and on ground motion parameters as well.

2. BEHAVIOR FACTORS FOR SINGLE INPUT GROUND MOTIONS; CYCLING LOADING EFFECT

Currently it is usual to estimate the actual force demand by dividing the base shear force that corresponds to a fully elastic response by the behavior factor.

Early studies revealed the fact that the equal displacement assumption and the equal energy assumption provide a fairly good estimation of the force reduction factors at long and short periods, respectively. These developments accounts for

ductility properties only. A study by Newmark and Hall (1973) using 10 ground motions records of 1940 El Centro earthquake, proposed reduction factors that include the effect of both, ground motion and structural properties. Nassar and Krawinkler (1991), Miranda and Bertero (1994), Watanabe and Kawashima (2002) have been conducted studies on the force reduction factors that give fairly good estimates on q factors especially for routine buildings. Ordan *et al.*, 1998 and Arroyo *et al.*, 2003 found that the value of q strongly depends on ductility and natural vibration period, and is significantly influenced by the soil type.

Inelastic behavior depends on many parameters, associated to the excitation and the structural system. In order to uniformly grasp the effect of multiple earthquake ground motions, and for the sake of clarity we used spectral representations of SDOF systems response, having 5% damping ratio, and bilinear restoring force characteristics, with stiffness degradation and 10% post-yielding stiffness ratio; all systems have equal displacement ductility. For flexible structures however, SDOF models are expected to reproduce with some degree of inaccuracy the actual response. For routine buildings we expect however realistic estimates.

By definition, the behavior factor is given by

$$q = \frac{F_{el}(\xi_{el}, T)}{F_y(\mu, \xi_{nl}, T)} \tag{1}$$

where F_{el} and F_y are the maximum linear and nonlinear base shear force respectively, μ is the displacement ductility factor, ξ_{el} and ξ_{nl} are the damping ratios in the linear and nonlinear behavior range respectively, and T is the vibration period of the model. By simplicity, usually ξ_{nl} is taken same as ξ_{el}.

We first compared the formulations of Newmark and Hall (1973) and Miranda and Bertero (1994), with q factors obtained from analysis for low and high displacement ductility systems, using the NS component accelerograms recorded during 1977, 1986 and 1990 at the INCERC Bucharest station (fig.1).

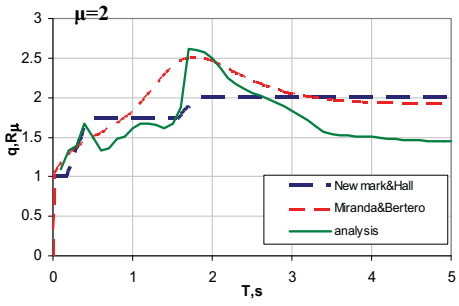

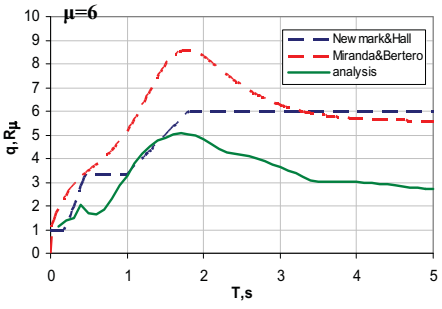

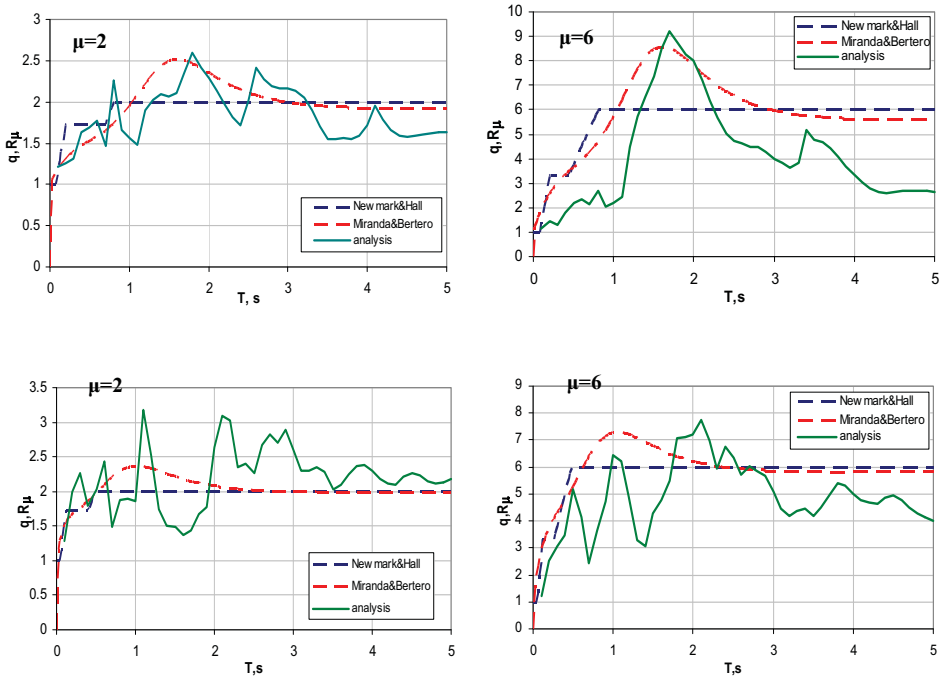

Figure 1. *q* factors for VN77NS, VN86NS, VN90NS records (INCERC Bucharest station)

From the above plots can be observed that q tends to one as T approaches zero. Proposed relationships fairly estimate the analysis results, especially for short-medium vibration period and for low-medium displacement ductility; for flexible structures with high ductility, the results are grossly overestimated, especially in the case of 1977 strong ground motion. On the other hand, a large variability of q in terms of T and μ can be observed. The variability of spectral response was more detailed investigated, using a number of 15 accelerograms of 1986 Vrancea earthquake, recorded in Bucharest (fig.2).

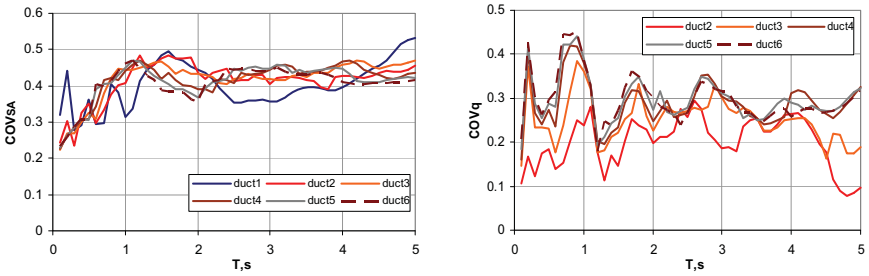

Figure 2. COV of *SA* and *q* factors for 1986 EQGM (15 records, Bucharest)

The results are showing a larger variability corresponding to high ductility in small vibration period region. As for the q factor, the scattering is much more pronounced; the variability is lower for low ductility structures.

From the definition, one of the major disadvantage of q factor is that does not account for the effect of hysteretic demand, as a powerful damage indicator (Uang *et al.,* 1990; Iancovici, 2005). The mass normalized hysteretic energy is given by

$$EH(t) = (1 - \beta_k)\omega^2 \int_0^t z(\tau)\dot{x}(\tau)d\tau \tag{2}$$

where, β_k is the ratio of pre- and post-yielding stiffness, ω is the natural circular frequency and $z(t)$ is the nonlinear (hysteretic) displacement. For the sake of investigating the patterns of q factors and hysteretic energies, we plotted their mean plus one standard deviation values on the same graph (fig.3).

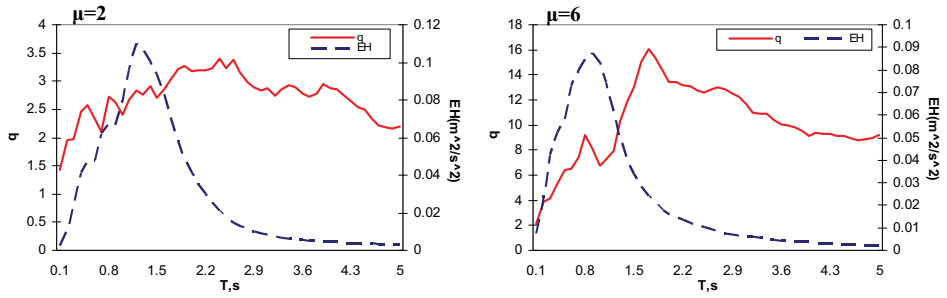

Figure 3. q factor and hysteretic energy spectral representations (15 records, Bucharest)

As suggested, the variation pattern differs considerable; generally q factor could not correctly reproduce the hysteretic energy distribution over the whole vibration periods range. The coefficients of variation for the input energy that the structure will receive and the hysteretic energy that the structure will absorb are plotted in fig. 4.

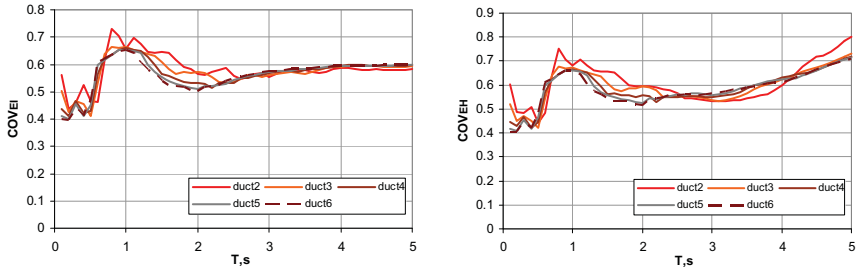

Figure 4 . COV of input and hysteretic energies 1986 EQGM (15 records, Bucharest)

A high coefficient of variation can be observed for both parameters. For short natural periods range the variation is higher for low ductility; for flexible systems, the ductility effect on COV nearly vanishes.

3. MULTIPLE GROUND MOTIONS EFFECT ON STRUCTURAL RESPONSE

The multiple input ground motion effect was introduced by a set of two and three accelerograms respectively. The effect of longer duration motions was removed from analyses by considering 40 seconds relaxation time intervals between excitations. We chose for our purpose again the NS component accelerograms recorded at the same site, INCERC Bucharest station during 1977, 1986 and 1990 earthquakes and the generated pulses are shown below.

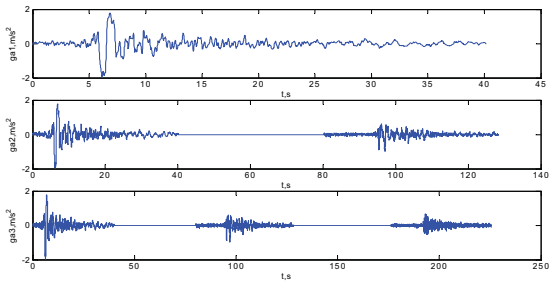

Figure 5. Multiple input motions of 1977, 1986 and 1990 EQGM, NS components (INCERC Bucharest station)

The spectral representation corresponding to low and high displacement ductility show that there is no sensitivity on q factors for the considered multiple input motions.

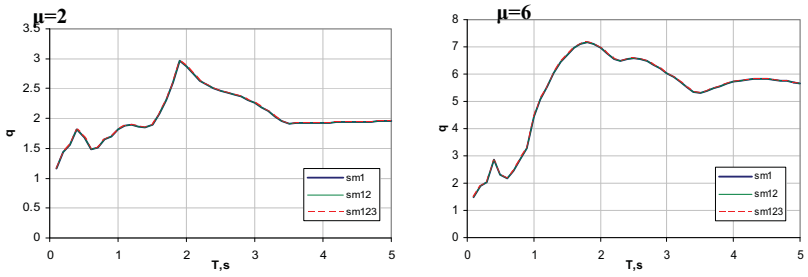

Figure 6. q factors for 1977, 1986 and 1990 EQGM, NS components (INCERC Bucharest station)

Taking the VN77NS record as reference and representing the ratios of the corresponding hysteretic energies (fig. 7), it can be observed that the variation is pronounced for *SM12* and has almost doubled values for *SM123*, especially in the case of low-medium vibration periods. This fact is not reproduced by the behavior factors ratios.

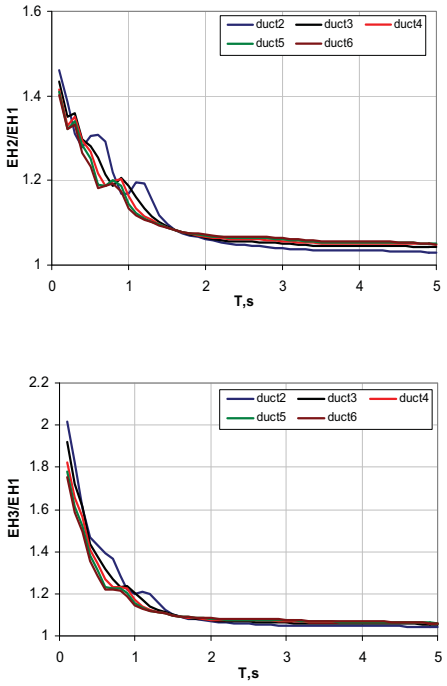

Figure 7. Hysteretic energy ratios for 1977, 1986 and 1990 EQGM, NS components (INCERC Bucharest station)

It is therefore desirable to relate the behavior factors with damage. Earthquake structural damage may be expressed as a contribution of excessive inelastic deformation and cyclic reversal loading effect. For the purpose of studying the correlation that might exist between behavior factors and damage, we used an improved damage model developed by Bozorgnia and Bertero, 2001. This addresses to inelastic SDOF systems and tends to eliminate the disadvantages of the well known Park and Ang damage index (Williams *et al.,* 1995; Mehanny *et al.,* 2000).

By definition, the Bozorgnia and Bertero damage index is given by

$$DI = (1-\alpha_1)\frac{\mu-\mu_e}{\mu_{mon}-1} + \alpha_1 \frac{EH}{EH_{mon}} \tag{3}$$

where μ is the displacement ductility, μ_e is the ratio of maximum elastic portion of deformation to yield displacement, μ_{mon} is the monotonic displacement ductility capacity, EH_{mon} is the hysteretic energy capacity under monotonic load and $0<\alpha_1<1.0$ is a constant. The associated damage index ratios are represented in fig. 8.

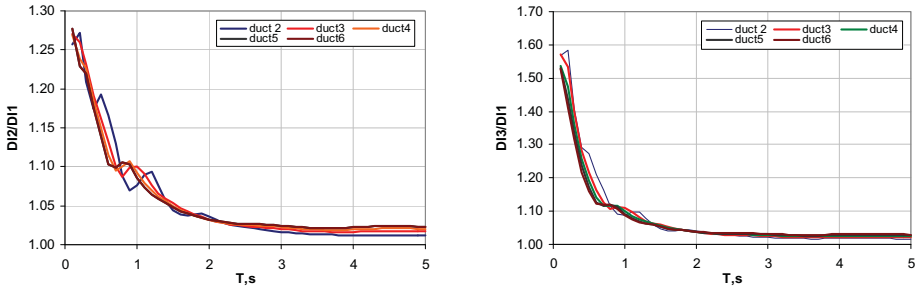

Figure 8. Damage index ratios for 1977, 1986 and 1990 EQGM, NS components (INCERC Bucharest station)

The spectral distribution of damage shows attenuation with the vibration period, with small influence of ductility. However the increase in damage ratio is up to 25% for *SM12* and up to 60% for *SM123*.

There are a very limited number of records that can serve to our purpose, able to drive the structure up to the desired performance level.
We chose then to simulate a large number of artificial strong ground motion accelerograms which realistically aim to reproduce a prescribed structural response and have similar amplitude, frequency content and duration as the real ones, recorded in Bucharest on soft soil conditions (fig. 9).

Artificial ground motions were simulated using the procedure described by Gasparini *et al.* 1976), who's response spectra match the elastic acceleration response spectra, given in the Romanian seismic design code P100-2006.

Sokolov and Bonjer (2006) proposed a procedure to estimate the ground motion parameters based on site-dependant Fourier spectra, obtained by attenuation relationships. Based on this procedure, estimates of peak ground accelerations, for 1940 event in Bucharest, were made as 0.24g. Comparisons with recorded accelerograms during 1977, 1986 and 1990 events were proven the availability of the proposed technique.

Based on these estimates, we generated three sets of 20 accelerograms compatible with the elastic response acceleration spectra for Bucharest, having peak ground accelerations of 0.24g (first and last) and 0.20g (middle). Since the problem of generating artificial ground motions has many issues, our simulation intends to reproduce the possible succession of events that occurred and may occur in the

future, primarily focusing on the structural response and ground motion characteristics from engineering point of view (fig. 9)

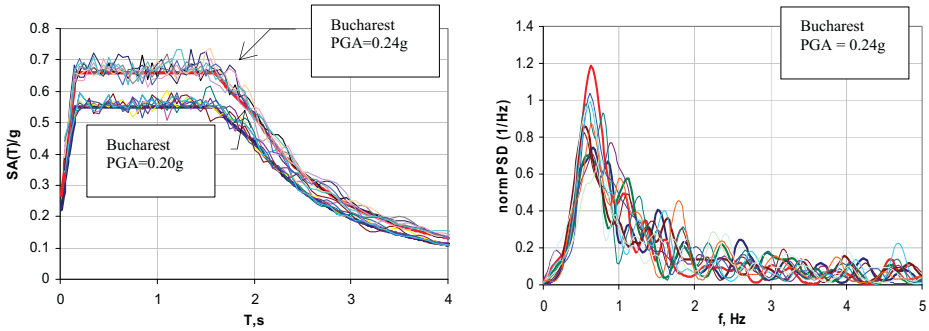

Figure 9. Code spectra compatible accelerograms and corresponding normalized PSD functions

Typical simulated accelerograms are presented below (fig.10).

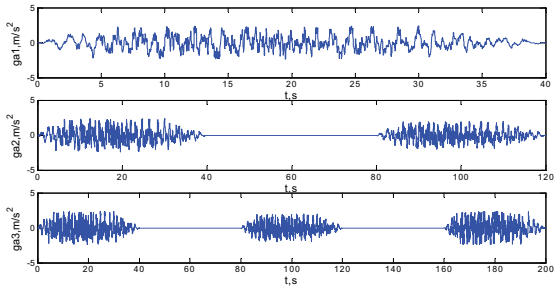

Figure 10. Typical code spectra compatible simulated accelerograms

By analyses, means plus one standard deviation values of *q* factors were obtained and are represented in fig.11.

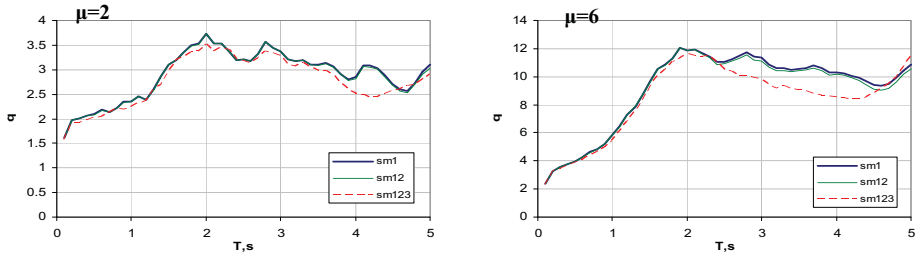

Figure 11. *q* factors (means plus one standard deviation), artificial accelerograms

The results are showing a general decreasing trend of the *q* factor; a slight decrease of *q* factor corresponding to *SM12* and a more pronounced decrease in the case of *SM123*, especially in the case of flexible structures.

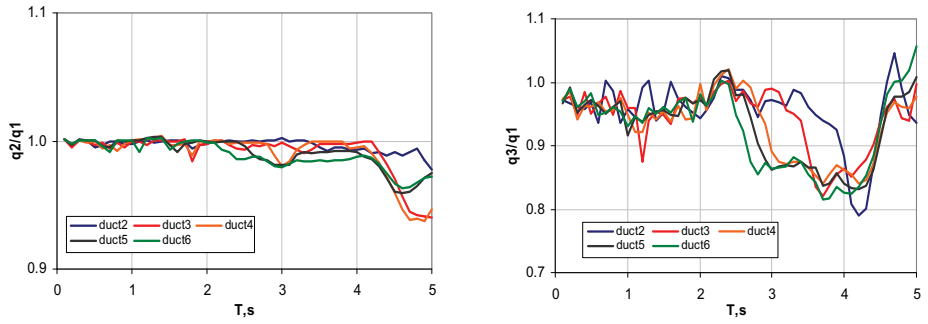

Figure 12. *q* factors ratios

Similarly, we computed the ratios of means plus a standard deviation of the behavior factors, corresponding to *SM12* and *SM123*, taking as reference those corresponding to *SM1* (fig.12).

One can be observed that generally, in the case of two input motions, the decrease of behavior factor goes up to 6% and up to 21%, in the case of three input motions, for flexible structures having low ductility. In the range of low-rise buildings, the variation is rather uniform and goes up to 2-3% for two input motions and up to 12% for three input motions. Consequently the decrease of *q* will generate an increase in the force and drift demands, that the structure should be able to supply. Slight increases of *q* can be observed in the case of high-rise buildings with low ductility.

4. CONCLUSIONS

The behavior factors cannot reproduce the effect of hysteretic energy demand. We have shown that for a typical multiple strong motions recorded at the same site, INCERC Bucharest station during 1977, 1986 and 1990 Vrancea earthquakes, there is no variation on behaviour factors. However, in the same time, the hysteretic energy demand goes up to 40% and 80% respectively. Same tendency was observed in the case of associated damage indices.

For a large number of artificially generated accelerograms, the effect of repeated ground motions on *q* factor might be considerable, especially in the case of three input motions, for the flexible structures having low ductility. Consequently, the

base shear demand would increase considerably. This could be the case of some reinforced concrete buildings in Bucharest, designed in the pre-code or low code era, with low inelastic deformation capacity and low hysteretic energy performance.

These are however estimates that might be reliable for routine buildings. For flexible buildings however changes are expected due to the higher modes effect and the effect of over-strength.

Amadio *et al.,* 2002 suggested that the reduction on *q* factor is even larger than for SDOF systems, in the case of steel moment resisting frames. A seismic design procedure that does not take into account the cumulative inelastic deformation demand that a structure will likely undergo during severe ground motion could lead to unreliable performance.

References

1. Amadio, C., Fragiacomo, M., Rajgelj, S. , The effects of repeated earthquake ground motions on the non-linear response of SDOF systems, Earthquake Engineering and Structural Dynamics, 32:291-308, 2003
2. Gasparini, D.A., Vanmarcke, E.H., Simulated Earthquake Motions Compatible With Prescribed Response Spectra, Department of Civil Engineering, Research Report R76-4, Masschusetts Institute of Technology, Cambridge, Massachusetts, 1976
3. Iancovici, M. , Evaluarea performantei structurale a cladirilor de beton armat, Ph.D. thesis, Technical University of Civil Engineering Bucharest (in Romanian), 2005
4. Miranda, E. Bertero, V., Evaluation of strength reduction factors for earthquake resistant design, Earthquake Spectra, 10(2), 357-379, 1994
5. Nassar, A. A., Krawinkler, H., Seismic demands for SDOF and MDOF systems, Report No. 95, The John A. Blume Earthquake Engineering Center, Stanford University, California, USA, 1991
6. Newmark, N. M., Hall, W. J., Seismic design criteria for nuclear reactor facilities, Report No. 46, Building Practices for Disaster Mitigation, National Bureau of Standards, U.S. Department of Commerce, 209-236, 1973
7. Sokolov, V., Bonjer, K-P., Modeling of distribution of ground motion parameters during strong Vrancea (Romania) earthquakes, 1st ECCES, Geneva, 2006
8. Terán-Gilmore, A., Jirsa J., The concept of cumulative ductility strength spectra and its use within performance-based seismic design, ISET Journal of Earthquake Technology, Paper No. 446, Vol. 41, No. 1, pp. 183-200, 2004
9. Uang, C.M. and Bertero, V.V., Evaluation of Seismic Energy in Structures, Earthquake Engineering and Structural Dynamics, Vol. 19, pp. 77-90, 1990
10. Watanabe, G., Kawashima, K., An Evaluation of the Force Reduction Factor in the Force-Based Seismic Design, Tokyo Institute of Technology, O-Okayama, Meguro, Tokyo, Japan, 152-8552, 2002
11. Romanian Seismic Design Code P100/2006, Ministry of Transport, Construction and Tourism, Romania, 2006

"Computational Civil Engineering 2007", International Symposium
Iaşi, România, May 25, 2007

Databases- business support for the Civil Engineering

Irimia Roxana-Adina[1], Vlăsceanu Alina Nicoleta[1]
[2]*Department of Computer Science, Christian University"Dimitrie Cantemir", Bucharest, Romania*

Summary

The current changes in modern society and the evolution of the market, defined by the generalization of the Internet-Intranet-Extranet technologies, produce significant changes in the management of large databases and new ways of exploring the huge potential of information provided by Internet interactions must be found. Companies that need to develop predictive models using business expertise use the concepts of Data Mining and Web mining into business operations to improve decision making. In addition, Data mining software allows them to find relationships and patterns in raw data and use it in an automated decision supports system; they also can extract knowledge from real-time and historical data and predict outcomes of future situations.
The actual development trend regarding the Databases Management Systems must focus on:
-using intensively the integration of the Information Systems;
-obtaining open applications;
-ensuring interoperability and communication for the Information Systems;
-focusing on the global performances;
- Databases Management Systems must become platforms for the databases.
The technology of data bases have interfered with others Computer Science-based technologies, generating new types of hybrids DBMS, such as evolved (advanced) data bases.
Related with the Civil Engineering field, it can be mentioned the spatial databases (which have resulted by combining the technology of data bases with geographical systems and assisted design) and the multimedia databases (which store and process classical data-text and graphics and also multimedia data-images, audio and video).

KEYWORDS: spatial databases, multimedia databases Data Mining, Internet, digital economy.

1. INTRODUCTION

One of the factors that stimulated the development of database technology was the need to guarantee the consistency of the stored data. On the other hand, the demand to process more complex data with more semantic content have also lead to a better understanding of the properties of the data and motivated the evolution of the Data Base Management Systems (DBMS) toward the inclusion of facilities to handle such properties.

The handling of data properties within the context of a database engine faces two main difficulties: 1) Properties are hard to identify, especially those obvious in the actual world; 2) Data property presentation varies during the process of design of the software.

The proper requirements elicitation of a software product is a key factor in the success of the whole software development process. However, these requirements are not easy to deal with. They have different intrinsic natures and they may appear showing different faces. In many cases, some requirements are totally or partially hidden in the information collected by the software developers.

Pragmatic issues such as the degree of adhesion of a given DBMS or others related with performance may introduce additional mutations. The understanding of the evolution from actual world data properties to database world integrity restrictions is another key factor in the success of the software artifact during its life cycle. This understanding must be accompanied with a well defined traceability mechanism, which must clearly identify the actual world data property behind every database integrity restriction. Traceability is also a key factor especially during software maintenance activities.

Not every data property must be modeled, but each property must be looked at carefully to see if modeling is needed in the context of the scope and in the objective of the software artifact. A more analytical approach may order the data properties by taking into account their importance.

2. EVOLUTION OF DATA PROPERTIES

Figure 1 shows all possible mappings from data properties in the actual world to database integrity restrictions. It should be noticed that there are neither arrows from Business Rules to Object Restrictions, nor from Attribute Properties to General Rules. These mappings are extremely hard to find. Also, some other mappings shown in Figure 1 occur very seldom, while others are common.

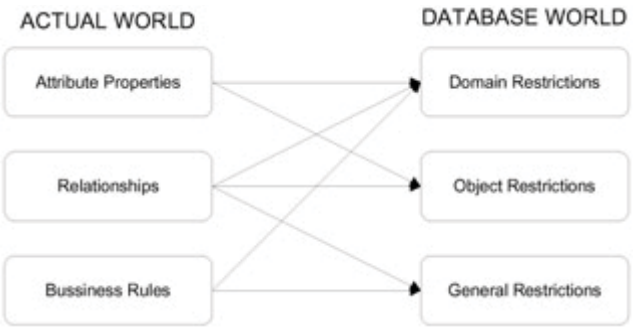

Figure 1. Mappings data properties into integrity restrictions

Attribute Properties. Database Engines have a set of built-in data types whose main purpose is to deal with the Attribute Properties of the data to be stored. These data types are useful and have been used for decades, helping users to take care of their data processing needs.

Relationship Properties. The connection among different attributes is the source of most of the data processing richness and problems. These connections have a scope larger than Attribute Properties since they involve several attributes, at least two, usually belonging to different objects or entities.

Business Rules. Every organization restrains behavior in some way. This is strongly associated to constraints that define which data may (or may not) be actualized. A Business Rule is a declarative sentence usually describing a correct state of a piece of data.

3. METHODS TO ORGANIZE THE DATA AND DBMS (DATA BASE MANAGEMENT SYSTEMS)

As mentioned above the need to guarantee the integrity of the stored data was and still is one of the key factors driving the evolution of the Data Base Management Systems (DBMS), creating different Database paradigms. The following paragraphs give a brief summary about how most popular paradigms see the Database integrity problem.

Relational Databases. A rich theory for constraints has emerged in relational databases, mainly based on a fundamental class of constraints called dependencies. Its main motivation is to incorporate more semantics into the relational model. The term relational model has thus come to refer to the broad class of database models that have relations as the data structure and that incorporate some or all of the query capabilities, update capabilities, and integrity constraints. Many ideas of

other database paradigms already in the scenario (and in their own evolution process) have been borrowed by researchers and vendors, and introduced in current relational products. This fact has created types of incomplete and extended relational engines, which started to be known as post relational databases. They are incomplete because not all the prescribed issues for the relational model are satisfied, and extended because they go further in some other areas such as active characteristics.

Active Databases. Supporting reactive behavior implies that a database management system may be viewed from a production rule system perspective. These production rules are well known today, in database terminology, as active rules or simply triggers. It is a form of computation, which is motivated by the occurrence of some event, typically a database operation, executing a reaction to that stimulus. Active rules may pose queries to the database to collect information about events and database objects and decide whether events require an action. Then they may execute actions, normally any sequence of database operations. Reactive behavior is seen as an interesting and practical way to check for satisfaction and enforcement of integrity constraints. Nevertheless, integrity constraint maintenance, materialized view maintenance (especially useful in the warehousing area) and implementation of Business Rules are not the only areas of application of data repositories with reactive behavior. Other interesting applications areas are replication of data for audit purpose, data sampling, workflow processing, scheduling, real-time applications and many others. In fact, practically all products offered today in the marketplace support complex reactive behavior on the client side.

Spatial Databases. Even though there is a very active research area interested in the design of robust and efficient spatial databases, the inability of current GIS regarding the implementation and management of spatial integrity constraints is still evident. This is due to the fact that within the scope of geographic applications, special problems come up due to the location aspects of data. A modification in a spatial database may cause simultaneous updates in a large number of records in multiple files, making it hard to manage the entire environment. A very sophisticated control is required to avoid redundancy and loss of integrity.

Object-Relational Databases. Object-oriented literature typically uses the term "relationship" to mean, specifically, relationships supported by foreign keys in a relational system. Various levels of support for referential integrity have been implemented in those systems. As in the relational paradigm, triggers are very effective in supporting data integrity in a database, especially for dealing with those restrictions that cannot be expressed declaratively. ORDBMSs demand a system of triggers even more flexible than the relational one.

Object-Oriented Databases. Given that in an OO environment, objects are collected into classes and relationships are established at the class level. A

relationship between classes denotes a set of relationships between the objects of the respective classes. Relationships may have attributes. A model is always a compromise to achieve the right amount of expressive power while keeping simplicity and clarity. Domain Restrictions, keys, and referential integrity constraints may all be used straight-forwardly in OODBMSs. Other kinds of constraints are peculiar to OODBMSs, for instance: constraints of the migration of objects between classes (roles); exclusivity constraints between classes; constraints on the definitions of subclasses; and existence dependencies. The last ones are the key to semantic integrity checking since they allow the designers to track and solve inconsistencies in an object-oriented conceptual schema.

Distributed Databases. A distributed database managing system (DDBMS) is a database management system (DBMS) that supports characteristics of a distributed database, that is, the possibility of handling information contained in multiple locations, and preserving data integrity at the same time. A DDB differs from a centralized DB mainly in that data are placed in a number of locations instead of being located in only one site. This characteristic of DDBs causes the control of data integrity to be more complex than for centralized environments. Each transaction can involve more than one location, and it is hard to keep an execution order of the instructions of the transaction to preserve data integrity.

The strength of the SQL standards induces one to think that in the future the object relational paradigm will continue to be dominant in the field of DBMS. Improvements to check-and-trigger mechanisms are strongly needed to integrate data properties in a more friendly way with the data itself. Development platforms where data properties become a concern of the engine and the data integrity is fully factorized will form application programs leading to an evolution and the maintenance of less traumatic DBMS-based software artifacts. Naturally, this process will require very active participation on the part of researchers and DBMS producers.

4. SPATIAL DATABASES AND GIS-USEFULL INSTRUMENTS FOR CIVIL ENGINEERING

A *spatial database* is a database that is optimized to store and query data related to objects in space, including points, lines and polygons. While typical databases can understand various numeric and character types of data, additional functionality needs to be added for databases to process spatial data types. These are typically called geometry or feature. The Open Geospatial Consortium created the Simple Features specification and sets standards for adding spatial functionality to database systems. Database systems use indexes to quickly look up values and the way that most databases index data is not optimal for spatial queries. Instead,

spatial databases use a spatial index to speed up database operations. In addition to typical SQL queries such as SELECT statements, spatial databases can perform a wide variety of spatial operation. The following query types and many more are supported by the Open Geospatial Consortium:

- Spatial Measurements: Finds the distance between points, polygon area, etc.
- Spatial Functions: Modify existing features to create new ones, for example by providing a buffer around them, intersecting features, etc.
- Spatial Predicates: Allows true/false queries such as 'is there a residence located within a mile of the area we are planning to build the landfill'
- Constructor Functions: Creates new features with an SQL query specifying the vertices (points of nodes) which can make up lines.
- Observer Functions: Queries which return specific information about a feature such as the location of the center of a circle.

In the category of Spatial Database Systems, it can be mentioned Oracle Spatial, PostgreSQL DBMS (which uses the spatial extension PostGIS to implement the standardized data type geometry and corresponding functions) and MySQL DBMS (which implements the data type geometry plus some spatial functions that haven't been implemented according to the OpenGIS specifications. Functions that test spatial relationships are limited to working with master bounding rectangles rather than the actual geometries. MySQL versions earlier than 5.0.16 only supported spatial data in MyISAM tables. As of MySQL 5.0.16, InnoDB, NDB, BDB, and ARCHIVE also support spatial features).

A *geographic information system* (GIS) is a system for capturing, storing, analyzing and managing data and associated attributes which are spatially referenced to the earth. In the strictest sense, it is a computer system capable of integrating, storing, editing, analyzing, sharing, and displaying geographically-referenced information. In a more generic sense, GIS is a tool that allows users to create interactive queries (user created searches), analyze the spatial information, edit data, maps, and present the results of all these operations. Geographic information science is the science underlying the applications and systems, taught in degree programs at many universities. Geographic information system technology can be used for scientific investigations, resource management, asset management, Environmental Impact Assessment, Urban planning, cartography, criminology, history, sales, marketing, and route planning. For example, a GIS might allow emergency planners to easily calculate emergency response times in the event of a natural disaster, a GIS might be used to find wetlands that need protection from pollution, or a GIS can be used by a company to find new potential customers similar to the ones they already have and project sales due to expanding into that market.

Civil Engineering projects involve the management, analysis and integration of large amounts of geographic information to ensure success. This can include a wide range of information such as detailed design drawings originating from CAD

solutions, detailed mapping, air photography, geological investigations, population information, traffic flows and environmental models.

With increasingly complex projects, the interaction of often international multidisciplinary functions requires the introduction of effective and efficient data management and sharing solutions. GIS provides the civil engineer with tools for creating, managing, analysing and visualising all types of geographic information. GIS is now being used by Civil Engineers in every application domain and throughout every aspect of the enterprise, be it on the desktop, in the field, or in collaboration with others.

The Geographical Information Systems provides a rich set of databases and spatial tools needed to manage civil information for design, modeling and maintenance. Data is taken from many different sources and file formats and integrated into a single application platform to support complex civil engineering workflows.

A *geodatabase* is a spatially enabled relational database that has the ability to represent various types of geographic data, manage attributes associated with that data, maintain spatial relationships (topology and networks), and keep track of user-defined thematic layers and datasets. GIS typically supports three different "views" of geographic information: the geodatabase view, the geovisualization view, and the geoprocessing view.

Spatial relationships, such as topologies and networks, are also crucial parts of a GIS database. Topology is employed to manage common boundaries between features, define and enforce data integrity rules, and support topological queries and navigation

Networks are used to describe a connected graph of GIS objects. The graph, or network, can be used to model transportation pathways, pipelines, utilities, hydrology, and many other network based applications.

5. MULTIMEDIA DATA BASES AND OPEN COMUNICATIONS IN THE INTERNET ENVIRONMENT

Nowadays, we are witnessing an explosive growth in use of multiple media forms (voice, data, images and video etc.) in varied application areas including entertainment, communication, collaborative work, electronic commerce, and Civil Engineering. The increasing computing power, integrated with multimedia and telecommunication technologies, is bringing into reality the dream of real time, virtually face-to-face interaction with collaborators sitting far away from us. In the process of realizing the technological ambitions, it's necessary to address a number of technology, management and design issues and to be familiar with exciting current applications. It is impossible to track the magnitude and breadth of changes

that the multimedia and communication technology is bringing daily to us in many different ways throughout the world. The major multimedia networking areas includes: Development and management of real time distributed multimedia applications; Audio/video applications and streaming issues; Protocols and technologies for building Internet multimedia applications; QOS (Quality of Service) frameworks and implementation; Collaborative applications; Multimedia synchronization in distributed environment; Multicasting technology and applications; Use of mobile multimedia over wireless network.

The Internet has evolved from a provider of the simple TCP/IP best-effort service to an emerging integrated service Internet. This development provides tremendous opportunities for building real-time multimedia applications over Internet, although they are often large and complex. The CORBA Media Streaming Framework and Java Media Framework are the two emerging environments for implementing Internet multimedia. They provide applications with a set of APIs to hide the underlying details of Internet real-time protocols. The Internet multimedia applications developed using these two frameworks are expected to appear in the near future.

In addition to HTML (Hyper Text Markup Language) pages and web sites, a number of new and more sophisticated technologies have been developed for creating and developing Web pages:

- Dynamic HTML introduces movement and the ability to react to a user's actions to Web pages;
- JavaScript, Java, and ActiveX are technologies that provide a way of performing complex tasks within a Web page and can even function as full-featured programs;
- CGI scripts is a technology used on some Web servers to provide server-based features such as visitor counters and discussion groups;
- XML (Extended Markup Language) provides a way of giving detailed content information about a Web page, allowing for more meaningful searching and information gathering.

In the last few years the rapidly growing Internet has pushed new multimedia applications in the field of communication and Civil Engineering. The next step in the information age is the mobile access to multimedia applications: everything, everywhere any time, using data transmission for mobile multimedia applications in wireless cellular networks.

Multimedia services are offered by service providers in the field of: broadcast (TV and audio channels, editors); information on demand (video, audio, weather, documents); communication (voice and video telephony); commerce (banking, electronic commerce, publicity); and industry (collaborate work, VPN).

Multimedia has the intrinsic goal of improving the effectiveness of computer-to-human interaction and, ultimately, of human-to-human communication. While the

human-computer interaction community looks predominantly at the application layer and the telecommunications community at the lower end of the ISO/OSI stack, little work has been published in bridging the gap between these two communities. Indeed, the human element is often neglected in quality of service negotiation protocols. Not only does this have a negative and undesirable impact on the user's experience of multimedia, it also discards the potential for more economical resource allocation strategies. With the proliferation of ubiquitous multimedia in predominantly bandwidth-constrained environments, more research is needed towards integrating and mapping perceptual considerations across the protocol stack and building truly end-to-end multimedia communication solutions.

6. CONCLUSIONS

The new vision over the knowledge based society increases the importance of knowledge, information and communication, presented in a multidimensional form, all these creating the nucleus of humanity's progress. The digital revolution based on these new values has transformed the business and governmental environment, revolutionizing the educational processes and generating new ways of memorizing, storing, and sharing information and data to a global level, causing an irreversible transformation in the social and individual level.

The new knowledge-determined society is inclusive, which means that any person, without any kind of discrimination, has the right to create, receive and use information and knowledge, no matter what media it being used and without border restrictions. The new form of social organization is individually-centered, focusing on citizens and communities as creators and beneficiaries of large- scaled dissemination of information. This implies a restructuring of the social organization in the sense of increasing social equity and democracy, mainly by increasing the transparency offered by the wide access to information, resulting in improving the quality of life. The new perspective, the openness of communication, also implies new forms of solidarity and cooperation, together with an increase of the degree of responsibility in using and spreading information.

Civil Engineering companies are recognizing the significant productivity gains to be obtained through the introduction of project intranets/extranets for the management, and publishing of shared project information. Geographic information is at the heart of all engineering projects and is by many different departments or organizations during any successful project. Geographic information collected during the planning stage is then necessary for detailed design, construction and maintenance phases of any project. The creation of a geoportal to share centralized data allows all project team members to access the relevant geographic information as and when required.

References

1. Jorge H. Doorn J., *Database Technologies*, Idea Group Inc, Argentina, 2005.
2. Shashi Shekhar and Sanjay Chawl, *Spatial Databases*, Prentice Hall, 2003.
3. Philippe Rigaux, Michel Scholl and Agnes Voisard, *Spatial Databases - With Application to GIS*, 2000
4. Mehdi Khosrow-Pour, *Encyclopedia of Information Science and Technology*, Idea Group Publishing, 2005
5. Syed Mahbubur, RahmanIdea, *Multimedia Networking: Technology, Management and Applications*, Group Publishing, 2002
6. Bruce Kogut, *The Global Internet Economy*, The MIT Press, 2003
7. Alan Simon and Steven Shaffer, *Data Warehousing and Business Intelligence for e-Commerce*, Morgan Kaufmann Publishers, 2001.
8. Mahesh Raisinghani, *Business Intelligence in the Digital Economy: Opportunities, Limitations, and Risks*, IGI Publishing, 2004.
9. *IBM Framework for e-business Technology, Solution, and Design Overview*, IBM Redbooks, 2001.

"Computational Civil Engineering 2007", International Symposium
Iaşi, România, May 25, 2007

Foundation solutions for a marketing center in Cluj

Nicolae Boți[1], Irina Lungu[2] and Ioan Boți[3]
[1]*Department of Roads and Foundations, Technical University, Iaşi, 700050, Romania*
[2]*Department of Roads and Foundations, Technical University, Iaşi, 700050, Romania*
[3]*Department of Geotechnical Eng., Technical University of Civil Eng., Bucureşti, 020396, Romania*

Summary

The construction of the marketing center is set on the left bank of the river Somes, in difficult site conditions. The underground water table increases from approximately 2.4-3.5m deep to 1.0-1.8m from the ground surface.

The lithological succession consists of clayey soils with various thicknesses and a significant swelling and contraction potential continued by silty sands, sand and gravels up to 10m deep. The cohesive soil layers display a reduced consistency index, less than 0.5, as for the fat clay, the void ratio may result in values up to 1.5.

In order to accommodate the site conditions three foundation solutions has been discussed: open caissons, embedded 0.3m into the good foundation soil; drilled short piles or precast driven piles inserted into the good foundation soil at lest 15d; foundation beam networks onto an improved soil by a granular material cushion.

The technology to perform the granular compacted layer is set in order to allow the heavy machines to enter the excavated area that transformed into a swamp. In this respect, the principle of the reversed filter method is required, by laying coarse materials at the bottom and finer materials on top.

The thickness of the granular cushion is set to prevent a deformation limit state at the footing level as well as at the cushion base level. The effective pressure should be less than the plastic pressure developed within the granular material first and second, into the natural foundation soil.

The design of the cushion concluded that a 2m thickness will comply with the restrictions set to prevent reaching a deformation limit state under the foundation system.

The solution proved to be efficient in case of poor soil conditions such as unconsolidated earth fillings, mud and loose sands, a non-uniform soil layering which is specific to swampy areas, to prevent the frost sensitivity and to ensure the presence of a drainage layer.

KEYWORDS: active clays, soil improvement, granular compacted cushion, deformation limit state, equivalent layer method.

1. GEOTECHNICAL SURVEY

1.1. Geological and geomorphological data

The construction site is situated at the South border of the Somes's Plateau limited at North-East by Transilvania Field, on the left side terrace of the river Somes. The geological eras are considered a necessary base for this survey due to the fact that a texture is a result of the deposit conditions and the successions of the events. At high depths there is a salt formation which, in its ascension generated the folding of the strata into an anticline with West-East direction. Marls are found above the salt deposits, which are visible on the Desmir hills. The quaternary is represented by the alluvial deposits of the second terrace of the river Somes. With ages, the other streams created a swamp in the area of interception with the river Somes.

1.2. Hydrogeological data

Within the three boreholes performed at the construction site, water is present in sand and gravel strata, at depths between 2.4-3.5m and the level increased from 3.5m to 1.0m (F_1), from 3.1m to 2.1m (F_2) and from 2.4m to 1.8m (F_3) from the ground surface. Water is strongly sulphurous, with very low carbonide, very low salts content.

The fluctuating underground water level influences the geotechnical category together with the foundation solution: the excavation goes below the water table and consequently gravitational drainage works are required, without any risks of damaging the surrounding buildings.

1.3. Soil profile

Based on the performed boreholes and borehole logs, the soil profile consists of the following layers:

- clayey soil, brown-black, 0.2m thickness (F_1, F_3) and 1.2m (F_2);
- fat clay, black, with high plasticity, variable thickness 2.3m (F_1), 1.2m (F_2), 0.5m (F_3) – γ = 16.41-17.83 kN/m^3, I_c = 0.41-0.77, e = 1.06-1.49;
- grey clayey sand, with metal insertions, 1m thickness in F_1 borehole only – γ = 18.6 kN/m^3, I_c = 0.33, e = 0.78;
- yellowish grey gravel, only in the F_2 borehole, 3.1m thickness – γ = 20.36-21.37 kN/m^3;
- fat marly clays with fine gravel, 0.6m thickness in F_3 borehole – γ = 21.74 kN/m^3, I_c = 0.8, e = 0.84;
- brownish silty sands, 1.2m thickness – γ = 19 kN/m^3, e = 0.59, $\Phi = 37^0$;

- fine gravel with sand, 3.5m (F_1), 1.5m (F_2), 2.0m (F_3) thickness – γ = 22.8kN/m^3;
- brownish gravel, 1m thickness in F_1 borehole only – γ= 20 kN/m^3;
- coarse gravel and sand, 2m thickness in F_1 borehole only – γ = 22.8 kN/m^3;
- yellowish-brown sand, below 10m depth all over the place – γ = 18.11 kN/m^3, e = 0.77

2. FOUNDATION SOLUTIONS

According to the site conditions previously presented the following foundation solutions were considered appropriate:

- open caissons,
- short piles – drilled or precast driven,
- foundation beam network onto a granular material compacted cushion.

2.1. Open caissons

Caissons ensure the crossing of the soft soils, preferable used in river beds, since the soil removal from the inside is easily done by a ship scraper and the developed friction force is low. It is considered an efficient solution where piling is difficult due to the presence of large boulders or other obstacles. It is important to maintain the verticality of the caisson advance into the ground. By using hydro-mechanically excavation under the water table in sands or silty sands, a hydraulic fracture of the ground may develop immediately under the cutting edge of the caisson.

2.2. Short piles

The limited use of a pile foundation according to this site conditions can be explained by the difficulties during piling – drilling or driving – and also by the fact that such short piles result with a good behaviour during service when designed to carry loads up to 250-300 kN with an optimum pile interdistance of 1.5 – 2.0m. A subevaluation of the pile bearing capacity can happen when using tables for the point resistance and side friction in case of coarse sands, gravels, and high consistency clays.

2.3. Foundation beam network onto a granular material compacted cushion

As a soil improvement method of the initial soft soil, a granular compacted cushion is considered appropriate, the layering process beginning over an initial layer made

of crushed stones and boulders that is stable enough to ensure the access of the heavy machines to start the compaction process.

The composition of the ballast cushion is dictated by: the nature and composition of the soil, the groundwater table, and the construction design parameters [1]. In case the cushion is built under the water table, on permeable soils the reverse filter principle has to be applied to avoid hydraulic fracture of the soil underneath, by layering a coarser material at the bottom and finer material on top.

3. DESIGN PRINCIPLES FOR THE GRANULAR COMPACTED CUSHION

The foundation soil design subjected to a shallow foundation was performed using the conventional pressure according to the Romanian STAS 3300/2-1985 of 350kPa. In figure 1, the cushion dimensions are presented in order to support a shallow foundation: the thickness h_p and the enlargement (the width of the guard area) c with respect to the foundation edges, with a total of B_p under the footing.

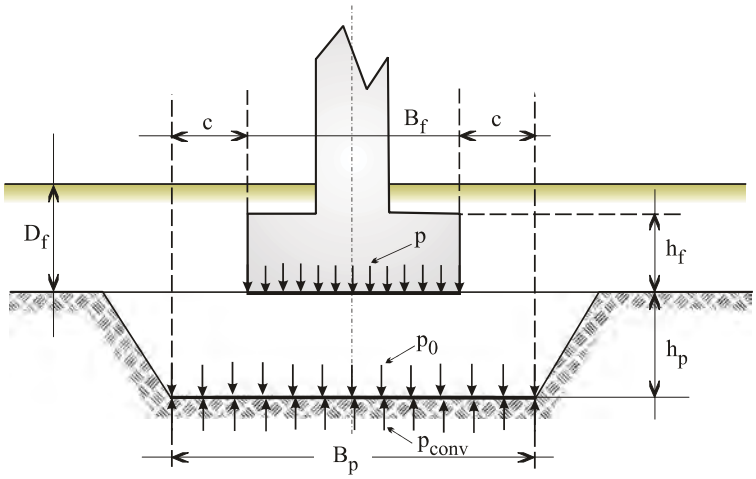

Figure 1. The load transfer from the footing to the cushion and then to the foundation soil

The minimum thickness of a granular compacted cushion is considered to be 1.00m and in case the cushion acts as a reverse filter, the cushion is designed over the entire building and with a minimum thickness of 1.50m. In this hypothesis of cushion's pre-dimensioning, the pressures verification at the base of the cushion is given by:

$$p_0 = \gamma \cdot D_f + \gamma_p \cdot h_p + \alpha \cdot p \leq p_{conv} \quad (1)$$

where: γ is the soil unit weight of the soil filling above the ground level, γ_p is the unit weight of the granular material compacted into the cushion, D_f the foundation depth, h_p the cushion's thickness, p the pressure deliver from the footing, α the distribution coefficient for the vertical normal stress along the footing axis.

The final verification of the cushion is made based on the isobar curves, with the restriction that the cushion shall be set between the isobars of 0.2p of the vertical normal stress σ_z and 0.3p of the horizontal normal stress σ_y, as well as for the shear stress τ (figure 2) [2].

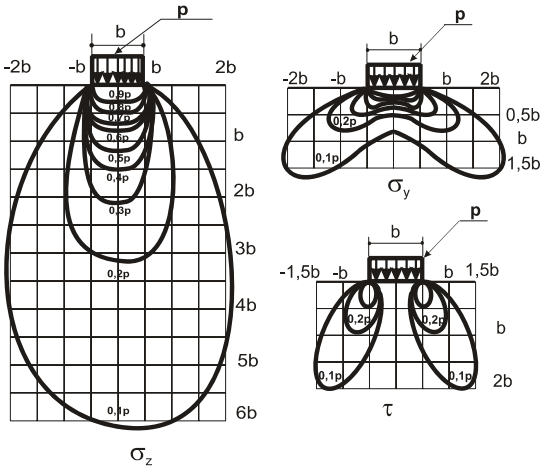

Figure 2. Isobar curves for a continuous flexible footing with the width b

The method of the equivalent stratum is applied by using Odemark's relationship in order to asses the distribution of the stress along the thickness of the cushion based on the pressure delivered from the footing to the cushion (figure 3) [2], [3].

$$h_{equivalent} = \alpha \cdot h_1 \cdot \sqrt[n]{\frac{E_1 \cdot \gamma_2}{E_2 \cdot \gamma_1}} \tag{2}$$

where: γ_1, γ_2 are the unit weight of the two layers involved, α a coefficient experimentally set, E_1 and E_2 are the corresponding moduli of the materials within the two layers, h1 the thickness of the layer for which the equivalent thickness is established. For the present case $\gamma_1 \cong \gamma_2$, $\alpha = 1$ and $n = 2.5$. The granular material is considered to be a ballast with the following characteristics: $\gamma_d = 20.5 - 21.5 kN/m^3$, $w_{opt} = 6 - 8\%$ and a modulus $E_1 = 400 daN/cm^2$. The thickness of the cushion is set initially to 1.00m, a foundation depth of 1.50m and a deformation modulus of the soil underneath $E_2 = 100 daN/cm^2$.

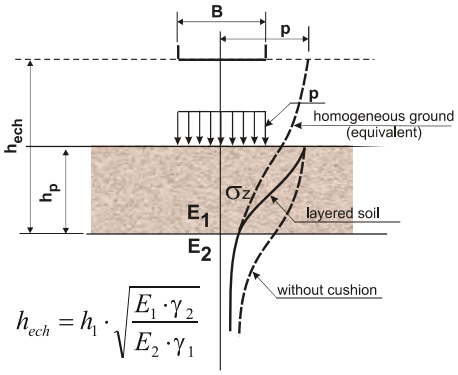

Figure 3. The method of the equivalent stratum

The bearing capacity of the foundation soil is set as p_{conv} = 350kPa, the pressure delivered by the footing p = 250kPa, the distribution coefficient 0.55 and consequently, the pressure at the base of the cushion p_0 = 137.50kPa. The resulted equivalent thickness is set as $h_{equivalent}$ = 1.50m. This case is similar with the ones mentioned in literature, where the ration between deformation modulus of the soil is smaller 1.8-2.5 the cushion modulus, 150-200daN/cm^2, the ground can be considered homogeneous.

3. CONCLUSIONS

Based on the analysis performed on the foundation solutions, the foundation system is recommended to consist of flexible continuous footing for the external shear walls and a foundation beam network of the columns inside, all performed on a compacted ballast cushion. The thickness is finally set at 2.0m to accommodate poor soil conditions such as unconsolidated earth fillings, mud and loose sands, a non-uniform soil layering which is specific to swampy areas, and to ensure the presence of a drainage layer.

References

1. Mihu, A., Silion, T., Ciubotaru, V., Boți, N., Muşat, V., Grecu, V., Beche, V., Sîrbu, G., Folosirea pernelor de balast la fundarea unor construcții de clădiri pe pământuri puternic compresibile şi saturate cu apă, *Revista nr. 1 Construcții*, INCERC Bucureşti, 1976. (in Romanian)
2. Boti, N., Silion, T., Raileanu, P., Cijevschi, Maria, Musat, V., Grecu, V., Stanciu, A., Nicuta, Ana, Criterii de dimensionare a pernelor de pamant, *Sesiunea Ştiințifică Jubiliară „40 de ani de Învățământ Superior de Construcții la Iaşi"*, 1981. (in Romanian)
3. Pop, V., Popa, A., Maniu, I., Popa, A., Fundații de suprafață pe pernă de balast, *Rotaprint IP Cluj Napoca,* 1978. (in Romanian)

"Computational Civil Engineering 2007", International Symposium
Iaşi, România, May 25, 2007

The Expertise of Offshore Structures

Ludovic G. Kopenetz, Ferdinand-Zsongor Gobesz
Department of Structural Mechanics, Faculty of Civil Engineering and Building Services, Technical University of Cluj-Napoca, Cluj-Napoca, 400020, Romania

Summary

The problem of energy in tight liaison with ecology is representing one of the greatest problems of humanity. Considering an exponential broaden of marine production in the following years, the international organizations have imposed the adoption of some highly strict internal and international prescriptions in order to avoid environmental accidents (pollution). In this context, the structural safety of the offshore-type complex plants and equipments is quite actually.

The structural expertise must cover, beside the vastness of interfering random variables, all-important aspects in order to avoid the pollution of the pelagic environment.

The present paper wishes to bring a humble contribution to the clarification of the aspects which are producing sensitive alterations of structural safety (quality of material, global and local stability, fatigue, corrosion and erosion etc.), using advanced and lifetime oriented analysis concepts.

KEYWORDS: offshore structure analysis safety stability assessment

1. INTRODUCTION

The behavior in situ of the steel offshore structures (figure 1) and the ecological aspects are tightly bonded to structural safety. In this way, the structural expertise must answer to the problems of structural safety [1], [2], [3]. At its turn, the concept of structural safety is bundled to the design, construction and operation of offshore structures, considering the extent of interfering random variables (wind waves, earthquake, construction faults, corrosion, fatigue etc.).

The international standards concerning the conservancy of the planetary ocean (covering approximately 70% of the Earth's surface) are very severe [4]. In this context the structural expertise of the offshore structures which are located in the area of the coastal shelf of the Black Sea has a peculiar importance, considering the fact that these structures were conceived and erected at the level of knowledge of the years 1970-1980 [5].

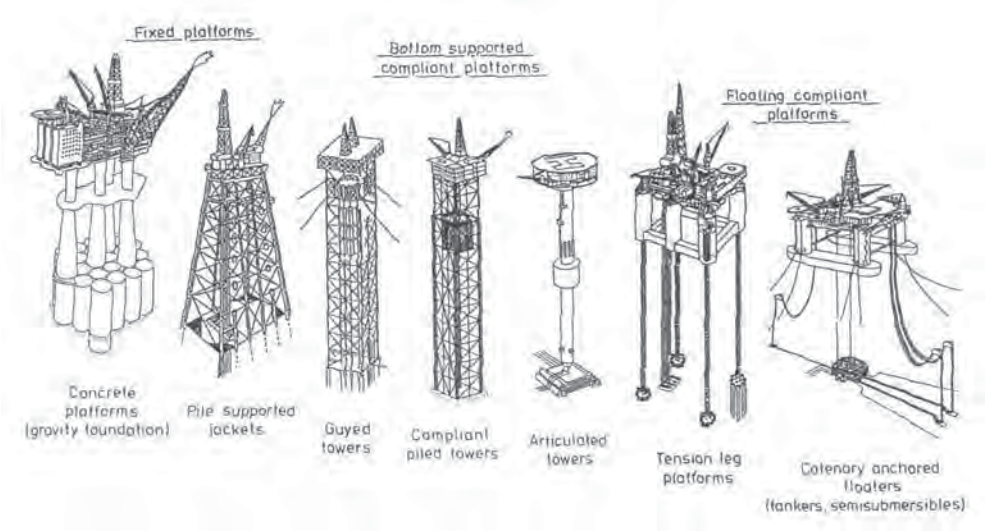

Figure 1. Offshore structure types.

It is known that during the years of 1990 a series of such structures collapsed worldwide, such as the Sleipner platform made from reinforced concrete) in the North Sea (figure 2, 3), an offshore structure made from steel in the area of Brazil's territorial waters etc.

During construction Perspective view Section views

Figure 2. Illustrations of the Sleipner platform.

The following factors underlay the occurrence of such accidents:

- misconceived structural analysis aspects (even using the most advanced computing programs and supercomputers);
- corrosion due to severe operating conditions in marine environment;
- imperfections during construction and assembling;
- great number of parameters which were hard to control;

- post critical structural behavior;
- mismatches between lab-test results and the real situation.

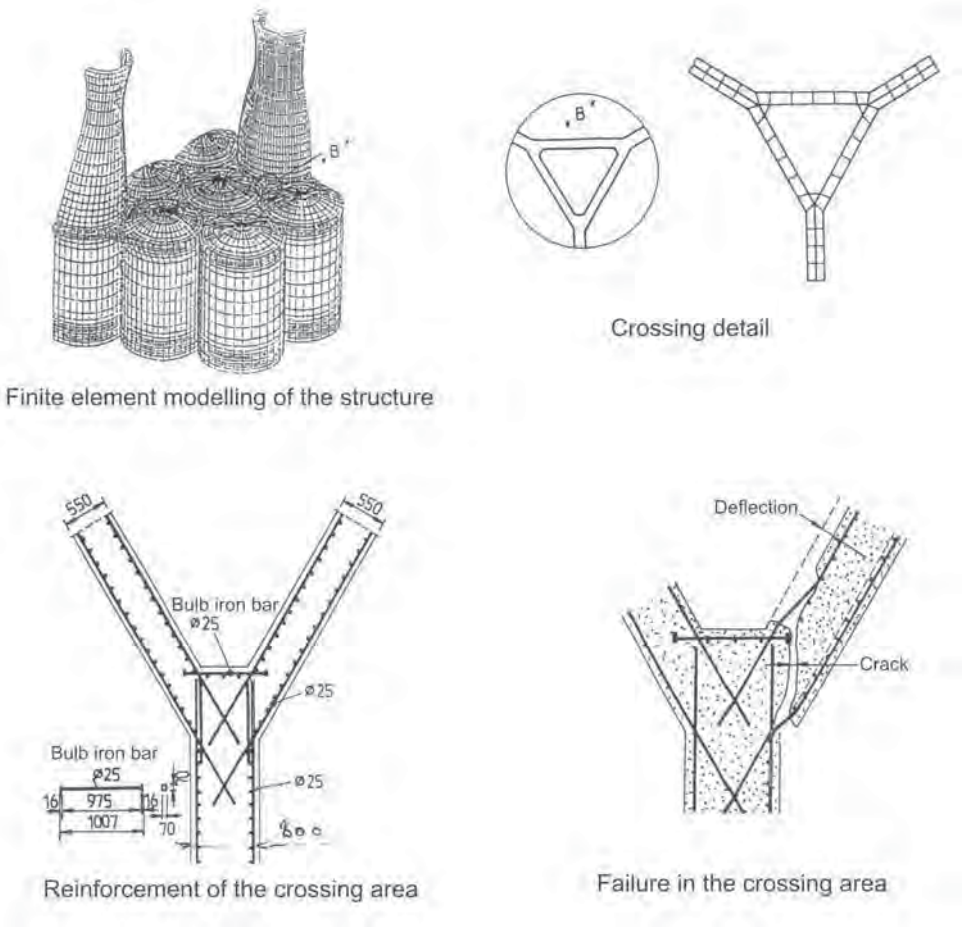

Figure 3.

In this paper the authors square up structural analysis aspects which are required for structural expertise in order to assess the level of safety of these kinds of structures in situ.

2. LOAD EVALUATION ASPECTS [6], [7], [8]

The permanent and non-persistent actions will be considered both by their lasting time and their time variation.

The evaluation aspects will relay upon a sternly hydro mechanical analysis (wave theory, hydrostatics and hydrodynamics). In case of floating offshore structures, the Archimedean modification of pushing forces will be considered

Model experiments and the simulation of some regular loadings on such structures have a distinctly relevance:

- sea rolling waves generated by intermittent wind having 150 ÷ 175 km/hour traveling speed,
- seismic waves (tsunami).

3. STRUCTURAL ANALYSIS ASPECTS AND PROBLEMS CONCERNING FATIGUE TEST [9], [10], [11], [12], [17]

Stresses in offshore structures are highly dependent from global stiffness (jackets coupling manner, cable inclination and tension etc.).

A dissimilar effect on stresses is coming from the vibration of these structures [13]. The effects of vibrations are originated from the frequency of the acceleration as well as from the reversing speed of the acceleration. These vibration effects are acting not only on the bearing structure, but also on the operating crew (there are persons to whom 0.01·g acceleration at a 1Hz frequency causes sensitivity).

The stress ranges are determined upon an elastic analysis of the structure from loadings caused by waves, wind etc. [14], [15], [16]. The action of waves has a dynamic character, similar to seismic action, but having a quasi-permanent persistence. These loads are determined from the hydrodynamic analysis considering the FROUDE-KRYLOV components, the incidental hydrodynamic mass etc.

The coupling between stress status and corrosion is well known. There is a slackness of the corrosion in case of compressive stress, and an accelerated corrosion in case of tensile stress.

In the same way there is a connection between fatigue loading and corrosion speed. The methodologies used for fatigue examination are based on the principle of the linear cumulating of damages (MINER), based on the prescriptions from:

- DNV – Det Norske Veritas (Norway);
- GL – the German Lloyd (Germany);
- ECCS – the European Convention for Constructional Steelwork,
- API – the American Petroleum Institute (USA).

In order to trail in site these kinds of structures, the authors are advising the permanent monitoring of the essential joints of the structure and the comparison of the behavior with a synthetically WÖHLER curve.

At the point when the loading spectrum is approaching to the curve, intervention can be instantly made.

This procedure allows displaying the contribution of corrosion on the level of the stress spectrum. The special tensomatic markers which are able to withstand marine environment are already on the market at a reasonable cost, the problem being resumed to the mounting and to the procurement of proper software.

The quantification or numerical computation of the stress spectrums can be done through the RESERVOIR method.

4. CONCLUSIONS

The recent collapses of some offshore platforms, although these were made using highly advanced technology, shows that structural expertise and examination works are indispensable for the existing platforms.

The emergence of any damage and the modification of the threshold for structural collapse impose a reasonable limitation of hazards. Lowering the risk to a certain level is done usually with uncommon financial exertion. Considering risk limitation actions, the expertise and eventually monitoring of these structures have an incommensurably lower cost than other measures, adopted usually on probabilistic bases.

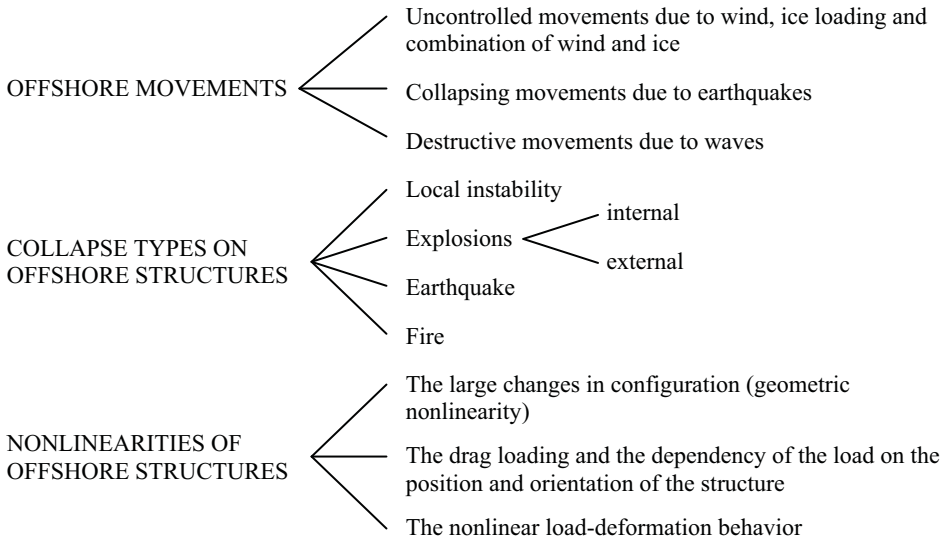

Figure 4.

In case of steel offshore structures, the actions which are causing sensitive modifications of the structural safety can be grouped in the following classes (figure 4):

- problems concerning base material quality (cold-flow, different brittle fracture types, lamellar fracture);
- problems concerning global and local stability (curling of thin walls and plates etc.);
- fatigue and repeated stress;
- creeping;
- problems concerning deformations induced by static and dynamic loads;
- corrosion and erosion problems.

The actual prescriptions need improvements in the way of extending the computing concepts related to the so called "structural" and "specific imperfections".

The fabrication and maintenance costs of the offshore structures made from steel are huge, due to the aspects mentioned in this paper. In such conditions o possible way and with spectacular results appears to be the using of reinforced concrete by the accomplishment of the offshore constructions. Alternative structures in this direction are presented in figures 5, 6 and 7, having the decisive advantage of corrosion withstanding, relatively simple erection ashore, simple anchoring in comparison with the special ones from steel structures.

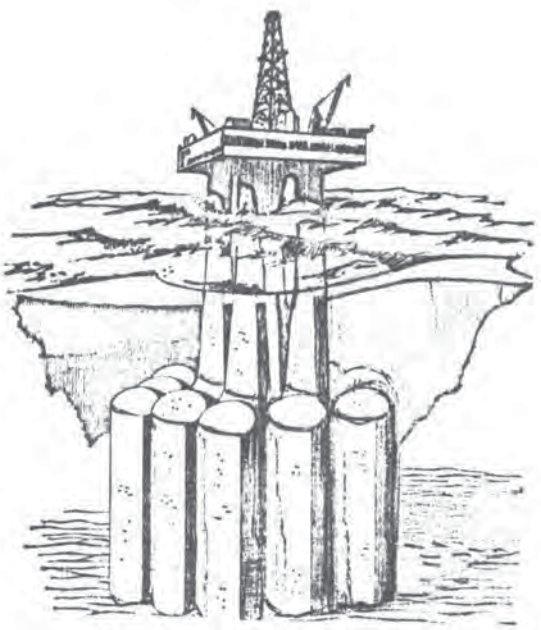

Figure 5.

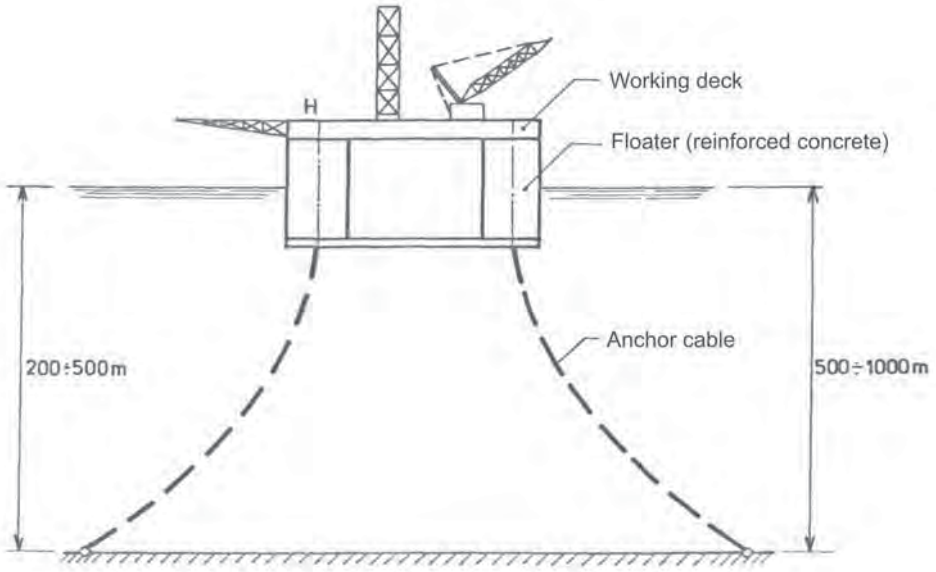

Figure 6.

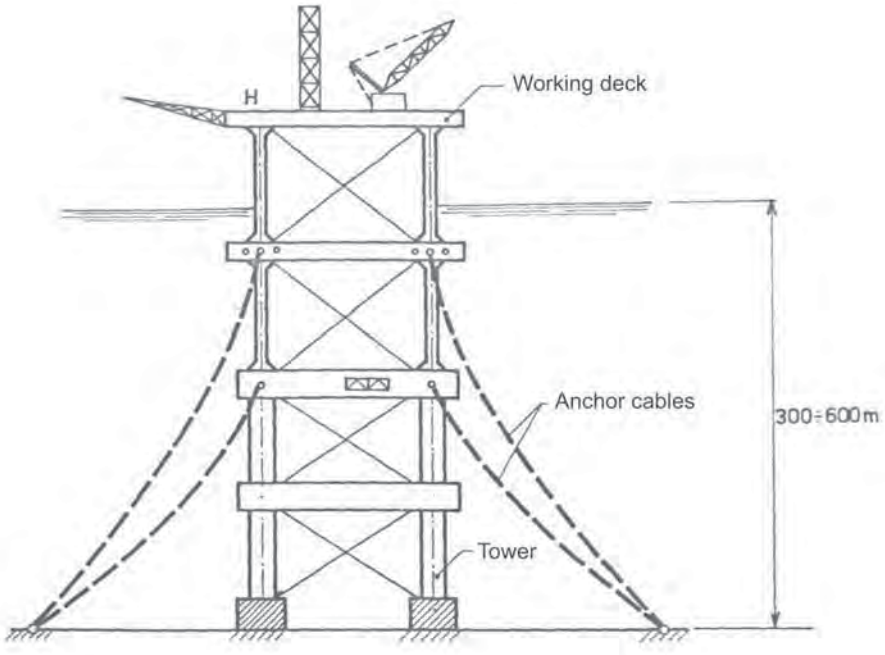

Figure 7.

The tackling of fatigue problems is advisable to be done through permanent monitoring and by comparing the stress spectrum with a synthetically WÖHLER curve.

Structural engineers dealing with such structures are advised to accept only those results which are confirmed by a simplified, but not shallow structural analysis.

References

1. Clauss, G., Lehmann, E., Östergaard, C., *Offshore Structures*, Springer Verlag, London-Berlin-New York, 1992.
2. Cătărig, A., Kopenetz, L., Alexa, P., Analysis Problems of Tubular Offshore Structures, *Proceedings of the Seventh International Symposium on Tubular Structures*, A. A. Balkema, Rotterdam, Brookfield, 1996.
3. Kopenetz, L., Cătărig, A., Practical Structural Dynamics of Marine Cables, *Ovidius University Annals, Series: Civil Engineering*, vol. 1, No. 6, 2004.
4. Kopenetz, L., Cătărig, A., Comportarea "in situ" a structurilor din oțel de tip Offshore, *Revista Construcțiilor*, Nr. 1, 2005.
5. CECM–TC6, *Recommandations pour la vérification à la fatigue des structures en acier*, CTICM Centre technique et industriel pour la construction métallique, Saint-Rémy-lès Chevreuse, France, 1987.
6. Brebbia, C. A., Walker, S., *Dynamic Analysis of Offshore Structures*, Nekines-Butterworths, London-Boston, 1981.
7. Kinsman, B., *Wind Waves, their Generation and Propagation on the Ocean Surface*, Prentice-Hall, 1965.
8. Hauptmanns, U., Werner, W., *Engineering Risks*, Springer Verlag, Berlin-London-New York, 1991.
9. Haibach, E., *Betriebsfestigkeit*, VDI-Verlag, Düsseldorf, 1989.
10. EUROCODE-3, *Design of Steel Structures*, 1993.
11. STAS 10108/0-1978, *Design of Steel Structures* (in romanian), 1978.
12. Dalban, C., et alii, *Construcţii metalice*, EDP, Bucureşti, 1983.
13. Kopenetz, L., Cătărig, A., Probleme de analiză structurală pentru consolidarea podurilor, *Simpozion Reabilitarea Drumurilor şi Podusilor*, Cluj-Napoca, 2000.
14. British Standard–BS5400, Part 10, Steel, Concrete and Composite Bridges, *Code of Practice for Fatigue*.
15. RP2A, *Recommended Practice for Planning, Designing and Constructing Fixed Offshore Platforms*, Washington, American Petroleum Institute, 1987-1989.
16. API-RP2A, *LRFD, its consequences for adoption to North Sea Offshore design practice*, Advanced Mechanics & Engineering Ltd, 1991.
17. EUROCODE-1, *Basis of Design and Actions on Structures*, 1991.

"Computational Civil Engineering 2007", International Symposium
Iaşi, România, May 25, 2007

Scenario and impact of global warming in building energy performance simulation

Petr Kotek[1,2], Jordán[1]
[1]*Department of Microenvironmental and Building Services Engineering, CTU Technical University in Prague, Czech Republic*
[2]*contact: kotek.petr@centrum.cz*

Summary

Building performance simulation (BPS) tools are more and more widely used in practice and developers are trying to facilitate and anticipate the settings of input parameter for ordinary users. BPS tools are used to determine the energy consumption, indoor environment and to diagnose heating and cooling load for relevant HVAC systems in the building under investigation. Every simulation model is still under a big uncertainty in input setup data in case of using BPS tool before the building is built. An uncertainty and sensitivity analysis (UASA) was performed in our latest research by using MonteCarlo simulation (with Latin Hypercube sampling). The aim of this research was to estimate the most influential input parameter for building envelop and other boundary condition.

From UASA was assumed the most influential input parameters such as outside temperature and sun radiation (OT, SR) which we (i.e designer) can not change or optimize. And moreover, these outside climate data are different every year. It means that if we use some reference climate database we will put a big uncertainty in simulation model and outputs are with a big different uncertainty every year.

This paper is focused in impact of different OT, SR during the year and mainly in point of view: "WHAT IF IN FUTURE". The climate is lunatic every year and we can see and feel that the temperature is slowly rising all over the world. Nowadays the question of global warming is more and more discussed. According Intergovernmental panel on climate change (IPCC) we performed a study how the energy consumption will change in predicted years according to IPCC scenario.

Two case studies were chosen for different scenarios of climate change First and second cases are one real administration building in Czech Republic, Prague. One is performed without thermal insulation on the wall construction and second with and is shown their appropriate sensitivity in point of view of climate change

KEYWORDS: climate change, IPCC scenario, sensitivity analysis, Monte Carlo simulation, Latin Hypercube sampling

1. INTRODUCTION

Uncertainty and sensitivity analysis by using MonteCarlo (MCA) simulation is a powerful method for estimation the most influential parameters and for clarifying how big the uncertainty in results is. The simple crude MCA simulation technique is shown on Figure 1. Inputs X_i can be for example thickness, density and conductivity of thermal insulation, transmittance of transparent construction, emissivity of opaque envelope or some inputs for HVAC components etc. [2]

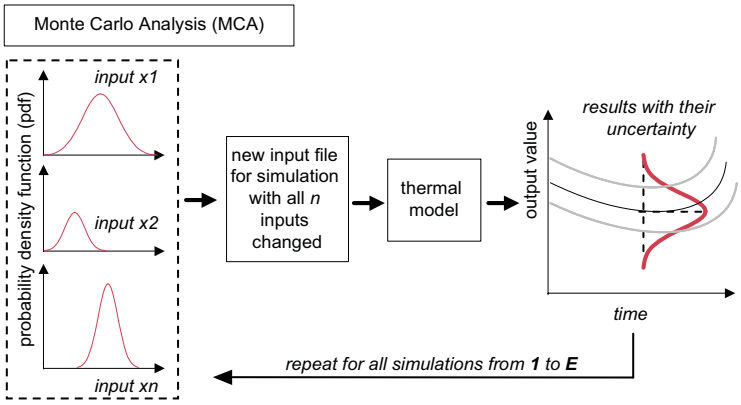

Figure 1. basic principle of MonteCarlo (MCA) simulation.

Many of them can be future optimize by using some optimization algorithm but some of these like outside dry bulb temperature and sun radiation could not. These not "predictable" inputs can bring huge uncertainty in results and they can influent heating and cooling load for HVAC equipment and change heating and cooling energy consumption every year. Whence it follows that if we use BPS tool for assessment energy consumption we have to present range of values where the real energy consumption per year probably will be. It means, that if we use some "old" climate database with average temperature for 50 or 30 years, we have to analyze these values, compare with measured values for 5 years backwards for example and performed new ones.

From Figure 2. we can see the difference between 30 years observation in Prague and actual measure temperature. From the chart we can also see, that the long term observation is little bit "colder" than nowadays temperature. From this we can say, that the distribution of the temperature is not normal during the year but more Beta distribution (with α=2 , β=5). It is obvious that if we use the "red" values for the building performance simulation we will have different output values instead of using the "blue" one.

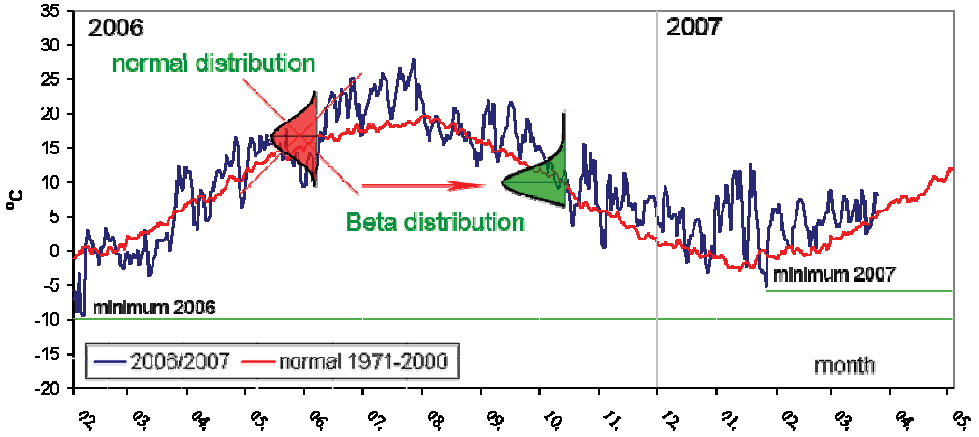

Figure 2. difference between long term observation and actual temperature in Prague

From the Figure 2. we can feel about, that the climate is wormer and wormer than long term observation. Also this winter 2007 a lot of people save money for paying heating bills because the temperature was so high.

And moreover in 2003, 2004, 2005, 2006 was the annual average temperature higher than observation among years 1971-2000 in Czech Republic (CR). Nobody knows if our planer will rapidly warming-up but all over the world we can see, that rising temperature changing a lot of thing just now.

In 1988 United Nations Organization (OSN) established Intergovernmental Panel on Climate Change (IPCC) by World Meteorological Organization (WMO) and by the United Nations Environment Programme (UNEP). IPCC reports are widely cited in almost any debate related to climate change.

The IPCC published a first assessment report in 1990, a supplementary report in 1992, a second assessment report (SAR) in 1995, and a third assessment report (TAR) in 2001. A fourth assessment report (AR4) is currently under way.

The IPCC has made a series of reports and scenarios related to climate change and these it can be find out in TAR. Statements of the IPCC or information from the TAR are often used as a reference showing a scientific consensus on the subject of global warming. An increasing body of observations gives a collective picture of a warming world and other changes in the climate system *(The global average surface temperature has increased over the 20th century by about 0.6°C)*

The TAR estimate for the climate sensitivity is 1.5 to 4.5 °C over the period 1990 to 2100. Each scenario then has a range of possible outcomes associated with it. The most optimistic outcome assumes an aggressive campaign to reduce CO_2 emissions, while the most pessimistic is a "business as usual" scenario. The more realistic scenarios fall in between. [6]

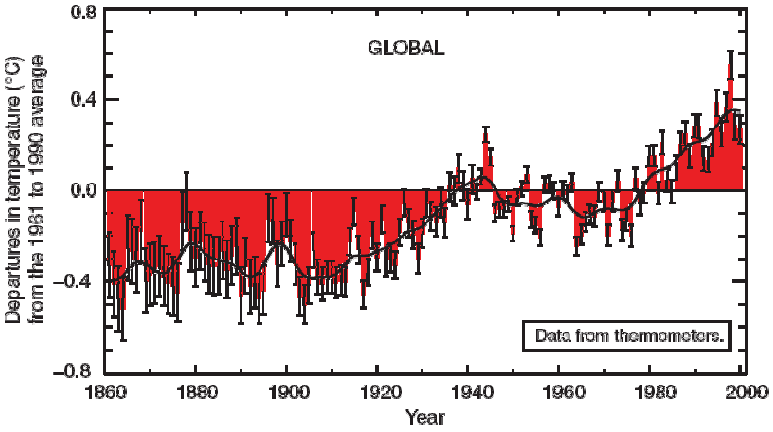

Figure 3. The 140 years observation of global temperature (IPCC)

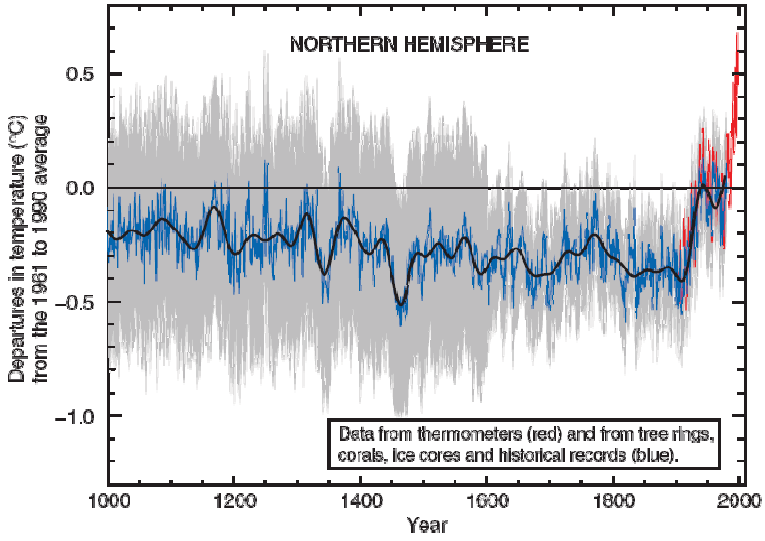

Figure 4. The 1000 years climate model observation of global temperature (IPCC)

According the IPCC long term observation (Figure 3., Figure 4.) we can see, that the Earth is really warming-up but maybe this is the normal "behavior"of our planet and it happened many times in the past. But maybe is it true and every single human on our planet making our planet warmer by driving car for example. This paper is based on work of 2500 scientist all over the world in 120 countries and we used the IPCC outcomes from their climate model as an input for our investigation. Investigation in point of view: How the heating and cooling energy consumptions will change over the period 1990 to 2100.

2. IPCC SCENARIOS

From TAR outcomes we used the scenarios

- Global mean temperature change (ºC) (Figure 5a.)
- Radiative solar forcing (W/m^2) (Figure 5b.)

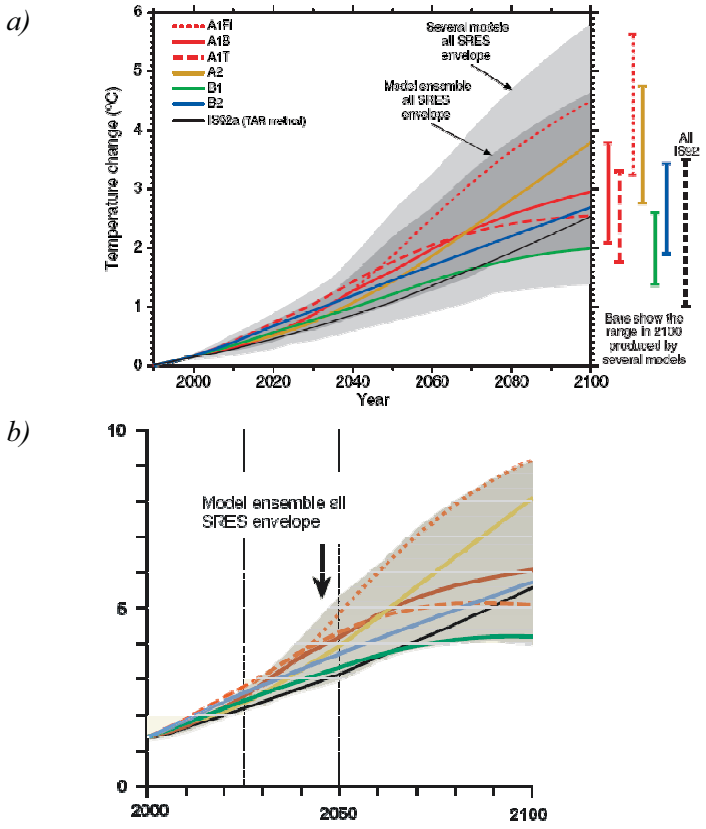

Figure 5. The IPCC scenarios *a)* temperature *b)* solar radiation

For creating new climate database it can be used crude MCA (via analysis in Figure 2. and prediction in Figure 5). But the pure MonteCarlo simulation cannot be applied for time-consuming problems such as dynamic BPS tool, as it requires a large number of simulations. A small number of simulations can be used for the acceptable accuracy of statistical characteristics of response using the stratified Latin Hypercube sampling technique LHS [1]. For our aim is enough to create climate database based on scenario B1 (lower bound) and A1Fl (upper bound) with uncertainty shown in Figure 2. The IPCC report also includes one inconsiderable

fact. Fact, that annual temperature is rising and also every year occur more days with extreme temperature in winter and summer. This fact can be seen on Figure 6.

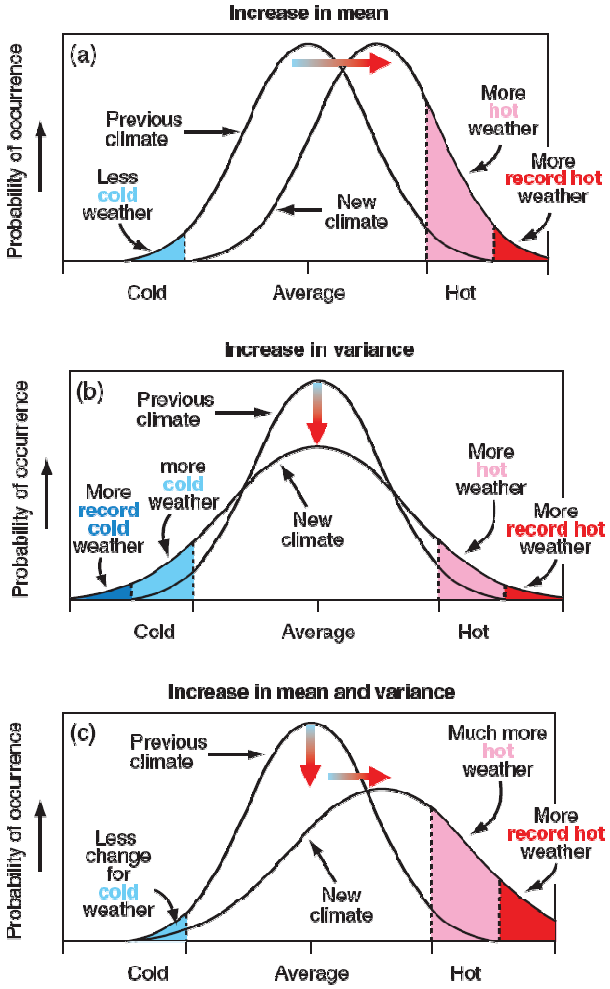

Figure 6. Globe mean temperature change and variance in future

3. PROGRESSION

For Czech Republic exist two *.epw climate databases – for Prague and for Ostrava city (see Figure 7.). These *.epw files can be download from EnergyPlus website free of charge. [8] and used for every king of BPS tool (ESP-r, Trnsys, DOE-2, Design Builder, IES<VE>, etc).

Figure 7. Czech Republic and marked two cities with available climate database

Sometimes these two climate databases are used for the whole Czech Republic and hereby bring big uncertainty in results. But this has not been considered in this paper. The case study (administration building) is in the capital city Prague and we will modify the downloaded climate file *CZE_Prague_IWEC.epw* with Weather Statistics and Conversions (WSC) tool developed by EnergyPlus. [8]

The statistical values for both climate databases are shown in Table 1.

Table 1. Statistical report of *CZE_Prague_IWEC.epw*

GPS / elevation	50°44' N, 14°29' E/ 364 m
Annual mean temperature	7.9 °C
Days in heating period	245
Average temperature during heating period	4.09 °C
min / max temperature	-15.2 / 30.5 °C
Hours with temperature > 0°C /year	7078 hours (295 days)
Hours with temperature ≤ 0°C /year	1682 hours (70 days)

By using EnergyPlus WSC tool the files were converted to the *.csv and exported to the MS Excel → modified for two scenarios (step 10years) and uncertainty made by SimLab [7]. These new weather files (12 for each scenario) were converted back to the *.epw file with WCS tool and used for simulations.

Table 2. Statistical report of *CZE_Prague_IWEC.epw* in 2100 according IPCC

	scenario B1 in 2100	scenario A1Fl in 2100
Annual mean temperature	10.4 °C	12.7 °C
Days in heating period	204	180
Average temperature during heating period	3.86 °C	4.22 °C
min / max temperature	-16.3 / 36.7 °C	-17.8 / 42.6 °C
Hours with temperature > 0°C	7393 hours (308 days)	7596 hours (317 days)
Hours with temperature ≤ 0°C	1367 hours (57 days)	1164 hours (48 days)

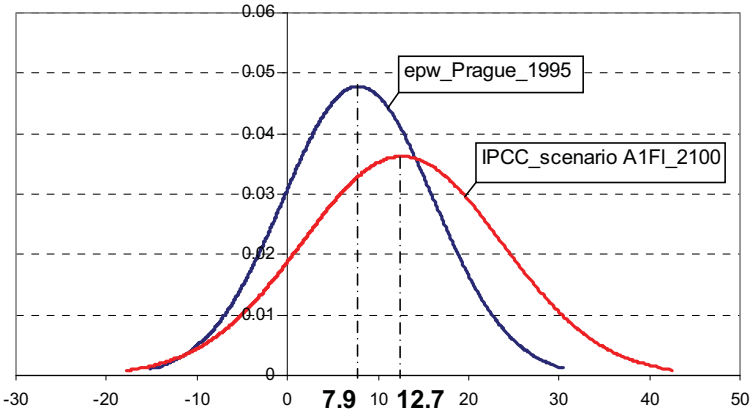

Figure 8. Globe mean temperature change and variance according IPCC for Prague

For this prototype we used IES <VE> [5] which incorporates ApacheSim, a dynamic thermal simulation tool based on first-principles mathematical modeling of building heat transfer processes. It has been tested using ASHREA Standard 140 [4] and qualifies as a Dynamic Model in the CIBSE system of model classification [3].

4. CASE STUDIES - ADMINISTRATION BUILDING

For the real administration building in Prague was performed two possible situations.

- **Adm.case A** without thermal insulation like many old building in CR
- **Adm.case B** with 8cm insulation on the wall.

Another construction and setting were used the same for both cases.

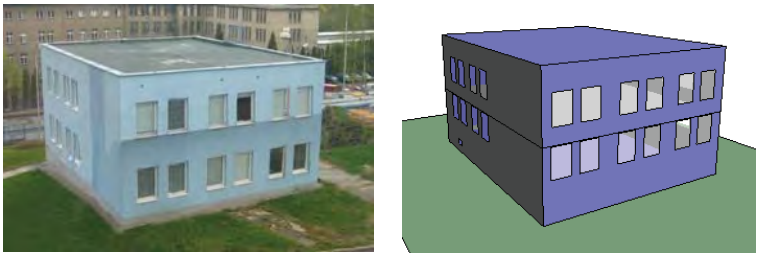

Figure 9. Photo of administration building and energy model in IES <VE>

The material prosperities for both cases can be found in Appendix 1.

Table 3. Basic proportions and settings of the building

Width x length x hign	12.4 x 15.3 x 8.1 m
Volume	1537 m^3
Area of glazing	18 %
Set point for heating - day / night, weekend	20ºC / 15ºC
Set point for cooling - day / night, weekend	24ºC / 32ºC
Working hours	6 - 18 hours

For these cases (adm.case A, adm.case B) were made new 48 “IPCC weather files” and for each one made 20 “uncertainty files” according probability distribution. The automatic simulation were performed during approximately 4 hours on Intel Core2 CPU T5500, 1.66 GHz, 1GB RAM.

5. RESULTS

Results shown in Figure 10 represents both cases in point of view energy load for heating (red curve) and cooling (blue curve) and annual energy consumption.

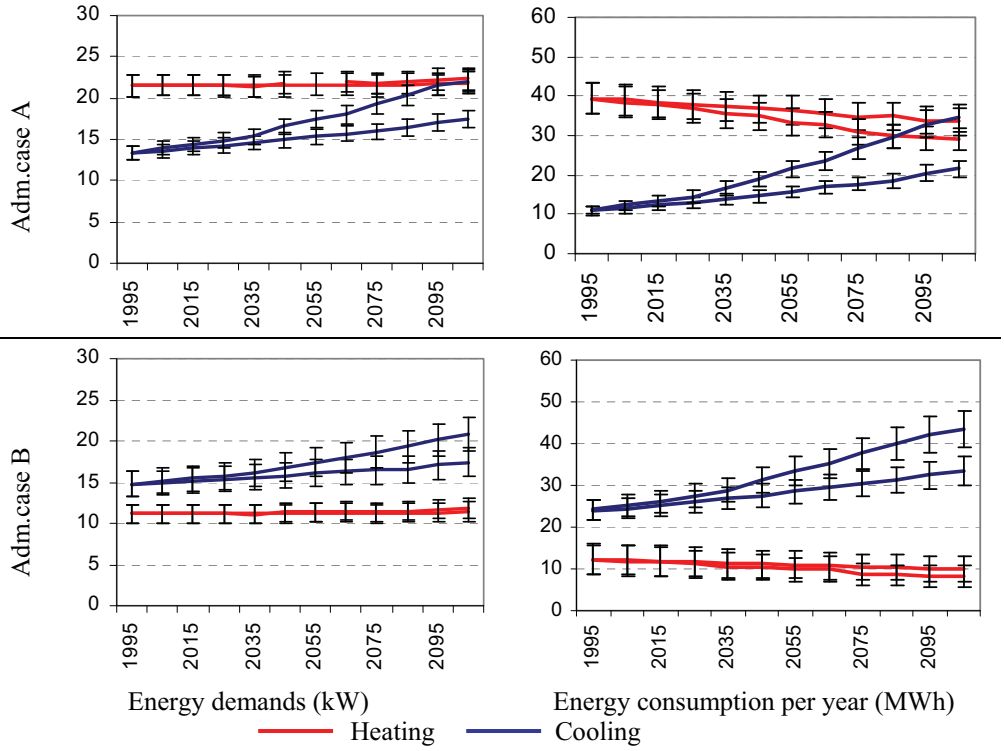

Fiure 10. Impact of global warming according scenario IPCC - the uncertainty in results on the basic shown in Figure 2 represents the black boundary.

From results in Figure 10 can be seen, that if the temperature and solar radiative forcing rise up, than heating load will stay almost the same. The annual heating will little bit fall down because of warmer winter. Obviously the huge impact will be in cooling demand and consumption. If we compare the results for non insulated and insulated building it is nice to see, that cooling demand will rise up from now in 2100 about 70%±10% (without insulation) and 40%±9% (with insulation) and consumption will be higher about 218%±21% (without ins.) and only 82%±12% (with ins.) This big difference is because of easier accumulation in the brick wall without insulation.

6. CONCLUSIONS

The aim of this paper is to show how big the impact of global warming can be in total annual energy consumption per year. The fact, that we will need more power for cooling bring together with higher temperature also higher pollution from cooling sources and the ozone hole will be bigger and bigger because of greenhouse gases. It is not obvious, that thermal insulation can also cut down the cooling consumption and it is time to do it for every single building not only because of reducing heating demand.

Acknowledgements

The authors thank for support CTU research aim No. CEZ MSM 6840770003

References

1. McKay M.D., Conover W.J. and Beckman R.J., A Comparison of Three Methods for Selecting Values of Input Variables in the Analysis of Output from a Computer Code, *Technometrics Vol. 21: 239-245.*, 1979.
2. Kotek, P., Jordán, F., Kabele, K., Hensen, J., T*echnique of uncertainty and sensitivity analysis for thermal and HVAC calculations*, IBPSA 2007, Beijing, Sep/2007. (not published yet)
3. Crawley, B.D., Hand, W.J., Contrasting the capabilities of building energy performance simulation programs, United States Department of Energy, University of Strathclyde, Wisconsin, 2005.
4. ANSI/ASHRAE Standard 140-2001, Standard Method of Test for the Evaluation of Building Energy Analysis Computer Programs.
5. IES <Virtual Environment> 5.1. Building performance simulation tool, http://www.iesve.com/content/ , last visited May 2007
6. IPCC-The Scientific Basis, Published by the press syndicate of the university of cambridge for the Intergovernmental Panel on Climate Change (IPCC), www.cambridge.org ISBN 0521 01495 6, 2001
7. SIMLAB Version 2.2. 2004. Simulation Environment for uncertainty and sensitivity analysis, developed by the Joint Research Centre of the European commission. http://simlab.jrc.cec.eu.int
8. EnergyPlus website: http://gundog.lbl.gov/

Appendix 1 - Thermal prosperities of administration building

Adm.case A - without thermal insulation

Wall Construction (outside to inside)

Layer	Conductivity [$W.m^{-1}.K^{-1}$]	Thickness [m]	Capacity [$J.kg^{-1}.K^{-1}$]	Density [$kg.m^{-3}$]	EN-ISO U-Value [$W.m^{-2}.K^{-1}$]
Outside plaster	0,190	0,0125	1000	800	
Brickwork	0,800	0,450	900	1700	1,21
Inside plaster	0,350	0,010	1000	1000	

Adm.case B - with thermal inslutaliton

Wall Construction (outside to inside)

Layer	Conductivity [$W.m^{-1}.K^{-1}$]	Thickness [m]	Capacity [$J.kg^{-1}.K^{-1}$]	Density [$kg.m^{-3}$]	EN-ISO U-Value [$W.m^{-2}.K^{-1}$]
Outside plaster	0,190	0,0125	1000	800	
Polystyrene	0,044	0,080	1270	20	0,38
Brickwork	0,800	0,450	900	1700	
Inside plaster	0,350	0,010	1000	1000	

Other construction	EN-ISO U-Value [W.m-2.K-1]
Roof	0,28
Ground Floor	0,9
Floor	0,84
Window	1,7
Glass door	1,7

"Computational Civil Engineering 2007", International Symposium
Iaşi, România, May 25, 2007

Settlement prediction of a pile group based on design charts

Irina Lungu[1], Nicolae Boți[2] and Anghel Stanciu[3]
[1]*Department of Roads and Foundations, Technical University, Iaşi, 700050, Romania*
[2]*Department of Roads and Foundations, Technical University, Iaşi, 700050, Romania*
[3]*Department of Roads and Foundations, Technical University, Iaşi, 700050, Romania*

Summary

The rehabilitation of transportation infrastructure is an on-going process that involves an increased complexity of bridges and retaining structures with corresponding complex requirements to comply with during service.

When the necessary bearing capacity is not provided by means of a shallow foundation, a deep foundation, i.e. a piles group is considered appropriate for both bearing and deformation requests.

Pile foundations represent current foundation solutions for these constructions, given the poor soil conditions often encountered on the construction site. Their design is based on the soil limit states – both deformation and bearing capacity. Settlement restrictions that are included with the deformation limit state require an accurate evaluation of the settlement prediction regarding the pile group.

Depending on the purpose of using piles for the foundation system, one of the following three cases will be the most suitable in a practical design: (a) the piles are supposed to carry the full load; (b) the piles will act as settlement reducers for the raft which is a less important bearing element of the foundation system; the piles are required to have a factor of point and shaft capacity safety somewhat greater than unity; (c) the piles are provided as settlement reducers but they will operate at a shaft factor of safety of unity, and piles of different length or stiffness are used . The raft is the principal bearing element of the foundation.

Sometimes, simple settlement calculations seem to be adequate for practical purposes provided that the appropriate in-situ soil properties have been carried out with engineering judgment. The errors introduced by the simple methods are usually small compared with those that can occur during sampling and testing.

The laboratory and field tests on single piles and pile groups as well as a careful monitoring activity of buildings with pile foundation have known a tremendous evolution, implementing all this in data base systems used in the computer field and advanced numerical methods for engineering purposes.

KEYWORDS: pile group, settlement, design charts, pile-soil interaction, single pile, Finite Element Method, Boundary Element Method.

1. INTRODUCTION

There is a strong intention to modify the actual capacity based design to a settlement based design when foundation systems on piles are concerned [1],[2],[5]. In pursuing this issue there are the following arguments:

- bearing capacity of the single pile is very sensitive to the pile installation procedure while its stiffness is less affected;
- bearing capacity of an individual pile in a pile group may significantly vary when piles have different dimensions and spacings, or when due to soil variation, the installation procedure may introduce some differences among them, while pile group behavior under loading intend to make this differences less significant;
- the connecting raft may deliver a significant part of the load to the subsoil by direct contact and in the same time, its influence on the foundation settlements may be less important [5],[39];
- when piles act as settlement reducers the most important factor that decide on the necessary number of piles is the differential settlement.

2. SETTLEMENT PREDICTION OF A PILE GROUP BASED ON THE SINGLE PILE BEHAVIOR

Considering that the single pile rigidity was established by load tests on single piles, the stiffness of a pile group may be quantified through the use of an efficiency, η, the inverse of the group settlement ratio, R_s, defined as:

$$\eta = \frac{1}{R_s} = \frac{k_p}{nk_1} \tag{1}$$

with k_1 - pile-head stiffness of a single pile; k_p - stiffness of the pile group (in terms of average settlement).

To a first approximation, the group efficiency was taken as a simple power law of the number of piles in the group, as: $\eta \approx n^{-e}$, therefore the group stiffness becomes: $k_p \approx n^{1-e}k_1$ [3].

The exponent, e, generally lies in the range of 0.3-0.5 for primarily friction piles, rising to 0.6 or higher for end bearing piles. Fleming presented a set of design charts (figure 1) in terms of a base value ,e_1, and four correction factors c_1 to c_4, as indicated in the equation:

$$e = e_1(l/d)\cdot c_1(E_p/G)\cdot c_2(s/d)\cdot c_3(\rho)\cdot c_4(\nu) \tag{2}$$

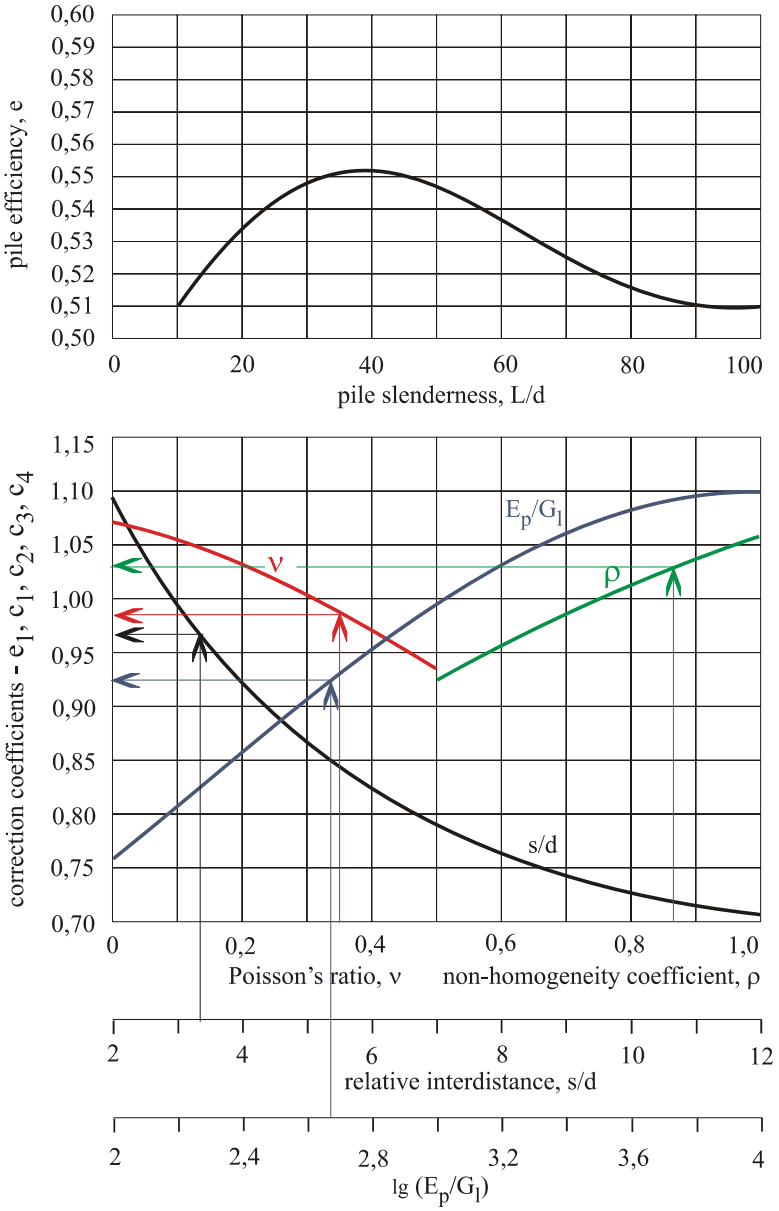

Figure 1. Design chart to evaluate the pile efficiency

The simple use of efficiency factors does not provide any indication of the increased proportion of load carried by the pile bases in a group of piles - and thus the greater importance of underlying soil strata compared with the case of a single pile [5].

Poulos [2] pointed out that since the base response is generally more non-linear than the shaft response, this may lead to lower group efficiency than using linear elasticity. But ignoring non-linear effects will overestimate the interaction between piles, which will compensate for overestimation of the base stiffness.

3. COMBINATION OF BOUNDARY ELEMENT WITH FINITE ELEMENT APPROACH

Hain and Lee [4] developed a method for pile raft settlement prediction which included a finite element approach for the raft and a boundary element approach using Mindlin's solution for the pile group interaction (so called raft on a pile reinforced continuum).

The model considers a variable stiffness raft of any geometry supported by a random group of identical piles and a soil mass idealized as an elastic continuum.

Consideration is given for a deep homogeneous mass, a modified linear elastic analysis for a layer of finite thickness, a failure of individual piles at load less than the total group capacity by applying an excess load cut-off procedure.

Four types of interactions are included in this approach and represented in figure 2.

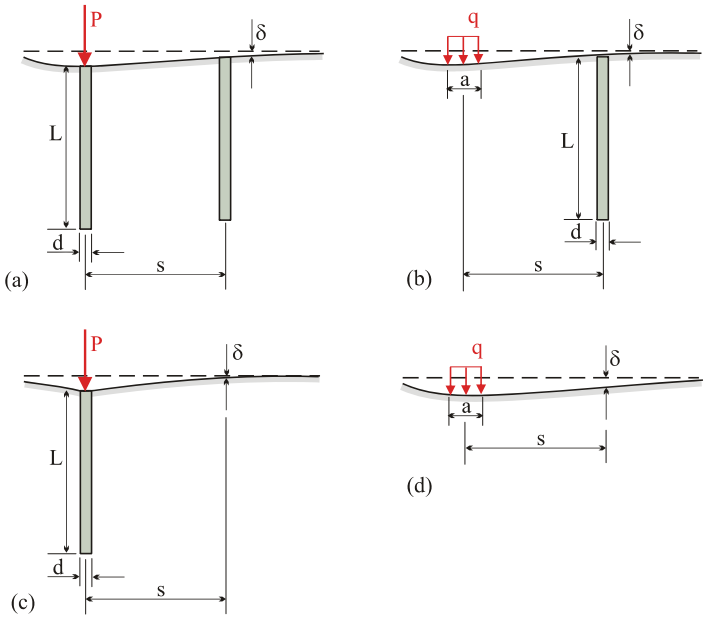

Figure 2. Pile-soil-raft interactions – basic representations

Imposing the compatibility and equilibrium conditions between the soil-pile group system and the raft a set of stiffness equations can be formed. Two assumptions are involved:

- only vertical forces are transmitted from the raft to the pile heads;
- each pile occupies the whole of the "constant pressure" area around a particular node.

These assumptions can not be appropriate to be applied for the analysis of piled isolated footings where lateral forces and overturning moments are the major proportion of the applied loads.

The pile compressibility is also considered and as a conclusion, the author stated that the percentage of load suported by the pile group diminishes as the pile compressibility increases.

A decrease in the length of the piles had the similar effect on the load distribution in the foundation system. The final results with all the influences assessed at the begining are presented in figure 3 as design charts.

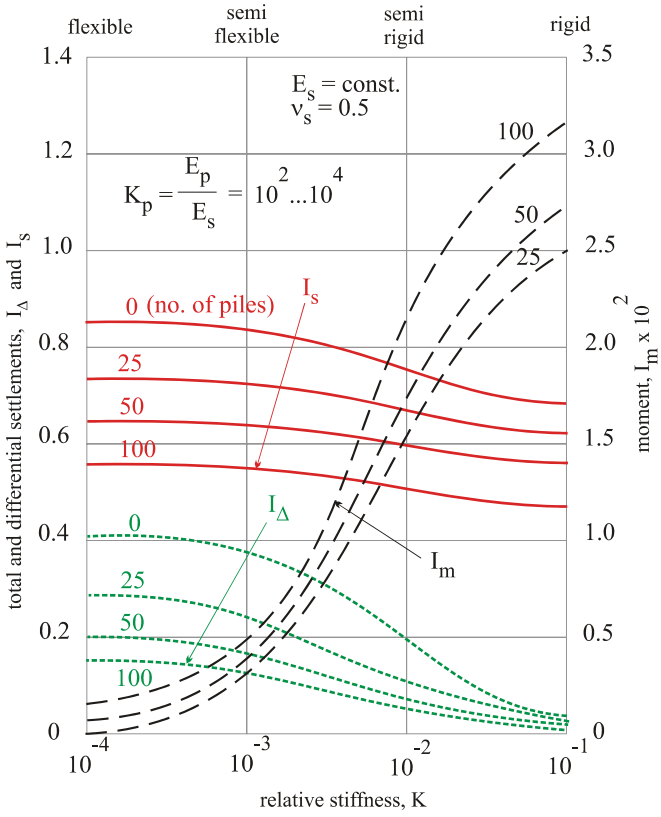

Figure 3. Design charts with parameters influencing the pile group behavior under vertical loads

The method is considered the first attempt in considering a sound interaction in a piled raft foundation with the limitations of a linear elastic behavior of the soil, a regular pile arrangement: the raft and piles with the same length and geometry [5].

4. CONCLUSIONS

The stiffness of a single pile becomes more important in design practice not only by its value but for learning the motivation of a suggested procedure in the available literature and thus to be able to make a sound engineering judgement each time a new case comes up.

Design charts proved to be useful tools to set comparative values at work in order to select the foundation elements in the best combination to face even the most pessimistic hypothesis of soil-foundation interaction. A successful and economic design is reached only when the interaction effects are taken into account.

References

1. Van Impe, W.F., *Developments in pile design*, DFI Conference, Stressa, 1991
2. Poulos, H.G., *Foundation economy via piled-raft systems*, Piletalk International, K. Lumpur, Malayesia, pp 97-106, 1991
3. Fleming, W.G.K., A new method for single pile settlement prediction and analysis, *Géotechnique*, vol 42, no 3, pp 411-425, 1992
4. Hain, S.J. and Lee, I.K., The analysis of flexible raft-pile systems, *Géotechnique*, vol 28, no 1, pp 65-83, 1978
5. Lungu, I., Teză de doctorat, *Contribuții privind conlucrarea între terenului de fundare, fundație şi structura de rezistență*, Iaşi, 1997

"Computational Civil Engineering 2007", International Symposium
Iaşi, România, May 25, 2007

The importance of controlling subsystem in information systems for building industry

Peter Mesároš[1], František Mesároš[2]
[1]*Department of Management Sciences, Faculty of Business Economics, University of Economics, Košice, 04130, Slovakia*
[2]*Research Institute of Building Informatics Ltd., Košice, 04001, Slovakia*

Summary

The paper presents various aspects and opportunities of using information systems and information technologies in building industry considering their impact on competitiveness. Especially we focus on new subsystem of controlling and its integration in corporate information system. It is a contribution to the research project Nr. 2330256/07 of University of Economics in Bratislava, named Knowledge Management as Assumption of Successful Development of Slovak Enterprises.

KEYWORDS: information systems, information technologies, controlling system, building industry

1. INTRODUCTION

An increasingly rapid change and development in the business environment of building firms have been noted in recent years. The growth of domestic as well as foreign competition creates a constant pressure on intensive exploitation of the latest information technology, innovation of products and increase in the quality of construction performance. This appears to be the way of acquiring a competitive advantage and achieving the building firm prosperity. Important factors of prosperity are mainly composed of:

- profit which is not formed at the expense of the future gains,
- short-term liquidity and long-term capacity of funding,
- economy of the whole firm with an accent on economization and quality of the construction performance,
- effectiveness in using relevant information and information technologies for its processing in order to achieve competitiveness.

Managers in the building firms, even despite the fact that various programme systems have already been introduced in the corporate information systems, report on the lack of relevant current and exact information related to the corresponding dates and suitable form of decision making in an efficient and effective way. The current corporate information systems in the building industry are not capable of

providing the information that is needed by managers. In connection with this, it is particularly the information required for:

- comparing the plan and reality as to the ongoing conduct of the building i.e. the information necessary for the ongoing management of profit and costs of the construction,
- making the deviations analysis as compared to the planned state,
- rapid conduct of calculation with providing the data for the needs of further measures to eliminate the deviations from the plan.

The current information systems do not assure a rapid indication of problems and analysis of their causes with the proposal for their elimination (Čarnický, 1999). Managers can find this information in a huge amount of data concerned with the plan, accounting, marketing, various reports, etc. They select only certain information, make their own analysis in order to make the optimum decisions. However, this activity is rather time-consuming and not so effective, as a result of this process – making a relevant directing decision – appears to be frequently rather subjective and intuitive. Similar associations are also mentioned by various other authors (M. Kozlovská, 2002). In recent years a large business has grown up around the subject of information systems and information technologies and its implementation in business practice of all industries of national economies. ICT companies and management consultants have developed methods and techniques for identifying and agreeing investment in information systems that support business strategy and create new strategic options and build the competitiveness. Information technology has changed the nature of competition and has created new opportunities for using information services. Using a technology to reduce the cost of building company activities or to add value to existing products and services can provide a competitive advantage.

2. INFORMATION SYSTEMS FOR BUILDING INDUSTRY

2.1. ERP systems and its exploitation in building companies

According to Wikipedia definition, Enterprise Resource Planning systems (ERPs) integrate all data and processes of an organization into a unified system. A typical ERP system will use multiple components of computer software and hardware to achieve the integration. A key ingredient of most ERP systems is the use of a unified database to store data for the various system modules.

Enterprise Resource Planning is a term originally derived from manufacturing resource planning (MRP II) that followed material requirements planning (MRP). MRP evolved into ERP when routings became major part of the software

architecture and a company's capacity planning activity also became a part of the standard software activity. ERP systems typically handle the manufacturing, logistics, distribution, inventory, shipping, invoicing, and accounting for a company. Enterprise Resource Planning or ERP software can aid in the control of many business activities, like sales, marketing, delivery, billing, production, inventory management, quality management, and human resource management. ERPs are cross-functional and enterprise wide. All functional departments that are involved in operations or production are integrated in one system. In addition to manufacturing, warehousing, logistics, and Information Technology, this would include accounting, human resources, marketing, and strategic management.

Implementing ERP software is typically not an internal skill, so even smaller projects are more cost effective if specialist ERP implementation consultants are employed. The length of time to implement an ERP system depends on the size of the business, the scope of the change and willingness of the customer to take ownership for the project.

2.2. Controlling subsystem – new component in ERPs for building industry Special applications

In our view, controlling presents a specific form of work with information, its gathering, processing, evaluating and providing for the needs of managerial performance and decision-making. From the point of view of time, two main directions have been formed, namely the strategic and operational controlling. The strategic controlling is aimed at direction of a long-term detecting of the business company potentials. Externally, it analyzes the threats and opportunities. The operational controlling directs its activities within the given profit potential. Its aim is the optimisation of subject, time and value parameters of the corporate activities aimed at achieving the prosperity and profit in the process of building production conduct.

2.2.1. Assumptions of Controlling Subsystem Implementation

In the controlling subsystem the existing databases are used that have been formed within the calculation-planning subsystem (ex ante information) and the database of personal and economic information subsystem (ex post information). A simplified connection of the given subsystems and their groups is illustrated in Fig.1 and Fig. 2.

The data are taken from the group of tasks *Production calculation* that presents the proposed economic and capacity expression of technical, technological, material and organizational performance of the object construction or just a part of it. A whole range of data can be found here, namely the limit ones, the norm/standard/ and planned data for the whole construction, an object, or a part of it. Continuously

once a month, these data are taken from the group of tasks *Production billing* for the concretely undertaken volume in the given construction, object, part, or an order.

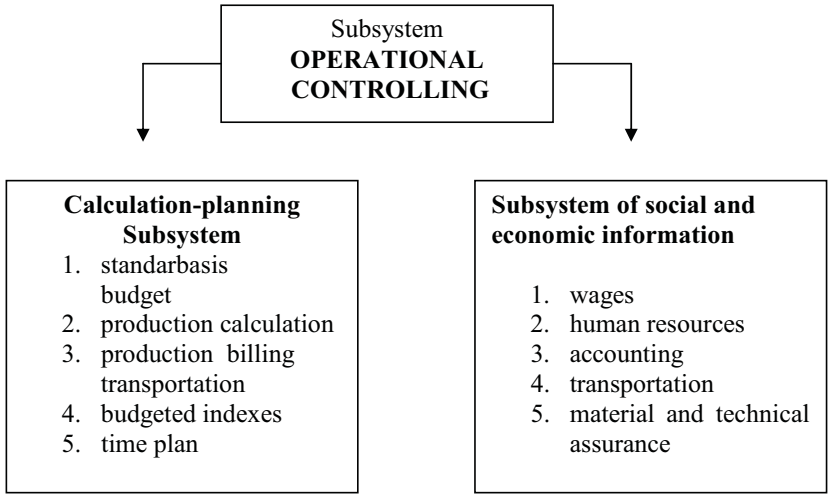

Figure 1. Operational controlling as a subsystem of the information system

The production billing uses the same standard basis as the production calculation. The production billing (PB) is calculated as a multiplication of the data of the real vector of production (Q sk) and the data from the standard basis (SB).

$$PB = Qsk * SB \tag{1}$$

The production billing can be processed from:

- organizational points of view for orders, or objects when the order includes more objects (constructions, centres, centre of costs, division, plant),
- the point of view of time in a month, exceptionally even a shorter time period (summarized quarterly, annually, for the whole order).

The area of drawing the building costs: The tool for performing this activity is accounting. Even smaller enterprises should have an independent area of the so-called (managerial) accounting of costs. The accounting of costs enables to use such procedures and methods of accounting that are not allowed for financial accounting. The objective of this procedure is to enable to define the respective volume of variable costs and to find the so-called contribution profit (a contribution to cover the fixed costs from the profit production) at every calculation unit, centre, etc.

The essential difference between adding the costs to the financial accounting and accounting of costs consists in the fact that:

- financial accounting is managed by the accounting classes for the needs of making a record on the profit and losses. The so-called balance sheet and therefore the main criterion here, is a strict evidence of documents;
- accounting of costs is more governed by the principle of causality. The basic kinds are classified with an accent and in dependence on certain decisions so that they could directly enable the respective management measures.

The data on the reality are mainly taken from the group of tasks of intracorporate accounting in the structure defined within the calculation-planning subsystem in connection with the organizational structure of the given building firm. For example:

EC - economic centre

CC - costs centre

EA - economic activity

CU - calculation unit/entity (construction – object)

Therefore, it is inevitable to create a code of numbers of the actual suppliers in the structure - a plant, EC, CC, EA.

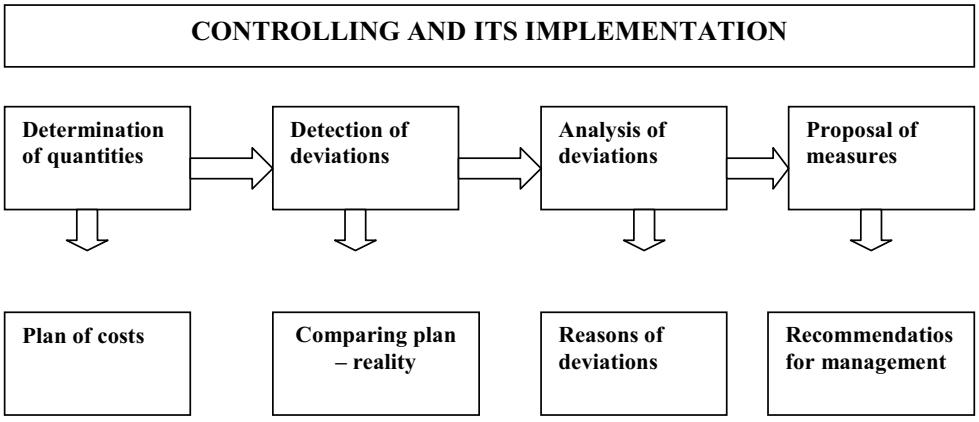

Figure 2. Content of activities and procedural steps in the controlling subsystem

Within the controlling subsystem even the links to the material and technical supply for the purposes of continuous comparing the planned material need with the real material use, not only in the financial but also in the material expressing, are defined as well.

When selecting the followed indexes the individual building firms themselves determine the type of indexes, as well as the extent and degree of details. However,

their extent is given by the principle of effectiveness of the information system. It is required that the costs for their provision are lower than the effects provided by the detected deviations and accepted decisions.

2.2.2. Advantages of implementing and exploiting the controlling subsystem

The advantages arise from technically calculated and justified norms of manufacturing and technical character of unit costs elaborated by the Department of manufacturing and technical preparation of production. Thus, controlling

- contributes to the prosperity of a building firm,
- creates presumptions for acquiring a higher quality of building work
- help achieve rapid outcomes of costs drawing in the course of construction (once a month at the minimum), i.e. not after the completion of construction,
- serves to common check-up of drawing the individual costs for the construction,
- enables to carry out a detailed analysis of deviations, provides the possibility of analysing the causes of their origin and points to the divisions responsible for their origin,
- has a psychological significance since it upgrades the motivation of workers towards savings (as this method enables a preventive check-up of costs drawing, it also motivates the workers towards higher responsibility for their own economic behaviour),
- creates pressure towards the perfect arrangement of organizational relations among divisions, sticking to the technical, technological and organizational conditions of the construction performance,
- enables to evaluate the effectiveness of production divisions activities as well as the activities of divisions of pre-production and production preparation (Trávnik, 1998), e.g. incomplete project documentation of the construction with a poor quality, on the basis of which the technical preparation of the construction is elaborated. The production calculation may thus cause rather great deviations from the norms that are not due to production but are generally ascribed to production,
- enables to analyse continuously the objectivity of understanding the right overheads for the respective construction job,
- provides important data for the analysis of the secondary budgeted costs that are often incorrectly accounted within the construction overhead costs.

In the context of the above said it is highly recommended to set up a position of the controller who, on the basis of his knowledge and practical experience, could analyse the detected deviations between the plan and reality. He thus assures the working of information flows, i.e. provides objective information for decision-making on the basis of real processes taking place in the construction.

Within his work capacity, the controller assures the following tasks, in particular:

- prepares supporting documents for planning and decision-making,
- processes the methodological materials, regulations for processing the normative basis of the enterprise, production calculations, budgets, production billing, budgeted indexes, supporting papers for a follow-up of production cost indexes in the intracorporate accounting,
- follows the legal acts in the field of pricing, accounting, calculations, statistics, taxes, etc., and tries to implement them into the corporate information system as soon as possible,
- provides methodological counselling in the given areas for the enterprise workers.

The setting of the controller tasks provides only a framework of his activities. Therefore, it is rather necessary to take into account the specific features of every building firm as well.

3. CONCLUSIONS

Application of the controlling subsystem appears to be a relatively simple and transparently conceptual fact. It assures the complex approach and presents an effective form of acquiring, processing and interpreting the information on the costs and profit, which support decision-making and formulating the strategy by managers. It gives presumptions for increasing the efficiency of a building firm and its prosperity according to the objective indexes. It enables to act successfully in the competitive environment as well as to respond to constantly increasing requirements of investors to the quality of building production.

References

1. Čarnický, Š., Why the top management workers need executive information systems? *Acta Oeconomica Cassoviensia N3*, Faculty of Business Economics Košice of the University of Economics in Bratislava, 1999.
2. Kozlovská, M., Management of purchasing, *Eurostav*, vol. 8, 2002.
3. Mesároš, F., Mesároš, P., Information Systems Strategy in Building in Industry, *Economics and Business Management*, vol. 1, 2003.
4. Trávnik, I., et al., *Directing the building work value,* Slovak Technical University in Bratislava, Bratislava, 1998.

"Computational Civil Engineering 2007", International Symposium
Iaşi, România, May 25, 2007

Analysis of Water Consumption in Residential Building

Roman Musil
CTU in Prague, Faculty of Civil Engineering, Department of Microenvironmental and Building Services Engineering, Thákurova 7, 169 34 Prague 6,e-mail: roman.musil@fsv.cvut.cz

Abstract

This paper consider about measurement consumption of cold water in residential buildings. In the year 2005 ran over extensive monitoring cold water consumption in 62 residential building in Pilsen implement by waterworks Pilsen with cooperation department of microenvironmental and building services systems in Prague. The paper considers about analysis this measurement and comparsion with Czech norm and prescriptions. There will be evaluate daily and hourly maximal coefficient cold water take-off and daily and hourly cold water consumption profiles for residential buildings.

Keywords

monitoring, residential building, water consumption

1. INTRODUCTION

Need and consumption of cold water in residential building is magnitude which is not initial only for dimension supply water systems but it shows life style and user consumer habits. This value is evolving and changing with society development. Impact on user behaviour is in relation prices development. The second aspect is technical building facilities development in hot water preparation which enables using flexible facilities reacting on variable water needs.

2. WATER NEED

Water need is supposed take-off while consumption is the real take-off water amount for certain time period. Water consumption assessment is input value which is covered with sufficient equipment capacity for water supplying. Problem is when consumption is function of time and we have to observe it in different time scale. Therefore water need assessment isn't possible simplify to one value but time period has to be written by more parameters which are:

- water need during the chosen period (specific water need)
- water take-off during time period distribution

Basic statement is specific water need qp. This value is given in dependence on kind of operation and activity in designed building. It is water need per basic consumption unit (person, bed, eat,…) and it is in liter/(unit*day). Probably water losses from source to consumer are included in specific water need. Probably water losses are supposed about 20%. State specific water need for residential buildings according to valid Czech public notice number 428/2001 sb. are in table 1.

Table 1. Specific water need [m^3/person/year] according to valid Czech notice 428/2001 for residential buildings.

Specific water consumption for flats during the year	Specific water need in m^3/year
flats with only cold water outflows	16
flats with only cold water outflows and collective WC	25
flats with only cold water outflows and WC (without bathroom)	31
flats with only cold water outflows,WC, bathroom with solid fuel stove	41
flats with only cold water outflows,WC, bathroom with flow heater or electric boiler	46
flats with WC and bathroom with central hot water preparation	56

3. WATER NEED ASSESSMENT

We calculate with subsequent values for assessment of water need whichever object:

1) Daily average water need

$$Q_P = q \,.\, n \;\; [\,l/d] \qquad [1]$$

Where:

q – specific water need (liter/unit/day)

n – number of unit

3.1 Daily maximum water need

Facilities for water take–off from source, capacity of water and water pipelines for supplying water to water–supply tank are designed on maximal water need.

$$Q_m = Q_P \,.\, k_d \;\; [\,l/d] \qquad [2]$$

Where:

Q_p – average daily water need

k_d – daily inequality coefficient

Table 2. Take-off daily inequality coefficient [ČSN 736701]

size of urban area (people)	do 1000	1000 - 5000	5000 - 20 tis.	20 tis. - 100 tis.
$k_{d\,(-)}$	1,5	1,4	1,35	1,25

3.2 Hourly maximum water need

We dimension facilities for supply water to consumers on this value. Running of vary hourly need is use for dimension of pumping device which supply water directly to consumers (for example pumping station for increasing water pressure). Hourly water need is one value from component for assessment of water-supply tank value.

$$Q_{h,\,max} = Q_m \,.\, k_{h,\,max} \,.\, z \;\; [\text{ l/hod}] \qquad [3]$$

3.3. Hourly minimum water need

$$Q_{h,\,min} = Q_m \,.\, k_{h,\,min} \,.\, z \;[\text{ l/hod}] \qquad [4]$$

Where: Qm – daily maximum water need [l/day]

kh, max – hourly maximum inequality coefficient

kh, min – hourly minimum inequality coefficient

z – take-off water period – residential building a hotels z = 24 hours

– administrative buildings z = 10 hours

Balance values Q_m and Q_h serve to accumulate reservoir and automatic pumping station designing which are components of internal water-supply. Determination of daily and hourly inequality coefficient is very complex for residential and civil buildings. These coefficients depend on various factors. Water need during day is unequal and depends on building operation character, on yearly season, temperature change, flat and house furniture of building services water systems, on social and age of user groups and their behavior. Water take-off varies during week too.

In 2005 year went ahead wide monitoring water consumption in 62 residential buildings in Pilsen practiced by the waterworks Pilsen in cooperation with Department of Microenvironmental and Building Services Systems, CTU in Prague. Monitoring on cold water was done in 3 week period by water meter fixed on building foot with hourly period saving measured values. These values are primarily determined for processing stochastic loads profiles and mathematical urban space modelling. Final values don´t include hot water which is supplied to building by centralized heating system. Evaluate measurement results are in next graphs.

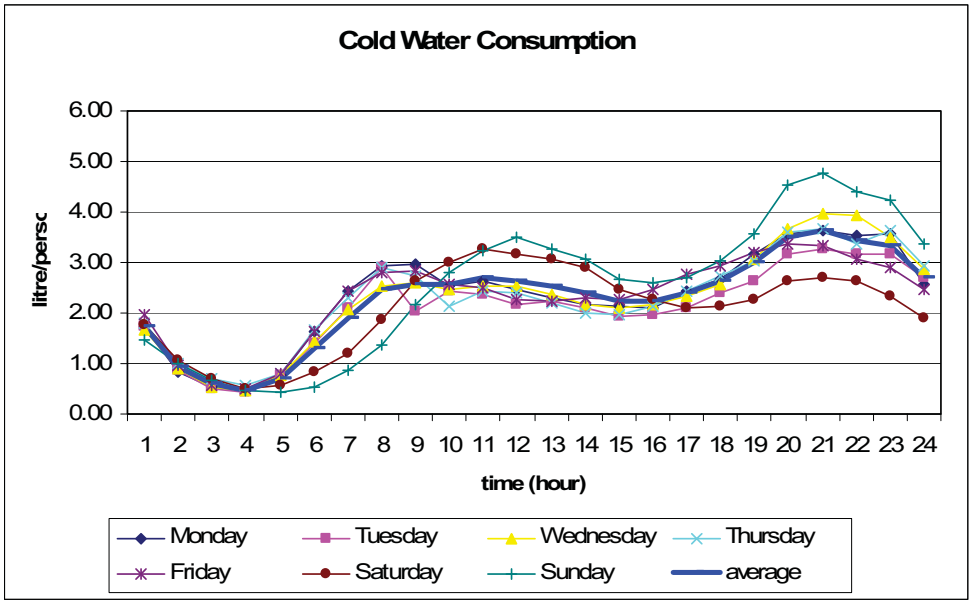

Figure 1. Daily cold water consumption during week

Table 3. Comparsion of hourly inequality coefficient in several days with average value

number of inhabitants	50	75	300	400	500
Monday	108%	100%	100%	98%	103%
Tuesday	109%	104%	108%	107%	108%
Wednesday	96%	113%	100%	98%	99%
Thursday	96%	100%	96%	102%	97%
Friday	106%	90%	92%	88%	90%
Saturday	85%	87%	98%	97%	96%
Sunday	101%	106%	106%	110%	107%

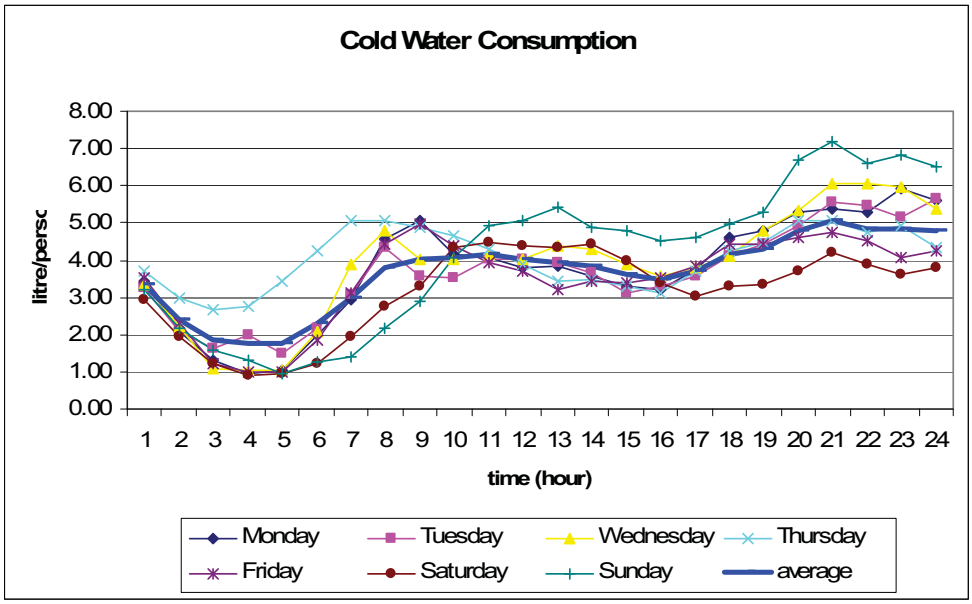

Figure 2. Maximal cold water consumption during week – envelope curve [2].

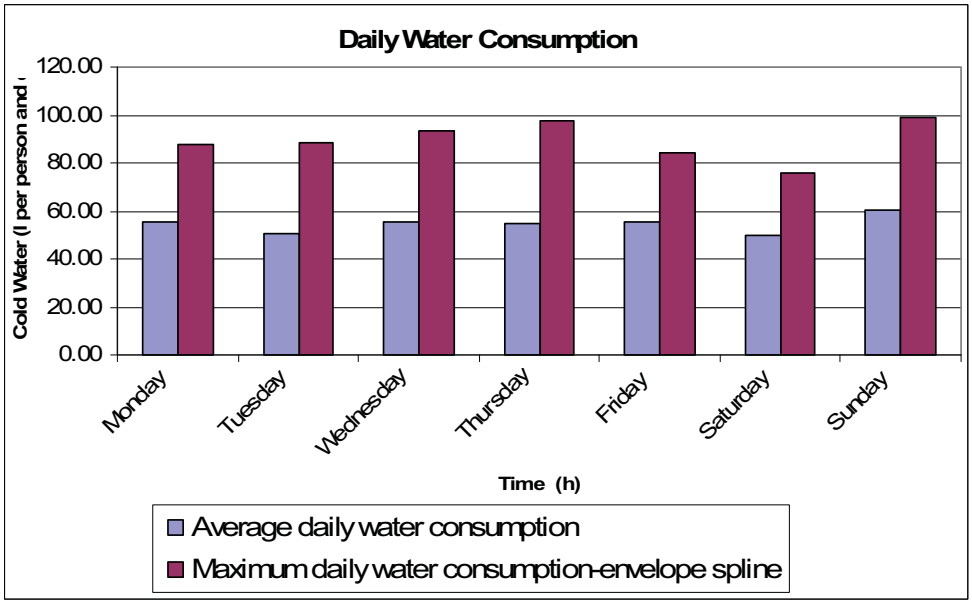

Figure 3. Total daily cold water consumption

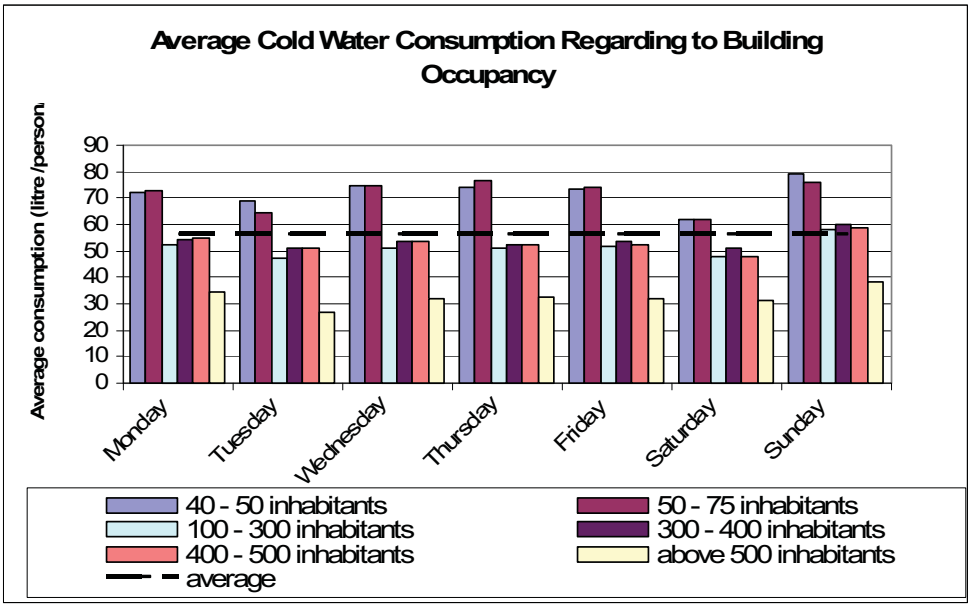

Figure 4. Total daily cold water consumption divided according to number of occupant in the building

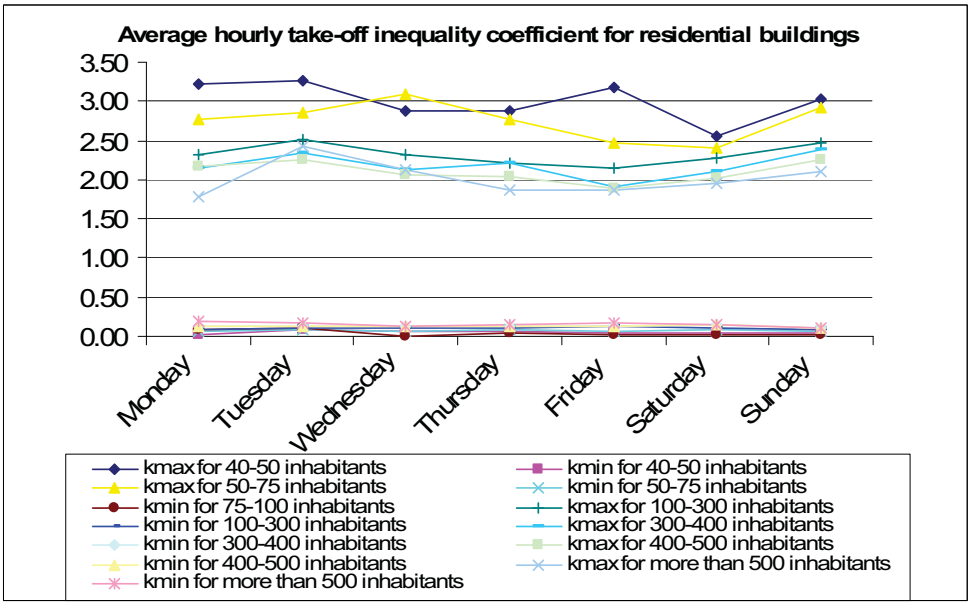

Figure 5. Hourly inequality coefficient according to flat occupancy

4. CONCLUSION

From measurement results result that total yearly water consumption from all 62 measurement is 56 liter/person/day (Fig. 3 and Fig 4.). Average water consumption in same object type is for us important at total water need evaluation and is very depended on concrete measured residential buildings, its inhabitants and technical equipment. For building services systems designing average value doesn't have predicative value. As well as in other technical areas for example structural mechanics for beam calculation we have several load states which are partly covered and results is maximum load envelope curve. It is similar with water consumption, in this case we have 62 load states (done measurement) where envelope curve copy maximal take-off values in separate hours (Fig. 2). Average maximal take-off is 90 liter/person/day. From equation [2] is coefficient inequality 1,6 which in comparable with Czech norm value (for 1000 inhabitant is k_d=1,5). From Fig. 3 is possible to see that average daily water consumption during week has minimum difference. Differences are in time period of take-off (Fig. 1 and Fig.2) where is possible to see extreme in noon and in the evening. Greatest take-off peak is in Saturday (noon) and in Sunday (noon and evening). In Saturday evening is surprisingly lowest from the whole week. Measurement results shows also number of inhabitants influence on average cold water consumption in object (Fig. 4). Average cold water consumption in object with lower number of inhabitant is bigger than by bigger occupancy of building. The next important indicator is hourly inequality coefficient (Fig.5) which is in most of groups expressively other than ČSN 736701 values, how is shown in consequent table.

Table 4. Comparsion of hourly inequality coefficient in several days with average value

number of inhabitants	50	75	300	400	500
$k_{h,max\ Czech\ norm\ value}$	6,7	6,3	4,4	3,4	2,6
$k_{h,max\ calculated\ from\ metering}$	3	2,75	2,3	2,2	2,1
comparison [%]	45%	44%	52%	65%	81%

Values were calculated from measured dates always for every day in week and were averaged for compare with Czech norm values. Table shows that values given by calculation from measured cold water consumption in residential buildings are extensively different. Residential building with smaller number of inhabitants has bigger differences (as far as about 55%) and other way round with more people in object is difference smaller. Smaller daily inequality coefficient values mean lower hourly take-off water differences which is influenced by fact that was measured only cold water and there are no taken in peak hot water take-offs. In table 4, we can see percentage comparison calculated k_{hmax} for individual days with average hourly maximal coefficient during week. Table shows, that weekly average value

of hourly inequality coefficient is with regard to small daily value differences sufficient.

Acknowledgement

This paper would not be created without excellent cooperation and technical facilities of Waterworks Pilsen, a.s which ensured measurement and date collection. Paper was created with support of investigative intention CEZ MSM 6840770003.

References

1. Kadlecová M., Notices to new Czech norm of hot water design, Topenářství Instalace 3/99
2. Kabele K. and collective, Energy and Environmental building systems, CTU 2005
3. Czech notice of Agriculture Ministry 428/2001
4. Vrána J. Water and Sewerage in Home and Flat, Grada publishing 2005
5. Musil V.and collective, Technical Buildings Facilities I

"Computational Civil Engineering 2007", International Symposium
Iaşi, România, May 25, 2007

Improving Civil Engineering Physics Teaching-Learning with Mathematica 5.1

Irina Radinschi[1], Brindusa Ciobanu[2]
[1]*Department of Physics, "Gh. Asachi" Technical University, Iasi, 700050, Romania*
[2] *Department of Physics, "Gh. Asachi" Technical University, Iasi, 700050, Romania*

Summary

In this paper we present some important examples of Mathematica 5.1 techniques for studying physical concepts and phenomena and for plotting a general class of physics phenomena. We point out that a computer algebra system like Mathematica is very useful for physics studies. We have a long-term experience in using this program in physics teaching and learning, as in approached fields as mathematical physics and computational physics.

Mathematica 5.1 is described through some examples of plotting waves interference, constructive interference and destructive interference. These examples highlight the power and versatility of Mathematica and indicate its application to a much wider range of problems in computational physics.

Mathematica 5.1 assists the students for solving differential equations, differentiating, integrating, making sums, finding roots, plotting and producing animations. We emphasize the graphical capability of Mathematica and use its power to go beyond finding solutions and performing length calculations and bring the studies alive with animations, and other graphical tools. This is possible because Mathematica 5.1 provides a good environment for computation, a high-level programming language, text, graphics, and animation. Further, GrTensorM which is embedded in Mathematica is a package which allows us carrying out length calculations and evaluating the components of some tensorial and pseudotensorial quantities.

For these reasons we implement Mathematica 5.1 in our course of physics, for exploring, teaching, and applying powerful mathematical methods in physics. This computer algebra system allows the students to develop their ability to learn physics, to solve difficult problems with a symbolic computing engine, and to review the basic mathematics. We introduce Mathematica program into our courses for students who major in technical fields because is a reliable tool for teaching and learning physics in a modern way.

KEYWORDS: Mathematica 5.1, engineering physics teaching-learning,computer algebra system, physics, physical concepts and phenomena.

1. INTRODUCTION

It is well-known that nowadays, physics studies are not allowed without using adequate software. Mathematica is a powerful mathematical software system for teachers and students. In the recent years, Mathematica has changed the way physics is taught and teached. Mathematica 5.1 gives the possibility to visualize and display physics concepts and phenomena, to perform length calculations and to generate numerical and graphical solutions to physics problems. It also provides modern techniques and for plotting 2D and 3D having many options for graph drawing.

Our experience in computational physics [1]-[6], [10]-[14] and particularly in using Mathematica 5.1, make us to decide that a better way for engineering physics teaching-learning is to incorporate this computer algebra system in our course of physics. Mathematica 5.1 is a very powerful and useful general purpose program [7]-[8] which can find solutions to algebraic equations, it can do calculus, it can evaluate equations numerically and it can plot and generate animations and sounds. Mathematica 5.1 also covers essential physical situations and phenomena. This allows the students leaving the length calculations to Mathematica and pay more attention to the physics studies. Mathematica has also a powerful online help built in, which can be used even by the new users [7]-[8].

Mathematica is a reliable tool of choice, in engineering analysis and modeling, and in technical education in universities. Mathematica 5.1 combines powerful computing software with a convenient user interface. Mathematica's features include symbolic and high-performance numeric computation, 2D and 3D data visualization, broad programming capabilities, and one-step creation of web documents [9].

2. PRESENTATION OF MATHEMATICA 5.1 APPLICATIONS

2.1. Applications of Mathematica 5.1 in physics

Mathematica 5.1 includes advanced programming methods from modern computer science as well as adding a host of new ideas of its own [9].

Mathematica 5.1 applications in physics studies allow the students to test their understanding of the concepts and phenomena, and applying them to many physical situations. It also allows solving rapidly physics problems without performing length calculations, and plotting and producing animations. We show how Mathematica 5.1 will be applied to take the students beyond the limitations of

traditional instruction. We present some Mathematica 5.1 applications in physics which are implemented in our courses.

2.2.1. Mathematica 5.1 commands for studying the wave interference. Plotting 2D interference.

The wave interference is an interesting topic, and with the graphical and animation capability of Mathematica, we can improve our physics courses. Once the students are able to handle the equations which describe the wave interference, they also discover results on their own by varying the amplitudes, the values of pulsation, initial phase and time, and generating constructive and destructive interference.

Mathematica 5.1 is also a reliable tool for graph drawing. It has many options for the color of the curves and for the color of the background. These can be set by using the option Graphics`Colors` and choosing from there the colors. The built-in *Mathematica* color directives RGBColor, Hue, and CMYKColor handle the most common systems. This package gives color directives using other standard systems. For axes we use the option AxesLabel and we plot the physical quantities on Z-axis, Y-axis and X-axis.

The Mathematica 5.1 commands for plotting 2D the wave interference are given below. We give some examples for constructive and destructive interference.

-Graphics-

ln[1]:=Plot[{0.2*Sin[Pi/4*t+Pi/3],-0.2*Sin[Pi/4*t+Pi/3]},
{t,1,10},PlotStyle→{{Hue[0.1]},{Hue[0.2]}},Background→RGBColor[0.94174`,
1.`,1.`],AxesLabel→{t, Ψ}]

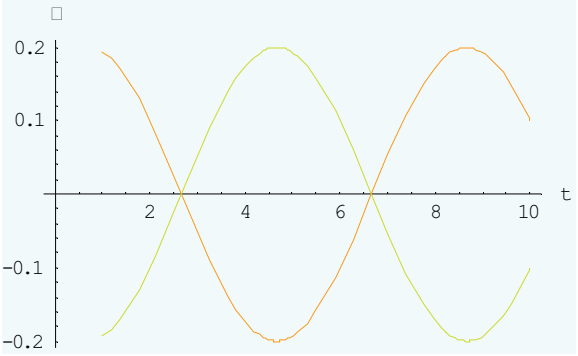

Figure1. Plotting two waves

Out[1]= -Graphics-

ln[2]:=Plot[{0.2*Sin[Pi/4*t+Pi/3],0.4*Sin[Pi/4*t+Pi/7],0.2*Sin[Pi/4*t+Pi/3]+0.4*Sin[Pi/4*t+Pi/7]},{t,1,10},PlotStyle→{{Hue[0.1]},{Hue[0.2],{Hue[0.3]}},Background→RGBColor[0.94174`,1.`,1.`], AxesLabel→{t, Ψ}]

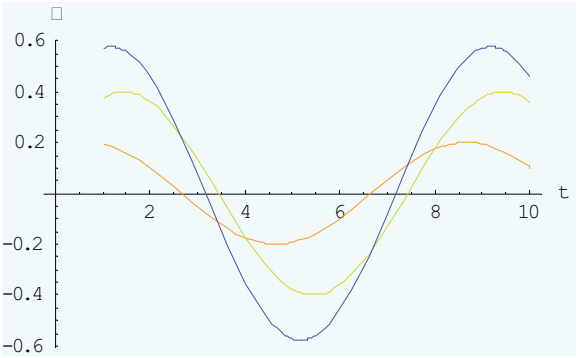

Figure 2. Plotting 2D interference

Out[2]= -Graphics-

In this case, the resultant wave function is evaluated using the command

ln[3]:= TrigExpand[0.2*Sin[Pi/4*t+Pi/3]+0.4*Sin[Pi/4*t+Pi/7]]

Out[3]=0.346759*Cos[Pi/4*t]+0.460388*Sin[Pi/4*t]

$$\text{Out[3]= } 0.346759\,\text{Cos}\left[\frac{\pi t}{4}\right] + 0.460388\,\text{Sin}\left[\frac{\pi t}{4}\right]$$

ln[4]:=Plot[{0.2*Sin[Pi/4*t],0.4*Sin[Pi/4*t],0.2*Sin[Pi/4*t]+0.4*Sin[Pi/4*t]},{t,0.1,50},PlotStyle→{{Hue[0.1]},{Hue[0.2]},{Hue[0.7]}}, Background→RGBColor[0.94174`,1.`,1.`],AxesLabel→{t,ψ}]

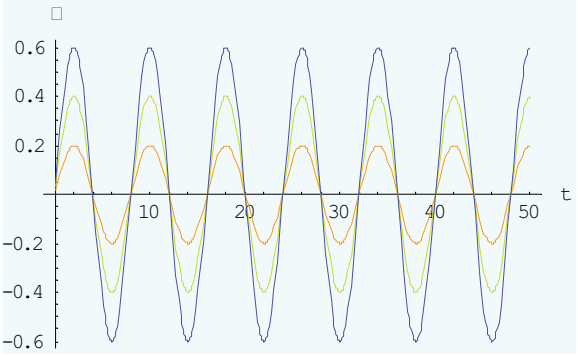

Figure 3. Plotting constructive interference

Out[4]= -Graphics-

The resultant wave function is computed with the command

ln[5]:= TrigExpand[0.2*Sin[Pi/4*t]+0.4*Sin[Pi/4*t]]

Out[5]=0.6*Sin[Pi/4*t]

$$\text{Out[5]= } 0.6\,\text{Sin}\left[\frac{\pi t}{4}\right]$$

ln[6]:=Plot[{0.2*Sin[Pi/4*t+Pi/3],-0.2*Sin[Pi/4*t+Pi/3], 0.2*Sin[Pi/4*t+Pi/3]-0.2*Sin[Pi/4*t+Pi/3]}, {t,1,10}, PlotStyle→{{Hue[0.1]}, {Hue[0.2]}}, Background→RGBColor[0.94174`,1.`,1.`], AxesLabel→{t, Ψ}]

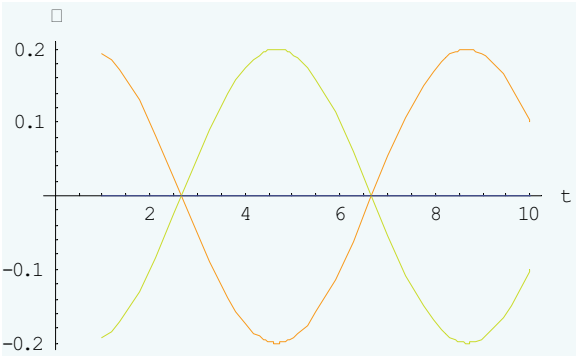

Figure 4. Plotting destructive interference

Out[6]= -Graphics-

ln[7]:=Plot[{0.2*Sin[Pi/4*t],0.2*Sin[Pi/4*t+Pi],0.2*Sin[Pi/4*t]+0.2*Sin[Pi/4*t+Pi]},{t,0.1,50},PlotStyle→{{Hue[0.1]},{Hue[0.2]},{Hue[0.7]}}, Background→RGBColor [0.94174`,1.`,1.`],AxesLabel→{t, Ψ }]

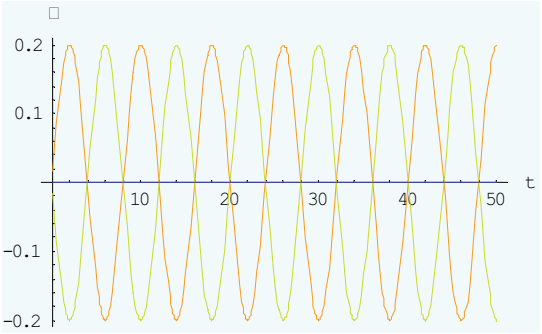

Figure 5. Plotting destructive interference

Out[7]= -Graphics-

2.2.2. Mathematica 5.1 commands for plotting 3D wave interference

We give an example of plotting 3D the interference. The Mathematica 5.1 commands for plotting 3D waves interference are presented.

ln[8]:=p1=Plot3D[0.2*Sin[ω*t],{t,1,10},{ω,Pi/7,Pi/4},Background→RGBColor [0.94174`,1.`,1.`],AxesLabel→{t,ω,Ψ}]

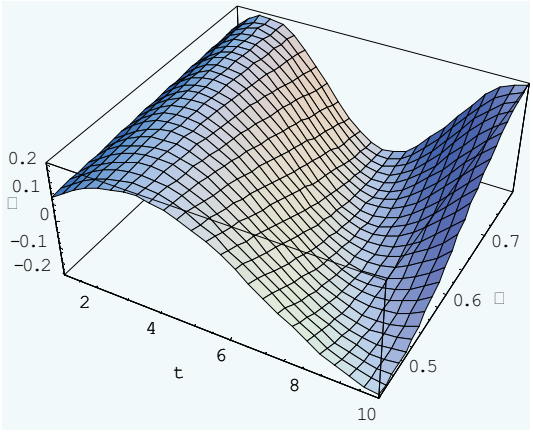

Figure 6. Plotting 3D wave function

Out[8]= -SurfaceGraphics-

ln[9]:=p2=Plot3D[0.2*Sin[ω*t+Pi],{t,1,10},{ω,Pi/7,Pi/4},Background→RGBColo r [0.94174`,1.`,1.`],AxesLabel→{t,ω,Ψ}]

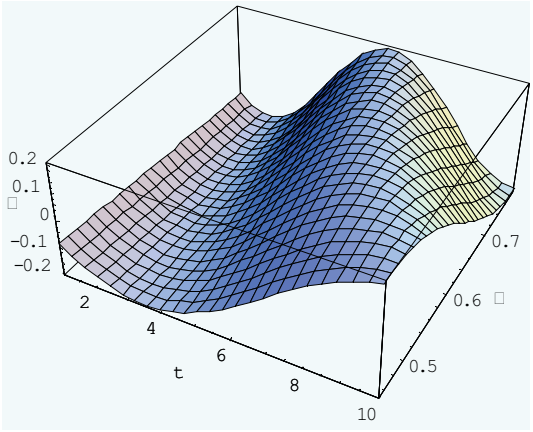

Figure 7. Plotting 3D wave function

Out[9]= -SurfaceGraphics-

ln[10]:= -SurfaceGraphics-

Show[{p1,p2},Axes→True]

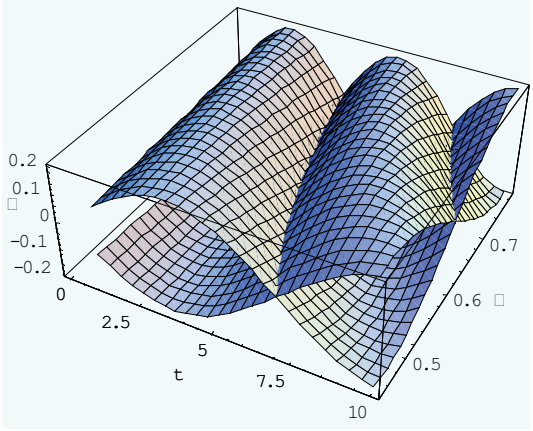

Figure 8. Plotting 3D destructive waves interference

Out[10]= -SurfaceGraphics-

The sum of two wave functions can also be plotted using the commands given below.

ln[11]:=p3=Plot3D[0.2*Sin[ω*t]+0.2*Sin[ω*t+Pi],{t,1,10},{ω,Pi/7,Pi/4},Backgro und→RGBColor [0.94174`,1.`,1.`],AxesLabel→{t,ω,Ψ}]

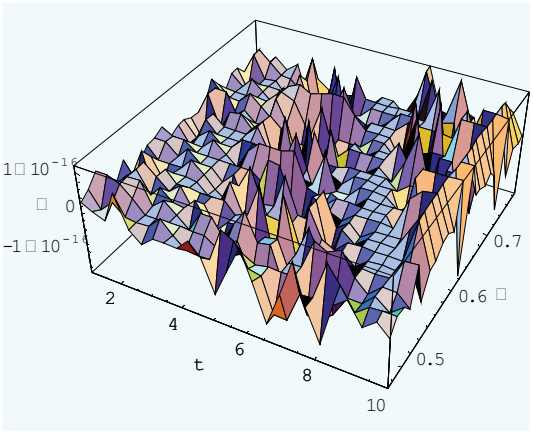

Figure 9. 3D graph for destructive waves interference

Out[11]= -SurfaceGraphics-

The resultant wave function for destructive waves interference is computed using the command

ln[12]:= TrigExpand[0.2*Sin[ω*t]+0.4*Sin[ω*t]]

Out[11]=0*Sin[ω*t]

For plotting constructive interference we use the next commands.

ln[13] =p3=Plot3D[0.2*Sin[ω*t+Pi/3],{t,1,10},{ω,-Pi/4,Pi/4},Background→RGBColor [0.94174`,1.`,1.`],AxesLabel→{t,ω,Ψ}]

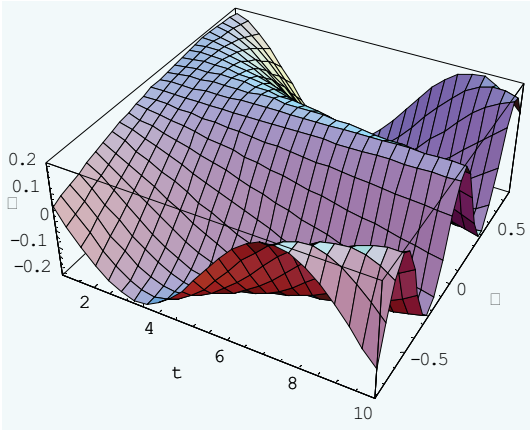

Figure 10. Plotting 3D wave function

Out[13]= -SurfaceGraphics-

ln[14] =p4=Plot3D[0.2*Sin[ω*t-Pi/4],{t,1,10},{ω,-Pi/4,Pi/4},Background→RGBColor [0.94174`,1.`,1.`],AxesLabel→{t,ω,Ψ}]

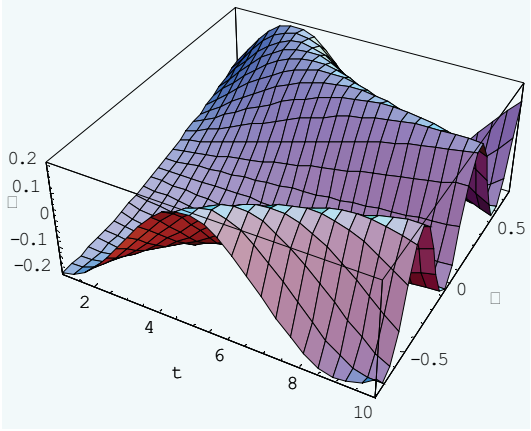

Figure 11. Plotting 3D wave function

Out[14]= -SurfaceGraphics-

The resultant wave function is computed using the command

ln[15] =TrigExpand[Sin[ω*t+Pi/3]+0.2*Sin[ω*t-Pi/4]]

Out[15]=0.0317837*Cos[ω*t]+0.241421*Sin[ω*t]

ln[16] Plot3D[0.0317837*Cos[ω*t]+0.241421*Sin[ω*t],{t,1,10},{ω,-Pi/4,Pi/4},Background→RGBColor [0.94174`,1.`,1.`],AxesLabel→{t,ω,Ψ}]

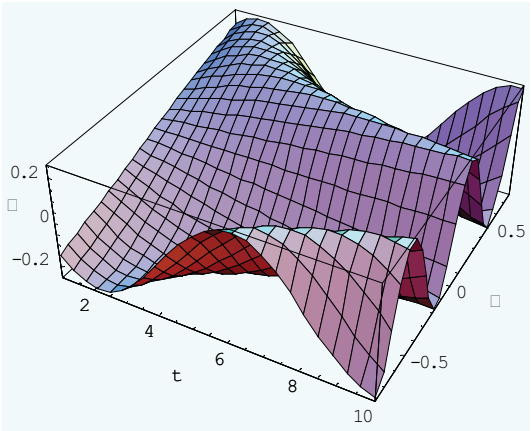

Figure 12. Plotting 3D constructive waves interference

Out[16]= -SurfaceGraphics-

Plot3D includes a setting for the PlotPoints and one for the Mesh option. For the graph from the Figure 12 we use these options and we obtain

ln[17] Plot3D[0.0317837*Cos[ω*t]+0.241421*Sin[ω*t],{t,1,10},{ω,-Pi/4,Pi/4}, Background→RGBColor [0.94174`,1.`,1.`], PlotPoints→40, Mesh→False, AxesLabel→{t,ω,Ψ}]

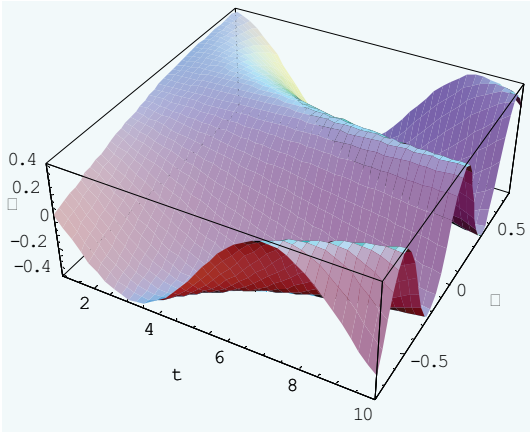

Figure 13. Plotting 3D constructive waves interference

Out[17]= -SurfaceGraphics-

3. CONCLUSIONS

The latest version Mathematica 5.1 raises the level in mathematical software, providing more than 50 new functions, toolkits, and performance improvements in a powerful program [15]-[16]. The Mathematica 5.1 version adds a host of new capabilities, especially for working with large-scale, diverse types of data. New innovative algorithms are introduced to deliver unmatched performance for all steps in the data handling process, importing, analyzing, manipulating, or plotting.

We have introduced Mathematica 5.1 as a teaching and learning tool in our course of physics for civil engineering. Mathematica 5.1 is a powerful program and has many advantages. It provides a good environment for computation, a high-level programming language, text, graphics, and animation. We assume that the students are already familiar with Mathematica, but we also offer a basic training in this computer algebra system for beginers.

The cases of Plot and Plot3D wave interferences was illustrated with some examples and commands for plotting 2D and 3D waves interference, and also

options like PlotStyle, Background→RGBColor, AxesLabel, PlotPoints, and Mesh have been added for improving the graph drawing.

Our main goals are to implement Mathematica 5.1 and Maple 9.5 programs to assist students in physics learning and for solving problems. We want our students to make progresses and we also want them to make these progresses rapidly. On the other hand, we'll give them the possibility to choose between Mathematica 5.1 and Maple 9.5, or to work with both programs.

References

1. Ciobanu B., Radinschi I., One Computational Algorithm for Physics Modeling, P*roceedings of 5th International Conference on Electromechanical and Power Systems*, SIELMEN, Chisinau, Rep. Moldova, October 6-8, 2005, pp. 222-225.
2. Radinschi I., Ciobanu B., *Testing Physics*, Junimea Publishing House, Iasi, Romania, 2006.
3. Radinschi I., Ciobanu B., *Physics for Engineers*, Junimea Publishing House, Iasi, Romania, 2006.
4. Ciobanu B., Radinschi I., A Sequential Programming Algorithm – a Tool for Study the Standing Waves, *Proceedings of International Symposium IEEI 2006*, Iasi, Romania, Bulletin of IP Iasi, Vol. LII(LVI), Fasc.5, pp. 129-134.
5. Radinschi I., Scripcariu L., Ciobanu B., Frunza M. D., Online Teaching-while-Quizzing Test, *Proceedings of the 2nd National Conference on Applied Physics*, June 9-10, Galati, Romania, 2006, in press Romanian Journal of Physics
6. Ciobanu B., Radinschi I., Teaching and Learning Physics for Engineers by Aid Computers, *Proceedings of International Symposium IEEI 2006*, Iasi, Romania, Bulletin of IP Iasi, Vol. LII(LVI), Fasc.5, pp. 135-140.
7. Mathematica for Scientists and Engineers: Using Mathematica to do Science, by Richard Gass (Prentice Hall).
8. www.wolfram.com.
9. http://www.pugh.co.uk.
10. Radinschi I., Frunza M. D., Ciobanu B., Online Virtual Model for Testing the Knowledge, *Proceedings of INTED 2007*, March 7-9, Valencia, Spain.
11. Radinschi I., Ciobanu B., Implementation of Computational Methods in Physics Learning, *Proceedings of 4th International Symposium Computational Civil Engineering 2006*, Iasi, Romania, 2006, pp. 251-257.
12. Frunza M. D., Radinschi I., A Virtual Model for Testing Mathematics, Physics and Chemistry, *Proceedings of International Symposium for Design and Technology of Electronic Packages*, SIITME, 2006, p. 154, Iasi, Romania.
13. Ciobanu B., Radinschi I., The Electrical Properties of sample Investigation by Computational Programs, *Proceedings of 5th International Conference on Electromechanical and Power Systems*, SIELMEN, October 6-8, 2005-Chisinau, Rep. Moldova, 2. p. 218-221.
14. Ciobanu B., Radinschi I., One computational program for predictions of properties of the yarns, *Proceedings of International Symposium Present and Perspective in Textile Engineering*, November 10-12, 2005, Iaşi, Romania, p. 563-569.
15. www.gtpcc.org
16. www.pcmag.com; www.usc-b2b.com; www.cambridge.org; www.uc.edu.

"Computational Civil Engineering 2007", International Symposium
Iaşi, România, May 25, 2007

Physics with Maple 9.5

Irina Radinschi[1], Brindusa Ciobanu[1], Mircea Daniel Frunza[2]
[1]*Department of Physics, "Gh. Asachi" Technical University, Iasi, 700050, Romania*
[2] *Faculty of Electronics and Communications, "Gh. Asachi" Technical University, Iasi, Romania*

Summary

In this paper we sketch how computer algebra systems like Maple 9.5 can be used to helping the students connecting physical concepts and phenomena with powerful mathematical formalisms and graphical representations. We demonstrate that a computer algebra system like Maple is very useful for physics studies. The experience in this area demonstrated that computational physics, together with traditional theoretical and experimental physics, is a reliable tool which helps students to explore a wide variety of phenomena and give them a deeper understanding of these topics.

Maple 9.5 provides a good environment for computation, a high-level programming language, text, graphics, and animation. Maple 9.5 is also capable of, and used for, high-level computation by students and this making it an ideal computer assisted teaching and learning tool. It is also a comprehensive environment for exploring, teaching, and applying mathematical methods in physics. Using Maple the students will be unconstrained by traditional mathematical and physical limitations, and they will also be capable of a better understanding of computational methods. Maple 9.5 for physics helps the students to develop their ability to learn physics, to solve difficult problems with a symbolic computing engine, and to review the basic mathematics. Maple 9.5 assists the students for solving differential equations, differentiating, integrating, making sums, finding roots, plotting and producing animations. In this work are presented some applications of Maple 9.5 in physics, which help the students to bridge the gap between mathematical formalism and physical phenomena.

Step by step we want to introduce Maple program into our courses for those who plan to major in technical fields. The main features of our course are the use of computer program like Maple for teaching and learning physics, and for solving physics problems. The students can also use the computers outside class for further instruction and problem solving. In this way we want to take our students beyond the limitations of traditional instruction and make them to become familiar with high-level computer algebra systems.

KEYWORDS: Maple 9.5, computer algebra system, physics, physical concepts and phenomena.

1. INTRODUCTION

Analyses of current developments in physics teaching and learning have shown the importance of implementation of high-level computer algebra systems like Maple [7] in our courses. Maple is a mathematical application package that supports symbolic and numeric computation and graphics. Maple 9.5 helps students connecting physical concepts and phenomena with powerful mathematical formalisms and graphical representations. The extensive mathematical assistance, symbolic manipulations, computational power and graphical abilities of programs like Maple [11]-[14] can greatly help students to explore physical topics and experiment with ideas without performing cumbersome calculations.

We have a long-term experience in computational physics [1]-[6], [8]-[10] and particularly in using Maple 9.5 program, with applications in many fields of physics. Our course will be designed to incorporate the use of Maple for solving differential equations, differentiating, integrating, making sums, finding roots, plotting and producing animations.

Students use Maple V software to achieve a better conceptual understanding of the material of the course while still gaining a good knowledge of the methods of problem-solving. Further, this computational method allows a rapid learning of physics and is also a powerful tool for solving problems.

2. PRESENTATION OF MAPLE 9.5 APPLICATIONS

2.1. Applications of Maple 9.5 in physics

Maple 9.5 applications in physics gives students the opportunity to show what they have learned by testing their understanding of the concepts and phenomena, and applying them to real situations. Further, it allows solving rapidly physics problems without performing length calculations, plotting and producing animations. We present some Maple 9.5 applications in physics which are implemented in our courses.

2.2.1. Evaluation of speed and displacement

```
> ode1 := m*diff(x(t),t)=4*t^2/3;
```

$$ode1 := m\left(\frac{d}{dt}x(t)\right) = \frac{4}{3}t^2$$

```
> ans1 := dsolve(ode1);
```

$$ans1 := x(t) = \frac{4\,t^3}{9\,m} + \_C1$$

and

```
> diff(4*t^3/(9*m),t);
```

$$\frac{4\,t^2}{3\,m}$$

2.2.2. Plotting the speed and displacement

The commands of Maple 9.5 for plotting 2d, for producing animations and for plotting 3d for the speed are:

a) plotting 2d

```
>with(plots);
>plot(4*t^2/3,t=0...10);
```

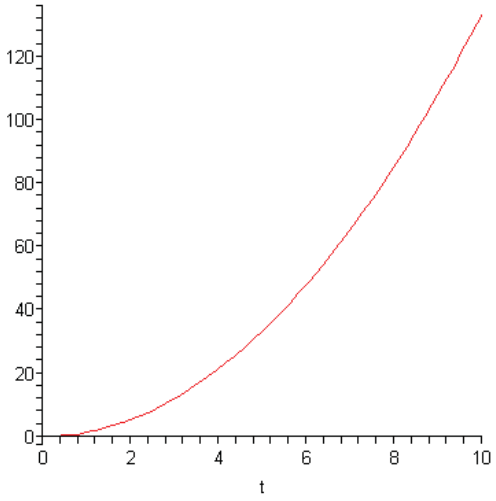

Figure 1. Graph 2d of the speed

b) producing animations

```
>with(plots);
>animate(plot,[A*(4*t^2/3),t=0...10], A=-5...5);
```

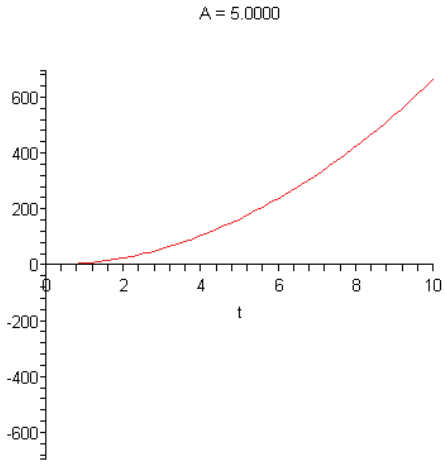

Figure 2. Animation 2d graph of the speed

c) plotting 3d

```
>with(plots);
>plot3d(4*t^2/(3*m),m=0.1...1,t=0...10);
```

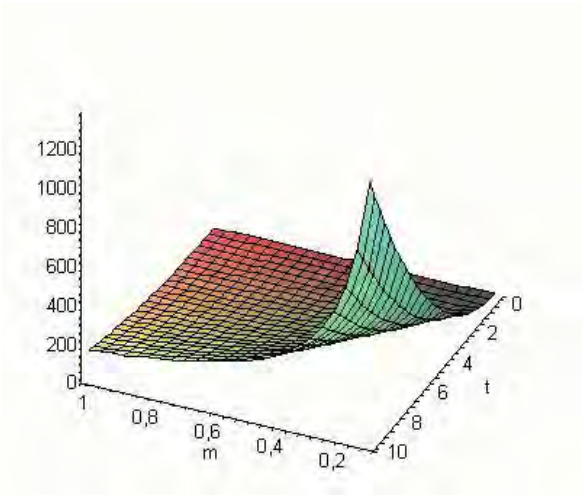

Figure 3. Plot 3d of the speed

The commands of Maple 9.5 for plotting 2d, for producing animations and for plotting 3d (in this case we consider that the integrating constant is C_1=0) for the displacement are

a) plotting 2d

```
>with(plots);
>plot(4*t^3/9,t=0...10);
```

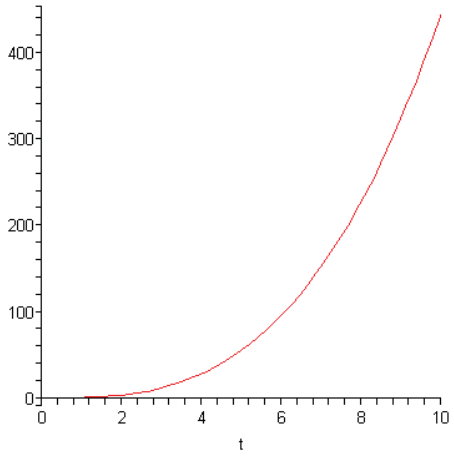

Figure 4. Plot 2d of the displacement

b) producing animations

```
>with(plots);
>animate(plot,[A*(4*t^3/9),t=0...10], A=-5...5);
```

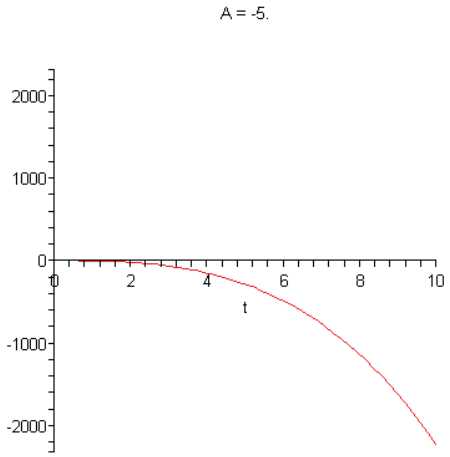

Figure 5. Animation 2d graph of the displacement

c) plotting 3d

```
>with(plots);
>plot3d(4*t^3/(9*m),m=0.1...1,t=0...10);
```

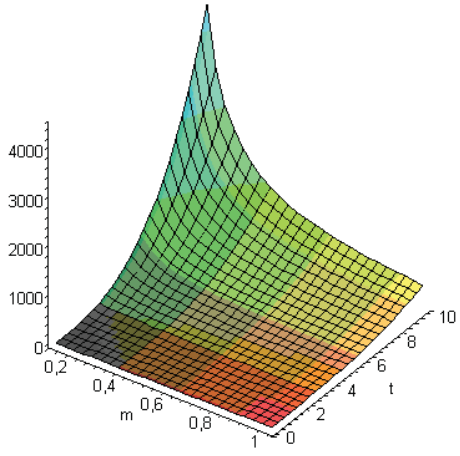

Figure 6. Plot 3d of the displacement

2.2.3. Plotting the wave propagation

There are considered three wave functions. The commands of Maple 9.5 for plotting the waves propagation in 2d and 3d cases are given below.

a) plotting 2d

```
>with(plots);
>f:=4*sin(Pi/4*t+Pi/7);
>h:=2*cos(Pi/4*t+Pi/3) ;
>g:=0.7*sin(2*Pi/3*t+Pi/7);
> plot({f(t),g(t),h(t)},t=0...10);
```

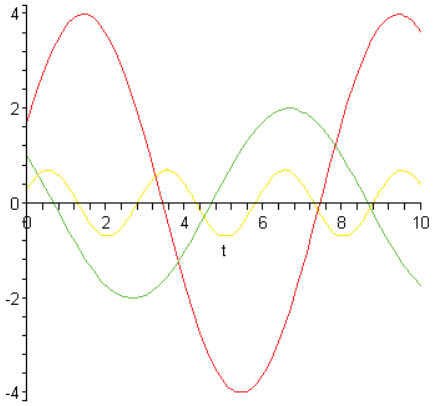

Figure 7. Plot 2d of the wave propagation

b) plotting 3d

```
>with(plots);
>f:=4*sin(omega*t+Pi/7);
>g:=0.7*sin(omega*Pi/3*t+Pi/7);
>h:=2*cos(Pi/4*t+Pi/3) ;
>plot3d({f,g,h},omega=0...Pi/4,t=0...10);
```

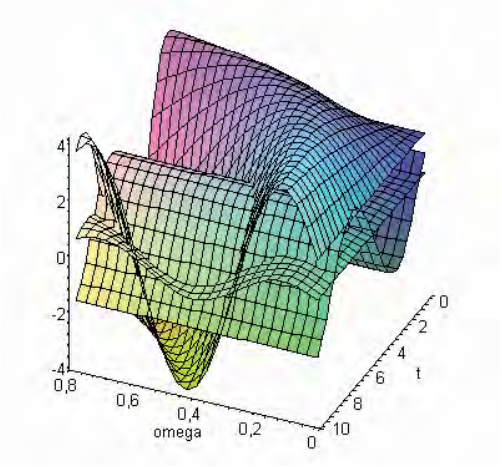

Figure 8. Plot 3d of the wave propagation

2.2.4. Plotting the kinetic and potential energy

The commands of Maple 9.5 for plotting the kinetic energy and the potential energy (with respect of SI units) are given bellow

```
>with(plots);
>plot3d({m*v^2/2,m=0.1...1,v=0...10);
```

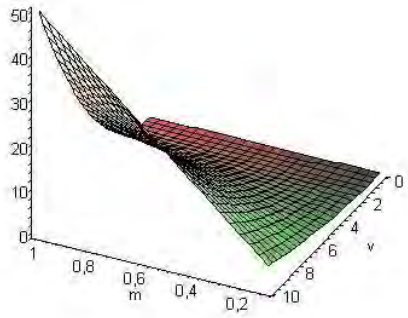

Figure 9. Plot 3d of the kinetic energy

```
>plot3d({k*x^2/2,k=0.1...10,x=1...100);
```

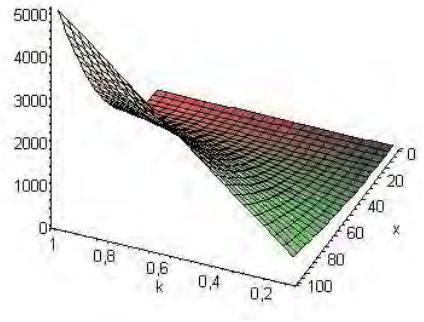

Figure 10. Plot 3d of the potential energy

We gave some examples which demonstrate the usefulness of Maple 9.5 for teaching and learning physics.

Maple 9.5 can also be used as a powerful tool for solving physics problems. After the students will become familiar to most of Maple commands they will be capable to solve more complicated problems.

3. CONCLUSIONS

This paper points out some advantages of using Maple [7], [11]-[14] in studying physics. We presented some examples from our course to demonstrate the usefulness of this high-level computer algebra system. We used Maple 9.5 for evaluating the speed and displacement in a particular case, for plotting 2d and 3d of the speed and displacement, and for producing animations. The program was also used for plotting the wave propagation of three waves in 2d and 3d cases, and for plotting the kinetic energy and the potential energy in 3d case.

The main goals are to allow students the ability to learn physics, to perform length calculations, to make graphical representations and introduce animations, and also to solve physics problems using Maple 9.5. The applications will be introduced step by step, firstly students have to learn how to handle with derivatives and integrals, solving equations and making graphs. At a higher level, they will be able to solve challenging and physically realistic problems.

References

1. Ciobanu B., Radinschi, I., One Computational Algorithm for Physics Modeling, P*roceedings of 5th International Conference on Electromechanical and Power Systems*, SIELMEN, Chisinau, Rep. Moldova, October 6-8, 2005, pp. 222-225.
2. Radinschi I., Ciobanu B., *Testing Physics*, Junimea Publishing House, Iasi, Romania, 2006.
3. Radinschi I., Ciobanu B., *Physics for Engineers*, Junimea Publishing House, Iasi, Romania, 2006.
4. Ciobanu B., Radinschi I., A Sequential Programming Algorithm – a Tool for Study the Standing Waves, *Proceedings of International Symposium IEEI 2006*, Iasi, Romania, Bulletin of IP Iasi, Vol. LII(LVI), Fasc.5, pp. 129-134
5. Ciobanu B., Radinschi I., Teaching and Learning Physics for Engineers by Aid Computers, *Proceedings of International Symposium IEEI 2006*, Iasi, Romania, Bulletin of IP Iasi, Vol. LII(LVI), Fasc.5, pp. 135-140.
6. Radinschi I., Scripcariu L., Ciobanu B., Frunza M. D., Online Teaching-while-Quizzing Test, *Proceedings of the 2nd National Conference on Applied Physics*, June 9-10, Galati, Romania, 2006, in press Romanian Journal of Physics
7. http://grtensor.org; http://www.maplesoft.com/maplebooks.html.
8. Radinschi I., Frunza M. D., Ciobanu B., Online Virtual Model for Testing the Knowledge, *Proceedings of INTED 2007*, March 7-9, Valencia, Spain.
9. Radinschi I., Ciobanu B., Implementation of Computational Methods in Physics Learning, *Proceedings of 4th International Symposium Computational Civil Engineering 2006*, Iasi, Romania, 2006, pp. 251-257.
10. Frunza M. D., Radinschi I., A Virtual Model for Testing Mathematics, Physics and Chemistry, *Proceedings of International Symposium for Design and Technology of Electronic Packages*, SIITME, 2006, p. 154, Iasi, Romania.
11. http://www.wfu.edu/physics/cel/maple.html
12. http://www.maplesoft.com/applications/
13. www-teaching.physics.ox.ac.uk
14. www.adsabs.harvard.edu

"Computational Civil Engineering 2007", International Symposium
Iaşi, România, May 25, 2007

Physics Studies – Computational Methods, a Strong Connection

Irina Radinschi[1], Brindusa Ciobanu[2]
[1]*Department of Physics, "Gh. Asachi" Technical University, Iasi, 700050, Romania, radinschi@yahoo.com*
[2] *Department of Physics, "Gh. Asachi" Technical University, Iasi, 700050, Romania, bciobanu2003@yahoo.com*

Summary

The aim of this paper is to point out the importance of the connection between theoretical physics and computational methods. At national and international level, considerable efforts have been made for implementing the computational methods in the study of physics. This work is focused on the use of Mathematica and Maple programs for physics studies. Because our applications are part of the algebraic computations in physics, new calculation programs in Mathematica and Maple are conceived. We also used methods of animated graphs for illustrating the physics phenomena. The calculations are performed with Mathematica and Maple programs. In some particular cases of our applications, these programs have attached the GrTensor packages. Many graphs were also made using the Mathematica and Maple programs. This goal will be reached easily establishing good collaborations with specialists in the field from our country and from abroad. On the other hands, undergraduate physics implies to work with students and in this way they have the possibility to enlarge the circle of collaborations and gather a lot of information in the field and in adjacent areas. Platforms as Mathematica and Maple have some advantages as flexibility and speed, and more advanced graphical facilities. GrTensorII which is embedded in Maple is a package which allows us carrying out length calculations and evaluating the components of some tensorial and pseudotensorial quantities. This is because it has the facility for defining new tensors. Furthermore, it allows the simplication of large terms. The duration of the calculations is shorter compared to that which used other software such as REDUCE. GrTensorM runs under Mathematica. GrTensorM has a large number of predefined objects, with automatic index generation and facilitates the creation of new objects with a compact intuitive interactive definition facility. An important step is the development of the existing methods, and in this light we intend to enlarge the areas of study by using the Mathematica and Maple programs to more classes of applications. In this way a powerful connection between physics studies and computational methods is established.

KEYWORDS: physics studies, computational methods, Mathematica, Maple, GrTensorII, GrTensorM.

1. INTRODUCTION

The connection between the physics studies and the computational methods is one of the most important issues at national and international level. The mathematical methods implemented in our physics course represent the main way of instruction and provide the skills needed for advanced studies in physics. Mathematica and Maple have the potential to strongly impact the way problem solving methods are taught in undergraduate physics and the curriculum of such courses. In order to perform length calculations, evaluate the components of some tensorial and pseudotensorial quantities and make graphs we use powerful programs like Mathematica and Maple. In physics we want to use more animated graphs for illustrating the phenomena. Nowadays, physics studies are not allowed without using adequate software. Because the use of good software is very important, this is the reason why specialists in the field from our country and from abroad have been consulted. Further, special attention was paid for involving our students in this interactive study: physical phenomena-computational methods.

We consider that this work can be extended to many physical situations and a lot of information in the field can be achieved. Because the study of physics requires in many cases making graphs and carrying out calculations which can be performed using computer algebra methods, we strongly recommend programs like Mathematica and Maple.

We have a long-term experience in computational physics [1]-[3], [5]-[7] and particularly in using these programs, with applications in many fields of physics. Our course will be designed to incorporate the use of the Mathematica and Maple programs as the primary means of teaching mathematical methods for solving physics problems. Further, we want to understand how this course impacts the students' understanding of the course material, and to what extent Mathematica and Maple can be reliable problem solving tool for students at a similar level in their study of physics. This is an important point, because one of the main problems that would arise is how will be the course instruction affected by the use of these two computer programs and what are the strengths and weaknesses of Mathematica and Maple as teaching and learning tools.

These studies imply to work with students, and in this way they have the possibility to enlarge the circle of collaborations and gather a lot of information in the field and in adjacent areas. Further, the computational methods allow a rapid learning of physics and our viewpoint is they can succesfully replace the traditional methods. We hope that our students will feel confident and they will be able to handle with the Mathematica and Maple programs, in order to easily and rapidly solve and explore most problems they encounter in their physics studies, and enrich their knowledge.

2. CONNECTION BETWEEN PHYSICS STUDIES AND COMPUTATIONAL METHODS

2.1. Presentation of Mathematica and Maple programs

As we pointed out in Introduction, the study of physics requires adequate software. In recent years computer algebra systems have become increasingly powerful tools in teaching physics. The extensive mathematical assistance, symbolic manipulations, computational power and graphical abilities of programs like Mathematica and Maple [4] can greatly help students to explore physical topics and experiment with ideas without performing cumbersome calculations. We consider that we are able to obtain reliable results in teaching and learning physics, and this is due to the good connection between the physics studies and the methods of computer calculation and graphic simulation. The applications which are obtained for many physical situations also allow to propose some useful suggestions for future studies. Concerning our courses and seminars we want to perform the calculations with Mathematica and Maple. Many graphs will also be made using the Mathematica and Maple programs. Special attention will be paid to animated graphs for illustrating the physics phenomena. In the whole process of teaching and learning physics we will take into account that many of our students are novice users of these programs, and will choose the adequate level of applications.

Platforms as Mathematica and Maple have some advantages as flexibility and speed, and more advanced graphical facilities. GrTensorII is a package which allows calculating the components of tensorial and pseudotensorial quantities, and is embedded in Maple. This is because it has the facility for defining new tensors. Furthermore, it allows the simplification of large terms. GrTensorM runs under Mathematica. GrTensorM has a large number of predefined objects, with automatic index generation and facilitates the creation of new objects with a compact intuitive interactive definition facility. We have a long-term experience in using these programs in physics teaching and learning, as in approached fields as mathematical physics and computational physics.

2.2. Advantages in using Mathematica and Maple for teaching and learning physics

We sketch the advantages of these powerful programs in teaching and learning physics. It is obviously that Mathematica and Maple program have to satisfy some requirements which indicated them as powerful tools. These requirements are:

1) to be a good mathematical tool for solving equations, carrying out length calculations, and writing tensorial and pseudotensorial quantities,

2) Mathematica and Maple computer algebra systems have to allow the students to easily and quickly change the mathematical models and the parameters and then generate new answers,

3) giving the possibility to be applied for a large number of applications and yielding meaningful results,

4) facilitating to make predictions and analogies between different physical situation,

5) giving the possibility to make graphs and animated graphs in order to illustrate the physical phenomena,

6) having the entire documentation electronically searchable.

These features make Mathematica and Maple ideal for use in upper-level physics courses for students completing assignments.

3. APPLICATIONS OF MATHEMATICA AND MAPLE

3.1. Maple 9.5 applications

We present some examples from a typical calculus course. Further, some graphs are inserted. The topics that we have chosen are solving differential equations, evaluating the first and second derivative of some physical quantities and making graphs and animated graphs. The following examples, solutions and graphs demonstrate such cases.

3.1.1. Maple commands for simple harmonic oscillations and damped harmonic oscillations

Firstly, we consider the simple harmonic oscillations and damped harmonic oscillations and we give the Maple sequences for dsolve – solve ordinary differential equations (ODEs). The first example is using the command dsolve(ode1) which yields the roots of ode1. In the second case we use the command dsolve(ode2) which yields the roots of ode2.

```
> ode1 := diff(x(t),t,t)+omega^2*x(t);
```

*ode1 := (diff(x(t),(t, 2)))+omega^2*x(t)*

```
> ans1 := dsolve(ode1);
```

ans1 := $x(t) = \_C1 \sin(w\,t) + \_C2 \cos(w\,t)$

and

```
> ode2 := diff(x(t),t,t)+2*gamma*diff(x(t),t)+omega^2*x(t);

ode2 := (diff(x(t),(t, 2)))+2*gamma*(diff(x(t), t))+omega^2*x(t)

> ans2 := dsolve(ode2);

ans2 := x(t) = _C1*exp((-gamma+(gamma^2-omega^2)^(1/2))*t)+_C2*exp((-
gamma-(gamma^2-omega^2)^(1/2))*t)
```

3.1.2. Maple commands for evaluating the first and second derivative of displacement for the simple harmonic oscillations

Secondly, we give some examples of evaluating the first and second derivative of displacement for the simple harmonic oscillations. This will give the velocity and acceleration for the simple harmonic oscillations.

```
> diff(A*sin(omega*t+phi),t);
```

$$A \cos(\omega t + \varphi)\,\omega$$

```
> diff(A*sin(omega*t+phi),t,t);
```

$$-A \sin(\omega t + \varphi)\,\omega^2$$

3.1.3. Maple commands for plotting 2d and 3d for simple harmonic oscillations

Thirdly, we make the graphs for simple harmonic oscillations. We make a 2 – dimensional graph and a 3 – dimensional graph.

For the 2 – dimensional case we plot the expression for the displacement with the amplitude A=2, the pulsation ω=Pi/4 and the initial phase φ=Pi/3 and t=0…10, and we obtain the graph from the Figure 1.

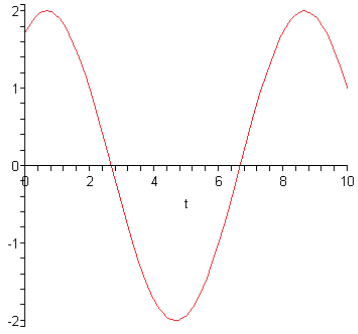

Figure1. Simple harmonic oscillations, the 2d graph

```
> with(plots);
> plot(2*sin(Pi/4*t+Pi/3),t=0...10);
```

For the 3 – dimensional case we plot the expression for the displacement with the amplitude A=0.1…1, the pulsation ω=Pi/4, the initial phase φ=Pi/3, and t=0…10.

We give the sequences bellow and in the Figure 2 we plot the displacement for different values of the amplitude and time.

```
> plot3d(A*sin(Pi/4*t+Pi/3),A=0.1...1,t=0...10);
```

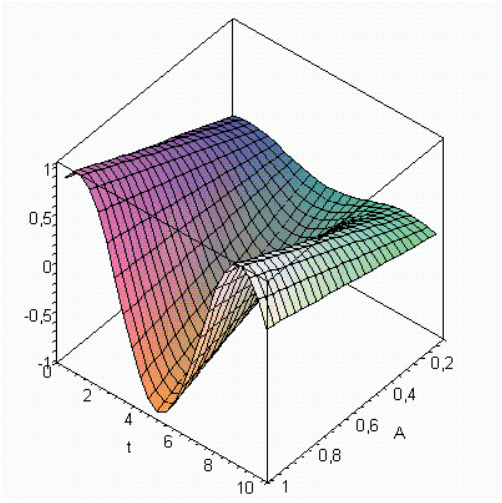

Figure 2. Simple harmonic oscillations, the 3d graph

For the graphs the selection animate or animate3d can be selected.

3.2. Mathematica 5.1 applications

We give some examples connected to the topics of solving differential equations, evaluating the first and second derivative of some physical quantities and making graphs and animated graphs.

3.2.1. Mathematica commands for simple harmonic oscillations and damped harmonic oscillations

We present the simple harmonic oscillations and damped harmonic oscillations and we give the Mathematica sequences for DSolve. We obtain

ln[1] DSolve[x''[t] == -ω^2 x[t], x, t]

Out[1] {{x→Function[{t},C[1] Cos[ω t]+C[2] Sin[ω t]]}}

and

ln[2] DSolve[x''[t] == 2 δ x'[t] + ω^2 x[t], x, t]

Out[2] {{x→Function[{t}, $e^{(-\delta-\sqrt{\delta^2-\omega^2})t}C[1]+e^{(-\delta+\sqrt{\delta^2-\omega^2})t}C[2]$

3.2.2. Mathematica commands for evaluating the speed and acceleration for the simple harmonic oscillations

In this case the first and second derivatives of displacement for simple harmonic oscillations are computed. They will give the velocity and acceleration for the simple harmonic oscillations.

ln[1] D[A*Sin[ω*t+φ],t]

Out[1]A ω Cos[ω*t+φ]

ln[2] D[A*ω*Cos[ω*t+φ]]

Out[3] -A ω^2 Sin[ω*t+φ]

3.2.3. Mathematica commands for plotting 2d and 3d for simple harmonic oscillations

c) We plot the displacement for the simple harmonic oscillations. We make a 2-dimensional graph and a 3-dimensional graph, and use the same values for the amplitude, pulsation, initial phase and time parameters as in the case of Maple program.

For the 2-dimensional case we obtain the graph from the Figure 3.

ln[1] Plot[2*Sin[Pi/4*t+Pi/3],{t,1,10}, PlotStyleHue[.1], Background→RGBColor [0.94174`,1.`,1.`], AxesLabel→{t, Ψ }]

Out[1]-Graphics-

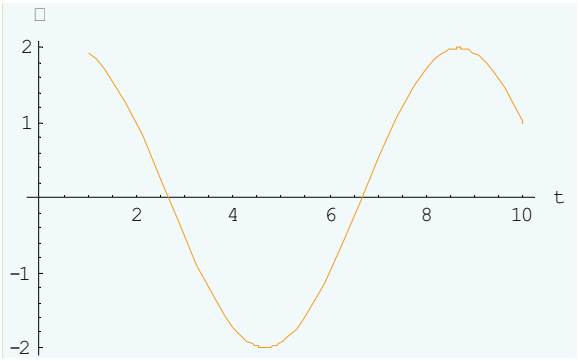

Figure 3. Simple harmonic oscillations, the 2d graph

There are many options for the color of the curve and for the color of the background. These can be set by using the option Graphics`Colors` and choosing from there the colors. The built-in *Mathematica* color directives RGBColor, Hue, and CMYKColor handle the most common systems. This package gives color directives using other standard systems. For axes we use the option AxesLabel and we plot the wave function Ψ on Y-axis against time t on X-axis.

The 3-dimensional case is illustrated in Figure 4. We plot the expression for the wave function using the same option for RGBColor as in the 2d case. For axes we use the option AxesLabel and we plot the wave function Ψ on Z-axis, against amplitude A on X-axis and time t on Y-axis.

ln[2] Plot3D[A*Sin[Pi/4*t+Pi/3], {A,0.1,1}, {t,1,10}, Background→RGBColor [0.94174`,1.`,1.`], AxesLabel→{A,t,Ψ}]

Out[2] -SurfaceGraphics-

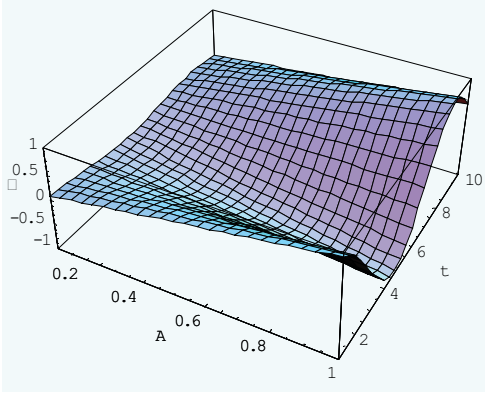

Figure 4. Simple harmonic oscillations, the 3d graph

ln[3] Show[f,Mesh→False]

Out[3] -SurfaceGraphics-

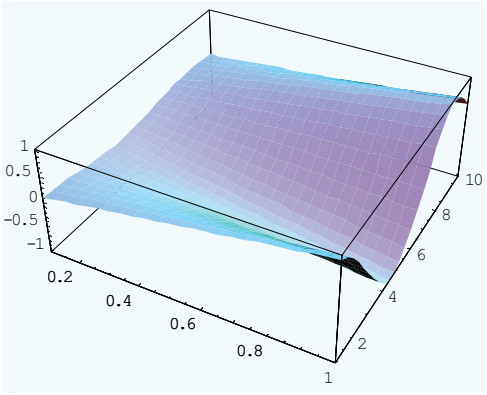

Figure 5. Simple harmonic oscillations, the 3d graph

Further, the SelectionAnimate or Sound Generation can be selected. Mathematica is a powerful computational tool which provides a large spectrum of choices for SelectionAnimate and for Sound Generation. It also provides simulations of relevant concepts.

In some particular cases of our applications, Mathematica and Maple programs have attached the GrTensor packages. These are useful for evaluating the components of some tensorial and pseudotensorial quantities. Important calculations can be carried out with GrTensorII and GrTensorM for studies concerning the general relativity. These packages allow evaluating the determinant of a metric, the covariant and contravariant components of the metric tensor, the components of the Einstein and Ricci tensor, and also to define new tensors and pseudotensors.

We also strongly encouraged the students to use either Mathematica or Maple to work on the homework problems.

4. CONCLUSIONS

In this paper, we examined the connection between physics studies and Computer Algebra Systems. Teaching and learning undergraduate physics using Mathematica 5.1 and Maple 9.5 is described through examples. Both Mathematica 5.1 and Maple 9.5 are very useful for learning, teaching, and carrying out research in physics.

We presented some examples from our course to demonstrate the usefulness of these computer programs. We have chosen the cases of simple harmonic oscillations and damped harmonic oscillations. Mathematica and Maple are used for solving the equation of motion in these two cases, for evaluating the velocity and acceleration in the case of simple harmonic oscillations and for plotting the displacement in both cases. We work with Mathematica 5.1 and Maple 9.5. For evaluating tensorial and pseudotensorial quantities the GrTensorII and GrTensorM packages are attached to Mathematica and Maple programs, respectively.

We will implement Mathematica and Maple as teaching and learning tools in our course of physics for civil engineering taking into account the advantages of these programs.

References

1. Ciobanu B., Radinschi I., One Computational Algorithm for Physics Modeling, P*roceedings of 5th International Conference on Electromechanical and Power Systems*, SIELMEN, Chisinau, Rep. Moldova, October 6-8, 2005, pp. 222-225.
2. Radinschi I., Ciobanu B., Implementation of Computational Methods in Physics Learning, *Proceedings of 4th International Symposium Computational Civil Engineering 2006*, Iasi, Romania, 2006, pp. 251-257.
3. Frunza M. D., Radinschi I., A Virtual Model for Testing Mathematics, Physics and Chemistry, *Proceedings of International Symposium for Design and Technology of Electronic Packages*, SIITME, 2006, p. 154, Iasi, Romania.
4. http://grtensor.org; http://www.maplesoft.com/maplebooks.html.
5. Ciobanu B., Radinschi I., Teaching and Learning Physics for Engineers by Aid Computers, *Proceedings of International Symposium IEEI 2006*, Iasi, Romania, Bulletin of IP Iasi, Vol. LII(LVI), Fasc.5, pp. 135-140.
6. Radinschi I., Scripcariu L., Ciobanu B., Frunza M. D., Online Teaching-while-Quizzing Test, *Proceedings of the 2nd National Conference on Applied Physics*, June 9-10, Galati, Romania, 2006, in press Romanian Journal of Physics
7. Ciobanu B., Radinschi I., A Sequential Programming Algorithm – a Tool for Study the Standing Waves, *Proceedings of International Symposium IEEI 2006*, Iasi, Romania, Bulletin of IP Iasi, Vol. LII(LVI), Fasc.5, pp. 129-134.
8. Radinschi I., Frunza M. D., Ciobanu B., Online Virtual Model for Testing the Knowledge, *Proceedings of INTED 2007*, March 7-9, Valencia, Spain.
9. Radinschi I., Ciobanu B., *Testing Physics*, Junimea Publishing House, Iasi, Romania, 2006.
10. Radinschi I., Ciobanu B., *Physics for Engineers*, Junimea Publishing House, Iasi, Romania, 2006.

"Computational Civil Engineering 2007", International Symposium
Iaşi, România, May 25, 2007

Computer Algebra System for Energy-Momentum Localization

Irina Radinschi[1], Brindusa Ciobanu[1]
[1]*Department of Physics, "Gh. Asachi" Technical University, Iasi, 700050, Romania, radinschi@yahoo.com*
[2] *Department of Physics, "Gh. Asachi" Technical University, Iasi, 700050, Romania, bciobanu2003@yahoo.com*

Summary

The aim of this paper is to sketch how computer algebra systems like Maple 9.5 with the GrTensorII package is used for performing calculations for energy-momentum localization. This computer algebra platform Maple and GrTensorII allows defining new objects like tensorial and pseudotensorial quantities, and for this purpose there are created procedures with GrTensorII 1.50 version. As the software Maple allows the use of complicated graphical methods, they were used to make the graphical representations. Maple has some advantages as flexibility and speed, and also advanced graphical facilities as animation. GrTensorII which is embedded in Maple is a package which allows us carrying out length calculations and evaluating the components of some tensorial and pseudotensorial quantities. This is because it has the facility for defining new tensors and pseudotensors. Furthermore, it allows the simplification of large terms and gives the possibility to evaluate the energy and momentum density components for a given metric. The duration of the calculations is shorter compared to that which used other software such as REDUCE. At international level, considerable efforts have been done to find a generally accepted expression for the energy-momentum density. This includes working with superenergy tensors, energy-momentum complexes, quasi-local expressions and tele-parallel quantities. Concerning the development of the existing theories and methods, we mention the enlargement of the areas by applying the energy-momentum complexes and their tele-parallel versions in the case of different 2, 3 and 3+1 dimensional space-times. Special attention has been paid to the connections between the results and furthermore to the connections with the tele-parallel theory of gravitation. In this context, we present some programs elaborated in GrTensorII which have been used for evaluating the energy and momentum components for the Einstein, Landau-Lifshitz and Møller energy-momentum complexes and make an investigation of the connection between physics studies and computational methods. We point out several important results that the energy-momentum complexes have yield for different geometries and some scientific perspective for future research in this area. Further, special attention was also paid for involving our master students in this interactive study: physical phenomena-computational methods.

KEYWORDS: computer algebra system, Maple, GrTensorII, energy-momentum localization.

1. INTRODUCTION

It is well-known that a computer algebra system like Maple is very useful for physics studies, and GrTensorII package [1] can be used for performing length calculations and evaluating the components of some tensorial and pseudotensorial quantities. Further, GrTensorII is a reliable tool for evaluating the energy and momentum components of the energy-momentum complexes of Einstein [2], Landau-Lifshitz [3] and Møller [4] and gives a deeper understanding of these prescriptions.

The different attempts at constructing an energy-momentum density don't give a generally accepted expression. The “center” of general relativity is one of the most interesting and challenging ideas in modern science, the one that gravity is the geometry of curved four-dimensional space-time. In conclusion, gravity is geometry. For localizing the energy there have been used many definitions, including superenergy-tensors, the energy-momentum complexes, the quasi-local quantities, and the tele-parallel theory of gravitation. The energy-momentum complexes definitions include the Einstein [2], Landau-Lifshitz [3], and Møller [4] prescriptions. These prescriptions have been criticized because of their drawback, they are coordinate dependent. Except the Møller energy-momentum complex which allows evaluating the energy distribution in any coordinate system, the other prescriptions give meaningful results only if the calculations are restricted to quasi-Cartesian coordinates. There are doubts that these pseudotensorial definitions yield good results for a given space-time. In this light, some remarks are needed: 1) the energy-momentum complexes (ELL) are non-covariant, coordinate dependent expressions and yield acceptable results only the calculations are carried out in quasi-Cartesian coordinates, 2) only the Møller energy-momentum complex enables one to calculate the energy in any coordinate system and 3) this agrees with the equivalence principle which states that gravity cannot be detected at a point. Chang, Nester and Chen [5] showed that the energy-momentum complexes are actually quasi-local and legitimate expressions for the energy-momentum. They concluded that there exist a direct relationship between energy-momentum complexes and quasi-local expressions because every energy-momentum complexes is associated with a legitimate Hamiltonian boundary term. In the last decades the issue of the energy-momentum localization by applying the energy-momentum complexes was re-opened and many interesting results have been obtained [6], which demonstrate that these prescriptions are powerful concepts for energy-momentum localization. All these considerations point out the significance of these prescriptions and stress the usefulness of Maple program and GrTensorII package which allow calculating the energy and momentum components for a given space-time, and also making graphical representations.

2. GRTENSORII PACKAGE AND ENERGY-MOMENTUM COMPLEXES

2.1. Energy-momentum complexes

2.2.1. General comments

As we pointed out in Introduction, the lack of the pseudotensorial prescriptions is connected to the dependence of the energy-momentum complexes on the coordinate systems. Only the Møller prescription allows evaluating the energy and momentum in any coordinate system. The other energy-momentum complexes of Einstein and Landau-Lifshitz yield reliable results if the calculations are carried out in quasi-Cartesian coordinates. In this context, another important problem appears. According to recent studies, although the energy-momentum complexes behave under general coordinate transformations like non-tensorial objects, the local conservation laws obtained by them hold in all coordinate systems. The Einstein and Landau-Lifshitz energy-momentum complexes give the same energy distribution as the Penrose definition for a general non-static spherically symmetric metric of the Kerr-Schild class [7]. In the case of the most general non-static spherically symmetric metric these definitions disagree concerning the expression for the energy distribution [7].

2.2.2. Maple and GrTensorII platform for the Einstein, Landau-Lifshitz and Møller prescriptions

The GrTensorII programs for the Einstein, Landau-Lifshitz and Møller energy-momentum complexes are given below. Further, examples for a class of solutions belonging to the string theory are presented [8]-[10].

GrTensorII for the Einstein energy-momentum complex:

```
>readlib(grii):
>grtensor();
> grdef(`H{k^m^l^n}:=(-detg)*(g{^k^m}*g{^l^n}-g{^l^m}*g{^k^n})`):
Created definition for H(dn,up,up,up)
> grdef(`H1{i^k^l}:=1/sqrt(-detg)*g{i m}*H{k^m^l^n,n}`):
Created a definition for    H(dn,up,up,up,pdn)
Created definition for H1(dn,up,up)
```

GrTensorII for the Landau-Lifshitz energy-momentum complex:

```
>readlib(grii):
>grtensor();
> grdef(`S3{^m^j^n^k}:=-detg*(g{^m^n}*g{^j^k}-g{^m^k}*g{^j^n})`):
Created definition for S3(up,up,up,up)
> grdef(`S4{^m^n^k}:=S3{^m^j^n^k,j}`):
Created a definition for    S3(up,up,up,up,pdn)
Created definition for S4(up,up,up)
```

GrTensorII for the Møller energy-momentum complex:

```
> grdef(`M{i^k^l}:=sqrt(-detg)*(g{i m,n}-g{i n,m})*g{^k^n}*g{^l^m}`):
Created definition for M(dn,up,up)
```

The first two commands in these procedures are for starting the GrTensorII package. The command grdef is used for defining the required energy-momentum complexes.

The Einstein, Landau-Lifshitz and Møller energy-momentum complexes are used for evaluating the energy and momentum components for the space-time which describes a magnetic stringy solution. The metric is used in the initial form for the Møller prescription and is transformed in quasi-Cartesian coordinates for the Einstein and Landau-Lifshitz prescriptions. The following results are obtained:

```
> qload(kar1);
Calculating ds for kar1 ... Done. (0.000000 sec.)
> grcalc(M(dn,up,up)):
Calculating g(dn,dn,pdn) for kar1 ... Done. (1.000000 sec.)
Calculating detg for kar1 ... Done. (0.000000 sec.)
Calculating g(up,up) for kar1 ... Done. (0.000000 sec.)
Calculating detg for kar1 ... Done. (0.000000 sec.)
Calculating M(dn,up,up) for kar1 ... Done. (0.000000 sec.)
> grdisplay(M(dn,up,up));
```

$$M_{\theta}{}^{r}{}_{\theta} = -2\frac{\sqrt{\frac{M^2 r^6 \sin(\theta)^2}{(Mr-Q^2)^2}(Mr-Q^2)(r-2M)}}{r^3 M}$$

$$M_{\phi}{}^{\phi}{}_{\theta} = 2\frac{\sqrt{\frac{M^2 r^6 \sin(\theta)^2}{(Mr - Q^2)^2}}\cos(\theta)}{r^2 \sin(\theta)}$$

$$M_{\phi}{}^{r}{}_{\phi} = -2\frac{\sqrt{\frac{M^2 r^6 \sin(\theta)^2}{(Mr - Q^2)^2}}(Mr - Q^2)(r - 2M)}{r^3 M}$$

$$M_{t}{}^{t}{}_{r} = \frac{\sqrt{\frac{M^2 r^6 \sin(\theta)^2}{(Mr - Q^2)^2}}(2M^2 - Q^2)}{Mr^2}$$

```
> qload(kar);
```

Calculating ds for kar ... Done. (0.000000 sec.)

```
> grcalc(H1(dn,up,up)):
```

Calculating g(dn,dn,pdn) for kar ... Done. (1.000000 sec.)

Calculating detg for kar ... Done. (0.000000 sec.)

Calculating g(up,up) for kar ... Done. (0.000000 sec.)

Calculating detg for kar ... Done. (0.000000 sec.)

Calculating H1(dn,up,up) for kar ... Done. (0.000000 sec.)

```
> grdisplay(H1(dn,up,up));
```

$$Hl_{t}{}^{t}{}_{x} = 2(rQ^2 + 2M^2 r - 2MQ^2)xM/\left(r^2(Mr - Q^2)^2\left(M(r^4 M - r^3 Q^2 - 2r^3 M^2 + 2r^2 MQ^2 + 2z^2 M^2 r + 2y^2 M^2 r + 2x^2 M^2 r + z^2 rQ^2 + x^2 rQ^2 + y^2 rQ^2 - 2z^2 MQ^2 - 2y^2 MQ^2 - 2x^2 MQ^2)/\left(r^2(Mr - Q^2)^2\right)\right)^{1/2}\right)$$

$$Hl_{t}{}^{t}{}_{y} = 2My(rQ^2 + 2M^2 r - 2MQ^2)/\left(r^2(Mr - Q^2)^2\left(M(r^4 M - r^3 Q^2 - 2r^3 M^2 + 2r^2 MQ^2 + 2z^2 M^2 r + 2y^2 M^2 r + 2x^2 M^2 r + z^2 rQ^2 + x^2 rQ^2 + y^2 rQ^2 - 2z^2 MQ^2 - 2y^2 MQ^2 - 2x^2 MQ^2)/\left(r^2(Mr - Q^2)^2\right)\right)^{1/2}\right)$$

$$Hl_{t}{}^{t}{}_{z} = 2(rQ^2 + 2M^2 r - 2MQ^2)zM/\left(r^2(Mr - Q^2)^2\left(M(r^4 M - r^3 Q^2 - 2r^3 M^2 + 2r^2 MQ^2 + 2z^2 M^2 r + 2y^2 M^2 r + 2x^2 M^2 r + z^2 rQ^2 + x^2 rQ^2 + y^2 rQ^2 - 2z^2 MQ^2 - 2y^2 MQ^2 - 2x^2 MQ^2)/\left(r^2(Mr - Q^2)^2\right)\right)^{1/2}\right)$$

$$Hl_t{}^{x}{}_{t} = -2\left(r Q^2 + 2 M^2 r - 2 M Q^2\right) x M \Big/ \Big(r^2 \left(M r - Q^2\right)^2 \Big(M \big(r^4 M - r^3 Q^2 - 2 r^3 M^2 + 2 r^2 M Q^2 + 2 z^2 M^2 r + 2 y^2 M^2 r + 2 x^2 M^2 r + z^2 r Q^2 + x^2 r Q^2 + y^2 r Q^2 - 2 z^2 M Q^2 - 2 y^2 M Q^2 - 2 x^2 M Q^2 \big) \Big/ \left(r^2 \left(M r - Q^2\right)^2 \right) \Big)^{1/2} \Big)$$

$$Hl_t{}^{y}{}_{t} = -2 M y \left(r Q^2 + 2 M^2 r - 2 M Q^2\right) \Big/ \Big(r^2 \left(M r - Q^2\right)^2 \Big(M \big(r^4 M - r^3 Q^2 - 2 r^3 M^2 + 2 r^2 M Q^2 + 2 z^2 M^2 r + 2 y^2 M^2 r + 2 x^2 M^2 r + z^2 r Q^2 + x^2 r Q^2 + y^2 r Q^2 - 2 z^2 M Q^2 - 2 y^2 M Q^2 - 2 x^2 M Q^2 \big) \Big/ \left(r^2 \left(M r - Q^2\right)^2 \right) \Big)^{1/2} \Big)$$

$$Hl_t{}^{z}{}_{t} = -2\left(r Q^2 + 2 M^2 r - 2 M Q^2\right) z M \Big/ \Big(r^2 \left(M r - Q^2\right)^2 \Big(M \big(r^4 M - r^3 Q^2 - 2 r^3 M^2 + 2 r^2 M Q^2 + 2 z^2 M^2 r + 2 y^2 M^2 r + 2 x^2 M^2 r + z^2 r Q^2 + x^2 r Q^2 + y^2 r Q^2 - 2 z^2 M Q^2 - 2 y^2 M Q^2 - 2 x^2 M Q^2 \big) \Big/ \left(r^2 \left(M r - Q^2\right)^2 \right) \Big)^{1/2} \Big)$$

```
> qload(kar);
```

Calculating ds for kar ... Done. (0.000000 sec.)

```
> grcalc(S3(up,up,up,up,pdn),S4(up,up,up)):
```

Calculating g(dn,dn,pdn) for kar ... Done. (1.000000 sec.)

Calculating detg for kar ... Done. (0.000000 sec.)

Calculating g(up,up) for kar ... Done. (0.000000 sec.)

Calculating detg for kar ... Done. (0.000000 sec.)

Calculating S3(up,up,up,up,pdn) for kar ... Done. (0.000000 sec.)

Calculating S4(up,up,up) for kar ... Done. (0.000000 sec.)

```
> grdisplay(S4(up,up,up));
```

$$S4^{t\,t}{}_{x} = -2\,\frac{x\left(r Q^2 + 2 M^2 r - 2 M Q^2\right)}{r^2\left(M r - Q^2\right)(-r + 2 M)}$$

$$S4^{t\,t}{}_{y} = -2\,\frac{y\left(r Q^2 + 2 M^2 r - 2 M Q^2\right)}{r^2\left(M r - Q^2\right)(-r + 2 M)}$$

$$S4^{t\,t}{}_{z} = -2\,\frac{z\left(r Q^2 + 2 M^2 r - 2 M Q^2\right)}{r^2\left(M r - Q^2\right)(-r + 2 M)}$$

The command qload in these procedures is for loading the metric, grcalc is designated for calculating the energy and momentum components for the aforementioned energy-momentum complexes, and the command grdisplay is used for displaying the results. The energy components of the Einstein, Landau-Lifshitz and Møller energy-momentum complexes are involved in calculating the expression for energy in the case of the aforementioned magnetic stringy solution.

For plotting the expressions for energy obtained in the Einstein, Landau-Lifshitz and Møller prescriptions on the same graph the next Maple 9.5 commands are used. We denote with f, g and h the expressions for energy in the Landau-Lifshitz, Einstein and Møller prescriptions, respectively. In all expressions we consider the case M=1.

```
> with(plots);
> f:=r/2*(r*Q^2+2*r-2*Q^2)/((r-2)*(r-Q^2));
> g:=1/2*(r*Q^2+2*r-2*Q^2)/(r-Q^2);
> h:=r/2*(2-Q^2)/(r-Q^2);
> plot3d({f,g,h},r=0...100,Q=0.1...1);
```

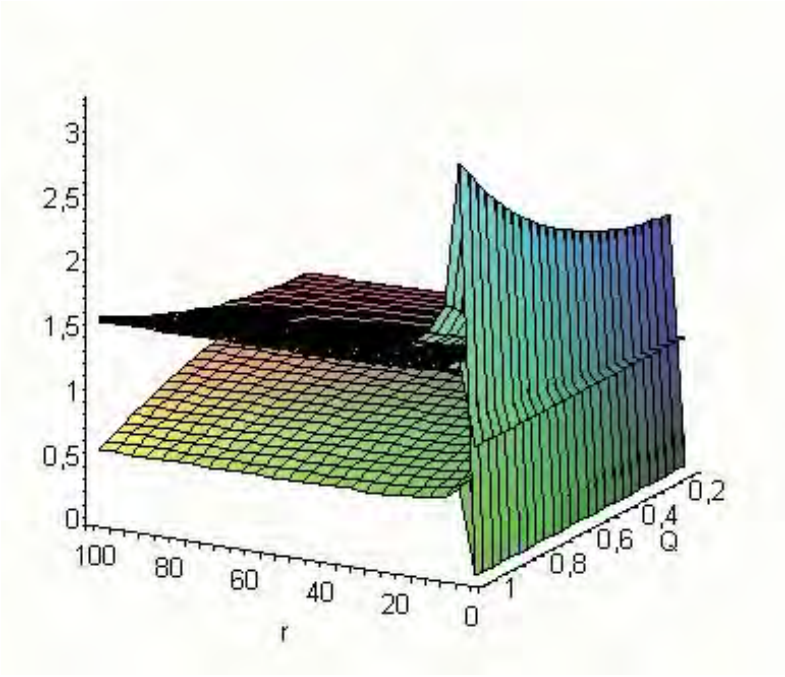

Figure 1. Energy on Z-axis plotted against r on X-axis and Q on Y-axis

3. CONCLUSIONS

In the last decade the problem of the energy-momentum complexes has been re-opened and acceptable results have been obtained [6] for different space-times. Many authors used different energy-momentum prescriptions to investigate the energy distributions for a given geometry. They demonstrated that in many cases several energy-momentum complexes yield the same and acceptable result. Chang, Nester and Chen [5] showed that the energy-momentum complexes are actually quasi-local and legitimate expressions for the energy-momentum. Their idea supports the energy-momentum complexes and the role which these are playing in energy-momentum localization. Furthermore, important studies have been done about the new idea of quasi-local approach for energy-momentum complexes [11]-[12] and a large class of new pseudotensors connected to the positivity in small regions have been constructed [13]. In this light, the quasi-local quantities are associated with a closed 2-surface (L. B. Szabados, [12] and http://relativity.livingreviews.org/Articles/lrr-2004-4/). The Hamiltonian boundary term determines the quasi-local quantities for finite regions and the special quasi-local energy-momentum boundary term expressions correspond each of them to a physically distinct and geometrically clear boundary condition [14].

Maple and GrTensorII procedures are used for evaluating the energy and momentum components of the Einstein, Landau-Lifshitz and Møller energy-momentum complexes. Some of our results are presented, and the metric under consideration describes a magnetic stringy solution. GrTensorII yields the energy and momentum components which are involved in the expression for energy and momentum densities. The expressions for energy in the Einstein, Landau-Lifshitz and Møller prescriptions are plotted on the same graph using Maple 9.5 commands for 3d graphs. The computer algebra platform Maple 9.5 and GrTensorII package is used for performing the calculations and graphical representations, and in this way a powerful connection between physics studies and computational methods is established. The young master students play an important role in this activity and their tasks are clearly defined. They are mostly needed to clarify the problems related to theoretical physics and computational and mathematics demands. Their contributions are meant to be strictly related to their dissertation papers. They also have the possibility to enlarge the circle of collaborations abroad and gather a lot of information in the field and the adjacent topics.

References

1. http://grtensor.org; http://www.maplesoft.com/maplebooks.html.
2. Einstein, A., *Preuss. Akad. Wiss.* Berlin 47, 778, 1915; Addendum-ibid. 47, 799, 1915; Trautman, A. in *Gravitation*: *an Introduction to Current Research*, ed. L. Witten, Wiley, New York, p. 169, 1962.
3. Landau, L. D., Lifshitz, E. M. *The Classical Theory of Fields*, Pergamon Press, p. 280, 1987.

4. Møller, C. *Ann. Phys.* (*NY*) 4, 347, 1958.
5. Chang, Chia-Chen, Nester, J. M., Chen, Chiang-Mei, *Phys. Rev. Lett.* 83, 1897, 1999.
6. Aguirregabiria, J. M., Chamorro, A., Virbhadra, K. S., *Gen. Rel. Grav.* 28, 1393, 1996; Vagenas, E. C., *Mod. Phys. Lett.* A21, 1947, 2006; Sharif M., Fatima, Tasnim, *Astrophys. Space Sci.* 302, 217, 2006; Gad, Ragab M., *Gen. Rel. Grav.* 38, 417, 2006; Grammenos, Th., *Mod. Phys. Lett.* A20, 1741, 2005; Radinschi, I., *Mod. Phys. Lett.* A15, Nos. 11&12, 803, 2000; Radinschi I., Grammenos, Th., *Int. J. Mod. Phys.* A21, 2853, 2006; Aydogdu, O., Salti, M., *Astrophys. Space Sci.* 302, 61, 2006.
7. Virbhadra, K. S., *Phys. Rev.* D60, 104041, 1999.
8. Radinschi, I,. *Rom. J. Phys.* Vol.50, Number 1-2, 57, 2005.
9. Radinschi I., Ciobanu B., International Conference Fifty Years of Romanian Astrophysics, Bucharest, September 27-30, AIP, 2006
10. Radinschi, I., Yang, I-Ching, *On the Energy of Stringy Black Holes*, New Developments in String Theory Research, ed. Susan A. Grece, Nova Science Publishers, Inc New York, U.S.A., p. 17, 2006.
11. Chang, Chia-Chen, Nester, J. M., *Class. Quant. Grav.* 16, 1279, 1999.
12. Chang, Chia-Chen, Nester, J. M., Chen, *Grav. Cosmol.* 6, 257, 2000; Szabados, L. B., *Living. Rev. Relativity* 7, 4, 2004.
13. So, Lau Loi, Nester, James M., Chen, Hsin, gr-qc/0605150, to appear in Proceedings of the 7th International Conference on Gravitation and Astrophysics; Deser, S., Franklin, J.S., Seminara, D., *Class. Quant. Grav.* 16, 2815, 1999.
14. Nester, James M., *Class. Quant. Grav.* 21, S261, 2004; Chen, Chiang-Mei, Nester, J. M., Tung, Roh-Suan, *Phys. Rev.* D72, 104020, 2005.

"Computational Civil Engineering 2007", International Symposium
Iaşi, România, May 25, 2007

The state of stresses in RC beams with installation holes located in compressed zone

Przemysław Siwiec[1], Sebastian Toś[1]
[1]*Institute of Building Engineering, Wroclaw University of Technology*

Summary

This paper presents a question of influence of installation holes located in the compressed zone of the reinforced concrete beam on functioning. In order to research the actual functioning of the element a numerical model based on Finite Element Method has been created.

Two independent analyses were performed in which linear and nonlinear constitutive relations for concrete and for steel have been used. The results acquired have been compared and discussed.

KEYWORDS: RC beam, nonlinear FEM analysis, nonlinear material, numerical model, numerical analysis.

1. INTRODUCTION

Designing process of reinforced concrete structures (RCS) is based on current state of knowledge. Codes of Practice (CP) in many countries are based on this knowledge. It can be considered that if an element is designed according to requirements of the CP and it fulfills requirements of border states (in both phases: service and mount) as well as construction requirements, there is certain probability that it will be safe and will properly carry adequate loads.

The problem occurs when there is need to specify the state of safety of reinforced concrete element not designed in accordance with requirements of the CP and especially when it doesn't fulfill construction requirements. Then it is necessary to perform a complete analysis of stresses and strains according to rules of mechanics. And here a problem arises: according to rules of a linear analysis it is not possible to specify correctly the state of stresses in reinforced concrete elements in the II (2nd) phase. So there is a need to make the analysis based on physical and geometrical nonlinearities in reinforced concrete.

2. NONLINEAR MODEL

Fundamental physical stress-strains relations based on assumption of linear elastic relation come from the Hook's law. The structure deformations are not proportional to the loads and this irregularity in material of a structure. This kind of material is called plastic.

From the point of view of theory of elasticity, material turns to undetermined state after exceeding limit value of stresses (criterion of plasticity) defined by constitutive relationships between stresses and strains. There are many criteria of plasticity in complex state of stresses [1,2,3]. The most popular are: Trasca and Von Mises (M-H-V) yield criterion for describing materials such as steel and aluminum; and Coulomb and Druckner-Prager yield criterion for describing such materials as concrete, rocks, soils and sands. In literature, for describing plasticity in reinforced concrete the most popular are Von Mises criterion (M–H–V) for steel and Druckner-Prager criterion for concrete under compression. The most divergences among researchers of the problem have been caused by concrete under tension. The solutions used [4.5.6.7] are mainly connected with adopted calculation techniques. In this paper the Finite Element Method as a basic analytical tool has been used. Within a framework of this method the smeared crack approach for modeling concrete under tension has been used.

Basic assumption of theory of plasticity in FEM formulation is decomposition of strains to elastic and plastic parts:

$$\varepsilon = \varepsilon^e + \varepsilon^p \tag{1}$$

Such a model is called elasto-plastic. The most important consequence of adopting this material model relation between total stresses for certain time t and total strains for time t, is additional parameter – a function of stresses and strain history. This function is taken into account by internal parameter of state □, governed by a specific evolution law. Properties of elasto-plastic material are determined by assumptions:

- the elastic relation between total stresses and strains is given by:

$$\sigma = \mathbf{D}\varepsilon^e \tag{2}$$

- the yield condition determines the state of stresses when the plastic flow is initiated. This condition is determined by vector function of stresses and by the parameter of state κ, according to relationship:

$$f(\sigma, \kappa) = 0 \tag{3}$$

- the flow rule specifies the plastic strain rate vector as a function of the state of stresses in relationship:

$$\dot{\varepsilon}^p = \sum_{j=1}^{n} \dot{\lambda}_j \frac{\partial g_j}{\partial \sigma} \tag{4}$$

for n functions of plastic potential g_j which can also be considered as a function of the stress vector and state parameter $g_j(\sigma,\kappa)$.

The plastic multiplier $\dot{\lambda}_j$ is determined from Kuhn-Tucker conditions:

$$\begin{cases} f \le 0 \\ \dot{\lambda}_j \ge 0 \\ \dot{\lambda}_j f = 0 \end{cases} \tag{5}$$

- the hardening hypothesis describes evolution of the internal state parameter κ. Generally, changes of κ parameter are given by a function of the stresses vector and the plastic strain rate vector, i.e.:

$$\dot{\kappa} = h(\sigma, \dot{\varepsilon}^p) \tag{6}$$

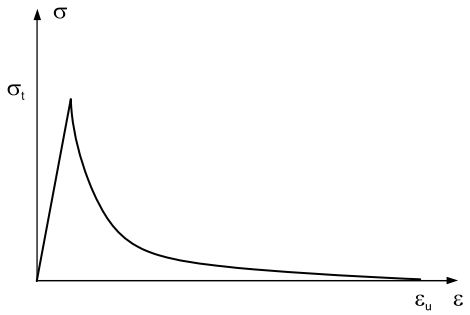

Fig. 1 – The stress-strain relation in crack.

The smeared crack approach puts forward two concepts: smeared cracks with fixed direction which is determined when the crack is initiated (constant direction of the crack during the whole iteration) and the rotated cracks (the crack direction changes during iteration according to redistribution of main stresses). Transient concept is multi-directional crack model which makes an assumption that a new crack arises when angle between direction of vector of actual main stresses and direction normal to the old crack exceeds certain value but the old one is still active.

The fundamental feature of smeared crack approach is taken from decomposition of the total strain into elastic strain and a crack strain as:

$$\varepsilon = \varepsilon^{e} + \varepsilon^{cr} \tag{7}$$

During increasing of loading, the new cracks simultaneously occur and everyone of them makes new local co-ordinate system n-t. For the crack strain for crack i which is given by:

$$e_i^{cr} = \left[\varepsilon^{cr}{}_{nn,i}, \gamma^{cr}{}_{nt,i} \right]^T \tag{8}$$

total strain vector in crack is given by:

$$e^{cr} = \left[e_1^{cr}, e_2^{cr}, \ldots, e_n^{cr} \right]^T \tag{9}$$

Basic cracking parameters of the smeared crack concepts are: tensile strength of concrete which determines when crack appears, fracture energy which determine how much of energy is dissipated when a unit of crack appears (the area under σ–ε curve in crack in fig. 1, shear retention relation in crack, the tension softening relations as a relation between crack stress and crack strain (shape of descending part of relations in fig. 1).

3. DESCRIPTION OF PROBLEM.

During the analysis of large precast concrete structure [8] it has been noticed that almost every beam has from 4 to 8 holes located in compressed zone. Through these holes go installation pipes.

Fig. 2 – Shown Precast concrete beams with installations holes.

Detailed analysis of the project has shown that no analysis of influence of these holes on load-carrying capacity and operating conditions had ever been carried out.

The analysis has been made for 11,54 m long precast concrete beam (0,40x1,025). It had 8 holes (see fig. 2) 3,60 m from the end of the beam 4 installation holes

(15cm in diameter), have been made. They have been placed 20cm from the upper edge (i.e. the compressed zone).

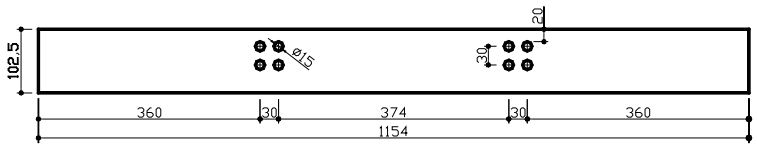

Fig. 3 – Draft of the beam. Installation holes displayed.

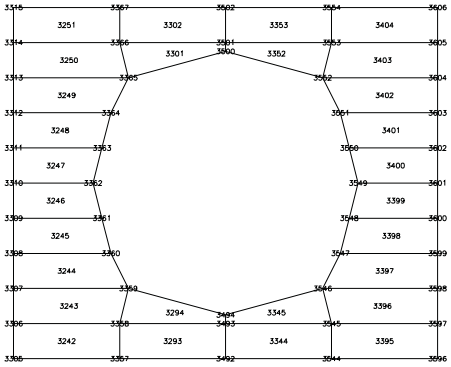

Fig. 4 – Scheme of nodes arrangement around the hole.

4. DESCRIPTION OF NUMERICAL MODEL.

The Finite Element Model has been designed with 4-node plain stress elements (fig. 4 and 5). Reinforcement has been modeled as embedded bars in structural elements – reinforcement strains have been computed on the basis of the displacement field of the mother element. This approach guarantees full connection of finite element and reinforcement (without any bond-slip). In numerical model both linear and nonlinear constitutive principles for concrete and steel have been used. The computer model has been performed only for a support zone 4 m long. It has been assumed that material was homogeneous – cross-sections only along neutral axis have been examined.

5. CALCULATIONS AND RESULTS.

For numerical calculation the actual load from the design project (216,78kN/m) has been taken into account. This load yields the bending moment at 3568,89kN/m.

In the figures 6 and 7 the linear static analysis results have been presented.

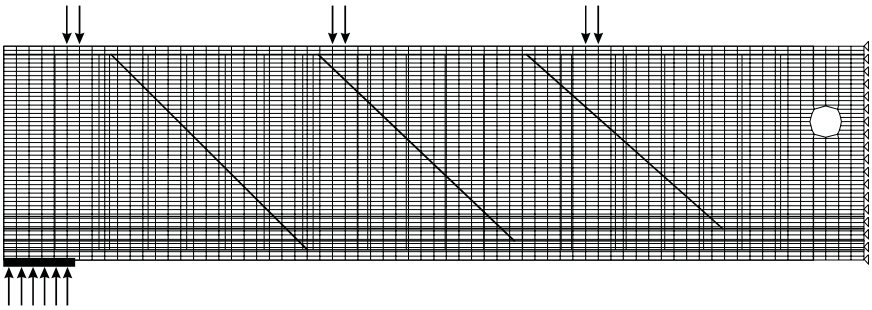

Fig. 5 – Scheme of finite elements arrangement.

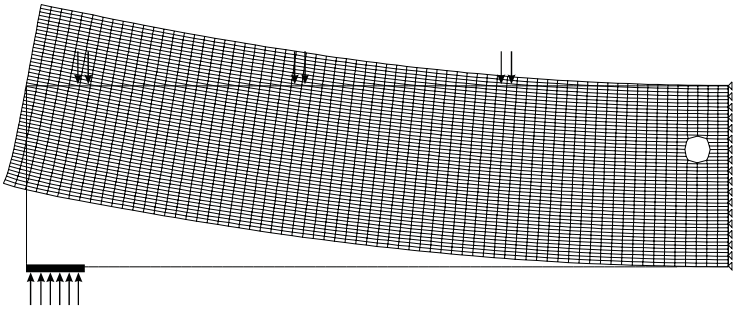

Fig. 6 – Beam deformations draft – linear static analysis.

It can be noticed that elastic relations in concrete don't allow to analyze properly the stress distribution in concrete. According to this analysis the tensile stresses reach 11,71 MPa, which is not true. Therefore the correctness of stress distribution and its values around the hole could be questioned.

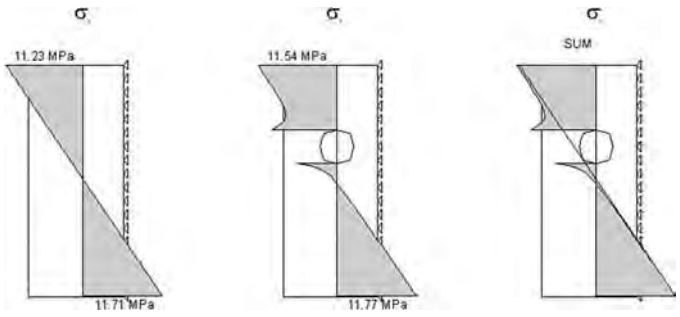

Fig. 7 – Stress distribution around the hole – linear static analysis.

In order to eliminate this problem the nonlinear analysis has been performed.

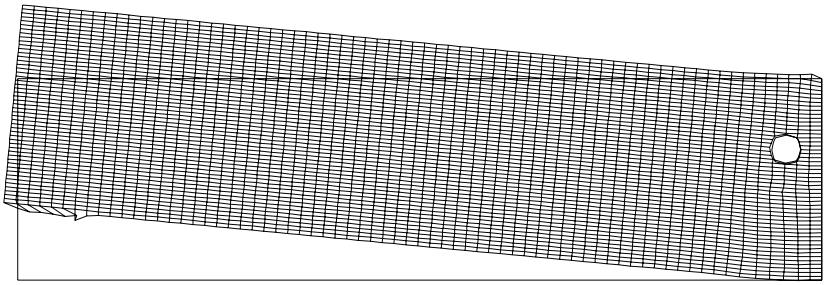

Fig. 8 – Element deformation for Lf= 2,496 (damage of the beam) – nonlinear analysis.

The numerical analysis has been carried out with use of Newton-Rawston iterative algorithm for solving a nonlinear system of equations. For iteration process the arc-length spherical method for prediction of load increment and energy norm criterion for convergence criterion of equilibrium iteration have been used. During numerical analysis load has been progressively increased in order to fulfill equation:

$$L_f \cdot \overline{\mathbf{K}} \times \overline{\mathbf{v}} = \overline{\mathbf{F}} \tag{10}$$

Where:
- L_f – scalar nonlinear load coefficient,
- K – global stiffness matrix,
- v – general displacements vector,
- F – general loads vector.

Response of the structure has been presented as a relation between selected degree of freedom in function of nonlinear load coefficient (Lf) which allows to determine critical values of loads at which structure fails (see fig. 10).

Structure damage mechanism can be observed through the research (albo investigation) of model deformation during the nonlinear analysis (fig. 8). The breaking of the beam close to the hole can be noticed very clearly. This has been caused by (the lack of) elastic recovery of other parts of researched element (no flexion).

Crack development has presented the state of stresses in the structure. In fig.9 areas of active cracks have been displayed.

An important fact is appearing of skew cracks (in the support zone) for coefficient of deformation Lf equal to 1,0 which has been observed in real structure as well. During damage phase almost the whole tensile zone of the beam has been cracked.

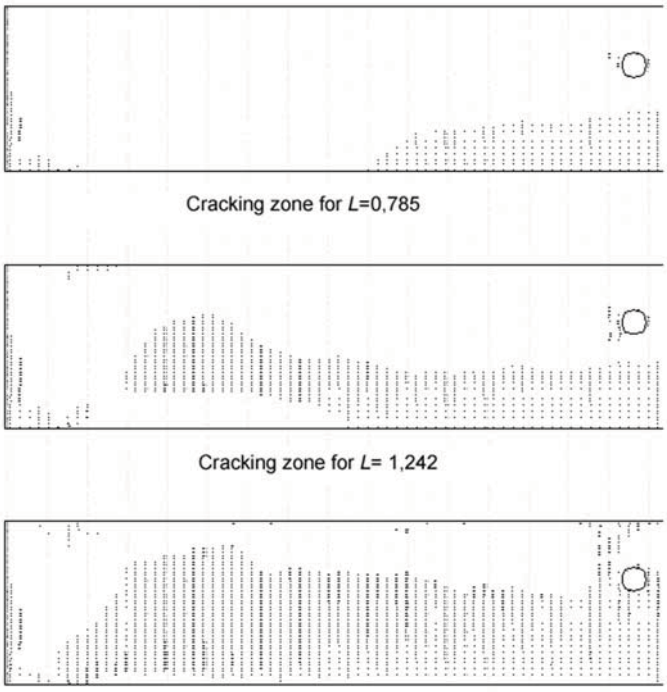

Fig. 9 – Development of cracking zone for different values of nonlinear loads coefficient Lf.

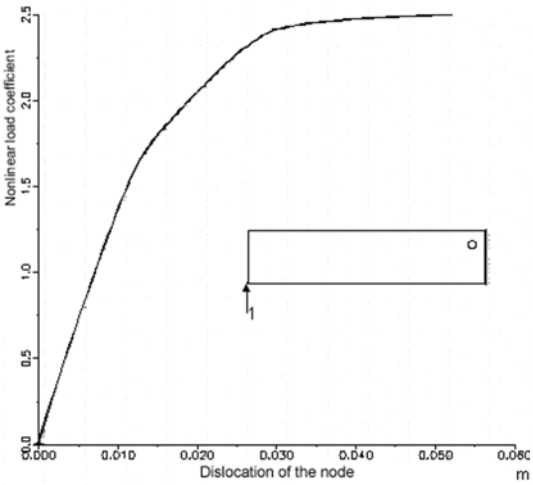

Fig. 10 – Relation between displacement of node 1 and nonlinear load coefficient L_f.

Through nonlinear analysis and stress distribution it is possible to determine crack development and neutral axis position of cross-section of RC beam (fig. 12). As contrasted with the nonlinear analysis, the linear analysis of RC structure has proved almost totally useless (fig. 11).

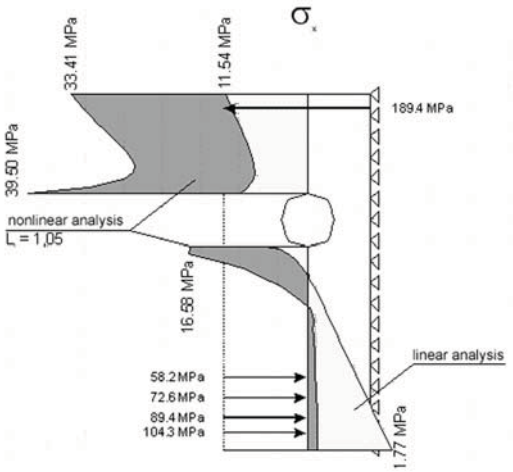

Fig. 11 – Stress distribution around the hole received from nonlinear analysis.

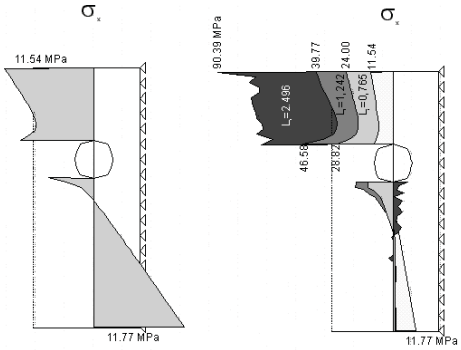

Fig. 12 – Stress distribution from linear and nonlinear analysis for various loads coefficients. Left – linear analysis, Right – nonlinear analysis.

6. CONCLUSIONS

In result of the analysis of the computer model an image of stresses around the hole has been received (fig. 7 and fig.11, 12). It can be seen very clearly there occurred a disorder in stress distribution around the hole. It is significant that stress increment at the edge of the hole reaches up to 70% of material strength (compression strength of concrete). However this disorder decays and about 10 cm from the hole edge stresses reach regular values (similar to those of elements without holes).

The analysis of a nonlinear loads coefficient has shown that the beam fails at large values of this coefficient (about 2,5 times of service load) which leaves large safety margin for the structure. Therefore it can be stated that the influence of the hole is not significant for decreasing of the beam safety.

Additionally the nonlinear computer model has been proved highly reliable for the analyses of cracked RC elements.

References

1 Blaauwendraad J.: *Numerical Methods in Structural Mechanics* – Delft University of Techniology – 1993

2 De Borst R.: *Computational Methods in Non-linear Solid Mechanics* – Delft University of Technology, seria B20, Delft – 1993

3 Feenstra P. H., De Borst R., Rots J. G.: *The application of various crack models to F.E. analysis of reinforced concrete panels* - Nonlinear Engineering Computation, ed. N. Bićanić, D.R.J. Owen, 1991

4 Grootenboer J. J., Leijten S. F. C. H., Blaauwenraad J.: *Concrete mechanics, Part C, Numerical models for reinforced concrete structures in plain stress* – Heron vol. 26, Delft – 1981

5 Rots J. G., Blaauwenraad J.: *Crack model for concrete: Discrete or smeard? Fixed, multi-linear or rotatin?* – Heron 34, Delft – 1989

6 Rots J. G., Nauta P., Kusters G. M. A., Blaauwenraad J.: *Smeared crack approach and fracture localization in concrete* – Heron, vol. 30, 1985

7 Siwiec P., Strouven P., Moczko A.: *Study of steel bar corrosion by experimental and analytical simulation* – DIANA Computational Mechanics '94, ed. Kusters M. A., Hendriks A. N., Kluwer Academic Publishers, Dordrecht – 1994

8 Szechiński M, Kamiński Kamiński.: *Research on reinforced Concrete structure after the damage*, Reports of Institute of Buiding Ingeneering of the Wrocław University of Technology, Wrocław. Poland. 2001.

"Computational Civil Engineering 2007", International Symposium
Iaşi, România, May 25, 2007

Computer Graphical Communication an Efficient Tool for Understanding the Design of Wooden Trusses

Andrei Slonovschi[1], Ion Antonescu[1] and Liviu Prună[1]
[1]*Department of Descriptive Geometry and Technical Drawing,*
Technical University "Gh. Asachi" Iasi, 6600, Romania

Summary

In design or workmanship the civil engineers (designers, chiefs of building yards, etc.) often encounter moments when they need to create or read technical drawing plans.

The skill of plan's reading is firstly due to the capacity of engineer to create mental images. This ability differs from one individual to another allowing it's exploiting and training in a manner that allow him to communicate with the other engineers, making him fully understood, by learning and training the concepts of Descriptive Geometry, Technical Drawing and Computer Graphics.

The routine of mentally converting space representations in plane drawings and reverse, by using an engineering common language or, in other words, to communicate through graphical approach engineering data, is achieved in Civil Engineering Faculty in the firs year of study.

Practical experience in teaching disciplines regarding graphical communication shows, as expected, that exclusive using of didactic charts using bi-dimensional representations isn't sometimes enough for students to understand the three-dimensional shape of complex construction elements.

Taking account of these factors three-dimensional didactic models for drawings with a high level of understanding difficulty were proposed and developed.

KEYWORDS: Computer Graphical Communication, Descriptive Geometry, Technical Drawing, Computer Graphics, 3D Model, AutoCAD, Triple Orthographic Projection, Axonometric Isometric Projection.

1. INTRODUCTION

In design and execution activity, a fundamental role in creation and understanding of technical drawing blueprints has the ability of person to create mental images, without which it be practically impossible to read and relate the views of a drawing for understanding the shape of existing or virtual parts composing the future buildings.

The bulk of first year students from technical faculties, hence the ones from Civil Engineering Faculties, don't have a trained ability for creating mental images, in other words, to see with their mind's eyes the three-dimensional shape of a part staring from it's 2D graphical representations and haven't any knowledge about existing conventions or standards referring to graphical communication.

This skill together with data related to graphical communication language is acquired in the firs year of study at Descriptive Geometry and Technical Drawing disciplines.

Introduction of computer graphics and CAD programs (e.g. AutoCAD) facilitate the acquiring of this skill by their capacity to create virtual images suggesting the 3D shape of bodies.

Let see further how computer graphics together with descriptive geometry and technical drawing help in developing of future engineers' 3D space vision.

2. THE NECESSITY OF USING COMPUTER GRAPHICS IN TRAINING OF ABILITY TO CREATE MENTAL VIEWS

At Technical Drawing discipline in workshop lessons the students have to create five blueprints referring to:

- Geometrical constructions;
- Wooden structures (wooden roof truss);
- Reinforced concrete steel structures (concrete steel beam);
- Metal structures (metal truss);
- Dwelling buildings representation (plan of current floor and façade).

These aim equally the training of capability to see with their mind's eyes and the gradual spreading of data referring to Technical Drawing, namely to the engineering graphical communication norms.

Because some students have a reduced capacity of creating mental images, and others with such an ability more developed don't have trained it at all, the blueprint which rises frequently understanding problems is the wooden truss referring to a portion of a roof, it's length being of 4 meters and it's span of 12 meters (fig. 1).

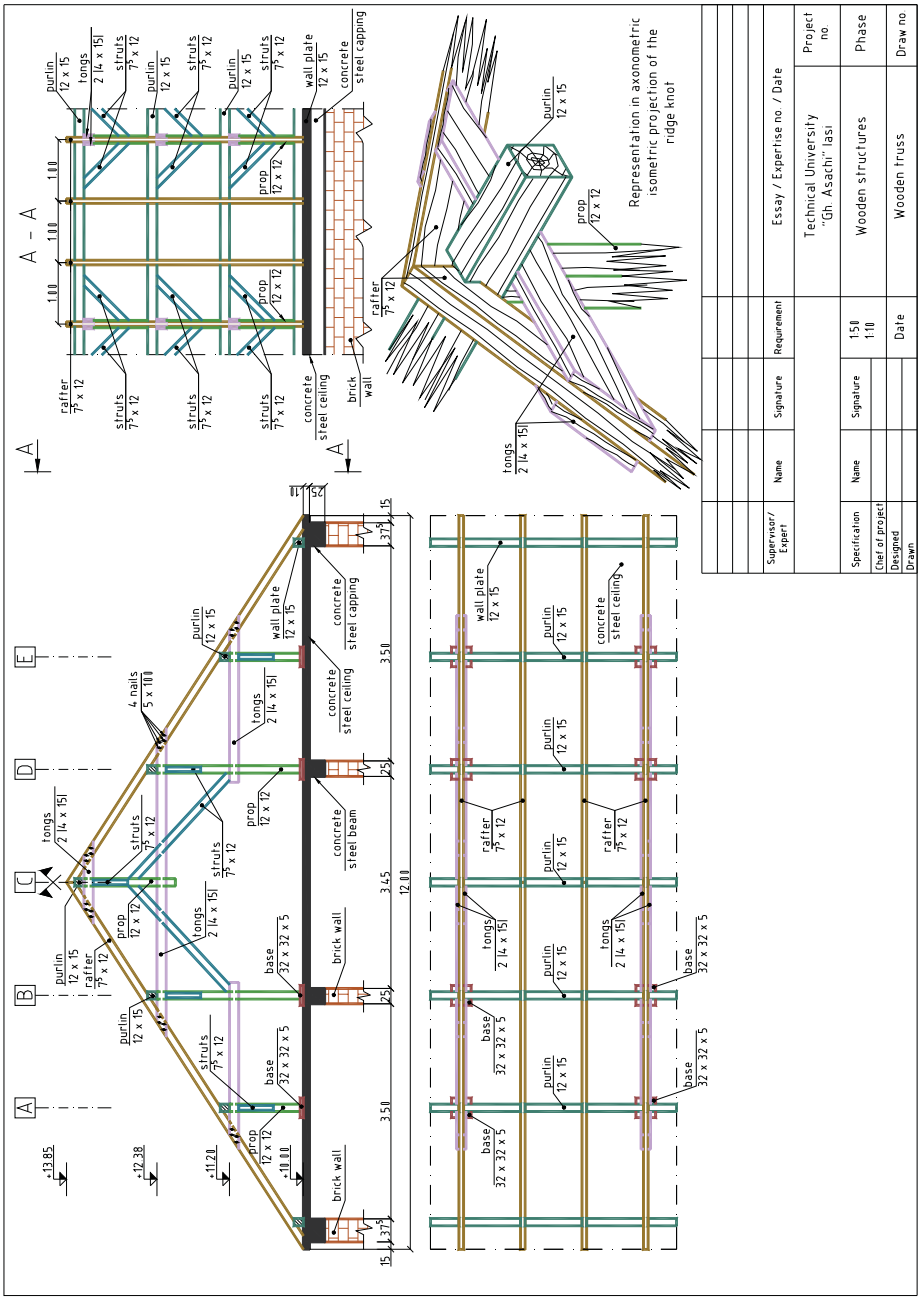

Figure 1. The Wooden Roof Truss

As noticed from figure 1 on the blueprint are drawn the front view, the plan (view from above), the profile (section view from the left) and the isometric representation of a ridge beam assembly knot detail of a wooden roof truss.

In the classical presentation variant of the theme referring to the wooden structures (with the help of presentation plans) the composing parts of the truss (rafters, purlins, ridge beam, props wall plates, tongs, struts, bases, etc.) are presented to the students together with the way of vertical loads transmission (rafters → purlins → props → bases→ ceiling → etc.).

From practical experience it is noticed that the students have major ambiguities in deciphering the 3D shape of the truss (the way of positioning the props, rafters, tongs, struts, bases, etc.). So, they partially understand the representing way of the front view but they do not understand the depicting of view from above, left view and of the ridge beam assembly knot detail. These facts demonstrate that there are major problems on the road of materializing the mental image of the body orthographical represented on the plan.

Starting from the above mentioned problems we have proposed that, by using computer graphics, to create a three-dimensional solid model of the wooden truss which to significant contributes to the smoothing of the above mentioned road. This model was developed with the support of AutoCAD program.

3. REALISING OF THE THREE-DIMENSIONAL MODEL OF THE WOODEN TRUSS

In the frame of the lesson dedicated teaching the "wooden truss" theme, parallel with the classical exposure, with the help of the plans containing it's orthographic plane representation, the presentation of the 3D model is made. This 3D model was realised at the 1:1 scale according to the dimensions from the 2D representation.

For a relatively rapid learning of the four representations from the didactic plan (front view, plan view, left view and isometric projection of the ridge beam assembly knot) the screen of AutoCAD program was split into four view-ports thus (fig. 2):

- front view in the upper left corner;
- view from above in the lower left corner;
- view from the left in the upper right corner;
- 3D model in the lower right corner.

If working is done in any view-port, the changes made are automatically updated in the others three view-ports.

The vision of 3D model take place on stages the model being structured using the AutoCAD layers technique.

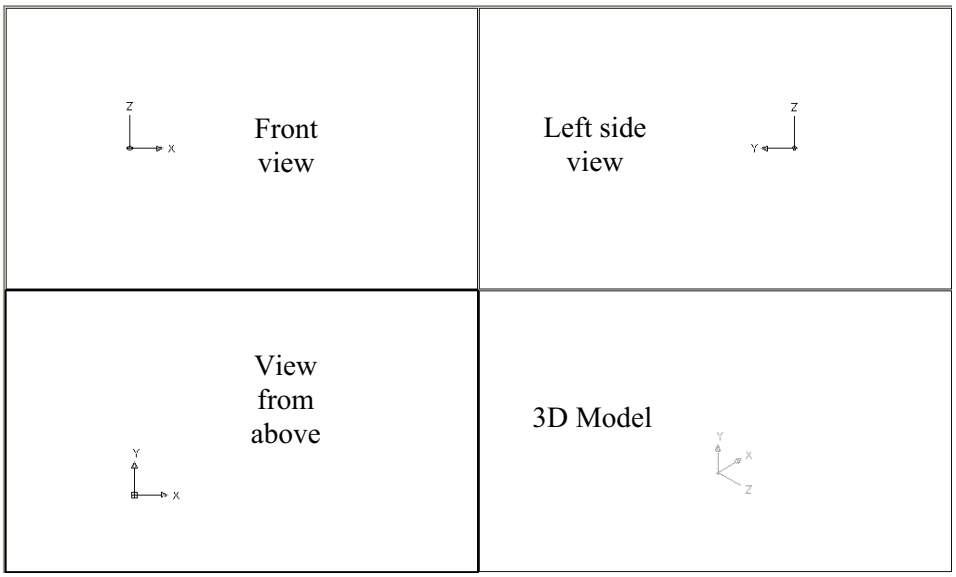

Figure 2. Projection disposal on view-ports

In the first step, taking in account the walls’ thickness and the distances between them, the slices from the walls supporting the cappings and the beams of the ceiling are depicted (fig. 3).

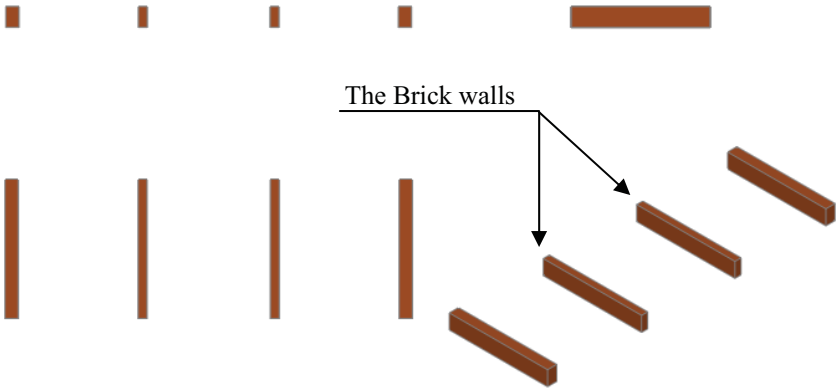

Figure 3. The Brick walls

As the upper and lower level dimensions of all walls are equal the picture appearing in the “left view” view-port can create confusion at first sight because a single wall is seen, the other ones being covered by the visible wall. This confusion is eliminated by the views appearing in the other three view-ports.

In the second stage the ceiling and its beams and cappings are shown. In the "view from above" view-port the walls, the beams and the cappings are not seen because the ceiling is placed above these elements. By the other hand in the "3D model" view-port some portions of these elements are seen because of the different location of the observer (fig. 4).

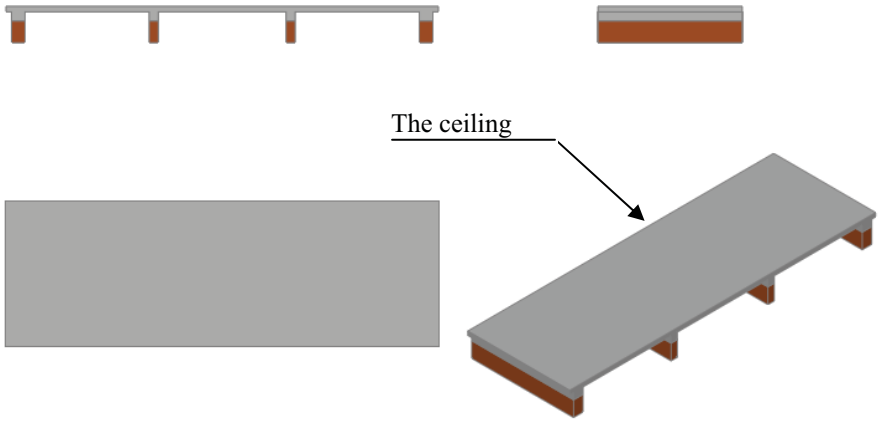

Figure 4. The Ceiling

In the third step the bases are positioned. These have a parallelepiped shape with 32 x 32 x 5 cm sizes and are placed on A, B, D şi E axes at 3 meters distances one axe from another along the building.

The only view-ports in which all bases are seen are the "view from above" and "3D Model". In "left side view" the bases are not seen because they are covered by the wall plates. In "front view" only the bases from the first row are seen, the others are overlapping in this view with these (fig. 5).

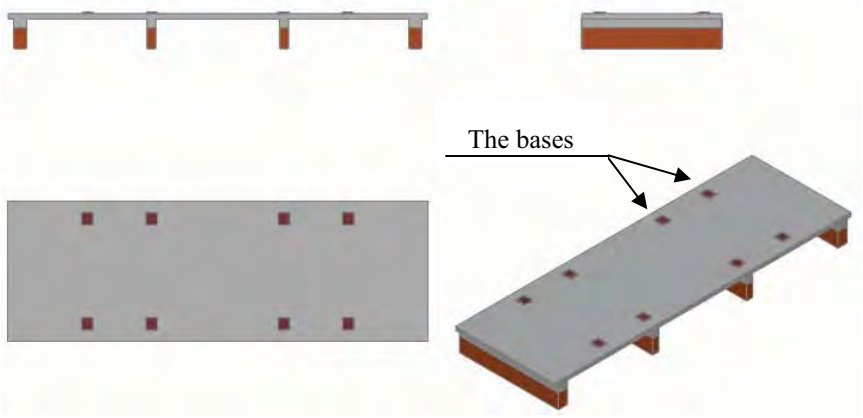

Figure 5. Bases position

In the fourth step the props located on A, B, D and E axes are depicted. The props from C axe are drawn after the drafting of the rafters and the ridge beam.

The props are structural parts of the roof taking the vertical loads from the purlins and transmitting them to the ceiling's girders. The adopted dimensions for the props' sections are 12 x 12 cm.

The props from A, B, D and E axes are centred positioned on bases (fig. 6). In fig. 7 the detail of a prop leaning on a base is depicted.

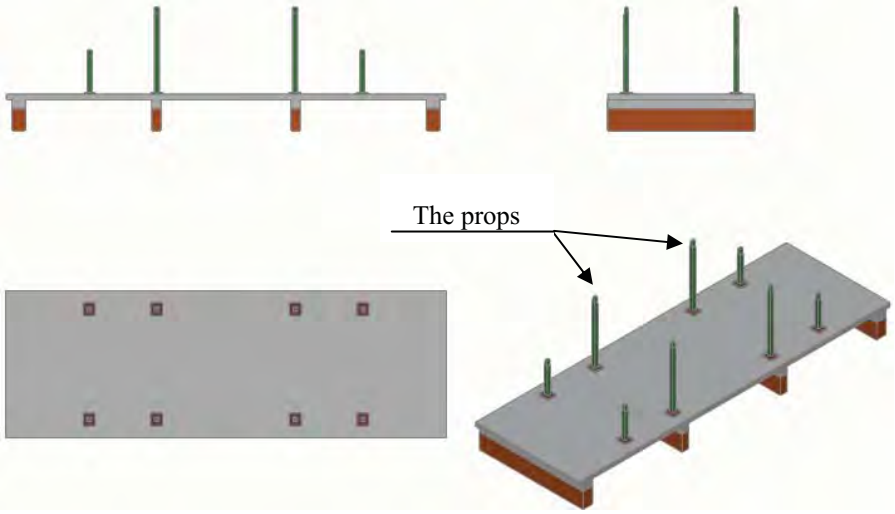

Figure 6. Placement of Props from A, B, D and E axes

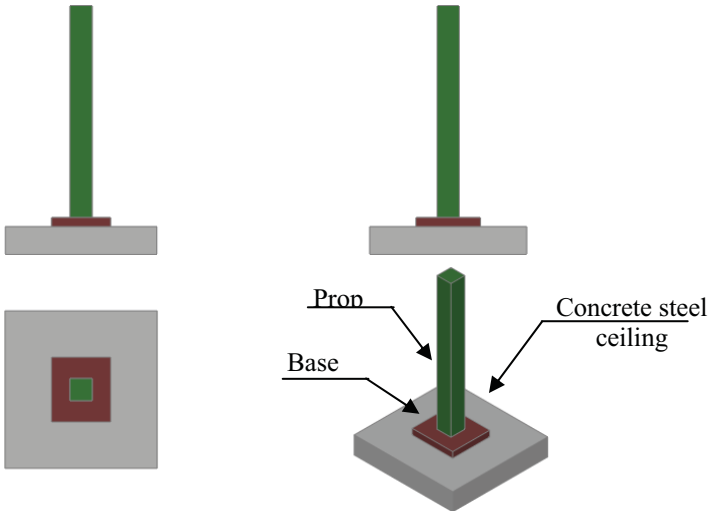

Figure 7. Detail of a prop leaning on a base

The only view-ports in which all props are seen are the "view from above" and "3D Model".

In "left side view" view-port the props from one half of the roof opening are seen, the others overlapping in view with these. In the "front view" only the props of the first rank are seen, the others being placed on rear of the ones from the first row (fig. 6).

In the fifth stage the purlins and the wall plates are positioned parallel with the building's edges. The purlins and the wall plates are structural part of the roof that take the vertical loads from the rafters and transmit them to the props and the capping of ceiling. The purlins lean on the props. The adopted section for purlins and wall plates is 12 x 15 cm.

Next the current purlins and the wall plates are represented (fig. 8). The view-ports in which all elements are seen are the "view from above" and "3D Model". In "left side view" view-port only two purlins and one wall plate from a total of four purlins and two wall plates are visible, the other elements overlapping with the visible purlins and wall plates.

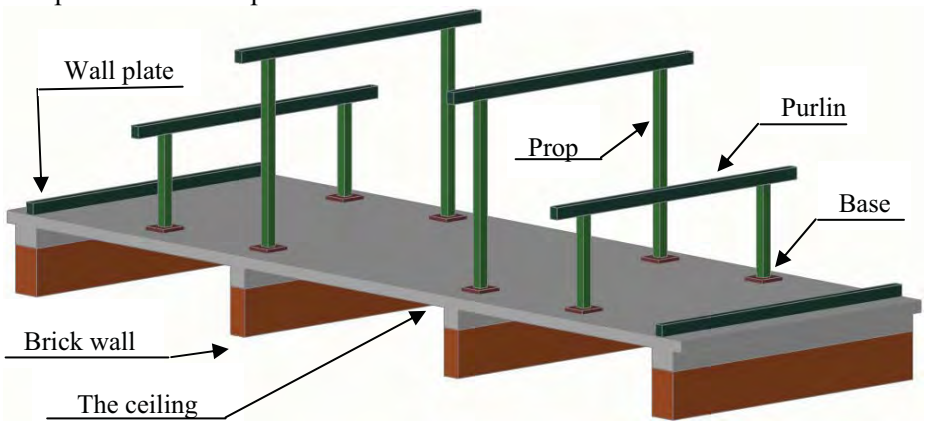

Figure 8. Current Purlins and the Wall Plates

In the sixth stage the rafters are drawn. The rafters are structural elements of the roof that transmit the vertical outside loads to the purlins and wall plates and giving shape to the roof.

As noticed in fig. 1 the roof is coupled thus for its construction on the opening will be pairs of two rafters positioned along the building. The axial distance between rafters is 1 meter.

The adopted sizes for rafters' sections are 7^5 x 12 cm. As these must be positioned on purlins on edge (the smaller size of the section) results that in the front view the section's dimension is 12 cm and in the left and upper views the dimension is 7^5 cm (fig. 9).

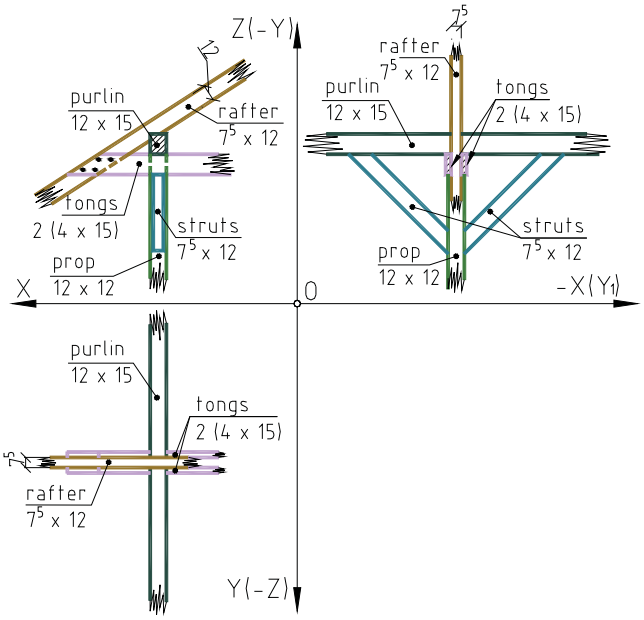

Figure 9. Knot detail in triple orthographic projection

For representing the rafters, the level assembly dimensions of these and the cutting-out of the rafters in order to lean them on the purlins and wall plates have to be taken in account. The cut-out is realised with a maximum deep of one third of the greater dimension of the section (fig. 10 and 11). Knowing this information and taking in account the upper and lower level positioning dimensions all the roof's rafters are represented.

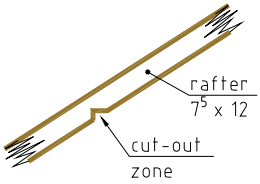

Figure 10. Detail of cut-out in a rafter

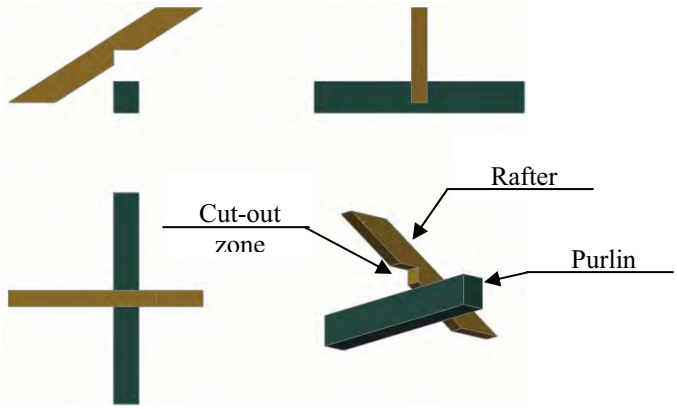

Figure 11. Exploded detail of purlin – rafter joint

The view-ports in which all rafters are seen are the "view from above" and "3D Model". In the "front view" only the front rafters are visible, the others being positioned behind them, and in the view-port "left side view" only the rafters positioned on one half of the roof opening are seen, the rafters positioned on the other half of the opening being behind them (fig. 12).

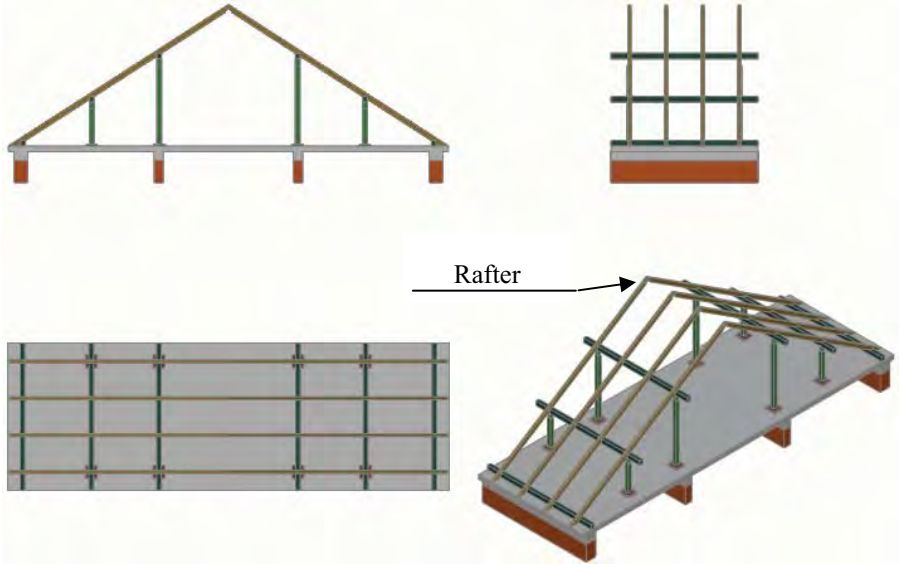

Figure 12. Rafters positioning

In the seventh step the ridge beam is positioned. The same conditions presented in case of mounting the purlins are taken in account for representing the ridge beam (fig. 13 ... 15).

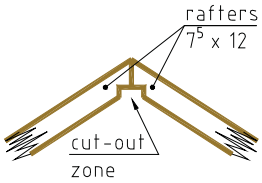

Figure 13. Detail of upper rafters joint

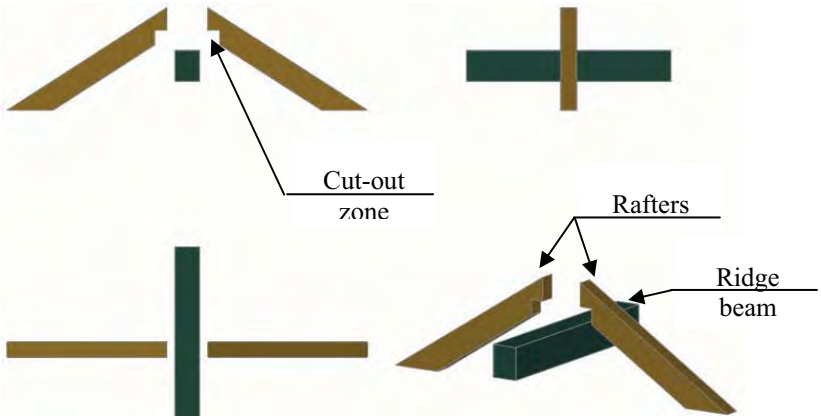

Figure 14. Exploded detail of upper knot

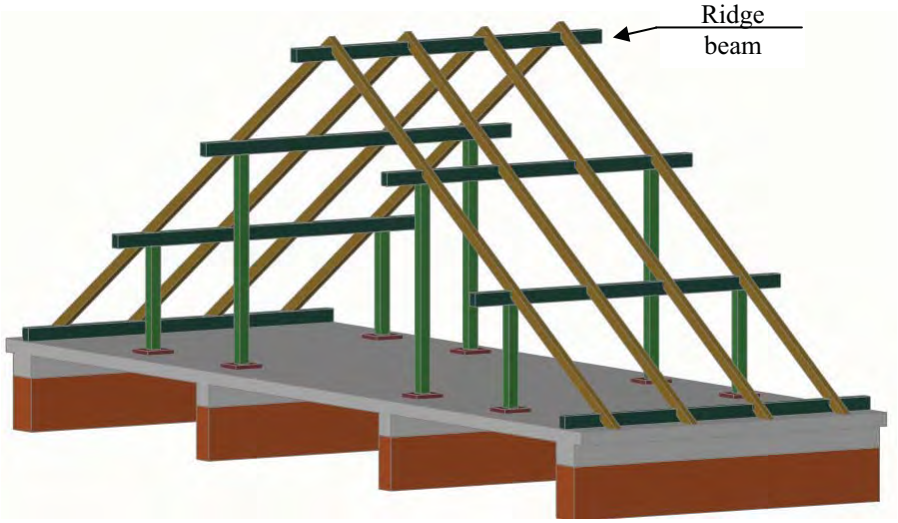

Figure 15. Positioning of Ridge Beam

In the eighth stage the props from C axe are depicted. The props are assembled under the ridge beam at a distance between axes of 3 meters in the same transversal planes as the existing props (fig. 16 and 17).

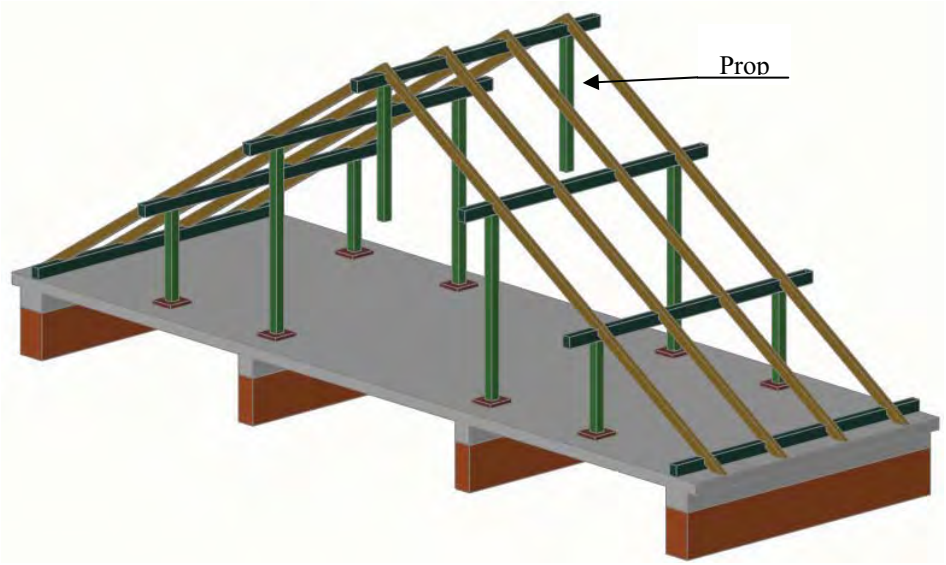

Figure 16. Placement of Props from C axe

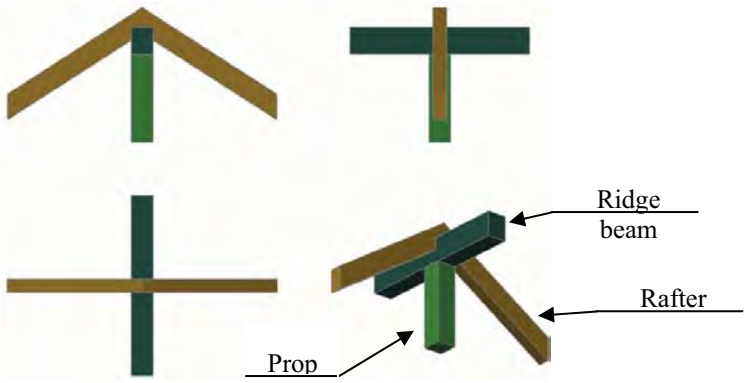

Figure 17. Detail of Ridge Beam mounting

In the ninth step the tongs are represented. The tongs are stiffness elements of the roof truss. These are positioned in pairs under the purlins, containing between them the rafters and the props (fig. 18).

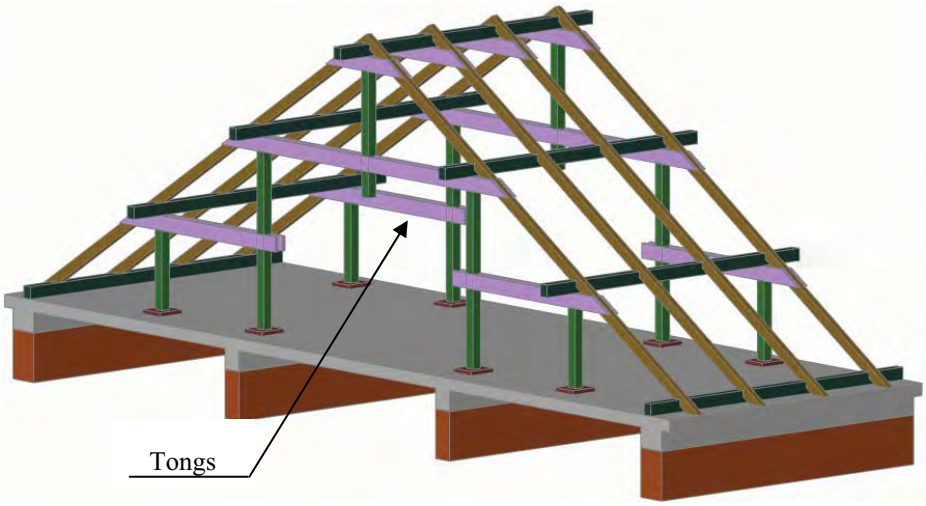

Figure 18. Placement of Tongs

The view-ports in which all tongs are seen are view from above" and "3D Model". In the "front view" only the front tongs are visible, the other tongs overlapping in this view with them. In the "left side view" the ends of the tongs from one half of the truss opening are seen.

In the overlapping zone between props and tongs, the props are cut out for tongs crossing (fig. 19).

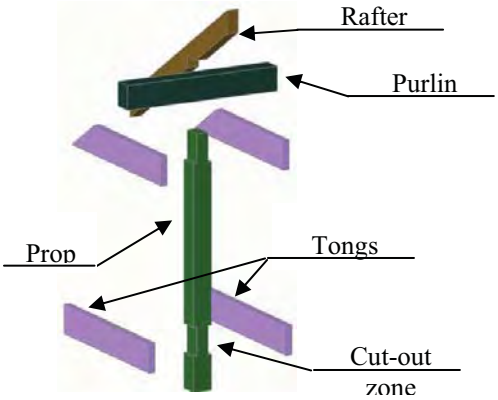

Figure 19. Exploded detail of prop's cut-outs for tongs mounting

In the last step the struts are positioned. The struts are stiffness elements of the truss also (fig. 20).

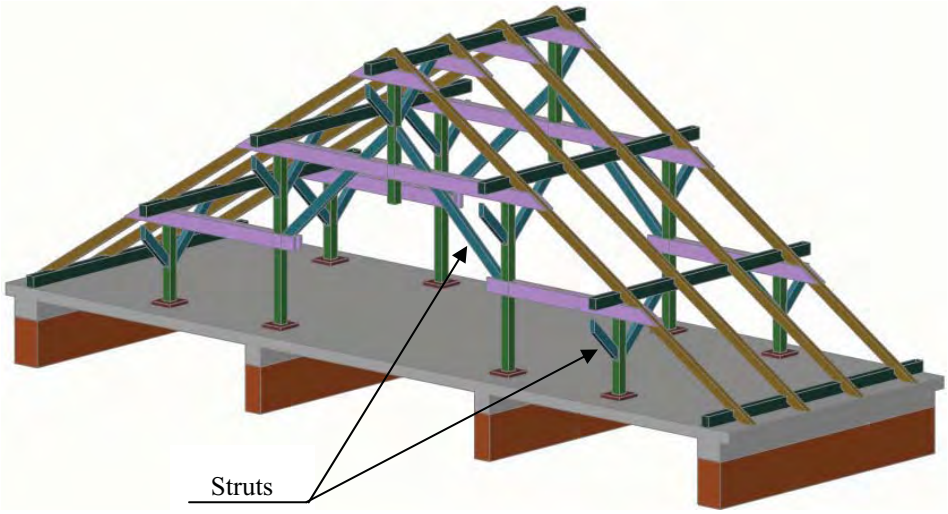

Figure 20. Positioning of Struts

The view-ports in which all struts are seen are view from above" and "3D Model". In the other two view-ports only the struts from the first rank are visible.

Using the AutoCAD program specific commands for space vision of the model (3DORBIT, VPOINT, ZOOM, PAN) some positions of the roof truss's 3D model are presented to the students for a better understanding of its structure and shape.

Also with the help of the 3D model the students better understand the way of structuring and depicting in axonometric isometric projection of the ridge knot (fig. 21 and 22).

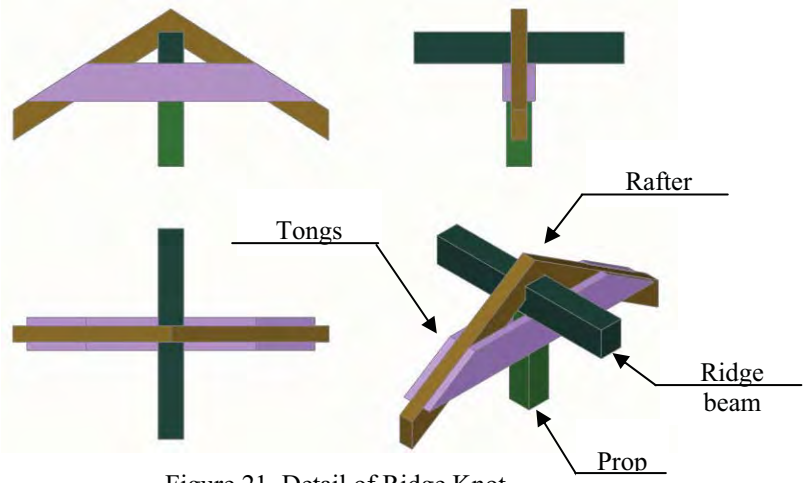

Figure 21. Detail of Ridge Knot

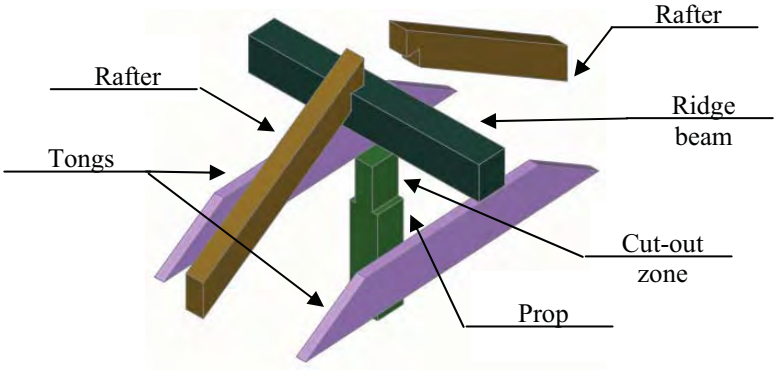

Figure 22. Exploded detail of Ridge Knot

3. CONCLUSIONS

Using of computer graphical communication and of CADD programs (like AutoCAD) together with classical graphical disciplines (Descriptive Geometry, Technical Drawing) is essential in forming and developing of spatial vision and the ability of reading triple orthographic projection drawings, tools useful for future design and execution engineers.

References

1. Stănilă, A., Hîncu, G., *Caiet de desen tehnic*, Editura Societății Academice "Matei-Teiu Botez", Iaşi, 2006. (in Romanian)
2. Gheorghiu, M., Chelcea, M., *Indrumator pentru desen tehnic de constructii,* Editura Matrix Rom, Bucureşti, 2001. (in Romanian)
3. Harrington, D., Burchard, B., Pitzer, D., *Inside AutoCAD 2002*, New Riders Publishing, 2002.
4. Simion, I., *AutoCad 2006 pentru ingineri,* Editura Teora, Bucureşti, 2006. (in Romanian)

"Computational Civil Engineering 2007", International Symposium
Iaşi, România, May 25, 2007

Analysis of dynamic parameters of rail fastening by Rihaczek transformation

Jaroslav Smutny[1], Lubos Pazdera[2]
[1]*Department of Railway Constructions and Structures, Faculty of Civil Engineering, University of Technology Brno, Brno, 602 00, Czech Republic*
[2]*Department of Physics, Faculty of Civil Engineering, University of Technology Brno, Brno, 602 00, Czech Republic*

Summary

For evaluation of response signals obtained by rail fastening analysis a new method using time and frequency related transformations has been developed. In the paper the laboratory measurements and dynamic parameter analyses of flexible fastening of Vossloh SKL14 type have been described. The method can also be used for designing new rail fastening systems and their parts.

KEYWORDS: Rail fastening, dynamic test, time frequency transform

1. INTRODUCTION

The basis for the selection and comparison of new components of rail superstructure are also theoretical analysis (simulation) and static and dynamic tests carried out in the laboratory and in the field (directly on the railway) [9]. It is necessary to mention that theoretical analysis of application of mathematical simulation is often based on idealized assumptions. Hence, when the real conditions on the railway or tramway superstructure are encountered, the model may be inaccurate.

For testing the railway superstructure construction, different methods and different criterions were applied. Dynamic testing [4] often uses the method of exciting the structure by mechanical shock. Exciting by shock is useful for the setting up a given set of frequencies as the shock, according to the theory, stimulates all frequencies, mainly resonant. Mechanical shock is often stimulated by a special hammer, which has an incorporated power sensor in radial direction to the railhead. The response is measured by accelerometer sensors at different points of the rail structure (rail foot, clip plate, clamp, sleeper etc). This method makes it possible to record frequency components in the range 1 Hz to 10 kHz. Recorded data are often recalculated and presented in the form of the frequency transfer function. This

shows important frequency components (mainly resonant) that include information about dynamic properties of particular parts of tested structure.

Often in the experimental investigation of dynamic properties [5] of rail fastening, the measurement and calculation of the transfer function is called accelerance (inverse function of dynamic weight). It is for that reason that the acceleration transducer is the most suitable electromechanical measurement device for the measuring of oscillation. Accelerance is defined by the relation

$$H_{aF}(f) = \frac{S_{aF}(f)}{S_{FF}(f)} \tag{1}$$

where $S_{aF}(f)$ is cross spectrum of response and entry signal, S_{FF} is auto-spectrum of entry signal. From the relation (1) it can be seen that measured acceleration is standardised for power measured during the shock.

In spite of the advantages, it is not possible to localise the time behaviour of frequency components included in the signal. Therefore for the evaluation of response signals when analysing the rails fastenings, the authors supplemented the methods of the measurements by utilising progressive processes of signal analysis, i.e. by utilising time frequency transformations.

One possible procedure to analyse time occurrence of frequency components of transfer and non-stationary signals, is the use of the so-called time frequency proceedings (transformations). These can be distributed according to two basic groups [3]:

- linear (including mainly Short Time Fourier Transformation, Wavelet Transformation etc.)
- non-linear (including mainly quadratic Cohen Transformations, Affine and Hyperbolic Transformation, eventually further special proceedings)

2. THEORY OF TIME FREQUENCY ANALYSIS

Given a time series, x(t), it can readily be seen how the "energy" of the signal is distributed in time. By performing a Fourier transform to obtain the spectrum, X (ω), it can also be seen how the "energy" of the signal is distributed in frequency. For a stationary signal, there is usually no need to go beyond the time or frequency domains. However, most real world signals have characteristics that change over time, and the individual domains of time and frequency do not provide a means for extracting this information. The general goal of this contribution is to demonstrate some lesser-known methods for creating functions that represent the energy of the signal simultaneously in time and frequency.

Example of linear time-frequency distributions is the Short Time Fourier Transformation. The main idea of the Short Time Fourier Transform (STFT) is to split a non-stationary signal into fractions within which stationary assumptions apply and to carry out a Fourier transform on each of these fractions. The STFT is defined by equation [3, 4]

$$STFT(\tau, f) = \int_{-\infty}^{\infty} [x(t) \cdot g^*(t-\tau)] \cdot e^{-j \cdot 2 \cdot \pi \cdot f \cdot t} \cdot dt \tag{2}$$

where '*' denotes the complex conjugate, g is the short time window, $x(t)$ is the signal, τ is the time location parameter, f is frequency and t is time. In the two dimensional time-frequency joint representation, the vertical stripes of the complex valued STFT coefficients STFT(τ, f) correspond to the Fourier spectra of the windowed signal with the window shifted to given times τ. The main disadvantage of linear time-frequency transform is that the time frequency resolution is limited to the Heisenberg bound. This is due to the imposition of local time window *g(t)*. If this window is more resolved in time, the frequency resolution suffers because the effective width of its Fourier transform *G(f)* increases, and vice-versa.

Quadratic (non-linear) methods present the second fundamental class of time frequency distributions. Quadratic methods are based upon estimating an instantaneous power (or energy) spectrum using a bilinear operation on the signal *x(t)* itself. The class of all quadratic time-frequency distributions to time shifts and frequency-shift is called Cohen's class. Similarly, the class of all quadratic time-frequency distributions covariant to time-shift and scales is called the Affine class. The intersection of these two classes contains time-frequency distributions, like the Wigner-Ville distribution, that are covariant to all operators.

Cohen [1] generalised the definition of the time frequency distributions in such a way as to include a wide variety of different distributions. These different distributions can be represented in several ways. Cohen's class definition like the Fourier Transformation, with respect to τ, of the generalised local correlation function is most common. With a two-dimensional kernel, the bilinear time frequency distribution of the Cohen´s class is defined according to equation [2]:

$$C_x(t,f) = \iiint e^{-j \cdot 2\pi \cdot \theta \cdot t' - j \cdot 2\pi \cdot f \cdot \tau + j \cdot 2\pi \cdot \theta \cdot t} \cdot \psi(\theta, \tau) \cdot x\left(t + \frac{\tau}{2}\right) \cdot x^*\left(t - \frac{\tau}{2}\right) \cdot d\theta \cdot dt \cdot d\tau \tag{3}$$

where x is the signal, t (t') is the time, τ is the time location parameter, ω is angular frequency, θ is shift frequency parameter, $\psi(\theta, \tau)$ is called the kernel of the time frequency distribution. A distribution C_x (t, f) from Cohen's class can be interpreted as the two-dimensional Fourier Transformation of a weighted version of the ambiguity function of the signal

$$C_x(t,f) = \iint A_x(\theta,\tau)\cdot\psi(\theta,\tau)\cdot e^{-j\cdot 2\pi\cdot f\cdot\tau}\cdot e^{-j\cdot 2\pi\cdot\theta\cdot t}\cdot d\tau\cdot d\theta \tag{4}$$

where $A_x(\theta, \tau)$ is the ambiguity function of the signal $x(t)$, given by equation:

$$A(\theta,\tau) = \int x\left(t+\frac{\tau}{2}\right)\cdot x^*\left(t-\frac{\tau}{2}\right)\cdot e^{-j\cdot\theta\cdot t}\cdot dt \tag{5}$$

We note that all integrals run from -∞ to ∞. The weighted function $\psi(\theta, \tau)$ is called the kernel. It determines the specific properties of the distribution. The product $A_x(\theta, \tau)\cdot\psi(\theta, \tau)$ is known as the characteristic function. Since the ambiguity function is a bilinear function of the signal, it exhibits cross components, which, if allowed to pass into time frequency distribution, can reduce auto-component resolution, obscure the true signal feature, and make interpretation of the distribution difficult. Therefore, the kernel is often selected to weight the ambiguity function such that the auto-components, which are centred at the origin of the (θ, τ) ambiguity plane, are passed, while the cross-components, which are located away from origin, are suppressed. This means that the suppression of cross-components might be understood as the frequency response of a two-dimensional low-pass filter.

When a low pass kernel is employed, there is a trade-off between cross-components suppression and auto-component concentration. Generally, as the band-pass region of the kernel is made smaller, the amount of cross-component suppression increases, but at the expense of auto-component concentration. There is definition of the kernel for Rihaczek Transformation in equation 6

$$\psi(\theta,\tau) = e^{\frac{j\cdot\theta\cdot\tau}{2}}. \tag{6}$$

Equation 4 can also be rewritten into the following form [5]

$$C_x(t,f) = \int_{-\infty}^{\infty}\int_{-\infty}^{\infty}\Pi(\tau-t,\theta-f)\cdot WVT(\tau,\theta)\cdot d\tau\cdot d\theta \tag{7}$$

where

$$\Pi(t,f) = \int_{-\infty}^{\infty}\int_{-\infty}^{\infty}\psi(\theta,\tau)\cdot e^{-j\cdot 2\cdot\pi\cdot(f\cdot\tau-\theta\cdot t)}\cdot dt\cdot d\omega \tag{8}$$

is the two-dimensional Fourier transform of the kernel ψ and WVT presents Wigner-Ville transform. Cohen's class has a simple interpretation as a smoothed Wigner-Ville distribution [5].

3. ANALYSIS OF DYNAMIC PARAMETERS

The model used for laboratory measurements and analysis of dynamic parameters of a sample of rail fastening is presented below. The rail grid model was constructed of concrete sleepers B 91, on which there were fastened rails of construction shape UIC 60 by flexible fastening Vossloh SKL14.

For the testing of the dynamic properties of the sample, the method of measuring the response to mechanical shock was used. Mechanical shock was stimulated by a special hammer in the radial direction on the railhead. A part of this hammer is a force detector.

The response was measured by accelerometers at different points of the rail structure, on the rail foot and sleepers (10 cm from fastening). Figure 1 show the location of detectors. From the response time signals frequency transfer functions (accelerance) were calculated in order to obtain standardised responses [5].

Figure 1 General view of the working place

Signals from measurements on the rail and sleepers were used for the presentation of particular analyses in this contribution. The measuring system consisted of a Brüel and Kjaer PULSE modular analyses for recording the vibration parameters together with B&k cubic acceleration detector and a B&k shock stimulation hammer (Figure 1).

The accelerometers were fastened to the measured construction by means of bee wax. The results were recorded digitally.

The analysis of the response to mechanical shock was evaluated by means of the following methods and parameters [5]:

- Time records of the duration of impulse response function (in principle standardized acceleration value)
- Frequency analysis with the use of frequency response function (according to equation 1)
- Time-frequency method of spectral analysis (for the transfer from time to time- frequency domain, the algorithm of Short Time Fourier Transformation and Rihaczek Transformation was used)

Time histories of the impulse response function, recorded by accelerometers, located on the rail foot, are depicted on the upper graph of Figure 2. The maximum positive value of acceleration of 300 $m \cdot s^{-2}$ is reached 1 ms from the observed beginning. The maximum negative value of acceleration of -300 $m \cdot s^{-2}$ is reached 2 ms from the beginning. Damping of the signal from the acceleration 300 $m \cdot s^{-2}$ to the acceleration lower than 30 $m \cdot s^{-2}$ took 15 ms.

In the left graph of Figure 2 is depicted the amplitude spectrum of this frequency response function calculated according to equation 1. In the graph, six important frequencies (0.2 kHz, 0.7 kHz, 1.9 kHz, 2.4 kHz, 3.3 kHz and 3.7 kHz), are visible. The important values are taken as those which have the damping up to 20 dB from the maximum value of amplitude spectrum.

Time frequency amplitude spectrum estimated by application of Short Time Fourier Transformation to the impulse response function is depicted in the middle graph in Figure 2. As shown on this graph, the time history of important frequency components essentially differ.

Frequency component 1.9 kHz reaches the highest values for a relatively long time (compared to other frequency components). It appears in the signal nearly in its full history, i.e. approximately 40 ms by damping up to 40 dB. The second most important component is the frequency 3.3 kHz. This appears in signal up to the time of 20 ms from the above. Other notable frequencies 2.4 kHz and 3.7 kHz are in the signal for the time of 5 ms up to 15 ms.

Similar conclusions are visible from the middle graph of Figure 3, which present the analysis of impulse response function on the rail foot by the use of Rihaczek Transformation. This transform belong to the category of non-linear time frequency proceedings from the Cohen class.

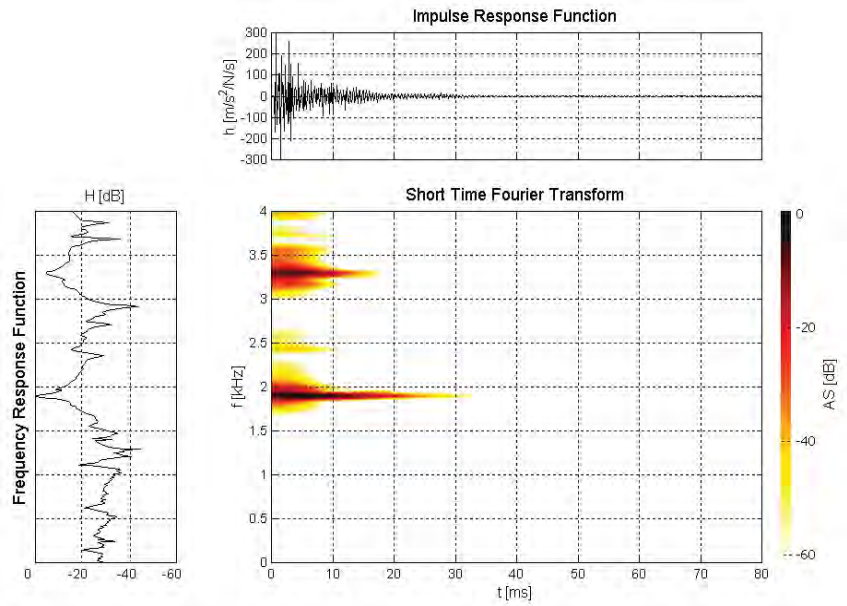

Figure 2 Accelerometric detector located on the rail foot, time frequency analysis by Short Time Fourier Transformation

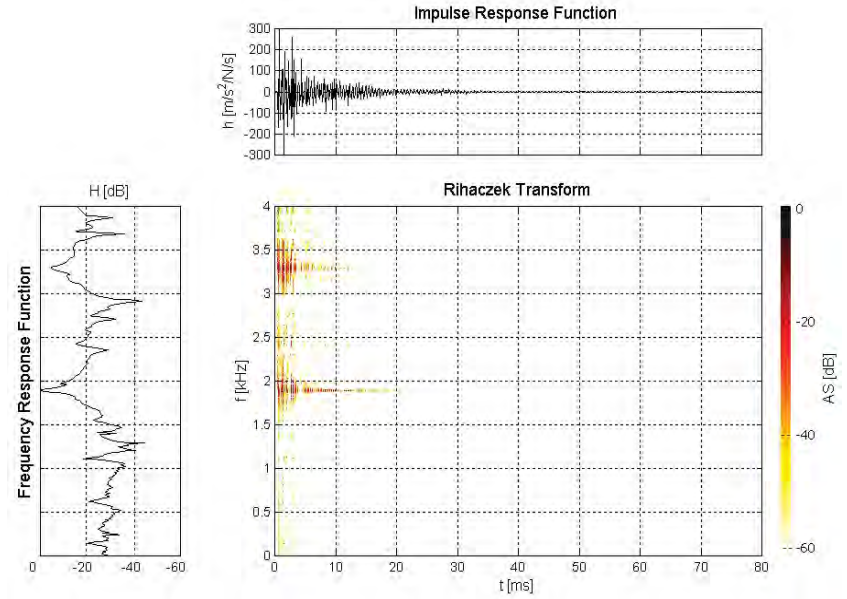

Figure 3 Accelerometric detector located on the rail foot, time frequency analysis by Rihaczek Transformation

Signals (impulse response function) taken by a second transducer, located on the concrete sleeper, have different character. From the time record (see upper graph of Figure 4) it is apparent that the maximum impulse response function amplitude acquires lower frequency values as a result of the influence of the transformation of the signal through the fastening of rail, clip plate, sleeper to the accelerometer and reaches values of 50 $m \cdot s^{-2}$. These values were reached 2 ms from the first rise time from "amplitude pack". Values of acceleration are considerably lower than those by the transducer located on the rail foot which was located nearer to the source of mechanical impulse.

In the left graph of Figure 4 is depicted the amplitude spectrum of frequency response function. The form of spectrum considerably differs from the characteristics measured by the first transducer located on the rail foot. The most important components appear in the lower frequencies from the transducer located on the rail foot: in the interval of 0.2 kHz up to 2 kHz, there are also more in number.

Similar conclusions are given by the middle graph of Figure 4 which presents the time frequency amplitude spectrum estimated by the application of the Short Time Fourier Transformation. From this graph it can be seen that time occurrence of significant components included in signal is considerably shorter (the longest is approx. 20 ms from the imaginary beginning) than it is from the signal from transducer located on the rail foot.

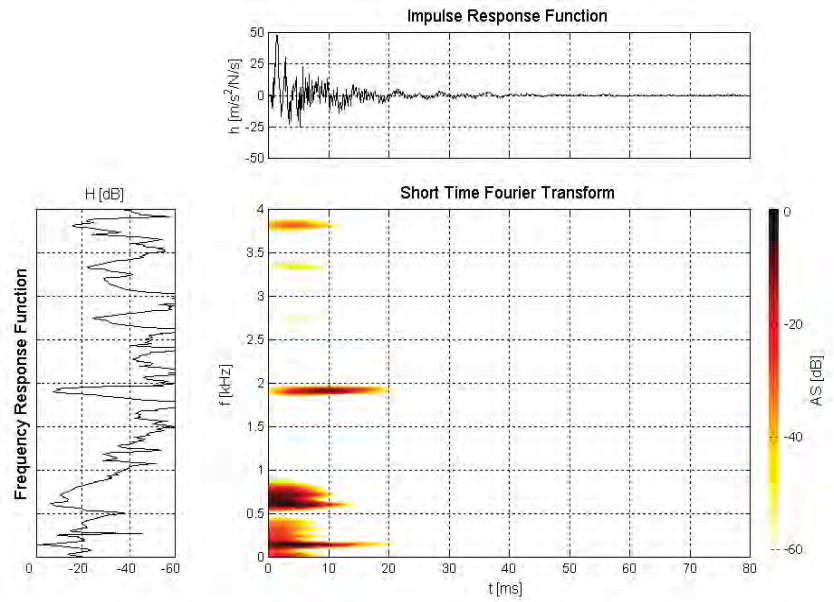

Figure 4 Accelerometric detector located on concrete sleeper, time frequency analysis by Short Time Fourier Transformation

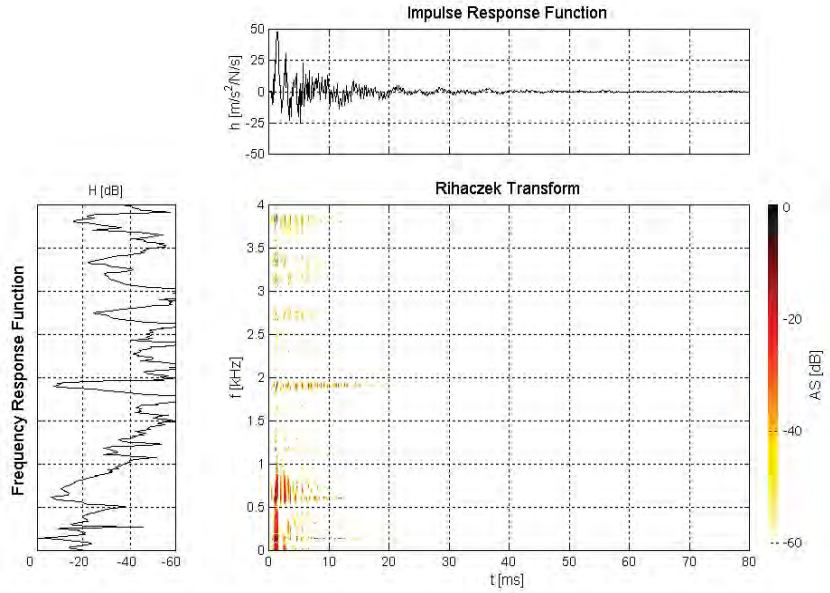

Figure 5 Accelerometric detector located on concrete sleeper, time frequency analysis by Rihaczek Transformation

Similar conclusions apply to the middle graphs of Figure 5 which present the analysis of signals from transducers located on the sleeper by the use of Rihaczek Transformation. The significant frequency components which are calculated by the Rihaczek Transformation (Figure 6) are frequencies of 0.2 kHz, 0.7 kHz, 1.9 kHz, 2.7 kHz, 3.2 kHz, 3.4 kHz and 3.7 kHz. The most significant spectrum component is the frequency component 0.2 kHz which appears within this spectrum for a relatively long time in relation to the activity of other components.

On the whole, it is possible to state from the middle graphs in Figure 2 to Figure 5 that in contrast to linear methods whose ability to resolve the frequency elements in the time region is limited by certain window functions, quadratic methods can achieve this objective. Higher distinguishing makes more favourable localization of significant frequency components in time possible. The quality of time and frequency achieved by measuring the signal response to mechanical shock and applying by these transformations is a good choice.

4. CONCLUSIONS

Based on measurements and analyses, it is possible to state that the methods presented above are very good for the measurement of dynamic parameters of rail

fastenings. The use of these methods enables the testing of new types of rail fastenings and different types of rail washers under rails and the opportunity to optimise the geometric location of damping elements on rail etc. From the mathematical means of signal analysis it is possible to utilise both Short Time Fourier Transformation and Rihaczek Transformation for time-localisation of the occurrence of frequency elements of stationary and non-stationary signals.

Based on the experience acquired, it is of great advantage for the analysis of real signals to utilise the properly selected time and frequency sections. This procedure seems to be more suitable than the spatial arrangement. It is possible for more precise localisation of time records to separate significant frequency components or to depict all important frequencies. Analysis of signals, acquired by measurement and analysis of response to mechanical shock gives new, more detailed insights to transition characteristics of railway and tramway structures. Hence, it grants valuable knowledge for a thorough analysis of these constructions, which can be important for consequent optimisation of construction and operational conditions. Also the fact that by time frequency proceedings analysis of dynamic load of railway and tramway constructions provides real data for consequent formulation of mathematical models. From this point of view, both linear and non-linear time frequency transformations are applicable. These methods give a fast and accurate localisation of frequency components included in the measured signal. It is possible to apply the described method successfully not only on samples of several constructions of railway and tramway superstructure but also directly in the field on real tracks.

Acknowledgements

This research has been supported by the research project 103/07/0183 ("The investigation of dynamic effects due to the rail transport by the method of quadratic time and frequency invariant transformations ") and by research project MSM 0021630519 (“Progressive reliable and durable load-bearing structural constructions”)

References

1. Cohen L., Time-frequency distributions, Proc. IEEE, 1989, vol. 77 no. 7, pp. 941-981
2. O'Neill J.C., Quartic Functions for Time-Frequency Analysis with Applications to Signal Adaptive Kernel Design, SPIE - Advanced Signal Processing Algorithms, 1997
3. Poularikas A. D.: The Transform and Applications Handbook, IEEE Press, 1996
4. Melcer, J., Kucharova, D. : Mechanical properties of rubber pads under static and dynamic load, proceedings of International Conference on Materials Science and Engineering, BRAMAT 2003, Romania, Brasov, 3/2003, University of Brasov, 2003, pp. 18-314.
5. Smutný J., Pazdera L.: New techniques in analysis of dynamic parameters rail fastening, InSight, The Journal of The British Institute of Non-Destructive Testing, Vol 46, No 10, October, 2004, pp. 612-615, ISSN 13542575

"Computational Civil Engineering 2007", International Symposium
Iaşi, România, May 25, 2007

The use of time frequency transformations in testing structural elements

Jaroslav Smutny[1], Lubos Pazdera[2]
[1]*Department of Railway Constructions and Structures, Faculty of Civil Engineering, University of Technology Brno, Brno, 602 00, Czech Republic*
[2]*Department of Physics, Faculty of Civil Engineering, University of Technology Brno, Brno, 602 00, Czech Republic*

Summary

The paper deals with the non-destructive testing of structural elements by means of the acoustic response using the jointed time and frequency transforms. These methods make it possible to localize the beginning and the end of frequency components contained in the measured signal and in this way, they enable us to analyze perfectly the spectrum of the non-stationary noise. In this way, this mathematical procedure enables us to distinguish a good specimen from a defective one.

KEYWORDS: Time Frequency Transform, Wavelet Transform, Acoustic Response Analysis, Ambiguity Function

1. INTRODUCTION

Many times we have already been able to convince ourselves that utilising the experience and knowledge having their roots even in the far past have brought surprisingly good results. One of such experience is the knowledge that noise resulting from the shock applied to a structure with cracks (disturbances) is significantly different from the same subject without cracks. This phenomenon has been known for a long time. As early as in the Middle Ages this phenomenon was used to detect cracks in ceramic pots after their firing. The phenomenon mentioned makes it possible to detect cracks in metallic materials as well. Its very old application in the railway transport is generally known. However, in the development and application of the methods used to detect defects in structural elements and materials, this phenomenon has often been neglected. The absence of the advanced measuring techniques and appropriate mathematical instruments necessary for the evaluation of measured signals were the main reasons.

There are only the methods of the time-frequency analysis in connection with the classic spectral analysis that make a thorough analysis of the signals measured with good possibilities of classifying and identifying possible defects. The noise excited

by force impulse to the tested construction or element is a very interesting phenomenon since it contains a number of mutually independent and well recognisable symptoms according to which it is possible to differentiate materials with cracks from those without cracks [8, 9].

These symptoms are particularly included multi-spectra of the measured noise signals. The composition of the spectrum of noise of each material is given by several characteristics with their own side elements with respect to time and frequency. The spectrum of the measured noise is changed for the duration of the process. The symptoms of cracks are as follows:

- Changes of the amplitudes of particular characteristic frequency components
- Frequency shifts of characteristic frequency components
- Appearance of new frequency components
- Presence of modified spectrum in comparison with a good product

2. THEORY OF TIME FREQUENCY ANALYSIS

Information relating to any technical or physical occurrence is represented in the signal by time changes of immediate values or physical phenomena described. The direct evaluation of the time-amplitude representation often appears not to be easy. That is why there is a practice of the signal transform from the time domain to some different ones. In some cases, some important pieces of information from the frequency area may be obtained. There are a lot of various transforms applied for transition between time, frequency and jointed time frequency domain. The best known method is the Fourier transform and some of its modifications.

The Fourier transform and some of its modifications are the techniques which are especially suitable for processing stationary signals. These methods can analyse transient and non-stationary signals as well as in the cases when we are interested only in the frequency components contained in the whole time behaviour of signal. However, these do not provide us with information on the occurrence of important frequency components in the time flow.

One of the possible way how to analyse the time occurrence relating to the frequency components of transient and non-stationary signals is the use of the so-called time-frequency analysis method.

The goal of this paper is to demonstrate some less-known methods for creating functions representing the energy of the signal simultaneously in time and frequency domain.

The Short Time Fourier and Wavelet Transforms represent the examples of the linear time-frequency distributions. The main idea of the Short Time Fourier Transform (STFT) is to split a non-stationary signal into segments where the signal

is considered to be stationary. The Fourier transform on each of these segments is computed. The STFT is defined by equation [3]

$$STFT(\tau, f) = \int_{-\infty}^{\infty} [x(t) \cdot g^*(t-\tau)] \cdot e^{-j \cdot 2 \cdot \pi \cdot f \cdot t} \cdot dt \tag{1}$$

where '*' denotes the complex conjugate, $g(t)$ is a short time window, $x(t)$ is a signal, τ is a time location parameter, f is a frequency and t is a time. In the two dimensional time-frequency joint representation, the vertical slice of the complex valued STFT coefficients STFT(τ, f) correspond to the Fourier spectra of the windowed signal with the window shifted by time τ. The time frequency resolution is limited to the Heisenberg principle, which is the main disadvantage of the linear time-frequency transform. The signal component cannot be presented as a point in the time frequency space. Only its position inside the $\Delta t \cdot \Delta f$ rectangle region may be determined. This is due to the imposition of local time window $g(t)$. If the width of the window is increased, frequency resolution improves but time resolution becomes poor and vice-versa.

The Wavelet transform (WT) is a new mathematical tool developed mainly since the middle of the 1980s. It is efficient for the local analysis of non-stationary and fast developing transient signals. Similarly to the STFT, the Wigner distribution, ambiguity function and the Wavelet transform map the signal to the time-scale (frequency) joint presentation. The temporal aspect of the signal is preserved. The WT provides a multi-resolution analysis with a dilated window. The high frequency analysis is made using a narrow window and the lower frequency analysis is made using a wide window. The Wavelet analysis is similar to the Fourier analysis because it breaks a signal down into its constituent parts for the analysis. Whereas the Fourier transform decomposes the signal into a set of sine waves of different frequencies, the Wavelet transform decomposes the signal into its "wavelets", scaled and shifted versions of the "parent Wavelet". The Wavelet transform allows us an outstanding localisation in both the time domain via translation of the parental wavelet and in the scale (frequency) domain via dilatation. The translation and dilatation operations applied to the parent wavelet are performed to calculate the wavelet coefficients representing the correlation between the wavelet and the localised section of the signal. The wavelet coefficients are calculated for each wavelet segment, giving a time-scale function relating to the wavelets correlation to the signal [6, 7].

$$WT(\tau, s) = \frac{1}{\sqrt{|s|}} \cdot \int_{-\infty}^{\infty} x(t) \cdot \psi^* \left(\frac{t-\tau}{s} \right) \cdot dt \tag{2}$$

where '*' denotes the complex conjugate, $x(t)$ is a signal, t is a time, τ is a translation factor, s is a scale factor (frequency) and $\psi(x)$is a wavelet. This transform is called Continuous Wavelet Transform because the analysing wavelet can be used at any scale, and its position can also be shifted continuously over the entire time domain of the signal being analysed.

As the parent wavelet (which is obviously the most suitable especially for transient processes) the Morlet Wavelet and the Mexican Hat Wavelet are often used. The parent Morlet Wavelet is preferred for the analysis of the vibration measurement. The Morlet's basic wavelet function is a multiplication of the Fourier basis with a Gaussian window according to equation (3)

$$\psi = e^{-j\cdot\omega_0\cdot t}\cdot e^{-\frac{t^2}{2}} \tag{3}$$

Its real part is a Cosine-Gaussian function and the imaginary part is a Sine-Gaussian function. The Wavelet transform is of a particular interest for the analysis of non-stationary and transient signals. The Wavelet transform provides an alternative to the classic Short Time Fourier Transform or the Gabor transform, and it is more efficient than the Short Time Fourier Transform.

The Wigner-Ville transform [2, 4] is another alternative method for a Short-Time Fourier Transform and the Wavelet Transform for processing both the stationary and non-stationary signals. The Wigner distribution was proposed by Wigner in 1932 for the region of quantum physics, and about 15 years later, this was modified for the region of the signal analysis by Ville. The Wigner-Ville transform is defined for the time frequency region by relation

$$WVT_x(t,f) = \int_{-\infty}^{\infty} x\left(t+\frac{\tau}{2}\right)\cdot x^*\left(t-\frac{\tau}{2}\right)\cdot e^{(-j\cdot 2\cdot\pi\cdot f\cdot\tau)}\cdot d\tau \tag{4}$$

where '*' is a complex conjunction, t is a time, τ is a shift along the time axis, $x(t)$ is a time representation of the signal and $WVT_x(t,f)$ is a jointed time and frequency representation of the signal. In contrast to the linear time frequency transforms in which the resolution is limited by the window function, the Wigner-Ville spectrum offers us an excellent resolution both in the frequency and time domain. The calculation is not limited by the Heisenberg principle of uncertainty which is its important characteristic since it is a more general transformation that does not utilise the weighing function.

Quadratic (non-linear) methods represent the second fundamental class of time frequency distributions. The quadratic methods are based upon estimating an instantaneous power (or energy) spectrum using a bilinear operation on the signal *x(t)* itself. The class of all quadratic time-frequency distributions to time-shift and frequency-shift is called the Cohen's class. Similarly, the class of all quadratic time-frequency distributions covariant to time-shift and scale is called the Affine

class. The intersection of these two classes contains time-frequency distributions like the Wigner-Ville distribution that are covariant to all operators [2]. Cohen [1] describes the non-linear time frequency transformation (especially shift-invariant class) that can be derived from the Wigner distribution.

Cohen [1] generalised the definition of the time frequency distributions in such a way which includes a wide variety of different distributions. These different distributions can be represented in several ways. The Cohen's class definition like the Fourier Transform, with respect to τ, of the generalised local correlation function, is the most common. With a two-dimensional kernel, the bilinear time-frequency distribution of the Cohen´s class is defined according to equation [1, 10]

$$C_x(t,f) = \iiint e^{-j\cdot 2\pi\cdot\theta\cdot t' - j\cdot 2\pi\cdot f\cdot\tau + j\cdot 2\pi\cdot\theta\cdot t}\cdot\psi(\theta,\tau)\cdot x\left(t+\frac{\tau}{2}\right)\cdot x^*\left(t-\frac{\tau}{2}\right)\cdot d\theta\cdot dt\cdot d\tau \quad (5)$$

where x(t) is a signal, t is a time, τ is a time location parameter, ω is an angular frequency, θ is a shift frequency parameter, a function ψ(θ, τ) is called the kernel of the time frequency distribution. Distribution Cx (t,ω, ψ) from the Cohen's class can be interpreted as the two-dimensional Fourier Transform of a weighted version of the ambiguity function of signal

$$C_x(t,f) = \iint A_x(\theta,\tau)\cdot\psi(\theta,\tau)\cdot e^{-j\cdot 2\pi\cdot f\cdot\tau}\cdot e^{-j\cdot 2\pi\cdot\theta\cdot t}\cdot d\tau\cdot d\theta \quad (6)$$

where $A_x(\theta, \tau)$ is the ambiguity function of the signal $x(t)$, given by equation:

$$A(\theta,\tau) = \int x\left(t+\frac{\tau}{2}\right)\cdot x^*\left(t-\frac{\tau}{2}\right)\cdot e^{-j\cdot\theta\cdot t}\cdot dt \quad (7)$$

Note that all integrals run from -∞ to ∞. The weighted function $\psi(\theta, \tau)$ is called the kernel. It determines the specific properties of the distribution. The product $A_x(\theta, \tau)\cdot\psi(\theta, \tau)$ is known as the characteristic function. Since function $A_x(\theta,\tau)$ represents a bilinear operation for processing the signal, the contributions from the so-called cross components are exhibited during its calculation, which consequently deteriorates the differentiation of the given transformation. This effect may be limited by a suitable choice of the so-called kernel function. Then the kernel function unambiguously determines the properties of a given transformation.

Therefore, the kernel is often selected to weight the ambiguity function such that the auto-elements that are centred at the origin of the (θ, τ) ambiguity plane are passed, while the cross-elements that are located away from origin are suppressed. This means that the suppression of cross-elements might be understood as the frequency response of a two-dimensional low-pass filter.

When a low-pass kernel is employed, there is a trade-off between the cross-elements suppression and the auto-element concentration. Generally, as the band-

pass region of the kernel is made smaller, the amount of the cross-element suppression increases, however, at the expense of the auto-element concentration. Table 1 presents definitions of the kernels for various time frequency distributions [5].

Table 1 Definitions of the kernels for various time frequency distributions

Distribution	Kernel function $\psi(\theta, \tau)$
Rihaczek	$\psi(\theta,\tau) = e^{\frac{j\cdot\theta\cdot\tau}{2}}$
Margenau-Hill	$\psi(\theta,\tau) = cos\left(\frac{\theta\cdot\tau}{2}\right)$
Page	$\psi(\theta,\tau) = e^{\frac{j\cdot\theta\cdot\lvert\tau\rvert}{2}}$

Equation 6 can also be rewritten into the following form [5, 10]

$$C_x(t,f) = \int_{-\infty}^{\infty}\int_{-\infty}^{\infty}\Pi(\tau - t, \theta - f)\cdot WVT(\tau,\theta)\cdot d\tau\cdot d\theta \tag{8}$$

where

$$\Pi(t,f) = \int_{-\infty}^{\infty}\int_{-\infty}^{\infty}\psi(\theta,\tau)\cdot e^{-j\cdot 2\cdot\pi\cdot(f\cdot\tau-\theta\cdot t)}\cdot dt\cdot d\omega \tag{9}$$

is the two-dimensional Fourier transform of the kernel ψ and *WVT* presents the Wigner-Ville transform. Cohen's class has a simple interpretation as a smoothed Wigner-Ville distribution.

3. ANALYSIS OF DYNAMIC PARAMETERS

The text to follow pursues the determination of the quality of structural elements (in this case the "hurdis" brick) by the method of acoustic response analysis. The basis for the methodology designed by the author is the analysis of the response of the noise signal to a mechanical impulse, particularly by time-frequency procedures. The measured specimen was placed on a special device fixed to supports (Figure 1). The mechanical shock was excited by a special pendulum with a defined choice of the shock intensity. The measuring device (made by the Bruel & Kjaer Company) consisted the PULSE 3360C signal analyser, a

microphone and the measuring software. The sampling frequency was 12 kHz. The electric signal detected and digitally recorded resulted from the measurement, and it was adequate to the amplitude of the acoustic pressure in the place of the microphone location.

After completing the analysis, the check measurement and calculations, the following methods and parameters were used to the analysis of the response to the mechanical shock:

- diagram time history of the acoustic pressure
- frequency analysis with help of behaviour of the power spectral density (the algorithm of the fast Fourier transform was used)
- linear jointed time and frequency methods of the spectral analysis (the algorithms of the Wavelet transform were used)
- non-linear jointed time and frequency methods of the spectral analysis (the algorithms of the Rihaczek transform were used)

The analyzed figures are composed of three diagrams. The upper diagram shows the time history of the acoustic pressure. In the left diagram, the amplitude spectrum of the acoustic response calculated by the direct employing of the Fourier transform on measured signal is shown. The middle diagram shows the 3D view of jointed time and the frequency spectrum of the amplitude spectrum of the acoustic pressure. The spectra in particular diagrams in Figures 2 to 5 were gradually calculated by means of the Wavelet transform or more precisely by the Rihaczek transforms.

The values of the acoustic pressure in the decibel scale are depicted in the middle diagrams in different colours. It should be said that the maximum value is in black colour. Figures 2 to 5 present three groups of diagrams of the signals measured by the microphone using the impact-echo method used to a defective product and for the defect-free one.

Comparing the time records of a good and a defective specimen, it may be considered that the signal coming from the good product has a lower damping, i.e. the specimen sounds for a longer time.

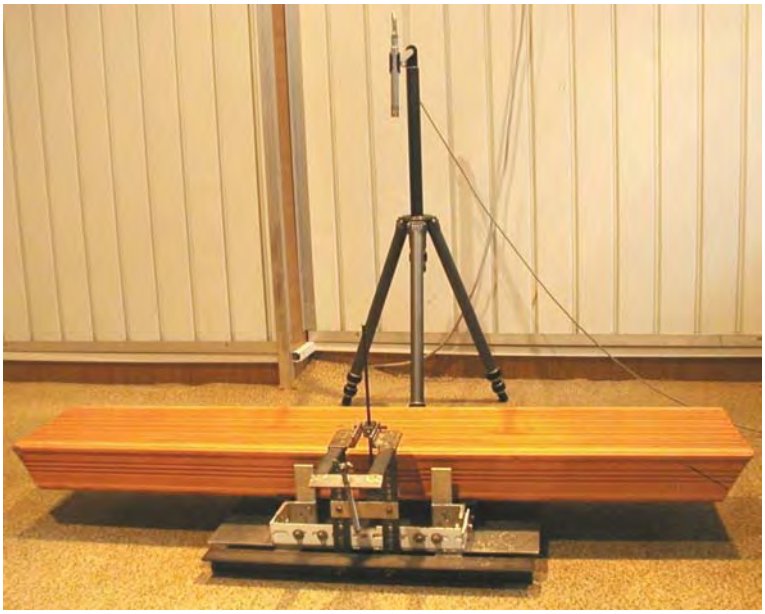

Figure 1 General view of the working place

Then the frequency characteristic shows that in a defective specimen the distinctive frequency components have "moved" in the direction of the lower frequency values and that the spectrum is wider compared with defect-free specimens. The comparison of the course of the time-frequency transform clearly shows the different characters of the spectra of the defective specimens and the defect-free specimens.

The text to follow will only deal with the diagram of the time-frequency characteristics obtained by means of different mathematical procedures. The Wavelet transform will be considered as a basic transform. The time-frequency curve for the defect-free product (Figure 2) clearly shows two frequency components on frequencies 2.5 kHz and 3.3 kHz. The component on frequency 2.5 kHz is damped by 20 dB approximately in 30 ms, while the frequency component 3.3 kHz is damped in 50 ms. These two frequency components compared with other frequency components are remarkable in their spectra. The change of the time-frequency spectrum of a defective specimen (Figure 3) can easily be distinguished. The distinctive frequency region, approximately from 700 Hz to 3.2 kHz contains more than two important frequency components – e.g. it is possible to choose the values on 700 Hz, 1.1 kHz, 1.8 kHz, 2.2 kHz, 2.5 kHz, 2.8 kHz and 3.2 kHz – their values are less than one order lower than the value of the maximum component. The time periods for damping of these frequency components by 20 dB are usually shorter than the periods for selected components

in defect-free specimens. These periods reach the values of damping approximately between 15 ms and 30 ms.

Let us mention that the Wavelet transform is one of the basic and also fast procedures for the time-frequency analysis of signals. However, the accuracy and appropriateness of this method depends upon the choice of the window function. The application of the method requires a certain experience gained for the “rational” definition of input parameters and also in the interpretation of its spectrum.

Therefore it is often more advantageous to use non-linear time frequency transformations for this analysis of the transient signals. The characteristic feature of non-linear transformations rests in their resultant resolution in time and frequency which is not limited by the Heisenberg uncertainty principle. This fact includes a high resolution capability in the time frequency level which demonstrates itself by the “accurate” localisation of important frequency components in time.

The Rihaczek transforms applied to both signals (defective ones in Figure 4 and defect-free ones in Figure 5) show a similar jointed time-frequency spectrum of the standardised acoustic pressure level as in case of the Wavelet transform. The time-frequency spectrum (the Rihaczek transform) shows local frequency maximums of particular frequency components in time more distinctively (precisely) than it is with the spectrum calculated by the Wavelet transform. This is given especially by the type of transform where mainly the kernel and the local auto-correlation function participate in the phenomenon presented.

The time-frequency spectrum calculated by the Rihaczek transform shows sharper courses of particular distinguished frequency components ("slighter lines") than it is with the spectra calculated by the Wavelet transform.

As apparent from Figures 2 to 5, the whole process of response may be roughly divided into three stages. In the first stage, a very fast growth of the amplitudes of the key frequency components to maximum values is apparent. In the second stage, the descent and extinguishing of higher frequency components occur. However, in both phases of the response the contents of the frequency cross-sections remain approximately the same. In the third stage, the fading of the response occurs. This is usually characterised by the existence of the lowest frequency component.

If some material cracks occur, the speed of the growth and the declination of amplitudes of the spectrum are higher than for a defect-free material. It should, however, be stated that the speed of the growth and declination of amplitudes of particular important elements are not the same. The frequency or the time-frequency spectrum of defective materials is generally much wider, and the so-called clusters of important frequency components occur there. This phenomenon is properly interpreted by particular diagrams in Figures 2 to 5.

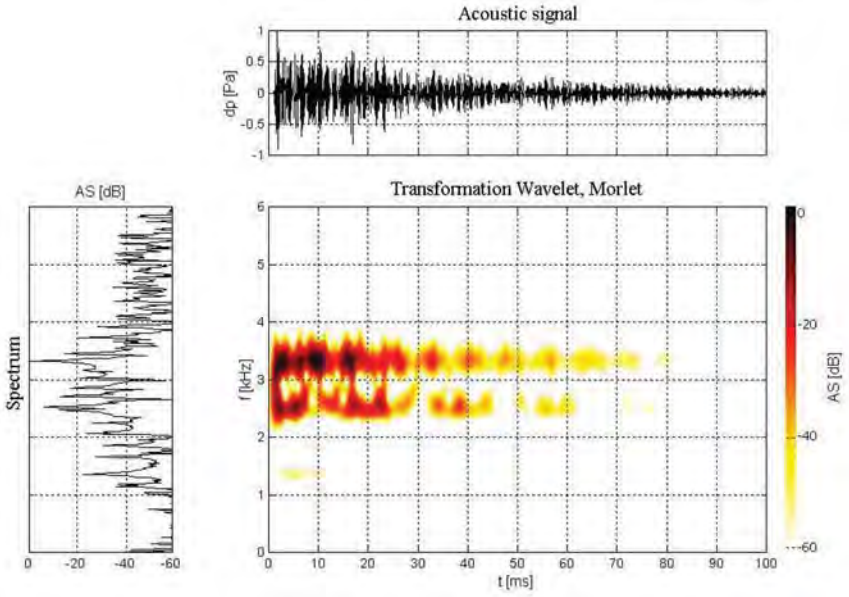

Figure 2 Defect-free product - time behaviour signal from microphone, frequency spectrum and time - frequency analysis by Wavelet transform

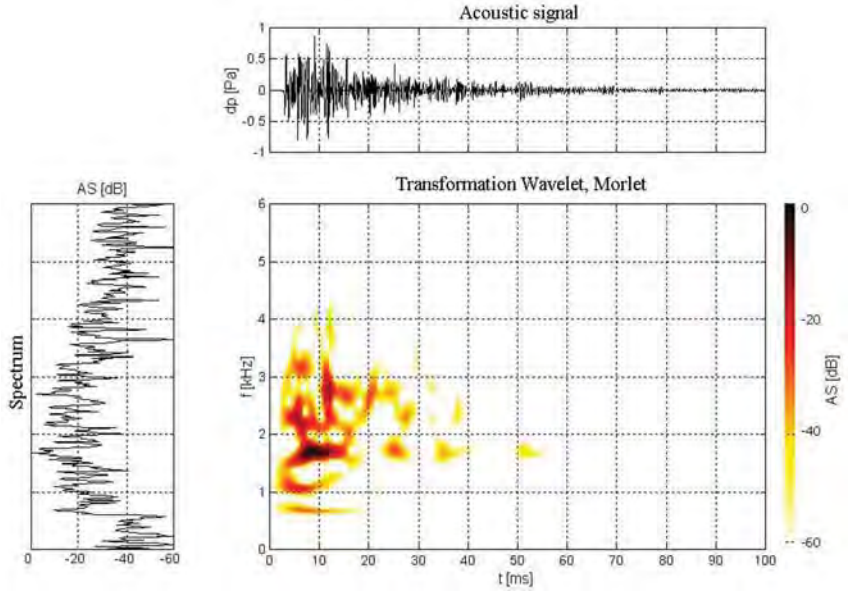

Figure 3 Defective product - time behaviour signal from the microphone, frequency spectrum and time - frequency analysis by the Wavelet transform

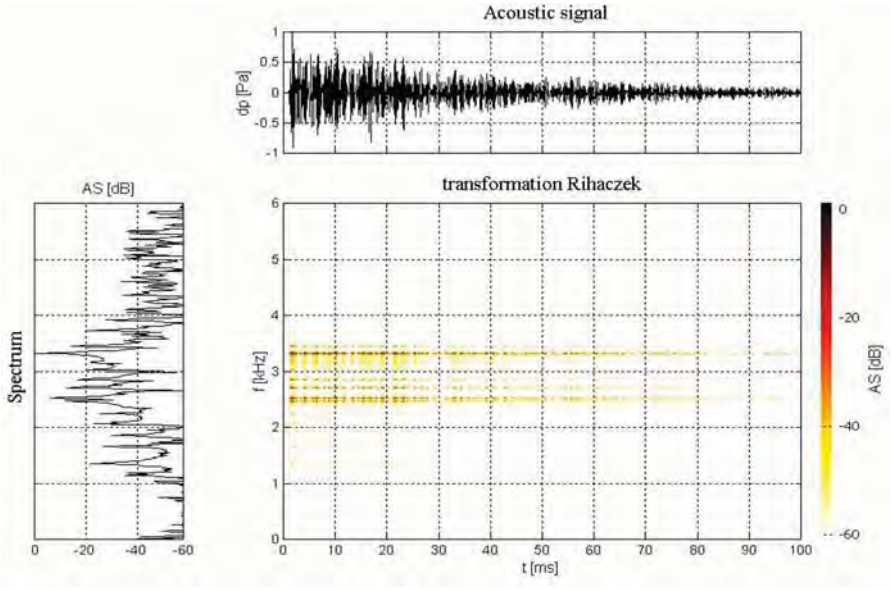

Figure 4 Defect-free product - time behaviour signal from the microphone, frequency spectrum and time - frequency analysis by the Rihaczek transform

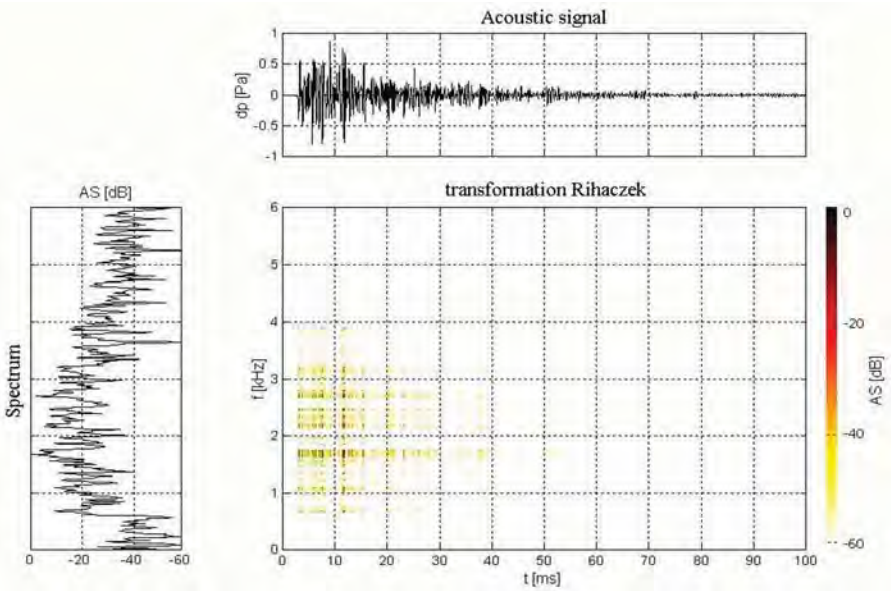

Figure 5 Defective product - time behaviour signal from the microphone, frequency spectrum and time - frequency analysis by the Rihaczek transform

4. CONCLUSIONS

Based on the measurement and analyses made, it is possible to state that the experiment checked the possibilities of using the given methodology for the detection of structural defects of the measured products and materials from the homogeneity and the cracks formation points of view. The analysed parameters enable us to distinguish a good product from a defective one. The given methodology may be successfully applied to all ceramic and concrete products. It can also be established that modern means of signal analysis, especially the time-frequency transforms highly contributed to a quality processing of the measurement. These methods provide us with a time localisation of frequency components contained in the measured signal. In this way, these methods offer new possibilities in the experimental analyses of structural elements and materials. This possibility is included in both the linear and the non-linear time-frequency procedures. By comparing the obtained results we can clearly observe that when analysing the responses to the mechanical shock (heavily damped time signals) the procedures, namely those including into the class of the Cohen time-frequency transforms, show a very good time localisation of significant frequency components contained in the analysed signal.

In some particularly important cases the depicting of results of the computes and analyses by the time and frequency sections may be completed. Thus, these provide us with a profound support in the analysis of the time-frequency results. This procedure often appears as more suitable than e.g. a separate space arrangement. This makes it possible to locate very precisely the time behaviour of particular important frequency components or to show all important frequency components contained in the spectrum in a given time.

In conclusion it may be mentioned that the given methodology can also be incorporated in the process of the half-automated quality control of products under in the production line. When using the above methodology together with the methods of qualitative analysis or the artificial intelligence (fuzzy and rough sets, neural networks, genetic algorithms etc.), then the process of evaluating the quality of products can fully be automated.

Acknowledgements

This research has been supported by the research project 103/07/0183 and by research project MSM 0021630519 ("Progressive reliable and durable load-bearing structural constructions")

References

1. L. Cohen: Time-frequency distributions - a review, Proc. IEEE, Vol. 77 No. 7, 941-981, 1989
2. Wahl T. J.: Bolton J. S., The Application of the Wigner Distribution to the Identification of Structure-Borne Noise Components, Journal of Sound and Vibration, pp. 101-122, 1993, ISBN 0022-460X/93/100101
3. Poularikas A. D.: The Transform and Applications Handbook, IEEE Press, 1996
4. J.C. O'Neill: Quartic Functions for Time-Frequency Analysis with Applications to Signal Adaptive Kernel Design, SPIE - Advanced Signal Processing Algorithms, 1997
5. Hammond J. K., White P. R.: The Analysis of Non-Stationary Signals Using Time-Frequency Methods, Journal of Sound and Vibration, pp. 419-447, 1996, and ISBN 0022-460 X/93/100101
6. Marasek C., Piotrkowski R., Serrano E., Ruzzante J. E.: Monitoring of the tool condition with acoustic emission signal analysis using wavelet packets, Insight - Non-Destructive Testing and Condition Monitoring Vol. 44 No. 12, December 2002, ISSN 13542575
7. Chang Y. F.: Wavelet deconvolution before scanning in ultrasonic non-destructive testing, Insight - Non-Destructive Testing and Condition Monitoring Vol. 44 No. 11, November 2002, ISSN 13542575
8. Young S. Cho: Non-destructive testing of high strength concrete using spectral analysis of surface Wales, NDT & E International, Volume 36, Issue 4, June 2003, pp. 229-235, ISSN 0963-8695
9. Allen G. Davis : The non-destructive impulse response test in North America: 1985–2001 NDT & E International, Volume 36, Issue 4, 2003, pp. 185-193, ISSN 0963-8695
10. Smutný J., Pazdera L.: New techniques in analysis of dynamic parameters rail fastening, InSight, The Journal of The British Institute of Non-Destructive Testing, Vol. 46, No 10, October, 2004, pp. 612-615, ISSN 13542575

"Computational Civil Engineering 2007", International Symposium
Iaşi, România, May 25, 2007

Design of reinforced soil works – Textomur structures – based on the computer program Cartage

Anghel Stanciu[1], Oana Colţ [2] and Irina Lungu[3]
[1]*Department of Roads and Foundations, Technical University, Iasi, 700050, Romania*
[2]*Department of Roads and Foundations, Technical University, Iasi, 700050, Romania*
[3]*Department of Roads and Foundations, Technical University, Iasi, 700050, Romania*

Summary

Reinforced soil represents an alternative solution to consolidate earth massifs and perform retaining structures included in the present transportation infrastructure.

One of the advantages consists in applying this type of structure in poor foundation soil conditions, due to the fact that the induced pressures are small and uniformly distributed. Construction costs may also be decreased by using the local material from the construction site as filling material within the reinforced soil work. Finally, the resulted platform may also be support for additional construction works.

Regarding the construction method, the variety of the reinforcements (steel, geosynthetics, geogrids) or of the facing elements (precast concrete blocks, steel structures, reversed geogrids or geosynthetics) allows various performing procedures to develop when building reinforced soil structures.

Textomur system is included in the category of reinforced soil with geosynthetics, developed mainly in France. The main difference between this system and other reinforcing techniques consists in building up the facing element, by using prefabricated steel elements.

The design of the reinforced soil works in Textomur system is implemented via a computer program – Cartage. This program was initiated in 1985 LCPC (Laboratoire Central du Ponts et Chaussée), France and it is based on the analytical calculation method developed also at LCPC, considering the limit equilibrium.

By running this computer program stresses within the reinforcements can be evaluated, the displacements of the soil massive, and the safety coefficients at anchorage as well, based on the stability analysis of the massive in case of cylindrical failure surfaces going through the toe of the reinforced soil structure.

KEYWORDS: reinforced soil, retaining structures, geosynthetics, Textomur, Cartage.

1. INTRODUCTION

The first modern system of soil reinforcing was initiated and developed in the mid '60s by the French engineer Henri Vidal, with the name *Terre Armeé* (reinforced soil), using steel reinforcements. Beginning with 1970, geosynthetics have been created as an alternative of the steel reinforcements. The acceptance of geosynthetics in reinforced soil construction has been triggered by a number of factors, including aesthetics, reliability, cost, simple construction techniques, good seismic performance, and the ability to tolerate large deformations without structural distress.

In Romania, the first attempts of performing retaining walls by reinforced soil were made in 1973...1974, when such a construction work was designed and built over 50m length. After 1990 many retaining walls have been performed as soil reinforced with geotextiles and geogrids within road rehabilitation works.

Textomur system is included in the category of reinforced soil with geosynthetics, developed mainly in France. The main difference between this system and other reinforcing techniques consists in building up the facing element, by using prefabricated steel elements.

2. TEXTOMUR REINFORCING SYSTEM

Textomur is essentially a reinforcing technique of soil using geogrids or geotextiles. There are many variants of the Textomur system and the name corresponds to Textomur system with mineral, vegetal, or neutral facing elements.

The facing elements of Textomur have a length of 4.75m the steel within has a diameter of 6 and 8mm. For the Textomur system with mineral facing the formworks are galvanized after welding and bending at the appropriate angle. The height of one layer is 60-65cm, being variable depending on the requirements of the project. The slope of the formwork may vary between 40° to 90°. The reinforcement length is established for each project but an initial 0.7 of the total height is recommended.

2.1. Advantages

- Local material from the construction site may be used as filling material.
- Flexibility – curves, edges, terraces of variable length may be performed.
- Long lasting life – the life span is estimated for approximately 120 years.
- Easy to built, without a foundation.
- Construction may be performed without additional bracing.

2.2. Textomur with mineral facing

Textomur with mineral facing includes galvanized welded steel facing elements behind which large boulders of 30-100cm are manually placed over a width of 30cm and along the entire height of the facing (figure 1). The boulders are preferred to be with plan surfaces and consequently the arrangement will display less voids.

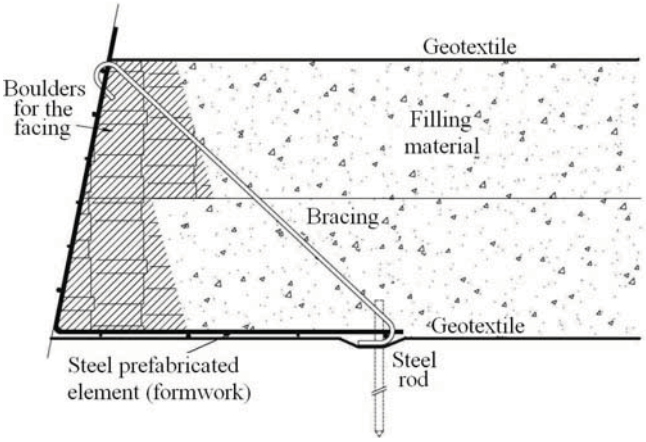

Figure 1. Cross section of a Textomur system with mineral facing

This type of Textomur is best applied for retaining structures (figure 2), the ensure slope stability, for significant height, reinforced soil works in steps can be performed, with an aesthetic role as well.

Figure 2. Retaining wall of Textomur with vertical mineral facing

3. COMPUTER PROGRAM - CARTAGE

The computer program Cartage is based on the LCPC calculation method of the reinforced soil [1], [2], considering the limit equilibrium of the massive. Slope stability is analyzed based on circular failure surfaces through the toe of the massive. The program computes the stresses within reinforcements, considering each failure surface. The safety coefficient for internal stability is set as 1.5. The maximum stress in each reinforcement resulted from the program is considered the service stress for the corresponding failure surface. The calculation continues until the safety requirements are met, altering the reinforcing scheme or the reinforcement type.

3.1. Calculation method of L.C.P.C.

The method is based on Rankine's theory to compute the active earth pressure on the retaining element (figure 3). The soil layer horizontally placed between the *i*-1 and *i* reinforcements is considered to establish the tension force within the reinforcement [3], [4]. Regarding the main stress as the vertical one ($\sigma_v = \gamma \cdot H$), the tension force in the *i* reinforcement would counteract the active earth pressure acting on the facing of height ΔH.

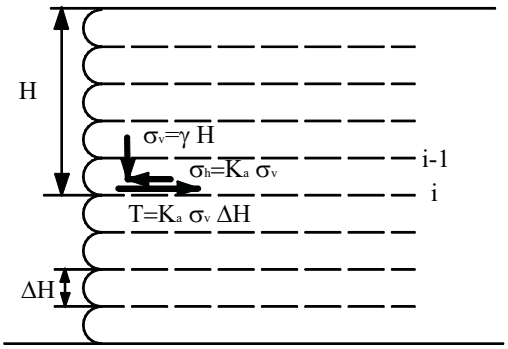

Figure 3. Principle of L.C.P.C. method

Consequently the tension force is given by:

$$T_i = \gamma \cdot H \cdot K_a \cdot \Delta H + \frac{1}{2} \cdot K_a \cdot \gamma \cdot (\Delta H)^2 \tag{1}$$

but $H = i \cdot \Delta H$ and thus the final relationship is the following:

$$T_i = \left(1 + \frac{1}{2}\right) \cdot K_a \cdot \gamma \cdot \Delta H^2 \tag{2}$$

3.2. Design hypotheses

The stability analysis is performed considering the simultaneous action of several pessimistic factors the highest height, a horizontal platform at the top, the service load as close as possible towards the facing, and ignoring the presence of the material in front of the reinforced structure toe.

A case study is presented as a retaining wall on the road RN 94, Embrun, France. The less favourable case is adopted in the design profile (figure 4), height of 5,40m corresponding to 9 levels of Textomur formwork, with an inclination of 27^0 [5]. The presence of soil over the first formwork height was disregarded.

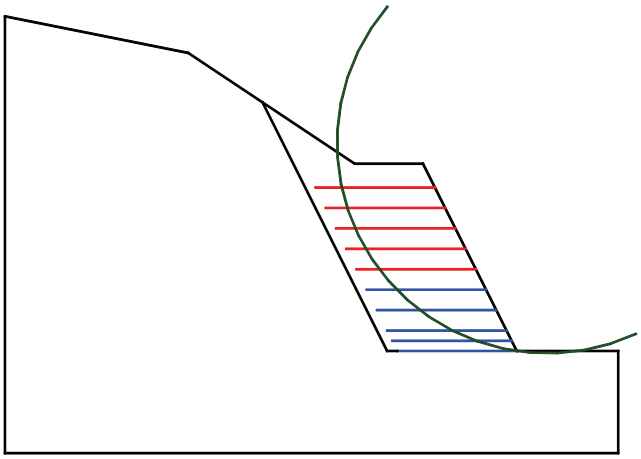

Figure 4. Design profile for Cartage, considering one potential failure surface

The geotechnical parameters of the local material are: unit weight - $\gamma = 21 kN/m^3$; internal friction angle - $\phi = 35^o$; cohesion - $c = 5$kPa.

For filling the space between reinforcements, the local material is considered cohesionless.

Initially, 5 layers of geotextile were considered, with strength in tension of 100kN/m, with 0.60m interdistance, 2 layers with 200kN/m strength at 0,60m interdistance and 3 layers of 200kN/m strength at 0,30m interdistance.

The input data for Cartage are represented by: geometry of the massive; characteristics of the filling soil, foundation soil and soil behind the retaining structure; characteristics of the reinforcements; coordinates of the failure circles; displacement value at the massive top; the presence of underground water.

The input data are presented in figure 5, a verification of their accuracy being easily done.

```
                    RAPPEL  DES  DONNEES
                    ********************
                    tableau des segments
                    ====================
numero   point   point   numero
segment  gauche  droit    sol
--------------------------------
  1        1       2        2
  2        2       3        2
  3        3       4        1
  4        4       5        1
  5        5       7        1
  6        3       6        2
  7        6       7        2
  8        7       8        2

                    tableau des points
                    ==================
numero
point    abscisse   ordonn,e
----------------------------
  1         .00       12.83
  2        5.37       11.75
  3        7.55       10.30
  4       10.25        8.50
  5       12.25        8.50
  6       11.20        3.00
  7       15.00        3.00
  8       26.74        3.00

                    tableau du bed-rock
                    ===================
numero
point    abscisse   ordonn,e
----------------------------
  1         .00         .00

                    tableau des sols
                    ================

numero   poids                angle
 sol     terres   cohesion    frot.int.      up
-------------------------------------------------
  1       21.00        .00       35.0     .02000
  2       21.00       5.00       35.0     .02000

******CARACTERISTIQUES DU RENFORCEMENT******

 ***MASSIF GEOTEXTILES  NO  1***
  le massif est form, de   5 lits
  de     3.50 mStres de longueur
    Raideur du g,otextile      1000.00
    Rapport TgPhi geot/TgPhi sol =   .70000
    Rapport Cohe geot/Cohe sol =   .00000
    Segment mini en Traction =  .2000
    Valeur de DELTA EN TETE   .050000

 ***MASSIF GEOTEXTILES  NO  2***
  le massif est form, de   2 lits
  de     3.50 mStres de longueur
    Raideur du g,otextile      2000.00
    Rapport TgPhi geot/TgPhi sol =   .70000
    Rapport Cohe geot/Cohe sol =   .00000
    Segment mini en Traction =  .2000
    Valeur de DELTA EN TETE   .050000

 ***MASSIF GEOTEXTILES  NO  3***
  le massif est form, de   3 lits
  de     3.50 mStres de longueur
    Raideur du g,otextile      2000.00
    Rapport TgPhi geot/TgPhi sol =   .70000
    Rapport Cohe geot/Cohe sol =   .00000
    Segment mini en Traction =  .2000
    Valeur de DELTA EN TETE   .050000

  ***rupture circulaire***
  ===--------------------===
```

Figure 5. Format of the input data for the computer program Cartage

3.3. Results

By running the program the output data are presented in a table consisting of the extreme values for the safety coefficients according to the failure surfaces considered, for the displacement, coefficient of anchorage and maximum stress. Based on the required values by the designed norms, the necessity of altering the reinforcing scheme is analyzed.

The alteration of the reinforcing solution is made according to the difference between the imposed and obtained values and not in the least, based on the design experience of the engineer.

Within the presented case study, the final values are set in a table for the first 12 failure circles as in figure 6 [5].

T A B L E A U R E C A P I T U L A T I F

RU	F0	FSOL	DELTA	ANCR	TENR
1	.53	.53 ******	.05000	(0, 0) 999.00	(0, 0) .000E+00
2	.44	1.49	.00853	(1, 1) 17.26	(1, 3) .496E+01
3	1.36	1.50	.01413 ******	(1, 4) 3.01	(1, 5) .104E+02
4	1.29	1.49	.00970	(1, 3) 5.38	(1, 5) .708E+01
5	1.18	1.49	.01194	(1, 2) 3.39	(1, 5) .812E+01
6	.95	1.49	.01083	(1, 1) 6.54	(1, 5) .845E+01
7	.86	1.50	.01011	(1, 1) 9.29	(1, 5) .864E+01
8	.69	1.50	.01008	(1, 1) 11.52	(1, 5) .903E+01
9	.59	1.50	.01273	(1, 1) 10.19	(1, 5) .938E+01
10	.42	1.49	.00837	(1, 1) 16.81	(1, 2) .404E+01
11	1.39	1.50	.01311	(1, 4) 2.42 ******	(1, 5) .997E+01
12	1.23	1.49	.01406	(1, 3) 3.50	(1, 5) .960E+01

Figure 6. Final values as output data from the Cartage program

LEGEND:

- Values between parantheses (,) - number of the massive and reinforcement with the smallest value of the coefficient of anchorage (ANCR), respectively the maximum stress (TENR) for each failure circle.
- DELTA – displacement value ;
- F0 – value of the safety coefficient with reinforcing the massive ;
- FSOL – value of the safety coefficient after reinforcing the massive.

4. CONCLUSIONS

Using computer programs to design retaining structures made of reinforced soil decreases significantly the design time. In order to perform an efficient design it is required to master correctly the behaviour of the reinforced soil generally, and especially the response of such structures subjected to various external loads.

References

1. Silion T., P. Răileanu, A. Stanciu - Fundații - *Pământ armat*, Institutul Politehnic Iaşi, Facultatea de Construcții, 1980.
2. *Cartage* – manual de utilizare, L.C.P.C, 1985.
3. Schlosser F - *La terre armée, Recherches et realisations*, Bull. liaison Labo P. et.ch. 62, nov. – dec., 1972.
4. Schlosser F., Long T.N. – *Dimensionnement de murs en terre armee*, Session de formation permanente, E.N.P.C., 1974.
5. Proiect tehnic şi detalii de execuție - „*RN 94 - Déviation d'Embrun*", Geonove, Franța.

"Computational Civil Engineering 2007", International Symposium
Iaşi, România, May 25, 2007

Computer program for Pipe Section Column Sizing

Dragos Voiculescu[1], Daniela Preda[1]
[1]*Steel Structures, Technical University of Civil Enginering, Bucharest, Romania*

Summary

The paper presents the Excel Program for Pipe Section Column Sizing. The program has three main parts: the first one is the data input, where the proposed size of the column is set; the second one is the load section, where the maximum loads are input from the structural analysis program, such as SAP or ETABS; the third part gives the results of the structural checks on the proposed section.

The program is interactive, meaning that if one of the checks is wrong, it can be corrected by changing the size of the Pipe section.

The program is very useful in applied engineering design, as it gives immediately the final section of a specific column.

KEYWORDS: pipe section; column; sizing.

1. INTRODUCTION

The computer program was developed in Microsoft Excel in order to be used without major problems on any machine. It has some Visual Basic features to make it very easy to use; also it was realized in such a manner to be printed as calculation notes in real projects.

2. PROGRAM PRESENTATION

The program has three main parts, interconnected. The first part is the data input, where the initial geometrical characteristics of the column are given. This data is used to compute all sectional characteristics of the pipe section, which will be used later in the program. Also the section class is shown. (Fig.1)

Immediately after, the pipe steel grade is input. The user may choose in between the two common steel grades for pipes. After choosing the steel grade, the factored strength is shown. All strength checks will be reported to this strength.

Figure 1.Input data

After this data is established, the program demands the input of the buckling length factors (Fig.2). These ones are computed using another program, according to the column end supports and beam characteristics. The buckling length factors will be used to compute the buckling coefficient which will be used further.

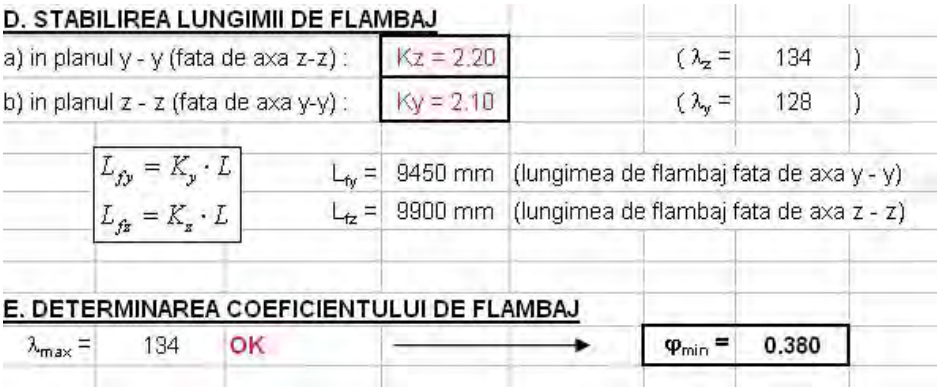

Figure 2.Buckling data input

Then the second part of the computer program starts, the part where the column loads are input. These loads are taken from a structural analysis program such as SAP or ETABS. The data is input in a table, and is used in all the strength and stability checks. (Fig.3)

Loads are given in three hypothesis: The first one is the maximum axial load with the correspondent bending moments; the second one is the maximum z-z bending moment with the correspondent others and the third one is the maximum y-y bending moment with the correspondent others. All further calculations is referred to these hypothesis.

F. EFORTURI DE CALCUL (IN MODUL)

a) IPOTEZA 1

N_{max} (kN)	M_{ycor} (kNm)	M_{zcor} (kNm)	T_{ycor} (kN)	T_{zcor} (kN)
-341.0	-3.60	-0.64	0.11	-4.05

b) IPOTEZA 2

N_{cor} (kN)	M_{ymax} (kNm)	M_{zcor} (kNm)	T_{ycor} (kN)	T_{zcor} (kN)
-148.30	21.15	19.80	3.19	4.81

c) IPOTEZA 3

N_{cor} (kN)	M_{ycor} (kNm)	M_{zmax} (kNm)	T_{ycor} (kN)	T_{zcor} (kN)
-191.84	21.07	19.80	3.18	4.81

Figure 3.Load input

The third part of the computer program starts with the strength checks for the proposed pipe section. Here the applied formulas are written and the result is given for each hypothesis. (Fig.4)

G. VERIFICAREA DE REZISTENTA A STALPULUI

a) IPOTEZA 1

$$\sigma_x = \frac{N}{A} + \frac{M_y}{W} + \frac{M_z}{W} = \quad 65\ \text{N/mm}^2 \quad \text{OK}$$

$$\tau_{res} = \frac{T_{res}}{A} = \frac{\sqrt{T_y^2 + T_z^2}}{A} = \quad 0.6\ \text{N/mm}^2 \quad \text{OK}$$

$$\sigma_{ech} = \sqrt{\sigma_x^2 + 3\tau_{res}^2} = \quad 65\ \text{N/mm}^2 \quad \text{OK}$$

b) IPOTEZA 2

$$\sigma_x = \frac{N}{A} + \frac{M_y}{W} + \frac{M_z}{W} = \quad 147\ \text{N/mm}^2 \quad \text{OK}$$

$$\tau_{res} = \frac{T_{res}}{A} = \frac{\sqrt{T_y^2 + T_z^2}}{A} = \quad 0.9\ \text{N/mm}^2 \quad \text{OK}$$

$$\sigma_{ech} = \sqrt{\sigma_x^2 + 3\tau_{res}^2} = \quad 147\ \text{N/mm}^2 \quad \text{OK}$$

c) IPOTEZA 3

$$\sigma_x = \frac{N}{A} + \frac{M_y}{W} + \frac{M_z}{W} = \quad 154\ \text{N/mm}^2 \quad \text{OK}$$

$$\tau_{res} = \frac{T_{res}}{A} = \frac{\sqrt{T_y^2 + T_z^2}}{A} = \quad 0.9\ \text{N/mm}^2 \quad \text{OK}$$

$$\sigma_{ech} = \sqrt{\sigma_x^2 + 3\tau_{res}^2} = \quad 154\ \text{N/mm}^2 \quad \text{OK}$$

Figure 4.Strength checks

Also the buckling checks are given in this part of the program (Fig.5).

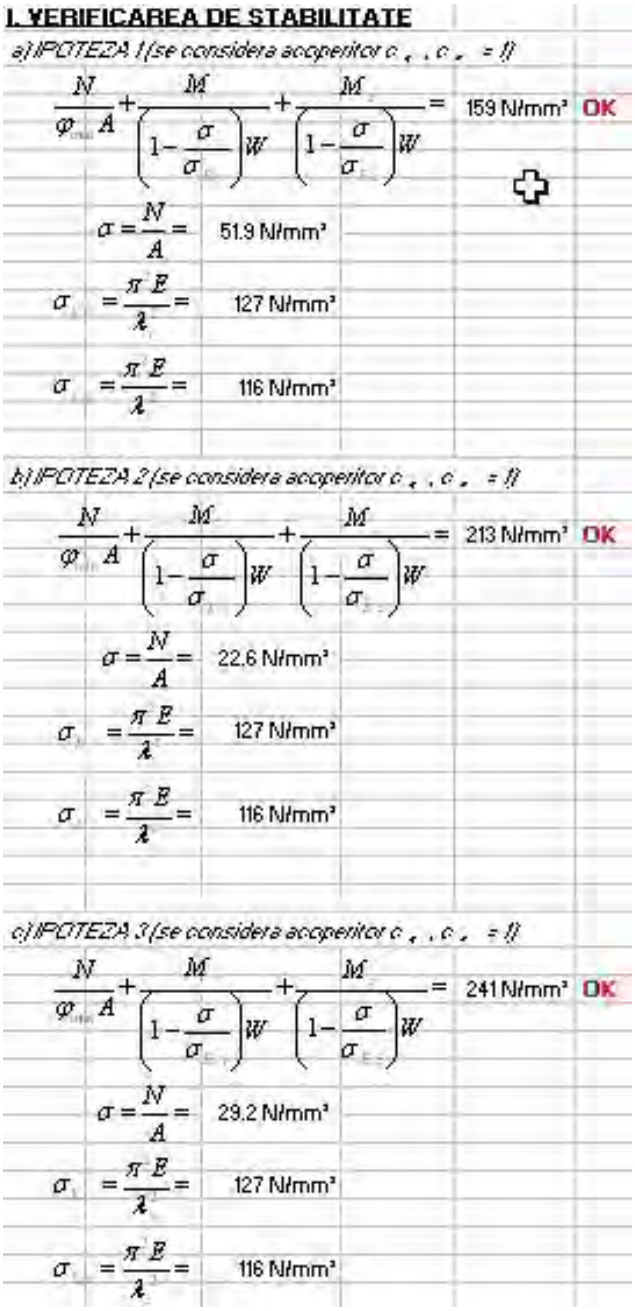

Figure 5.Buckling checks

3. CONCLUSIONS

This program is very useful when fast section sizing is demanded. It may be printed and gives the calculation sheet for the specific column.

References

1. STAS 10108/0-78.

"Computational Civil Engineering 2007", International Symposium
Iaşi, România, May 25, 2007

Computational method and application using Newton Algorithm

Cornelia Victoria Anghel
Computer Science Department, "EFTIMIE MURGU" University, Resita, 320085, Romania

Summary

The article presents some aspects about Newton method and algorithm and a numerical example. The C++ program illustrated the important steps and advantages to apply the Newton method to solve the nonlinear equations.

KEYWORDS: Newton (tangent) method, Newton algorithm, C++ program.

1. INTRODUCTION NEWTON METHOD (TANGENT METHOD)

The Newton Method (or Tangent Method) is used to solve the un-linear equations, and to reduce substantially the number of iterations.

If we considered $\mathbf{x}^*$ **-** a separate solution of equation **f(x) = 0** on [a, b] interval and **f(x)** is continue and monotone on this interval, the values of function in a and b points **f(a)** and **f(b)** have opposed signs (such as in Figure 1).

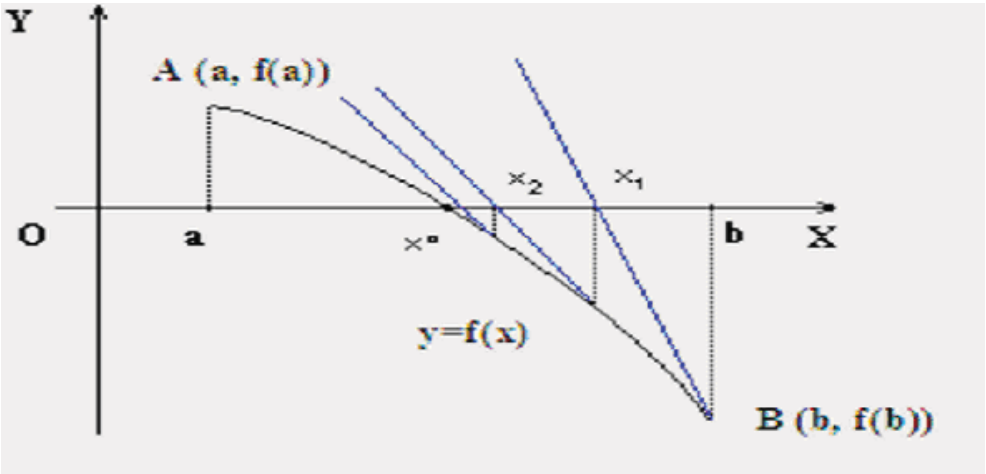

Figure 1.

We write the tangent equation in **A(a, f(a)),** point

$$y - f(a) = f'(a) \cdot (x - a)$$

intersect the Ox axis.

We obtain $x = a - \frac{f(a)}{f'(a)}$ or $x_1 = a - \frac{f(a)}{f'(a)}$.

From geometrical point for view (figure 1) signifies the fact that the arch/spring curve is replaced by the tangent, and the place of the exact value solution x_1 (the abscissa/x-coordinate of the intersection point of the curve and the axis Ox) it is taken as an approximate value x_1 (the abscissa of the intersection point of the tangent at the curve with the axis Ox).

By repeatedly applying Newton's method we can correct the first approximation, finding closer values to the exact one.

The approximate values result from the series:

$$x_n = x_{n-1} - \frac{f(x_{n-1})}{f'(x_{n-1})}$$

2. THE ALGORITHM OF THE TANGENT METHOD (NEWTON)

- We draw the tangent at the curve in the point **B(b, f(b))** and we find the intersection point of the tangent and the axis OX – $(x_1, 0)$. The abscissa of this point **x1** is taken as I the solution approximation.
- Computing the function value in $\mathbf{x_1}$ we could deduce the tangent at the curve in the point with the coordinates $(\mathbf{x_1}, \mathbf{f(x_1)})$. The tangent will intersect the axis OX in the point with the coordinates $(\mathbf{x_2}, \mathbf{0})$. The abscissa of this point $\mathbf{x_2}$ **0** taken as I solution approximation.
- Continuing this process several times, we can observe that we obtain a value series **x1, x2, x3, ... ,** which tend towards the equation solution **x°.**

3. NUMERICAL APPLICATION

We propose to solve the equation $x^3 - 2x - 5 = 0$.

Solution: We notice that if we note $f(x) = x^3 - 2x - 5$, then
$f(1) = -6$; $f(2) = -1$; $f(3) = 16$.

From the conditions $f(2) < 0$ and $f(3) > 0$ we deduce that a solution of the equation appears in the interval (2, 3).

We consider the first approximation $x_1 = 2$.

We determine $x_2 = 2 - \frac{f(2)}{f'(2)}$.

For $f(x) = x^3 - 2x - 5$, $f'(x) = 3x^2 - 2$ and $f(2) = -1$; $f'(2) = 10$

$$x_2 = 2 + \frac{1}{10} = 2 + 0.1 = 2.1.$$

We repeat the sentence and we get: $x_3 = 2.1 - \frac{f(2.1)}{f'(2.1)}$

where $f(2,1) = (2,1)^3 - 2\cdot(2,1) - 5 = 0,061$.

$f'(2.1) = 3\cdot(2,1)^2 - 2 = 3\cdot 4,41 - 2 = 13,23 - 2 = 11,23$.

It results $x_3 = 2.1 - \frac{0.061}{11.23} = 2.1 - 0.0054 = 2.0946$

Then we determine $x_4 = x_3 - \frac{f(x_3)}{f'(x_3)}$

By substitution we get: $x_4 = 2.0946 - \frac{f(2.0946)}{f'(2.0946)} = 2.09455.$

We approximate $x_4 = 2,095$.

The value of the function is:
$f(2,095) = (2,095)^3 - 2\cdot(2,095) - 5 = 9,195 - 4,190 - 5 = 9,195 - 9,190 = 0,005$
hence $f(2,095) > 0$.

From the conditions $f(2) = -1 < 0$ and $f(2,095) > 0$ we determine that the value $x = 2,095$ can be considered the solution of the given equation.

As an observation, we can affirm that if the graphic of the function f(x) is almost parallel to the ax Ox, i.e. the size of the derivative f'(x) is closed of zero, then the Newton method is not applicable, but another method is recommended, for example the string/cord method.

4. PROGRAM C++

The program written in C++ which determines the solution of the function given in the above mentioned example, using the algorithm of the tangent method (Newton) is:

```
#include <stdio.h>
#include <conio.h>
#include <math.h>
```

```
float Func(float x)
{
 return x*x*x-2*x-5;
}
int Newton(float Func(float, float *x), float *x)
{
 const float eps=1e-6;
 const int itmax=100;
 float df, dx, f;
 int it;

 for(it=1; it<=itmax; it++){
          f=Func(*x, &df);
          dx=(fabs(df) > eps) ? -f/df : -f;
          *x += dx;
          if (fabs(dx) <= eps*fabs(*x)) return 0;
           }
 printf("maximum no. of iterations exceeded within the Newton method! \n");
  return 1;
  }
```

The following notations were used:

Func – for the user function
a, b - the limits for the search interval
***x** - the found zero (output)
it - the number of iterations
itmax – the maximum number of iterations

The error number is returned:

0 – for a normal execution
1 – if the maximum number of iterations is exceeded
2 – when the interval does not contain a root.

After each partition of the interval, not only the ends of the interval are upgraded, but also the corresponding values of the function $f(a_i)$ and $f(b_i)$.

5. CONCLUSIONS

This method helps us to efficiently obtain the solution of the problem. The small number of iterations necessary for the determination of the equation solution from the presented example indicates that the choice of the tangent method (Newton) in

the solving of this equation was the right one. These observations can be picked out from the analysis of the results obtained after the development of the program implemented in the above presented programming language C++.

If the graphic of the function f(x) is almost parallel to the Ox axis, i.e. the size of the derivative f'(x) is closet o zero, then the Newton method is not applicable, but another method is recommended, for example the string/cord method.

References

1. Anghel C.V. – *Metode numerice. Algoritmi şi programe de calcul*. Ed. Orizonturi Universitare, Timişoara 2005 (in Romanian);
2. Anghel, I., Anghel, C.V.- *Algebra liniară. Programare liniară*, Curs vol.1, Ed. Eftimie Murgu, Reşiţa, 2003 (in Romanian);
3. Precup, R. ş.a – *Matematici asistate de calculator. Aplicaţii*. Ed. Politehnică, Timişoara, 2002 (in Romanian);
4. Kilyeni, Şt. – *Metode numerice*, vol.1, Ed. Orizonturi Universitare, Timişoara, 1997 (in Romanian).

"Computational Civil Engineering 2007", International Symposium
Iaşi, România, May 25, 2007

Partial substitution of Cement in Concrete by Finely Ground Brick Body

Libuše Beckerová, Gergely Bölckei and Jiří Brožovský
[1,2,3] *Faculty of Civil Engineering, Brno University of Technology, Brno, 602 00, Czech Republic*

Summary

Brick chippings are the waste which can partially substitute the cement. Therefore this waste is utilized, in light of the environment, into the useful new product - the concrete. The finely ground brick body is characterized by certain pozzuolana activity which enables the partially substitution of the energetically demanding binder which is the cement. The paper indicates the observations concerning the tests of concrete in which the cement was substituted by 10% and 20% of finely ground brick bodies from the brick plants Kryry and Šlapanice.

KEYWORDS: brick body, concrete, additive to concrete, pozzuolana activity.

1. INTRODUCTION

The brick plants produce on the average 1 till 5 % of waste, which is recycled only in low range and utilized as opening material. The rest is stored in deposits. The price of this waste material rarely overreaches 5 till 10% of the cement price. It is true that for the utilization as substitute for cement it is necessary to prepare it (by grinding, separation etc.). However also after this preparation its price does not overreach 20% of cement production costs. The finely ground brick body shows pozzuolana activity so that we can hold it for the active pozzuolana admixture and we can substitute the part of binder in cement composite by this material.

By the addition of finely ground brick body we can achieve, with comparable concrete parameters, the decrease of production costs.

The reaction extent of the burned brick body with the hydrating cement is given on the one hand by the composition of raw materials and on the other hand by the burning conditions.

The brick products are on the present as a rule burned at the temperature 1000 – 1100°C. The brick body is formed by raw glass surrounded by other crystals and it can show variable pozzuolana activity in dependence on the used earth and on the burning temperature. The greatest portion in the resulting product forms as the rule the glassy phase with high content of silicon and of alkalis and it contents further

also aluminiuum, different iron oxides, calcium and magnesium surrounded by crystals of mullite, silicon and sometimes also cristoballite. The brick products with high lime content can also contain considerably amounts of feldspars which support the increase of activity.

The reaction activity is highest mostly in the temperature range between 600 – 900°C. Higher temperature causes nucleation and crystallization of new phases in the body and the reaction activity rather decreases. The glassy phase excels during cooling and it is in dependence on the composition more or less active [4].

The following active admixtures were applied in practice:

- Finely ground brick body from the brick plant KRYRY
- Finely ground brick body from the brick plant ŠLAPANICE

The effect of the cement substitution in concrete by finely ground brick body, on its physico-mechanical characteristic, was tested in experimental work.

2. METHODS OF EXPERIMENTAL WORK AND THE COMPOSITION OF CONCRETE

The experimental work is based on the properties comparison of concrete made with different batch of finely ground brick body (substitution 10 % and 20 % of the cement weight) with the properties of reference concrete which was made without the use of brick body.

2.1. Input materials:

The following components were used for the production of concrete:

- cement CEM 42,5R from cement plant Mokrá
- sand fraction 0-4 mm from the locality Žabčice
- crushed aggregate fraction 4-8 mm from the locality Želešice
- crushed aggregate fraction 8-16 mm from the locality Želešice
- admixture: finely ground brick body from the brick plant KRYRY and ŠLAPANICE
- The volume weight of these brick bodies are 2750 kg/m^3
- Additive: poly-carboxyl-ether ACE 40, from the firm BASF which shows liquefying effects, increases the initial and the final strength of concrete
- batch water – it fulfils the demands of the EN 1008.

The basic parameters of the aggregate are in table 1.

Table 1: Basic parameters of the aggregate

Parameter	Unit	Žabčice 0/4 mm	Želešice 4/8 mm	Želešice 8/16 mm
Volume weight	[kg/m^3]	2630	2650	2730
Bulk weight in shed state	[kg/m^3]	1770	1670	1710
Porosity	[%]	32,7	37,0	37,4

2.2. Composition of concrete

The composition of concrete is in table 2.

Table 2. Composition of concrete in 1 m^3

Component	Reference concrete	Concrete with10% of brick body	Concrete with 20% of brick body
CEM I 42,5 R Hranice cement	400 kg	360 kg	320 kg
Finely ground brick body	0 kg	40 kg	80 kg
Sand 0 to 4 mm from the Žabčice Gravel Pit	745 kg	740 kg	739 kg
Aggregates 4 to 8 mm from the Želešice Gravel Pit	235 kg	230 kg	229 kg
Aggregates 8 to 16 mm from the Želešice Gravel Pit	980 kg	972 kg	971 kg
Plasticizer BASF ACE 40	4 kg	4 kg	4 kg
Mixing Water	151 kg	147 kg	141 kg
Water/Cement Ratio	0,38	0,37	0,35

2.3. Observed parameters

The following parameters were observed with tested concrete:

- fresh concrete - flow table test $\boldsymbol{F}$ (EN 12350-5 Standard)
- density of fresh concrete $\boldsymbol{D}$ (EN 12350-6 Standard)
- density of hardened concrete $\boldsymbol{D}$ (EN 12390-7 Standard)
- compression strength $\boldsymbol{f_{c,cu}}$ (EN 12390–3 Standard) in the age of concrete 1, 3, 7, and 28 days
- bending strength $\boldsymbol{f_{cf}}$ (EN 12390–6 Standard) in the concrete age 28 days
- depth of penetration of water under pressure $\boldsymbol{h_{tv}}$ (EN 12390–8 Standard)
- dynamic modulus of elasticity $\boldsymbol{E_{bu}}$ (CSN 731371 Standard) in the age of concrete 1, 3, 7, 14 a 28 days.

Marking of individual tested concrete:

REF - reference concrete (strength class C 55/67)

S10 - concrete with 10% substitution of cement by finely ground brick body from brick plant Šlapanice

S20 - concrete with 20% substitution of cement by finely ground brick body from brick plant Šlapanice

K10 - concrete with 10% substitution of cement by finely ground brick body from brick plant Kryry

K20 - concrete with 10% substitution of cement by finely ground brick body from brick plant Kryry

3. TEST RESULTS

The test results are in table 3 and for selected parameters they are represented graphically in figures:

- Fig.1: Effect of the finely ground brick body addition on the compression strength of concrete with different age

  Fig.2: Effect of the finely ground brick body addition on the bending strength of concrete and on the ingress of pressure water - age of concrete 28 days

- Fig.3: Effect of the finely ground brick body addition on the dynamical elasticity modulus – for different ages of concrete.

Table 3: Results of concrete tests

Properte	Age [days]	Unit	REF	S10	S20	K10	K20
FRESH CONSCRETE							
F	--	[mm]	370	435	450	420	435
D	--	[kg/m^3]	2500	2480	2460	2470	2460
HARDENED CONCRETE							
D	28	[kg/m^3]	2520	2490	2480	2490	2480
$f_{c,cu}$	1	[MPa]	39,8	30,2	20,8	28,6	20,4
	3		49,8	40,4	34,9	36,5	33,6
	7		59,6	54,6	43,1	52,6	44,1
	28		74,0	68,6	56,6	69	52,1
f_{cf}	28		7,8	6,5	5,5	6,6	5,5
h_{tv}	28	[mm]	11	8	6	10	7
E_{bu}	1	[GPa]	47,5	42,8	40,3	40,8	40,7
	3		52,2	46,5	44,5	44,6	44,5
	7		56,7	52,8	50,3	51,1	49,8
	14		57,1	53,0	51,7	52,2	51,5
	28		57,4	54,6	52,0	52,5	52,5

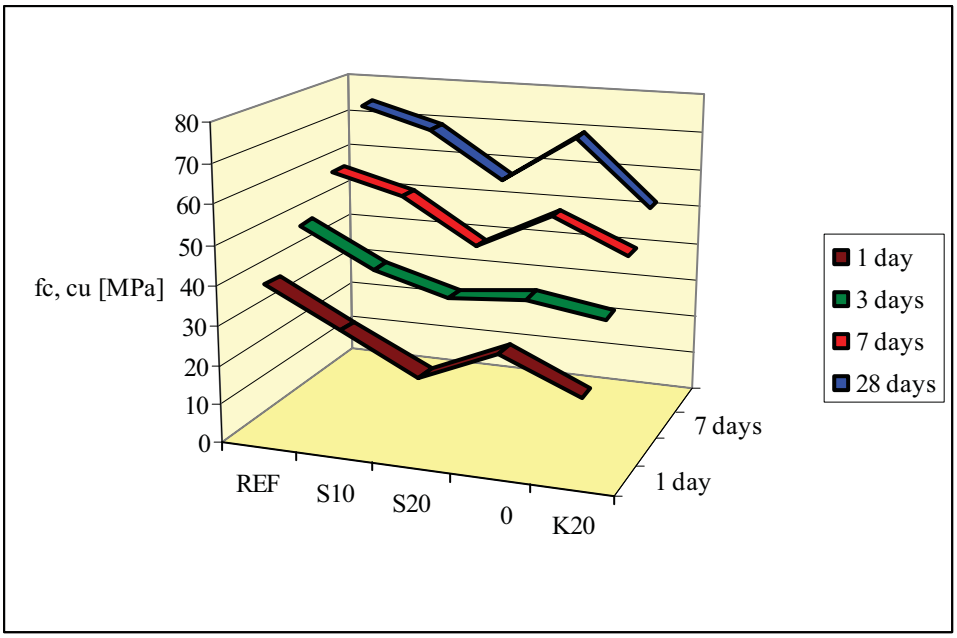

Figure 1.Compression strength in dependence on the quantity of added brick body and on the hardening time of concrete

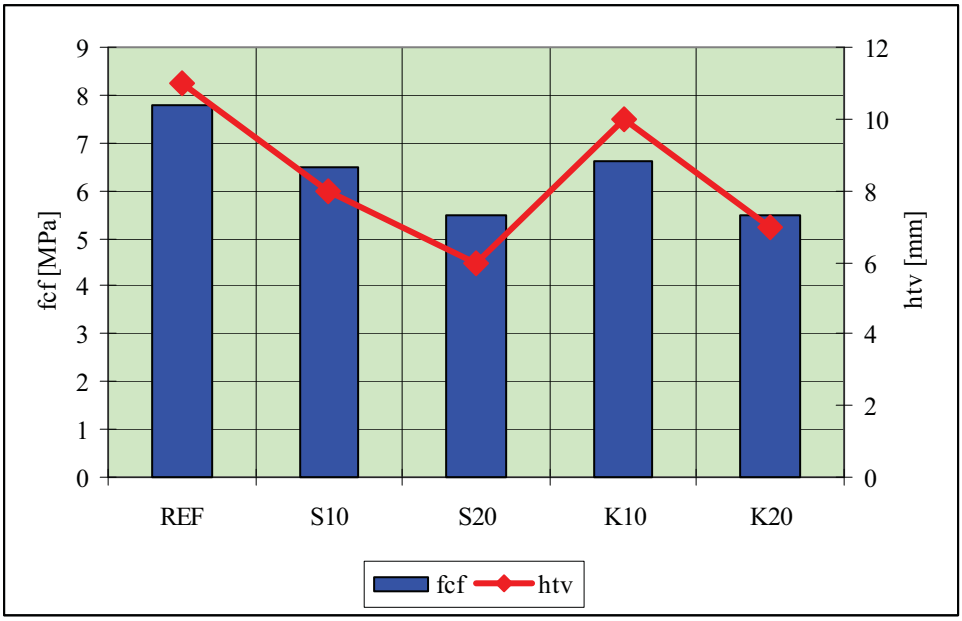

Figure 2.Effect of the quantity of added brick body on the bending strength and on the depth of the pressure water ingress

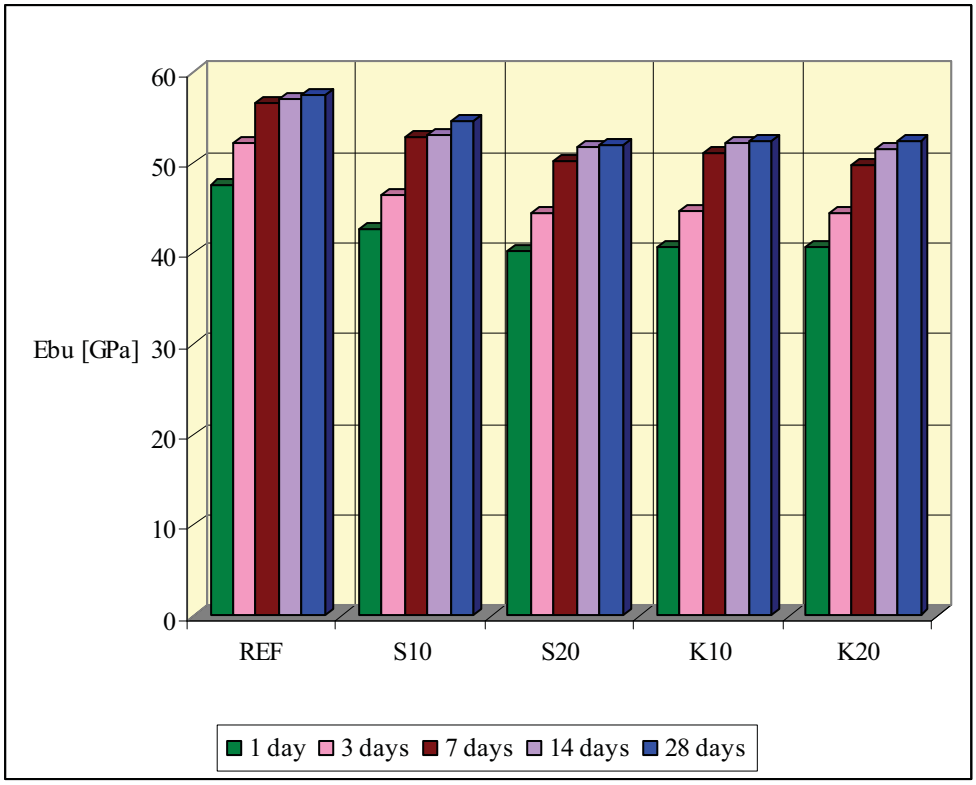

Figure 3.The dynamical elasticity modulus in dependence on the quantity of added brick body and on the hardening time of concrete.

4. CONCLUSION

Experimental works proved the usability of finely ground brick body as active admixture into concrete. The test results showed that the utilization of this active admixture is also adequate for the improvement of some special concrete properties.

a) Compression strength:

The concrete with the substitution of 10 % cement by finely ground brick body achieved after 28 days 92 - 93% of the reference concrete compression strength values.

The concrete with the substitution of 20 % of cement by finely ground brick body achieved after 28 days 71 – 73% of the reference concrete compression strength values.

b) Bending strength:

The bending strength decreases with the increasing content of the brick body. The highest strength had the reference concrete.

c) Depth of the pressure water ingress:

The depth values of pressure water ingress into the reference concrete were comparable with the water ingress into concrete with the addition of brick body and they are very favourable.

d) Dynamical modulus of elasticity:

The dynamical modulus of elasticity decreases with the increasing content of the brick body. The reference concrete had the highest value.

The results of experimental works show that better values of compression strength are achieved in the case of 10 % cement substitution by brick body – the concrete class corresponds with the concrete class of the reference concrete. Concrete with 20 % cement substitution by brick body achieves values which are by a class lower.

We can conclude that the utilization of finely ground brick body in concrete is useful from the ecological and also from the economical point of view.

ACKNOWLEDGEMENTS

The work was supported by the MSM 0021630511 Plan: Progressive Building Materials with Utilization of Secondary Raw Materials and Impact their on Structures Durability.

References

1. Drochytka, R.et al. Progressive Building Materials with Utilization of Secondary Raw Materials and their Impact on Structures Durability. Brno University of Technology, *Final report of the project VVZ CEZ MSM: 0021630511*, Brno 2006. Brožovský, J.: Subtask 3 (in Czech).

2. Brožovský, J. and Martinec, P. Durabbility of Concrete with Fly Ash. *In Proceedings of the 2d International Conference* on Concrete and Reinforced Concrete: Concrete and Reinforced Concrete – Development Trends. NIIZHB, Moscow, Russia, Vol. 4, 2005. (in Russian).
3. Brožovský, J., Zach, J., Brožovský, J., Jr.: Durability Of Concrete Made From Recycled Aggregates. *In Proceedings Of The International Rilem Jci Seminar Concrete Durability And Service Life Planning: Curing, Crack Control, Performance In Harsh Environments*, Ein-Bokek, Dead Sea, Israel, 2006
4. Wild, S., Gaillius, A., Hansen, H., Pederson , L. , Szabowski, J. : Pozzolanic proprietes of a variety of european clay bricks. *Building research and information* vol. 25, number 3, 1997
5. EN 12350-5 Testing fresh concrete - Part 5: Flow table test
6. EN 12350-6 Testing fresh concrete - Part 6: Density
7. EN 12350-3 Testing hardened concrete - Part 3: Compressive strength of test specimens
8. EN 12350-5 Testing hardened concrete - Part 5: Flexural strength of test specimens
9. EN 12350-7 Testing hardened concrete - Part 7: Density of Hardened Concrete
10. EN 12350-8 Testing hardened concrete - Part 8: Depth of penetration of water under pressure
11. CSN 73 1371 Method of Ultrasonic Pulse Testing of Concrete
12. EN 1008 Mixing Water for Concrete. Specification for Sampling, Testing and Assessing the Suitability of Water, Including Water Recovered from Processes in the Concrete Industry, as Mixing Water for Concrete

"Computational Civil Engineering 2007", International Symposium
Iaşi, România, May 25, 2007

Minimum weight buildings design using inequalities method

Constantin Amariei[1], Iulian Gabriel Mihai[2]
[1]*Structural MechanicsDepartment, TU"Gh.Asachi"Iaşi, 700050, România*
[2] *S.C.EdilConst S.A Câmpina, Prahova, 105600, România,*

Summary

Based on inequalities method and on possibilities of solving by automatic computation mathematical computation model of minimum weight steel structures is presented.

KEY WORDS: optimum design, minimum weight, inequalities method, linear algorithm.

1. GENERAL PROBLEMS

Optimization computation due to weight criterion can be done in many ways, according to structure equilibrium equations which are designed function of weight reduction condition formulation. Most important ways are presented below:

1. Establishment, function of a certain cross-section previously chosen, of all possible solutions, determination for each of it of the allowable load and choosing from all "sure" (for which the capable load is bigger than real load) of the one with the smallest one. The procedure is very elaborated and represents an empirical way for obtaining of some economic solutions.

2. The computation is based on choosing the most efficient solution from a variety of solutions, using one of the post-elastic computation methods. Such a possibility is given by the bending moments distribution in plastic domain, in its usual form or in a generalized operation form with mechanical work measures. [1] Using of this method supposes a certain experience in choosing the adjusting way of nodes, bars and kinematic chains equilibration, respectively in choosing of some combinations and constructive constraints which have to be taken in view.

3. Static methods, based on plastic yielding conditions (safety) corresponding to critical cross-sections of the structure, as presented below:

$$-S_{p(i)} \le S_i \le S_{p(i)} \tag{1}$$

where: $S_{p(i)}$ is the capable effort (plastic) of the critical cross-section "i";

S_i is the effective effort in the critical cross-section "i".

In the case of bar structures subjected mostly in bending, relation (1) becomes:

$$-M_{p(i)} \le M_i \le M_{p(i)} \qquad (2)$$

Choosing a statically determined system and writing the bending moments M_i as:

$$-M_i = M_{0i} + \lambda \cdot M'_{0i} + \sum_{h=1}^{n} x_h \cdot m_{0i}^h \qquad (3)$$

where: M_{0i} - bending moments on the base system, produced by permanent loads;

λ - loading coefficient;

M'_{0i} - bending moments in the base system by $\lambda = 1$;

x_h - statically undetermined values;

m_{0i}^h - bending moments produced in the base system by each $x_h = 1$.

The limit state computation is reduced to a linear algorithm problem consisting in increasing at maximum the loading factor λ in obtained relations by replacing the equations (3) and (2). By utilizing bending moment diagrams in equilibrium with external loads, disposed on base systems, judiciously choused, and which can differ from a load case to another, the plastic yielding conditions become $[7]$:

$$-M_p \le M_p^0 + \sum x_i \cdot m_i \le M_p \qquad (4)$$

where (for a critical cross-section "i"):

M_p - plastic moment of the cross-section;

M_p^0 - bending moment produced by several loads on a certain base system;

x_i - proportionality coefficients (statically undetermined values);

m_i - bending moments from auto equilibrium diagrams.

Using unknown factors decomposing or axes translations, are obtained resolvable formulations by simple procedure, due to which is determined the minimum of weight function.

4. The method based on using the elementary mechanisms combination and on the minimum weight solution theory elaborated by J.Foulkes and B.G.Neal.

5. The method proposed by J.Heyman and W.Prager, based on the general conditions of the limit state computation and on the minimum weight design theories and following the static way, in a two cycles of solving, each cycle consisting of two stages.

Generally, additionally to general hypothesis of the post elastic computation domain, at minimum weight structures design are also taken into consideration some supplementary hypothesis:

a) There exist an infinite variety of cross-sections (rolled steel shapes or composed cross-sections);

b) It is known the variation law on the weight per unit length of elements (q), due to plastic strength modulus (W_p). If there are graphically represented the pairs of values of (q, W_p) for the usual :I" rolled steel shape, is obtained the curve presented in figure 1 (approximated as being a continuous curve), which can be expressed by an exponential relation as :

$$q = k \cdot W_p^{\alpha} \tag{5}$$

or:

$$q = k\left(\frac{M_p}{\sigma_c}\right)^{\alpha} = k' \cdot M_p^{\alpha} \tag{6}$$

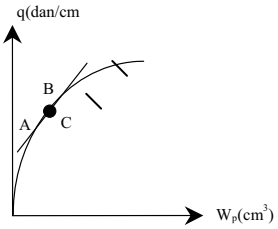

Fig. 1

The coefficients k and α vary function of the cross-section type.

Since for a certain structure the used cross-sections don't vary generally between very high limits, the curve (q, W_p) can be approximated with a polygonal diagram. For example, if the values of plastic module corresponding to points A and B from the figure 1 have a 1:2 ratio, the error coming from the approximation of the curve on the specified portion with a straight line, is only of 1%. Due to this assumption, the weight per unit length of the element can be written as a linear function:

$$q = a + b \cdot M_p \tag{7}$$

The total weight of the structure is:

$$Q = \sum_{i=1}^{n} q_i \cdot l_i = \sum_{i=1}^{n} \left(a + b \cdot M_{p(i)}\right) \cdot l_i = a \cdot \sum_{i=1}^{n} l_i + b \cdot \sum_{i=1}^{n} M_{p(i)} \cdot l_i \tag{8}$$

where l_i represents the lengths of the bars, $M_{p(i)}$ are the plastic bending moments of the bars cross-sections, and the number „n" is the number of bars having different values of plastic bending moments.

Because $a \cdot \sum_{i=1}^{n} l_i$ and b are constant, results that the determination of the minimum weight is reduced to determination of the minimum solution of the equation:

$$X = \sum_{i=1}^{n} M_{p(i)} \cdot l_i \tag{9}$$

called weight function.

Regarding the loads considered for minimum weight structures computation, according to American norms, they will be considerate as follows:

- for the combination consisting of permanent and live loads, they will be multiplied with a unic coefficient 1,7;
- for the combination consisting of permanent loads, live loads and wind action or earthquake action, they will be multiplied with a unic coefficient 1,3.

2. COMPUTATION MODEL BASED ON INEQUALITIES METHOD

Adaptation of the inequalities method for optimization computation

Inequalities method, usually used as determination way of loading limit factor can be adapted for a structure weight optimization computation, representing some important advantages, as simple and direct way of writing the constraining relations (especially of plastic yielding conditions), and the fact that it can be taken into consideration in the optimization computation of axial force influence, fact that can influence a lot the conceiving and behavior of certain structures categories.

Adaptation of inequalities method for weight optimization computation requires two important elements:

a) Taken in consideration as unknowns – in the relations that express plastic yielding conditions – of the plastic moments and introducing in these relations of the loading factor with imposed values by real loads acting on the structure.

b) Joining to these relations the weight function (linear or nonlinear) which has to be optimized.

The relations which compose the mathematic model for optimum design in this way are the following:

1. Static equilibrium equations:

a) for loaded bars (figure 2.a):

$$M_s^{(k)} \cdot b_k + M_c^{(k)} \cdot l_k + M_d^{(k)} \cdot a_k = \lambda_k \cdot a_k \cdot b_k \qquad (10)$$

where: k=1,2,…b (*b* being the number of loaded bars over the length).

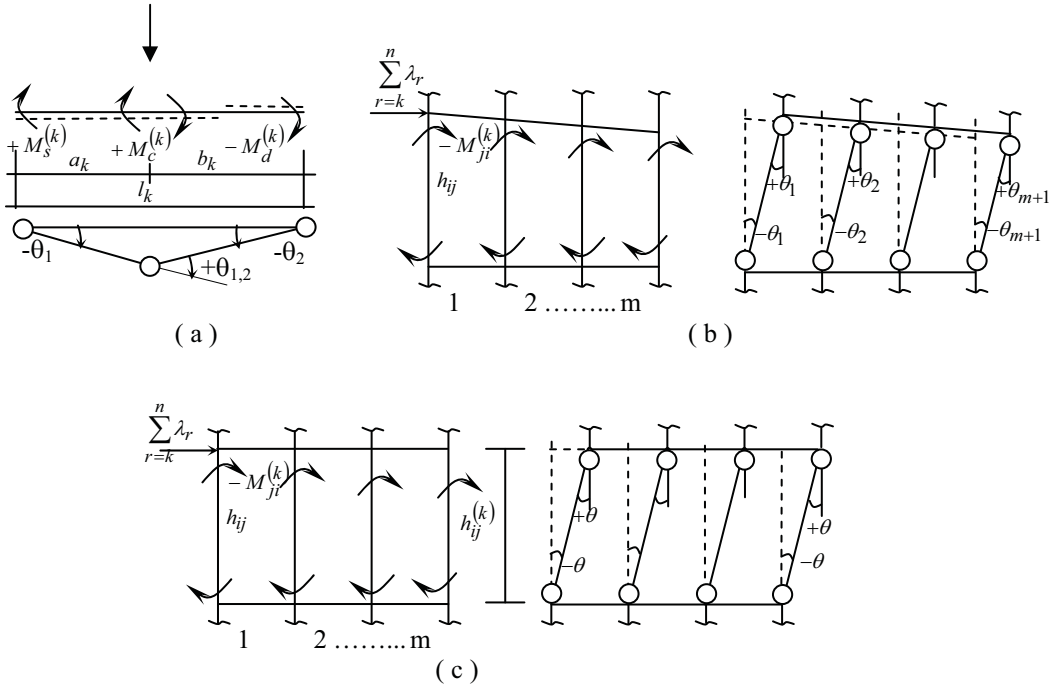

Fig. 2

b) for kinematic chains:

-unequal columns over the level (figure 2.b):

$$\sum_{i=1}^{s} \left(\frac{M_j^{(i)} + M_s^{(i)}}{h_i} \right) = H_k \qquad (11)$$

where: i=1,2…s (s being the number of the columns from a level);
k=1,2…m (m being the number of levels of the structure);
hi=column height;
Hk=sliding load for a level.

- unequal columns over the level (figure 2.c):

$$\sum_{i=1}^{s}\left(M_j^{(i)} + M_s^{(i)}\right) = h_k \cdot H_k \tag{12}$$

h_k level height.

c) for nodes:

$$\sum\left[\pm M_{ij}^{(k)}\right] = 0 \tag{13}$$

k=1,2…n (n being the number of nodes).

2. Relations which express plastic yielding conditions:

$$-M_{p(i)} \le M_i \le M_{p(i)} \tag{14}$$

where: $M_{p(i)}$ is the plastic moment of the critical cross-section"i" (the unknowns of the problem);

M_i is the effective bending moment in the critical cross-section "i", i=1,2…c (c being the number of critical cross-sections).

Totally are written a number of (e) statically equilibrium relations (e=b+m+n) and a number of (2c) inequalities – plastic yielding conditions.

3. Weight function, which has the usual form:

$$X = \sum_{i=1}^{p} l_i \cdot M_{p(i)}^{\alpha} \tag{15}$$

i=1,2…n (n being the established number of different plastic bending moments of the structure).

In a matrix form, the relations can be written as:

- statically equilibrium relations:

$$[B]\cdot\{\mathrm{M}\} = \{\overline{\lambda}\} \tag{16}$$

- plastic yielding conditions:

$$-\{M_p\} \le \{\mathrm{M}\} \le \{M_p\} \tag{17}$$

- weight function:

$$X = \{C\}^T \cdot \{M_p\} \tag{18}$$

where:

$[B]$ is the matrix of coefficients from the statically equilibrium relations;

$\{M\}$ vector of bending moments in the critical cross-sections;

$\{\bar{\lambda}\}$ is the vector of constants from statically equilibrium;

$\{M_p\}$ is the vector of plastic moments in critical cross-sections;

$\{C\}$ is the vector of plastic moments coefficients from the weight equation.

Removing from the plastic yielding conditions a number of (e) bending moments by their replacing with the values obtained in the (e) statically equilibrium equations, function of the other (c-e) bending moments, will result (2c) inequalities with [p+(c-e)] variables, [p necessary plastic bending moments and (c-e) bending moments in the critical cross-sections, as:

$$[A]\cdot\{M\}\geq\{\lambda\} \tag{19}$$

Some inequalities will be eliminated, obtaining a reduced number of constraining conditions which, together with the weight function, compose the relations of programming problem for minimum weight determination.

From the constraints number reducing problem, the most important are the following:

a) Imposing – constructively taking – of some ratios between necessary plastic moments, meaning:

$$M_{p(i)}>_{<}M_{p(k)} \tag{20}$$

which will have as effect the decreasing of the unknowns number of the optimization problem and also will eliminate some constraining relations referring to plastic joints appearance possibility on each bar in nodes.

b) "Selection" of inequalities meaning eliminating the least restrictive relations (which are satisfied including the remained inequalities).

c) Partially or totally knowing the shape of failure bending moments distribution (based on static and loading schemes), which makes possible to write – for critical cross-sections where is certainly known the sign of bending moment – only some simple inequalities, instead of double ones which usually appear in plastic yielding conditions:

$$-M_{p(i)}\leq M_i \tag{21}$$

or:

$$M_i\leq M_{p(i)} \tag{22}$$

In case of a linear weight function, **simplex method** can be used for solving, when is necessary the transformation of constraints inequations in equalities relations, by introducing of some compensation variables $\overline{M}$, so the matrix relation $[19]$ becomes (eventually after elimination of some constraints conditions):

$$[A]\cdot\{M\}-[E]\cdot\{\overline{M}\}=\{\lambda\} \tag{23}$$

where: $\{\overline{M}\}$ is the vector of compensation variables;

$[E]$ is the unit matrix.

Or, can be used the extended form of the problem, by introducing of some auxiliary variables $M^{'}$:

$$[A]\cdot\{M\}-[E]\cdot\{\overline{M}\}+[E]\cdot\{M^{'}\}=\{\lambda\} \tag{24}$$

or:

$$[A]\cdot\{M\}+[E]\cdot\{M^{*}\}=\{\lambda\} \tag{25}$$

where:

$$\{M^{*}\}=\{M^{'}\}-\{\overline{M}\} \tag{26}$$

in this case, is necessary to respect the negativity conditions for all three variables categories:

$$M,\overline{M},M^{'}\geq 0 \tag{27}$$

and the extended weight function (the lower bound of the weight function X) is:

$$X^{*}=\{C\}^{T}\cdot\{M_{p}\}+\{0\}^{T}\cdot\{M_{i}\}+\{\mu\}^{T}\cdot\{M^{*}\} \tag{28}$$

where: $\{M_{p}\}$ is the vector of necessary plastic bending moments, which makes the minimum weight structure;

$\{M_{i}\}$ is the vector of remain bending moments;

$\{M^{*}\}$ is the vector of auxiliary compensation variables.

The simplex solution contains also the values of “p” necessary plastic bending moments, and the values of remain bending moments in (c-e) critical cross-sections; the other (e) values of bending moments are determined with statically equilibrium equations, so it is possible a complete statically analyze for checking the plastic yielding conditions fulfill, and also the failure mechanism establishment.

In case of some big dimensions, the problem will be solved with a linear or nonlinear computer program.

3. COMPUTATION EXAMPLE

Determination of minimum weight solution for the frame in the figure 3.a.

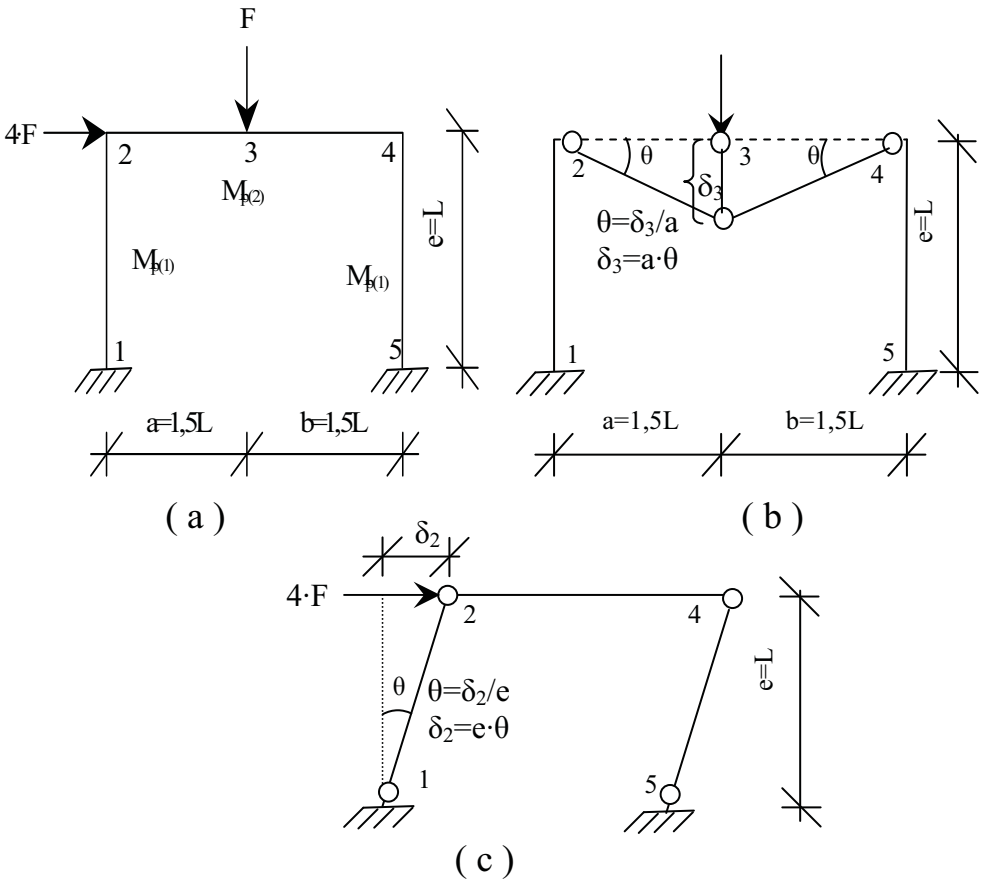

Fig. 3

It is considered: F=1; L=1.

It will be noted: $M_{p(1)}=Y_1$ şi $M_{p(2)}=Y_2$ which are the necessary plastic bending moments for the columns and beams.

Will be noted the bending moments in the five critical cross-sections **(1,2,3,4,5)** of the frame, as**:** $M_3=Y_3$; $M_4=Y_4$; $M_5=Y_5$; $M_1=Y_6$; $M_2=Y_7$

The relations which compose the mathematical model of the minimum weight frame design problem by **inequalities method** are the following:

1) Statically equilibrium relations:

a) bar equilibrium (figure 3.b):

$M_2\cdot\theta+ M_3\cdot\theta+M_3\cdot\theta+M_4\cdot\theta=F\cdot\delta_1$

or: $M_2+M_3+M_3+M_4=F\cdot a$

having the established notations:

$Y_7+Y_3+Y_3+Y_4=F\cdot 1{,}5\cdot L$

or $Y_7+2\cdot Y_3+Y_4=1{,}5$

b) displacement equilibrium (figure 3.c):

$M_1\cdot\theta+ M_2\cdot\theta+M_4\cdot\theta+M_5\cdot\theta=4\cdot F\cdot\delta_2$

or:$M_1+M_2+M_4+M_5=4\cdot F\cdot e$

having the established notations:

$Y_6+Y_7+Y_4+Y_5=4\cdot F\cdot L$

$Y_6+Y_7+Y_4+Y_5=4$

2) Plastic yielding conditions:

$-Y_1\le Y_6\le Y_1$;$-Y_1\le Y_7\le Y_1$; $-Y_2\le Y_7\le Y_2$;$-Y_2\le Y_3\le Y_2$;$-Y_2\le Y_4\le Y_2$;$-Y_1\le Y_4\le Y_1$; $-Y_1\le Y_5\le Y_1$

These relations can also be written:

$Y_1+Y_6\ge 0$; $Y_1+Y_7\ge 0$; $Y_2+Y_7\ge 0$; $Y_2+Y_3\ge 0$; $Y_2+Y_4\ge 0$; $Y_1+Y_4\ge 0$; $Y_1+Y_5\ge$

respectively:

$Y_1-Y_6\ge 0$; $Y_1-Y_7\ge 0$; $Y_2-Y_7\ge 0$; $Y_2-Y_3\ge 0$; $Y_2-Y_4\ge 0$; $Y_1-Y_4\ge 0$; $Y_1-Y_5\ge 0$

3) Weight function:

$$X=\sum_{1}^{n} l_i\cdot M_{p(i)}$$

so: $X=2\cdot M_{p(1)}+3\cdot M_{p(2)}+0\cdot M_3+0\cdot M_4+0\cdot M_5+0\cdot M_1+0\cdot M_2$

or: $X=2\cdot Y_1+3\cdot Y_2+0\cdot Y_3+0\cdot Y_4+0\cdot Y_5+0\cdot Y_6+0\cdot Y_7$

Using a usual computation program for solving linear problems, will be obtained the following results:

-plastic bending moments values:

$Y_1=M_{p(1)}=1.625$; $Y_2=M_{p(2)}=0.375$

-valorile momentelor din secțiunile critice:

$Y_3=M_3=0.375$; $Y_4=M_4=0.375$; $Y_5=M_5=1.625$; $Y_6=M_1=1.625$; $Y_7=M_2=0.375$

-value of the weight function:

X=4.375

Knowing the values of plastic bending moments on the columns and beams will be established the cross-section of bars:

a) the column:

$$M_{p(1)} = \sigma_c \cdot W_{column} \quad so: W_{column} = \frac{M_{p(1)}}{\sigma_c}$$

or: $W_{stalp} = \dfrac{b_{column} \cdot h_{column}^2}{4}$

Will be imposed: $h_{column} = 1{,}5 \cdot b_{column}$

and results : $\dfrac{b_{column} \cdot (1{,}5 \cdot b_{column})^2}{4} = \dfrac{M_{p(1)}}{\sigma_c}$

where $b_{column} = \sqrt[3]{\dfrac{4 \cdot M_{p(1)}}{2{,}25 \cdot \sigma_c}}$

$$h_{stalp} = 1{,}5 \cdot \sqrt[3]{\frac{4 \cdot M_{p(1)}}{2{,}25 \cdot \sigma_c}}$$

b) the beam:

$$M_{p(2)} = \sigma_c \cdot W_{beam} \quad deci: W_{beam} = \frac{M_{p(2)}}{\sigma_c}$$

or: $W_{beam} = \dfrac{b_{beam} \cdot h_{beam}^2}{4}$

It will be imposed: $h_{beam} = 1{,}5 \cdot b_{beam}$

and results: $\dfrac{b_{beam} \cdot (1{,}5 \cdot b_{beam})^2}{4} = \dfrac{M_{p(2)}}{\sigma_c}$

where: $b_{beam} = \sqrt[3]{\dfrac{4 \cdot M_{p(2)}}{2{,}25 \cdot \sigma_c}}$

$$h_{beam} = 1{,}5 \cdot \sqrt[3]{\frac{4 \cdot M_{p(2)}}{2{,}25 \cdot \sigma_c}}$$

References

1. Amariei C. – Calculul structurilor în domeniul plastic, I.P.Iaşi, 1974 (in Romanian)
2. Bălan Şt, Petcu V. – Calculul structurilor în domeniul plastic – Optimizări, Editura Academiei R.S.R., Bucureşti, 1979 (in Romanian)
3. Dancea I. – Metode de optimizare, Editura Dacia, Cluj Napoca, 1976 (in Romanian)
4. Gheorghiu Al. – Concepţii moderne în calculul structurilor, Editura Tehnică, Bucureşti, 1975 (in Romanian)
5. Mihăilă N. – Introducere în programarea liniară, Editura Didactică şi Pedagogică, Bucureşti, 1980 (in Romanian)
6. Nădejde I. – Probleme de cercetare operaţională. Programare matematică, Editura Academiei R.S.R., Bucureşti, 1971 (in Romanian)
7. Răutu S., Chiroiu V. – În legătură cu calculul construcţiilor cu greutate minimă (in Romanian)
8. Vuc I. – Modele matematice în proiectarea construcţiilor, Editura Facla, Timişoara, 1981 (in Romanian)

"Computational Civil Engineering 2007", International Symposium
Iaşi, România, May 25, 2007

Scientific Perspectives for Future Research Work in Fundamental Properties of Short-Lived Radionuclides from Decay and from in-Beam Studies

Brindusa Ciobanu[1], Ion Silisteanu[2] and Irina Radinschi [3]
[1] *Department of Physics, "Gh. Asachi" Technical University, Iasi, 700050, Romania*
[2] *"Horia Hulubei" Natl. Inst. of Physics & Nuclear Engrg., 077125, Bucharest-Magurele, Romania*
[3]*Department of Physics, "Gh. Asachi" Technical University, Iasi, 700050, Romania*

Summary

The aim of this paper is to point out some scientific perspectives for future research work in fundamental properties of short-lived radionuclides from decay and from in-beam studies, arisen in the frame of our research project. The project approaches one of the most important themes of nuclear physics. In recent years the investigation of unstable short-lived nuclei has gained world-wide interest as well on the experimental as on the theoretical side. These nuclei are characterized by unique structure properties: the weak binding of the outermost nucleons and the effects of the coupling between bound states and the particle continuum. Particularly, the modification of the effective nuclear potential leads to the formation of the nuclei with very diffuse nucleon densities, to the occurrence of the nucleon skin and halo structures. Our first goal is to formulate a reaction theory for cluster decay in which the clustering and reaction amplitudes will be represented by means of resonance formulas. A brief outlook of the experimental results and theoretical ideas which define the field is presented toghether with quantitative estimations for the resonance decay widths and relative intensities. The resonance solution of systems of coupled equations is obtained by a direct numerical integration using step-by-step methods on computer. Thus, we obtain most complete information on the development of typical structures from stable to exotic losely-bound nuclei by: improving the structure models in order to describe essential features and to obtain spectroscopic information on a number of nuclei that can then tested against data extracted from decay and in-beam studies; extending the range of applicability of reaction models by using accurate reaction channels methods (e.g. via additional channels including deformation, exchange effects, antysimmetrisation, etc); including microscopic structure information in coupled channel reaction models and treating more carefully of "intermediate" systems that are more or less bound or have mixed composition.

KEYWORDS: short-lived radionuclides, cluster decay, numerical integration of coupled channel equations, computational methods.

1. INTRODUCTION

In recent years the investigation of unstable short-lived nuclei has gained world-wide interest as well on the experimental as on the theoretical side. These nuclei are characterized by unique structure properties: the weak binding of the outermost nucleons and the effects of the coupling between bound states and the particle continuum. Particularly, the modification of the effective nuclear potential leads to the formation of the nuclei with very diffuse nucleon densities, to the occurrence of the nucleon skin and halo structures. These phenomena will also affect collective vibrations and rotations of unstable nuclei, particularly the electric dipole and quadrupole excitations, and new modes of excitations and decay might arise in nuclei near the drip line.

Apart from general structure aspects in the physics of nuclei far from stability, there is also strong relations to the question of clustering in nuclei and to few-body physics. Furthermore, there will be a strong coupling to the continuum both in static and dynamic descriptions. Nuclear clustering and fine structure are two of the most important typical structures in nuclear physics which are strongly connected to the stability and deformation.

Superheavy elements (SHE) probe the extremes of nuclear structure with respect to the number of nucleons that can form a bound system. Their existence and decay properties are one of the most fundamental problems in nuclear physics [1-4]. There are data that confirm the existence of Z=111 and 112 and their connection to lighter decay chains [1]. The first data for Z=113,114, 115 and 116 also exist [3, 4], with suggested A=288-292, respectively, but the A values are not certain since the connection to lighter nuclei is not known. A new element with atomic number 118 was synthesized for the first time in the $^{249}Cf + ^{48}Ca$ reaction.

Atomic and mass numbers of the isotope of element 118 were determined from the measured excitation functions and decay characteristics of the daughter nuclei produced in cross-bombardments [5]. Theoretical models for SHE have evaluated from microscopic-macroscopic models [6] to fully microscopic deformed Hartree-Fock (HF) models [7]. In addition to their importance for many-body nuclear structure, theoretical models for the prediction of the decay properties of the SHE are important when designing experiments since the technique used will depend on half-life and decay mode.

In order to obtain the most complete information on these new nuclei, effects and phenomena a use of radioactive beams in a wide range of isospin and energy is necessary. High energy beams produced byin- flight fragmentation and post-accelerated beams proved to be complementary with the respect to their intensity, purity, and optical quality. When one analyses a proper reaction model, the measurements of core or halo momentum distributions after breakup, can provide important information on the structure of a such nucleus. The detection of gamma-

rays from outgoing fragments allows to access experimentally whether core excited components are present in a halo state.

The experimental signatures of clustering and "fine structure" (FS) far from stability are supported by data from selective excitation in nucleon and α-transfer reactions, α-decay, heavy cluster decay, and by rotationally spaced energy levels, enhanced transition strengths and intensities, and appreciable emission width for the resonant states above the decay threshold. Recent decay and in-beam studies of unstable nuclei are revealing an unexpected diversity and richness of shapes, and new decay modes and typical structures which are related to very low binding energy and the strong influence of the continuum.

To treat the decay rates for these nuclei we describe the nuclear clustering and penetration of the particle through the potential barrier taking into account the correspondence between different decay channels and different final states of the daughter nucleus.

The decay process being governed by nuclear clustering and quantum tunneling over the Coulomb barrier is strongly influenced by couplings of the relative motion of the fragments to several nuclear intrinsic motions. We address to effects of coupling between the intrinsic degrees of freedom and relative motion by solving numerically the coupled channel equations, including all the relevant reaction channels.

Our first goal is to formulate a reaction theory for cluster decay in which the clustering and reaction amplitudes will be represented by means of resonance formulas. A brief outlook of the experimental results and theoretical ideas which define the field is presented together with quantities estimations for the resonance decay widths and relative intensities. The resonance solution of systems of coupled equations is obtained by a direct numerical integration using step-by-step methods on computer.

Thus, we obtain most complete information on the development of typical structures from stable to exotic loosely-bound nuclei by: improving the structure models in order to describe essential features and obtain spectroscopic information on a number of nuclei that can tested against data extracted from decay and in-beam studies; extending the range of applicability of reaction models by using accurate reaction channels methods (e.g. via additional channels including deformation, exchange effects, anti-symmetrization, etc); including microscopic structure information in coupled channel reaction models and treating more carefully of "intermediate" systems that are more or less bound or have mixed composition.

The modern facilities (EUROBALL, GAMMASPHERE, RIA, etc.) or recent research projects (SPIRAL-2, etc.) of the important international centers in Oak

Ridge (USA), Darmstadt (Germany), Dubna (Russia), etc., are mainly devoted to the laboratory investigation of exotic nuclear structures [6].

The very large number of publications and conferences in this field underlines its importance and define it as an excellence research area. The research team has a long-term experience in the research fields approached by the project, as:

- short lived nuclear production with secondary beams;
- spectroscopy of exotic nuclei by transfer and breakup reactions. One notes experimental methods like resonant particle spectroscopy (RPS) method [8], recoil decay tagging (RDT) method [9], cross-sections measurements in breakup reactions and theoretical methods (highly unstable states spectroscopy, semiclassical models for the evaluation of one-nucleon breakup reactions at intermediate energies, calculation and design for detection methods, RPS and RDT);
- theoretical modelling of spontaneous decay, transfer and break-up reactions (clustering and "fine structure" at limits of stability, coupled channel approximation for cluster decay including rotational degrees of freedom, quantum tunneling induced by rotational coupling, multichannel resonant decay).

In the following we will shortly present the current status and directions within the topics related to our project.

2. RESULTS AND PERSPECTIVES

2.1. Short lived nuclei production with secondary beams

One tries to estimate the most favourable projectile - target combination to maximize the fusion cross section at energies near the Coulomb barrier, taking into account the deformation degrees of freedom and mass assymetry.

These thematics investigate the orientation effect by considering the role of quadrupolar and hexadecapolar deformations for the projectile and the role of rotational degrees of freedom for the target. In this propose one developes coupled channel approximation for the Schrödinger equation, treating the cold fusion as a scattering problem with appropriate boundery conditions.

Both Numerov and Runge-Kutta numerical methods will be use for the computing of the radial wave functions. One establishes the succesfull application to the description of fusion of ^{48}Ca on actinide nuclei ^{238}U and ^{248}Cm, recently performed at the Flerov Laboratory Dubna. It was estimated that this projectile-target combination is one of the most promising one to reach the superheavy island of stability [1,2,10].

2.2. Spectroscopy of decay, transfer and breakup reactions

One attempts to measure one nucleon breakup cross sections for proton and neutron rich nuclei. One estimates breakup cross sections for weakly bound exotic nuclei. One performes the design and simulation of complex experimental setup for reactions with secondary beams.

Exotic nuclei (far from stability valley) play an important role in the structure studies, as well in the modern astrophysical studies (nucleosynthesis, structure an evolution of neutron stars, black holes, etc.)

One of the most sophisticated and succesful experimental methods has been proposed by Romania (C. Borcea et al.) in which a measurement of total reaction cross section and the inclusive breakup one nucleon cross section for ^{8}B and ^{11}Be have been proposed for the definite establishment of the existence of halo states [11]. In these experiments, a secondary beam of (e.g.) ^{11}Be has been produced by fragmentation of a primary beam of ^{18}O at 70 MeV/nucleon on a thick target of ^{9}Be. Fragmentation products have been separated with the doubly achromatic LISE separator in GANIL (France). An approximately 1000 ^{11}Be counts/sec has been obtained in impinged on a stack of 17 Silicon detectors which served as a degrader, target and analysing media for reaction products. In front of the telescope a position sensitive detector x-y (position sensitive parallel plate avalanche detector-PPAD) has been placed to define the beam spot on the detector. The telescope segmentation allowed identification of the reaction products as well as the identification of reaction mechanisms such as stripping or nuclear dissociation. The first mechanism has been identified by an increased rate of reaction events in adiacent segments of the telescope, following an reaction event in a given segment. Later on in a subsequent experiment at Michigan the nuclear dissociation mechanism has been identified by a supplementary energy loss deposition by the proton in the breakup reaction of ^{8}B on a silicon target. The method is based on the assumption that to a good approximation after breakup the heavy fragment will have 10/11 or 7/8 from the incident energy. This is based on the common understanding of halo states (i.e. low separation energy and low angular momentum characterising the state). This small change in the energy translates into a different range in the detector which can be measured. Backwards to the telescope an array or 32 neutron detectors has been placed in an attempt to better identify reaction mechanism such as nuclear dissociation.

A similar experiment has been performed recently in a Oberlin -Michigan - Bucharest collaboration. A cocktail of proton rich nucleai has been impinged on a silicon telescope. The experiment allowed identification of new candidates for proton halos, weakly bound nuclei, close to the proton drip line, which shows a very low separation energy and a wave function dominated by low angular momenta (p-waves). This work is in progress. These exeperments have a very nice future. New plannigs are projected at GANIL for studies of neutron rich nuclei in

the f-shell with the improvements that core states will be identified by an array of efficient gamma detetectors [12-16].

2.3. Spontaneous decay, transfer and breakup theoretical modelling

The experimental results and theoretical ideas which define the clustering and "fine structure" is presented together with quantitative estimations for the resonance emission widths. We present both formal considerations, derived from a microscopic (shell model) formulation of the reaction theory, and practical computational programs based on coupled channel methods, with many-body effects included in formation and reaction amplitudes, energy shifts and total decay widths.

The main conceptual issues in reaction theory are identified and their relative importance is assessed: these include, couplings between the relative motion of the fragments and several nuclear collective motions, the existence and convergence of the resonance scattering solution, account the effects of non-linear couplings to all orders, self-consistence of the scattering potential, and the rotational excitation of nuclei by the cluster transfer.

The cluster decay properties of heavy drip-line nuclei are considered and some spectroscopic information on the continuum states populated in the unbound intermediate systems in the decay channel is obtained. The limitations and advantages of current computational approaches are addressed, with particular regard to quantitative experimental comparisons for superheavy nuclei [1- 4], [17, 18].

2.4. Numerical computer codes for nuclear reactions with exotic nuclei

The aim is to obtain with good accuracy the eigenstates (bound and resonant) of deformed nuclei for realistic studies of phenomena like fission, alpha decay and proton emission.

The motion of a particle in a deformed potential is governed by the tri-dimensional Schrödinger equation. When the potential is axially symmetric, the wavefunction can be expanded in partial waves with angular and radial components. The radial wavefunctions are the solutions of a set of coupled differential equations of second order. In order to obtain the eigenstates (either bound, resonant or antiresonant) one has to solve (numerically) the eigenvalue problem for this system subject to some physically consistent boundary conditions. For this purpose several tasks should be accomplished: the calculation of the solution at the boundaries of the numerical domain (near the origin and at large distances), the propagation of the solution on the integration interval, the determination of the eigenvalues and the construction of the normalized wave functions. Many investigations have been devoted to this

subject. See for example [19-24], including our own experience [4,17,18,25]. In the present project one intendes to improve the existing procedures, increasing the accuracy and reducing the amount of computer time and memory requirements. Thus realistic cases with important deformations and large number of equations could be handled, allowing the study of nuclear processes in complex systems (like exotic and heavy nuclei).

2.5. Role of charge density in cold fusion reactions

Cold fusion barriers are studied with respect to the change of the charge density within the overlapping region. Charge evolution from separated target and projectile up to the compound nucleus is taken into account by meaning of a deduced transition formula which depends on geometric parameter variation defining the shape. Macroscopic shell correction and total deformation energy for fusion like configurations are calculated for different charge density paths.

The way geometric parameters influence on the total deformation energy is also studied and compared with already published work [26, 27]. Influence of changes on isotopic composition of the reaction is emphasized in final shell corrections, and an analogy is made with isospin equilibration observed and calculated in [28]. Total barriers are computed as a function of charge density taken as free parameter, a procedure also accounted in [29]. Minimization along this coordinate produces variations of about 4 MeV for light nuclei and up to 8 MeV for superheavy synthesis, for the deformation energy in the last part of the process.

4. CONCLUSIONS

The aim of this paper is to point out some scientific perspectives for future research work in fundamental properties of short-lived radionuclides from decay and from in-beam studies, arisen in the frame of our research project. Our first goal is to formulate a reaction theory for cluster decay in which the clustering and reaction amplitudes will be represented by means of resonance formulas. A brief outlook of the experimental results and theoretical ideas which define the field is presented toghether with quantitative estimations for the resonance decay widths and relative intensities. The resonance solution of systems of coupled equations is obtained by a direct numerical integration using step-by-step methods on computer.
The degree of novelty is given by the field of the proposal itself: exotic nuclear systems are intensively investigated by different experimental and theoretical groups in all important international centers during the last decade. Important experimental and computing facilities were assigned to this field in this period and many conferences and workshops were organized in order to analyse the obtained

results. The complexity is given by sophysticated experimental techniques and theoretical methods.
The participants are well recognized scientists in several related to this field areas. This project is a good opportunity to enlarge the international cooperation with our foreign partners and to prepair the participation within the framework of various international projects.

Acknowledgements

Research of authors was supported by MedC- CERES in the framework of the grant CEX05-D10-08/03.10.2005.

References

1. Yu. Ts. Oganessian, et al., *Phys. Rev. Lett,* 83, 1999, pp. 3154.
2. Yu. Ts. Oganessian, et al., *Phys. Rev.,* C70, 2004, pp. 242.
3. S. Hofmann and G. Münzenberg, *Rev. Mod. Phys.,* 72, 2000, pp.733.
4. I. Silişteanu, W. Scheid, A. Sandulescu, *Nucl. Phys. A*, 679, 2001, pp. 317.
5. Yu. Ts. Oganessian, et al., Synthesis of the isotopes of elements 118 and 116 in the ^{249}Cf and ^{245} Cm+ ^{48}Ca fusion reactions, C 74, 2006, 044602.
6. G. Münzenberg, Perspectives for nuclear structure research at GSI- from halo nuclei to superheavy elements, Proceedings of the 174. WE- Heraeus- Seminar*, Il Nuovo Cimento,* Vol. 110 A, N. 9- 10, 1997, pp. 1103.
7. S. G. Nilsson, I. Ragnarsson, *Shapes and Shells in Nuclear Structure,* Cambridge University Press, ISBN-13 978-0-521-01966-8, ISBN-10 0-521-01966-4, 2005, pp. 50, 72, 157.
8. D. Robson, *Nucl. Phys.*, A 204, 1973, pp. 204.
9. R. S. Simon et al., *Z. Phys.,* A 325, 1986, pp. 197.
10. Y. S. Tsyganov, Detection of ultra rare α decays of super heavy nuclei, *Nuclear Instruments and Methods in Physics Research,* A 573, 2007, pp. 161-164.
11. N. K. Skobelev, R. Anne, C. Borcea, D. Guillemaud - Mueller, S. Grevy, Z. Dlouhy, F. Carstoiu, M. Lewitowicz, S. M. Lukyanov, A. C. Mueller, F. Negoita, Yu. E. Penionzhkevich, M. G. Saint - Laurent, O. Sorlin, Reactions of breakup of ^{11}Be Nuclei interacting with ^{28}Si Nuclei, *Bull. Rus. Acad. Sci. Phys.*, 63, 1999, pp. 771.
12. A. De Vismes, P. Roussel-Chomaz, F. Carstoiu, Global analysis of proton nucleus cross sections, *Phys. Rev.,* C 62, 2000, 064612.
13. E. Sauvan, F. Carstoiu, N. A. Orr, J. C. Angelique, W. N. Catford, N. M. Clarke, M. Mac Cormick, N. Curtis, M. Freer, S. Grevy, C. Le Brun, M. Lewitowicz, E.Liegard, F. M. Marques, M. Mac Cormick, P. Roussel-Chomaz, M. G. Saint Laurent, One-neutron removal reactions on neutron-rich psd-shell nuclei, *Phys. Rev.*, C 69, 2004, 044603.
14. E. Sauvan et al., *Phys. Rev.*, C 69, 2004.
15. L. Trache et al., *Phys. Rev. Lett.*, 271102, 2001, pp. 87.
16. L. Trache et al, *Phys. Rev.*, C 69, 2004, 032802(R).
17. I. Silisteanu, A. O. Silisteanu, W. Scheid, B. I. Ciobanu, Alpha Half-Time Estimates for the Superheavy Elements, Proceedings of the Carpathian Summer School of Physics 2005, *Exotic Nuclei and Nuclear/ Particle Astrophysics,* World Scientific, 2006, pp. 423.
18. I. Silisteanu, A. Sandru, A. O. Silisteanu, B. Popovici, A. Neacsu, B. I. Ciobanu, Alpha Half-Time Estimates for the Superheavy Elements, Proceedings of the Predeal International Summer School in Nuclear Physics, *Collective Motion and Phase Transition in Nuclear Systems,* World Scientific,

2006, pp. 569.
19. S. Cwiok, J. Dudek, W. Nazarewicz, J. Skalski, T. Werner, Single particle energies, wave functions, quadrupole moments and g-factors in axially deformed Woods - Saxon potential with applications in the two - centre - type nuclear problems, *Comp.Phys.Commun.*, vol. 46, 1987, pp.379.
20. E. Maglione, L. S. Ferriera, R. J. Liotta, Nucleon decay from deformed nuclei, *Phys.Rev.Letters*, vol. 81, 1998, pp. 538.
21. K. Rykaczewski, J. C. Batchelder, C. R. Bingham, T. Davinson, T. N. Ginter, C. J. Gross, R. Grzymack, M. Karny, B. D. MacDonald, J. Mas, J. W. McConnel, A. Piechaczek, R.C. Slinger, K.S. Toth, W. W. Walters, P. J. Woods, E. F. Zganjar, B. Barmore, L.Gr. Ixaru, A.T. Kruppa, W. Nazarewicz, M. Rizea, T. Vertse, Proton Emitters: Probing the Structure of Unbound Nilsson Orbitals, *Phys.Rev.,*C, vol. 60, 1999, 011301.
22. T. Vertse, A. T. Kruppa, B. Barmore, W. Nazarewicz, L. Gr. Ixaru, M. Rizea, Proton emission from Gamow resonance, *AIP Conference Proceedings 518*, Proton-Emitting Nuclei, First International Symposium, Oak Ridge, Tennessee U.S.A., 2000, pp. 184.
23. H. Esbensen, C. Davids, Coupled-channel treatment of deformed proton emitters, *Phys.Rev.,*C, vol. 63, 2000, 014315.
24. M. Rizea, PERSYS - A program for the solution near the origin of coupled channel Schrödinger equation with singular potential, *Comput. Phys. Commun.*, vol.143, 2002, pp. 83.
25. I. Silişteanu, W. Scheid, A. O. Silisteanu, *Rom. Rep. Phys.,*57, 2005, pp. 4.
26. C. Y. Wong, *Phys. Rev. Lett***.**, 31, 1973, pp. 766.
27. L. C. Vaz, J. M. Alexander, *Phys. Rev.,* C 18, 1978, pp. 2152.
28. B-A. Li, S. J. Yennelo, *Phys. Rev.,* C52, 1995, R1746.
29. K. Satou, H. Ikezoe, S. Mitsuoka, K. Nishio, S. C. Jeong, *Phys. Rev.*, C 65, 2002,054602.

Experimental and numerical analysis of compressed concrete elements confined with FRP composites

Gabriel Oprisan, Nicolae Taranu and Vlad Munteanu
Civil Engineering Department, "Gh. Asachi" Technical University, Iasi, 700054, Romania

Summary

Confinement of concrete by suitable selection of transverse internal reinforcement or by externally bonded reinforcement results in significant increase in both the compressive strength and the ductility of concrete subjected to compressive loading. Traditional confinement solutions have been developed using steel hoops or steel jackets and only recently fibre reinforced polymer composites (FRP) have been perceived as reliable confinement solutions for concrete elements. Extensive research projects have been performed since 1990s and theoretical and experimental results confirm the validity of confinement with FRP composites jackets. An experimental program has been initiated at the Faculty of Civil Engineering, the Technical University of Iasi, to evaluate the confining effect with glass fibre/epoxy and carbon fibre/epoxy composites. The influence of the material type and the thickness of FRP confining jacket were the variables involved.

The results obtained have proven the effectiveness of confinement solutions based on FRP composites. Both compressive strength and ductility of the confined specimens have shown dramatic increase compared to unconfined concrete specimens. The experimental set-up, the testing procedure and the main results are presented, emphasizing the influence of the composite nature and the thickness of the confining jacket.

KEYWORDS: confining, FRP jackets, compressive strength, ductility

1. INTRODUCTION

To establish the mechanical characteristics of unconfined concrete, cylindrical specimen and standard cubes adequate to compression test were cast. Also in order to determine the concrete class and the compressive strength, 9 concrete cylinders, 100 mm in diameter and 250 mm high, and 9 cubes, 100 mm in side, have been tested in uniaxial compression under standard condition. To avoid a rapid failure of the unconfined concrete cylinder and determine the complete stress-strain curve including the post peak strength domain of the material it was necessary to use a special installation for the post elastic testing of brittle materials. The arrangement

of all transducers is illustrated in figure 1, for both unconfined and confined samples.

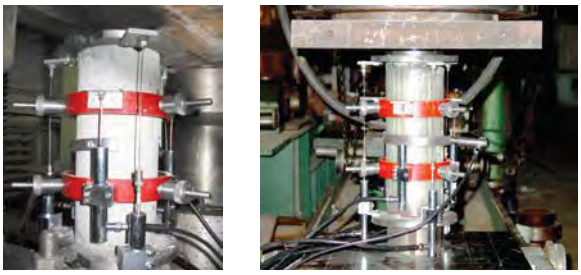

a. b.

Figure 1. Instrumentation of test samples with LVDTs a. unconfined concrete cylinder specimen; b. confined concrete cylinder specimen

The compressive strength determined on plain concrete samples, after 28 days is 31.64 N/mm2 on the concrete cylinders and 32.16 N/mm2 on the concrete cubes, and a complete stress-strain curve for unconfined concrete is illustrated in Figure 2.

2. EXPERIMENTAL PROGRAM

To avoid a rapid failure of the unconfined concrete cylinder and determine the complete stress-strain curve including the post-yielding domain of the material it was necessary to use a genuine installation for the post elastic testing of brittle materials. Before the experimental testing of the specimen, the testing machine had been calibrated and the equipment had been prepared for data acquisition, fig. 2. Data processing was done with a developed soft based on "Test Point" program.

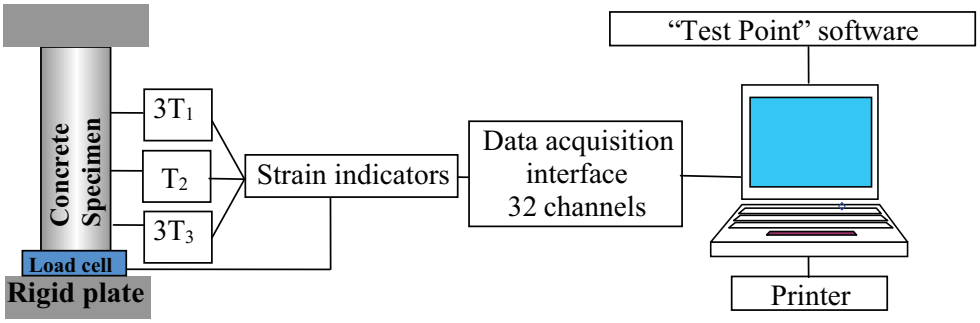

Figure 2. Acquisition and processing experimental data

Stress-strain curve obtained on unconfined concrete cylinders (fig.3) has two branches, a rising one associated with elastic, viscous and plastic strains, and a

falling one corresponding to pseudo plastic strain and characterized by an accelerated decrease in load and increase in strain over time. The maximum value on the curve corresponds to the ultimate compressive strength of concrete. The compressive strength determined on plain concrete samples, after 28 days was 31.64 N/mm^2 on the concrete cylinders and 32.16 N/mm^2 on the concrete cubes.

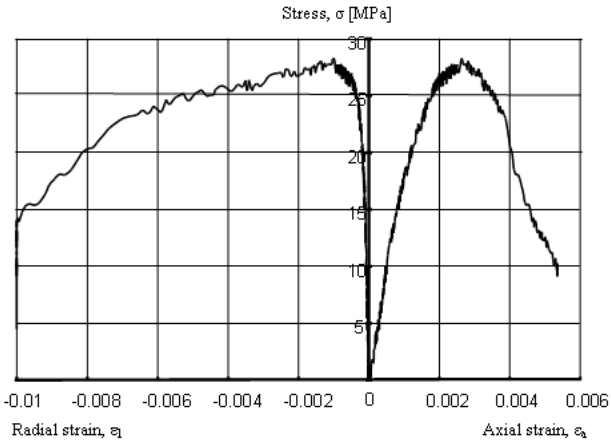

Figure 3. The complete stress-strain curves for unconfined concrete specimens

Nine specimens with 2, 3 and 4 unidirectional CFRP and GFRP layers (three of each type) with main fibers orientated in the hoop direction have been prepared using a wet hand lay-up technique. Prior to the application of the FRP layers the surface of the samples has been properly prepared to provide a hard, dry and clean surface. The main characteristics of GFRP for epoxy resins are presented in table 1 whilst the properties for glass and carbon fibers are given in table 2 and table 3.

Table 1 - Properties of epoxy resin

Appearance	Component A: light/yellow to amber Component B: pale yellow to clear liquid
Mixing ratio	A:B = 100:34,5
Density	1,16 g/cm^3
Tensile strength (ASTM D 638)	7 days at +21 ^{0}C: 55N/mm^2
Tensile modulus (ASTM D 638)	7 days at +21 ^{0}C: 2000N/mm^2
Fracture elongation (ASTM D 638)	7 days at +21 ^{0}C: 3,2%

Confined concrete specimens with GFRP and CFRP have been tested with the same installation used for the unconfined concrete samples. The confined specimens have been kept under laboratory conditions kept for 7 days to enable the complete cure of the polymeric resin after confinement.

Table 2 - Properties of glass fiber reinforcement

Fiber type	E-Glass fibers
Fiber orientation	0^0C (unidirectional)
Construction	93% warp, 7% weft
Areal weight	920 g/m^2
Fabric thickness	0,36 mm
Density of glass fibers	2,58 g/cm^3
Tensile strength of fibers	2250 N/mm^2
Tensile E-modulus	72400 N/mm^2
Ultimate fiber strain	3,7 %

Table 3 - Properties of carbon fiber reinforcement

Fiber type	Carbon fibers - high modulus
Fiber orientation	0^0C (unidirectional)
Construction	97% warp, 3% weft
Areal weight, [g/m^2]	610
Fabric thickness, [mm]	0,34
Tensile strength of fibers, [N/mm^2]	3900 (nominal) 3700 (minimal)
Tensile E-modulus, [N/mm^2]	231000
Ultimate fiber strain, [%]	1,5

Three stages have been observed on the stress-strain curve of confined concrete specimens:

- the first stage is linear and it corresponds to the stiffness of the unconfined concrete specimens, fig.4;
- in the second stage the concrete specimen exhibits larger lateral strains and the GFRP jacket creates a confining pressure on the concrete core. When the concrete specimen is cracked, a dramatic change in curve configuration occurs. At this stage much higher stresses and strains are attained than in the case of unconfined concrete;
- in the third stage, the concrete specimen is thoroughly cracked and the GFRP maintain the concrete confined specimen intact till the explosive failure of the jacket occurs. The stress-strain curve increases by a constant angle up to the rupture, fig.4.

A comparative set of curves for unconfined and CFRP confined samples is illustrated in fig.5; the confined samples have been wrapped with 2, 3 and 4 layers of CFRP composites.

The stress-strain curves of the CFRP composites have a bilinear shape with sharp softening in the transition area around the strength of the unconfined concrete. In the first stage the slope of the stress-strain curve is similar to that of the unconfined concrete. In the second stage the concrete is cracked and the confinement is activated. The stress of the confined concrete linearly increases with increasing the

CFRP strain. All experimental results confirm the similar work published in the field of structural rehabilitation with composites [1].

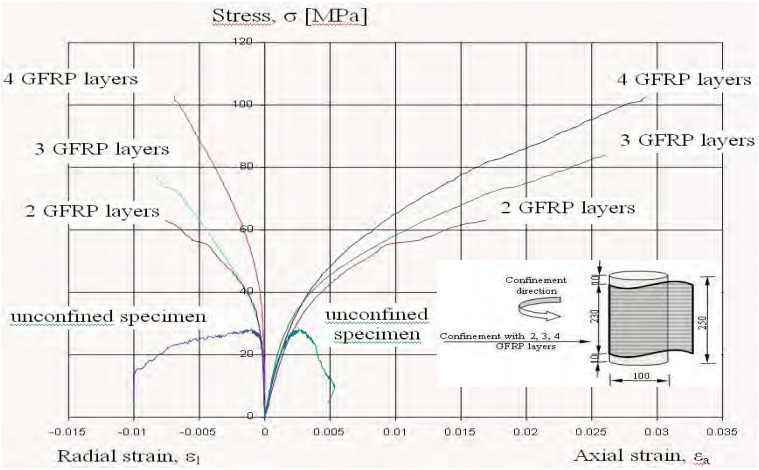

Figure 4 - Stress-strain curves of compressed unconfined and confined concrete specimens with GFRP

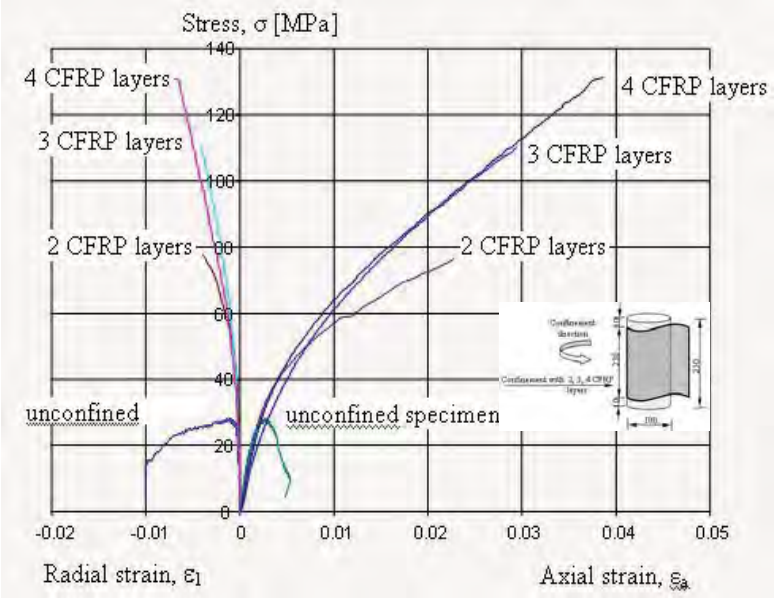

Figure 5 - Stress-strain curves of compressed unconfined and confined concrete specimens with CFRP

When the test is properly carried out the maximum stress is reached at the CFRP rupture. Some samples failed prematurely due to separation of the composite layers

at the lap joints. A step forward of the experimental program has been the cyclic loading of the confined samples as a first stage to seismic retrofit with polymeric composites. Some preliminary results are shown in fig.6 [2].

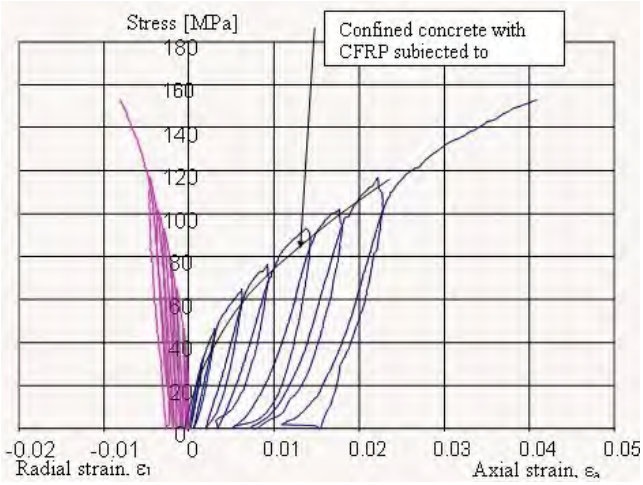

Figure 6 - Stress-strain curves of confined specimens subjected to cyclic load

3. NUMERICAL ANALYSIS

In order to verify the suitability of a FEM based software (LUSAS) for modelling concrete confinement problems, a numerical analysis was performed.

A statical non-linear analysis was conducted on a model that was built under the same dimensional conditions with the experimental program.

The concrete cylinder was modelled as a 3D solid element. In order to obtain a radial regular meshing it was first modelled a quarter of the final concrete element. The CFRP jacket was modelled as a sum of thick shell elements, "glued" onto the concrete surface using the SLIDELINE option, proper for contact problems, as in this case. The attributed thickness of the jacket was equivalent to a 3 layers disposal of CFRP sheets.

3D solid elements were used for the concrete cylinder meshing, as long as for the jacket, 3D surface elements were used. Although the software allows the use of higher order finite elements, only linear interpolation between nodes option was used in order to reduce the total number of elements and nodes for having a reasonable solving time.

The cylinder was considered as simply supported at the top end and totally restrained at the bottom end. The load was applied as a uniformly distributed force at the top end of the concrete element. In order to ensure a good convergence of the load increments, an initial value of 1 N/mm^2 was used and variable load increments (3 and 10) were used afterwards in the Solution Software Manager.

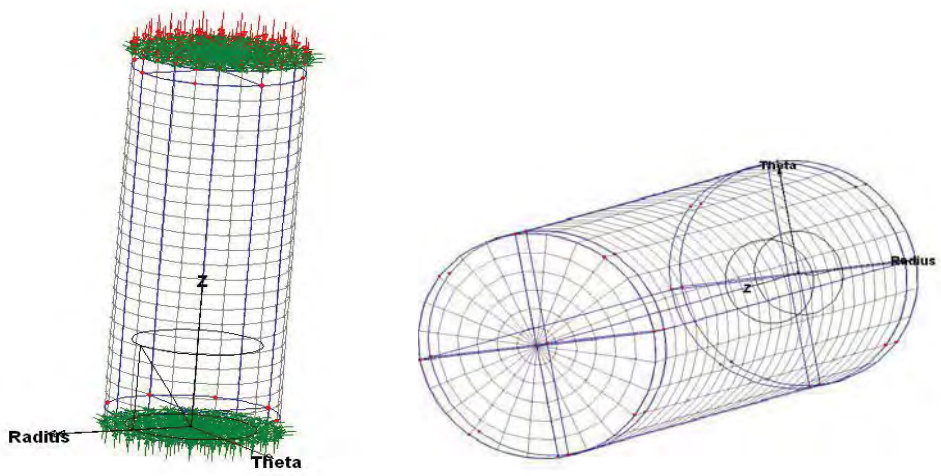

Figure 7 Support and load conditions of the concrete cylinder; radial meshing of the concrete volume

A Ducker-Prager material model based was used for defining the material properties for concrete as long as for the composite CFRP jacket an orthotropic material model available in the software's material options was used.

The mechanical properties for both concrete and composite jacket were defined in accordance with the materials that were used in the laboratory tests, and then attributed to the geometric elements.

From the large range of numerical and graphical results available after performing the run of the program, representative data charts and maps were selected and presented below. They are related to stresses, strains, displacements data needed in order to realise a good picture of the confined concrete cylinder behaviour under axial loading.

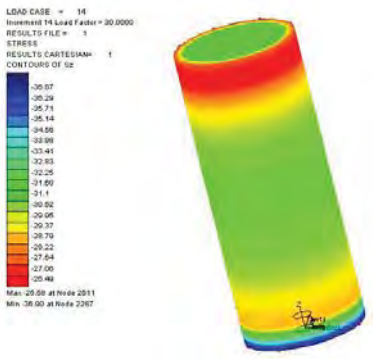

Figure 8. Normal stresses (unconfined concrete cylinder)

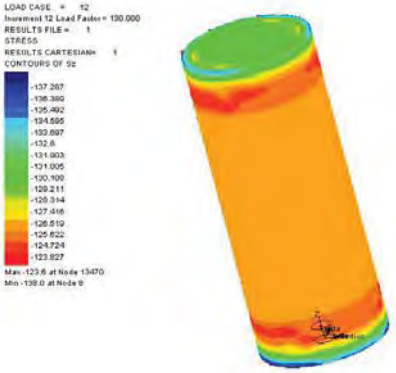

Figure 9. Normal stresses (CFRP confined concrete cylinder)

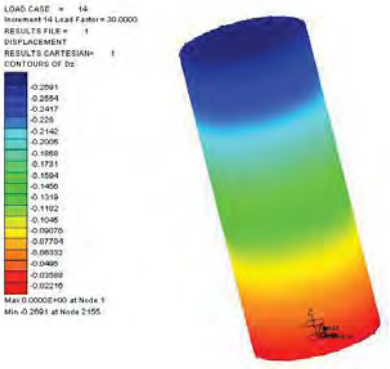

Figure 10. Longitudinal displacements (unconfined concrete cylinder)

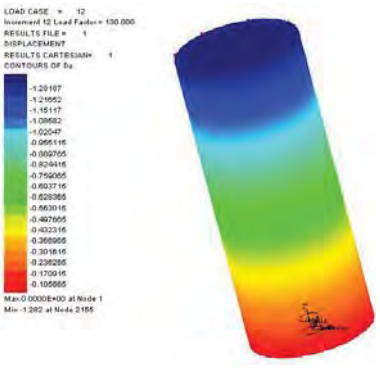

Figure 11. Longitudinal displacements (CFRP confined concrete cylinder)

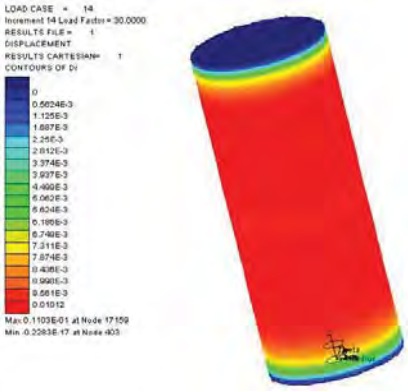

Figure 12. Transversal displacements (unconfined concrete cylinder)

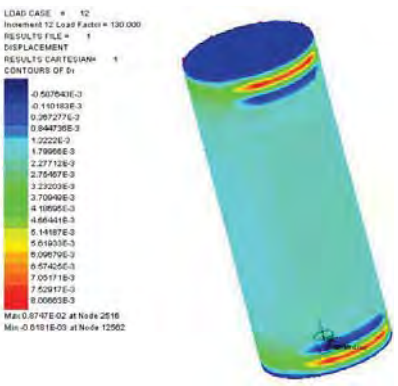

Figure 13. Transversal displacements (CFRP confined concrete cylinder)

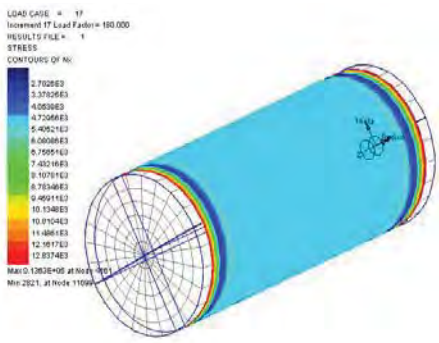

Figure 14. Longitudinal stress resultants in the CFRP jacket

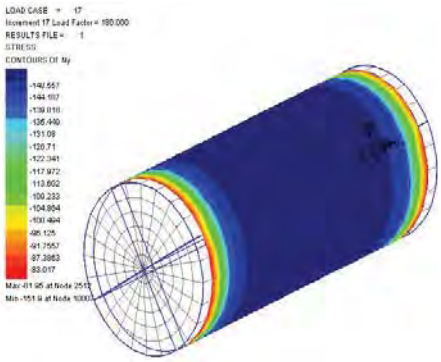

Figure 15. Transversal stress resultants in the CFRP jacket

Characteristic stress-strain curves for both confined and unconfined concrete were obtained; they are very similar to those obtained from the experimental analysis.

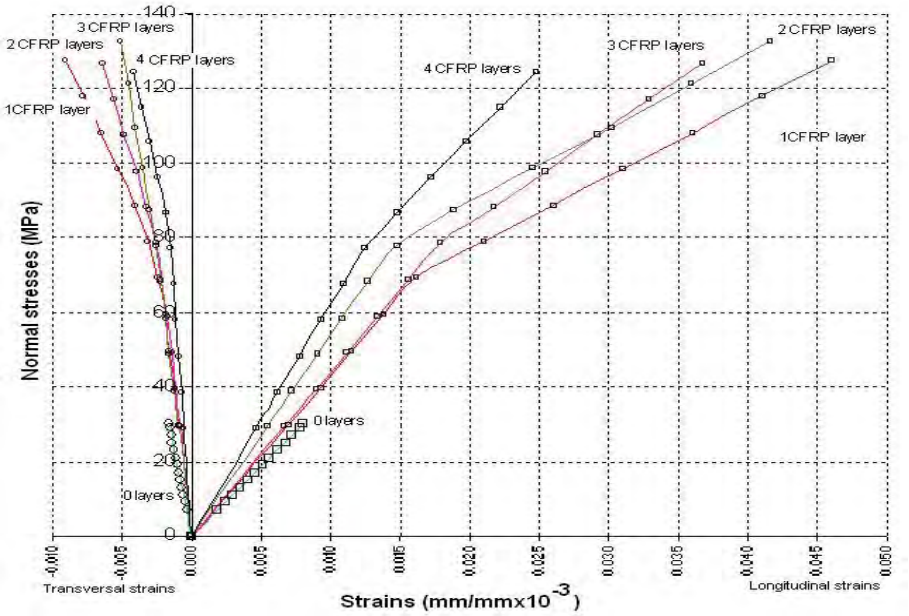

Figure 16. Stress-strain characteristic curves (CFRP confined / unconfined cylinder)

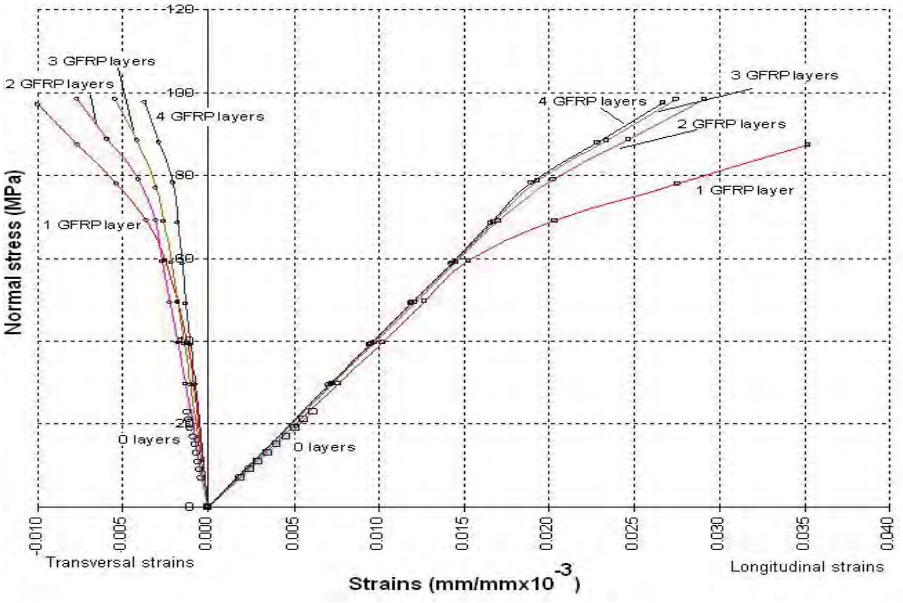

Figure 17. Stress-strain characteristic curves (GFRP confined / unconfined cylinder)

4. CONCLUSIONS

The use of FRP confinement significantly improves compressive strength and ductility of concrete. It should be noted that epoxy resins adhere well to the concrete surface, being also an excellent adhesive. Strengthening solutions with FRP used for reinforced concrete columns prove to be very good for several reasons. On the one hand, the strength and ductility values obtained are favourable and on the other hand, the weight of the consolidated system and the cost related to execution time and work are considerably reduced. Experience has shown that the failure modes of FRP are different and they depend on a series of factors which can influence the results obtained, such as: the characteristics of the concrete to be confined, casting moulds and vibration methods, fibre volume fraction, confinement techniques and accurate application by qualified workers.

References

1. Teng, J.G., Chen, J.F., Smith, S.T., Lam, L., *FRP strengthened RC structures*, John Wiley, Chicester, 2002.
2. Oprisan, G. *Soluții moderne de consolidare a structurilor penrtu construcții industriale*, Teză de doctorat - U.T. Iasi, (2002). (in Romanian)

"Computational Civil Engineering 2007", International Symposium
Iaşi, România, May 25, 2007

Rayleigh models coefficients

Florin Ţepeş Onea

Universitatea "Ovidius" Constanţa

Summary

The propose of this work is to study the effect of the superior vibration modes on the energy dissipation in the backlash between two plots of a idealized concrete dam.

The intern energy dissipation inside the structural material is generating material internal variations or hysterical damping. For viscous damping this energy is frequency balanced. The Rayleigh damping could be considered as a linear combination between structural masses matrix and stiffness matrix. The damping matrix is obtained from the Cauchy sequence:

$$C = M\sum_{k=0}^{p-1} a_k (M^{-1}K)^k \tag{1}$$

Where the coefficients a_k *k=1,2..p are obtained from p simultaneous equations:*

$$\xi_i = \frac{1}{2}\left(\frac{a_0}{\omega_i} + a_1\omega_i + a_2\omega_i^{\,2} + \ldots + a_{p-1}{}^{2p-3}\right) \tag{2}$$

For p=2:

$$C = \alpha M + \beta K \tag{3}$$

Where α and β are constants that can be obtained from two dumping ratios of two different frequencies.

This study is made for an idealized symmetric concrete dam

It was used two calculus models for the dam-foundation ensemble; a plain one and spatial model, with simultaneous calculation.

KEYWORDS: Rayleigh, spatial mesh, excitation, dumping

1. STRUCTURAL ANALYSYS

The plane finite element mesh is made by 80 quadrilateral elements for the foundation and 56 elements for the dam. The elasticity modulus for the dam was pick $E_b = 300000 daN/cm^2$ and for the foundation $E_f = 150000 daN/cm^2$, with the dam's high of 30m and the slope $\lambda_1 = \lambda = 0,5$.

The dam is made by two plots 15m width each other separate for a backlash of 1mm. The two plots adjacent nodes, corresponding with the space, have the same quota on x and z axis. This nodes can be connected with the help of springs in order to model the friction.

We can notice that in the case of plane mesh the fundamental vibration mode is flexural on upstream-downstream, the second mode is flexural too but on the high of the dam, the others modes are of torsion.

For the spatial mesh the first vibration mode implies a symmetrical displacement and flexural on upstream- downstream direction of the two plots, and for the second mode a antisymmetrical displacement. To start with the 6's vibration mode it appear also a rotation of the two plots, imples a relative moving of the plots surfaces in the spae between them. The propose of this work is to study the effect of the superior vibration modes on the energy dissipation in the backlash between the two plots.

Because both masses and stiffness matrix are orthogonal, damping matrix is orthogonal too. From orthogonal condition we obtain:

$$\phi_i^T (\alpha M + \beta K)\phi_j = 2\omega \tag{4}$$

Where ϕ_i, ϕ_j are eigenvectors, ω_i is circular frequency, ξ_i fraction of critical dumping. The equation become:

$$\alpha + \beta\omega_i^2 = 2\omega_i\xi_i$$

For determine the α and β coefficients influence, it was made a parametric study for plane and spatial dam- foundation discrete mesh. Critical damp fraction was taken as constant $\xi = 0,05$ for whole vibration modes because of the fact that massive structure as a concrete dam is, it is possible to obtain, after the structure excitation (with a value lower that the seismic value), only the fraction of critical dumping corresponding to the first vibration mode.

The calculus was made in both cases of finite elements, for the first 10 vibration modes.

If we coupled $\omega_1 + \omega_i$ and solving the equation systems obtained result α and β coefficients. So for plane discrete mash $\alpha = 1,44, \beta = 1,51E-3$ for ω_1 and ω_3 and $\alpha = 1.97, \beta = 5.66E-4$ for ω_1 and ω_{10} . We can observe that the effect of the mass matrix increase and the effect of stiffness matrix decrease in the same direction with the increase of the second frequency taken into account.

In spatial mesh case, the fundamental vibration mode is reduce $\omega_1 = 13,48 rad/s$ and for the plane mesh $\omega_1 = 21.3 rad/s$. This difference appears because in spatial mesh we take account of the torsion vibration modes also.

For the spatial mesh and for the frequency ω_1 and ω_3 α=0,893 and $\beta = 2,5E-3$ while if use the frequency ω_1 and ω_9 $\alpha = 1,063$ and $\beta = 1.56E-3$.

In the case of spatial discrete mash we can notice a mass matrix influence grow and a stiffness matrix influence diminution in the same time as the pulsation value grow. The variation of the α and β factors is much reduce when is use the spatial mash. For the spatial mash case we obtain a mean value $\alpha_{Ed} = 0,99$ and for the plane mesh $\alpha_{med} = 1.72$. All the results are presented in tables 3.1 and 3.2

Table 1 Plane mesh

Num.	Ω_i (rad/s)
1	21.3
2	38.59
3	44.43
4	79.44
5	87.59
6	96.43
7	109.0
8	118.8
9	121.3
10	155.1

$\omega_1 + \omega_i$	α	β
1+3	1,44	1,519E-3
1+5	1,71	9,17E-4
1+7	1,78	7,67E-4
1+10	1,97	5,66E-4

Table 2 Spatial mesh

Num.	ω_i
1	1
2	17,44
3	26,49
4	34,28
5	37,21
6	42,17
7	45,64
8	49,8
9	50,25

$\omega_1 + \omega_i$	α	β
1+3	0,893	2,5E-3
1+5	0,989	1,97E-3
1+7	1,041	1,689E-3
1+9	1,063	1,567E-3

The calculus was resumed for a critical dump fraction 8% in witch case we obtain for spatial mash and the pears ω_1 and ω_9 the following results α=1.69 and β=2.51E-3, results with no big difference compare with the case of critical dump fraction of 5%.

It is obvious that only for a spatial discrete mash the obtained results are close to reality. The influence of superior modes use in the case of spatial mash have no significant effect on the α and β coefficients as it presented in table 2.

It is noticed that in the same time with the increase of the frequency the mass matrix effect increase to and also the stiffness matrix effect decrease.

So, we can say that the stiffness matrix effect connected with frequency is major.

After coefficients calculus, it was analyzed the dam response at the same excitation with and without damping matrix effect. It was followed the effect of using vibration modes 1-3, 1-5,1-7,1-10 in mass end stiffness matrix coefficients on the stress and displacement response. In the table 3,4,5,6 are presented stress and displacement values for different coefficient pairs α and β, for plane and spatial mesh.

1.1 Plane mesh-displacements compare

(nods was select on a vertical for the coping of the weir to the foundation of the dam)

Table 3

Node	Without damping	$\omega_1+\omega_3$	$\omega_1+\omega_5$	$\omega_1+\omega_7$	$\omega_1+\omega_{10}$
161	0.728E-2	0.4200E-2	0.4184E-2	0.4178E-2	0.4104E-2
152	0.6079E-2	0.3508E-2	0.3495E-2	0.3490E-2	0.3429E-2
143	0.4149E-2	0.2407E-2	0.2399E-2	0.2396E-2	0.2876E-2
124	0.3706E-2	0.2154E-2	0.2147E-2	0.2144E-2	0.2107E-2
94	0.2404E-2	0.1406E-2	0.1401E-2	0.1399E-2	0.1375E-2

1.2 Plane mesh-stress compare (stress are presented in upstream-downstream points)

Table 4

	Without damping	$\omega_1+\omega_3$	$\omega_1+\omega_5$	$\omega_1+\omega_7$	$\omega_1+\omega_{10}$
σ(-)daN/cm^2	-18.2	-10.93	-10.92	-10.91	-10.75
σ(+)daN/cm^2	14.9	7.57	7.54	7.53	7.37

1.3 Spatial mesh-displacements compare (nods was select on a vertical for the coping o the weir to the foundation of the dam)

Table 5

	Without damping	$\omega_1+\omega_3$	$\omega_1+\omega_5$	$\omega_1+\omega_7$	$\omega_1+\omega_{10}$
161	0.433E-2	0.3319E-2	0.3326E-2	0.3325E-2	0.3326E-2
152	0.3646E-2	0.2778E-2	0.2783E-2	0.2786E-2	0.278E-2
143	0.3096E-2	0.2352E-2	0.2357E-2	0.236E-2	0.236E-2
124	0.2328E-2	0.1764E-2	0.1769E-2	0.1771E-2	0.1773E-2
94	0.1593E-2	0.1205E-2	0.1209E-2	0.1212E-2	0.1213E-2

1.4 Spatial mesh – stress compare (stress are presented in upstream – downstream points)

Table 6

	Without damping	$\omega_1+\omega_3$	$\omega_1+\omega_5$	$\omega_1+\omega_7$	$\omega_1+\omega_{10}$
σ(-)daN/cm^2	-12.03	-9.2	-9.2	-9.2	-9.2
σ(+)daN/cm^2	7.16	5.2	5.2	5.2	5.2

It is presented in the table 7 displacement comparative values for the spatial mesh for two critical dumping ratios of 5% and 8%.

Table 7

	5% Rayleigh	8% Rayleig	Diference %
323	-0.3878E-3 -0.8799E-2 -0.2340E-2	-0.3623E-3 -0.7545E-2 -0.2272E-2	-6.57 -14.25 -2.9
314	-0.2895E-3 -0.7398E-2 -0.2276E-2	-0.2678E-3 -0.6348E-2 -0.2210E-2	-7.49 -14.19 -2.89
299	-0.1890E-3 -0.5644E-2 -0.2144E-2	-0.1738E-3 -0.4849E-2 -0.2082E-2	-8.04 -14.08 -2.89
278	0.1383E-3 -0.4047E-2 -0.1965E-2	0.1354E-3 -0.3480E-2 -0.191E-2	-2.09 -14.01 -2.79
256	0.1032E-3 -0.2943E-2 -0.1779E-2	0.1024E-3 -0.2529E-2 -0.1731E-2	-0.77 -14.06 -2.69

The displacement comparative graphics are presented in figures 1 and 2 and the stress calculus points in figure 3.

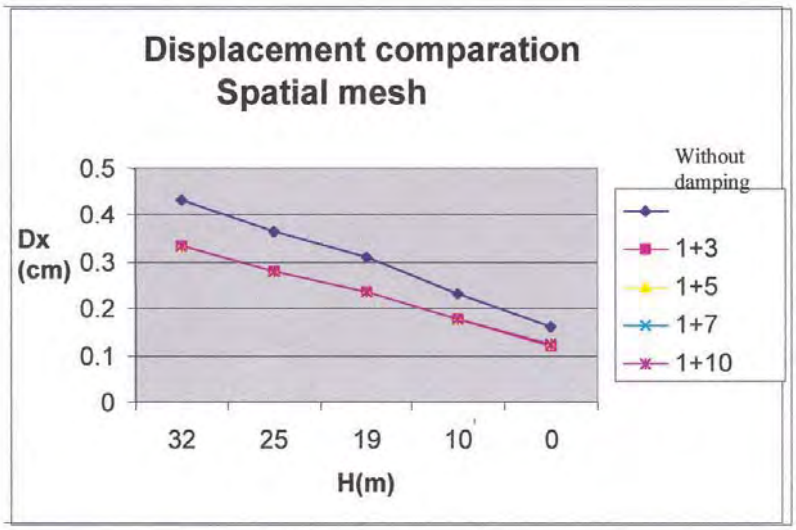

Figure 1 Displacement comparison for spatial mesh

It is also notice that as well as for plane and spatial discrete mash, if damping matrix is used, the stress and efforts values are almost similar for all the coefficient pairs α and β used. It was also noticed that for Rayleigh models use, only the first 3 vibration modes are required.

Major response differences of 14% are obtained only between 2 critical dams of 2% and 8%.

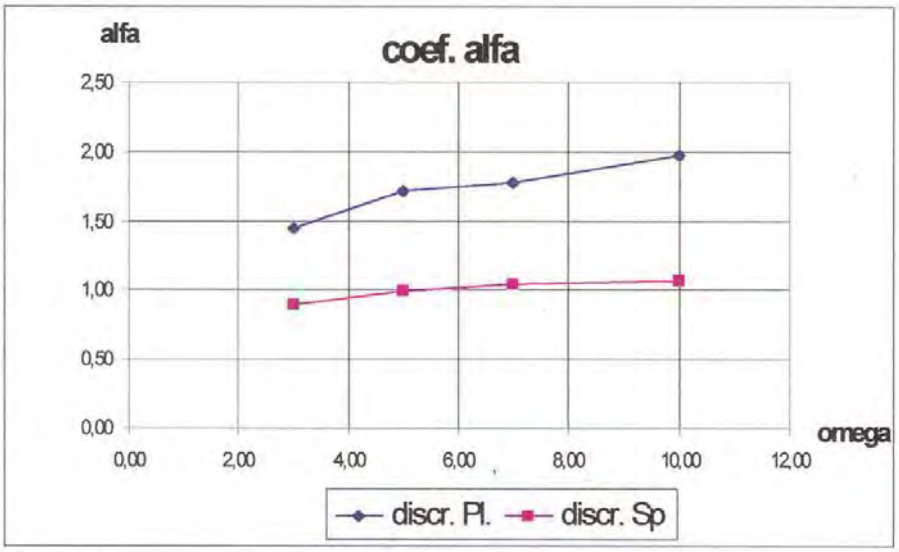

Figure 2 $\alpha(\omega)$ for plane mesh and spatial mesh

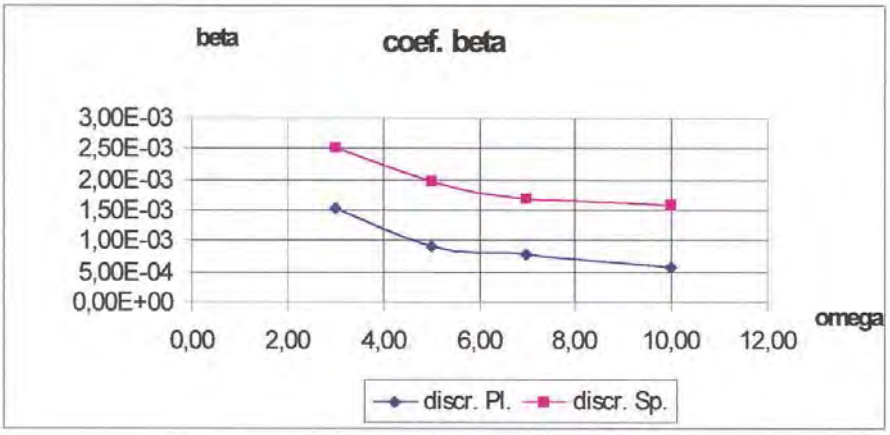

Figure 3 $\beta(\omega)$ for plane mesh and spatial mesh

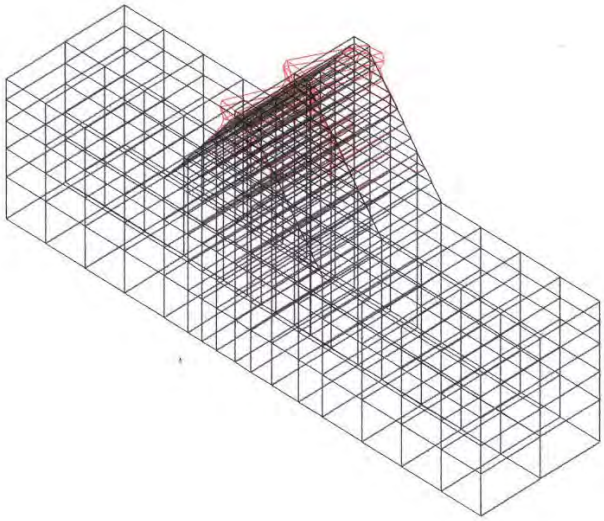

Figure 4 Modal analyze. Spatial mesh for a concrete dam. The six vibration mode Freq=42.17rad/s; T=0.149s

References

1. Clough. R.W., Penzien J., Dynamics of Structures, New York: McGraw-Hill Book Co.1975
2. Bathe. K.J. and Wilson, E.L. Numerical Methods in Finite Element Analysis. Englewood Cliffs, N.J.: Prentice-Hall,Inc.,1976
3. D.Stematiu, Calculul structurilor hidrotehnice prin metoda elementelor finite, Editura Tehnică Bucureşti, 1988. (in Romanian)

"Computational Civil Engineering 2007", International Symposium
Iaşi, România, May 25, 2007

NDT Devices as Long-Term Vision in Assessing of Old Masonry Buildings by Probabilistic Approach

Magda Brosteanu[1] and Teodor Brosteanu[2]
[1]*CCI Department, Faculty of Civil Engineering, Technical University of Iasi, Romania*
[2]*CFDP Department, Faculty of Civil Engineering, Technical University of Iasi, Romania*

Summary

Assessment and retrofitting of existing buildings made by masonry structure represent a huge engineering challenge as a distinct problem versus the design of a new building. Structural Strengthening and Thermal Renovation have to be applied at the same time.

This article refers to Two Non-Destructive Testing Devices in Diagnostic and Assessing under realistic conditions of Old Masonry Buildings evaluated to the real performance. It focuses on flat-jacks technique to determine the state of stress in masonry, and on monitoring of buildings health using IR thermal-graphic method. Minimum Equipment for Compressive Strength Qualifying Test on Masonry Large Specimen, and Minimum Equipment for Infrared Thermal-Graphic Test in Quality Control of Thermal Insulation are presented.

The results deal with the Masonry Strengths of walls and columns for the computation of Nominal Assurance Degree of Seismic Action of the existing masonry dwellings and monumental buildings according to the Strengthening Structural Design for Compressing Loading and Lateral Loading of damaged buildings.

Other results deal with the Surface Temperature Distribution and Moisture Content in Visible and Infrared Images for Quality Control of Thermal Insulation according to the Thermal Renovation Design for Heat Losses and Yearly Thermal Balance of damaged buildings.

The measured values are random variables. The characteristic values of random variables as fractiles for a given probability will be computed using the Probabilistic Approach.

KEYWORDS: monitoring, non-destructive testing (NDT), flat-jacks technique, infrared thermal-graphics, masonry characteristic compressive strength, surface temperature, random variables, input data in strengthening design.

1. INTRODUCTION

Many masonry structures were built over long periods of time using different technologies and materials. There are hidden damages out of a professional control. There are dwellings and monumental buildings made by masonry structure, placed on seismic hazard zone that need to be retrofitted at new performance levels.

The Romanian law L10:1995 concerning the quality in constructions defines one main component from 11 ones of quality system such as serviceability behavior and remedies during the life span of buildings.

Investor and/or owner or users have to be able to define correctly the users' requirements on custom mode offer and contract form of technical project for assessment or retrofitting.

Structural Safety (strength and stability) and Thermal Protection (thermal insulation and moisture protection for heat energy saving) are two essential performance requirements of buildings. Assessment and retrofitting of existing buildings made by masonry structure represent a huge engineering challenge as a distinct problem versus a new building design. Framing of damages into potential risk degrees has a cultural, social and economic impact.

Structural Strengthening and Thermal Renovation have to be applied at the same time.

The existing buildings are big consumers of energy. The volume of existing buildings is so big and it contains many masonry buildings that need an upgrading of the insulating by thermal retrofitting that means no interstitial condensation risk and no surface dew point temperature. There are almost 8.0 million of dwellings as 2.8-rooms conventional apartments with an amount of fuel required for one season's heating of 10.4-21.5 mil tones conventional fuel per year. By summing-up almost 20% for other buildings, the Romanian annual energy consumption for the heating of buildings is between 12.5-25.8 mil tones conventional fuel per year.

There are damaged old buildings placed on seismic hazard zones. Local remedies were been applied from economic reasons. Few local inventories were been performed with modest results. The existing buildings with classified damages need an upgrading of cross walls structure in order to reduce the seismic risk for users' safe.

No general rules are expected. Case-studies will be performed. Few official inventory and preliminary decisions of alternative spaces of living or working about were been performed. This is a worried factor.

There will be a sustainable activity to restore old buildings and monuments, not matter where. The trends in building costs in Germany (7) for new buildings and existing buildings are presented in the Fig.1.

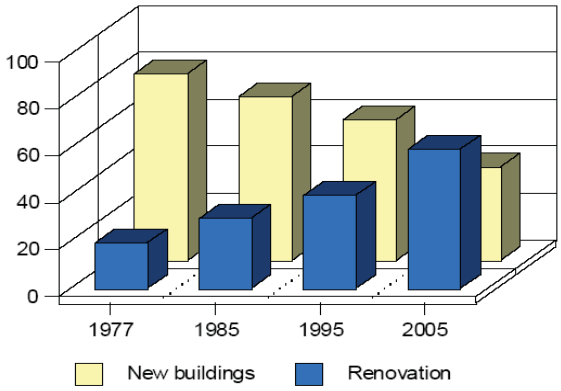

Fig.1. Trends in building costs in Germany

This article refers to the non-destructive testing device in assessing of old masonry buildings which were originally built over a long time ago, and it is focuses on flat-jacks technique to determine the state of stress in masonry, and on health monitoring using IR thermal-graphic method, as input data for strengthening structural design of masonry members in compression, and thermal renovation design.

2. DIAGNOSTIC SURVEYS

Diagnostic strategy is presented in the Fig.2. Keywords of diagnostic strategy using the probabilistic approach are the followings: sources of risk, damages, weak points, indicators, probability of failure, limit states, monitoring, early damages survey, random variables, input re-design data, costs etc.

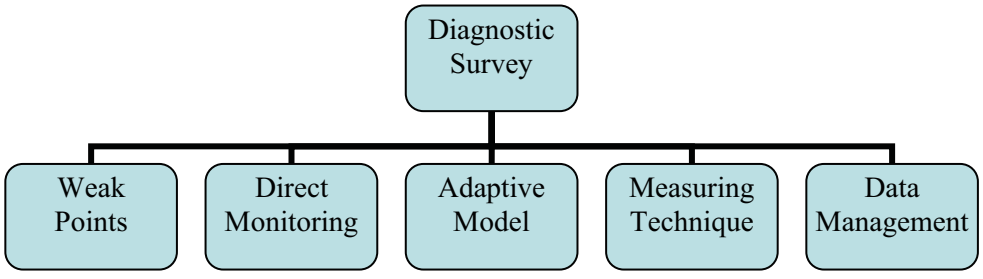

Fig.2. Diagnostic Strategy

Preliminary surveys focus on:

(i) geometric survey using topographic method and photogram-metric technique to identify the geometry of building;
(ii) crack-detection using piezoelectric arrays to identify static pattern and probable causes of instability.

Final aim of preliminary surveys of the overall pattern of cracks is the framing of existing buildings with classified damages into 4 potential classes of seismic risk **RS** /5/. **RS1** means a high risk of collapse. **RS2** means a low probability of collapse but there are major damages of bearing elements. **RS3** means that the damages of bearing elements do not disturb the structural safety but there are major damages of nonbearing elements. **RS4** means that the expected seismic answer of the existing building and the designed seismic answer for a new building are the same.

Note that should be kept in mind the influence factors of quantifying: the design seismic zone, the structural pattern on height, the aseismic conformity of structure, the nominal assurance degree to seismic action, the probable nature of collapse of bearing elements (either a ductile nature, a semi-ductile one or a breakable one), the reinforcement details, the building importance factor, the building life span, and the building inventory.

Diagnostic surveys focus on:
(iii) coring survey using coring and sampling technique to provide specimens for material testing;
(iv) X-ray survey inside the boreholes using a rotating micro-camera to provide 3-D image of wall;
(v) non-destructive testing using flat-jacks technique (6) to determine the state of stress in masonry realistic specimen, and the strengths of masonry: the $\mathbf{f_k}$ compressive strength, the $\mathbf{f_{vk}}$ shear strength, and the $\mathbf{f_{xk}}$ tensile strength in bending, and the $\mathbf{f_{vk}}$ shear strength of mortar layer;
(vi) sonic testing using an ultrasonic pulse excitation through, to perform a detailed survey of sound velocity distribution over;
(vii) radar-screen survey using high frequency electro-magnetic waves to investigate the interfaces between material layers having different dielectric constants;
(viii) health monitoring using fiber optical sensors and IR thermal-graphics for data capture to control any change in behavior, such as temperature distribution, moisture distribution, strains in all directions, relative movements, inclination etc;
(ix) material-destructive testing on coring samples using axial compression and other tests to assess the masonry strengths, and the degree of physical-chemical damages.

The calibration is a very important step.

3. FLAT-JACKS TECHNIQUE

Characteristic values of the compressive strength for the computational design purpose of new masonry structures are only regulated by design codes. Hence, the behavior of old masonry structures in compression has to be investigated to provide strength values.

Flat-jacks technique is a non-destructive testing method for quantification of phenomenon with regard to the state of stress in masonry.

Minimum Equipment for Compressive Strength Qualifying Test on Masonry Large Specimen consists of:

Loading Devices: Electric Drill, Core Drill, Hydraulic Pump, Hydraulic Flat-Jacks, Hydraulic Presses, Service Gauges, and Flexible Hose;

Recorder and Dataloggers: Data Acquisition Board, Inductance Strain Gauges Transducers, Wheastone Bridge Circuit, Graphic Recorder (Printer), Deformeters (Comparing Devices), Micrometers, Dilatometers, Sonic Detector, and Software.

Testing Method consists of: Stress-Strain Analysis of Large Specimen in Compression, Modulus of Elasticity, Shear and Dilatometer Tests on Masonry Sample Area, Diagnostic Surveys, Sonic Surveys, Structural Monitoring, and Structural Strengthening.

Fig.3. Flat-Jacks Compressive Starter Kit

Flat-Jacks Compressive Starter Kit is shown in the Fig.3. It contains: 5 flat-jacks, 10,000 psi capacity hydraulic hand pump, 1,000 psi test quality pressure gauge, 2,…,6 feet hydraulic hoses with quick connect fitting, removable extensometer of 0.0001 inch resolution, inch reference bar, marking gauge, 100 extensometer gauge points, rugged field case, where 1 psi=10^{-3} ksi=10^{-3} kip.sqin^{-1}=0.006895 MPa=0.006895 N.mm^{-2}, 1 in=25.4 mm, 1 ft=12 in=0.3048 m.

Fig.4. Flat-Jacks Shear Starter Kit

Flat-Jacks Shear Starter Kit is shown in the Fig.4. It contains: 10,000 psi capacity hydraulic hand pump, 10,000 psi test quality pressure gauge, 5,000 psi test quality pressure gauge, 10 feet hydraulic hose, 10 tones capacity hydraulic ram with tilt saddle, 2-3.5 inch x 2.0 inch x 0.5 inch hardened steel bearing plates, 2 inch Φ x 1.4 inch cylindrical aluminium spacer, 2 inch Φ x 4.0 inch cylindrical aluminium spacer, rugged field case.

Fig.5. Survey to perform flat-jacks test

The survey using flat-jacks technique carried out without scaffolding is presented in the Fig.5.

Masonry sample will be marked by two horizontal cuts into which two flat jacks will be inserted and it will be subjected to an axial compression. The pressure of flat-jacks will be increased up to the re-establishment of the initial degree of deformation. It is possible to find the masonry compressive strength $\mathbf{f_k}$ in

MPa=N.mm^{-2} by increasing of compression load until the first vertical crack will arise in the brick (1), (2), (3) because the lateral strain of mortar will only meet the effect of adhesion and friction between bricks and mortar.

Masonry sample will be marked by two vertical cuts, a brick will be removed out, and two small horizontal-acting hydraulic flat jacks will be inserted. It is possible to find either the shear strength of mortar layer f_{vk} or the friction angle between bricks and mortar by modifying the vertical and horizontal stresses.

Masonry strengths are random variables. By the probabilistic approach (9), the characteristic value of a material strength is the probability p=0.05 of lower values than this. The fractiles x_p will be computed as follows:

$$x_p = m_x \pm k\sigma_x \tag{1}$$

where,

m_x is the mean of random variables;

k is the factor or standard deviation number depending on the p probability and the type of distribution;

σ_x is standard deviation.

From the field data arranged into an increasing row, data selection, graphic probability distribution such as histogram and frequency polygon, on recommends Henry's line for checking of the theory-testing concordance, and the elimination of the absurd results. If the mean line that rectifies the plotted line is very close by the middle field points, it will be a concordance between the measured values distribution and the theoretical distribution. A few values will be rejected, and a few values will be kept.

The intersection of Henry's line with the abscissa is m_x point. The intersection of Henry's line with the 16% line is the a angle between Henry's line and the ordinate, where σ_x is tangent of a. The intersection between Henry's line with the 5% line means the x_p fractile.

Mean value with relative frequency named first moment or math hope and the variance named central second moment are computed using locating and spreading of statistical evaluation from Table 1 and Table 2, using Eq.2 and Eq.3.

Fractile is computed using Eq.1 for 0.05 probability of lower value than x_p.

Table 1. Data selection

Intervals	Central Value	Absolute Frequency	Relative frequency	Sum		Diagram of events on interval
R	$N.mm^{-2}$	N_i	$f_i=n_i/n$	Σn_i	Σf_i %	N_i
1.46-1.50	1.48	6	0.1111	6	11	x x x x x x
1.51-1.55	1.53	8	0.1482	14	26	x x x x x x x x
1.56-1.60	1.58	9	0.1666	23	43	x x x x x x x x x
1.61-1.65	1.63	12	0.2222	35	65	x x x x x x x x x x x x
1.66-1.70	1.68	8	0.1482	43	80	x x x x x x x x
1.71-1.75	1.73	6	0.1111	49	91	x x x x x x
1.76-1.80	1.78	5	0.0926	54	100	x x x x x
7	1.63	54	1.0000	54	100	5 10

Table 2. Mean and standard deviation computation

Central value	Relative frequency	Multiplication	Central deviation	Variance
X_i	$F_i=n_i/n$	$f_i X_i$	$A_i = X_i - m_x$	$\sigma^2 = f_i (X_i - m_x)^2$
1.48	0.1111	0.1644	-0.1424	0.0022
1.53	0.1482	0.2267	-0.0924	0.0012
1.58	0.1666	0.2632	-0.0424	0.0002
1.63	0.2222	0.3621	0.0076	0.0001
1.68	0.1482	0.2489	0.0576	0.0005
1.73	0.1111	0.1922	0.1076	0.0013
1.78	0.0926	0.1648	0.1576	0.0023
1.63	1.0000	1.6224		0.0078

$$m_x = \sum_{1}^{8} f_i X_i = 1.6224 \tag{2}$$

$$\sigma_x = \sqrt{\sum f_i (X_i - m_x)^2} = 0.0883 \tag{3}$$

The characteristic compressive strength of masonry large specimen f_k computed as fractile of 1.4771 MPa:

$$x_p = 1.6224 - (1.645)(0.0883) = 1.4771 \tag{4}$$

4. IR THERMAL-GRAPHICS

The key feature to reduce the amount of heat losses through the building envelope to a very low value is a very high standard of thermal insulation. Hence, the thermal behavior of masonry envelopes has to be investigated to provide thermal resistance $\mathbf{R}$ -values and thermal transmittance $\mathbf{U}$ -values (4).

Lock in thermal-graphics is a picture-based method for visualization and quantification of phenomenon with regard to the heat transfer.

The thermal energy caught by the IR camera from an object is focused by the radiation detector and the electronic system converts the electrical signal produced by detector into a video signal on monitor screen.

The total energy emitted by a body's surface is defined by Eq.5:

$$\mathbf{E_T} = \int_{\lambda=0}^{\infty} \varepsilon_\lambda \mathbf{E}_\lambda \mathbf{d}\lambda = \varepsilon_T \sigma \mathbf{T}^4 \tag{5}$$

where,

$\mathbf{E_T}$ is the total radiation energy emitted with the wavelength λ at $\mathbf{T}$ temperature;

ε_λ is the body's emissive power for the radiation with the wavelength λ;

$\mathbf{E}_\lambda$ is the radiation energy emitted with the wavelength λ;

ε_T is the body's emissive power for the radiation with the whole wavelength spectrum;

$\sigma = 5.672 \cdot 10^{-8}$ W. m $^{-2}$.K^{-4} is Stefan Boltzmann's constant.

Minimum Equipment for Infrared Thermal-Graphic Test in Thermal Insulation Quality Control consists of: Thermnocouples Meters and Probes, Equipment for Recording, Stocking, and Processing, Thermal CAM P-Series (professional infrared camera), and Thermal CAM Connect Software.

Testing Method consists of: Data Acquisition of Temperature, Temperature Control, and Thermal Imaging System.

IR equipment can catch the body's thermal image in real time using a receiving and recording system (IR camera), and a processing system of the thermal images (computer and software). IR camera consists of a scanning system, an infrared radiation detector, an electronic system, and a microprocessor.

Working parameters are as follows: temperature range from -20°C till 500°C with the sensibility increment of 0.1°C, working autonomy of 3 hours, and operation temperature from -15°C till 45°C. The calibration between the surface emissive power and the surface temperature is given.

A few results are presented (11). In the Fig.6, the visible image and IR image with cold bridges zones are presented. In the Fig. 7, the earth moisture infiltration at the building ground floor level (12) is presented. In the Fig.8, temperature values on a window with the layering effect are presented as screened results.

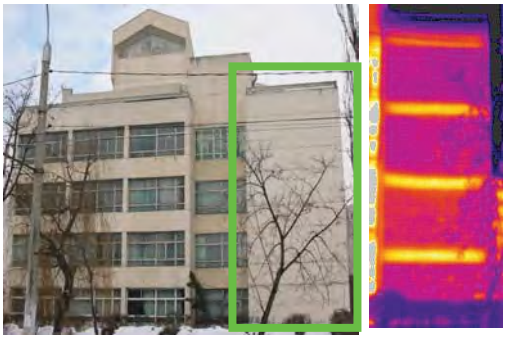

Fig.6. Visible and infrared images with defects due to the cold bridges

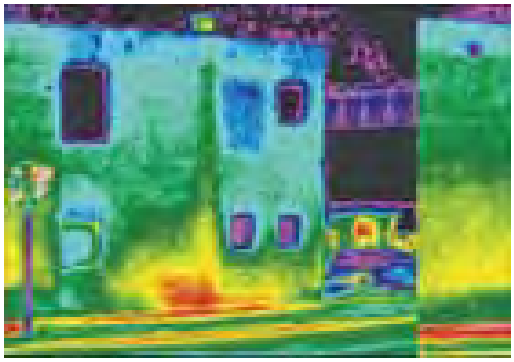

Fig.7. Infrared image of the earth infiltration tracing

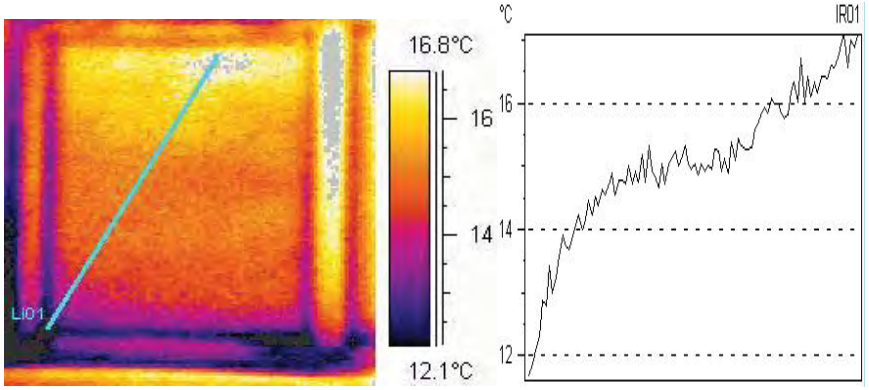

Fig.8. Screened results of temperature distribution

5. CONCLUSIONS

There will be a sustainable activity to restore old buildings and monuments, not matter where it will be. In Germany, trends in building costs for new and existing buildings confirm this.

Assessment and retrofitting of existing buildings made by masonry structure represent a huge engineering challenge as a distinct problem versus a new building design.

Inspection techniques via monitoring and parallel testing i.e. the diagnostic surveys under realistic conditions are presented.

Flat-jacks technique as a non-destructive testing method is suggested for input data capture of masonry strengths in strengthening design of damaged old buildings. Note that for high buildings, few experts have to be rock-climbers.

Lock in thermal-graphics as a picture-based method for visualization and quantification of phenomenon with regard to the heat transfer, but not only is suggested for input data capture of masonry thermal resistance in thermal renovation design of damaged old buildings. It is attractive. IR thermal-graphics is an important instrument to stimulate the interest concerning the quality of works. The right decision is taking the best insulation available. Note that for high buildings, few experts have to be rock-climbers, too.

Lock in acoustics and thermal-graphics is suggested for research.

On recommends the equivalent rigid frame pattern for simplified structural design (10), and for the best approximation to the specimen experimental behavior (8), and for actual brick shear walls structure, as well.

The equivalent rigid frame consists of columns with the same features as posts, and slabs with the same features as lintels. The frame columns will substitute the posts spanning between posts centre lines. The slabs will substitute the lintels on the entire span of columns centre lines.

References

1 xxx The EC 6-1-3:1996 *"Design of Masonry Structure-General Rules for Buildings-Rules for Reinforced Masonry".*

2 xxx CR 6:2006 *Codul de proiectare pentru structuri din zidarie.*

3 xxx The EN 1052-3:1996 "*Methods of tests for masonry".*

4 xxx SR EN ISO 13790:2005:2004 *Evaluarea performantei termice a cladirilor.*

5 xxx P 100:2006:2004 *Codul de proiectare seismica cap. 1"Prevederi de proiectare pentru cladiri", cap.3 "Prevederi pentru evaluarea si proiectarea consolidarii constructiilor vulnerabile seismic*, *cap.8 "Prevederi pentru proiectarea consolidarii monumentelor istorice si a constructiilor cu valoare arhitecturala".*

6 xxx The former ISMES spa "*Building and Monument Restoration-Surveys and Control",* Bergamo, Italy, 1996.

7 xxx Collaborative Research Center SFB 477, founded by the German Science Foundation (DFG), *"Life Cycle Assessment of Structures via Innovative Monitoring",* University Carola-Wilhelmina-Braunschweig, Germany, http://www.sfb477.tu-bs.de

8 Hendry, A.W., Sinha, B.P., Davies, S.R. -*Design of Masonry Structures*, Third edition of Load Bearing Brickwork Design, E& FN Spon Publishing House, An Imprint of Chapman & Hall, London, Weinheim, New York, Tokyo, Melbourne, Madras, 1997, ISBN0 419-21560-3.

9 Brosteanu, M. -*Constructions. Philosophy of Design*, The first edition. Cerni Publishing House, Iasi, 1998, ISBN973-9378-13-7.

10 Brosteanu, M., Brosteanu, T. -*Selection of theoretical method for lateral load analysis of brick shear walls structures,* In the Proceedings of International Symposium "Computational Civil Engineering", "Matei-Teiu Botez" Academic Society Publishing House, Iasi, May 26, 2006, ISBN(10)973-7962-89-3, ISBN(13)978-973-7962-89-8.

11 Avram, C. -*Investigatii IR pentru controlul calitatii protectiei termice,* Satisfacerea exigentelor de izolare termica si conservare a energiei in constructii, "Matei-Teiu Botez" Academic Society Publishing House, Iasi, 2003, ISBN973-85882-7-8.

12 xxx The former http://www.agema.com; http://www.flir.com.

"Computational Civil Engineering 2007", International Symposium
Iaşi, România, May 25, 2007

IT Approach in Heat Transmission Visualizing through Opaque Walls

Magda Brosteanu[1] and Teodor Brosteanu[2]
[1]*CCI Department, Faculty of Civil Engineering, Technical University of Iasi, Romania*
[2]*CFDP Department, Faculty of Civil Engineering, Technical University of Iasi, Romania*

Summary

This article refers to the 2-D thermal field computation in the steady-state conditions for thermal design of the building envelope. A procedure to analyze the heat transfer through the opaque wall is provided. The results are as follows: Heat Flow Image and Density, Surface Temperature Distribution, and Isothermal Lines. Computing programs are very useful instruments in the designing of adjustment to R-value and in the solving of problems.

KEYWORDS: building, envelope, opaque wall, heat transfer, steady-state conditions, computational analysis, surface temperature visualizing.

1. INTRODUCTION

The Romanian standard SR EN 10211-2:2001 /1/ is identical to the European Standard EN ISO 10211-2:2001-Thermal bridges in construction-Calculation of heat flows and surface temperatures-Part2: Linear thermal bridges.

Solving problems by 2-D analysis has required using the dedicated software and computer aided design systems.

2. THERMAL FIELD

The thermal field represents all temperatures $\theta(x, y, z, \tau)$-values, where x, y, z are the spatial co-ordinates of the point and τ is the time.

The thermal field is computed from the Laplace's Eq., as follows:

$$\lambda \Delta\theta = c\rho \frac{\partial\theta}{\partial\tau} + I \qquad (1)$$

where,

λ is the thermal conductivity of the material, in $W.m^{-1}.K^{-1}$;
c is the heat capacity of the material, in $J.\ kg^{-1}.K^{-1}$;
ρ is the density of the material, in $kg.m^{-3}$;
I is the source of heat, in $W.m^{-3}$.

There are many heat transfer problems from which **2-D** problem in steady-state conditions is the most useful formula for $\theta(x,y)$-values computation by the Numerical and Computational Techniques:

in steady-state conditions τ=0, and in transient ones $\tau \neq 0$;

in linear conditions with λ, c, ρ=constants, and non-linear ones with $\lambda(\theta), c(\theta), \rho(\theta)$;

1-D problem of $\theta(x)$, **2-D** problem of $\theta(x,y)$, and **3-D** problem of $\theta(x,y,z)$.

3. MATHEMATICAL MODEL

By the Finite Difference Method or Finite Element Method, the Differential Equations with second partial derivative of θ with respect to dx^2 squared at constants (m, n) have to be changed into a system of Algebraical Linear Equations using difference operators or finite operators:

$$\lambda \frac{\partial^2 \theta}{\partial x^2} + \lambda \frac{\partial^2 \theta}{\partial y^2} = 0 \tag{2}$$

The digitization after **x** and **y** in elementary layers supposes the nodes disposal at the borders, at intermediary surfaces between different materials, and in the same material. The differential operators could be approximated with the help of two levels schemes resulted from $\theta(x,y)$ development in the Taylor's series around the node with (m, n) co-ordinates.

Finally, the formulae have resulted by the imposed, uniqueness conditions, initial and at the limits ones:

the 1st case condition (Dirichlet's one) in steady-state conditions has indicated that the inside air temperature θ_i and the outside air temperature θ_e are fixed;

the 2nd case condition (Newman's one) has indicated the occurrence of a continuous density of heat flow q_s at the boundaries, i.e. we have to consider many nodes up to the breadth of the influence zone l_p of the cold bridge limited by the normal heat flow on both surfaces of the element:

$$q_s = \frac{\Delta\theta}{R} \tag{3}$$

the 3rd case condition (Fourier's one) has indicated the heat transfer on the internal surface and external surface of the element:

$$\alpha_i(\theta_i - \theta_{si}) = \lambda \frac{\theta_{si} - \theta_2}{\Delta y} \quad \text{and} \quad \lambda \frac{\theta_3 - \theta_{se}}{\Delta y} = \alpha_e(\theta_{se} - \theta_e) \tag{4}$$

the 4th case condition has indicated the heat transfer between different materials deduced from the conservation Eq.:

$$\sum q = 0 \tag{5}$$

4. HANDLING THE PROGRAM

There are thermal bridges as parts or portions of a built element, given by the technological or structural reasons, in which the insulating material is completely absent, i.e. **the insulation is bridged**.

The heat flow increases across the thermal bridges and the inside surface becomes cooler, giving the reason of **"the cold bridge term".** There is also an increased risk of condensation.

Sometimes, it is necessary to calculate the thickness of **the additional insulating material** in order to produce the same specified $\mathbf{R_0}$-value as in the current section. The best position of thermal insulating material is at the outside surface of building element.

Thermal resistance of the envelope $\mathbf{R_0}$ in $m^2.K.W^{-1}$ can be found from the Eq. as:

$$R_0 = R_i + R + R_e \tag{6}$$

All details selected can be developed for the claimed input data.

The results of computational approach are as follows:

- the image of heat flow;
- the density of heat flow q_s, in $W.m^{-2}$;
- the distribution of the outer surface temperature , $\theta_{es}(x, y)$ in ^0C ;
- the distribution of the inside surface temperature $\theta_{is}(x, y)$, in ^0C;
- the isothermal lines $\theta(x, y)$=constant;
- the zones of almost constant temperatures;
- the lines of almost constant densities of heat flow;
- the zones of almost constant densities of heat flow.

Considering a case-study /2/ of a building outer wall joint subjected to 2-D heat flow through, in the winter time conditions, for a masonry wall with a cold bridge due to a concrete column with and without adjustment at the outside surface using an EPS layer, the results are shown in the Fig. below. Wall structure thermal properties and indoor-outdoor surface resistances are taken, and the temperatures remain steady.

Wall Joint Digitization is presented in the Fig. 1.

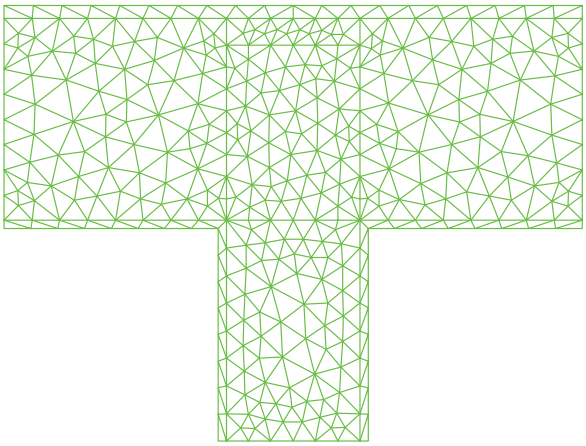

Fig.1. Wall Joint Digitization

The image of lines of conductive heat flow through the outer wall after the thermal adjustment is presented in the Fig.2. There is a non-uniform heat flow through because of the effect of lateral heat flow is significant.

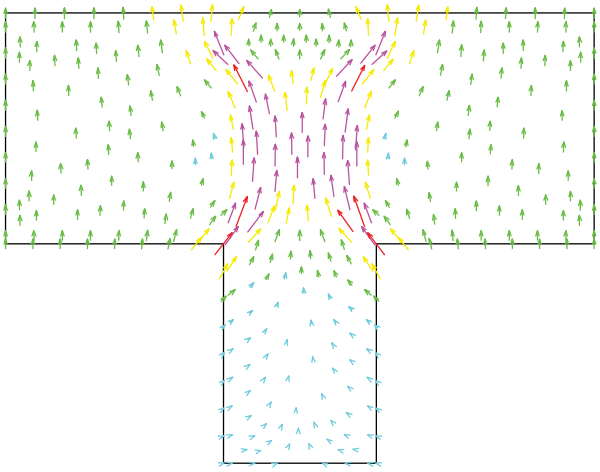

Fig.2. Image of Heat Flow through

The distribution of heat flow density and surface temperature on a wall joint with and without adjustment of R_0-value is compared in the Fig. 3, 4, 5, 6, 7, and 8.

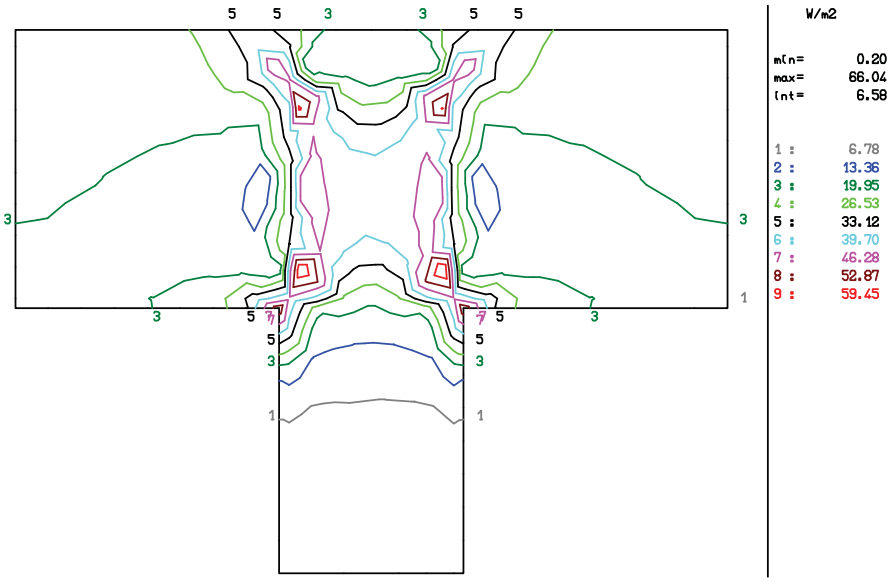

Fig.3. Variation of the Density of Heat Flow after the Adjustment

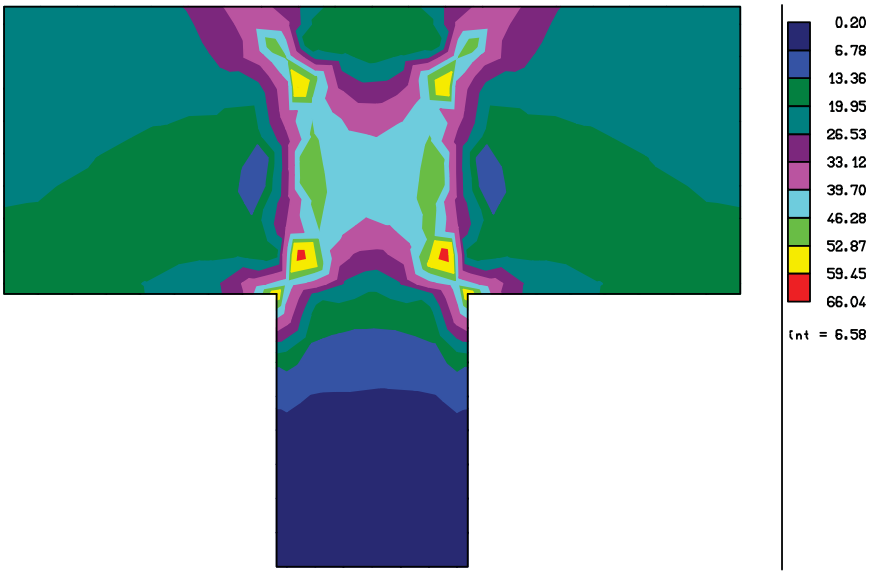

Fig.4. Zones of almost Constant Densities of Heat Flow after the Adjustment

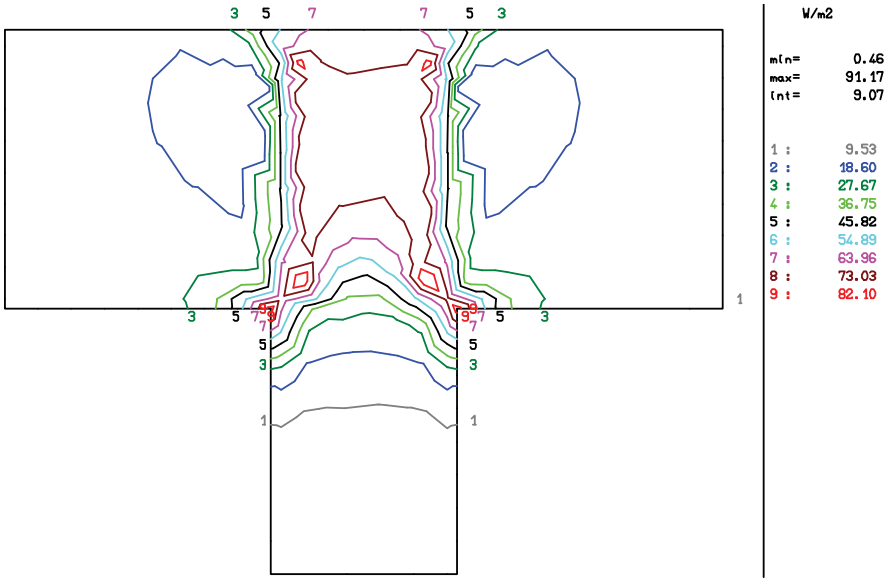

Fig.5. Variation of the Density of Heat Flow before the Adjustment

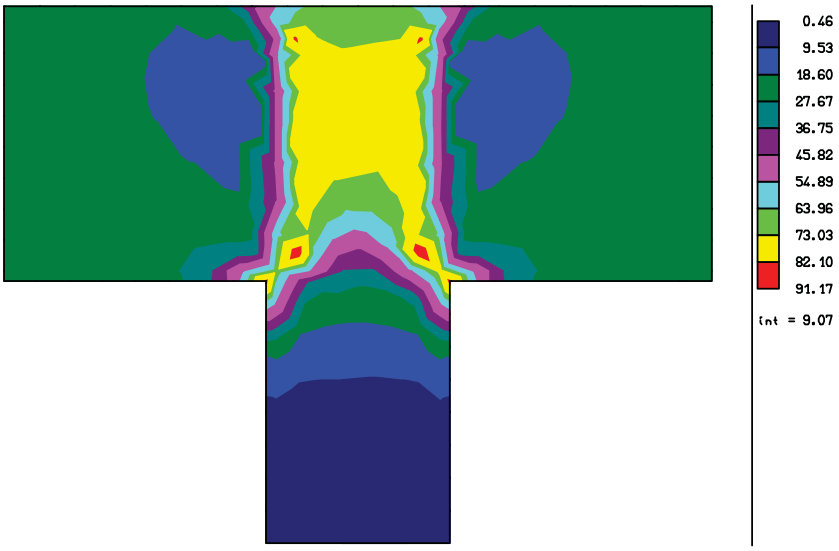

Fig.6. Zones of almost Constant Densities of Heat Flow before of the Adjustment

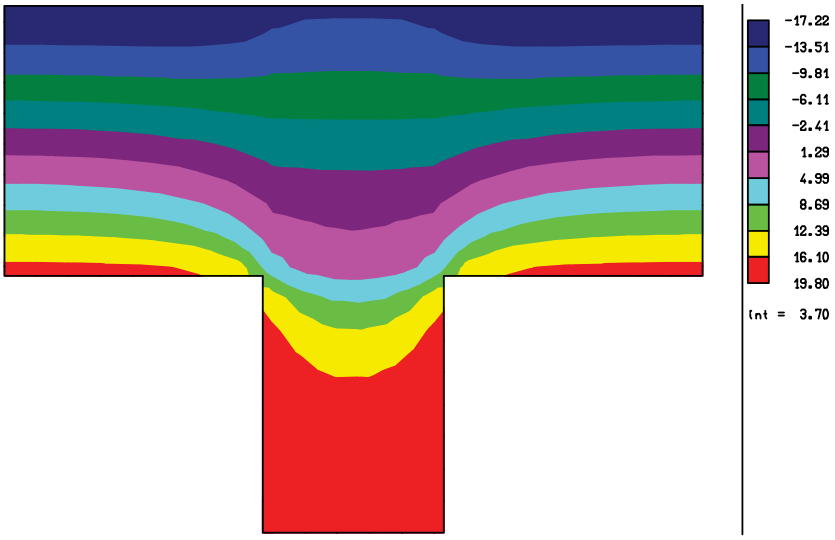

Fig.7. Zones of almost Constant Temperatures after the Adjustment

After the adjustment, the isothermal lines are almost parallel to the wall external surface and the effect of lateral heat flow is not significant.

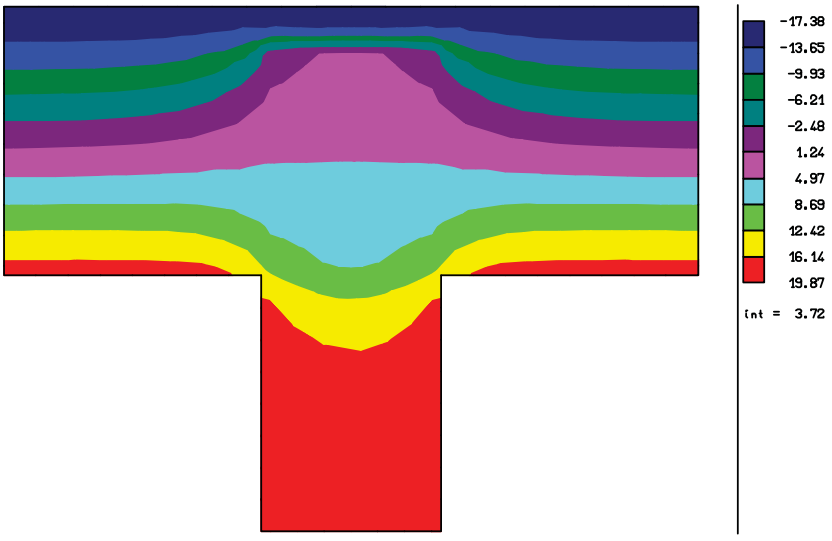

Fig.8. Zones of almost Constant Temperature before of the Adjustment

5. CONCLUSIONS

Thermal comfort and protection requirements mean a positive state of mind due to a friendly inside environment, and a lower cost of heating for energy conservation resulting from the best thermal isolation available concerning the improvement of relative humidity, condensation risk, comfort temperature, thermal resistance, thermal transmittance, and heat losses.

2-D FEM wall pattern in the steady-state conditions is suggested for the design of the adjustment of R_0-value. After the adjustment, the effect of lateral heat flow is not significant. Note that the best position of thermal insulating material is at the outside surface of building element.

IT Approach is an important instrument to stimulate the taking of right decision by heat transmission visualizing. It is attractive.

On recommends the dynamic heat transmission through the building envelope with solar gain and material thermal storage, for research and effective design, as well.

References

1 xxx The Romanian code SR EN ISO 10211-2:*2001 "Thermal bridges in construction-Calculation of heat flows and surface temperature. Part2: Linear thermal bridges"*.

2 Moss, J. Keith *–Heat and Mass Transfer in Building Services Design*, "E&FN Spon" Publishing House, an imprint of Routledge, London, 1998, ISBN 0 419 22650 8.

"Computational Civil Engineering 2007", International Symposium
Iaşi, România, May, 2007

Comparative Study on the Results of Analytical and Experimental Analysis of a Steel Taintor (Radial) Gate

Adrian Prodescu and Daniel Bîtcă

Steel Structures Department, University of Civil Engineering, Bucharest, Romania

Summary

The main load of a hydraulic gate is the water pressure, especially for the submerged gates. A good accuracy of the computation methods leads to a more secure structure.

The paper presents a comparison between different computation methods of this type of structures. A radial gate was analyzed. The size of the submerged outlet is 4,0 x 4,0 m and the water depth is 20,0 m

The following methods were used in the analysis:

- *The finite elements method, using a mesh of the structure of the gate.*
- *Model studies. An 1:4 scale model was built in order to perform this study. The model was subjected to water pressure. In several points of this model, strain measuring devices were installed and the strains were measured at several water pressure magnitudes.*

The results of the first two computation methods are compared in some points of the structure. With the aid of the second method, the strains were computed in order to compare them with the strains measured on the model.

These comparative studies try to establish the accuracy of each of the methods presented above.

KEYWORDS: radial gate, water pressure; experimental study

1. STUDY'S OBJECT

In this paper it is analyzed a depth radial gate, which have the dimensions 4,00x4,00m, located on 20,00m depth. The structure of radial gate is presented in figure 1.

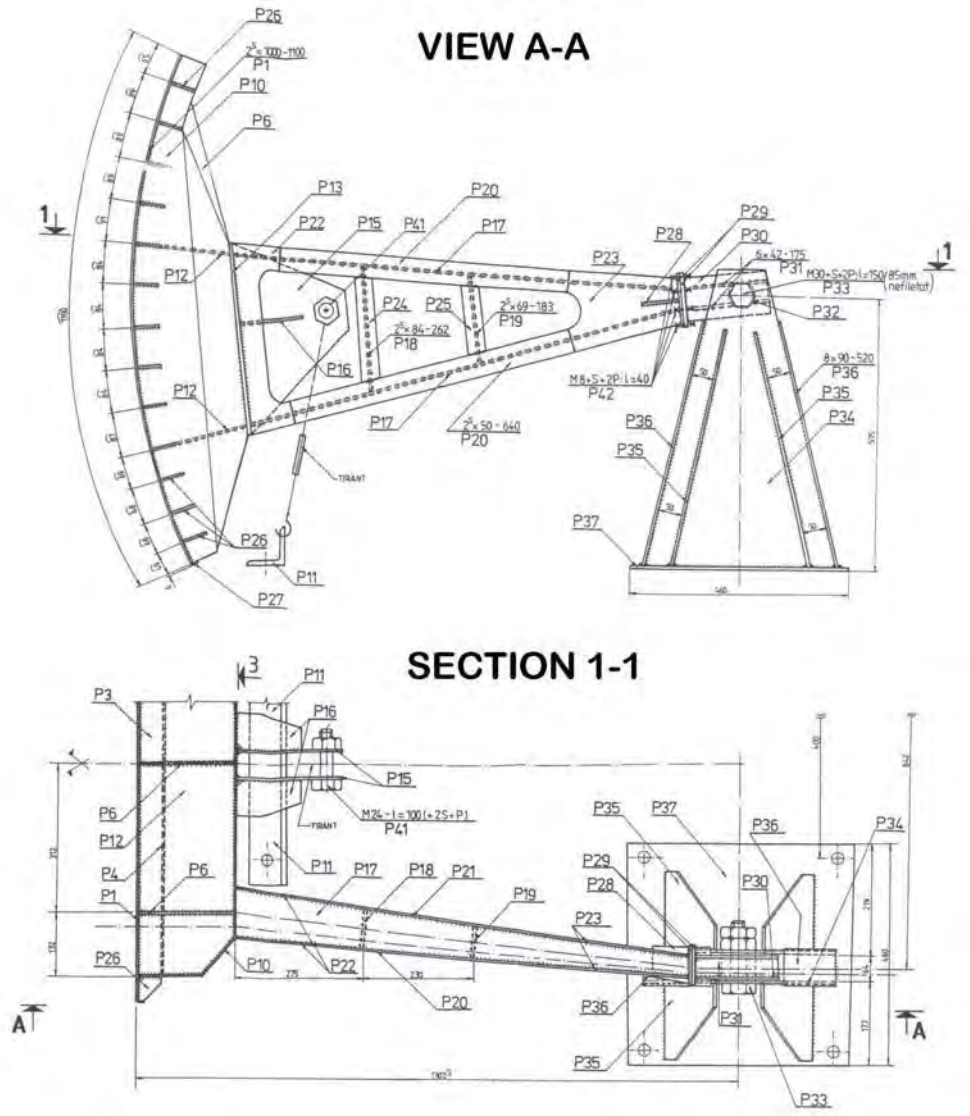

Figure 1. The structure of analyzed radial gate

The main dimensions of the 1:4 scale model are:

- the outlet dimensions Lxh = 1050x1000 mm;

- the plate radius is 1300 mm;

- the plate thickness is 2,5 mm, in order to be 1:4 by the thickness of the gate's plate (10 mm);

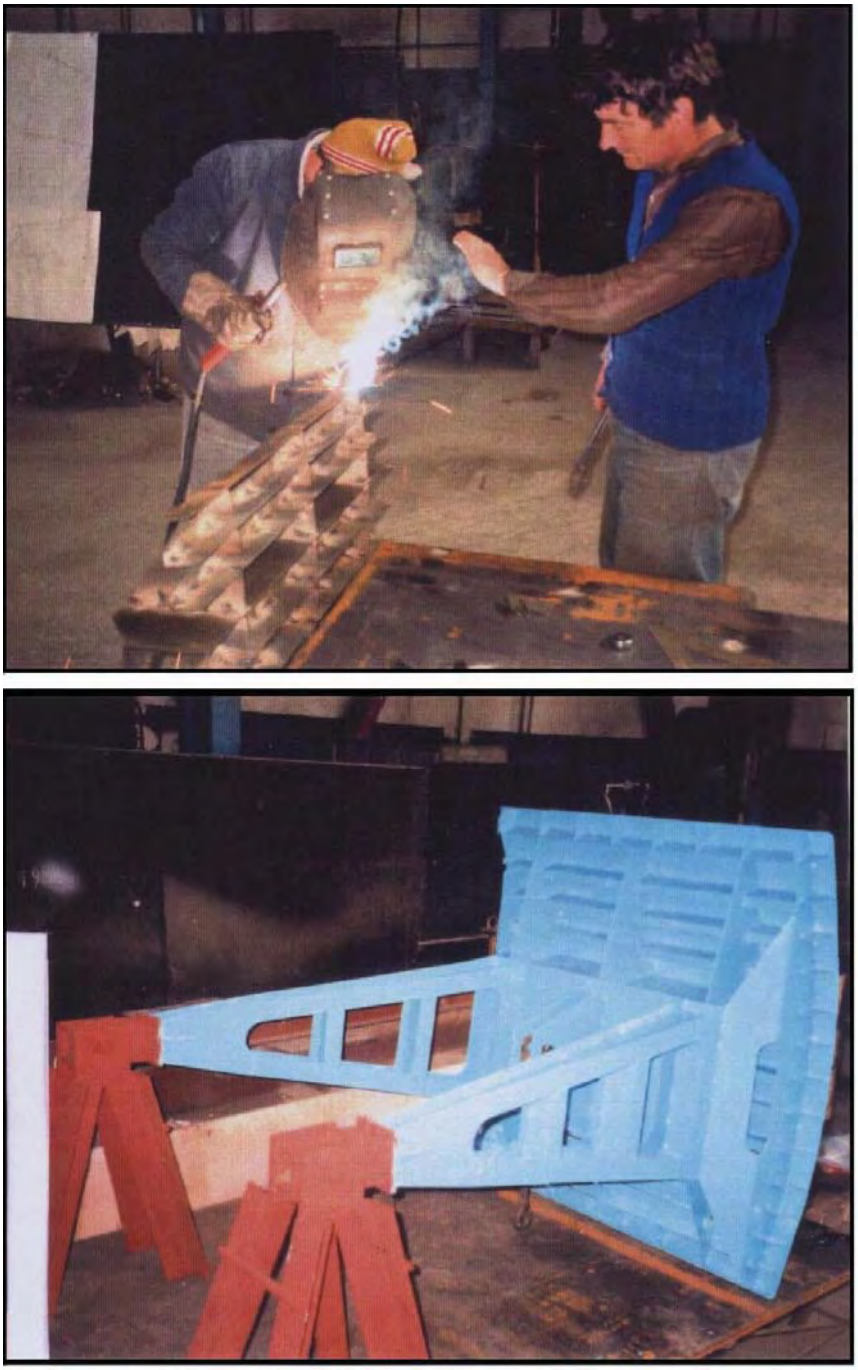

Fig 2 Assembling the scale model

2. THE HYDRAULIC PRESSURE TEST OF THE SCALE MODEL

In order to apply water pressure on the model, a steel tank was built such as the model would fit on one of the tank's lateral faces. The tank was made out of 6 mm thickness sheet, which was stiffened with angle steel shapes.

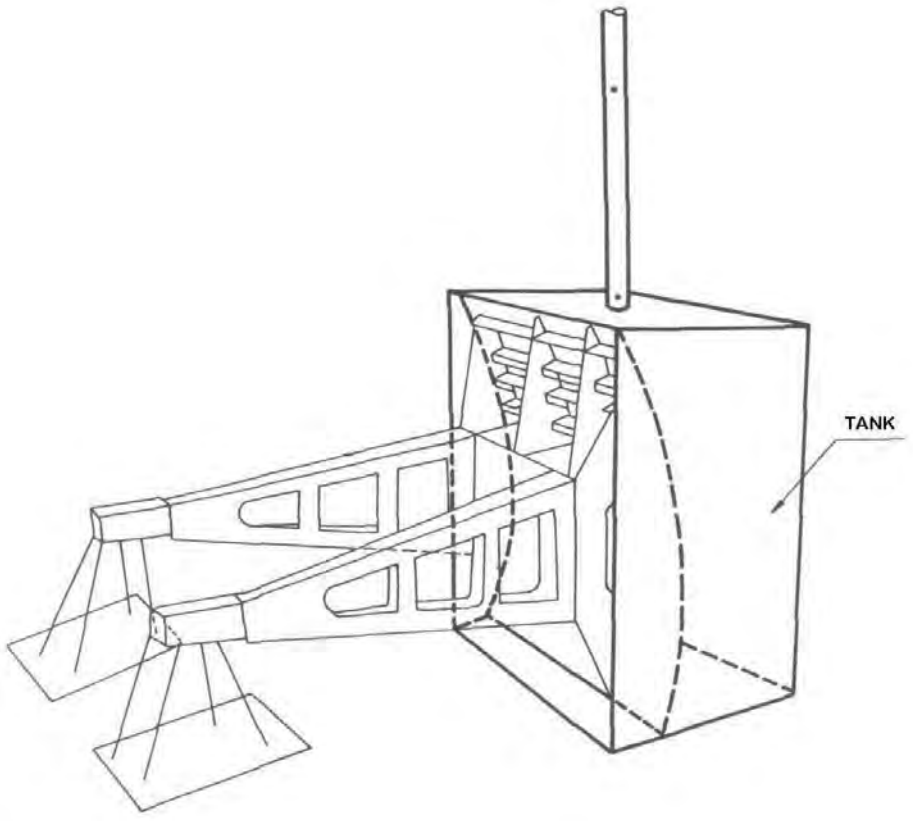

Fig. 3. The scheme of the hydraulic pressure test

The sealing between the model and the tank was made using siliconic sealant with good elastic properties, in order to allow the displacements between the tank and the model.

The boundary conditions were made similar to the real ones, when the gate is closed.

A vertical pipe was attached to the top face of the tank. This pipe allows the increase of water pressure in 1 m steps, the maximum pressure being 6 m above the tank.

The deflections of the model were measured in 6 load steps; the water pressure was increased with 1 m in each step.

The deflections of the model in the upstream - downstream direction were measured with the aid of some measuring devices with 1/100 mm precision. The points in which these measuring devices were placed are shown in fig. 4 and 5. In pts 1 and 2 (where the displacements should be 0) two measuring devices were installed in order to correct the other measured deflections.

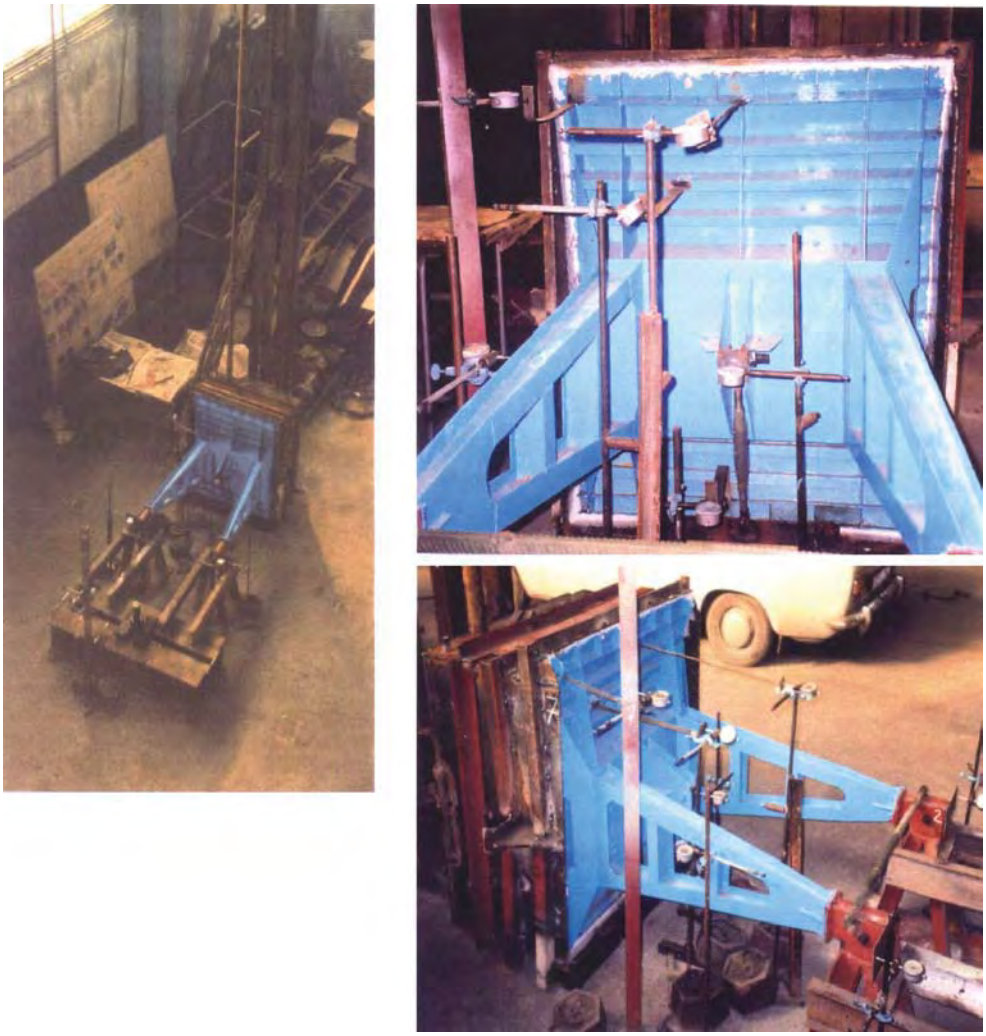

Fig. 4. Aspects during the test

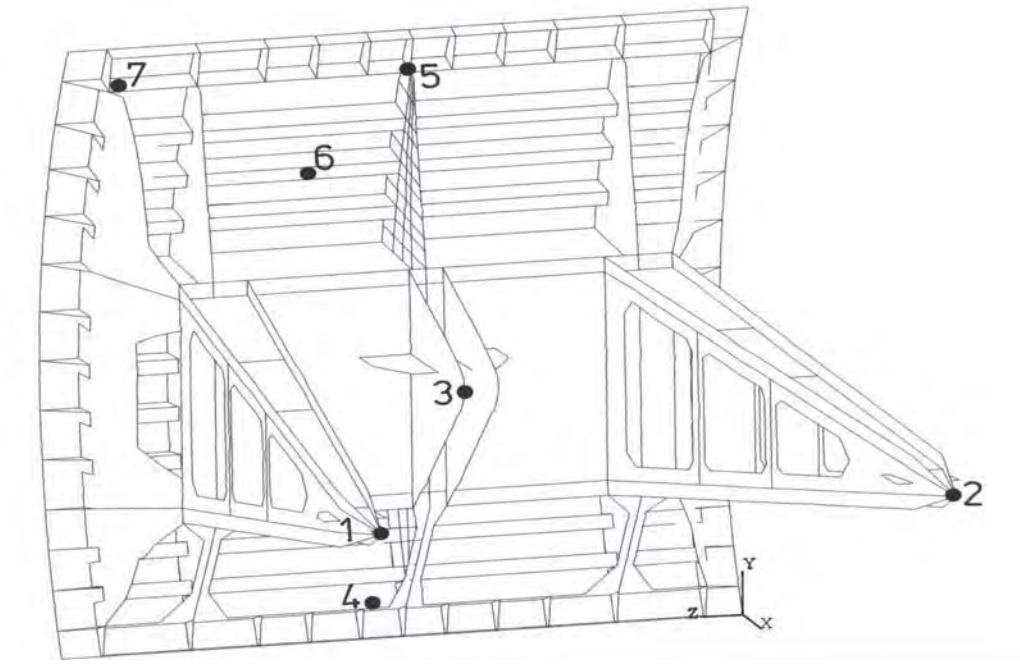

Fig. 5. The points where the measuring devices were installed

The corrected deflections in points 3 to 7 are shown in fig. 6. The corrections were made using the deflections measured in points 1 and 2 (which are the bearings where, theoretically, the displacement is null)

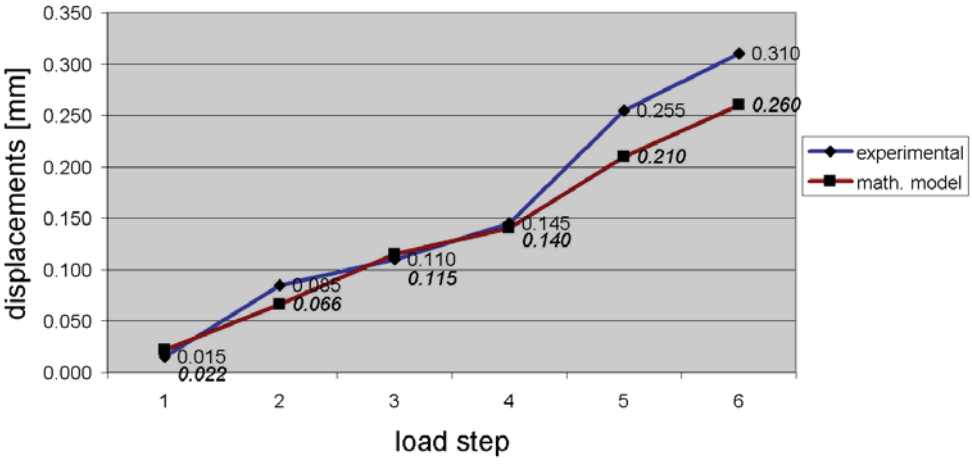

Figura 6. The corrected deflections in points 3 to 7.

3. COMPARRISON BETWEEN THE RESULTS OF THE TEST AND THOSE OBTAINED BY COMPUTATIONS

A finite elements model was build, having the same characteristics as the scale model. The load steps were similar to the ones from the test.

The graphs in fig. 7, 8 and 9 shows comparisons between the displacements obtained in the test and in the computations.

One can notice a good match between the results obtained using the two methods, especially in the first four loading steps.

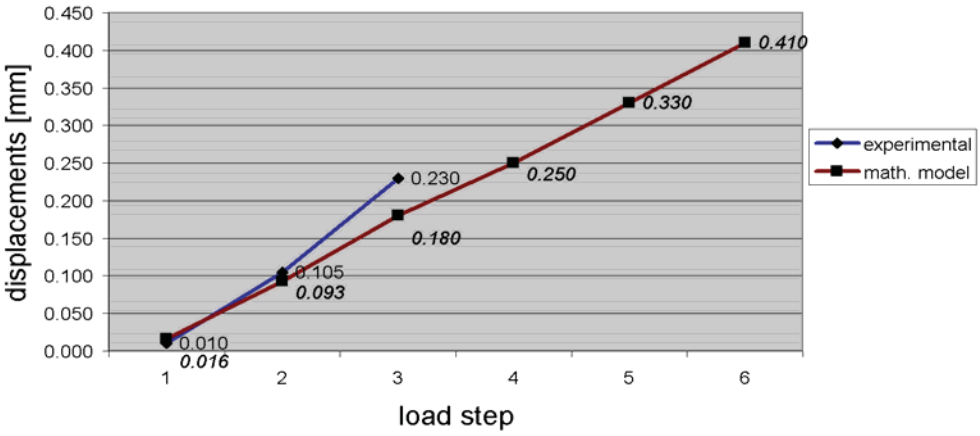

Fig 7. Displacements in point 3

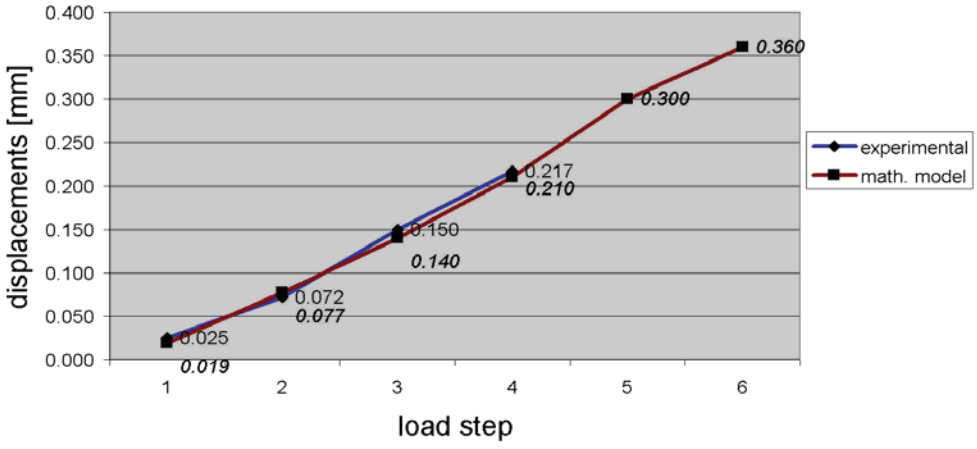

Fig 8. Displacements in point 6

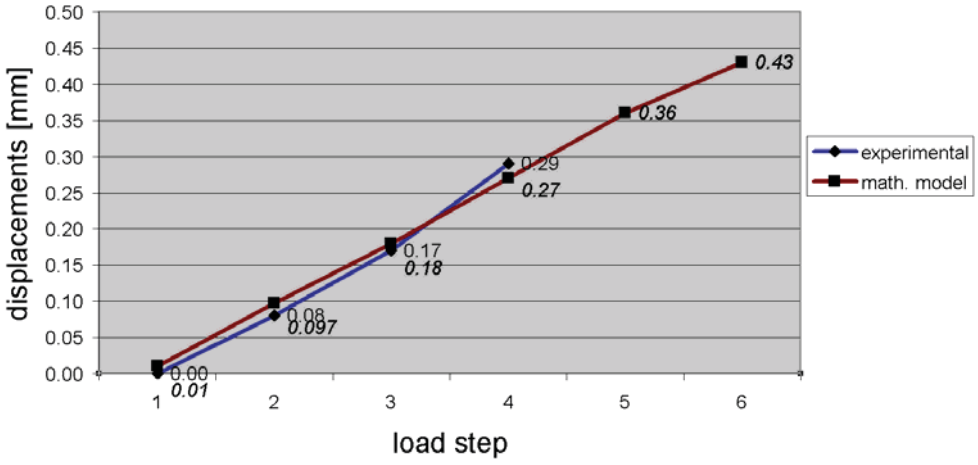

Fig 9. Displacements in point 7

In points 3 and 6, situated in areas of the structure having rather big stiffness, one can see the results are very close, the maximum differences being of about 19 % for point 3 and about 26% in point 6.

As a conclusion, the closeness between the results confirms the reliability of the finite element method, if the mesh is appropriate and sufficiently detailed.

References

1 Prodescu, A. *Acuratețea modelelor de calcul folosite la analiza stavilelor segment*, Teză de doctorat, Universitatea Tehnica de Construcții, Bucureşti, 1998

2 Beleş, I; Răduică, N. *Construcții metalice şi elemente de construcții; Stavile metalice* Institutul de Construcții Bucureşti 1979

"Computational Civil Engineering 2007", International Symposium
Iaşi, România, May 25, 2007

Contribution to non-linear constitutive modelling of masonry structures in 2D

Jiří Brožovský[1], Alois Materna[2] and Ivan Kološ[1]
[1]*Dept. of structural mechanics, VSB – Technical University of Ostrava, CZ708 33, Czech Republic*
[2]*Dept. of building structures, VSB – Technical University of Ostrava, CZ708 33, Czech Republic*

Summary

This paper discusses a non-linear constitutive model for modelling of masonry in 2D. The model consists from two independent parts: the model for mortar and the model for bricks or stones.

The reason of using two different constitutive models is our need to be able to modell individual bricks (or stones in the case of a stone masonry) and the mortar between the bricks.

We have decided to use a smeared crack approach for the modelling fo a mortar. It is an approach that is widely and successfully used for a constitutive modelling of concrete and we assume that it can be also applied to a mortar that is very similar to a concrete.

The model of mortar is based on an equivalent one-dimensional stress-strain relation that depends also on 2D state of stress (through the Kupfer's failure criteria that is used to obtain the limit stresses for the one-dimensional stress-strain relation) and on some special material properties such is fracture energy of mortar.

Bricks are modelled in a different way, As a generally brittle, they often can't be effectively modelly by the smeared crack approach. The damage of the brick (a crack) usually goes through the whole brick and it can be assumed that its occurrence depends on a stress intenzity on an area and not on the stress size in an individual material point. Thus we have decided to use a simple approach that can be describes as a very basic non-local material model.

After the ckack on the brick is detected the material properties are changed in a moment. Unlike the model for a mortar, it is assumed that there is no unloading curve for this model,

KEYWORDS: finite element method, constitutive modelling, masonry, mortar, bricks, crack band model, smeared cracks.

1. INTRODUCTION

The static analysis of masonry can be done in several ways. The most common is approach is a linear elastic constitutive modelling. It allows to provide a relatively simple computational analysis and many structures can be analysed with very simple computational models (beams and frames) and often even without need of a computer. Also the finite element analysis can relatively easy and non-complicated. It is often said that linear elastic modelling is enough for a design of masonry structures because they are not allowed to work in situations when their behaviour can be non linear (under tension loads, for example).

But there are situations when the assumption of the linear elastic behaviour is not sufficient. For example there are often needs of analysis of already existing buildings or of historic structures and monuments that can work in an non-optimal mode for masonry. For these cases a lot of different non-linear constitutive models have been developed by many authors (for example [1]). Many of these approaches are very complex and they can offer a high level of accuracy of results if they are properly used. But it isn't often easy (or even possible) to get all the necessary input data that are needed for such models. In these cases the results can be even less precise than the traditional computing approaches. There are also a lot of not so advanced models that cannot offer so high precision of results but they usually require lower number of input data and may they may be easier to use.

In this paper we present a constitutive model for masonry that we are developing. This model was designed as a compromise between needs and possibilities of computing and access to input data (however, the proposed model still can be too complicated in some cases).

2. CONSTITUTIVE MODEL DESCRIPTION

2.1. Overview

The constitutive model includes two independent parts: the model for mortar and the model for bricks. These parts are based on different assumptions and they are impemented in different ways. The mortar is implemented using the smeared crack approach and the crack-band model. Bricks are modelled with a simple variation of a non-local model approach. This division of the model into two parts allows us to create a models that can include individual bricks (or stones in a case of stone masonry that is common in historic buildings) and also locate the mortar in positions that are correspond with the real structure.

The proposed constitutive model is developed for 2D cases (for the plane stress case).

2.2. Model for mortar

The constitutive law for mortar is controlled by an equivalent uniaxial stress-strain relation. The simplification of the problem from 2D to 1D is not ideal but it is relatively easy to develop and understand. To make the uniaxial relation to be more corresponding with the real behaviour the limits of the relation (strenghts in tension and in compression) are computed from a 2D failure criteria (the Kupfer's criteria is used here) and depends on the actual 2D stresses.

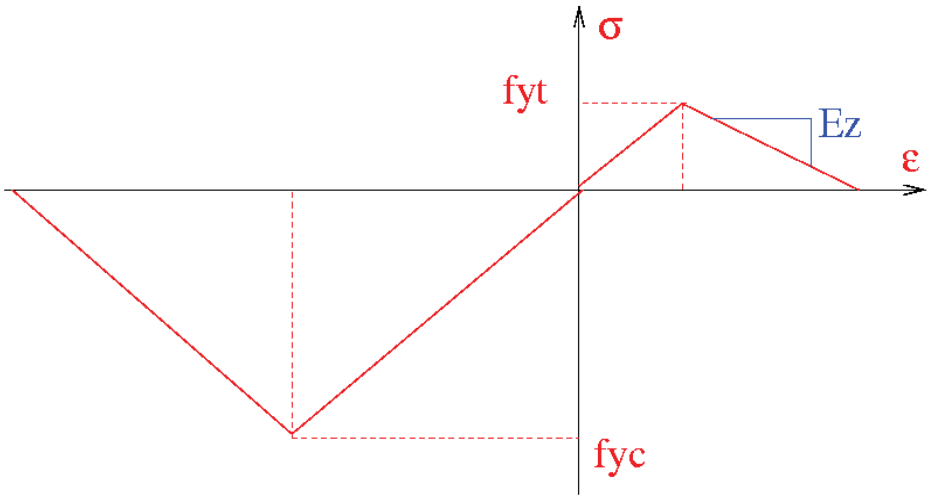

Figure 1. Uniaxial stress-strain relation for mortar

There used approach has several disadvantages. The one of the most important is that results depend of properties of a finite element mesh. It is obvious, because when a “damage” is detected the properties of the material became be reduced and they are reduced on whole area of the element (or – in our case – on a whole area that corresponds with an integration point of a finite element).

This issue can be minimized by usage of the Bazant's crack-band model when the properties of the stress-strain diagram (the “Ez” value in Figure 1) depends on the size of the cracked area (value L on Figure 2) and the material properties (the fracture energy G_F). The fracture energy can be obtained from special experiments or it can be (with limited precision) computed (Karihaloo []).

The behaviour of the material in the compression is modelled in a similar way.

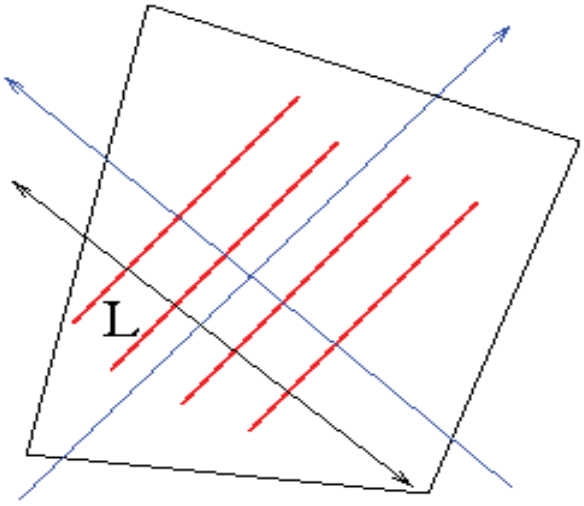

Figure 2. Lenght L of the cracked area

2.3. Model for bricks

The real bricks (or stones in stone masonry) have a different behaviour. They usually are much more brittle than the mortar. The material model for mortar can be also used for a modelling of bricks but it usually isn't ideal for this purpose.

We have prepared a different constitutive model. We assume that behaviour of bricks is linear elastic until the damage (crack) is detected. Usually, the crack goes throught the full height (or width) ob brick so it is obvious that the failure condition must respect this.

We have proposed a use an approach that is similar to non-local material models: the stresses in the brick are controlled on an area A with dimensions that are comparable with height of the brick. It should guarantee that crack is detected if the stresses in the brick are big enough to be able to create a crack. Thus a brittle demage of the brick should occur.

After the brick is damage the material properties should be changed. Now we have adopted the elasto-plastic behaviour of a material. After the crack is detected then the normal stiffness of the material (represented by Young's modullus) is reduced to zero. It is not an ideal approach because it means that the cracked material still carry the previous stresses but we selected it for the relatively ease of the implementation. After we will test the other parts ot the alghorithm (namely the computation of the failure condition) we will improve the behaviour of the cracked material to be more realistic.

3. ILLUSTRATIVE EXAMPLE

Model description

To show the behaviour of the model we have prepared a simple (not very realsisic) numerical example. The geometry is shown on the Figure 3. The sizes of bricks are 270x160 mm and the width of mortar is 10 mm in all cases.

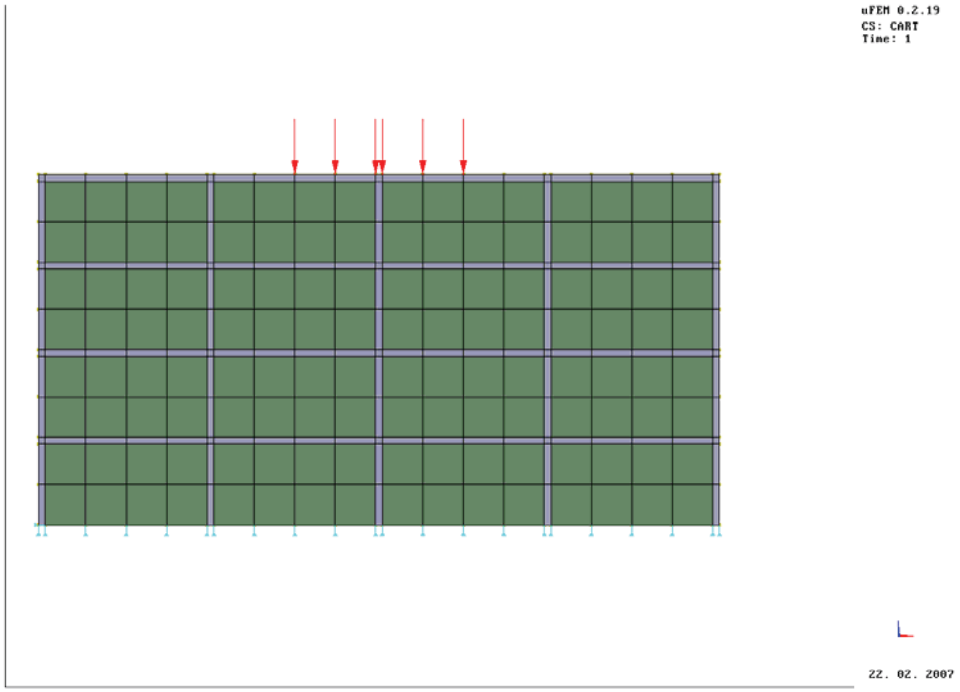

Figure 3. Illustrative example – finite element model

The Figure 4 shows the load-displacement relation that was obtained from the analysis of the model.

The relatively sharp change of the stress-strain curve is the result of a selected constitutive model of mortar – the bricks under the loading cracked in a moment and then the strength of the structure became reduced. From the Figure 4 it is obvious that the mortar has a relatively small influence of the results in this case.

The relatively high strength of a damaged material in this case was a result of a relatively large residual stiffness of a bricks (we used a elastoplastic model with hardening for the bricks here to help the convergence of solution).

The results show that the model features a behaviour that we have expected to obtain.

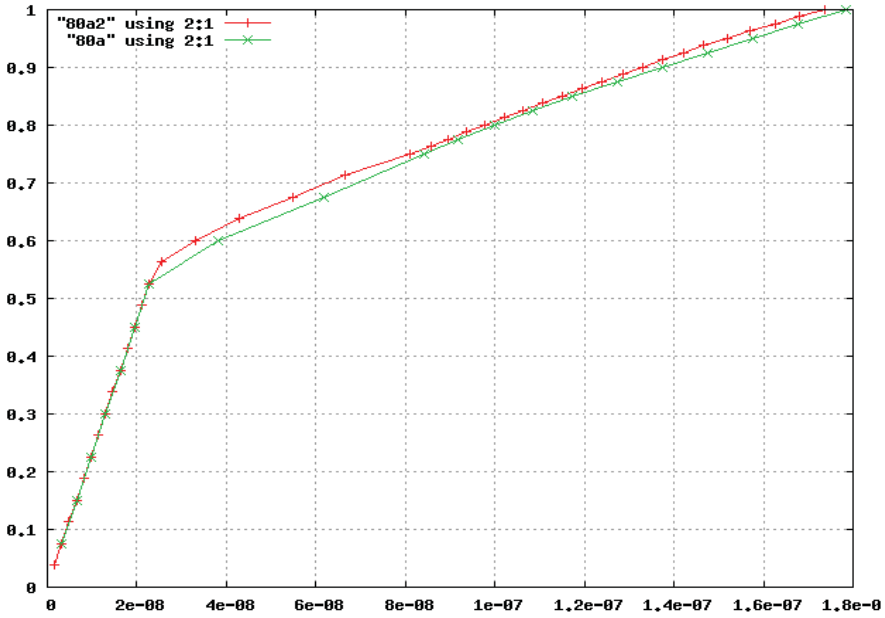

Figure 4. Computed stress-strain relation

4. CONCLUSIONS

The article shows a basic material model for masonry. It can be improved in several ways, namely in the area of the modelling of bricks.

Acknowledgements

The works are supported from the Czech state budget through the Czech Science Foundation. The project registration number is GA CR 103/03/P389.

References

1. Bazant Z. P., Planas, J., *Fracture and size effect in concrete and other quassibrittler materials*, CRC Press, Boca Raton, 1998.
2. Cervenka V., *Constitutive models for cracked reinforced concrete*, ACI Journal, vol. 82, 1985.
3. Cervenka V., *Inelastic finite element analysis of of reinforced concrete panels under in-plane load,* University of Colorado, Colorado, 1970

"Computational Civil Engineering 2007", International Symposium
Iaşi, România, May 25, 2007

Behavior of newly developed FRP reinforcement in structures under various load schemes

David Horak[1], Martin Zlamal[1], Petr Danek[2]
[1]*Department of Concrete and Masonry Structures, Brno University of Technology, Czech Republic*
[2]*Department of Building Testing, Brno University of Technology, Brno, Czech Republic*

Summary

An own reinforcement based on glass or carbon fiber reinforced polymers in frame a Czech ministry of industry and trade research task was developed. A set of experiments was made for reinforcing of concrete structures with this FRP internal reinforcement.

The developed reinforcement was used for reinforcing of several concrete elements. These elements were exposed to different types of loading. Their behavior was monitored to verify the functionality of new reinforcement. Based on this results it is possible to determine required properties of reinforcement used for every sort of reinforcing (longitudinal or shear reinforcement).

This reinforcement was also used to additionally strengthen the masonry vaults loaded with static and dynamic loads. Obtained results are compared with theoretic results of nonlinear numerical analysis of constructions.

KEYWORDS: Longitudinal and shear GFRP reinforcement, reinforced concrete structures, strengthened masonry vaults.

1. INTRODUCTION

At present non-metallic reinforcement is used very frequently (because of their resistibility) in constructions that are exposed to aggressive environment's influence. It makes possible to reduce costs needed for special arrangements for protection the common reinforcement and eventually consecutive repairs.

However the price of the non-metallic reinforcements is quite high (see Fig. 1). And because this reinforcement form the significant part of the final costs of the cross-section price, it is very advisable to (next to economical optimizing of the cross-section [1]) use local non-imported (i.e. probably cheaper) materials.

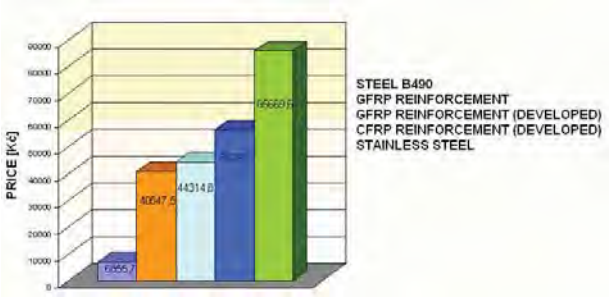

Figure 1. Comparison of the average prices in the Czech Republic (common materials and developed reinforcement)

The economic aspect mentioned above isn't in the Czech Republic so strong, because there isn't any native producer of this kind of reinforcement. While using it is necessary to import the reinforcement from abroad, which makes construction sometimes more expensive.

In terms of research in frame of the Czech Ministry of Industry and Trade, development of "home" reinforcement based on glass and carbon fibers has begun. It is of course necessary to check out functionality of this system – i.e. functionality of interaction of reinforcing bar and surrounding concrete.

But not only new concrete structures are in the centre of interest. Masonry continues to be popular because of its relative simplicity of application in the technical practice. Indeed, for a new use of structural masonry reasonable constructional rules are required, because conventional approach based on the experience is unacceptable nowadays. In addition, most methods of carrying capacity assessment and of strengthening for the existing masonry construction are increasingly based on analyses of mathematical simulation and appropriate (linear and nonlinear) computational models. One method of load-bearing elements strengthening is application of additional external non-prestressed reinforcement into chases in masonry on intrados of vaults, which will provide stiffening and increasing of load carrying capacity of the individual load-bearing elements.

The existing and especially historical masonry structures are nowadays considerably monitored. Many of them are in need of some retrofitting or strengthening. In such cases the non-metallic with minimal requirements for reinforcement cover even in aggressive environment could be the best solution. Therefore some tests were undertaken to learn about behavior of masonry vaults additionally strengthened with GFRP bars. These test logically followed previous research of the additionally strengthened masonry structures.

To achieve good usable results it is necessary to provide also statistical evaluation and theoretical backgrounds for further designs of such structures. Therefore all data obtained from the tests are used to create and verify the numerical model of

FRP reinforcement material used in calculations. This model should allow to predict as accurate as possible the behavior of concrete and masonry structures reinforced with FRP bars.

Mathematical model is created in physically non-linear FE software based on fracture mechanics of quasi-brittle materials. Results obtained from real tests are used as input data for all materials. It means all material characteristics for both concrete (strengths, modulus of elasticity, fracture energy, etc.) and non-metallic bars (tensile strength, load-deflection diagram, modulus of elasticity). The cohesion between reinforcement and concrete (grouting) is modeled via cohesion parameters for each type of the surfacing.

Comparison of the real and numerical results shows very good correspondence (some results are shown in the text below and in [2] and [3]).

1.1. Concrete reinforcement

Tests are performed in several partial fields:

- obtaining physical-mechanical characteristics of reinforcement,
- obtaining cohesion between reinforcement and concrete,
- monitoring behavior of specimens reinforced with non-metallic reinforcement (i.e. real function of reinforcement in loaded construction).

The first two research points were completed and all the results were analysed [2]. Choice of the most suitable type of reinforcement was achieved based on obtained results. The best cohesion with the concrete, material properties and demand factor of the production of the reinforcement and the surface preparation were confronted. All these parameters influence the price and the efficiency of the developed reinforcement.

After the decision about the surfacing of the reinforcement it was necessary to confirm the functionality of the reinforcement. Therefore several tests were performed on the concrete specimens. GFRP bars were used as both longitudinal and shear type of reinforcement.

1.2. Strengthening of the masonry structures

The method of additionally inserted non-prestressed reinforcement allows additional strengthening of masonry structures without a necessity of large intervention into vaults especially in case of external application. This system is capable redistributing newly originated stresses from load that act on a strengthened construction. The aim of reinforcement is to restrict the development of existing cracks and eliminate possibly an origin of the new ones, and to improve load-bearing capacity of vaulted masonry constructions.

From the static viewpoint, unreinforced masonry structure is unable to transfer tensile forces that can originate on existing structure from following action:

- action of the higher imposed load against the designed one,
- action of either identical or the lower load against the designed one.

Another consequence of the retrofit reinforcement application into masonry structures is the rigidity improvement. The effect is evident especially at the structures cracked by the previous traffic utilisation. Nevertheless, from the practical viewpoint this consequence could be smaller for railway bridges.

For reinforcing the masonry structures it were used two types of reinforcing materials (shape of this reinforcement bars can be seen in Figure 2):

- commonly used steel reinforcement (Helifix),
- non-metallic reinforcement (GFRP bars).

Figure 2. Shape of Helibar and wrapped surface GFRP

As a binding (transferring) medium between reinforcement and origin masonry was used special mortar (grouting substance). It is important to mention that it is essential the reinforcing bars compose with grouting substance and with origin masonry the reliable and durable system.

2. CONCRETE MEMBERS WITH LONGITUDINAL GFRP REINFORCEMENT

These tests are related to concrete beams (dimensions 350 x 100 x 2200 mm) reinforced only with longitudinal GFRP reinforcement (diameter 14 mm, one-side-wrapped bars).

This test was classical four-point bending test (Figure 3). The span of the beam was 2.2 m and the loading forces were applied at 1/3 of the length of the beam. Beams were designed to obtain failure caused by a bending moment. During the experiment following input data were monitored – force load, deflection on several points and strain of the reinforcing bars (monitoring units build into the reinforcement [2]).

Three specimens with the longitudinal reinforcement were exposed to load forces. Also three specimens without the reinforcement were loaded to provide reference data and to make possible the comparison of effects of the reinforcement. Results

of specimens without reinforcement allowed also validating the input data (i.e. material model of the concrete) used in FEM numerical model.

Figure 3. Deflection of the loaded beam before the collapse

All three reinforced beams collapsed because of exceeding the tensile strength of the GFRP bars. Two of them collapsed under the load force, one beam collapsed in the middle. Maximal average load carrying capacity of this beam improved from total 6.11 kN (calculation presumption 6.09 kN) to 17.19 kN (calculation presumption 16.38 kN - according to ACI 440.1R-03 without any safety factors). The tests results demonstrated the functionality of the developed non-metallic reinforcement.

The development of the load-deflection curve is in Figure 4. Also comparison of the behavior between reinforced beams (specimen 1-3), non-reinforced beams (reference specimens 1-3) and numerical model of the reinforced beam (Atena 3D results) can be found there.

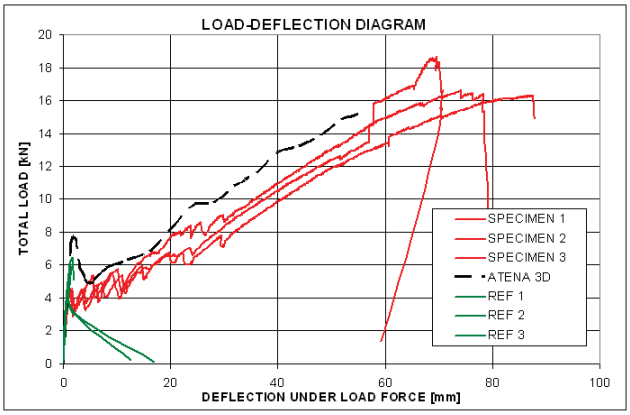

Figure 4. Deflection of the beam with longitudinal GFRP reinforcement

2. CONCRETE MEMBERS WITH LONGITUDINAL AND SHEAR GFRP REINFORCEMENT

The non-metallic reinforcement was tested also as shear reinforcement. The longitudinal reinforcement in these beams were the GFRP bars (diameter 14 mm, one-side-wrapped bars – same as mentioned before). The shear reinforcement was created from one GFRP bar (diameter 8 mm, one-side-wrapped bars) shaped into spiral looped around all longitudinal reinforcement bars – see Figure 5.

This reinforcement had to be shaped before hardening. Thus the curing method was changed and the curing of the already shaped and fixed reinforcement proceeded at the room temperature. The hardening of the bar took more time, but the material characteristics were not reduced.

Figure 5. Shear reinforcement shaped into spiral

All beams (dimensions 115 x 240 x 2100 mm) were loaded by the same way as the beams with longitudinal reinforcement only. It means the load scheme was classical four-point bending test with load points at 1/3 of the span. Supposed failure mode was exceeding the shear capacity in the area near supports.

Again the test set was made from three test specimens with shear reinforcement and from three "reference" specimens without shear reinforcement. The reinforcement influenced positively the shear capacity of the tested beam and confirmed its functionality. The shear capacity improved from 54.7 kN (reference specimens without shear reinforcement) to 82.2 kN (reinforced specimens).

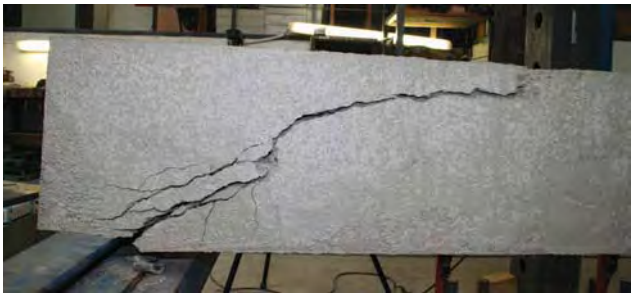

Figure 6. Cracked beam with GFRP shear reinforcement

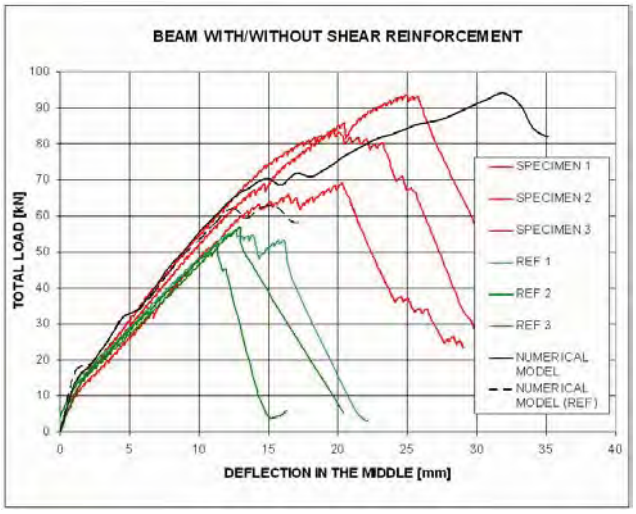

Figure 7. Deflection of the Beam with GFRP Shear Reinforcement
(REF Specimens are Reference Specimens Without Shear Reinforcement)

The tests results demonstrated the functionality of the developed non-metallic reinforcement.

3. MASONRY STRUCTURES STRENGTHENED WITH GFRP BARS

Within experimental parts of the project three sets of masonry vaults with for various loading types were manufactured. For the distinction of individual vaults are used notation jKi, where „j" corresponds to series number (1-3) and „i" to the strengthening method (1-3). The vaults were symmetrically loaded in ½ of the span

- 1.series (j=1), asymmetrically in ¼ of the span - 2.series and symmetrically in both quarters of the span - 3.series (j=3).

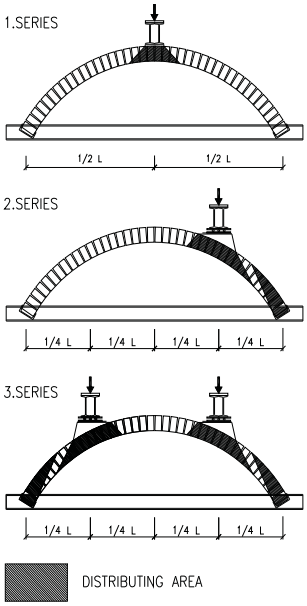

Figure 8. Loading scheme of the vaults and distribution zones of the load in the vaults

Each series consists of three vaults: non-strengthened – comparative (i=1), a vault reinforced in two chases (i=2) and a vault reinforced in three chases (i=3). The vaults were bricked up from full burnt bricks on lime-cement mortar of the width 890 mm, span 2600 mm, deflection 750 mm and radius 1500 mm.

Into every reinforcing chases were embedded 2 bars. First experiments were performed with reinforcement HeliBar of special helical shape of diameter 8 mm and the second set of test specimens were reinforced with GFRP bars of diameter 6 mm (one-side wrapped). Only unsymmetrical loading in ¼ of the span was used for testing vaults with non-metallic reinforcement (it is the case of the biggest influence of the additional strengthening [4]).

3.1. Behavior under static load

From the comparison of the load-bearing capacity of the individual vaults in the series results that essential growth of the load-bearing capacity was achieved especially in the case of 1st series and 2nd series of the vaults, namely more than eight multiple growth. This growing of carrying-capacity can be watch for both cases of reinforcement – helical metallic and non-metallic. It was related to the

vaults stressed by either concentrated or one-sided load, at which the vaults were loaded by the interaction of normal forces and bending moments.

In the case of 3rd series the experiments did not prove the effects of strengthening by additionally inserted reinforcement on the vaults load-bearing capacity; no effects of reinforcement demonstrated themselves because the vaults were mainly compressed.

In the case of non-strengthened vaults of 1st and 2nd series the failure was acute, main crack was opened and the vault ruptured. In the case of the strengthened vaults of 1st and 2nd series came to the gradual opening of separate cracks until the failure, which was accompanied by the rapture of the metallic reinforcement from the chases. All glass reinforcing bars were in the ultimate limit state ruptured.

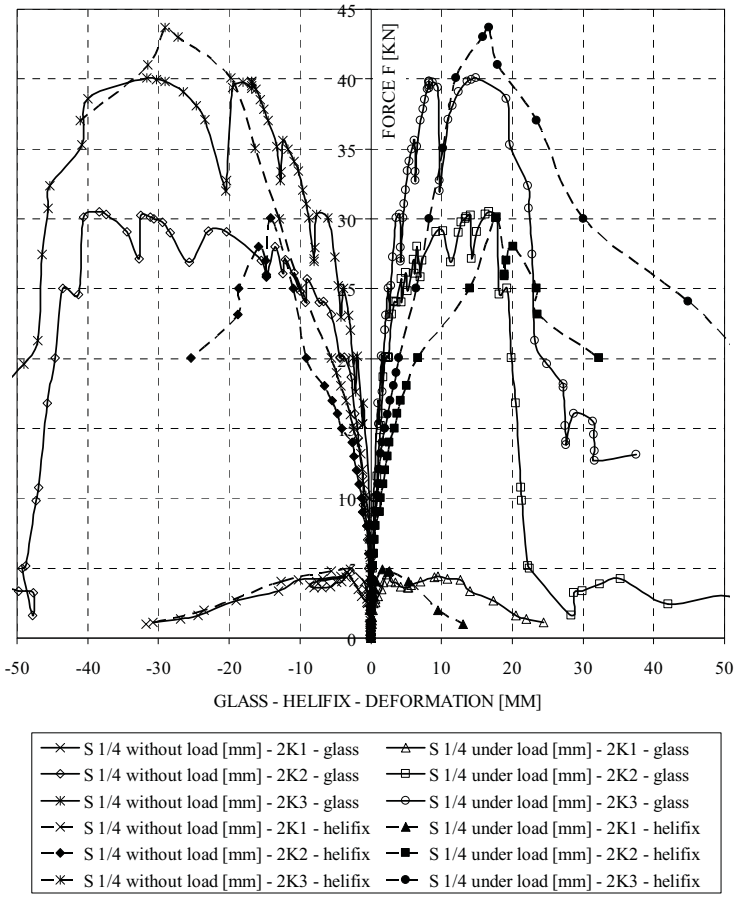

Figure 9. Comparison of deformations on vaults loaded in ¼ of the span strengthened with GFRP and metallic helical reinforcement

On the basis of thus obtained results from numerical studies and on the base of the designed algorithm, it will be possible to obtain (substantiate) simple constitutive relations for the evaluation and design of strengthening by simplified designed methods used in the practice and to set up simple algorithms for design and checking calculation of the masonry vaulted construction with additional reinforcement for the practice.

3.2. Behavior under dynamic load

Dynamical tests were performed on vaults loaded asymmetrically in 1/4 of the span and reinforced with glass reinforcement (GFRP) only. From results of first dynamical tests it is visible increasing of load-bearing capacity of the reinforced vaults (2K2, 2K3) compared to the non-reinforced vault (2K1) (Figure 10).

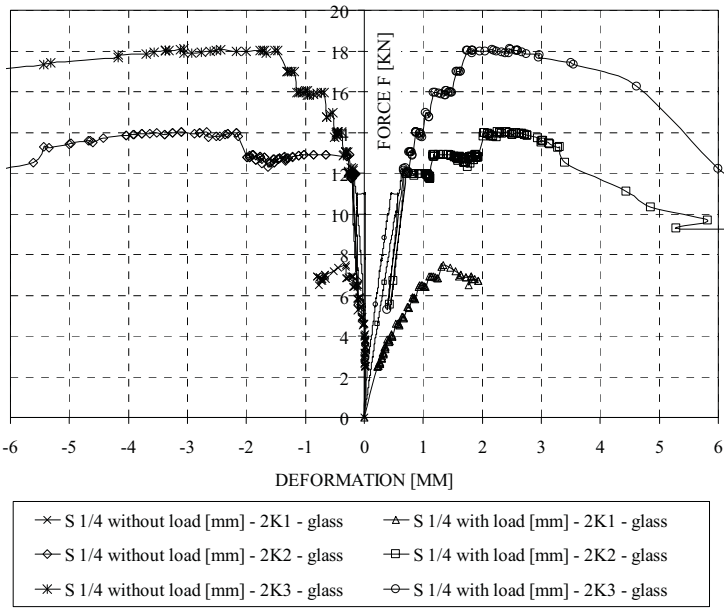

Figure 10. Comparison of deformations on vaults loaded in ¼ of the span strengthened with GFRP reinforcement – dynamical test

Unfortunately the low set of tested specimen prohibited comparison with the test data from statical experiments. The results are also influenced by the big non-homogeneity of masonry structure. Also the fracture mode (i.e. failure of the vault by opening of tension cracks in the bed joint) is not uniform and the position of cracks can influence the final load bearing capacity.

Strengthened vaults can be partially compared by relation of their load-bearing capacity. Ratio of the load-bearing capacity of the vaults with three reinforcing chases and with two chases (2K3/2K2) at statical loading is 1,33 and at dynamical loading is 1,29.

3. CONCLUSION

The tests showed that the developed system is functional. The reinforcement bars can work as concrete reinforcement and they are capable to transfer the load forces generated in the construction during the loading.

There is also very positive benefit for the strengthening of the masonry vaults. This system can be used to repair the historical structures with minimal impact to the structure itself (thanks to low requirements for cover – there is no need to provide additional layers of cover materilas).

So far only short term tests were performed. To fully confirm the functionality and safety of the newly developed reinforcing system it will be necessary to verify the long term characteristics of the reinforcement. The main subjects of research will be the behavior of the reinforced structures under the long term loads. Also the resistibility of the reinforced structures in the aggressive environment has to be verified.

Acknowledgements

This research has been proceeded with support of Czech ministry of industry and trade (MPO) in frame research task 1H-PK2/57 – “Durable concrete structures” and also has been prepared with the financial support of Ministry of Education, Youth and Sports, project No. MSM0021630519 “Progressive reliable and durable load bearing structures”.

References

1. Plsek, J., Stepanek, P., Optimisation of design of croos-section in concrete structures, *Procceding of the 4th International Conference Concrete and Concrete Structures*, 2005.
2. Stepanek, P., Fojtl, J., Horak, D., Pull-out test of non-metallic FRP reinforcement for concrete structures, *Proceedings of the 4th International Specialty Conference on Fibre Reinforced Materials*, 2006, Hong Kong.
3. Horak, D., Krupa, P., Stepanek P., Prokes, J., Development of the new methods of measurement of the strain in GFRP concrete reinforcement, *Worshop NDT 2006 – Non-destructive testing in engineering practice*, 2006, Brno, Czech Republic.
4. Stepanek, P., Zlamal, M.: Additional strengthening of masonry vaults with non-prestressed additional reinforcement, *Proceeding “STRUCTURAL FAULTS + REPAIR-2006”*, 2006, Edinburgh, Scotland.

"Computational Civil Engineering 2007", International Symposium
Iaşi, România, May 25, 2007

New Shear Connectors for Composite Girders – Experiences with ABAQUS Push-Out Test Simulations

Josef Fink [1], Lubomir Ondris [2]
Institute of Steel Structures, TU Vienna, Karlsplatz 13/212, A-1040 Vienna, Austria

Summary

Composite structural members consisting of steel and concrete parts utilize the advantages and suppress the disadvantages of individual material components. The shear loading between steel and concrete parts is transferred by shear connectors. They have to be designed to maximize the shear load capacity and ductility and to minimize the overall manufacturing costs.

At the Technical University of Vienna, Institute of Steel Constructions, new shapes of shear connectors for composite steel and concrete beam structures are being developed. The composite structure consists of steel I-beam with connector welded lengthwise in the middle of the flange and surrounded by a concrete reinforced slab. The first sheet-type crown shaped connector has already been accepted for patent procedure. To verify its efficiency both numerical analyses and physical experiments with push-out tests were carried out. For numerical analyses of composite structures the well-established FE-program ABAQUS is used. Results depend on many material and control parameters therefore first an extensive parametric study was necessary /1/. Here missing information is given, originally suppressed in /1/ because of patent protection procedure. Further numerical experiences with different loading velocities, with ABAQUS option NLGEOM and experiences relating to results evaluation are described. Different results of ABAQUS versions 653 and 662 are mentioned. Necessity of a very careful preparation of numerical simulation and of using realistic material data for concrete is emphasized.

A comparison in /2/ shows a very good matching between physical tests and numerical simulation.

KEYWORDS: Composite steel and concrete beam structure, welded shear connector, push-out test, finite element modeling, ABAQUS, material model for concrete, loading velocity, geometric nonlinearity, kinetic energy, total strain energy, new shape of shear connector.

1. INTRODUCTION

Developing of new sheet-type connectors at the Technical University of Vienna, Institute of Steel Structures consists of physical tests with push-out specimens and of their numerical simulation as well. A recent extensive parametric study /1/ of options given in the known FE-program ABAQUS /3-5/ was concerned with a new sheet-type crown shaped connector. After accepting it by European Patent Office in Vienna for patent procedure under proposed name "VieCro", the information originally suppressed in /1/ can here be given for completeness.

The welded steel parts of the specimen can be seen in Fig. 1. In Fig. 2 the complete specimen with reinforced concrete slabs is ready for testing in a horizontal loading machine. In Fig. 3 the basic parts of the FE-model utilizing twofold symmetry are shown. Because of their very high stiffness, the head plate and the I-beam could be removed from the FE-model and replaced by corresponding boundary conditions. The loading was simulated by prescribing boundary condition on the lower surface of the steel connector (welded to the I-beam) in longitudinal direction. ABAQUS static and dynamic nonlinear procedures have been invoked, using quadratic FE-elements C3D20R and linear FE-elements C3D8R, respectively.

In /1/ results of 123 FE-calculations are given in form of P-d diagrams, d being the actual value of the prescribed connector displacement, P being the corresponding total reaction force in supported right side surface in Fig. 4. In diagrams the influence of ABAQUS material parameters, of friction coefficient in frontal and lateral contact surfaces and of clamped or contact support while using static and dynamic solution procedures can be observed.

2. DIFFICULTIES WITH NUMERICAL SIMULATIONS

The difficulties are caused by highly nonlinear character of the problem and by missing specific material parameters for concrete. If there is no P-d diagram from physical test and/or if the material data are not reliable then it is not easy to decide whether the calculated peak load, post-peak response and failure load are "true" i.e. whether they correspond to the parameters chosen only or whether they are influenced also by potential "internal" numerical instabilities.

In a recent EU-Project FE-packages ABAQUS, ANSYS, DIANA, GEFDYN and LUSAS used for solution of concrete dams have been compared /6/. It has been confirmed that the result of a complex highly nonlinear problem often depends on nonlinear control parameters used. According to /6/, correct estimating of the failure load using a non-convergence stopping criterion is problematic because with a "wrong" criterion the non-convergence on relatively small loads can occur. The quotation marks signalize some uncertainty always present while solving complicated nonlinear problems: The result depends on the solution path, this

again depends on a set of parameters used. Every change in parameters used means a different solution path, sometimes with surprising effects.

Because of problems described a very careful preparation of solution strategy and mesh data and a very thorough results evaluation is necessary. Even then it is always useful to carry out more calculations with slightly changed parameters to check the result sensitivity.

Throughout the study /1/ emphasis has been placed on the highest possible accuracy and reliability of the system answer rather than on efficiency of calculations. As far as possible, for the most control and material parameters ABAQUS default values were used uniformly throughout all calculations.

With static calculations maximum number of iterations as a general stopping criterion was set sufficiently high (and never reached), for starting and minimum increments very small values were set. With dynamic calculations the ABAQUS default automatic incrementation with global stable increment estimator was used.

3. SOLUTION PROCEDURES

From ABAQUS nonlinear procedures tested in /1/ (*STATIC,RIKS, *STATIC,STABILIZE, *DYNAMIC,EXPLICIT) the last one seems to be the most suitable for simulation of physical push-out tests. The reasons why just an explicit integration package like ABAQUS/Explicit should be used for solving highly nonlinear problems are convincingly given in /7/. Practical comparison of results obtained by particular procedures is given in /1/.

4. FE-MODEL FOR DYNAMIC ANALYSES

With the *DYNAMIC,EXPLICIT procedure of ABAQUS/Explicit package only linear elements can be used. However, the FE-model has to take into account material and contact nonlinearities and the geometry of the connection.

The authors prefer a rather conservative solution with some "FE-overkill". The mesh for dynamic analyses (Fig. 4) consists of following parts: steel connector: 6474 linear 8-node hexahedrons C3D8R (3 elements crosswise on the half-thickness of 10 mm), concrete slab: 30495 elements C3D8R, reinforcement: 525 elements T3D2, each anchor rod: 1 element T3D2. This mesh is able to register high stress gradients occurring in interactions between sheet connector and concrete parts near connector.

5. MATERIAL MODELS

ABAQUS material models used are completely described in /1/, thus the description will not be repeated here. It is to emphasize that for concrete parts a characteristic material curve with loss of strength after reaching the tensile strength has been used instead of artificial material features.

For steel parts an elastic-ideal plastic model without hardening was used.

6. FRICTION IN CONTACT SURFACES

In /1/ each calculation has been carried out three times with friction coefficients 0.3, 0.5, 0.7. For simplicity, between frontal surfaces (Fig. 5) the same friction coefficient was used as between lateral surfaces (Fig. 6). Generally, P-d curve from physical experiment, especially in post-peak area, can better be approximated in numerical simulation using small friction coefficient. Calculations in /8/ confirm this conclusion and analyse the contribution of frontal and lateral friction.

7. RESULTS EVALUATION – ENERGIES AND VISUAL INSPECTION

In dynamic calculations used for simulation of quasi-static processes an important role plays the ratio of kinetic energy to internal energy ALLKE/ALLIE with a peak value accompanying distortion. ABAQUS-recommendation that ALLKE/ALLIE should not be over 0,05-0,1 has to be used with some caution. The ultimate value can be different if the distortion is localized in a small area and the energy output in history output request is required for the whole FE-model. This is the way how the ratio ALLKE/ALLIE is judged usually, at least in first calculations. In all calculations described in /1/ and here energies were output for the whole model.

It turns out that in the curve ALLKE/ALLIE-d sometimes the existence of the peak regardless of its magnitude determines the distortion process. Usually, the peaks are very narrow and disappear soon. Often they can not be observed because of such a trivial reason as too big distance between output points. Also in such cases a careful visual inspection of deformed mesh using deformation scale factor > 1 can detect beginning of distortions or numerical difficulties since the accompanied oversized unnatural displacements do not disappear.

8. LOADING VELOCITY

Dynamic explicit calculations in /1/ have been carried out conservatively with a very small constant velocity of v=0.5 mm/s (prescribed connector displacement linear increasing with time). Using higher velocities can shorten the computer times substantially, on the other side inertial forces can arise and influence the result. Therefore it would be useful to find the upper bound of admissible velocities for quasi-static calculations of structures in question.

First, push-out test simulations based on an anvil connector shape (red in Fig. 7) and utilizing two planes of symmetry have been carried out. ABAQUS concrete material model CDP with dilation angle $\psi=30^{o}$, friction coefficient f=0.5 between interaction surfaces, clamped support surface and loading in the same way as in /1/ but using five constant loading velocities v were used. The corresponding Pmax-v diagram (Fig. 8) was however unacceptable, contradicting expectations. By detailed inspection of particular solutions it has been found out that, in contrary to /1/, the pre-peak response in P-d diagrams is characterized by several irregularities (Fig. 9). For example, upon velocity v=1 mm/s, the first peak value at d=0.5 mm (blue in Fig. 9) is followed by a downcome caused by local numerical problems which can clearly be seen in Fig. 7 (excessive local displacements; deformation scale factor: 10) and on ALLKE/ALLIE-d curve in Fig. 10. Just the curve for v=2 mm/s could be accepted for estimating Pmax as a measure for inertial effects. Differences in Pmax and irregularities are not caused by inertial forces directly but by the extreme numerical instability of the solution: Already a negligible parameter change (in this case the loading velocity v) effects on the solution path. Thus, simulations based on an anvil connector shape could not be used to identify the range of admissible velocities.

After this experience the influence of the loading velocity has been examined using the simplest possible example. The test beam 100x100x200 mm consisting of concrete only (without any contact interactions and steel parts) was clamped on one end and loaded by prescribed displacement of -25 mm on the opposite surface. Again, linear increasing displacement was prescribed. Following constant velocities were used: v=0 (static solution), 0.5, 5, 25, 100, 500, 1000 mm/s.

ABAQUS CDP material model and C3D8R elements were used. Because of twofold symmetry only 1/4 of the beam has been meshed. In Fig. 11 the final deformed shape with Mises stress upon v=5 mm/s can be seen. The corresponding Pmax-v diagram in Fig. 12 conforms to expectations. In Fig. 13 the pre-peak response up to v=5 mm/s is free of irregularities (diagram parts with d>2 mm do not contain any substantial information and are omitted). Clear visible is the force delay upon v=100, 500 and 1000 mm/s due to the distance between the surface on the left with applied displacement d and the clamped surface on the right with the reaction force P. Thus, upon higher velocities the solution is ever more dominated

by inertial effects unacceptable in a quasi-static structural response. ALLKE/ALLIE values in Fig. 14 confirm the conclusion that in this type of problems the constant loading velocity should not exceed, let's say, just to be sure, 10 mm/s.

However, also the difference between ABAQUS procedures is to be noticed. With the procedure *STATIC (v=0) the peak load of Pmax=115.2 kN is slightly higher than with the procedure *DYNAMIC,EXPLICIT (v=5 mm/s: Pmax=109.9 kN), both being used with NLGEOM=YES..

At last, push-out test simulations based on a crown shaped connector (in /1/ loaded by v=0.5 mm/s) have been recalculated using additional loading velocities v=5, 25, 100, 1000 mm/s. As in /1/, support with contact interaction, concrete material CDP M2, dilation angle ψ=36.31, friction coefficient f=0.3 and NLGEOM=YES were used.

Corresponding P-d curves can be seen in Fig. 15 (diagram parts with d>10 mm do not contain any substantial information and are omitted). The P-d curve for v=0.5 mm/s was already given in Fig. 27 of /1/.

Generally, P-d curves for support with contact interaction are characterized by oscillations, the same curves for clamped support are smooth (Fig. 28 in /1/). In Fig. 15 only the curves v=0.5 and v=5 mm/s are acceptable. The bifurcation of P-values after reaching peak area could not be explained yet. The reason is probably again an extreme numerical instability of the solution process.

With v=25 mm/s and more, oscillations become dominant and influenced by inertial effects. Also the force delay is clear visible. The ALLKE/ALLIE values in Fig. 16 are acceptable for v=0.5 and v=5 mm/s only.

In Fig. 17 Mises stress is shown to demonstrate the influence of inertial effects. Upon the velocity v=1000 mm/s the lower red part of the steel connector moving to the right is already upon d=0.76 mm (ideally) plastic, whereas the support reaction force on the specimen right side still equals zero. The yielding area in this case is not originating around contact points with concrete as usually but due to prescribed fast growing displacement on lower connector surface.

A general recommendation concerning the highest admissible loading velocity for numerical simulation of push-out tests can not be given. It is not easy to distinguish whether the difference in peak values and/or calculation break were really caused by inertial effects or by taking a different solution path. The critical velocity value depends on many parameters, e.g. connector shape, mesh quality, boundary conditions used, way how the loading is applied, and so on. Therefore, not only P-d curves should be compared but also ALLKE/ALLIE values have to be checked and the deformed mesh should be carefully visually inspected throughout the solution. At least two calculations with different loading velocities are to be carried out. If the results differ substantially, the reasons have to be investigated in more detail.

9. USING NLGEOM AND DOUBLE PRECISION

This option on the data card *STEP controls the inclusion of nonlinear effects of large displacements. With static procedures in ABAQUS/Standard default setting is NLGEOM=NO, with the procedure *DYNAMIC,EXPLICIT in ABAQUS/Explicit default setting is NLGEOM=YES.

In /1/ all calculations have been carried out taking into account the nonlinear effect of large displacements. In dynamic calculations in post-peak response this has led to very long calculations offering at last nonrealistic distorted FE-mesh by far not corresponding to the brittle behavior of concrete especially in situations with no or little reinforcement. E.g. the curve v=0,5 mm/s in Fig. 15 ends at d=23,6 mm, but between d=11,8 mm (expressive ALLKE/ALLIE-peak) and d=23,6 mm (calculation collapse) the structure in Fig. 18 (suppressed Fig. 30 in /1/) is nonrealistic distorted and the calculation does not give any real information. Therefore, using NLGEOM=NO can be a reasonable alternative generally, not only if BRITTLE material model is used.

Generally, always DOUBLE PRECISION solution should be used. Upon SINGLE PRECISION the solution process aborts prematurely and using NLGEOM=YES does not change the situation substantially.

10. ABAQUS VERSIONS 653 AND 662

For calculations in /1/ ABAQUS version 653 was used. At TU Vienna shortly a new computer system came into service using ABAQUS version 662. Calculations on both systems with the same input file showed in P-d diagram considerable differences in post-peak area. The reason could not be explained yet.

11. CONCLUSIONS

The basic question is which goals are to be fulfilled by numerical simulation of physical push-out tests. A pure matching of the P-d curve from an existing physical test can be achieved also by using a coarse FE-mesh, inadequate material model "sometimes without regard to the reasonableness of the material input variables" /9/ and controversial calculation parameters. Such a simulation, of course, keeps the simulation costs minimal. However, it proves rather the versatility of the FE-program and the user's inventiveness than an accurate representation of the physical behavior itself.

A consequent numerical simulation should not only match the data record from a foregoing physical test. It also should be able to reduce the number of physical tests in the course of selecting more effective connector shapes. This goal can be achieved only by a detailed visual inspection of analysis results get by a reliable FE-calculation. This has to be based on a sufficiently fine mesh (one linear finite element crosswise the modeled steel connector half-thickness is not sufficient to follow stress gradients), on a realistic material model (no "ideal plastic concrete" in tension), on a tolerable loading velocity (for safe excluding of additional inertial forces), etc. In case of doubts the influence of an unknown (e.g. material) parameter has to be checked by changing its value and repeating the calculation.

In near future the authors will continue developing of new connector shapes accompanied by exploring the influence of reinforcement location on properties of specific connector shape in composite steel and concrete beam structures.

Acknowledgment

The corresponding author thanks to Wojciech Lorenc for valuable and inspiring discussions /10/. Other research colleagues are encouraged to join and exchange experiences, too.

References

1. Fink J., Petraschek Th., Ondris L.: Push-Out Test Parametric Simulation Study of a New Sheet-Type Shear Connector, in: Projekte an den zentralen Applikationsservern, Berichte 2006, Zentraler Informatikdienst (ZID) der Technischen Universität Wien, Wien 2007, pp. 131-153, also: http://www.zid.tuwien.ac.at/projekte
2. Fink J., Petraschek Th., Ondris L.: Neuartige Schubverbinderleisten – experimentelle Untersuchungen und numerische Vergleichsbetrachtungen, ÖIAZ, accepted for publishing 2007
3. Hibbitt, Karlsson & Sorensen, Inc.: ABAQUS/CAE, ABAQUS/STANDARD, ABAQUS/EXPLICIT, Dokumentation Ver. 6.5.3, http://www.abaqus.com
4. ABAQUS Verification Manual, 2.2.24
5. ABAQUS Example Problems Manual, 2.1.15
6. Jefferson A.D., Bennett T. and Hee S.C.: Fracture Mechanics Based Problems for the Analysis of Dam Concrete, NW-IALAD-Final Technical Report-Task Group 2.4, Cardiff University (UWC), 15. March 2005
7. Zimmermann S.: Finite Elemente und ihre Anwendung auf physikalisch und geometrisch nicht-lineare Probleme, Report TUE-BCO 01.05, Technische Universität Eindhoven, Niederlande, März 2001
8. Iwancsics M.: Numerische Untersuchungen zu neuartigen Schubverbindern, Diplomarbeit, Institute of Steel Structures, TU Vienna 2007
9. Evaluation of LS-DYNA Soil Material Model 147, Report No. FHWA-HRT-04-094, November 2004, Federal Highway Administration, 6300 Georgetown Pike, McLean, VA 22101-2296
10. Lorenc W., Institute of Building Engineering, Wroclaw University of Technology: Private Communication 2006-2007

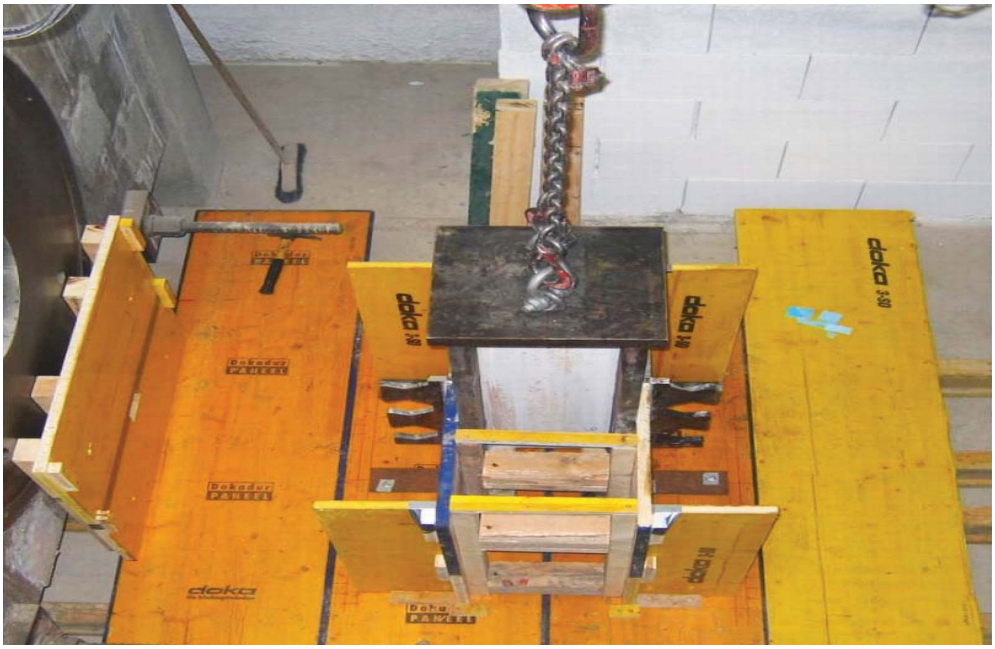

Fig. 1 Push-out specimen's welded steel parts

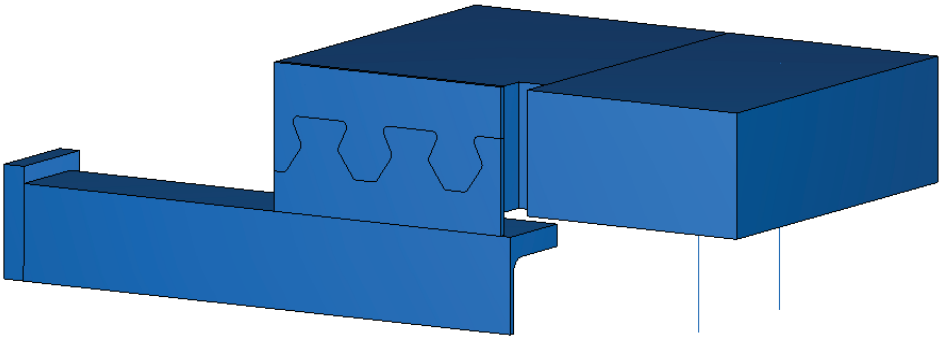

Fig. 3 Basic parts of the FE-model with twofold symmetry

Fig. 2 Complete push-out-specimen ready for testing

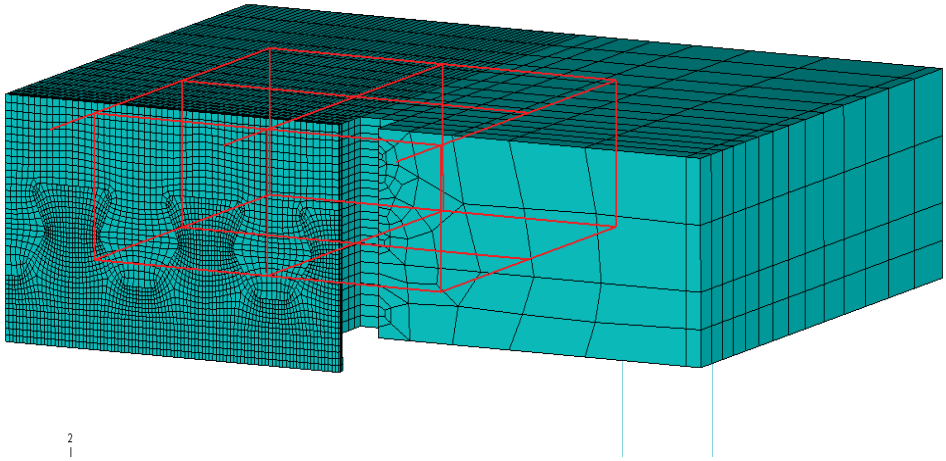

Fig. 4 FE-mesh for dynamic analyses incl. reinforcement, contact support on the right

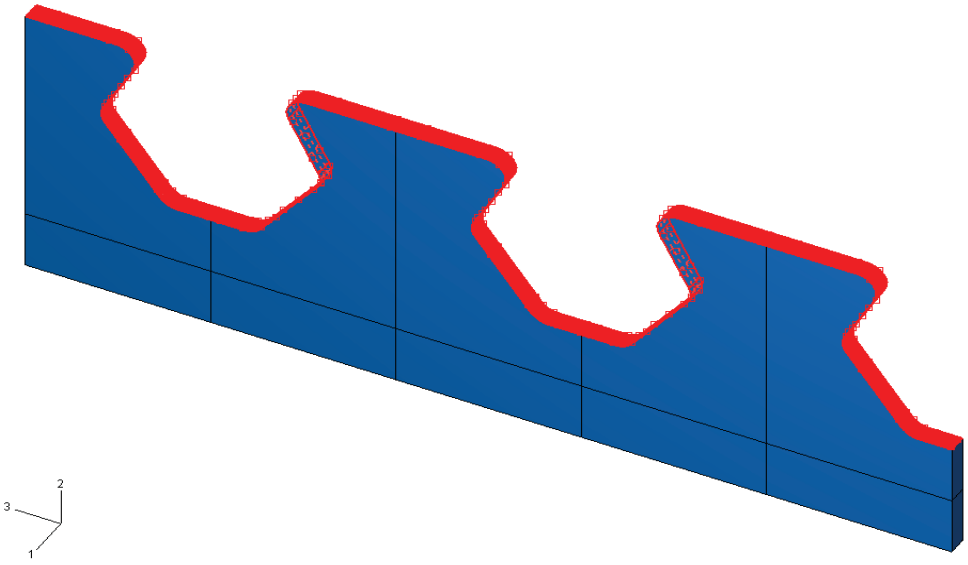

Fig. 5 Frontal master contact surface of the steel connector

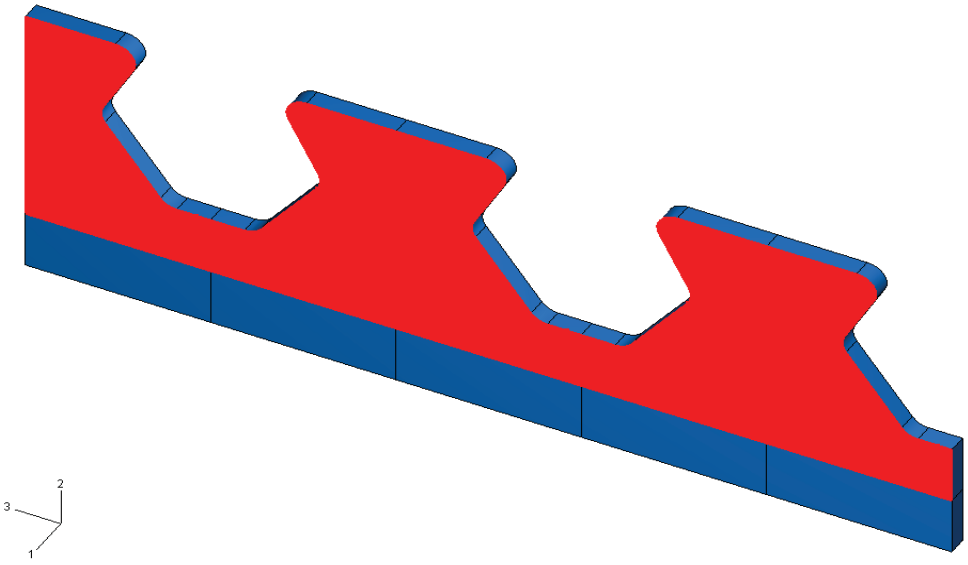

Fig. 6 Lateral master contact surface of the steel connector

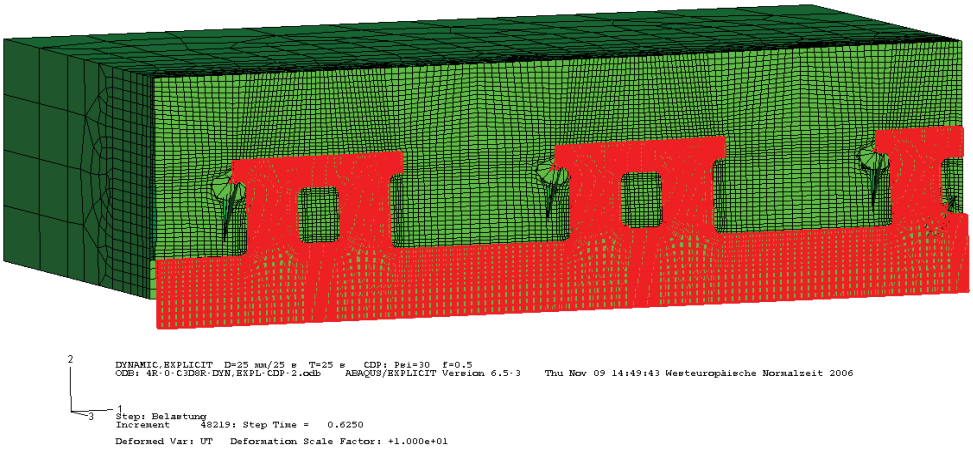

Fig. 7 FE-simulation with anvil shape connector, v= 1 mm/s, d=0.625 mm

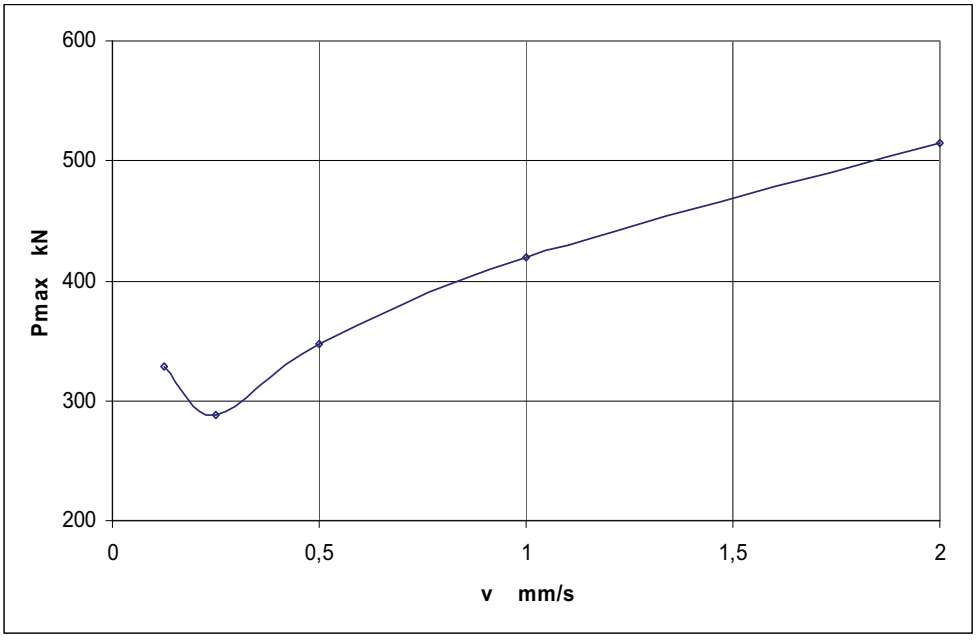

Fig. 8 Pmax – v curve, anvil shape connector

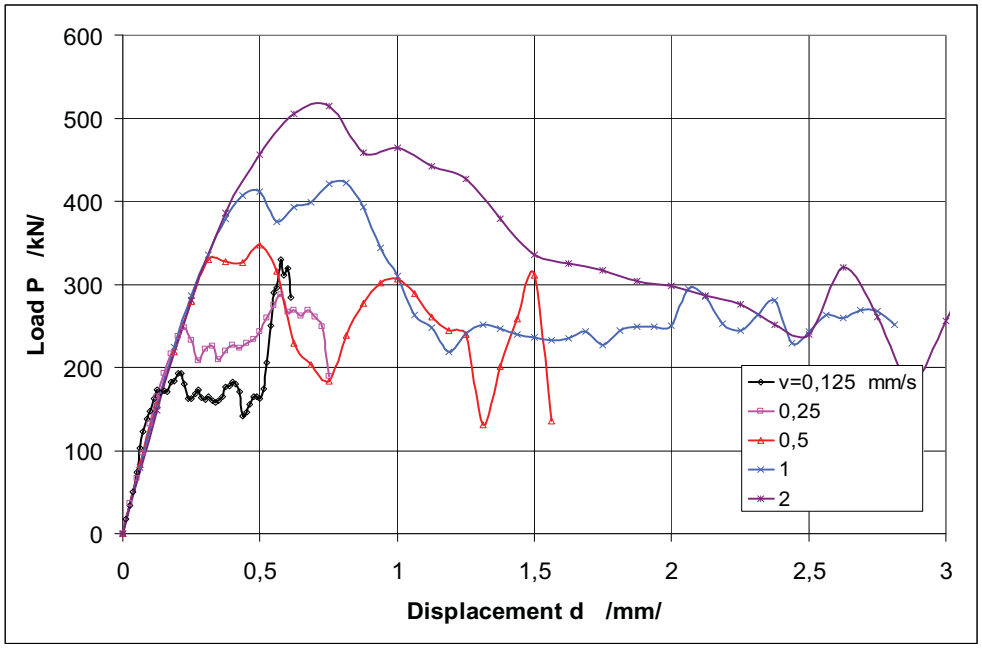

Fig. 9 P-d curves, anvil shape connector

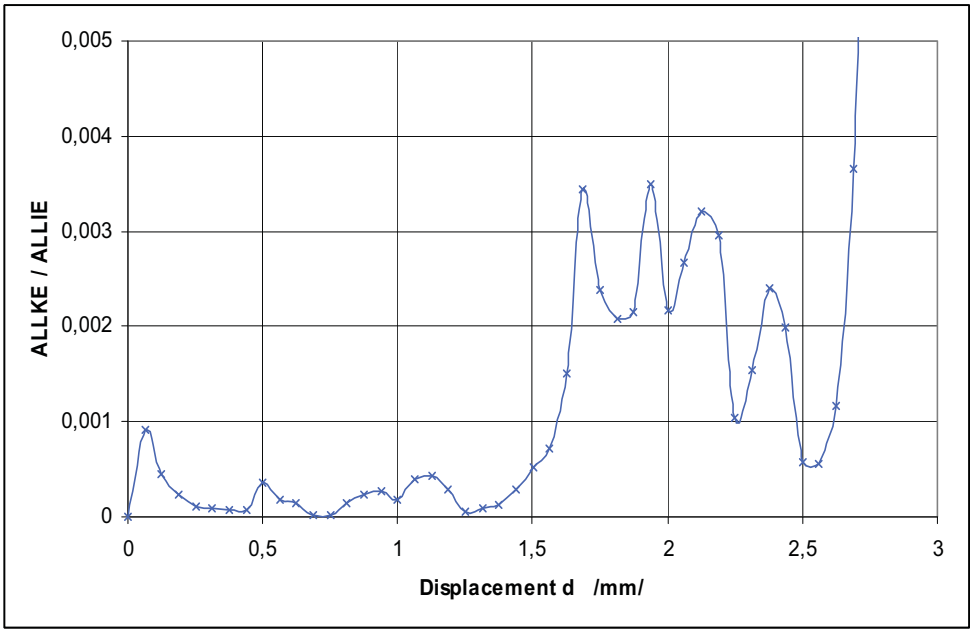

Fig. 10 ALLKE/ALLIE-d curve, anvil shape connector, v=1 mm/s

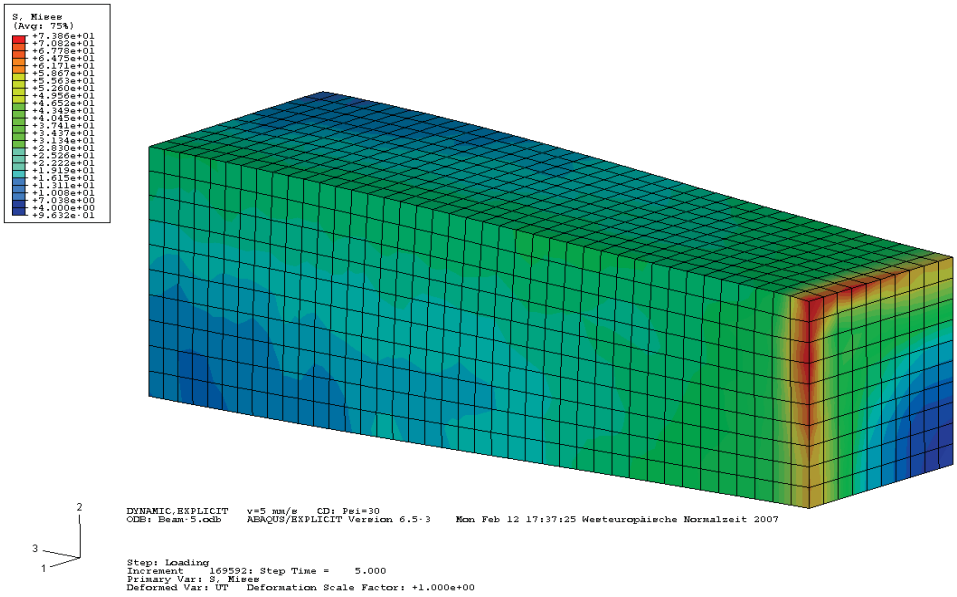

Fig. 11 Simple concrete beam with displacement controlled loading

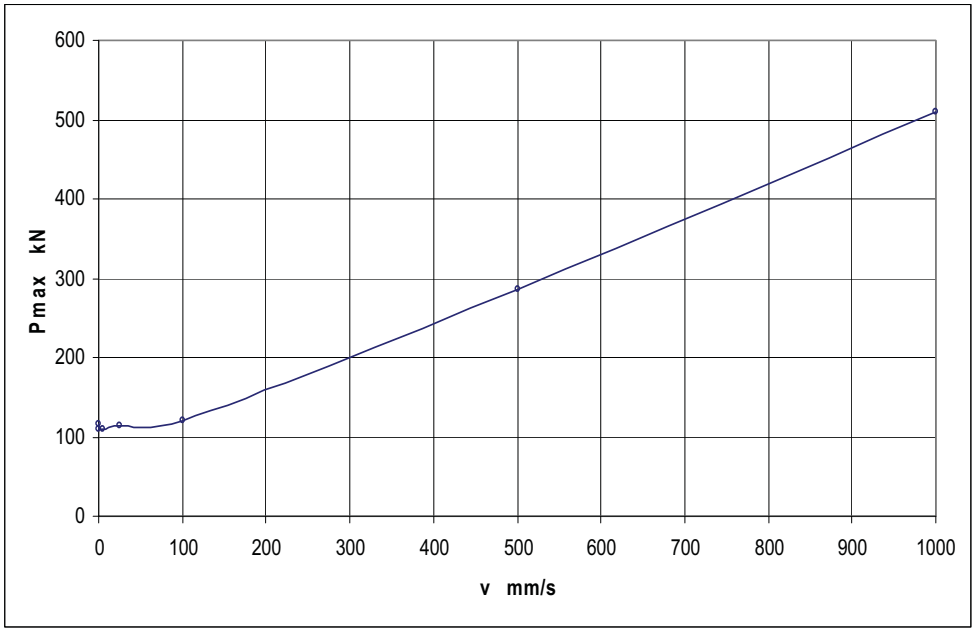

Fig. 12 Pmax – v curve, simple concrete beam

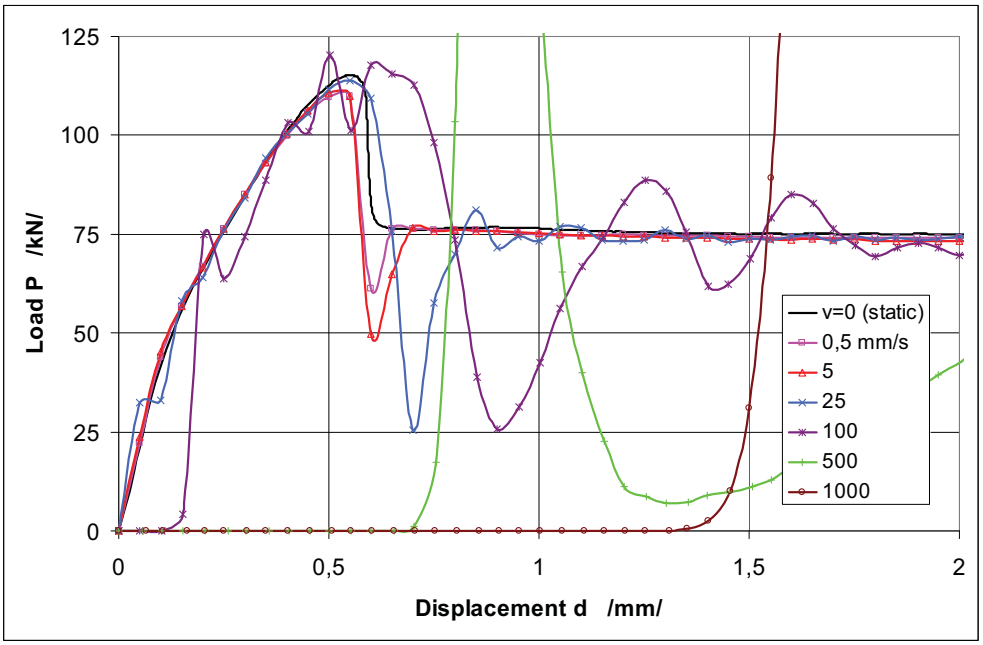

Fig. 13 P-d curves, simple concrete beam

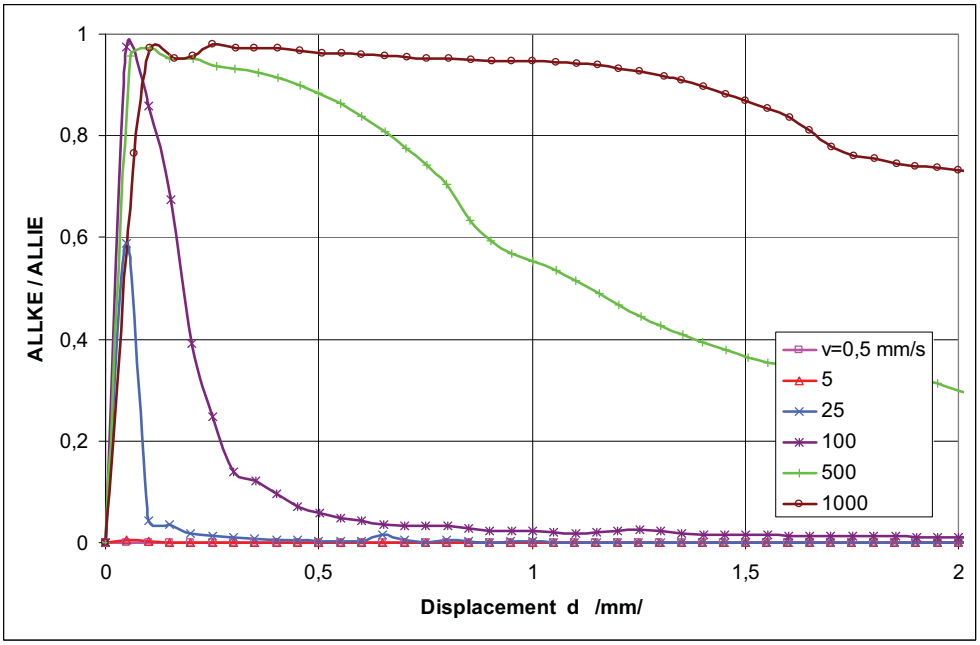

Fig. 14 ALLKE/ALLIE-d curves, simple concrete beam

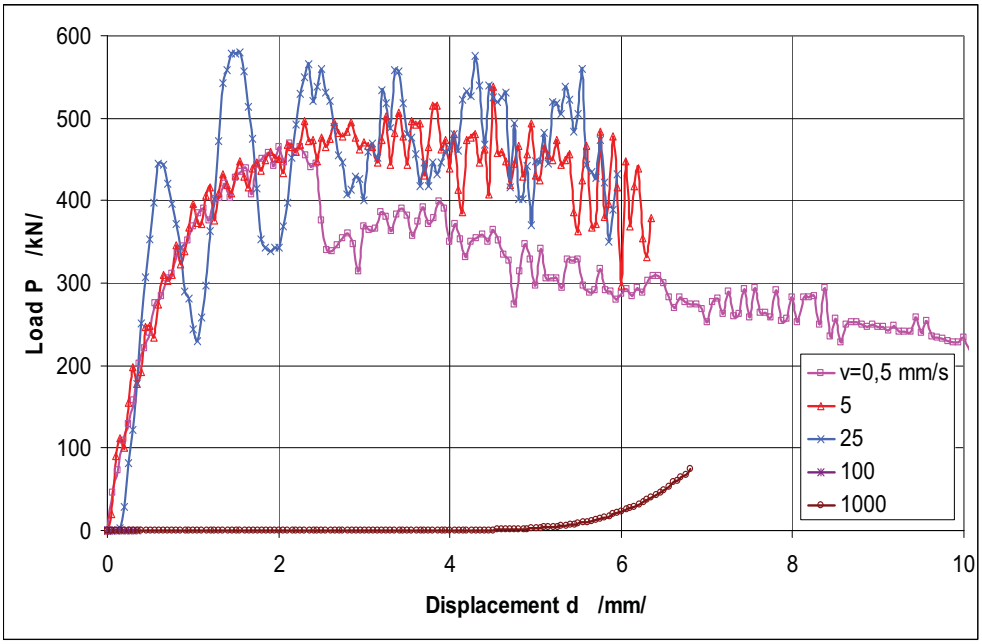

Fig. 15 P-d curves, crown shaped connector /1/, NLGEOM=YES

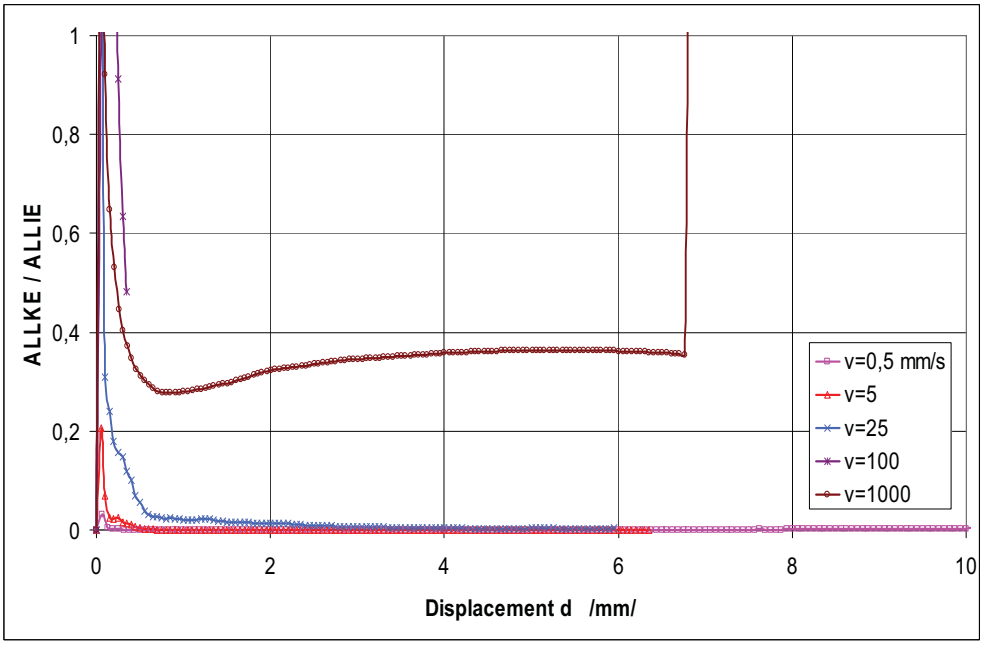

Fig. 16 ALLKE/ALLIE-d curves, crown shaped connector /1/, NLGEOM=YES

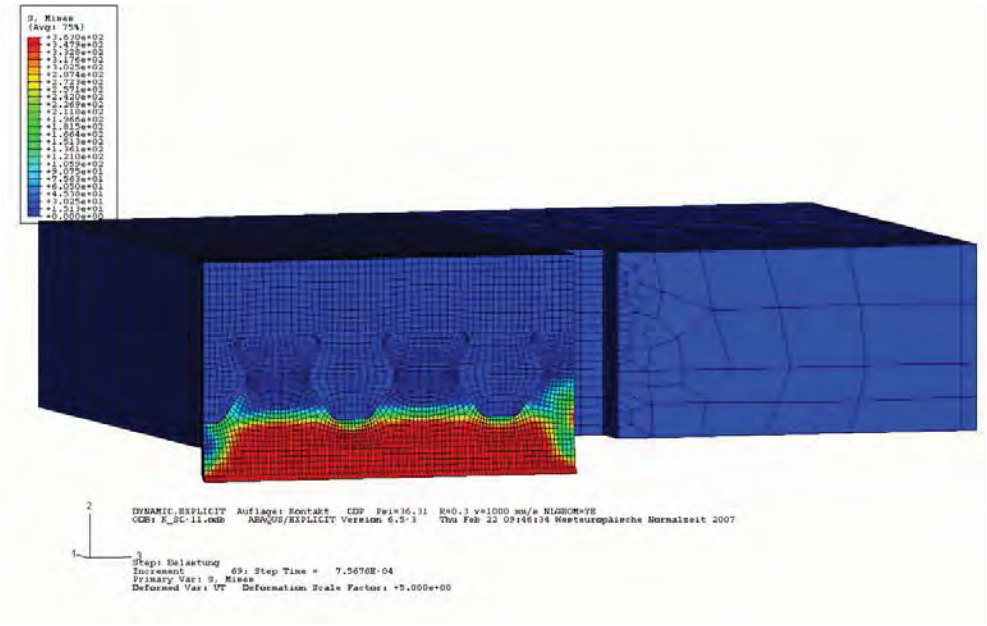

Fig. 17 Crown shaped connector /1/, NLGEOM=YES, v=1000 mm/s, d=0.76 mm

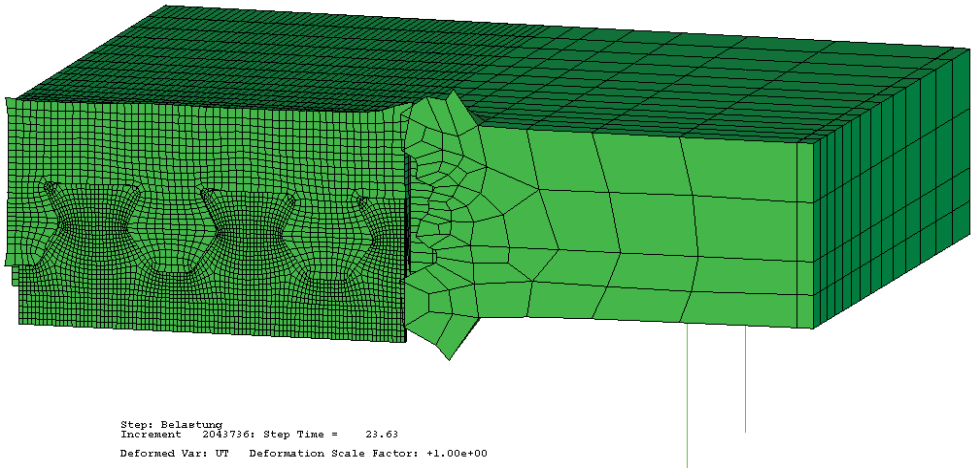

Fig. 18 Crown shaped connector /1/, NLGEOM=YES, v=0,5 mm/s, d=11,8 mm

"Computational Civil Engineering 2007", International Symposium
Iaşi, România, May 25, 2007

The Structural Expertise of Steel Cables

Ludovic G. Kopenetz, Ferdinand-Zsongor Gobesz
Department of Structural Mechanics, Faculty of Civil Engineering and Building Services, Technical University of Cluj-Napoca, Cluj-Napoca, 400020, Romania

Summary

Considering the fact, that steel cables are structural elements forming statically determinated systems, their rupture can lead to catastrophe. In this context, the structural assessment of steel cables represents a primary necessity, generated by the requirement to assure security and safety in use.

Generally the main causes which induce degradation/deterioration of cables are: fatigue and corrosion.

The effects of corrosion and fatigue are displayed usually through fiber laceration sequent to a certain service time, after which the number of ruptures and lacerations increases exponentially.

This paper covers some problems of structural expertise along with numerical simulation aspects of corrosion and fatigue, as well as a methodology for the deduction of the presumed service life of steel cables.

KEYWORDS: steel cable, structural expertise, corrosion, fatigue.

1. INTRODUCTION

The irrefutable qualities of bearing cable structures justify, from one part the extension of their application area, from another part the remarkable effort for world-over research concerning a better insight and knowledge about their behavior under corrosion and fatigue, envisioning a safer and more judicious design.

The aim of the authors through the submission of this paper is to present some aspects of their research done by the Faculty of Civil Engineering and Building equipments from the Technical University of Cluj-Napoca.

Since the middle of 70' the pursuit of this kind of research was focused in the following directions:

- Tests carried out in situ (generally considering only statical behaviour, just infrequently considering dynamical too), including the exact quantification of cable structure geometry based on survey techniques. Due to the fact that those kinds of structures are located usually at considerable heights, the applicable survey techniques have a dynamic character, recording also the swing and vibration of the structure and the movements induced by dynamic loads (wind, functioning equipment, traffic).
- Laboratory tests, in order to identify the structural materials through physico-mechanical and chemical analysis.
- Statical and dynamical analysis and calculus, including the evaluation of the service time for every structural component considering possible future loads and actions over the operative period.

It has to be pointed out the complex and time consuming character of any credible structural expertise in this field, considering the vastity of involved factors which are combined with the unstationary character of the loads (wind, temperature, vibrations from equipment and traffic etc.) [9], [10], [11].

Figure 1. The Agigea Bridge from Romania

2. CABLES AND TIE-BACKS IN MEMBRANOUS CABLE STRUCTURES

Common materials used in cable fabrication during history were: papyrus, camel hair, flax and hemp, until in 1834 when the first cables and ropes from steel wires were made. This new building material soon became indispensable in many fields, due to its special properties – high breaking strain compared to its self weight, great flexibility and durability [17]. In the field of construction, cables were used initially as bearing parts for suspended bridges, and much more lately for covering large areas without intermediate holders [18].

In the last period, in highly corrosive environments, cables made from polypropylene (specific cable weight / specific water weight = 0.91), polyester and nylon (specific cable weight / specific water weight = 1.14) are used.

2.1. Steel qualities and brands for cables and tie-backs [19], [20]

Cables and tie-backs are made from high- and very high-grade steel, with an average carbon content of 0.5% and a breaking strain around 60 daN/mm^2. Considerable growth of mechanical strength can be obtained through repeated deformations applied on steel rods during the fabrication process of wires. Thus, a cylindrical steel bar is transformed on the drawbench in wire, while its breaking strain rises up to 120 – 200 daN/mm^2. After that, the wire is subdued to a thermal treatment and hereby the material regains its plastic properties. The wire yarns are entwisted on a central wire, in one or more layers, composing strands. At their turn, the strands are coiled around a central core, forming the cable.

Nowadays in Romania two types of steel are used in the fabrication of wires which can be embodied in cables:

- carbon steel with 0.6 – 0.9% C and 0.3 – 0.7% Mn,
- thin alloyed steel, usually with manganese and silicon.

From carbon steel are wires with smooth (SBP) or marked (SBPA) surface made, each type in two qualities (I and II). From thin alloyed steel, high strength rods (PC90) are produced, with geometrical, chemical, mechanical and technological properties prescribed by the STAS438/1-74 standard.

The semi-product which is used in the fabrication of strands and cables is the proprietary carbon steel wire (through initial thermal treatment the steel is heated up to 880 – 930 °C, followed by a quick cooling to 450 – 500 °C in a lead bath after which the cooling continues slowly in the air) and drawn SBP type wire (the laminated wires are forced on a drawbench through a smaller hole than the actual diameter of the wire) without final annealing treatment.

The cables can be classified upon several criteria:

- Classification based on shape: The cables can be flat or round shaped. At their turn, round shaped cables can be simple (made from a single strand), double (composed from several strands) or coupled (formed by wrapping double cables around a central core).
- Classification according to the number of strands: Cables can be made from 1, 6, 8, 18 or 36 strands.
- Classification upon the core material: The cable core can be manufactured from vegetal, mineral, metallic or synthetic wires.
- Classification after the quality of fibers: Steel cables can be produced from uncoated (mat) or zinc coated wires.
- Classification upon the laying of strands: The wire yarns can be coiled in a strand towards right (Z) or left (S). At their turn, the strands can be wrapped within a cable towards right (Z) or left (S).

2.2. Bearing structures with cables

From the point of view of structural analysis, bearing structures with cables can be divided in the following two categories:

- isolated cables,
- cable nets and suspended structures.

Considering these structures, cables can be:

- isolated parallel or twisted wires,
- fascicles of stranded wires,
- ropes,
- thin steel rods,
- ribbons,
- chains,

arranged in one direction or in different directions (Fig. 2).

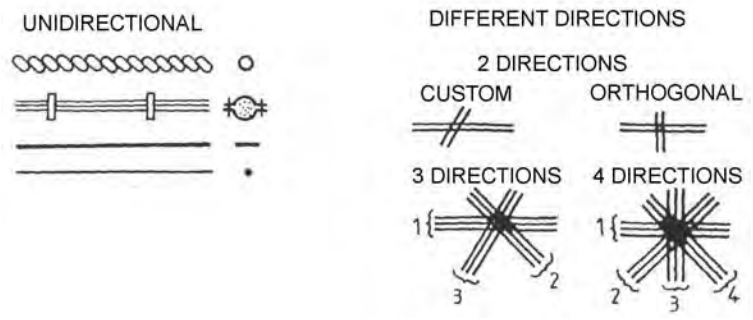

Figure 2. Different cable types

A synthetically exhibition of bearing structures with cables is presented in fig. 3.

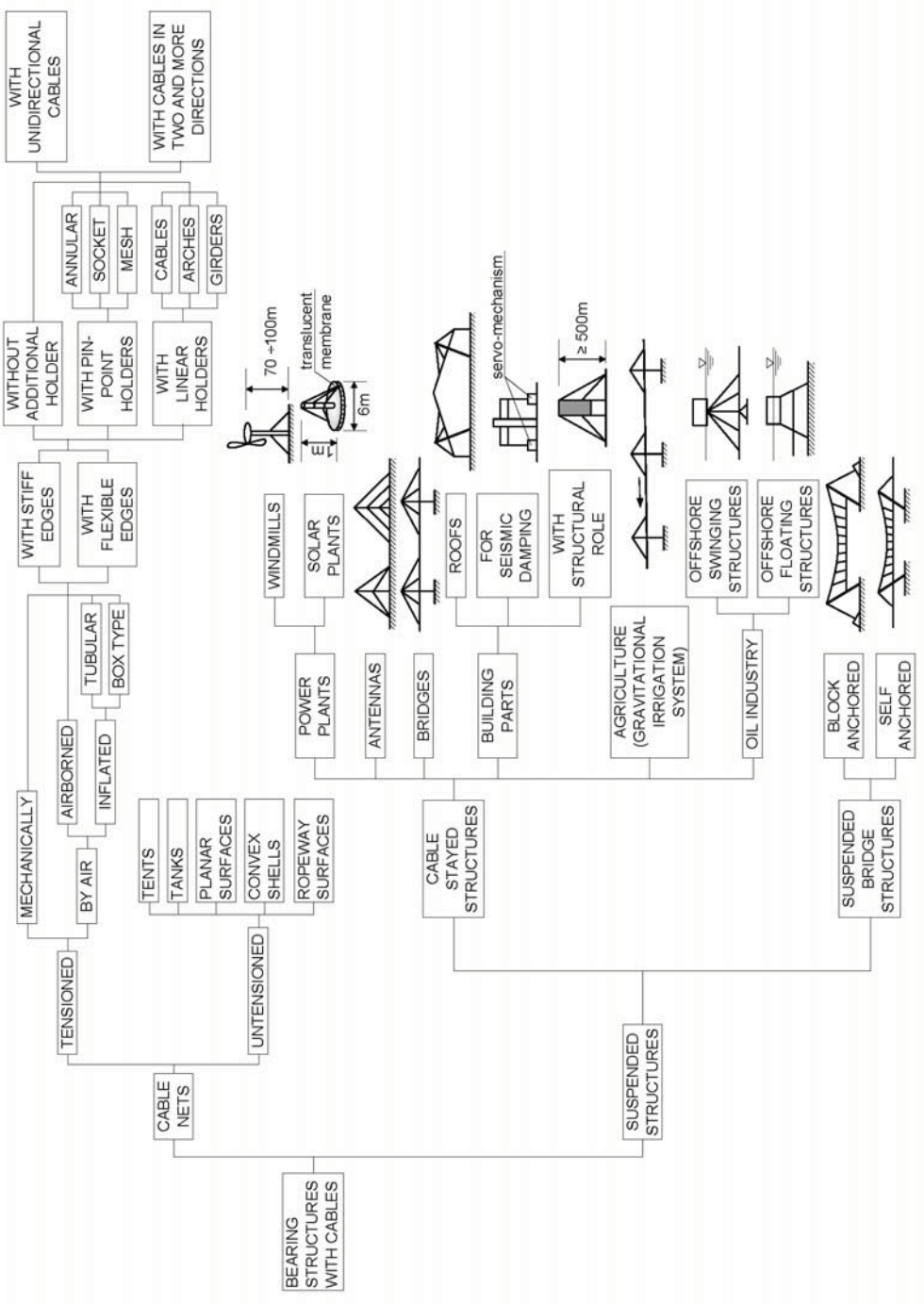

Figure 3. A classification of bearing structures with cables.

3. EXAMINATION FACETS FOR STRUCTURAL CABLES

In case of structural cables the problems which are generating noticeable modifications of the structural safety can be grouped in the following classes:

- Problems concerning the quality of the constitutive material (cold flow, brittle or breaking in different manners etc.).
- Fatigue problems due to repeated stress.
- The problem of considerable displacements caused by static and dynamic loads.
- Corrosion and erosion problems.

Bearing structures with cables are characterized by loads which are strongly depending from the basic geometry of the structure, namely by the initial balanced state (including also the geometrical and physical imperfections) induced by the steady and working loads and by eventual prestressing.

The expertise and checking of these structures must be done by studying the nonlinear geometrical (eventually physical) behaviour and all the factors upon which relies the structural safety. As a decisive element rises in this context the occurrence of corrosion and endurance to oligocyclic fatigue. The resistance to oligocyclic fatigue will be studied from secondary stresses (from vibrations or from daily thermal expansion – contraction) considering the intensity of the stress range.

3.1. Loads on structures with cables

The main loads applied on bearing structures with cables are arising from self weight, wind pressure, temperature, working loads with connected dynamic effects and support displacements.

3.1.1. The influence of weight

The following effects will be considered from dead load, combined also with other loads and forces from different causes:

- active loads, containing self weight and snow build-up, ice (frost);
- inactive loads, containing the self weight of the structural element and other permanent loads.

3.1.2. The influence of wind

This action will be considered in the context of KÁRMÁN vortices, combined from case to case with the phenomena of galloping and fluttering.

3.1.3. The influence of temperature

The low environmental temperature must be considered in any cases. Structural elements with lower working temperature than 0 °C will be additionally loaded with ice (frost) through the condensation of the moisture from the atmosphere.

In case of cable sustaining tubular structures with closed ends, through the cooling of the built-in gas or steam the inner pressure can drop enough to create vacuum inside the tube. In such case these tubular structural parts must bear up to the external pressure at low temperature.

3.1.4. The influence of dynamic effects

Buildings with structural cables are checked against the detrimal effects of vibrations that can arise from several sources, such as:

- impact forces;
- resonance developing from the operation of equipments (including air conditioning and ventilation appliances, loud musical gears, traffic etc.);
- seismic actions and wind.

3.1.5. The influence of thermal effects (expansion, contraction)

Thermal effects should be considered in combination with loads and forces from other causes:

- thermal actions through constraints and restraints;
- effects due to different coefficients of thermal expansion in case of structures with mixed materials (like steel and aluminium).

3.2. Case of laboratory-tests

The minimal bench tests which are carried out in a laboratory in order to identify the compounding materials of bearing structures with cables are:

- axial extension test, at different velocities;
- repeated bending test;
- torsion test;
- chemical test of the base material;
- simulation of corrosion and fatigue.

3.3. Site investigations [21]

Examining the behavior in time (ageing property) of steel cables is a special assay, imposed primary by the necessity to insure operational safety. In situ tests will pursue:

- Diminution of cable section, namely *loss of metallic cross sectional area* (LMA) due to corrosion, plastic deformation (afterflow) etc. [22].
- Modification of the shape (geometry).
- Broken wires, laceration and other *local faults* (LF) due to fatigue [22].

In principle the following methods are used for site investigations:

- visual inspection,
- electrochemical (potential, electrochemical sounds, magnetic etc.) methods,
- other nondestructive testing (microscopical examination, gravimetry, infrared thermography, gammagraphy, radiography and radar processing) [23], [24], [25].

For structural cables only a few of these methods give adequate results.

For visual inspection carried out in site, the authors are advising a new method: MOV_CAM (currently under patenting), using sliding digital cameras in order to view and process the image of the cable (fig. 4).

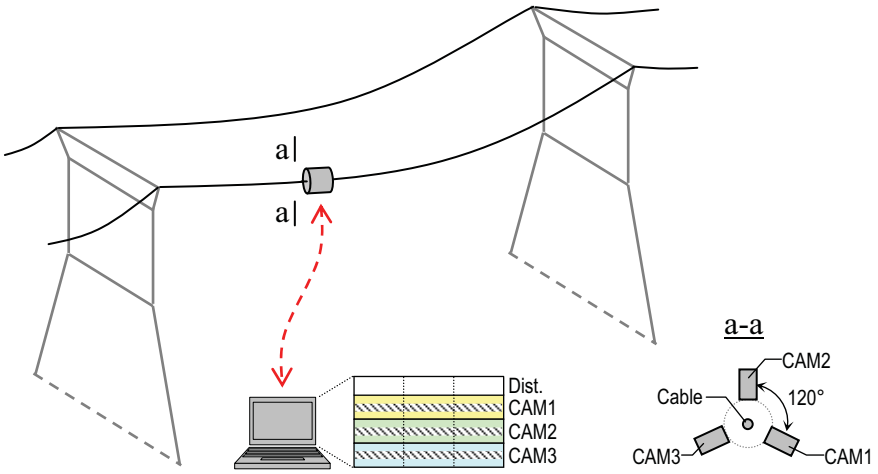

Figure 4. Visual investigation with digital cameras (currently under patenting).

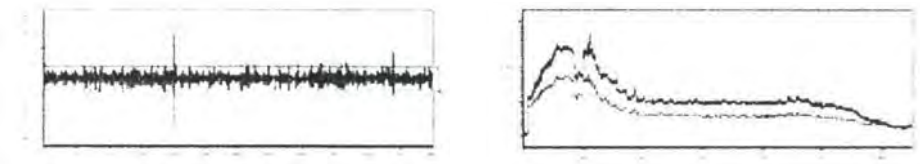

Figure 5. Sample results from LF and LMA testing.

For LMA and LF type investigations electromagnetic processes are successfully used lately, based on a magnetic head equipped with strong permanent magnets and sensors with distance meter. The software enables to inspect and to display the local faults (LF) and the sectional area diminishments (LMA) in a synthetically manner (fig. 5).

The investigation of the occurrence of corrosion in situ has a peculiar meaning, on one side due to the increasing intensity of the polluting agents in the environment, on the other side due to the requirement regarding the prolongation of the operational service time of cables.

Cables are highly sensitive to corrosion because their self constructional embodiment enables the penetration and stagnation of moisture.

One of the most delicate problems of structural engineering is to track and to keep under control the evolution of degradations caused by corrosion, because this aspect entail in time changes in the physico-mechanical properties and therefore in the strength of materials, leading also to stress redistribution in the structural elements. That is the reason why in the following part a method for monitoring the corrosion of steel cables and the principle of numerical simulation for this process will be described.

The acquisition of primary data about corrosion, in the case of cables, can be done with the method of electric resistance, which is easily applicable in situ. The method of electric resistance is based on the principle that cable corrosion is accompanied by cross sectional reduction. In this way, if there is no intercrystalline corrosion, the raising of electric resistance is produced by the diminution of the cross section.

In case of intercrystalline corrosion, the area of the cross section is not modified significantly, but the specific resistance increases. Thereby, measuring the electric resistance on different portions of a steel cable, considering 500 – 1000 mm long segments, the commencement of corrosion can be promptly recorded. Monitoring the corrosion of steel cables by the means of the electric resistance method enables the undelayed signaling of the occurrence of corrosion, including intercrystalline corrosion. This method is simple, safe and relatively cheap, implying low costs.

4. NUMERICAL SIMULATION OF CABLE CORROSION

The numerical simulation of corrosion can be done in order to study the phenomena in time, using probabilistic degradation functions or data acquired through monitoring. Some of the most frequently encountered fault types are presented in table 1.

Table 1. Typical patterns of wire rope degradation and failure [25]

Illustration	Short explanation
	A "bird cage" caused by sudden release of tension and resultant rebound of rope from overloaded condition. These strands and wires will not return to their original positions.
	A close-up of a rope subjected to drum crushing. The distortion of the individual wires and displacement from their normal position is noticeable. This is usually caused by the rope scrubbing on itself.
	A wire rope jumped from a sheave. The rope itself is deformed into a "curl" as if bent around a round shaft. Close examination of the wires show two types of breaks – normal tensile "cup and cone" breaks and shear breaks which give the appearance of having been cut on an angle with a cold chisel.
	Localized wear over an equalizing sheave. The danger of this type wear is that it is not visible during operation of the rope. This emphasizes the need of regular inspection of this portion of an operating rope.
	A wire which has broken under tensile load in excess of its strength. It is typically recognized by the "cup and cone" appearance at the point of the fracture. The necking down of the wire at the point of failure to form the cup and cone indicates that failure occurred while the wire retained its ductility.
	An illustration of a wire which shows a fatigue break. It is recognized by the squared off ends perpendicular to the wire. This break was produced by a torsion machine which is used to measure the ductility. This break is similar to wire failures in the field caused by excessive bending.
	A wire rope which has been subjected to repeated bending over sheaves, under normal loads. This results in "fatigue" breaks in individual wires, these breaks being square and usually in the crown of the strands.
	An example of "fatigue" failure of a wire rope which has been subjected to heavy loads over small sheaves. The usual crown breaks are accompanied by breaks in the valleys of the strands, caused by "strand nicking" resulting from the heavy loads.
	A single strand removed from a wire rope subjected to "strand nicking". This condition is the result of adjacent strands rubbing against one another and is usually caused by core failure due to continued operation of a rope under high tensile load. The ultimate result will be individual wire breaks in the valleys of the strands.

The SACOC (*Structural Analysis of Corrosion for Cables*) software package is based on the finite element method and it proved to be very useful in the study of the corrosion of structural cables. A schematic block diagram of this program is presented in figure 6 [21].

The user can take advantage of several available degradation functions simulating cable corrosion in time, or he can use quantifications from site investigations gathered in a data base.

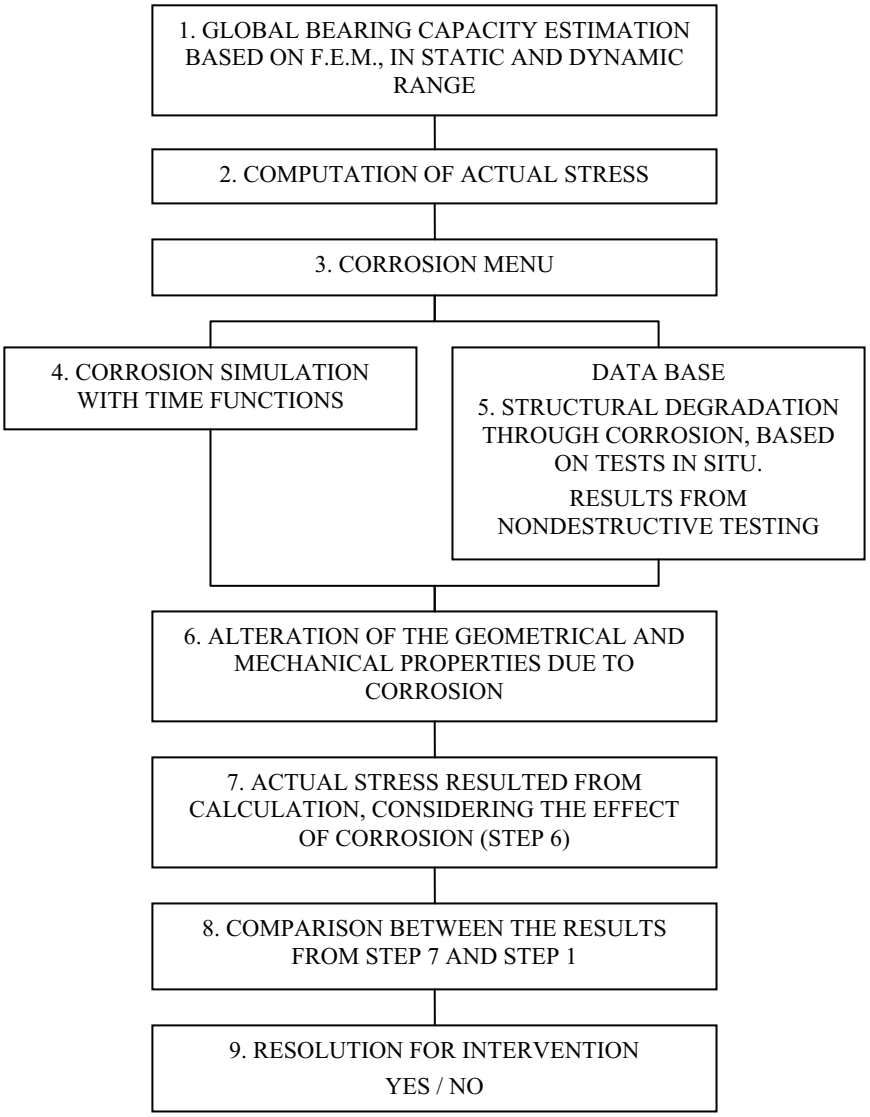

Figure 6. The schematic block diagram of the SACOC software.

5. CABLE QUALITY CERTIFICATION

The quality of cables is guaranteed by the manufacturer through quality assurance certificates, released for each product range. Deviations in dimensions, properties and shape shall not exceed the prescribed limits from the relevant Romanian technical regulations, nor those stated by the manufacturer. The list of standards for wires and steel cables is presented in table 2.

Table 2. The list of Romanian standards (STAS) in use

Pos.	Title	STAS code
1	Materials	880-66
2	Cold-drawn steel wires for drag ropes	1298-80
3	Steel cables. Concept and classification.	1710-79
4	Steel cables. Simple structure cables. Shapes and dimensions.	1513-80
5	Steel cables. Technical requirements.	1352-78
6	Steel cables. Double cables. Combined structure. Shapes and dimensions	1689-80
7	Steel cables. Combined cables. Double cables. Ordinary structure. Shapes and dimensions	1535-71
8	Steel cables. Combined cables. Triple structure. Shapes and dimensions	2693-80
9	Steel cables. Combined flexible double cables. Shapes and dimensions	1353-80
10	Steel cables. Flat cables. Shapes and dimensions	1559-80
11	Alternate bending test for steel wires	1177-74
12	Testing of metals. Torsion test for wires	1750-80
13	Testing of metals. Coiling test for wires	6622-70
14	Testing of metals. Tensile test for wires	6951-76
15	Testing of metals. Tensile test for steel cables	2172-74
16	Combined double concentric cables	2590-80
17	Steel wire for prestressed concrete	6484-77

6. CONCLUSIONS

Bearing structures with cables are liable to generate unappointed phenomena in comparison with conventional structures. Thus, beside the great displacements originated from their custom designed structural shapes, displacements arise due to the $\sigma_{breaking} / E$ ratio. While this ratio in case of conventional structures, considering OL37 steel is $3700 / 2100000 = 1 / 568$, in case of using cables becomes $15000 / 1650000 = 1 / 110$, namely five times bigger.

Zinc coated cables are able to withstand to corrosion approx. 10 – 15 years. For this reason, in case of highly corrosive environment should be remembered that high quality ropes and cables made from synthetic materials with outstanding endurance are available too.

The required anchoring of cables must be done by wrapping their end with cast zinc inside threaded pipes instead of using clamps, because the cable may slip out from the clamp at high dynamical stress.

Cables should be prestressed in a jointly manner with their anchors (thus the anchoring is tested) before installation, with a force equal to approx. 1.10 times the computed actual stress, in order to consume the significant remnant elongations and to avoid subsequent loosening and relaxation.

References

1. Falk, S., *Lehrbuch der Technischen Mechanik*, Springer Verlag, Berlin-Heidelberg, 1967.
2. Leonhardt, F., Zellner, W., Vergleiche zwischen Hängebrücken und Schrägkabelbrücken für Spannweiten über 600 m, *International Association for Bridge and Structural Engineering*, vol. 32, 1972.
3. ***, Bibliography and Data Cable-Stayed Bridges, *Journal of the Structural Division*, ST10, 1977.
4. Knut, G., Merkblatt-496, Ebene Seiltragwerke, *Beratungstelle für Stahlverwendung*, Düsseldorf, 1980.
5. Kopenetz, L. G., Ionescu, A., Lightweight Roof for Dwellings, *International Journal for Housing and its Application*, vol. 9, No. 3, Miami, Florida, USA, 1985.
6. Haug, E., Engineering Contributions to the Design of Lightweight Structures via Numerical Experiments, *2nd International Symposium Weitgespannte Flachentragwerke*, University of Stuttgart, 1979.
7. Jensen, J. J., *Das Dynamische Verhalten Eines Vorgespannten Kabelnetz*, University of Trondheim, Norway, 1972.
8. Goschy, B., Dynamics of Cable-Stayed Pipe Bridges, *Acier-Stahl-Steel*, No. 6, 1961.
9. Szabó, J., Kollár, L., *Függőtetők számítása*, Műszaki Könyvkiadó, Budapest, 1974.
10. Otto, F., *Das Hängende Dach*, Bauwelt Verlag, Berlin, 1959.
11. Oden, J. T., *Finite Elements of Nonlinear Continua*, McGraw-Hill, 1972.
12. Krishna Prem, *Cable-Suspended Roofs*, McGraw-Hill, London & New York, 1979.
13. Fuller, B. W., *Weathering of neoprene-coated Nylon fabric*, E. I. Dupont de Nemours & Co., Report BL-327, 1956.
14. Otto, F., Trostel, R., *Zugbeanspruchte Konstruktionen II*, Ullstein Verlag, Frankfurt-Berlin, 1966.
15. O'Brien, T., General Solution of Suspended Cable Problems, *Journal of the Structural Division*, ST1, Febr. 1967.
16. Sofronie, Ramiro, Vertical Deflection of Suspension Bridges, *Revue Roumain Scientique Technique-Mécanique Appliqué*, Tome 24, No. 3, Bucureşti, 1979.
17. Mollmann, H., *A Study in the Theory of Suspension Structures*, Copenhagen, 1965.
18. ***, *Recommendation for Guyed Masts*, The Working Group on Guyed Masts of I.A.S.S., 1981.
19. Kopenetz, L. G., Cătărig, A., *Cabluri structurale*, Simpozionul Tehnologie şi Siguranță, U.T. Pres, Cluj-Napoca, 2004. (in Romanian)
20. Kopenetz, L. G., Cătărig, A., *Teoria structurilor uşoare cu cabluri şi membrane*, U.T. Pres, Cluj-Napoca, 2006. (in Romanian)
21. Kopenetz, L. G., Cătărig, A., *Probleme ale coroziunii cablurilor din oțel*, Lucrările celei de a VII-a Conferințe de Construcții Metalice, vol. 2, Timişoara, 1994. (in Romanian)

22. ***, GTU Documentation, USA (Nondestructive Testing Technical Diagnostics).
23. Knut, G., On the Fatigue Strength of Wires in Spiral Ropes, *Journal of Energy Resources Technology*, vol. 107, 1985.
24. ***, Internal Report, Bethlehem Wire Rope, USA.
25. ***, Technical Report No. 107, Wire Rope Corporation, St.Joseph, MO, USA.
26. Bârsan, G. M., Kopenetz, L. G., Alexa, P., Theil, S., Gedanken zum Entwurf Leichter Zusamengesetzter Tragwerke, Proceedings of the 4th Conference on Steel Structures, Timisoara, Romania, 1985.

"Computational Civil Engineering 2007", International Symposium
Iaşi, România, May 25, 2007

Computer aided building diary

Mária Kozlovská[1] and Michal Danko[2]

[1]*Technical University of Kosice, Faculty of Civil Engineering, Slovakia*
[2]*Inzinierske stavby, a.s. Kosice, Slovakia*

Summary

One of the main and also generally obligatory tools for building site works management is the site diary. The building code orders to building manager the building diary leading. In the sense of the code, the building site diary is the document, which is the part of documentation available on building site and in the document are noticed all relevant events, which have happened on the site.

The article describes possibilities of better building diary leading, as the main document for managing and monitoring of works on building site by computer support. Also describes design, structure and architecture of electronic tool as well as collaboration of database environments. The article presents real examples of computer aided building site diary paper forms.

KEYWORDS: building, site diary, electronic tool

1. INTRODUCTION

The code also determines that the building diary has to be written from the first day of preparation works till construction works finish and also who is competent to write into the diary. According to law, by which are executed some dispositions of the building code, into the building diary are written all important conditions concerning a structure building up:

- notes about divergences from project documentation verified by surveyors office in building process or from conditions dedicated in building permission or in other resolution or proceeding,
- facts influencing building works and building process, especially time flow of works, temperature in relation to building works, especially with wet production process, weather,
- date of building site visit, found facts and steps of the person competent to do state building surveyor and the person doing state inspection,

- records of project engineer and of partial projects designer or of architectonic product author, geodesist and cartographer of the structure,
- records of investor or his empowered person or the structure owner, if he is not investor,
- records of the person making building inspection or capable person, which manages building process, building contractor,
- data about elimination of building faults and back-logs according to structure inspection decree conditions.

But the reality on many building site is such, that the records are not written daily, often are made after longer time period, sometimes only before the building disposition. Then they are only short information about weather, worker and equipments amount, in better case are written performed building processes but only in outline version.

2. THE BUILDING DIARY VALUE

The building site diary leading has its purpose, as well as irreplaceable value for all building participants. That is why are in following text presented some principles and good advices how write the diary in the manner, that the diary should be an effective management tool. The building diary presents also the most effective form of communication among building participants, which flows from law practice principles, demanding reliable presentation of all facts connected with building. The building diary in the sense of effective management tool must imply complex data, which are necessary not only for real state monitoring, but also for the building process management. The records written into building diary by particular building participants are the basis for follow change management what is inseparable part of every building activity. That is why the building site diary is the main tool of operative works management on building site.

The areas, which management is for the building diary essential:

- the building processes performance (data about workers, machines, products, materials, practices, ….)
- time schedule of works, building works quality
- occupational health and safety
- environment protection
- conditions of building site (production, social, operative, climatic…)
- financial controlling (performed works billing, internal accounting, …)
- contract parameters accomplishment (eventually change actions)

In small or technically simple buildings can be the diary retrieved by simple record about the structure, which investor writes and also person who special inspections do, signs the record. In the record must be written also building works amount, which perform on building site other corporate and natural persons besides the investor.

RECOMMENDED STRUCTURE (MAP) OF THE SITE DIARY	
INTRODUCTION PAPERS	
Cover front page	▫ Contractor ▫ Diary number ▫ Registration numbers of records sheets ▫ The building
General part	▫ **Main sheet** – the building name, place and date of the beginning, building number, contractor, project engineer, building manager, technical supervyor of investor, investor, subcontractors ▫ **List of main evidences about building:** contracts of building participants, protocol of building site transmission, additions and changes of contracts, … ▫ **List of building documentation –** evidence of documentation available on building site ▫ **Survey of performed exams and measurements –** evidence of protocols from exams and measurements of building constructions, technological equipments, nets, … ▫ **List of other documents originated in time of building production –** records from control negotiations, protocols, …
DAILY RECORDS	
Site diary establishment	▫ Record of contractor about works beginning ▫ Record of investor about empowered workers competent for records into the diary writing (building supervisor) and for the project engineer (author supervisor) ▫ Record of contractor about empowered workers to do notes into the diary ▫ Name of contractor employer responsible for OHS and FP on building site ▫ Verification of investor about acceptance of the diary front page

Beginning of works	▫ Works beginning date ▫ Found facts, which influence negatively the working process ▫ Requirements on the faults elimination (limitation)
Products, machines and equipments taking	▫ Appeal to investor into preparation of materials, machines and equipments, if they are not the part of contractor supplies ▫ Appeal to transport and supplying of supplies on building site in limitation ▫ Found inadequacies of investor supplies
Occupational health and safety and fire prevention insuring	▫ Skull session on building site including workers roster ▫ Record about control of workers certificates validity, special works performance competences ▫ Difference from safety arrangements in works race condition, with investor operations or with other contractors works ▫ Records about work accidents ▫ Records about building site control performed by occupational safety inspectorate
Works on building site performance	▫ Climatic conditions influencing works process and quality ▫ Type, amount and time schedule of performed works ▫ Works assurance by workers, machines and products, ... ▫ Building site readiness for subcontractor taking up ▫ Building parts finishing ▫ Requirements on investor in connection with restrictions in works performance
Works breaks and technological breaks	▫ Writing of all facts, which menace or preclude works continuance ▫ Writing of all and also short-time break
Continuation of works	▫ Date and time of interrupted works beginning and break reason record ▫ Requirements on correction and revisions performance
Works covering	▫ Appeal to control of quality and covered works integrity ▫ Record about control resuls
Auxiliary works specification	▫ Investor writes the works amount approved by him and by contractor ▫ Contractor specify amount and process of performed auxiliary works, capacity and terms point
Changes specification	▫ Record of all found divergences from executed and approved plans ▫ Record of performed divergences from previous plans, including their approbation, documentation and evidence
Coordination of (sub)	▫ In field of transport - requirements on transport with object and term introducing

contractors on building site	▫ In building works field – requirements on amount and terms, verification about their performance ▫ Works performance requirements – building site equipments demands ▫ Other works – lending of machines and equipments, method of using of building site objects, building site patrol, …
Facts necessary for billing	▫ working out hours amount (works charger by hour tariff) ▫ undone machines-hours, time of machines and equipments using ▫ increase of costs from reasons of impossibility of expected calculation incompliance because of changed organizational and technological conditions ▫ usage of energies (electrics, water, gas, …) taking method, operation time, used equipments
Exams and measurements performance	▫ time, process and results of exams and measurements ▫ investor statement into their result (in detail in control and exam plan of building)
Extraordinary events	▫ raised damages on possession – reason writing (natural forces, swag, …), damage amount, names and address of witnesses, performed arrangements ▫ illegitimate using of machines and equipments
The building acceptance and handover	▫ date of written appeal to transfer action beginning ▫ place, date and time of transfer action beginning ▫ transfer action process ▫ place, date and time of transfer action finish (writing of protocol about transfer and acceptance between contractor and investor, including list of faults and inadequacies
Competent institutions standpoints	▫ record of competent workers and institutes about their determinations ▫ competent institutes statements
Complex examination	▫ appeal on participation on equipments examination ▫ exams process, including achieved results ▫ complex examination beginning and finish date ▫ list of complex examination participants

Nowadays the form of the building diary can be various. From standard “blind” form, which can be bought in shops with paper forms (standardized notebooks) to structured forms, which form and structure is selected by firm itself in dependence on data management system. Basically the investor must accept the form of the building diary.

In contract relations writing, concerning often used formulation of commercial code "if contractor parties do not agree otherwise…" right and careful leading of the building diary has got big importance. The records in building diary are often only obligatory verification presenting real building process and accomplishment of duties among building participants. Timely and good made record in the building diary is also often an only entry basis for conventional sanctions, damages reparation, changes or additions of contract applying.

3. E-BUILDING DIARY – APPLICATION ENVIRONMENT

The building diary can be considered as some collection of information and records. In order to make work with these information and records easier and more effective, it is necessary to use computers with suitable software. This software must be dedicated specially for wok with information. Also it has to be able to observe all functions and conditions for the building diary leading. A useful alternative presents the product of company Microsoft – Access, which is part of today often used office packs Microsoft Office. By this program is possible to create database applications, which are the most suitable for work with information. Particular database applications are made from database objects namely from charts, into witch are inserted information, questions, paper forms, combinations, data pages, macros and modules.

The main characteristic of the program Microsoft Office is simple and especially wide possibility of work with information. Besides that it has got many other advantages, which in the case of the site diary leading as fully functional program, can do leading of the diary and work with it do more effective. At the present is communication by net and internet connection a common stuff. Similar possibilities provides also Access 2003, from which is possible to export data into different external database systems. Also is possible to install all database software Microsoft Access into computer net server or publish application data at the internet. The advantage is also the form of outgoing records by program Word or joining of tabs from program Excel. It is possible to join own databases of companies with the site diary database, by what is user work easier. User will not must write some data (about machines or employers), but only choose from database.

Next advantage of Access is database application insurance. There are many possibilities how to non-authorised entries. Database applications created in Access 2003 version is possible to sign by electronic signature. The user by his signature confirms that information contained in this file is valid and from sign immediate was not changed. If the file will not be changed, is possible to add signatures of other users. Added digital signature informs that, signature author insure the

project safety. This possibility is in case of the building diary very important, because records in the diary have to be signed.

4. E-BUILDING DIARY – APPLICATION OF STRUCTURE AND VISUAL ASPECT

Application of building diary e-form structure comes from higher presented map (tab. 1) of building diary. This application consists of 28 paper forms (fig. 1) which are each other connected. They are divided into two groups, into forms for data import into database and forms for browsing the data yet saved in database

The main structural element of electronic building diary is the forms. Each form consists of three parts: head-line, body and heel. In head-line is presented the name of database "Site diary" and "date" which is daily actualized. In place of heel of forms generality is inserted command button "Back" which can switch over the user into past form. Body of forms is different depending on contents and function. The forms dedicated for data insert are similar, only fields describes are different. In order to visual site of program will be agreeable for user, all forms are orange with black texts. Pictures 2 – 11 present selected forms (screens).

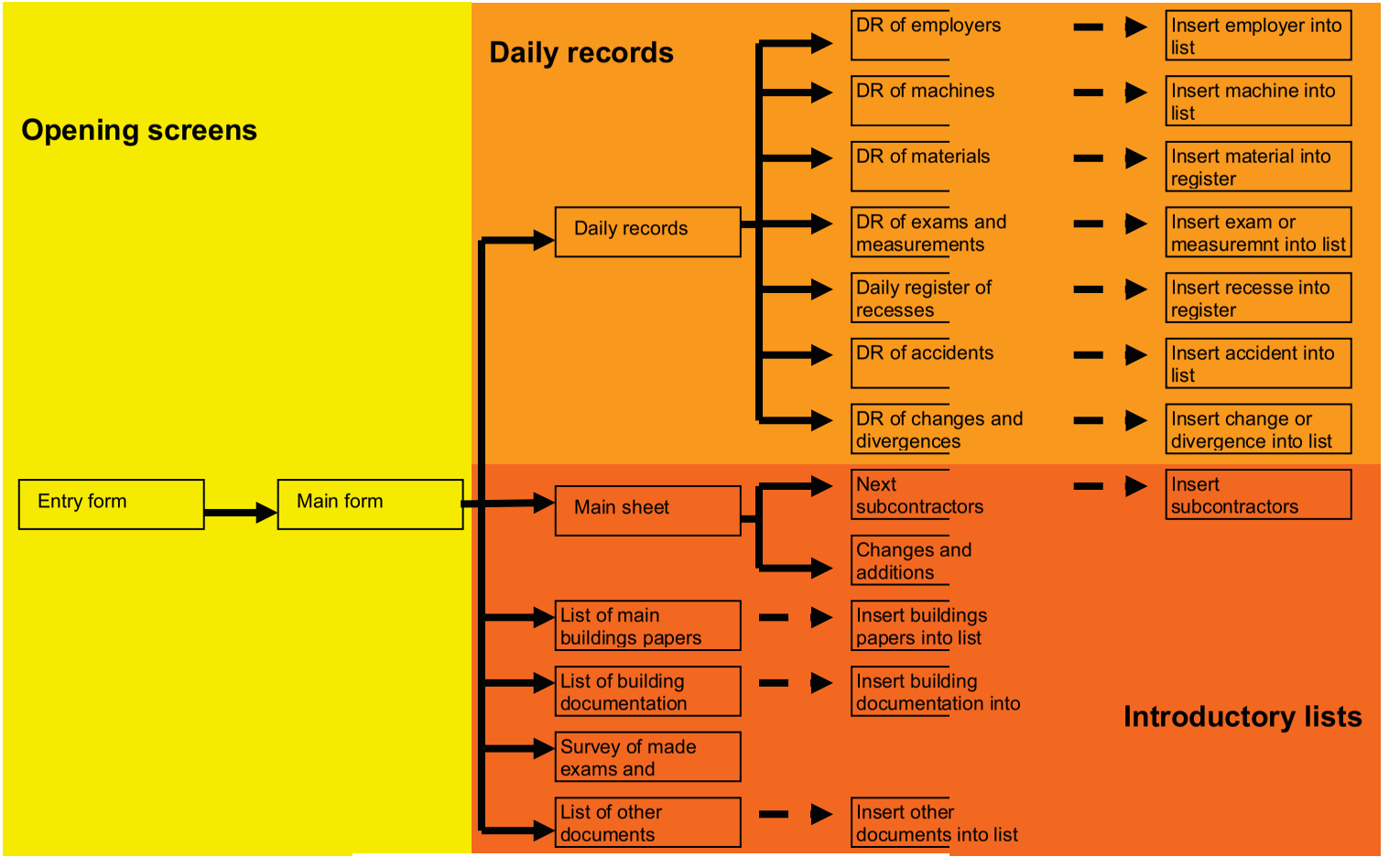

Fig.1 Structure of building diary

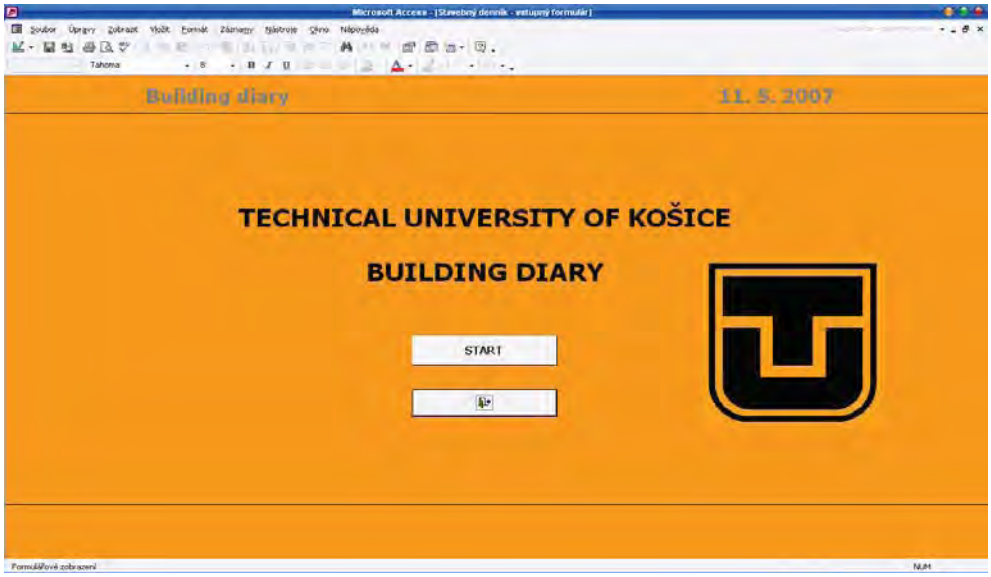

Fig.2 Opening screen

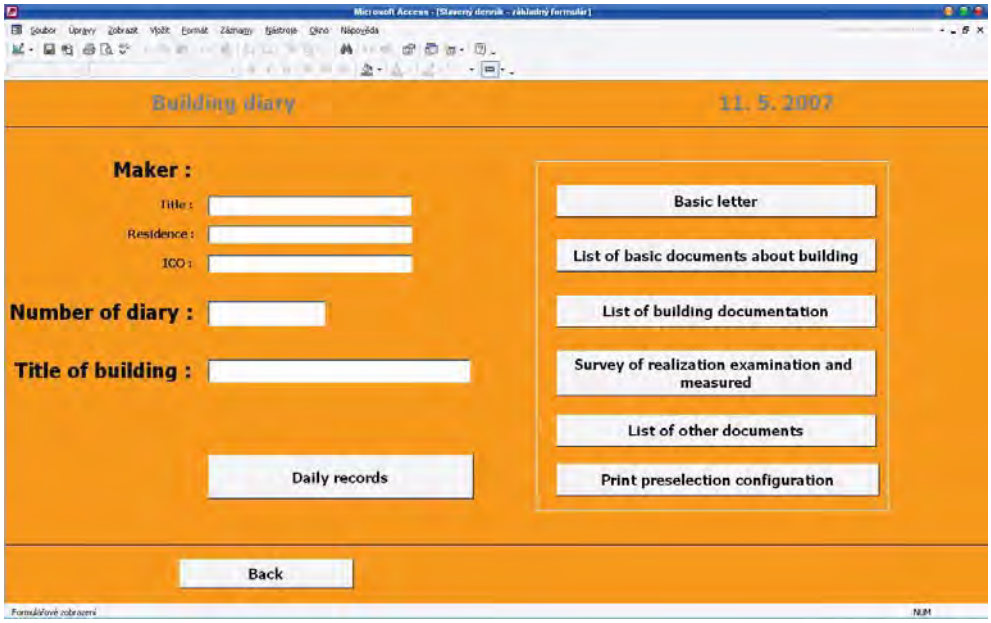

Fig.2 Main formular

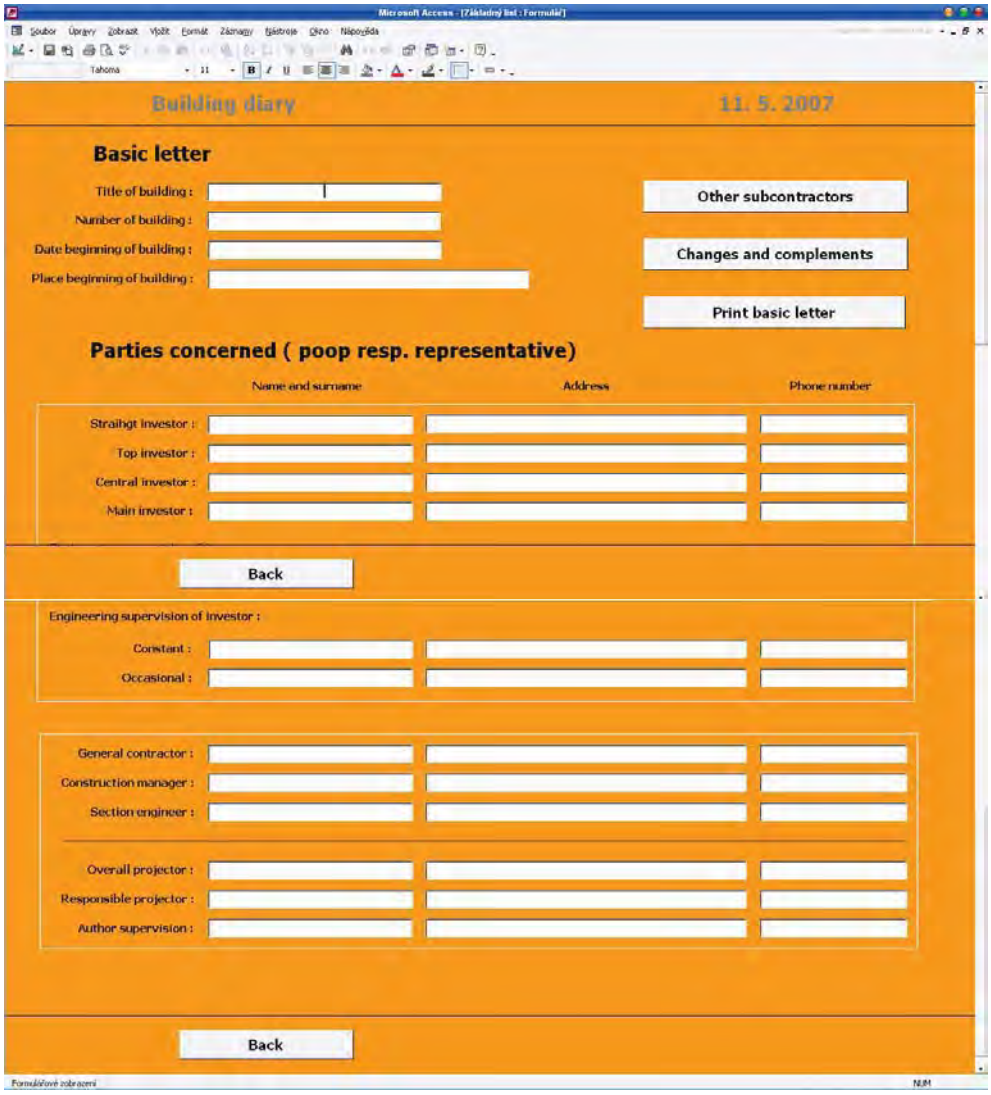

Fig.3 Basic information

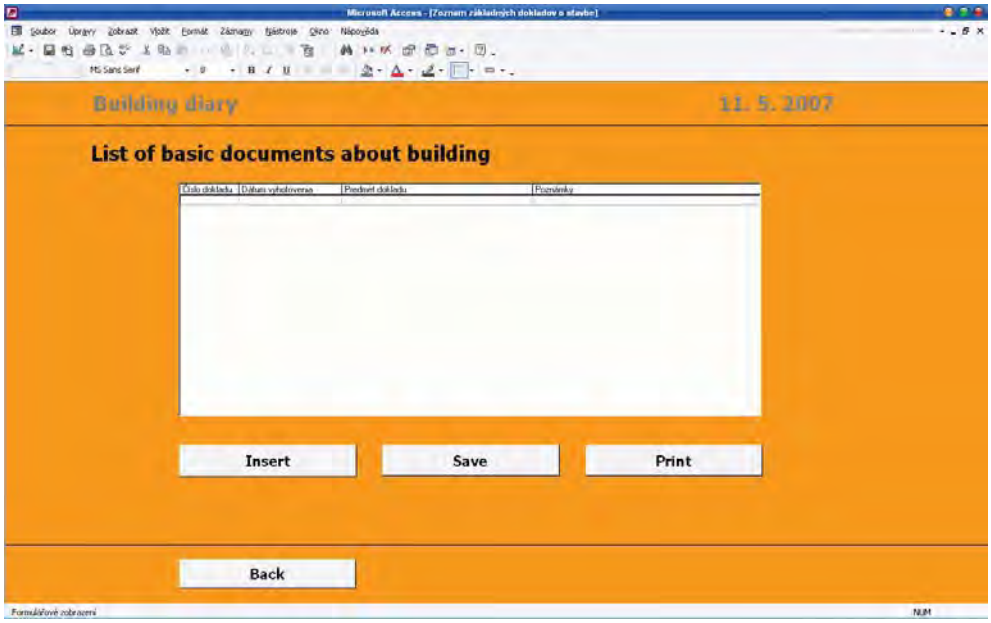

Fig. 4 List of basic documents about building

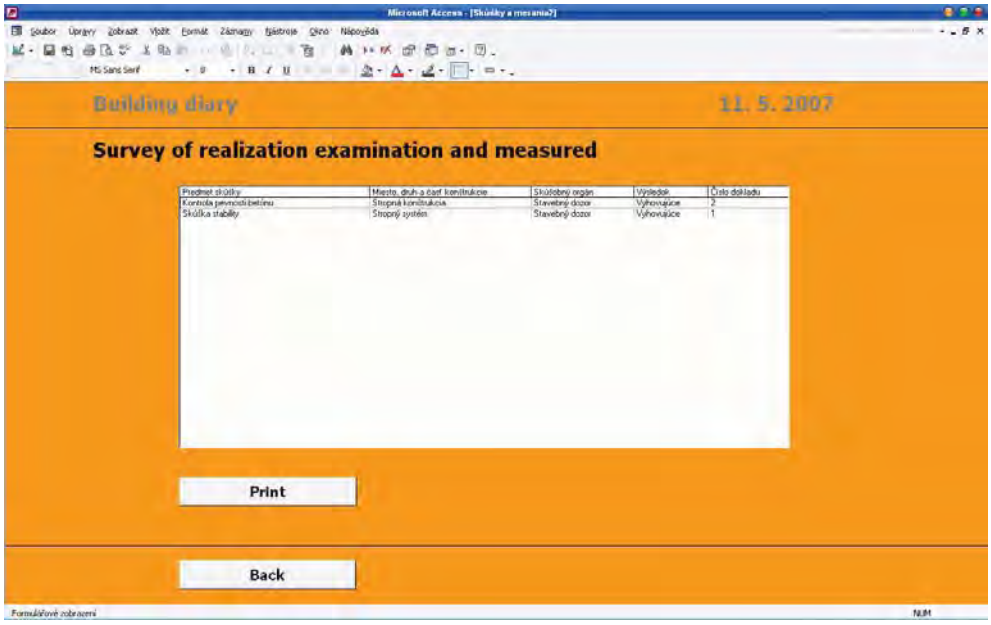

Fig.5 Survey of made exam and measure

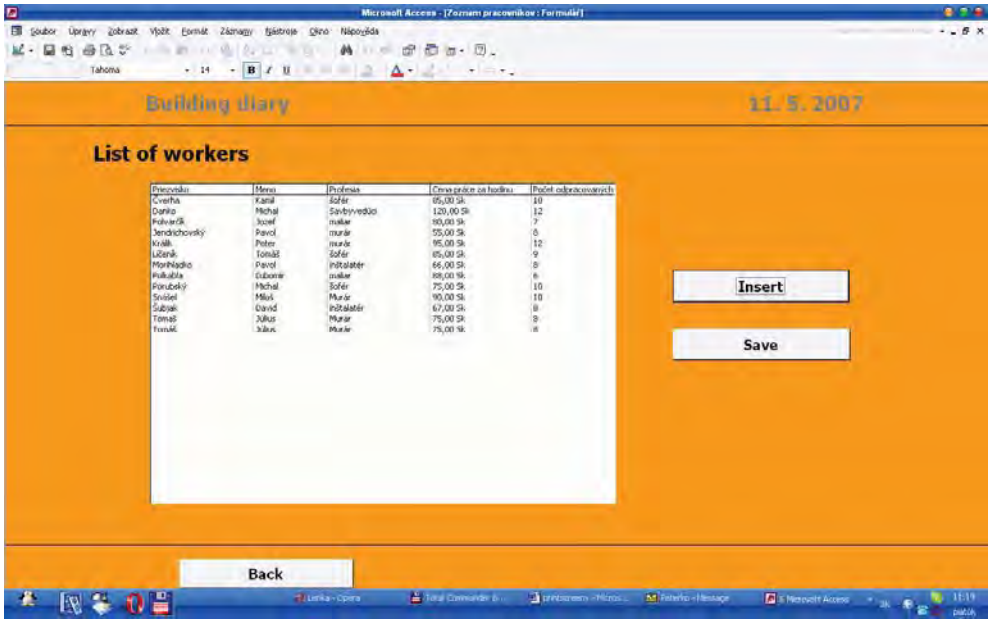

Fig. 6 List of workers

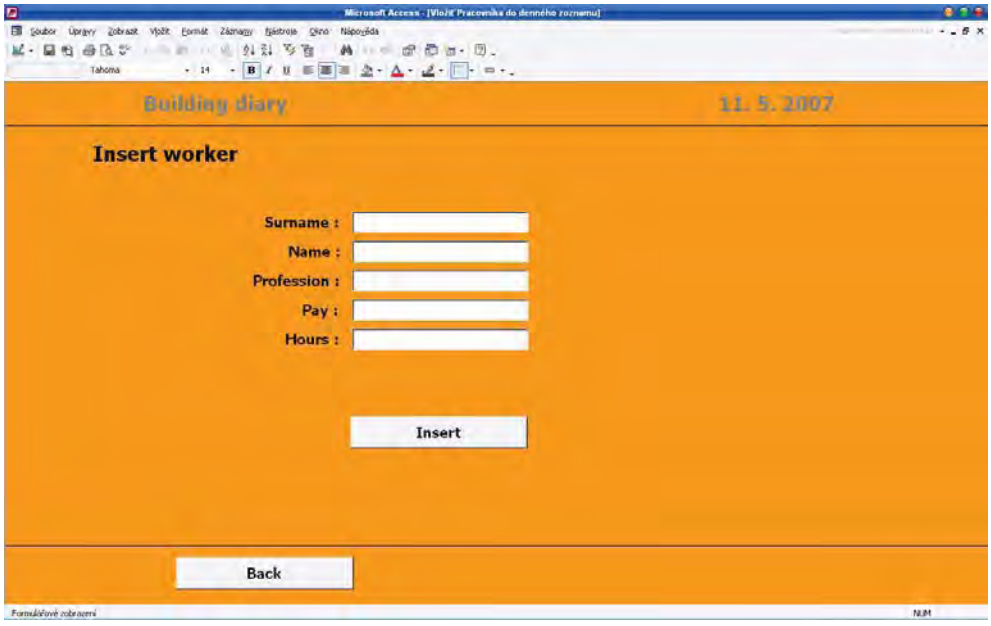

Fig.7 Formulary for workers inserts

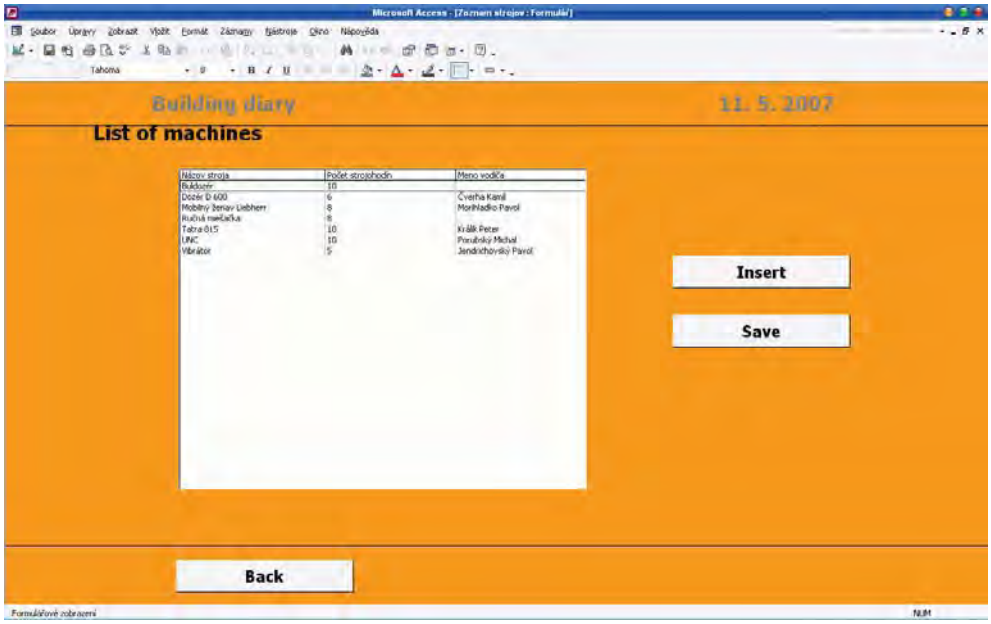

Fig.8 List of machines

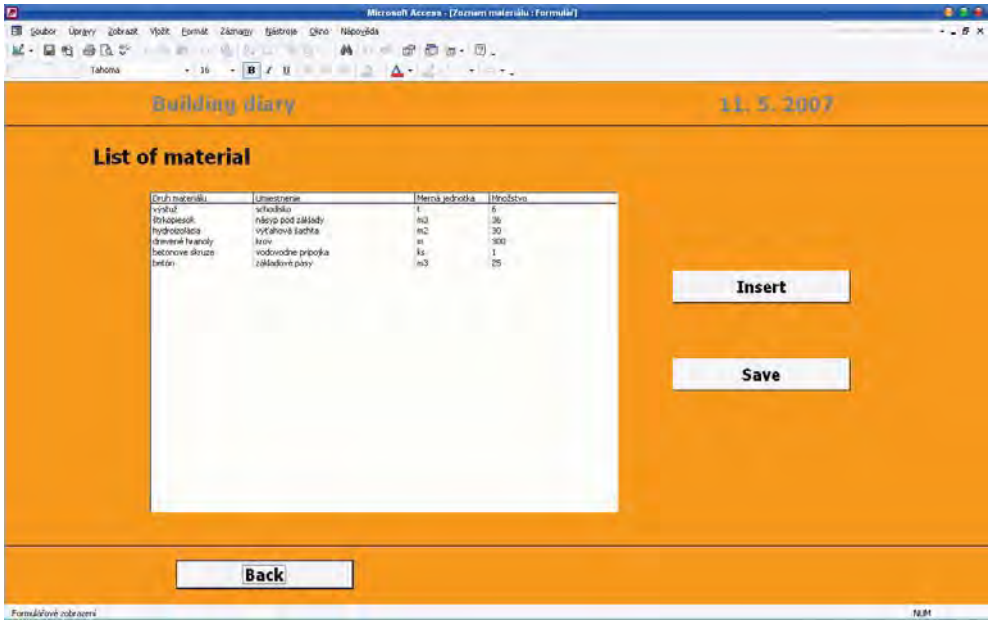

Fig.9 List of materials

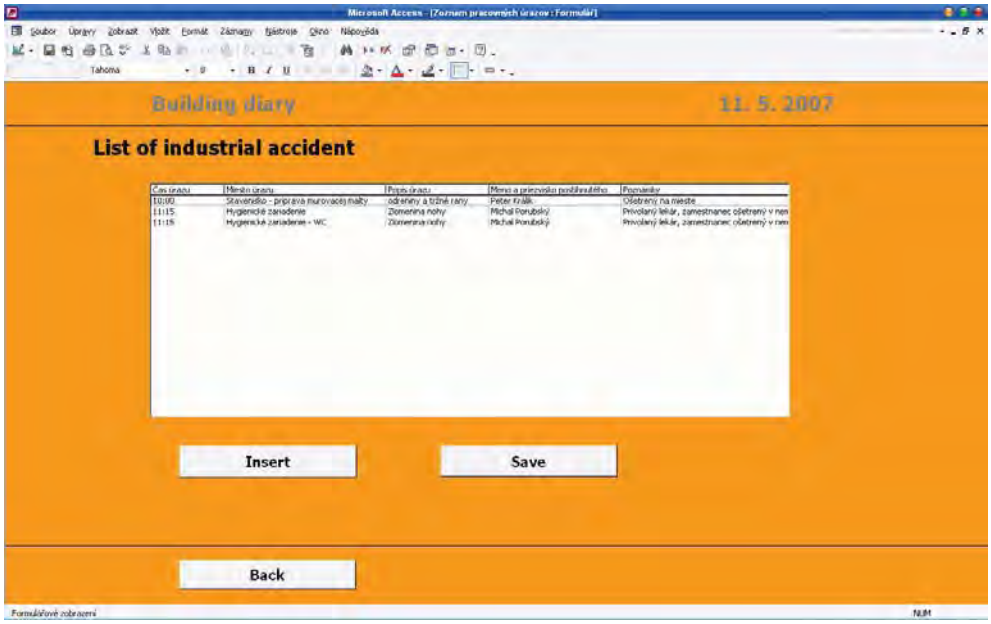

Fig.10 List of accidents

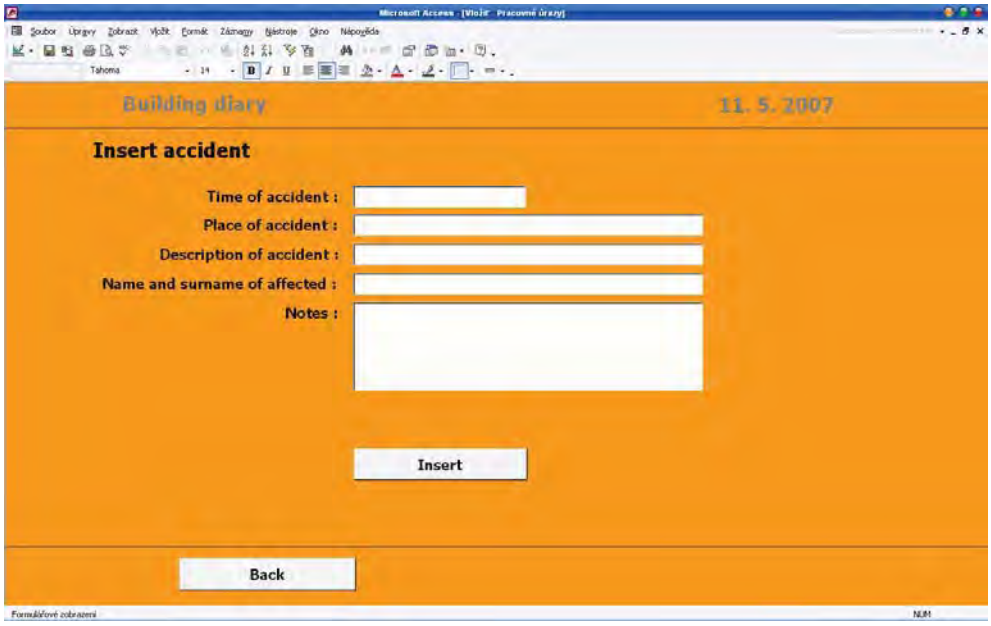

Fig.11 Formulary for accident inserts

5. CONCLUSION

The high rate of construction, necessity of fast transport of information, including their fidelity, create force on new tools development, which can effectively insure activities connected with building realization. Development and design of application supporting electronic leading of the site diary is a contribution, supporting these necessities. Nowadays information and communication technologies including personal computers are more often the natural "co-operator" of building managers. Developed application presents the tool, which can essentially do work of managers more effective.

The article is the part of the project KEGA 3/4004/06 MM program for building educate support.

References

[1] Kozlovská, M., Hyben, I.: *Works foreman – manager of the building process*. 1. edition. Bratislava: Eurostav, 2005.
[2] *Building law No.76/1976* in later regulations version.
[3] Korínek, M.: *Access 2000*. České Budějovice : Kopp, 2000.

Determination of the heat flows, of the solar and luminous characteristics of the glazing and of the devices for the solar protection. Automaton calculus program "SOLAR"

Ioan Moga and Ligia Moga
Physics of Constructions, Faculty of Civil Constructions and Installations, University of Cluj-Napoca, Cluj-Napoca, 400027,Romania

Summary

The automaton calculus program "SOLAR" has resulted from the activity for establishing the annex A94 from "THE METHODOLOGY FOR CALCULUS THE ENERGETICS PERFORMANCE FOR BUILDINGS - PART I", for the applying of the requirements of the law 372/2005.

The calculus program has at its basis the stipulations of the normative EN 13363-2:2005.

With the help of the automaton calculus program, it can be determined for any type of glazing with or without solar protection devices, the solar energy total transmission factor, luminous transmission factor and the normalized thermal emission flow.

KEYWORDS: heat engineering for constructions, solar protection devices, energy savings, rehabilitation of buildings.

1. CALCULUS ALGORITHM

1.1. Calculus program description

The calculus program is realized using the programming language Delphi under Windows system.

The calculus program was made out taking into consideration the stipulations from the normative SR ENISO 10211/1-98 concerning the geometrical model, the layout of the sectioning plans through the glazing system with the solar protection that forms the calculus network. Regarding the convergence conditions of the obtained solutions a more important requirement then the one in the normative SR ENISO 10211/1-98 was imposed. The requirement considers obtaining the convergence of the numeric calculus results by assuring the energy balance condition, in every

node of the calculus network, according to relation (17), with a accuracy of 0,0001W.

1.2. Glazing system and the solar protection devices

The glazing unit and the solar protection devices are made from a sequence of layers of material separated by spaces filled in with gas. The layers of the material are considered homogeneous and with thermal conductivities, that are not varying with temperature.

The heat and solar radiation flow are considered to transfer unidimensional. For the ventilated spaces, the expressions for the two-dimensional convection are converted into unidimensional formulas.

The layers for material and spaces are numbered with the subscript j from 1 to n, space n representing the interior environment and space O the exterior environment. The physical model does not limitate the number of layers.

The basis formulas indicated for the solar radiation and for the heat transfer express the energy balance for each layer.

For resolving the non-linear dynamic system of equations obtained, it is recommended the use of a iterative calculus process.

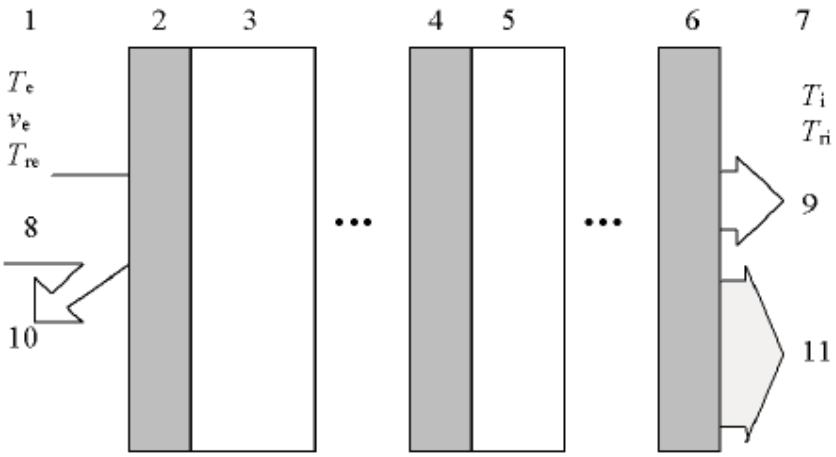

Figure 1 . System made of layers of material and spaces

Legend

T_e	Exterior air temperature	1	Exterior	8	Solar radiation
T_{re}	Exterior radiating temperature	2	Layer 1	9	Direct solar and luminous transmission factor

v_e	Exterior wind speed	3	Space 1		
T_i	Interior air temperature	4	Layer j	10	Direct solar and luminous reflection factor
T_{ri}	Interior radiating temperature	5	Space j		
		6	Layer n	11	Radiative and convective (direct and indirect) thermal transfer
		7	Interior		

NOTE: The interior and exterior environs are characterised by the interior air temperature and the radiating temperature; the exterior environment is also caracterised by the speed wind.

1.3. Solar and optical characteristics of the glazing

For each wave length λ and for each layer of the glazing j, next equilibrium equations can be written (Figure 2) for the normalized spectral radiative flow I_j si I'_j:

$$I_j(\lambda) = \tau_j(\lambda) \cdot I_{j-i}(\lambda) + \rho'_j(\lambda) \cdot I'_j(\lambda)$$
$$I'_j(\lambda) = \rho_j(\lambda) \cdot I_{j-i}(\lambda) + \tau'_j(\lambda) \cdot I'_j(\lambda) \quad (1)$$

where:

$\tau_j(\lambda)$ spectral transmission factor of the face exterior oriented ;
$\tau'_j(\lambda)$ spectral transmission factor of the face interior oriented ;
$\rho_j(\lambda)$ spectral reflection factor of the face exterior oriented ;
$\rho'_j(\lambda)$ spectral reflection factor of the face interior oriented ;
$I_j(\lambda)$ normalized spectral radiative flow interior oriented ;
$I'_j(\lambda)$ normalized spectral radiative flow exterior oriented ;

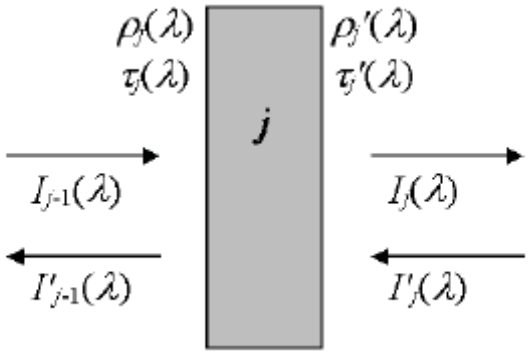

Figure 2. The scheme with the characteristic data of the layer j and related spectral flows

By writing the equation (1) for each layer *j* of the glazing, a system with n equations will result, having as unknowns the values for $I_j(\lambda)$ şi $I'_j(\lambda)$.

The limit conditions for resolving the system of equations will be:

$$I_0(\lambda) = 1 \text{ and } I_n(\lambda) = 0 \tag{2}$$

After resolving the system of equations and obtaining for each layer *j* the values for the spectral radiative flow $Ij(\lambda)$ şi $I'j(\lambda)$, the next factor will be obtained:

spectral transmission factor : $\tau_j(\lambda) = I_n(\lambda)$ (3)

spectral reflection factor : $\rho_j(\lambda) = I'_0(\lambda)$ (4)

spectral absorption factor:

$$\alpha_j(\lambda) = \left(1 - \rho_j(\lambda) - \tau_j(\lambda)\right) \cdot I_{j-1}(\lambda) + \left(1 - \rho'_j(\lambda) - \tau'_j(\lambda)\right) \cdot I'_j(\lambda) \tag{5}$$

The direct solar transmission factor τ_e, the direct solar reflection factor ρ_e, and the spectral absorption factor α_{ej} for each layer will be calculated taking into account the spectral data, determined according to the methodology from SR EN 410:1998;

In the same way the direct luminous transmission factor τ_v and direct luminous reflection factor ρ_v will be calculated.

1.4. Heat transfer

1.4.1 Thermal radiation

The heat flow through radiation depends upon the temperature of the system double with other heat flows that appear in the system.

For the thermal radiation the scheme from figure 3 is used, where the next characteristics are presented for each face of the layers that compose the system, glazing or solar protection layer.

T_j absolute temperature ;
$\tau_{th,j}$ direct solar transmission factor ;
ε_j effective emissivity of the face exterior oriented ;
ε'_j effective emissivity of the face interior oriented ;
$q_{th,j}$ radiative flow density towards interior ;
$q'_{th,j}$ radiative flow density towards exterior.

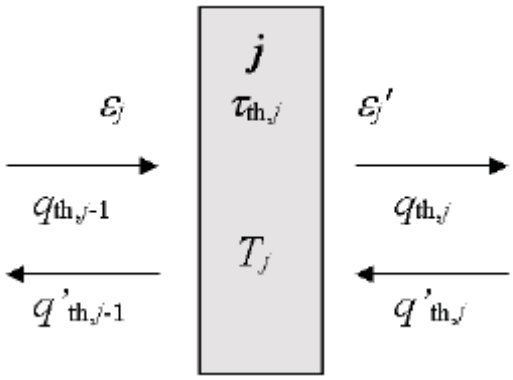

Figure 3. Characteristic data of the layer j and related radiative flow densities

The effective emissivity ε is derived from the normal emissivity ε_n, determined with the help of a infrared spectophotometer, with the related correction from the procedure described in SR EN 673 annex A.2.

For each layer *j* of the system of the glazing equations of radiative energy balance will be written resulting a complex equations system, where the temperature are at the forth value :

$$q_{th,j} = \tau_{th,j} \cdot q_{th,j-1} + \left(1 - \varepsilon'_j - \tau_{th,j}\right) \cdot q'_{th,j-i} + \varepsilon'_j \cdot \sigma \cdot T_{j-1}^4$$

$$q'_{th,j-1} = \left(1 - \varepsilon_j - \tau_{th,j}\right) \cdot q_{th,j-1} + \tau_{th,j} \cdot q'_{th,j} + \varepsilon_j \cdot \sigma \cdot T_j^4 \qquad (6)$$

Limit conditions are given by the interior and exterior radiative conditions, $T_{r,e}$ şi $T_{r,i}$:

$$q_{th,0} = \sigma \cdot T_{re}^4 \;;\; q_{th,n} = \sigma \cdot T_{ri}^4 \qquad (7)$$

After resolving the system of equations and determining the temperatures T_j, the next will be calculated :

the net radiative flow toward exterior

$$q_e = q'_{th,0} - q_{th,0} \qquad (8)$$

the net radiative flow toward interior

$$q_i = q'_{th,n} - q_{th,n} \qquad (9)$$

retained net heat, from thermal radiation, in layer *j*

$$q_{th,a,j} = \varepsilon_j \cdot q_{th,j-1} - \varepsilon'_j \cdot q'_{th,j} + \left(\varepsilon_j + \varepsilon'_j\right) \cdot \sigma \cdot T_j^4 \qquad (10)$$

1.4.2 Heat transfer through thermal conduction and thermoconvection in enclosed spaces with glazing surfaces

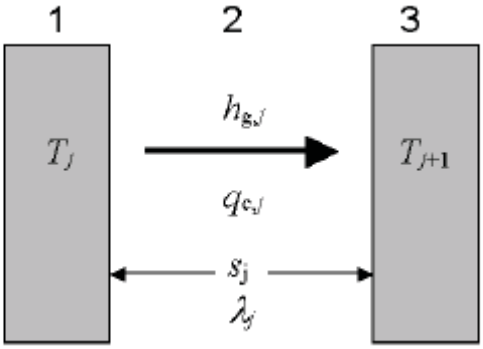

Figure 4. Scheme presenting the characteristic data for an enclosed space and the heat flow density through thermal conduction and thermoconvection

Legend
1 Layer j
2 Space of gas j
3 Layer j+ 1

λ_j Thermal conductivity of gas in a space j at temperature $T_m = \frac{(T_j + T_{j+1})}{2}$

s_j The thickness of the gas layer from the layer j

$h_{g,j}$ Thermal conductance of the gas in layer j

$q_{c,j}$ Heat flow density through thermal conduction and thermoconvection starting from layer j to j + 1

Thermal conductivity of gas in a limited space j, at medium temperature $T_{m,j} = \frac{(T_j + T_{j+1})}{2}$, enclosed between glazing surfaces (Figure 4), is given by the relation:

$$h_{g,j} = \frac{Nu_j \cdot \lambda_j}{s_j} \tag{11}$$

where:
- λj thermal conductivity of the gas from the enclosed space j ;
- sj the thickness of the gas layer ;
- λ thermal conductivity of the gas at the temperature Tm;

Nu Nusselt dimensionless number, determined according to the stipulations from the standard SR EN ISO 673:2000;

Limit conditions for exterior are:

for the air temperature : $T_0 = T_e$;
for the thermal transfer through thermoconvection:

$$h_{g,0} = h_{c,e} ; \tag{12}$$

Limit conditions for interior are:

for the air temperature : $T_{n+1} = T_i$;
for the thermal transfer through thermoconvection:

$$\text{hg,n} = \text{hc,i} ; \tag{13}$$

After resolving the system of equations and after determining the temperatures Tj, in each node of the calculus network, the next will be calculated :

resulted net heat in layer j (through thermal conduction and thermoconvection), is given by :

$$q_{c,aj} = h_{g,j-1} \cdot \left(T_{j-1} - T_j\right) + h_{g,j} \cdot \left(T_{j+1} - T_j\right) \tag{14}$$

heat flow density through thermoconvection toward exterior environs is given by :

$$q_{c,e} = q_{c,a,0} = h_{g,0} \cdot \left(T_1 - T_e\right) \tag{15}$$

heat flow density through thermoconvection toward interior environs is given by :

$$q_{c,i} = q_{c,a,n} = h_{g,n} \cdot \left(T_i - T_n\right) \tag{16}$$

A non-linear algebraic system of equations will result, after writting the equation for the energy balance, in each node of the calculus network. Because of the dynamic and non-linear nature of interaction between temperature and the radiative and convective heat transfer, for resolving the resulted system of equations, it is recommended the use of an iterative process. The dynamic nature is assess a rewritting for the system of equations, because of the modification of coefficients belonging to the system of equations, for each step of the iterative calculus.

2. VALIDATION OF THE "SOLAR" AUTOMATON CALCULUS PROGRAM

The validation of the automaton calculus program was made using the examples from annex C of the norm EN 13363-2:2005.

Next entry data were used:

1. exterior blind: blind- 50 mm air space- 4 mm glazing- 13 mm air space- 4 mm glazing
2. interior blind: 4 mm glazing- 13 mm air space- 4 mm glazing- 50 mm air space- blind.
3. inbuilt blind: 4 mm glazing - 13 mm air space- blind- 13 mm air space- 4 mm glazing.

Propeties of the materials:

Glass:

- 4 mm clear normal glass;
- solar energy transmission factor τ_e= 0,82, reflection factor ρ_e= 0,07;
- thermal emissivity ε= 0,84.

Blind:

- solar energy transmission factor τ_e= 0,2, reflection factor ρ_e= 0,4;
- thermal emissivity ε= 0,9;
- without thermal radiation transmission.

The obtained results depend on several factors:

- number of decimals with which the thermotechnic parameters are taken (2,3,4,...);
- number of decimals for working (algorithm calculus accuracy);
- number of calculus steps at which the thermotechnic parameters of air are changing numarul;
- interpolation manner of those parameters, when this operations are made etc .

After performing the calculus in double precision, is inferred that the values displayed in norm EN 13363-2:2005 in the annex C, are obtained as intermediate calculus values before the energetic balancing of the glazing system layers with solar protection.

After carrying out the calculus up to the energetic balance, until assurance with 3 decimals the energetic balance, the obtained results differ meaningful from the displayed values in annex C of the norm EN 13363-2:2005. The obtained results with the automaton calculus program “Solar” are the proper one by the thermotechnic point of view, taking into consideration the energy balance in each layer of the glazing assembly with solar protection.

The listing with the obtained results is given for the analyzed examples.

In the listing the results are obtained for: direct solar transmission factor τ, radiation factor G_h, convection factor G_c, ventilation factor G_v, secondary thermal transfer interior oriented G_{hcv}, total energy transmission factor G_{hcv+T}

On the right side of the tables in the listing is presented the energy balance for each surface of the glazing assembly- solar protection. It can be observed that the results

displayed in tables in annex C of the norm EN 13363-2:2005, are the intermediate calculus values before the energy balancing of the surfaces of the system.

3. CONCLUSIONS

The automaton calculus program "SOLAR" has a prompt practicability in the designing phase and also in the phase for energetic rehabilitation for new and existing buildings.

This program covers the required necessity of the experts in the field. Its applicability is general and can be taken into consideration for any type of glazing, filled with various gases, with the surfaces of the clear or treated glass, with or without solar protection in three variants of emplacement: in exterior, in interior and between leaves of glass.

References

1. SR EN 410:2003, *Glass for constructions. Determination of the solar and luminous characteristics of glazing.*
2. SR EN 673:2000, *Glass for constructions. Determination of the thermal transmittance U. Calculus method.*
3. SR EN 673:2000/A1:2002, *Glass for constructions. Determination of the thermal transmittance U. Calculus method.*
4. SR EN 673:2000/A1:2002/A2:2004, *Glass for constructions. Determination of the thermal transmittance U. Calculus method.*
5. SR EN ISO 10077-2:2004, *Pthermal perfomance of windows, doors and shutters. Calculus for the thermal transmittance- Second part: General method*
6. SR EN ISO 10211-1:1998, *Thermal bridges in constructonsi.Thermal flows and superficial temperatures. First part: General calculus method.*
7. SR EN ISO 10211-1:1998/AC :2003, *Thermal bridges in constructonsi.Thermal flows and superficial temperatures. First part: General calculus method.*
8. SR EN 13363-2:2006, Solar protection devices applied for glazings. The calculus of the solar and luminous transmission factor. Second part: The detailed calculus method.

Stor exterior si Doua geamuri (neventilat)

Ir = 0.0			Ir = 300.0			Rezultate						Echil. energetic Ir=0.0			Echil. energetic Ir=300.0		
Iter	Radiatie	Convecti	Ventilat	Radiatie	Convecti	Ventilat	Tau(T)	Gh	Gc	Gv	Ghcv	Ghcv+T	Suprl	Supr2	Supr3	Suprl	Supr2	Supr3
0	-22.385	13.500	0.000	-22.385	13.500	0.000	0.142	0.000	0.000	0.000	0.000	0.142	-90.217	99.587	13.300	32.783	105.587	19.300
1	-18.097	9.536	0.000	-42.574	22.954	0.000	0.142	-0.081	0.044	0.000	-0.037	0.105	-207.861	38.995	-7.538	377.226	33.737	-6.487
2	-16.182	8.231	0.000	-20.479	11.466	0.000	0.142	-0.014	0.010	0.000	-0.004	0.138	36.621	-35.392	-7.459	4.262	15.251	8.766
3	-22.742	12.248	0.000	-15.377	8.177	0.000	0.142	0.024	0.013	0.000	0.037	0.179	7.389	-13.643	-3.185	-3.432	0.338	2.983
4	-25.512	13.984	0.000	-14.777	7.699	0.000	0.142	0.035	0.020	0.000	0.055	0.197	2.057	-3.695	-1.079	-0.676	-1.273	0.938
5	-26.311	14.498	0.000	-14.781	7.661	0.000	0.142	0.038	0.022	0.000	0.060	0.202	0.686	-0.647	-0.322	0.055	-0.716	0.329
6	-26.470	14.606	0.000	-14.807	7.663	0.000	0.142	0.038	0.023	0.000	0.061	0.203	0.226	-0.031	-0.088	0.134	-0.320	0.128
7	-26.487	14.620	0.000	-14.818	7.665	0.000	0.142	0.038	0.023	0.000	0.061	0.203	0.057	0.035	-0.024	0.077	-0.135	0.053

Calculul Exact

Ir = 0.0			Ir = 300.0			Rezultate						Echil. energetic Ir=0.0			Echil. energetic Ir=300.0		
Iter	Radiatie	Convecti	Ventilat	Radiatie	Convecti	Ventilat	Tau(T)	Gh	Gc	Gv	Ghcv	Ghcv+T	Suprl	Supr2	Supr3	Suprl	Supr2	Supr3
0	-14.956	8.342	0.000	-21.804	11.550	0.000	0.142	-0.023	0.011	0.000	-0.012	0.130	-193.603	-2.406	2.596	120.299	-0.828	-0.257
1	-21.070	11.117	0.000	-18.079	9.765	0.000	0.142	0.010	0.005	0.000	0.014	0.156	-24.606	-5.653	-6.386	13.514	4.432	3.799
2	-24.623	13.386	0.000	-15.941	8.424	0.000	0.142	0.029	0.017	0.000	0.045	0.187	-6.542	-1.815	-2.586	3.796	1.655	1.699
3	-25.873	14.214	0.000	-15.100	7.882	0.000	0.142	0.036	0.021	0.000	0.057	0.199	-2.036	-0.595	-0.871	1.328	0.596	0.643
4	-26.286	14.488	0.000	-14.789	7.680	0.000	0.142	0.038	0.023	0.000	0.061	0.203	-0.659	-0.194	-0.285	0.479	0.216	0.236
5	-26.420	14.578	0.000	-14.676	7.607	0.000	0.142	0.039	0.023	0.000	0.062	0.204	-0.215	-0.063	-0.093	0.174	0.078	0.086
6	-26.464	14.607	0.000	-14.634	7.580	0.000	0.142	0.039	0.023	0.000	0.063	0.205	-0.070	-0.021	-0.030	0.063	0.028	0.031
7	-26.479	14.617	0.000	-14.619	7.570	0.000	0.142	0.040	0.023	0.000	0.063	0.205	-0.023	-0.007	-0.010	0.023	0.010	0.011
8	-26.483	14.620	0.000	-14.614	7.567	0.000	0.142	0.040	0.024	0.000	0.063	0.205	-0.007	-0.002	-0.003	0.008	0.004	0.004
9	-26.485	14.621	0.000	-14.612	7.565	0.000	0.142	0.040	0.024	0.000	0.063	0.205	-0.002	-0.001	-0.001	0.003	0.001	0.002
10	-26.485	14.622	0.000	-14.611	7.565	0.000	0.142	0.040	0.024	0.000	0.063	0.205	-0.001	-0.000	-0.000	0.001	0.000	0.001
11	-26.485	14.622	0.000	-14.611	7.565	0.000	0.142	0.040	0.024	0.000	0.063	0.205	-0.000	-0.000	-0.000	0.000	0.000	0.000

Doua geamuri Si Stor interior (neventilat)

Ir = 0.0			Ir = 300.0			Rezultate						Echil. energetic Ir=0.0			Echil. energetic Ir=300.0		
Iter	Radiatie	Convecti	Ventilat	Radiatie	Convecti	Ventilat	Tau(T)	Gh	Gc	Gv	Ghcv	Ghcv+T	Suprl	Supr2	Supr3	Suprl	Supr2	Supr3
0	-61.078	28.451	0.000	-21.854	0.142	0.000	0.142	0.130	0.094	0.000	0.224	0.366	-3.778	-24.668	-38.410	-75.256	54.222	-35.698
1	-62.332	31.637	0.000	-25.266	0.142	0.000	0.142	0.123	0.104	0.000	0.227	0.369	-42.602	-37.992	-7.145	-88.343	35.714	-25.266
2	-59.456	31.637	0.000	-24.990	0.142	0.000	0.142	0.114	0.104	0.000	0.218	0.360	-51.816	-21.690	11.449	-97.878	51.548	-25.166
3	-58.209	31.637	0.000	-14.415	0.142	0.000	0.142	0.145	0.104	0.000	0.249	0.391	-65.911	-11.435	19.352	-750.994	176.550	41.860
4	-57.601	31.637	0.000	1.269	0.142	0.000	0.142	0.196	0.104	0.000	0.300	0.442	-66.683	-9.427	23.424	-650.762	-7.774	158.729
5	-54.261	29.207	0.000	75.021	0.142	0.000	0.142	0.430	0.096	0.000	0.526	0.668	-67.282	-4.076	14.754	-641.857	50.573	-81.387
6	-54.035	29.207	0.000	52.879	0.142	0.000	0.142	0.356	0.096	0.000	0.452	0.594	-94.118	1.069	16.188	429.360	-160.092	-221.720
7	-54.038	29.207	0.000	40.311	0.142	0.000	0.142	0.314	0.096	0.000	0.410	0.552	-94.560	1.894	16.097	439.350	-192.316	-307.024
8	-51.469	27.274	0.000	-5.858	0.142	0.000	0.142	0.152	0.090	0.000	0.242	0.384	-94.644	5.445	8.463	450.954	-271.003	-201.572

Calculul Exact

Ir = 0.0			Ir = 300.0			Rezultate						Echil. energetic Ir=0.0			Echil. energetic Ir=300.0		
Iter	Radiatie	Convecti	Ventilat	Radiatie	Convecti	Ventilat	Tau(T)	Gh	Gc	Gv	Ghcv	Ghcv+T	Suprl	Supr2	Supr3	Suprl	Supr2	Supr3
0	-56.657	29.400	0.000	-31.031	9.341	0.000	0.142	0.085	0.067	0.000	0.152	0.294	-2.146	-3.516	-0.063	0.009	0.014	0.001
1	-56.986	29.603	0.000	-31.030	9.339	0.000	0.142	0.087	0.068	0.000	0.154	0.296	-0.474	-0.895	-0.010	0.000	0.000	0.000
2	-57.057	29.647	0.000	-31.030	9.339	0.000	0.142	0.087	0.068	0.000	0.154	0.296	-0.152	-0.299	-0.003	0.000	0.000	0.000
3	-57.080	29.661	0.000	-31.030	9.339	0.000	0.142	0.087	0.068	0.000	0.155	0.296	-0.054	-0.108	-0.001	0.000	0.000	0.000
4	-57.088	29.665	0.000	-31.030	9.339	0.000	0.142	0.087	0.068	0.000	0.155	0.296	-0.020	-0.040	-0.000	0.000	0.000	0.000
5	-57.091	29.667	0.000	-31.030	9.339	0.000	0.142	0.087	0.068	0.000	0.155	0.296	-0.007	-0.015	-0.000	0.000	0.000	-0.000
6	-57.092	29.668	0.000	-31.030	9.339	0.000	0.142	0.087	0.068	0.000	0.155	0.296	-0.003	-0.006	-0.000	0.000	0.000	0.000
7	-57.092	29.668	0.000	-31.030	9.339	0.000	0.142	0.087	0.068	0.000	0.155	0.296	-0.001	-0.002	-0.000	0.000	0.000	0.000
8	-57.093	29.668	0.000	-31.030	9.339	0.000	0.142	0.087	0.068	0.000	0.155	0.296	-0.000	-0.001	-0.000	0.000	0.000	0.000
9	-57.093	29.668	0.000	-31.030	9.339	0.000	0.142	0.087	0.068	0.000	0.155	0.296	-0.000	-0.000	-0.000	0.000	0.000	0.000

Geam Stor Geam (neventilat)

I t er	Ir = 0.0 Radiatie	Convecti	Ventilat	Ir = 300.0 Radiatie	Convecti	Ventilat	Rezultate Tau(T)	Gh	Gc	Gv	Ghcv	Ghcv+T	Echil. energetic Ir=0.0 Suprl	Supr2	Supr3	Echil. energetic Ir=300.0 Suprl	Supr2	Supr3
0	-14.753	13.500	0.000	-14.753	13.500	0.000	0.142	0.000	0.000	0.000	0.000	0.142	-77.982	248.809	58.736	-33.882	350.809	64.136
1	-338.562	490.932	0.000	-357.765	599.364	0.000	0.142	-0.064	0.361	0.000	0.297	0.439	97.805	-338.833	1207.277	198.309	-248.820	1360.504
2	-78.259	55.944	0.000	-64.621	49.500	0.000	0.142	0.045	0.021	0.000	0.066	0.208	-35.573	67.851	133.844	-38.646	102.068	168.965
3	-13.169	1.728	0.000	33.516	-42.264	0.000	0.142	0.155	0.146	0.000	0.301	0.443	12.826	142.289	-89.246	3005.241	-113.083	-430.448
4	-23.550	9.252	0.000	23.486	-16.380	0.000	0.142	0.156	0.085	0.000	0.241	0.383	10.568	77.569	-56.651	31.686	44.083	-51.419
5	-31.986	16.596	0.000	19.481	-13.572	0.000	0.142	0.171	0.100	0.000	0.271	0.413	-30.280	40.528	-16.112	-35.897	-74.251	-35.051
6	-35.468	19.404	0.000	12.302	-13.104	0.000	0.142	0.159	0.108	0.000	0.267	0.409	-26.166	31.957	-6.303	-2.666	14.123	-88.593

Calculul Exact

I t er	Ir = 0.0 Radiatie	Convecti	Ventilat	Ir = 300.0 Radiatie	Convecti	Ventilat	Rezultate Tau(T)	Gh	Gc	Gv	Ghcv	Ghcv+T	Echil. energetic Ir=0.0 Suprl	Supr2	Supr3	Echil. energetic Ir=300.0 Suprl	Supr2	Supr3
0	-33.524	18.565	0.000	-10.114	4.665	0.000	0.142	0.078	0.046	0.000	0.124	0.267	-0.128	0.428	0.258	-0.318	-0.986	-1.338
1	-33.394	18.471	0.000	-10.651	5.038	0.000	0.142	0.076	0.045	0.000	0.121	0.263	0.005	0.001	0.001	-0.086	-0.236	-0.230
2	-33.393	18.471	0.000	-10.752	5.106	0.000	0.142	0.075	0.045	0.000	0.120	0.262	0.000	0.000	0.000	-0.018	-0.049	-0.047
3	-33.393	18.471	0.000	-10.773	5.120	0.000	0.142	0.075	0.045	0.000	0.120	0.262	0.000	0.000	0.000	-0.004	-0.010	-0.010
4	-33.393	18.471	0.000	-10.777	5.123	0.000	0.142	0.075	0.044	0.000	0.120	0.262	0.000	0.000	0.000	-0.001	-0.002	-0.002
5	-33.393	18.471	0.000	-10.778	5.123	0.000	0.142	0.075	0.044	0.000	0.120	0.262	0.000	0.000	0.000	-0.000	-0.000	-0.000

Geam Stor Geam Vara (neventilat)

I t er	Ir = 0.0 Radiatie	Convecti	Ventilat	Ir = 500.0 Radiatie	Convecti	Ventilat	Rezultate Tau(T)	Gh	Gc	Gv	Ghcv	Ghcv+T	Echil. energetic Ir=0.0 Suprl	Supr2	Supr3	Echil. energetic Ir=500.0 Suprl	Supr2	Supr3
0	0.000	0.000	0.000	65.981	-29.500	0.000	0.142	0.132	0.059	0.000	0.191	0.333	0.000	0.000	0.000	77.000	537.104	-151.604
1	0.000	0.000	0.000	71.321	-29.500	0.000	0.142	0.143	0.059	0.000	0.202	0.344	0.000	0.000	0.000	1.871	-3.653	-81.638
2	0.000	0.000	0.000	71.366	-29.500	0.000	0.142	0.143	0.059	0.000	0.202	0.344	0.000	0.000	0.000	2.724	5.642	-80.785

Calculul Exact

I t er	Ir = 0.0 Radiatie	Convecti	Ventilat	Ir = 500.0 Radiatie	Convecti	Ventilat	Rezultate Tau(T)	Gh	Gc	Gv	Ghcv	Ghcv+T	Echil. energetic Ir=0.0 Suprl	Supr2	Supr3	Echil. energetic Ir=500.0 Suprl	Supr2	Supr3
0	0.000	0.000	0.000	52.193	-19.820	0.000	0.142	0.104	0.040	0.000	0.144	0.286	0.000	0.000	0.000	28.782	-13.284	-17.603
1	0.000	0.000	0.000	46.960	-17.316	0.000	0.142	0.094	0.035	0.000	0.129	0.271	0.000	0.000	0.000	5.643	-2.158	-1.409
2	0.000	0.000	0.000	46.671	-17.155	0.000	0.142	0.093	0.034	0.000	0.128	0.270	0.000	0.000	0.000	1.473	-0.106	-0.067
3	0.000	0.000	0.000	46.713	-17.164	0.000	0.142	0.093	0.034	0.000	0.128	0.270	0.000	0.000	0.000	0.503	0.049	0.029
4	0.000	0.000	0.000	46.748	-17.177	0.000	0.142	0.093	0.034	0.000	0.128	0.270	0.000	0.000	0.000	0.196	0.032	0.019
5	0.000	0.000	0.000	46.765	-17.183	0.000	0.142	0.094	0.034	0.000	0.128	0.270	0.000	0.000	0.000	0.080	0.015	0.009
6	0.000	0.000	0.000	46.772	-17.186	0.000	0.142	0.094	0.034	0.000	0.128	0.270	0.000	0.000	0.000	0.033	0.006	0.004
7	0.000	0.000	0.000	46.775	-17.187	0.000	0.142	0.094	0.034	0.000	0.128	0.270	0.000	0.000	0.000	0.014	0.003	0.002
8	0.000	0.000	0.000	46.777	-17.187	0.000	0.142	0.094	0.034	0.000	0.128	0.270	0.000	0.000	0.000	0.006	0.001	0.001
9	0.000	0.000	0.000	46.777	-17.187	0.000	0.142	0.094	0.034	0.000	0.128	0.270	0.000	0.000	0.000	0.002	0.000	0.000
10	0.000	0.000	0.000	46.777	-17.188	0.000	0.142	0.094	0.034	0.000	0.128	0.270	0.000	0.000	0.000	0.001	0.000	0.000
11	0.000	0.000	0.000	46.777	-17.188	0.000	0.142	0.094	0.034	0.000	0.128	0.270	0.000	0.000	0.000	0.000	0.000	0.000

Stor exterior si Doua geamuri Vara (neventilat)

I t er	Ir = 0.0 Radiatie	Convecti	Ventilat	Ir = 500.0 Radiatie	Convecti	Ventilat	Rezultate Tau(T)	Gh	Gc	Gv	Ghcv	Ghcv+T	Echil. energetic Ir=0.0 Suprl	Supr2	Supr3	Echil. energetic Ir=500.0 Suprl	Supr2	Supr3
0	0.000	0.000	0.000	29.664	-13.500	0.000	0.142	0.059	0.027	0.000	0.086	0.228	0.000	0.000	0.000	168.310	158.146	-65.156
1	0.000	0.000	0.000	38.213	-13.500	0.000	0.142	0.076	0.027	0.000	0.103	0.245	0.000	0.000	0.000	-234.837	70.656	4.321
2	0.000	0.000	0.000	35.707	-13.500	0.000	0.142	0.071	0.027	0.000	0.098	0.240	0.000	0.000	0.000	-4.669	-0.944	-11.977
3	0.000	0.000	0.000	35.586	-13.500	0.000	0.142	0.071	0.027	0.000	0.098	0.240	0.000	0.000	0.000	-0.293	-0.463	-12.815

Calculul Exact

I t er	Ir = 0.0 Radiatie	Convecti	Ventilat	Ir = 500.0 Radiatie	Convecti	Ventilat	Rezultate Tau(T)	Gh	Gc	Gv	Ghcv	Ghcv+T	Echil. energetic Ir=0.0 Suprl	Supr2	Supr3	Echil. energetic Ir=500.0 Suprl	Supr2	Supr3
0	0.000	0.000	0.000	45.827	-17.440	0.000	0.142	0.092	0.035	0.000	0.127	0.268	0.000	0.000	0.000	-46.260	2.477	-18.885
1	0.000	0.000	0.000	32.944	-12.204	0.000	0.142	0.066	0.024	0.000	0.090	0.232	0.000	0.000	0.000	-0.849	-0.114	-0.558
2	0.000	0.000	0.000	32.562	-12.047	0.000	0.142	0.065	0.024	0.000	0.089	0.231	0.000	0.000	0.000	-0.028	-0.004	-0.018
3	0.000	0.000	0.000	32.550	-12.042	0.000	0.142	0.065	0.024	0.000	0.089	0.231	0.000	0.000	0.000	-0.001	-0.000	-0.001
4	0.000	0.000	0.000	32.550	-12.042	0.000	0.142	0.065	0.024	0.000	0.089	0.231	0.000	0.000	0.000	-0.000	-0.000	-0.000

Doua geamuri Si Stor interior Vara (neventilat)

I t er	Ir = 0.0 Radiatie	Convecti	Ventilat	Ir = 500.0 Radiatie	Convecti	Ventilat	Rezultate Tau(T)	Gh	Gc	Gv	Ghcv	Ghcv+T	Echil. energetic Ir=0.0 Suprl	Supr2	Supr3	Echil. energetic Ir=500.0 Suprl	Supr2	Supr3
0	0.000	0.000	0.000	98.395	-45.000	0.000	0.142	0.197	0.090	0.000	0.287	0.429	0.000	0.000	0.000	62.806	46.753	-190.389
1	0.000	0.000	0.000	97.226	-45.000	0.000	0.142	0.194	0.090	0.000	0.284	0.426	0.000	0.000	0.000	64.361	36.899	-197.830
2	0.000	0.000	0.000	97.298	-45.000	0.000	0.142	0.195	0.090	0.000	0.285	0.426	0.000	0.000	0.000	62.327	37.244	-197.331
3	0.000	0.000	0.000	97.346	-45.000	0.000	0.142	0.195	0.090	0.000	0.285	0.426	0.000	0.000	0.000	61.265	37.306	-196.981

Calculul Exact

I t er	Ir = 0.0 Radiatie	Convecti	Ventilat	Ir = 500.0 Radiatie	Convecti	Ventilat	Rezultate Tau(T)	Gh	Gc	Gv	Ghcv	Ghcv+T	Echil. energetic Ir=0.0 Suprl	Supr2	Supr3	Echil. energetic Ir=500.0 Suprl	Supr2	Supr3
0	0.000	0.000	0.000	73.304	-31.781	0.000	0.142	0.147	0.064	0.000	0.210	0.352	0.000	0.000	0.000	-29.390	-38.773	-35.905
1	0.000	0.000	0.000	59.367	-26.005	0.000	0.142	0.119	0.052	0.000	0.171	0.313	0.000	0.000	0.000	-6.512	-13.835	-1.985
2	0.000	0.000	0.000	57.176	-25.228	0.000	0.142	0.114	0.050	0.000	0.165	0.307	0.000	0.000	0.000	-2.328	-3.165	-0.109
3	0.000	0.000	0.000	56.716	-25.079	0.000	0.142	0.113	0.050	0.000	0.164	0.305	0.000	0.000	0.000	-0.820	-1.064	-0.029
4	0.000	0.000	0.000	56.564	-25.030	0.000	0.142	0.113	0.050	0.000	0.163	0.305	0.000	0.000	0.000	-0.302	-0.390	-0.010
5	0.000	0.000	0.000	56.509	-25.012	0.000	0.142	0.113	0.050	0.000	0.163	0.305	0.000	0.000	0.000	-0.114	-0.147	-0.004
6	0.000	0.000	0.000	56.489	-25.005	0.000	0.142	0.113	0.050	0.000	0.163	0.305	0.000	0.000	0.000	-0.043	-0.056	-0.001
7	0.000	0.000	0.000	56.481	-25.003	0.000	0.142	0.113	0.050	0.000	0.163	0.305	0.000	0.000	0.000	-0.017	-0.021	-0.001
8	0.000	0.000	0.000	56.478	-25.002	0.000	0.142	0.113	0.050	0.000	0.163	0.305	0.000	0.000	0.000	-0.006	-0.008	-0.000
9	0.000	0.000	0.000	56.477	-25.001	0.000	0.142	0.113	0.050	0.000	0.163	0.305	0.000	0.000	0.000	-0.002	-0.003	-0.000
10	0.000	0.000	0.000	56.476	-25.001	0.000	0.142	0.113	0.050	0.000	0.163	0.305	0.000	0.000	0.000	-0.001	-0.001	-0.000
11	0.000	0.000	0.000	56.476	-25.001	0.000	0.142	0.113	0.050	0.000	0.163	0.305	0.000	0.000	0.000	-0.000	-0.000	-0.000

"Computational Civil Engineering 2007", International Symposium
Iaşi, România, May 25, 2007

Effect of moulding humidity on the properties of dry pressed ceramic tiles

Radomir Sokolar
Department of Technology of Building Materials and Components, Faculty of Civil Engineering, Brno University of Technology, City, Veveri 331/95, 602 00 Brno, Czech Republic

Summary

The aim of the work was to describe moulding humidity influence on the properties of dry pressed ceramic tiles from fly ash – clay mixture (70 % fly ash and 30 % stoneware clay). It was determined properties of green body (bulk density) and fired body (water absorption, bending strength, bulk density and apparent porosity according to EN ISO 10545 standards) by the mathematical functionalities.

KEYWORDS: Dry pressed ceramic tiles, pressing water content, bulk density, water absorption, green ceramic body, fired ceramic body.

1. INTRODUCTION

The enormous amount of fly ashes generated during mineral coal burning is still far from being used in its totality as a product or by-product, making technological alternatives needed in order to reduce its possible environmental impact. The paper present one of the possibilities how to use fly ashes – as a basic raw material for the production of ceramic tiles. It is evident, that moulding moisture influenced properties of dry pressed green or fired ceramic body very much. It was determined optimal water content to get maximal compact green body and the best properties of the firing fly ash - clay bodies according to EN ISO 10545 standards (e.g. water absorption, bending strength) and properties of the fly ash body microstructure. The properties of firing fly ash – clay body (water absorption, bending strength) were compared in accordance with requirements of EN 14411 for dry pressed for ceramic tiles (Table 1).

Table 1 - The choose properties of ceramic tiles - group B

Characteristics		BIa	BIb	B IIa	B IIb	B III
Water absorption [%]	average	≤ 0,5	0,5 - 3	3 - 6	6 - 10	> 10[2])
	individually	Max. 0,6	Max. 3,3	Max. 6,5	Max. 11	Min. 9
Bending strength [MPa]	average	≥ 35	≥ 30	≥ 22	≥ 18	≥ 15[1])
	individually	Min. 32	Min. 27	Min. 20	Min. 16	
Breaking strength (t ≥ 7,5 mm)		1300 N	1100 N	1000 N	800 N	600 N

2. RAW MATERIAL PROPERTIES

The fly ash utilized in this work was originated in the burning process of mineral brown coal in a pulverized coal-fired plant of Thermoelectrical Power Station, which is located in Melnik (Czech Republic). This thermoelectrical process has good efficiency in the combustion of the mineral coal and the residual carbon is very low - 1,2 wt%. Stoneware clay (from region Postorna CZ) was used as a binder for non plastic fly ash grains. The chemical composition of raw materials is showed in Table 2.

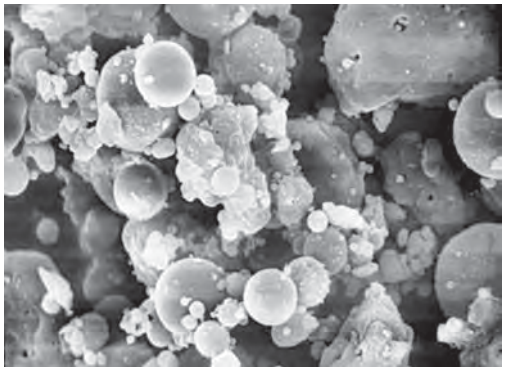

Figure 1. Microstructure of used fly ash (2000x).

Table 2. Average chemical composition of used raw materials

[mass-%]	**SiO_2**	**Al_2O_3**	**Fe_2O_3**	**TiO_2**	**CaO**	**MgO**	**K_2O**	**Na_2O**	**S**	**IL**
Fly ash	55,9	29,3	4,7	1,7	2,2	1,4	1,6	0,1	0,1	1,2
Clay	62,2	18,8	4,2	1,5	1,4	1,4	2,3			9,3

Particle size distribution of fly ash was studied by using of the floating method through the 0,063 mm sieve. The fly ash was grinded in the dry laboratory ball mill with clay together to get minimal residue on the 0,063 mm sieve.

Table 3. Particle size distribution of fly ash

	Original	After Ball grinding with clay
Sieve residue 0,063 mm [%]	43,2	5,9

3. SPECIMEN SHAPING AND FIRING

The mixture of raw materials (70 % mass fly ash + 30 % mass clay) was milled in dry ball mill together. Test specimens measuring 100 mm x 50 mm x 10 mm were

shaped in a laboratory press from granulate = moistened mixture with a different water content were pressed through a 1 mm sieve. The pressing pressure corresponds to used values for dry pressed ceramic tiles industrial production from spray-dried granulates (40 MPa).

The firing of test specimens proceed in the industrial tunnel kiln – maximal firing temperature 1020 °C with 5 hours soaking time in this temperature. After firing, It was determined properties of firing body: E – vacuum water absorption, B – bulk density (B_g – bulk density of green (not fired, only after drying) body, B_f – bulk density of fried body), P – apparent porosity, T – apparent relative density according to EN ISO 10545 – 3 and capillarity in dependence on moulding humidity. Frost resistance of firing body was determined by using indirect method - T – value (saturation value according to DIN 52253 – 3) describes the amount of open pores capable of filing with water under atmospheric pressure, in relation to the pores which fill with water at a vacuum of 30 mbar. Frost resisted bodies embody low T – values (under 0,75).

5. RESULTS

According to figures 2, 3 and tables 4, 5 it is evident, that all determined properties of green or fired bodies are depended on the pressing moisture of pressing granulate – it is concerned linear dependence. With increasing of pressing moisture the body is more compact and decreased the capillarity of fired fly ash – clay dry pressed body.

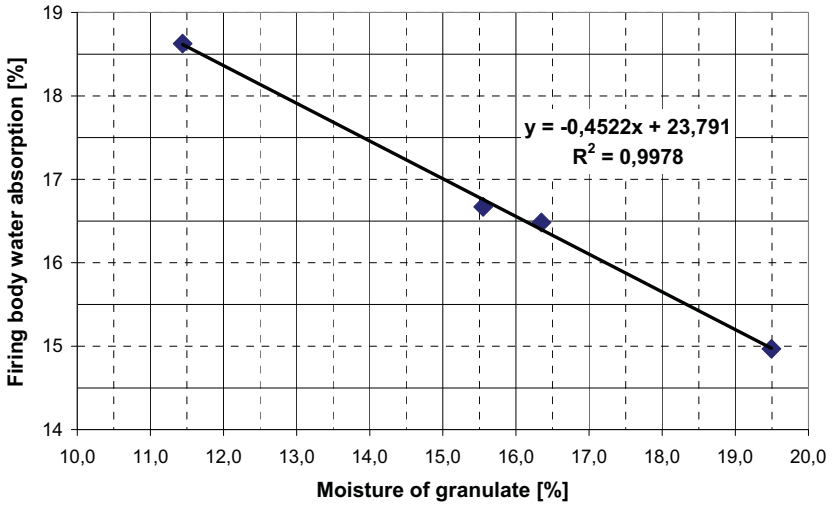

Figure 2. Fired body water absorption in dependence on pressing moisture of granulate

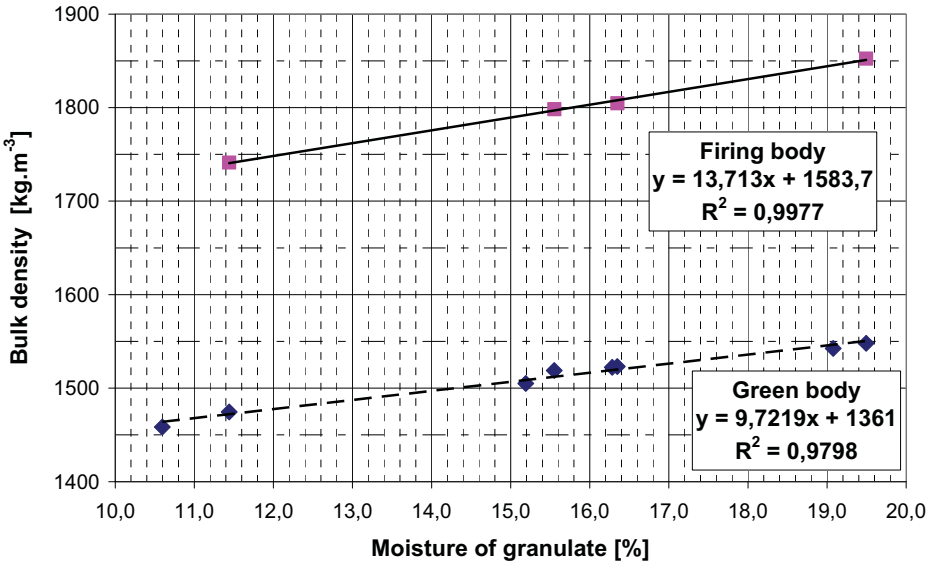

Figure 3. Bulk density of green and fired body in dependence on pressing moisture of granulate

Table 4. Properties of green and fired body

Moisture [%]	B_g [kg.m^{-3}]	B_f [kg.m^{-3}]	P [%]	E [%]	T [kg.m^{-3}]	T-value [-]
10,6	1458					
11,4	1475	1741	32,4	18,6	2577	0,988
15,2	1505					
15,6	1519	1798	30,0	16,7	2568	0,981
16,3	1523	1804	29,7	16,5	2569	0,976
19,1	1542					
19,5	1548	1852	27,7	15	2563	0,963

Table 5. Capillarity of fired bodied in dependence on pressing moisture of pressing granulate

Moisture [%]	Capillarity [mm] – after 5-10-20-30-40-50-60-70 min							
	5	**10**	**20**	**30**	**40**	**50**	**60**	**70**
11,4	47	64	76	85	all			
15,6	40	54	65	74	83	95	all	
16,3	36	50	60	69	77	83	all	
19,5	34	45	54	62	69	75	86	all

6. CONCLUSION

Possibility of dry pressed ceramic tiles production explicitly on base of Czech fly ashes is quite real. To get optimal properties of final fired body it must be determined optimal water content of pressing granulate.

Acknowlegements

This Research project was financed with MSM 0021630511 „Progressive Building Materials with Utilization of Secondary Raw Materials and their Impact on Structures Durability“

References

1. MAAGE M. Frost resistance and pore size distribution of bricks 1-2, Ziegelindustrie International, 1990, no. 9, p. 472-481, no. 10, p. 582-588.
2. BENTRUP H., FRANKE L.: Evaluation of the frost resistance of bricks in regard to long service life, Ziegelindustrie International, 1993, no. 7-8, p. 483-492, no. 9, p. 528-536.
3. FRIESE P.: Predictions of the Frost Resistance of Bricks, Ziegelindustrie International, 1995, no. 12, p. 952-963.
4. SOKOLAR, R. Dry Pressed Ceramic Tiles on the Basis of Fly Ash. Interceram 2007. DVS-Verlag GmbH, Vol. 56, no.1, p. 30-35, ISBN.

"Computational Civil Engineering 2007", International Symposium
Iaşi, România, May 25, 2007

Application of damage model for analysis of masonry structures

Jerzy Szołomicki

Department of Civil Engineering, Wrocław Universityof Technology, Wrocław, 50-370, Poland

Summary

The predictive modelling of the masonry structures behaviour, in the non-linear range represents a challenge due to their semi-discrete and composite nature. An adequate computational model should include the fundamental mechanisms that characterize the masonry behaviour at failure. This paper present the application of a damage model, based on the finite elements method, to simulate the ultimate response and the mode of failure of different masonry structures. To take into account the mechanical properties degradation, a damage variable is introduced in the constitutive law of the material.

KEYWORDS: Masonry structures, damage model, computational simulations

1. INTRODUCTION

The masonry structures are widely used in civil engineering. These structures are characterised by a softening response. Indeed, the non-linear behaviour of masonry is due to the damage and plastic micromechanical processes. From a microscopic point of view the damage is linked to the growth and coalescence of micro-cracks, leading to the formation of macro-cracks which can induce the collapse of the structure. The plasticity is due to intergranular displacements and accounts for inelastic deformations occurring during the loading process. Various nonlinear models have been proposed in the literature to describe the softening response of masonry structural elements. The available models adopted for structural computations are mainly based on macro-mechanical approaches using damage mechanics and plasticity theory.

As known, any macro-model of masonry structures always includes some approximations, since the different failure mechanisms of masonry (cracking of the mortar joints, sliding along bed and/or head mortar joints, cracking of the bricks under direct tension, masonry crushing) are not exactly reproduced, but are smeared out in the continuum.

This paper present the application of a damage model, based on the finite elements method, to simulate the ultimate response and the mode of failure of different masonry structures.

2. THE CONCEPTION OF DAMAGE MODEL

The nonlinear behaviour of masonry can be modelled using concepts of damage theory. In this case an adequate damage function is defined for taking into account different response of masonry under tension and compression states. Cracking can, therefore, be interpreted as a local damage effect, defined by the evolution of known material parameters and by one or several functions which control the onset and evolution of damage. The model takes into account all the important aspects which should be considered in the nonlinear analysis of masonry structures such as the effect of stiffness degradation due to mechanical effects and the problem of objectivity of the results with respect to the finite element mesh.

A useful concept for understanding the effect of damage is that of effective stress. The damaged $\boldsymbol{\sigma}_d$ and effective undamaged $\boldsymbol{\sigma}$ stress tensors are correlated, according to continuum damage mechanics, by the relation:

$$\boldsymbol{\sigma}_d = (1-d)\,\mathbf{D}\boldsymbol{\varepsilon} = (1-d)\boldsymbol{\sigma} \tag{1}$$

where d is a scalar value, ranging from 0 to 1 and representing the local damage parameter, **D** is the elastic stiffness matrix and $\boldsymbol{\varepsilon}$ is the strain tensor.

The damage function $g(\bar{\tau}, r)$ defines the limit of the region of undamaged response and is written at time t as:

$$\left(g(\bar{\tau}, r)\right)^t = \left(\bar{\tau}\right)^t - \left(r\right)^t \le 0 \tag{2}$$

where the undamaged complementary energy norm is defined as:

$$\left(\bar{\tau}\right)^t = \gamma\sqrt{2\Lambda^0\left(\left(\underline{\sigma}\right)^t\right)} \tag{3}$$

where $\Lambda^0(\underline{\sigma})$ is the elastic complementary energy.

For Simo's damage model $\gamma = 1$.

$\left(r\right)^t$ in the damage function of Equation (2) is the current damage strength measured with an energy norm and can be given as:

$$\left(r\right)^t = \max\left\{\left(r\right)^0, \left(\bar{\tau}\right)^t\right\} \tag{4}$$

where $\left(r\right)^0$ denotes the initial damage threshold of the material.

The initial damage threshold $\left(r\right)^0$, can be considered to carry out a similar function to the initial yield stress in an analysis involving an elasto-plastic material. However, in a damage analysis, the value of the damage threshold influences the degradation of the elastic modulus matrix. A value for $\left(r\right)^0$ may be obtained from:

$$(r)^0 = \frac{\sigma_d^t}{(E_0)^{1/2}} \tag{5}$$

where σ_d^t is the uniaxial tensile stress at which damage commences and E_0 is the undamaged Young's modulus. The damage criterion is enforced by computing the elastic complementary energy function as damage progresses:

$$\beta\left(\sigma^T D_e \sigma\right)^{1/2} - (r)^t \le 0 . \tag{6}$$

The damage flow rule defines the damage softening and is given by

$$\dot{d} = \dot{\mu}^t \frac{\partial\left(G(\bar{\tau}^t, d)^t\right)}{\partial \tau} \tag{7}$$

where $\dot{\mu} \ge 0$ is the damage consistency parameter and defines damage loading/unloading conditions according to the Kuhn-Tucker relations

$$\dot{\mu} \ge 0, g(\bar{\tau}, r) \le 0, \dot{\mu} g(\bar{\tau}, r) = 0 . \tag{8}$$

In addition, to simplify the calculations in damage analysis, the damage multiplier $\dot{\mu}$ is defined so that

$$\dot{\mu} = \dot{r} . \tag{9}$$

From the consistency of the damage condition in Equation (2) it is given that

$$\dot{\bar{\tau}} = \dot{r} = \dot{\mu} . \tag{10}$$

According to Equation (10), the definition (3) we have

$$\dot{\mu} = \frac{\gamma^2}{\bar{\tau}} \underline{\sigma}^T D_e^{-1} \dot{\underline{\sigma}} . \tag{11}$$

$(\partial G / \partial \bar{\tau})^t$ defines the damage rate with respect to the undamaged elastic complementary norm. If the damage potential function G is assumed to be independent of d, substitution of Equation (10) into Equation (7) will lead to:

$$d = G \tag{12}$$

with the undamaged condition being enforced so that

$$\left\{ G\left(r^t\right)_{(r)^t = (r)^0} \right\} = 0 . \tag{13}$$

Damage accumulation functions is given by:

$$\mathbf{G}\left((r)^t\right) = 1 - \frac{(r)^0 (1 - A)}{(r)^t} - A \exp\left[B\left((r)^0 - (r)^t\right)\right]. \tag{14}$$

For no damage, $\mathbf{G}(r)^t = 0$. The characteristic material parameters, A and B, would generally be obtained from experimental data.

3. DAMAGE CRITERION

The damage criterion is defined as a function of the free energy Ψ_0 of the undamaged material, expressed in terms of undamaged principal stresses $\sigma_i^{p,0}$:

$$\mathbf{F} = K\left(\sigma^{p,0}\right)\sqrt{2\rho_0\Psi_0} - 1 = \frac{K\left(\sigma^{p,0}\right)}{\sqrt{E^0}}\sqrt{\sum_{i=1}^{3}\left(\sigma^{p,0}\right)^2} - 1 \le 0 \tag{15}$$

where: ρ_0 is the density in the material configuration.

The terms of the above equation have the following meaning:

$$K\left(\sigma^{p,0}\right) = \frac{r}{\sqrt{2\rho_0\left(\Psi_t^0\right)_L}} + \frac{1 - r}{\sqrt{2\rho_0\left(\Psi_c^0\right)_L}}, \tag{16}$$

$$r = \frac{\sum_{i=1}^{3}\left\langle \sigma_i^{p,0} \right\rangle}{\sum_{i=1}^{3}\left|\sigma_i^{p,0}\right|}, \tag{17}$$

$$2\rho_0\left(\Psi_{t,c}^0\right)_L = \sum_{i=1}^{3}\left\langle \pm\sigma_i^{p,0}\right\rangle \varepsilon_i\,, \tag{18}$$

$$\left(\Psi_0\right)_L = \left(\Psi_t^0\right)_L + \left(\Psi_c^0\right)_L\,. \tag{19}$$

In these equations $\left(\Psi_{t,c}^0\right)_L$ represent the part of the free energy developed when the tension/compression limit is reached. Taking into account that the tension and compression strengths are $f_t = \sqrt{\left(2\rho_0\Psi_t^0 E_0\right)_L}$ and $f_c = \sqrt{\left(2\rho_0\Psi_c^0 E_0\right)_L}$ respectively, and substituting the last definition in the Equation (16), the damage function can be written as:

$$\mathbf{F} = \overline{\sigma} - f_c \le 0 \tag{20}$$

where

$$\overline{\sigma} = \left[1 + r\left(n - 1\right)\right]\sqrt{\sum_{i=1}^{3}\left(\sigma_i^{p,0}\right)^2} \tag{21}$$

with $n = \dfrac{f_c}{f_t}$. The advantage of the yield criterion written in Equation (21) is that any yield function $\mathbf{F}$ can be used always as long as it is homogeneous and of first order in stresses (Mohr-Coulomb, Drucker-Prager).

4. GLOBAL DAMAGE IMPLEMENTATION

The idea for global damage indices definition stemmed from a macroscale analogy with the microscale local damage index definition. Thus, the starting point for deducing a global structural damage index is Equation (22), which defines local damage as a relation between the actual free energy Ψ of the damaged material and the elastic free energy Ψ_0 of a fictitious undamaged material.

$$\Psi\left(\boldsymbol{\varepsilon}, d\right) = (1 - d)\Psi_0\left(\boldsymbol{\varepsilon}\right) = (1 - d)\left(\frac{1}{2\rho_0}\boldsymbol{\varepsilon}^T\boldsymbol{\sigma}^0\right). \tag{22}$$

It seemed natural to reach this objective by integrating the pointwise Equation (22) over a finite mass, as follows:

$$\Psi = (1 - d)\Psi_0 \Rightarrow \mathbf{W}_p = \int_V \rho_0\Psi dV = \int_V (1 - d)\rho_0\Psi_0 dV = (1 - D)\,\mathbf{W}_p^0 \tag{23}$$

where D^* is the global damage indices of the considered structural mass, $\mathbf{W}_p^0 = \int_V \rho_0\Psi_0 dV$ is its fictitious ever-elastic potential energy due to the actual strains and $\mathbf{W}_p$ is the actual potential energy. Solving Equation (23) for D, yields the final expression:

$$D^* = 1 - \frac{W_p}{W_p^0} = \frac{\int_V \rho_0\Psi_0 dV - \int_V (1 - d)\rho_0\Psi_0 dV}{\int_V \rho_0\Psi_0 dV} = \frac{\int_V d\rho_0\Psi_0 dV}{\int_V \rho_0\Psi_0 dV}. \tag{24}$$

In a finite element context, expression (24) takes the following operational form:

$$D^* = 1 - \frac{\sum_e \mathbf{a}^T \int_{V^{(e)}} \mathbf{B}^T\boldsymbol{\sigma} dV}{\sum_e \mathbf{a}^T \int_{V^{(e)}} \mathbf{B}^T\boldsymbol{\sigma}^0 dV} \tag{25}$$

where $\sum_{e}$ denotes the sum over a number of finite elements, **a** is the mesh nodal displacement vector, **B** is the strain displacement matrix, $V^{(e)}$ is the volume of each finite element (e), $\boldsymbol{\sigma}$ is the actual stress vector and $\boldsymbol{\sigma}_0$ is the stress vector should the material preserve its original characteristics and undergo the actual strains.

CONCLUSION

In this paper the author presented a damage model which can be applied successfully to asses the structural conditions and estimate the safety level and durability of historical masonry constructions under static and dynamic loading. The global damage indices provides accurate quantitative data on the state of any component subpart of a damaged structure and its importance to the overall structural behaviour, being of invaluable help to the task of assessing the reliability, safety and definition of adequate repair of retrofitting strategies.

References

1. Maier, G., Nappi, A. Papa, E. Damage models for masonry as a composite material: a numerical and experimental analysis. *Constitutive Laws for Engineering Materials*, ASME Press, New York, 1991.
2. Kachanov, L.M. Continuum model of medium with cracks. *ASCE J. Engng Mech.,* vol. 106: p. 1039-1051, 1980.
3. Park, Y.J., Ang, A.S. Mechanistic seismic damage model for reinforced concrete. *ASCE, J. Struct. Engng*, vol. 111: p. 722-739, 1985.
4. Pijaudier-Cabot, G., Bazant, Z.P. Non local damage theory. *ASCE J. Engng Mech.*, vol. 113: p. 1512-1533, 1987.
5. Gambarotta, L., Lagomarsino, S. Damage in brick masonry shear walls. *Fracture and Damage in Quasibrittle Structures: Experiments, Modelling and Computer Analysis,* p. 463-472, 1994.

"Computational Civil Engineering 2007", International Symposium
Iaşi, România, May 25, 2007

A New Form of the Active Moments Method

Constantin Ionescu
Civil Engineering, University, Iassy, Zip code: 700482, Romania

Summary

The paper desires to pay a tribute to Professors A. Şesan and N. Orlovschi, which professed last century at the Faculty of Civil Engineering and Installations from Iasi.

These professors imagined a calculation procedure for frames, named active moment method, as a response to the displacement (deformation) method.

The structure calculation by displacement methods is conducted on a base system, obtained by introducing fictive connections which deters the possible displacement of the nodes – revolutions and translations.

The elements in question in the displacement method are the nodes real displacements (written Z_i). Under the exterior forces action and displacements, on the elements in question direction, in the complementary connections appear reactions. Total reactions from complementary connections must be equal to zero. This way it can be obtained the condition equations.

Despite the active moments method, the basic system is similar to that in the displacements method, but the element in question are "active moments" of nodes $\boldsymbol{M_i}$ *and displacement (kinematic chains),* $\boldsymbol{M_A}$.

The active moment is defined as the moment which by its action on the base system, on the node ***"i"*** *or in the degree of freedom* ***"a",*** *creates the real displacement of the node* ***"i"****, and the real displacement of the nodes which are part of the kinematic chain* ***"a".***

The condition equations from the active moments method expresses the structure static equilibrium and has two types: nodes equilibrium equations and kinematic chains equilibrium equations. Must be mentioned the fact that none of the papers written by the authors didn't demonstrated the way in which the equilibrium equations have been obtained.

In the present paper have been obtained the equilibrium equations by active moments method by using the girder, node and nodes and beams chain equilibrium conditions with the help of the methodology "Gh. Em. Filipescu". This way has been obtained calculation relations for the extremity moments more general than the ones used in the displacements method, relations (4.6.) and (4.19.).

Also, it has been distinguished an alternative of the active moments method, where the elements in question are node active moments and active displacement forces.

KEYWORDS: structure calculus, condition equations, active moments, active forces, displacements, rigidities.

1. INTRODUCTION

The engineering technique evolution, in different time periods, has been determined by the necessity of refuge and attendance of the human activities which imposed a diversified volume of constructions. Due to this fact, has increased the number of problems connected to the search of different constructive forms which could better undertake the actions with a minimal construction materials consume.

The resistance structures composition and calculation has been made, long ago, based on the experience and only slightly on the theoretical elements.

Latter, based on the phenomena observation have been established constructive rules and calculation models, repetitively verified on the constructions. Generalizing the experience and development of the experimental researches have been developed the theoretical calculation basis for the constructions.

The current stage of theory development and structure calculus is due to engineers and science people who have discovered the solutions for the problems of the resistance structures design and execution for different constructions by experimental methods but also by theoretical ways.

Considering the investigations, have resulted general calculation methods, main principles of construction organization and future horizons of the researches in the area of one of the most interesting branches of the Construction Mechanics and Construction Dynamics.

In the science people gallery, which have contributed to the development of Construction Mechanics can be mentioned J.C.Maxwell, O. Mohr, K. Culman, L. Cremona, pe S. Timoşenko, I.P. Prokofiev and others.

In Romania, great engineers and professors as Gh. Em. Filipescu, A. Beleş, M. Hanganu, C. Avram, Alex. Gheorghiu, A. Şesan, M. Ifrim, N. Orlovschi and others have obtained remarkable results in the area of Constructions Static and Dynamics.

2. STATEMENT OF EQUILIBRIUM CONDITION

In the paper "The frame calculation by circumvolution method" published by A. Şesan and N. Popescu, in 1954, in the Journal of University "Al. I. Cuza" and

Polytechnic Institute in Iasi, are presented several definitions regarding the static structures calculus undetermined by displacements method.

It is mentioned that in that moment were known two methods of expressing the equilibrium equations. The first one had been published in Wien, in 1943, by R, Guldan. The equilibrium condition was expressed by two types of equations:

- Equilibrium equations on node ($\Sigma M_i = 0$):

$$d_i\varphi_i + \sum_k K_{ik}\varphi_i + K_{is}\Delta_{is} + K_{ij}\Delta_{ij} + S_i = 0 \qquad (2.1)$$

- Equilibrium equations of floor ($\Sigma T_k=0$) :

$$\sum_u \overline{K}\varphi_s + \sum_a \overline{K_j}\varphi_j + D_u + S_u = 0 \qquad (2.2.)$$

In these equilibrium equations have been made the notations:

- φ_i, φ_k, φ_s – nodes unknown angular displacements;
- Δ_k – unknown liniar displacements of the nodes;
- K_{ik} – rigidity at circumvolution of a bar extremity;
- $\overline{K}_s$ - rigiditatea la deplasare transversală a unei extremități de bară;
- S_i, D_u şi S_u – terms resulted from the actions effect.

Starting from the same base system with stucked displacements, I.P.Procofiev has published, in 1948, another form of static equilibrium equations:

- Node equilibrium equations:

$$\sum_{j=1}^{N} r_{ij}Z_j + \sum_{s=a}^{G} r_{is}Z_s + R_{ip} = 0 \quad \text{i} = 1,2,...,\text{N} \qquad (2.3.)$$

- Kinematic chain equilibrium equations:

$$\sum_{i=1}^{N} r_{si}Z_i + \sum_{e=a}^{G} r_{se}Z_e + R_{sp} = 0; \quad \text{s} = \text{a, b, . . ., G} \qquad (2.4.)$$

Where: $Z_1, \ldots, Z_j$ are nodes angular unknown displacements ,
$Z_k, \ldots, Z_n$ – nodes linear displacements.

Analyzing the two forms of the equilibrium equations statement, it can be observed that the first way in which it is used the forces equilibrium (T = 0), expressed by forces projections on perpendicular directions on beams, diminishes the application area only to frames with floors parallel beams. The second way, presented by Prokofiev, is based on effects overlapping (of the diagrams) and it is more general

than the first one, because it increases the methods area of application also to the frames with inclined pillars.

It must be mentioned also the paper of P. Mazilu, in Bucharest, in 1946, entitled: "The Frames Calculation – Displacements and Virtual Mechanical Work in Cross Method". The paper has been elaborated, as the author says, between 1942 –1943 and "introduces in Cross Method the principle of virtual displacements and virtual mechanical work".

In the same direction is written also the paper "Another Form of the Condition Equations for the Deformation Method" with the authors: A. Şesan and N. Popescu. The authors demonstrate that "the use of mechanical work for the condition equations establishment – node and displacement – can be generalized for any frames type".

The cited article and the paper named "Variants and Simplification of the Moments Distribution Method ", published by A. Sesan and N. Orlovschi, puts the basis of active moments method by introducing the notions of node and chain active moment.

In this paper, it is mentioned the use of "revolutions and displacements" as unknown elements of the condition equations which is a "disadvantage", because it operates with "insignificant" values, "modified" by multipliers and because of that the authors propose to express the equilibrium condition by elements in question - "active moments".

3. ABOUT THE "ACTIVE MOMENTS" METHOD

The "active moments" method was created in 1954 by professor A. Şesan and his collaborators: N. Orlovschi and N. Popescu. This is an alternative of displacements method which operates with unbalanced moments: "active moments" of nodes, $\mathbf{M_i}$ and displacement (kinematic chains), $\mathbf{M_A}$.

The active moment is defined as the moment which by activating, on the base system, on **"i"** node or in the liberty degree **"a",** determines the node **"i"** real displacement, also the real displacement of the node which are part from the kinematic chain "**a".**

The condition equations in the active moments method express the structure of static equilibrium and are of two types:

Nodes equilibrium equations:

$$\sum_i M = 0; \qquad -M_i + \sum_{j=1}^{N} \mu_{ij} M_j + \sum_a^G \mu_{ia} M_a + \eta = 0; \quad (i = 1, 2, ..., N); \quad (3.1.)$$

- Kinematic chains equilibrium equations:

$$\sum_a M = 0; \quad -M_a + \sum_{i=1}^{N} \mu_{ai} M_i + \sum_b^G \mu_{ab} M_b + m_a = 0; \quad (a = a,b,...,G); \quad (3.2.)$$

Where have been done the notations:

$$\mu_{ij} = -d_{ji} t_{ji}; \qquad \mu_{ji} = -d_{ij} t_{ij}; \qquad \mu_{ij} \neq \mu_{ji}; \qquad (3.3.)$$

$$\mu_{ia} = \sum_i \pm \nu'_{ij,a}; \qquad \nu'_{ij,a} = \frac{\overline{K_{ij}} \beta_{ij,a}}{\sum_A (\overline{K_{ij}} + \overline{K_{ji}}) \beta_{ij,a}}; \qquad (3.4.)$$

$$\mu_{ai} = \frac{1}{\beta_a} \sum_a d_{ij} (1 + t_{ij}) \beta_{ij,a}; \qquad \mu_{ia} \neq \mu_{ai}; \qquad (3.5.)$$

$$\mu_{ab} = -\frac{1}{\beta_a} \sum_{a,b} (\nu'_{ij,a} + \nu'_{ji,b}) \beta_{ij,a}; \qquad \mu_{ab} \neq \mu_{ba}; \qquad (3.6.)$$

$$m_i = \sum_i m_{ij}; \qquad m_a = \frac{1}{\beta_a} (\sum_a (m_{ij} + m_{ji}) \beta_{i,a} + \sum_k P_k \delta_{k,a}); \qquad (3.7.)$$

For these coefficients calculation are used the rigidities for the rotation of the bars extremities and for the transversal displacement of the bars extremities**,** $\mathbf{K_{ij}}$ şi $\mathbf{K_{ij}^{\psi}}$**,** the distribution and transmission: $\mathbf{d_{ij}}$**,** and $\mathbf{t_{ij}}$ and two proportionality coefficients: $\boldsymbol{\beta_{ij}}$ şi $\boldsymbol{\beta_A}$.

The proportionality coefficient of the bar rotation **ij** noted $\boldsymbol{\beta_{ij}}$ is calculated by considering a bar rotation which is equal to the unit, by which can be determined the other bars rotations.

If we consider that on a fictive bar acts an active moment, $\mathbf{M_A}$, than the proportionality coefficient of this bar is $\boldsymbol{\beta_A}$**.** The calculus is done with the relation:

$$\beta_a = \frac{\sum_a (\overline{K_{ij}^{\psi}} + \overline{K_{ji}^{\psi}}) \beta_{ij,a}^2}{\sum_a (\overline{K_{ij}^{\psi}} + \overline{K_{ji}^{\psi}}) \beta_{ij,a}} \qquad (3.8.)$$

4. DIRECT DEVICE FOR CONDITION EQUATION DEDUCTION IN THE METHOD OF "ACTIVE MOMENTS"

The deformed position of a certain frame can be defined by the mean of nodes displacements: rotations and translations.

The nodes angular displacements (**z_i, i = 1, 2, 3, ..., N**) are independent variables, while the linear displacements (**z_s, s = a, b, c, ..., G**) are interdependent by the mean of a number of parameters equal to the number of liberty degrees of the kinematic system, obtained by introducing articulations in nodes and in bearing constraint. The result is that the number of independent parameters, which geometrically define the deformed position of a structure, equals the nodes number to which is added the number of degrees of the frame elastic liberty. The nodes translations are part of a kinematic chain which relies on a single parameter, **z_s.**

For a bar **ij,** the rotation noted ψ_{ij} is expressed considering the parameter z_s with the relation:

$$\psi_{ij,s} = \beta_{ij,s} z_s \tag{4.1.}$$

Where $\beta_{ij,s}$ is the bar rotation ij when the parameter $z_s = 1$.

4.1. The girder equilibrium conditions

We extract a bar **ij** from a base system, of a certain structure, corresponding to the displacements method, activated by burdens and displacements (nodes rotation and bar rotation), fig.4.1. The general expressions of the end moments can be expressed as:

$$\begin{aligned} M_{ij} &= M_{ij}(z_i) + M_{ij}(z_j) + M_{ij}(\psi_{ij}) + M_{ij}(p) \\ M_{ji} &= M_{ji}(z_i) + M_{ji}(z_{jj}) + M_{ji}(\psi_{ij}) + M_{ji}(p) \end{aligned} \tag{4.2.}$$

Or as notations in fig.4.1:

$$\begin{aligned} M_{ij} &= K_{ij} z_i + t_{ji} K_{ji} z_j - \overline{K_{ij}^{\psi}} \psi_{ij} - \mathfrak{m}_{ij} \\ M_{ji} &= t_{ij} K_{ij} z_i + K_{ji} z_j - \overline{K_{ji}^{\psi}} \psi_{ij} + \mathfrak{m}_{ji} \end{aligned} \tag{4.3.}$$

In the case in which the bar **ij,** considered in the research, is component of different chains and nodes corresponding to the liberty degrees **a, b, c, ..., G,** than the expression of bar rotation can be written as a sum of rotations corresponding to each liberty degree:

$$\psi_{ij} = \psi_{ij,a} + \psi_{ij,b} + \psi_{ij,c} + ... = \sum_{s=a}^{G} \psi_{ij,s} \tag{4.4.}$$

or taking into consideration the relation (4.1):

$$\psi_{ij} = \sum_{s=a}^{G} \beta_{ij,s} z_s \tag{4.5.}$$

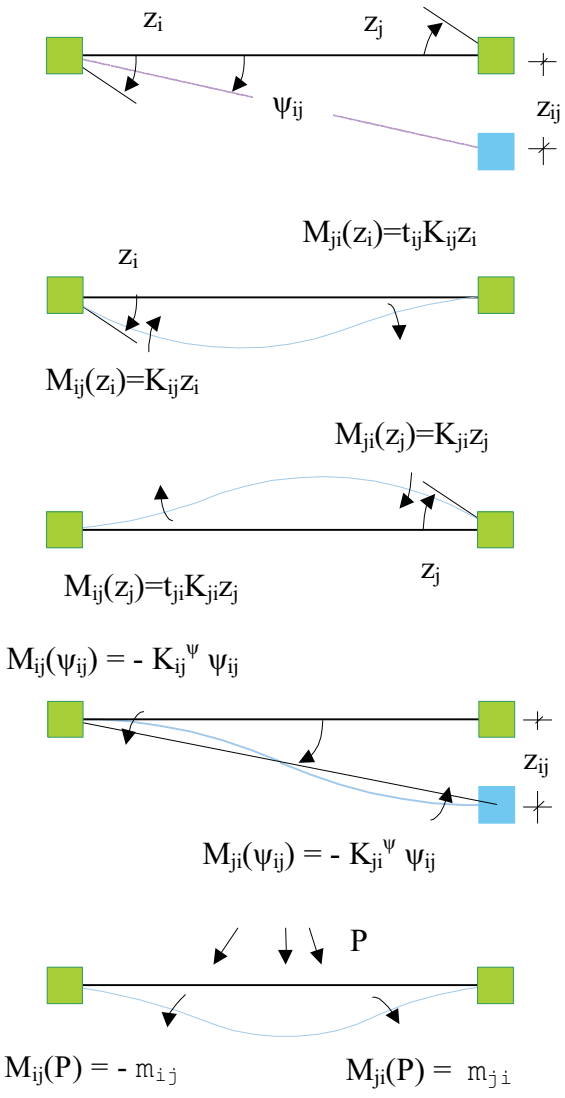

Fig. 4.1 Situations of girder and node loads considering the statement of equilibrium conditions – bar end moments *ij* for different load situations

The end moments, the relations (4.2.), as per relations (4.4.) and (4.5.) and notations from fig.4.1, become:

$$M_{ij} = K_{ij} z_i + t_{ji} K_{ji} z_j - \sum_{s=a}^{G} \overline{K_{ij}^{\psi}} \beta_{ij,s} z_s - m_{ij}$$
$$M_{ji} = t_{ij} K_{ij} z_i + K_{ji} z_j - \sum_{s=a}^{G} \overline{K_{ji}^{\psi}} \beta_{ij,s} z_s + m_{ji} \qquad (4.6.)$$

4.2. Node equilibrium conditions

Considering a node **i** taken from a certain structure, fig, 4.2., in which compete several bars, activated by a couple $\mathbf{M_i}$. The node will rotate. The node rotation measurement, $\mathbf{z_i}$, will equal each bar extremity rotation measure which competes in the node. In each bar extremity the end moments, which appear are proportional to the rotation measurement $\mathbf{z_i}$ ($M_{ij} = K_{ij}z_i$).

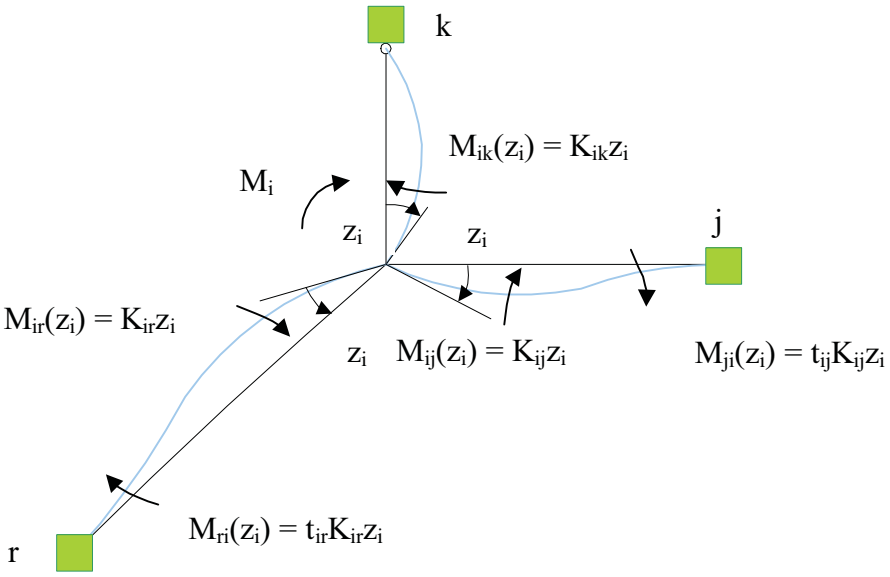

Fig. 4.2 The end moments of the bars which compete in node i when the node is loaded with a rotation of node, z_i, or with an active moment of node, M_i

Expressing the node **i** equilibrium, by a moment's equation:

$$\sum_i M_i = 0; \qquad \Rightarrow M_i = \sum_{j=1}^{N_i} K_{ij} z_i \qquad (4.7.)$$

Where:

$$z_i = \frac{1}{\sum_{j=1}^{N_i} K_{ij}} M_i \tag{4.8.}$$

Where - $\mathbf{N_i}$ represents the number of nodes connected by bars to node **i**.

4.3. Chain equilibrium condition

It is detached, from a certain frame, fig. 4.3.a., a chain of bars and nodes corresponding to a liberty degree, depending on the parameter $\mathbf{z_s}$**.** We act on this chain with an active moment, $\mathbf{M_s}$**,** which determines the real displacement, $\mathbf{z_s}$**,** or, the rotations, $\boldsymbol{\psi}_{\mathbf{ij,s}}$, without the node to have the possibility to rotate.

We express the equilibrium of these bars and nodes chain by a moment's equation:

$$\sum_s M = 0 \qquad \Rightarrow \mathrm{M_s} = \sum_{ij=1}^{B_s} (\overline{K_{ij}^{\psi}} + \overline{K_{ji}^{\psi}}) \psi_{ij,s} \tag{4.9.}$$

And considering the relation (4.1.) it is obtained:

$$M_s = z_s \sum_{ij=1}^{B_s} (\overline{K_{ij}^{\psi}} + \overline{K_{ji}^{\psi}}) \beta_{ij,s} \tag{4.10.}$$

Where:

$$z_s = \frac{1}{\sum_{ij=1}^{B_s} (\overline{K_{ij}^{\psi}} + \overline{K_{ji}^{\psi}}) \beta_{ij,s}} M_s \tag{4.11.}$$

Where - $\mathbf{B_s}$ number of bars for the chain s.

In order to determine the reaction from the connection of liberty degree it turns to the faulty in fig. 4.3.c. and the displaced in fig.4.3.d. The articulated scheme of the nodes and bars chain loaded with the moments on the bars and the reaction $\mathbf{R_s}$ is in equilibrium. The equilibrium is expressed by an equation of virtual mechanical work by producing a kinematic displacement compatible with the connections. It results:

$$R_s \Delta^{ar} - \sum_{ij}^{B_s} (\overline{K_{ij}^{\psi}} + \overline{K_{ji}^{\psi}}) \psi_{ij,s} \psi_{ij,s}^{ar} = 0 \tag{4.12.}$$

Or

$$R_s \Delta^{ar} - \sum_{ij=1}^{B_s} (\overline{K_{ij}^{\psi}} + \overline{K_{ji}^{\psi}}) \beta_{ij,s} z_s \beta_{ij,s} \Delta^{ar} = 0 \tag{4.13.}$$

Where

$$R_s = \sum_{ij=1}^{B_s} (\overline{K_{ij}^{\psi}} + \overline{K_{ji}^{\psi}}) \beta_{ij,s}^2 z_s \tag{4.14.}$$

And

$$z_s = \frac{1}{\sum_{ij=1}^{B_s} (\overline{K_{ij}^{\psi}} + \overline{K_{ji}^{\psi}}) \beta^2_{ij,s}} R_s \tag{4.15.}$$

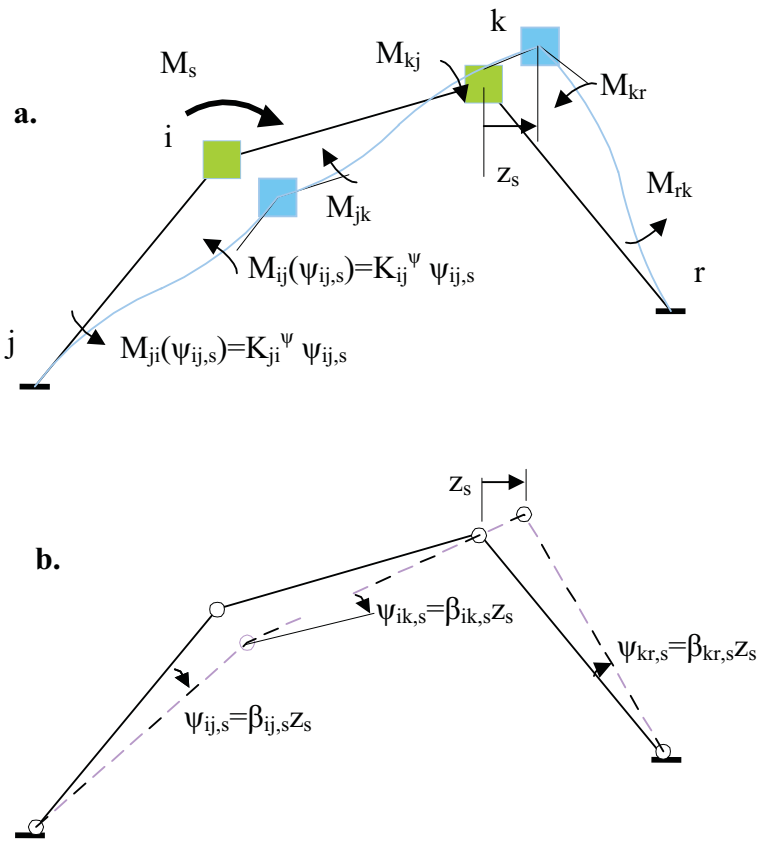

Fig.4.3. Loading situations for a nodes and bars chain in order to express the equilibrium condition: a. Bars and nodes chain loaded with the active moment of displacement, M_a; b. the connection between the bar rotation, $\psi_{ij,s}$ and displacement z_s;

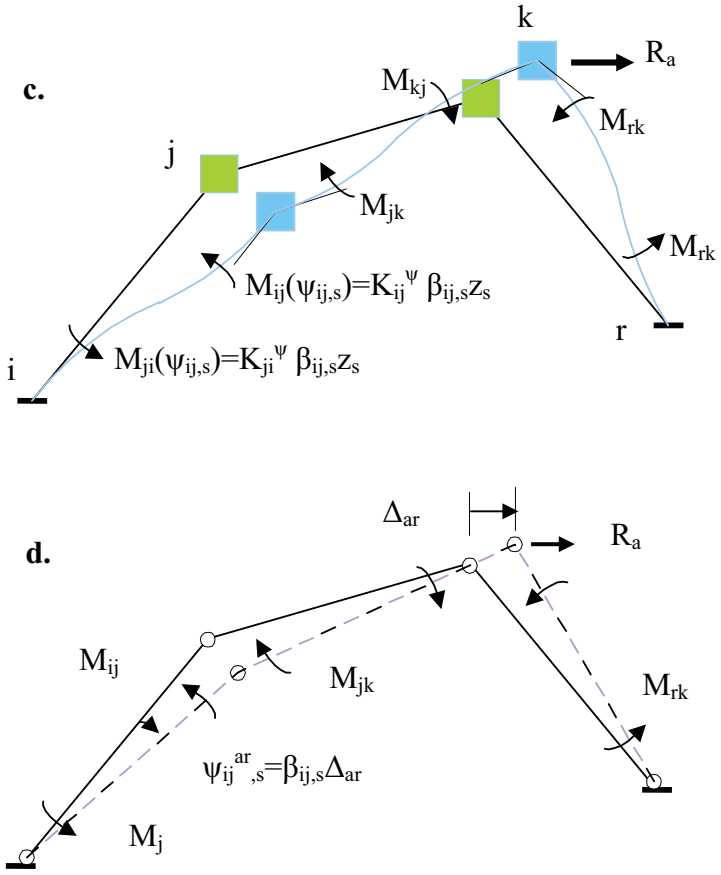

Fig .4.3 (continuance) Loading situations for a nodes and bars chain in order to express the equilibrium condition: d. The articulated scheme for a bars chain having in the bars extremities applied end moments, M_{ij} and the reaction from the liberty degree hardcore; c. Nodes and bars chain loaded with the real displacement z_s, on the liberty degree direction has been introduced the corresponding reaction R_a

Equalizing the relations (4.11.) and (4.15) it results:

$$\beta_s = \frac{R_s}{M_s} = \frac{\sum_{ij=1}^{B_s} (\overline{K_{ij}^{\psi}} + \overline{K_{ji}^{\psi}})\beta_{ij,s}^2}{\sum_{ij=1}^{B_s} (\overline{K_{ij}^{\psi}} + \overline{K_{ji}^{\psi}})\beta_{ij,s}} \tag{4.16.}$$

Or

$$R_s = \beta_s M_s = \frac{\sum_{ij=1}^{B_s} (\overline{K_{ij}^{\psi}} + \overline{K_{ji}^{\psi}}) \beta_{ij,s}^2}{\sum_{ij=1}^{B_s} (\overline{K_{ij}^{\psi}} + \overline{K_{ji}^{\psi}}) \beta_{ij,s}} M_s \qquad (4.17.)$$

β_s is, from the active moments method point of view, the rotation of a fictive bar on which would act the active displacement moment.

Based on the relations, (4.8.), (4.11.) and (4.16.) can be written the general expressions of bar moments loaded with burdens, with node active moments, **M_i,** and active displacement moments, **M_s,** or with node active moments and active displacement force, **R_s**:

$$M_{ij} = \frac{K_{ij}}{\sum_{j=1}^{N_i} K_{ij}} M_i + t_{ji} \frac{K_{ji}}{\sum_{i=1}^{N_j} K_{ji}} M_j - \sum_{s=a}^{G} \frac{\overline{K_{ij}^{\psi}} \beta_{ij,s}}{\sum_{ij=1}^{B_s} (\overline{K_{ij}^{\psi}} + \overline{K_{ji}^{\psi}}) \beta_{ij,s}} M_s - m_j \qquad (4.18.)$$

$$M_{ji} = t_{ij} \frac{K_{ij}}{\sum_{j=1}^{N_i} K_{ij}} M_i + \frac{K_{ji}}{\sum_{i=1}^{N_j} K_{ji}} - \sum_{s=a}^{G} \frac{\overline{K_{ji}^{\psi}} \beta_{ij,s}}{\sum_{ij=1}^{B_s} (\overline{K_{ij}^{\psi}} + \overline{K_{ji}^{\psi}}) \beta_{ij,s}} M_s - m_i \qquad (4.19.)$$

Also,

$$\begin{aligned} M_{ij} &= d_{ij} M_i + t_{ji} d_{ji} M_j - \sum_{s=a}^{G} \nu_{ij,s} M_s - m_j \\ M_{ji} &= t_{ij} d_{ij} M_i + d_{ji} M_j - \sum_{s=a}^{G} \nu_{ji,s} M_s + m_i \end{aligned} \qquad (4.20.)$$

And

$$\begin{aligned} M_{ij} &= d_{ij} M_i + t_{ji} d_{ji} M_j - \sum_{s=a}^{G} \nu'_{ij,s} R_s - m_j \\ M_{ji} &= t_{ij} d_{ij} M_i + d_{ji} M_j - \sum_{s=a}^{G} \nu'_{ij,s} R_s + m_i \end{aligned} \qquad (4.21.)$$

Where:

$$d_{ij} = \frac{K_{ij}}{\sum_{j=1}^{N_i} K_{ij}}; \qquad \nu_{ij,s} = \frac{\overline{K_{ij}^{\psi}} \beta_{ij,s}}{\sum_{ij=1}^{B_s} (\overline{K_{ij}^{\psi}} + \overline{K_{ji}^{\psi}}) \beta_{ij,s}}; \qquad \nu'_{ij} = \frac{\overline{K_{ij}^{\psi}} \beta_{ij,s}}{\sum_{ij=1}^{B_s} (\overline{K_{ij}^{\psi}} + \overline{K_{ji}^{\psi}}) \beta_{ij,s}^2}; \qquad (4.22.)$$

Observation: 1. the expressions 4.8 and 4.11 indicate the fact that the real displacements of the nodes can be determined based on the node and displacement active moments.

2. Analyzing the relations (4.3.), (4.6.) and (4.20.) we can say that the last two relations are more general, because the end moments are applicable to any straight bar from a static undetermined structure, with rigid nodes, loaded with burdens, node rotations and parameters of liberty degrees, node active moments and active displacement moments.

It is considered, a certain structure driven by a force system. The structure will deform and in the bars extremities appear bending moments, determined by the relations (4.5), (4.18) and (4.19). In order to determine the elements in question: nodes different displacements ($\mathbf{z_i}$ şi $\mathbf{z_s}$) or, node and displacement active moments ($\mathbf{M_i}$ şi $\mathbf{M_s}$) we will use the methodology of Gh. Em. Filipescu. In this method are being used the labile base systems activated by the given forces and the end moments ($\mathbf{M_{ij}}$, $\mathbf{M_{ji}}$). Are being used two types of equations:

- Continuity equations. In the case studied, here, in the paper, these equations reduced to the level of each bar, brought us to the relations (4.5), (4.18) and (4.19);
- Static equilibrium equations:

$$\sum_{j=1}^{N_i} M_{ij} = 0; \qquad \mathrm{i} = 1,2,3,..,\mathrm{N} \tag{4.23.}$$

$$\mathrm{LMV}_{(s)} = 0; \qquad \mathrm{s} = \mathrm{a,b,c,...,G} \tag{4.24.}$$

Explaining the equations (4.23) and (4.24) by end moments, the relations (4.5), (4.19), and (4.21), can be obtained these equation systems:

$$\sum_{j=1}^{N_i} K_{ij} z_i + \sum_{j=1}^{N_i} t_{ij} K_{ij} z_j - \sum_{s=a}^{G} \overline{K_{ij}^{\psi}} \beta_{ij,s} z_s - \sum_{j=1}^{N_i} \mathrm{m_j} = 0 \tag{4.25.}$$

$$\sum_{ij=1}^{B_s} K_{ij} \left(1 + t_{ij}\right) \beta_{ij,e} z_i + \sum_{ij=1}^{B_s} K_{ij} \left(1 + t_{ij}\right) \beta_{ij,e} z_j - \sum_{s=a}^{G} \sum_{ij=1}^{B_s} \left(\overline{K_{ij}^{\psi}} + \overline{K_{ji}^{\psi}} \right) \beta_{ij,s} \beta_{ij,e} z_s +$$

$$+ \sum_{ij}^{B_s} \left(-\mathrm{m_j} + \mathrm{m_i} \right) \beta_{ij,e} + \quad + \sum_{k=1}^{N_p} P_k \delta_{k,e} = 0; \quad i = 1,2,...,N: \quad i \neq j; \quad e = a,b,...,G; \tag{4.26.}$$

Or

$$r_{ii}z_i + \sum_j r_{ij}z_{jj} + \sum_s r_{is}z_s + R_{ip} = 0; \qquad i \neq j; \qquad i = 1,2,..., N; \qquad (4.27.)$$

$$\sum_i r_{si}z_i + \sum_j r_{ij}z_j + \sum_s r_{se}z_s + R_{sp} = 0; \qquad i \neq j; \qquad e = 1,2,...,G; \qquad (4.28.)$$

And

$$\sum_{j=1}^{N_i} d_{ij}M_i + \sum_{j=1}^{N_i} t_{ji}d_{ji}M_j - \sum_{s=a}^{G}\sum_{j=1}^{N_i} \nu_{ij,s}M_s - \sum_{j=1}^{N_i} m_{ij} = 0; \quad i \neq j; \quad i = 1,2,...,N; \qquad (4.29.)$$

$$\sum_{ij=1}^{B_s} d_{ij}\left(1+t_{ij}\right)\beta_{ij,e}M_i + \sum_{ij=1}^{B_s} d_{ji}\left(1+t_{ij}\right)\beta_{ij,e}M_j - \sum_{s=a}^{G}\sum_{ij=1}^{B_s}(\nu_{ij,s}+\nu_{ji,s})\beta_{ij,s}\beta_{ij,e}M_s +$$
$$+\sum_{ij}^{B_s}\left(-m_{ij}+m_{ji}\right)\beta_{ij,e} + \sum_{k=1}^{N_p} P_k\delta_{k,e} = 0; \quad i = 1,2,...,N; \quad i \neq j; \quad e = a,b,...,G; \qquad (4.30.)$$

Or

$$M_i + \sum_j \mu_{ij}z_j + \sum_s \mu_{is}M_s + m_{ip} = 0; \qquad (4.31.)$$

$$\sum_i \mu_{si}M_i + \sum_j \mu_{sj}M_j + \sum_e \mu_{es}M_e + m_{sp} = 0; \qquad (4.32.)$$

Also

$$\sum_{j=1}^{N_i} d_{ij}M_i + \sum_{j=1}^{N_i} t_{ji}d_{ji}M_j - \sum_{s=a}^{G}\sum_{j=1}^{N_i} \nu'_{ij,s}R_s - \sum_{j=1}^{N_i} m_{ij} = 0; \quad i \neq j; \quad i = 1,2,...,N; \qquad (4.33.)$$

$$\sum_{ij=1}^{B_s} d_{ij}\left(1+t_{ij}\right)\beta_{ij,e}M_i + \sum_{ij=1}^{B_s} d_{ji}\left(1+t_{ij}\right)\beta_{ij,e}M_j - \sum_{s=a}^{G}\sum_{ij=1}^{B_s}(\nu'_{ij,s}+\nu'_{ji,s})\beta_{ij,s}\beta_{ij,e}R_s +$$
$$+\sum_{ij}^{B_s}\left(-m_{ij}+m_{ji}\right)\beta_{ij,e} + \sum_{k=1}^{N_p} P_k\delta_{k,e} = 0; \quad i = 1,2,...,N; \quad i \neq j; \quad e = a,b,...,G; \qquad (4.34.)$$

Regarding the previous relations certain comments must be done, such as:

- The relations (4.27) and (4.28) represent the condition equations system for a structure static undetermined, in the displacement method. The elements in question are the displacements. The free terms are reactions, and the coefficients are unitary reactions and are determined with the above relations:

$$r_{ii} = \sum_{j=1}^{N_i} K_{ij}; \qquad \mathrm{r_{ij}} = t_{ij} K_{ij}; \tag{4.35.}$$

$$r_{is} = -\sum_{j=1}^{N_i} \overline{K_{ij}^{\psi}} \beta_{ij,s}; \qquad r_{si} = \sum_{ij=1}^{B_s} K_{ij}(1+t_{ji})\beta_{ij,s}; \tag{4.36.}$$

$$r_{es} = \sum_{ij=1}^{B_s} (\overline{K_{ij}^{\psi}} + \overline{K_{ji}^{\psi}})\beta_{ij,s}\beta_{ij,e}; \qquad \mathrm{R_{ip}} = -\sum_{k=1}^{N_i} \mathrm{m_{ij}}; \tag{4.37.}$$

$$R_{ep} = \sum_{ij=1}^{B_e} (-\mathrm{m_{ij}} + \mathrm{m_{ji}})\beta_{ij,e} + \sum_{k=1}^{N_p} P_k \delta_{k,p}; \tag{4.38.}$$

- The relations (4.21) and (4.32) represent the condition equation system for a structure static undetermined, in the method of active moments. The elements in question are node and bars active moments. The free terms and coefficients are determined with the relations:

$$\mu_{ii} = \sum_{j=1}^{N_i} d_{ij}; \qquad \mu_{\mathrm{ij}} = t_{ji} d_{ji}; \qquad \mathrm{i} \neq \mathrm{j}; \tag{4.39.}$$

$$\mu_{is} = -\sum_{j=1}^{N_i} \nu_{ij,s}; \qquad \mu_{\mathrm{si}} = \sum_{ij=1}^{B_s} d_{ij}(1+t_{ij})\beta_{ij,s}; \quad \mathrm{i} \neq \mathrm{j} \tag{4.40.}$$

$$\mu_{ej} = \sum_{ij=1}^{B_e} d_{ji}(1+t_{ji})\beta_{ij,e}; \qquad \mu_{\mathrm{es}} = -\sum_{ij=1}^{B_s} (\nu_{ij,s} + \nu_{ji,s})\beta_{ij,e}; \tag{4.41.}$$

$$\mathrm{m_{ip}} = -\sum_{j=1}^{N_i} \mathrm{m_{ij}}; \qquad \mathrm{m_{ep}} = \sum_{ij=1}^{B_e} (-\mathrm{m_{ij}} + \mathrm{m_{ji}})\beta_{ij,e} + \sum_{k=1}^{N_p} P_k \delta_{k,e} \tag{4.42.}$$

- The relations (4.33) and (4.34) represent the condition equations system for a structure static undetermined, in an alternative of active moments method. The elements in question are node active moments and active displacement forces.

4.5. The indirect device for condition equation deduction from active moment methods starting from the equation system of the displacement method.

Corroborating the relations (4.8) with (4.35) and (4.11) with (4.16) and (4.37) for e = **s**, can be obtained the expressions:

$$z_i = \frac{1}{r_{ii}} M_i; \tag{4.43.}$$

$$z_s = \frac{\beta_s}{r_{ss}} M_s; \tag{4.44.}$$

Are introduced the relations (4.43) and (4.44) in the condition equation system of the displacement method (2.3) and (2.4), results:

$$\frac{r_{ii}}{r_{ii}} M_i + \sum_j \frac{r_{ij}}{r_{jj}} M_j + \sum_s \frac{r_{is}}{r_{ss}} M_s + R_{ip} = 0; \tag{4.45.}$$

$$\sum_i \frac{r_{si}}{r_{ii}} M_i + \sum_j \frac{r_{sj}}{r_{jj}} M_j + \sum_s \frac{r_{se}}{r_{ss}} \beta_s M_s + R_{sp} = 0; \tag{4.46.}$$

After dividing the equation (4.46.) by β_s it is obtained:

$$\sum_i \mu_{si} M_i + \sum_j \mu_{sj} M_j + \sum_e \mu_{es} M_e + \eta_{sp} = 0; \tag{4.47.}$$

$$M_i + \sum_j \mu_{ij} z_j + \sum_s \mu_{is} M_s + \eta_{ip} = 0; \tag{4.48.}$$

The equation system (4.45) and (4.46) is identical with (4.31) and (4.32), and the system (4.47) and (4.48) is identical with the equation system formed from (2.3) and (2.4). Consequently, between the coefficients and free terms of displacement method and active moment method are the relations:

$$\mu_{ii} = \frac{r_{ii}}{r_{ii}} = 1; \qquad \mu_{ij} = \frac{r_{ij}}{r_{jj}}; \qquad \mu_{is} = \frac{r_{is}}{r_{ss}}; \tag{4.49.}$$

$$\mu_{si} = \frac{r_{si}}{r_{ii}} \frac{1}{\beta_s}; \qquad \mu_{sj} = \frac{r_{sj}}{r_{jj}} \frac{1}{\beta_s}; \qquad \mu_{se} = \frac{r_{se}}{r_{ss}}; \tag{4.50.}$$

$$\eta_{ip} = R_{ip}; \qquad \eta_{sp} = \frac{R_{sp}}{\beta_s}; \tag{4.51.}$$

3. CONCLUSION

Have been obtained the equilibrium equations from active moment method by using the equilibrium conditions for girder, node and nodes and bars chain by the mean of "Gh. Em. Filipescu" methodology. The equation system obtained in subchapter 4.2., and the relation (4.27.), has interchangeable lateral coefficients.

Has been identified a variant of active moments method, where the elements in question are node active moments and displacement active forces.

Have been obtained calculus relations for end moments more general than the ones used in displacement method, the relations (4.6) and (4.19).

References:

1. Orlovschi, N. I., Construction static, vol. II, Static undetermined structures, part 1,2,3, Rotaprint I.P. “Gh. Asachi” Iaşi, 1975 (in Romanian).
2. Şesan, A., Orlovschi, N. I., Variants and simplifications of moments distribution method, Construction theory and practice, Iaşi no. 1, 1954 (in Romanian).
3. Şesan, A., Orlovschi, N. I., A generalization of moments distribution methods. Studies and researches, Academia, R. P. Romania, filial Iaşi, nr. 3-4, 1955 (in Romanian).
4. Şesan, A., Popescu, N., Another form of the condition equations of deformation method, Construction Theory and Practice, Iaşi nr. 2, 1955 (in Romanian).
5. Amariei, C. I., Construction static – Static undetermined structures, vol. II, Rotaprint I.P. “Gh. Asachi” Iaşi, 1981 (in Romanian).

"Computational Civil Engineering 2007", International Symposium
Iaşi, România, May 25, 2007

Laboratory analysis in B.L.W.T. – priorities in insuring a safety curtain walling design

Elena Carmen Teleman, Elena Axinte
Civil and Industrial Constructions Dept., Faculty of Civil Engrg., T.U. "Gh. Asachi" Iasi, Romania

Summary

In the last half of century, the mankind is confronted with a new, most serious problem, determined by the global warming phenomenon and in particular, in the last years, Romania has already been confronted with the severe consequences of these climatic changes. A dramatic increase of the number of strong winds with speeds over 100 km/h in temperate climatic zones had been the cause of disastrous effects in terms of human lives and enormous material.

The design of very high buildings is a current modern concept but a greater complexity is imposed even from the first stage because of the importance of a realistic evaluation of the costs of investment. The balance between the investment costs and the safety level imposed during the service life time or in fact the risk involved by its exploitation is the designers most capital decision.

The latest solutions of steel glass façades are in fact glass panes of grate dimensions sustained in various manners by steel lattice structures or steel rods. Their important sensibility to every movement of the main structure, the influence of temperature variations upon the fixing details and hence upon the glass itself are almost exceeded by the effects of wind dynamic action directly supported by this envelope.

The last decades brought many scientific studies on these intricate systems and almost all of them are directed towards a more realistic evaluation of all the effects of the wind pressure upon light curtain walling.

Along the conditions imposed in the design of these elements in order to cope with wind pressure, the paper presents some of the results of several studies on models in the wind boundary layer wind tunnel of the Laboratory of Aerodynamics from the Faculty of Civil Engineering in Iasi. These results are directed towards a thorough evaluation of extreme values of wind pressure coefficients and also focus on the vibrations induced to the elements of the envelope by the dynamic effects of wind action, a most important comfort and safety criteria.

KEYWORDS: steel-glass envelopes, maxima wind pressure coefficients, spectral power, frequency of vibration, wind boundary layer tunnel

1. INTRODUCTION

Neglecting due to lack of knowledge of the extension of wind effects upon the antropic area had in the recent past year most disastrous consequences [1]. The last decades of the XX^{-th} century are marked by the development of the science of building aerodynamics, a domain where the meteorology and the theory of probabilities meet and mix together with the structural engineering concepts. The design of a multi-storey structure is a process with a high degree of complexity and the important effort involved in the project justifies the equilibrium between an economic cost of execution and the risk assumed for the exploitation period of time. After a rich experience has been achieved, it seems that the design of the envelope of a multi-storey building affects in a highest degree the safety level for the exploitation period of time. The light materials used for these envelopes, like glass, thermo-insulating materials, steel or aluminium skeleton vary widely their mechanical characteristics: dilatation coefficient, elastic modulus, strength and strain but in the process of design of the perimetral cladding the common factor of all these materials is that together they have to stand up against the effects of wind dynamic action.

In these conditions the design of a multi storey structure to strong wind gusts and their effects upon the envelope becomes an important preliminary stage because by modelling the interaction between the wind and the future structure and anticipating the structural response, benefic modifications of its aerodynamic shape may improve the dynamic behaviour. Also, by studying the environmental conditions imposed to the building important decisions may be taken in order to avoid unpleasant effects of the urban implantations. Notorious laboratories for the Aerodynamics of Structures from all over the world play an important role in this preliminary process.

For at least 50 years the humanity is confronted with a new and most serious problem: the dramatic climatic changes due to global warming, whose multiple and severe consequences Romania has already experienced. A rather realistic prognoses of wind motion at global scale along with the estimation of the local effects inside the structure of the boundary layer in different environments became priorities in insuring the security in the exploitation of the buildings because their consequences at the economic scale are huge. The amplification of the number of strong winds with speeds of more than 100 km/h in temperate zones and of the number of hurricanes with wind speeds of more than 200 km/h in tropical and subtropical zones increased dramatically the costs of reconstructions and repair in the last decades and unfortunately they were the cause of important human casualties, and sometimes disasters at human scale. In the same time, the insurances costs increased in some countries, like Great Britain ten times in the last 50years [2].

Many of the environmental conditions imposed to a high rise building amplify the effects of wind dynamic actions: increased speeds in shore areas, turbulences due to perturbations of urban wind profile in the big cities area, vicinity with other buildings of similar size etc., the implication being the distribution of the wind pressure/suction on the surface of the building [3]. Due to an important scientific knowledge accumulated in this respect, the architects and engineers are able to master the shape and types of structures adopted for these high rise buildings. A good example is the Milo Turning Tower, project of the Spanish architect Santiago Calatrava and for the time being, the highest building in Europe (245 m), whose torsioned shape reduces the vortices and diminishes the local pressures on the surface of the envelope [4].

2. PARTICULARITIES IN THE DESIGN OF MODERN CURTAIN WALLING

2.1. Types and design criteria

The requirements for transparent envelopes of the buildings are, no matter to which codes for practice we are referring to, based on the following criteria [5], [6], [7]:

- dimensions and tolerances;
- strength and serviceability;
- fire protection;
- thermal and physical functions insured;
- other specific criteria imposed by serviceability functions.

As steel and glass are preponderant in the structure of transparent facades, a fundamental need is to predict the glass behaviour in facades, in order to achieve both performance and economy.

The conventional supporting structures of steel-glass facades are those in which the glass pains carry their dead load and the afferent wind load depending on their surface; the panes are supported by steel window frames which transfer the loads to the main structure of the building. Normally, the glass frame producer designs the panes including glass, sealing and fasteners and gives the necessary requirements for the designer of the load bearing structure.

In the last decades, a very wide number of studies were directed towards the behaviour of the glass panels under different exploitation conditions. Vertical movements of the main structure of he building may be important but usually are situated between +5.0 mm and -25 mm but the expansion/contraction of the glass itself in vertical panels determine movements of 17.5 mm to -12 mm, important tension stresses being accumulated at the corners of the panels or on the edges, depending on the supporting system.

As the movements of the supporting system of the glass panels must follow the movements of the main structure of the building, after a rich experience was gathered in research studies, limitation of the maximum deformations of the glass under wind action in the middle of the panels are imposed: δ_1 is 1:175 from the span; also, deformations of the supporting frame must be limited so δ_2, δ_3 are no more than 1:175 of the span.

Also, preventing the lateral buckling phenomenon for the supporting elements under local pressure/suction impose limits for their slenderness; it was assumed of 1:100 from the span for steel beams and 1:360 from the span in the case of lattice girders [5].

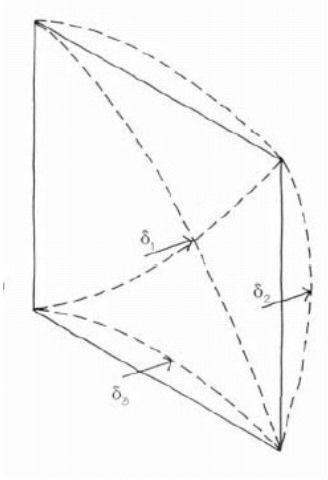

Fig. 1. Deflections of the steel-glass panels: δ_1- deflection in the middle of the panel; δ_2, δ_3 – deflections in the middle of the edges, on the supports [5]

The last decades imposed new solutions for transparent facades on the market, being the result of applicability of new technologies combined with the demand of higher performances. Hybrid –supported facades are greater surfaces of glazing whose supporting structure is characterized by the replacement of either a horizontal beam or a vertical column by a stainless steel cable or rod (fig.2.a., fig. 3) [6]. In the solution presented, the vertical cables take dead load of glass panes and the wind load also. If greater surfaces (higher glass facades) are considered, a horizontal truss (or more) is designed in order to take the wind action and to limit the deflections of the glass consequently. A particular type represents the suspended glass facades for which the cable supported mechanism prevents only wind loads, the glass panes supporting their own weight (fig. 2.b).

The hybrid-supported structure concept is based on the fact that the cables and rods remain in tension so one of the key structural design problems for these envelopes

is the thermal expansion, which might cause structural instability so normally, the cables are pre-stressed. If the height becomes too big, the pre-stressing force into the cables is not enough to overcome the effects of thermal expansion and for these situations, springs are used for each vertical truss to pre-stress the cables and rods. The design imposes for a non-linear analysis for obtaining the stresses, deformations and the natural frequency response. The literature specifies that a certain amount of trial and error is required to balance the rod and catenary system with the floor spring (fig. 4.).

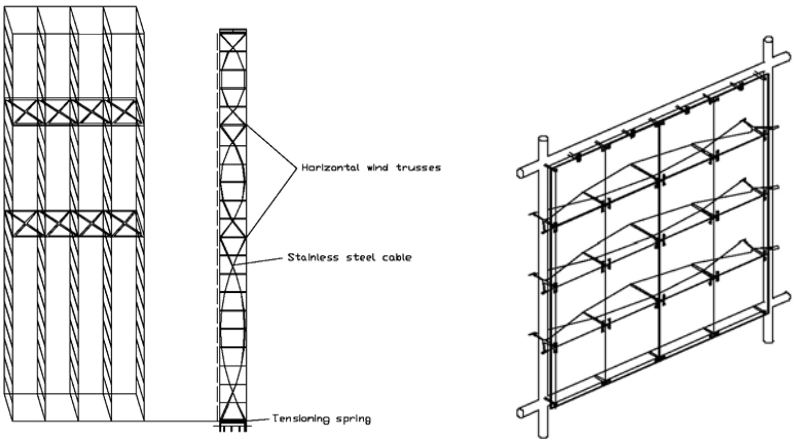

a b

Fig. 2.a, b. Steel-glass façades: a)-hybrid-supported glass façade; b)-cable supported suspended glass façade [6]

For these types of envelopes, deformation becomes of capital importance and the permissible deformation is established for the most frequent wind loads compatible not only with the glass or cladding system involved but also with the joints and the fastening systems. As the deflections of the cable truss are concentrated around the holes drilled in the glass, uncontrolled values of efforts may increase the risk of producing the fatigue phenomenon in the glass [6], [7].

Requirements for the design of the glass panels in limit states design impose the validation of the relationships for maximum stresses and maximum deflection defined with the following relationships [6], [7]:

$$\sigma_{\max} = k \cdot \left(\frac{a}{t}\right)^2 \cdot q_d \tag{1}$$

$$\delta_{\max} = k' \cdot \frac{a^4}{t^3} \cdot \frac{q^k}{E} \tag{2}$$

where:

- *a*-length of shorter edge of the pane;
- t- thickness of the glass pane;
- q_d – uniform pressure load on the panel in the ultimate state for design;
- k, k'- coefficient that takes into account the aspect ratio of the panel and also the normalized value of the load necessary to reduce the calculations from non-linear to linear case.;
- E-elastic modulus of the glass pane;
- q_k- the value of wind load pressure in the limit state of serviceability.

2.2. Studies considering the security in exploitation of light envelopes design

2.2.1. Accuracy in the determination of realistic values of wind pressure action

The cladding is generally designed to sustain the efforts due to wind dynamic action. Several factors influence the design criteria in this respect [7]:

- wind attack angle;
- internal pressure inside the building;
- risks involved by the presence of accidental wide openings in the facade which would lead to the alteration of internal pressure;
- amplification of wind suctions in the corners of buildings;
- effects of the alteration of the environmental conditions during the life time upon the distribution of wind pressures on the surface of the building and also, the effects of vicinity.

Imposed by the necessity of national standard regulations of design, execution and exploitation of curtain walling systems in Romania and in order to insure the security level imposed by the Romanian legislation a code for practice was elaborated: NP 102-04, issue nr. 170/15.02.2005 [8], according to which, whichever is the curtain walling system proposed by the designer, it must be tested for the comfort criteria, particularly from the wind action point of view (chapter 5.2.5. *Efforts upon curtain walls due to wind dynamic action*). The tests will consider for each system separately: local reference wind pressure according to the height above the ground, gust factor considering the specific dynamic behaviour of the structural main system and the peak factors applied to local pressure coefficients, considering the dynamic characteristics of the facade panel.

Serious lack of data makes these requirements onerous. For example, if a safety level is imposed, a reference wind pressure value superior to that corresponding to a 10 years recurrence will be adopted. The recommendation is to extrapolate the

values of a Gumbel I or Frechet II distribution of extremes based on the observation data from of I.N.M.H. Bucuresti, Filaret station. But since, the distribution regards only one station it will not correspond with accuracy for all over the surface of the Romanian territory and since the recommendation specify that the designer should adopt any other type of data in order to insure the security level, in fact it is non-operational for other zones than the one mentioned.

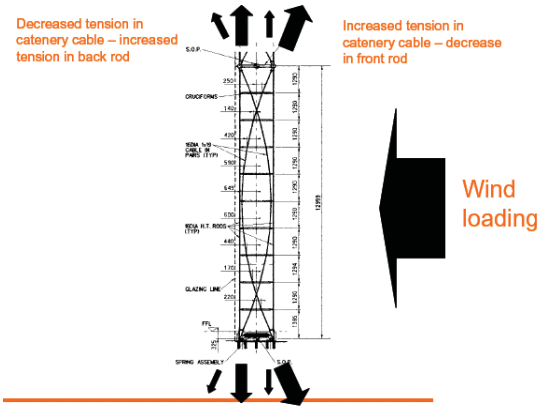

Fig. 3. Working system of a hybrid supported façade [5].

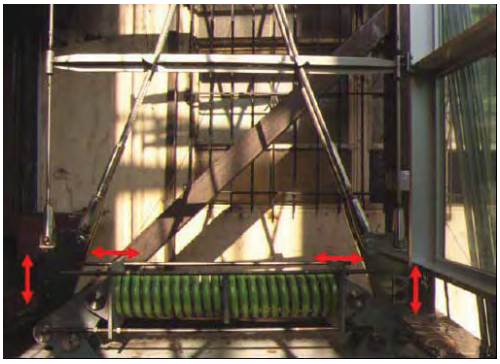

Fig. 4. Dissipative system for the wind: floor spring joint (Korean World Trade Center) [7].

Testing the curtain wall panels considering the cumulative effects of both dynamic behaviour of the main structural system and the dynamic behaviour of the steel-glass panel is difficult to achieve. The safety factor adopted in the limit state design theory is a function of two other random variables: safety index, β and the coefficient of variation of the wind action (speed/pressure), v. Considering a log-normal distribution, the safety factor is defined by [9]:

$$\phi = e^{0.75\beta v} \tag{3}$$

It is important to observe that, if a normal distribution is considered, then the safety index has usually values between 2.5 and 4.5; in this case the probability of failure during the service life is placed between 1/100 and $1/10^6$.

The usual formulation of the wind pressure in the codes for design against wind action all over the world is:

$$w = q_{ref} \cdot c_e \cdot c_g \cdot c_p \cdot A \tag{4}$$

where:

- q_{ref}- reference wind dynamic pressure;
- c_e-exposing factor;
- c_g-peak factor;
- c_p-pressure coefficient;
- A-surface of the area exposed to wind pressure.

Bearing in mind that all the measured values are random and analyzed through the statistics methods, a global coefficient of variation of wind action will be obtained from the formulae:

$$v = \sqrt{v_{q_{ref}}^2 + v_{C_e}^2 + v_{C_g}^2 + v_{C_p}^2} \tag{5}$$

In the process of design, the extreme values of wind pressure or suction themselves influence the security level imposed. Modern techniques of measuring in boundary layer wind tunnels have an increased degree of accuracy and the latest values of the variation coefficients reported are considerably lower than the ones stipulated by the various design codes, mostly due to the variation of the pressure coefficient c_p. As a general conclusion, the variation coefficient according to design code is 0.36 the partial safety factor being thus 2.25 in opposition with a variation factor of 0.18 obtained through wind tunnel measurements leading to a safety factor of 1.59 (β is 3.0 in both cases). An increased value of safety factor is based on local pressure coefficients obtained from general tests which are not giving a certainty of the pressure coefficients and offer only a rough and sometimes insecure evaluation of the wind action on the surface of the building [9], [10].

As the instantaneous pressure coefficient c_p is a process fully described through statistic methods, the maxima/minima values of pressure are defined by the algebraic sum between the mean pressure values and the product of the amplification of the variation factor which is named in all the codes for structural design to wind action as the peak factor, g or c_g with the value of the standard deviation (or the r.m.s.):

$$g_k(t) = \pm \frac{\hat{c}_{p,k}(t)(\breve{c}_{p,k}(t)) - \overline{c}_{p,k}(t)}{\sigma_{p,k}(t)} \tag{6}$$

where:

- $g_k(t)$ - local peak factor in the point *k* on the surface of the building at the time *t*;
- $\hat{c}_{p,k}(t)(\breve{c}_{p,k}(t))$ - local extreme values of maxima/minima of instantaneous pressure in the point *k* on the surface of the building at the time *t*;
- $\overline{c}_{p,k}(t)$ - local mean value of the instantaneous positive (or negative) pressure in the point *k* and at the time *t*;
- $\sigma_{p,k}(t)$ - root mean square (or standard deviation).

Although the codes specify that a conservative value of the peak factor may be taken as 3.5 to predict the extreme values of wind pressure from the mean values obtained for a certain position on the surface of the building, numerous studies developed showed that since in certain situations this peak factor may have values three times bigger, it is not wise however, when it comes for the design of the wall cladding of a high rise building to limit the evaluations of extremes only to the value mentioned above.

2.2.2. Consideration of wind-induced vibrations in design of light envelopes

In the design of glass facades slenderness and long spans are often imposed for both glass panes and frame structures and this may lead to dynamical problems when a flexible structure with low natural frequency is exposed to gusty winds [11]. Wind induced vibrations may damage the sealants, loosen fasteners and cause inconvenience to occupants of the building. In ENV 1991-2-4, 1995 it is stated that the fundamental natural frequency f_0 should be always higher than 5 Hz, regardless to the wind speed in order to avoid vibrations induced by dynamic wind loads [7]. Under the mentioned value, the dynamic behaviour of the structure must be separately analyzed, though the methods are not specified. A F.E.M. modelling of the glass pane and its frame provide an accurate analysis [6], [7], but in this case a time-history description of the wind dynamic action is desired as an input.

2. STUDIES IN THE LABORATORY OF BUILDINGS AERODYNAMICS CONCERNING CURTAIN WALLS DESIGN

During the last decade, the studies in the laboratory of Aerodynamics of the Civil Engineering Faculty were directed towards developing the local instantaneous pressure measurement techniques of sampling on rigid models of buildings placed

in urban environment and with different levels of height along with refining the acquisition methods and processing the data obtained [13], [14], [15].

In parallel, a calibration of the results was developed, showing where the accuracy of measuring must be increased. By elaborating a module of programs under MATLAB the statistic data were analyzed, mainly for the coefficients of wind pressure. Several programs were developed:

- TB1.M…TB3.M – program for the determination of the pressure/suction coefficients-mean, peak and standard deviations, tracing the isopleths with polynomial interpolation functions and graphics of variation of the aerodynamic coefficients on the surface of the models;
- GPD.M- program for the determination of the peak factor c_g of the local instantaneous pressure (mean, r.m.s. and maxima values, histograms and regression lines); also for the validation of the acquisition data (fig. 5.a, b);
- TREC.M – program of determination of the variation coefficient ν for different averaging periods;
- TST_PSD.M – program for the determination of the spectral power and spectral density in its normalized shape (fig. 6.a, b).

The last program enlighten the values of the frequencies that gather the majority of the spectral densities, the frequencies around 5 Hz being very important for the study as it was mentioned in the subchapter 2.2.1. This program was considered to be the best way to identify the critical values of frequencies that might superpose on the natural frequencies of the glass-steel panes.

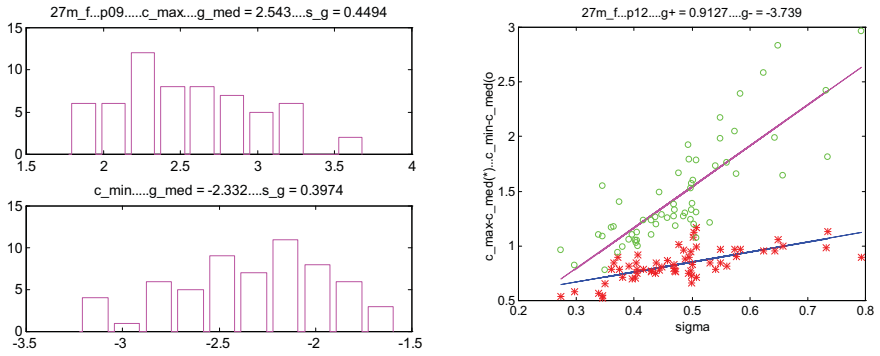

a b

Fig. 5.a, b. Programs under MATLAB elaborated during the studies in the boundary layer wind tunnel in the Civil Engineering Faculty in Iasi: a)-Program GPD.M for the determination of peak factors; b)- Calibration of the peak factor values.

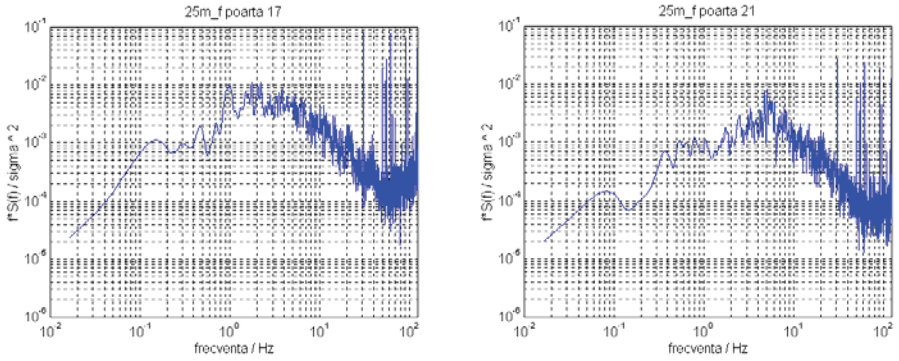

Fig. 6.a, b. Spectral densities normalized and traced in the program TST_PSD.M.: a) pressure signal processed; b)- suction signal processed.

3. CONCLUSIONS

Modeling the turbulences localized on the surface of the buildings and responsible of numerous accidents more or less severe was transferred into the numerical simulation sphere. The analysis of the fluctuating pressures was put into evidence by a spatial evaluation of the spectral density all over the surface of the structure, allowing the elaboration of an accurate method of design to wind dynamic action at least of the most common shapes of buildings [10] are presented in Eurocode 1 and also in the Romanian code NP 082-04. *Design Code. Basis of the structural design and evaluation of the actions on structures. Wind action* [16], [17].

Still, by refining the methods of evaluation of wind tunnel data of pressure on the surface of the buildings many precious data for specific situations imposed by the environmental conditions or architectural solutions are put into evidence.

The design of the transparent façades of glass and different solutions for the steel framing call for simulations by F.E.M. methods of the system dynamic behaviour using time history registrations of wind pressure. These simulations can be validated afterwards by tests on larger scales (or natural scales) of specimens of facade panels.

References

1. **www.news** softpedia.com, Sci/Tech News Staff - *Uragane mai multe din cauza încălzirii globale* (in Romanian)
2. Brian Smith, Tom Wyatt, *Structures, Dynamics and Wind a 10-th review*, 8th Biennal Scruton Lecture, Wind Engineering Society, 2003

3. Soligo, Michael, Vicepresident of Rowan Williams Davies & Irwin Inc.(RWDI) , Ontario, Canada- *High Rise Buildings in Hurricane Areas*, Technotes, Issue No. 2b
4. http: //www.turningtorso.com
5. Mike Otlet, Head of Structural Engineers ATKINS-*The role of a structural engineer in the design of a façade*, ATKINS, U.K. april 2006
6. Jusi Kallionieni-*Joints and fastenings in steel glass facades*, Helsinki University of Technology, Depart. of Civil and Environmental Engineering, Laboratory of Steel Structures, Ph.D. Thesis, 1999, Helsinki, Fnland
7. Aki Vuolio- *Structural Behaviour of Glass Structural in Facades*, Helsinki University of Technology, Laboratory for Steel Structures Publications, 2003, TKK TER 27, Helsinki, Finland
8. *"Normativ pentru proiectarea si montajul peretilor cortina pentru satisfacerea cerintelor de calitate prevazute de legea 10/1995",* NP 102-04, aprobat ord. nr. 170/2005
9. Peter A. Irwin- *Developing Wind Engineering Techniques to Optimize Design and Reduce Risk*, Conference on Wind Engineering 2006 (WES 06), Glasgow, U.K., www.ukwes.bham.ac.uk
10. Scott Gamble P. Eng.- *Wind Tunnel Testing – A Breeze Through*, Structure Magazine, nov. 2003
11. Peter Irwin, president of Rowan Williams Davies & Irwin Inc.(RWDI) , Ontario, Canada- *Motion Criteria in High Rise Buildings*, Technotes issue no. 2c
12. Scott L. Gamble, Roger J. Mittenburg, Michael D. Cicci, Marco Accardo (RWDI, Guelph, Ontario, Canada)-*Prediction of Local Exterior Wind Pressures from Wind Tunnel Studies Using Time History Analysis Approach,* Americas Conference on Wind Engineering, 2001.
13. Teleman, C.-*Contributii privind alcatuirea si calculul cladirilor multietajate cu structura metalica,* Teza de doctorat, 2000, U.T. "Gh. Asachi" Iasi (in Romanian)
14. Teleman, E.-C., Axinte, E., Silion, R.- *Trends of Actual Computer Assistance for Laboratory Studies in Boundary Layer Wind Tunnel,* "Computational Civil Engineering 2006", International Conference, Iasi, Romania 26 may
15. Carmen Teleman, Elena Axinte- *Calibration Methods of Data Obtained in Boundary Layer Wind Tunnel*, Buletinul Institutului politehnic din Iasi, Tomul XLVIII (LII), fasc 1-2. Constructii. Arhitectura, pp. 95-101
16. *Cod de proiectare. Bazele proiectarii si actiuni asupra constructiilor. Actiunea vantului* NP-082-04. (in Romanian)
17. XP ENV 1991-2-4/2000- Eurocode 1: *Bazele calculului si actiuni pe structuri – Partea 2-4: Actiuni asupra structurilor- Actiunea vantului (P 06-102-4)* (in Romanian)

"Computational Civil Engineering 2007", International Symposium
Iaşi, România, May 25, 2007

FEM 3D analysis of RC frame foundations of rotary cement kiln

Grzegorz Dmochowski, Przemysław Siwiec and Piotr Berkowski
Faculty of Civil Engineering, Wrocław University of Technology, Wrocław, PL50-370, Poland

Summary

Results of 3D finite element analysis of damaged foundations for cement tubular oven are presented in a paper. The foundation consists of four RC frames modeled for analysis using solid FE with 24 d.o.f. each. Serviceable and temperature loads, as well as loads from pre-stressing are taking into account. The frames, primary designed as 2D structures, are sensitive for out-off-plane and temperature loads. The additional effects of stresses from these loads should be taking into consideration during FEM analysis.

KEYWORDS: rotary cement kiln, RC foundation, spatial numerical model, FEM analysis

1. DESCRIPTION OF THE FOUNDATION

The support structure of rotary kiln under consideration was built in the early 1950s. It consists of four reinforced concrete solid frames spaced at equal intervals. The lowest frame is denoted by number 1 and the other by respectively 2, 3 and 4.

As part of rotary kiln retrofitting, frame 4 was to be torn down and an additional frame was to be placed next to frame 1 whereby the latter practically would not carry any loads. The other two frames: frame 2 and frame 3 were to continue to be in service and be subjected to additional loads. Because the two frames were considerably damaged it was necessary to determine their serviceability.

The foundation named frame 2 had been made as an RC frame embedded in the foundation plate. A static scheme with one column in the form of a rocker with both its ends articulated had been adopted. The other column had been rigidly fixed in the plate. The frame's spandrel beam had been thermally protected with an about 20 cm thick concrete overlay. In the course of its service considerable horizontal displacements of the kiln's foundation were observed. Therefore in the early 1980s the structure was strengthened by tensioning. The rigid-rigid column, the frame's spandrel beam and the joint connecting the members were subjected to tensioning.

The bowstrings were made from ϕ5 mm strings combined into L1+6+12+18 ropes, with two ropes running on each side of the foundation and concreted.

The technical condition of frame 2 varied. The foundation plate was found to be in good condition. The foundation had not undergone settlement and was undamaged. The columns were in satisfactory condition. The concrete reinforcement cover was found not to have loosened or cracked. The frame's spandrel beam was in bad condition. It was found to have sagged by 3-4 cm. The spandrel beam's undersurface was cracked and its reinforcement cover was loose over a considerable area. When the loosened cover was removed, reinforcement in the form of superficially corroded #35 square bars was revealed. Also the spandrel beam's entire top surface was found to be corroded.

The foundation named frame 3 had been built as a stiff frame, considerably long (8.6 m) along the kiln's axis, embedded in the RC plate. There were two platforms: one for a motor and one for the kiln's rotary bearing on the frame. The top surface of the frame was thermally protected with a 20 cm thick concrete overlay. The foundation plate was in good condition: no excessive settlements or damage were found. The columns were in satisfactory condition. They were uncracked and their reinforcement cover was found not to be loose. The frame's spandrel beam was in bad condition since it had been subjected not only to considerable service loads and temperature impacts but also to the destructive action of grease escaping from the motor driving the rotary kiln. Lubricant leaks were visible on the spandrel beam plate's undersurface.

2. FOUNDATION MATERIALS' STRENGTH PROPERTIES AND EXPLOITATION CONDITIONS

2.1. Concrete

On the basis of the fragmentary documentation which survived in the cement plant's archive it was found that the design strength of the foundation concrete had been assumed to be R_w = 160 kG/cm^2 which corresponds to current concrete grade B12.5-B15. According to non-destructive test results, the concrete in the frames could be classified as class B10 at the most. Therefore concrete parameters: R_{bb} = 4.8 MPa and R_b = 5.8 MPa were assumed for further calculations.

2.2. Reinforcing steel

In the surviving fragment of the design, smooth reinforcing steel ϕ20, ϕ30 and ϕ35 with allowable stress σ_d = 1200 kG/cm^2, corresponding to a design strength R_a of

about 106 MPa, was specified. The lower steel strength had probably been adopted in view of the considerable diameters of the structural reinforcement.

2.3. Foundation tensioning

The spandrel beam, the column and the joint of frame 2 had been tensioned using double steel ropes, made from ϕ5 mm strings forming a steel rope of type L1+6+12+18, running on both sides of the foundations. The nominal rope breaking force of 1130 kN had been assumed. The ropes were tensioned with a force amounting to 60% of the nominal force. Thus the tensioning force had been S = 2700 kN. From the way in which the ropes were secured it one could be concluded that the spandrel beam had been tensioned above the neutral axis, as shown in Figures 1 & 2.

2.4. Exploitation temperature

Considering that the concrete overlay protecting the foundation against temperature effects was 20 cm thick the foundation had been assumed to be subjected at its surface to a temperature field of +40°C, decreasing at every 10°C/m towards the column's base.

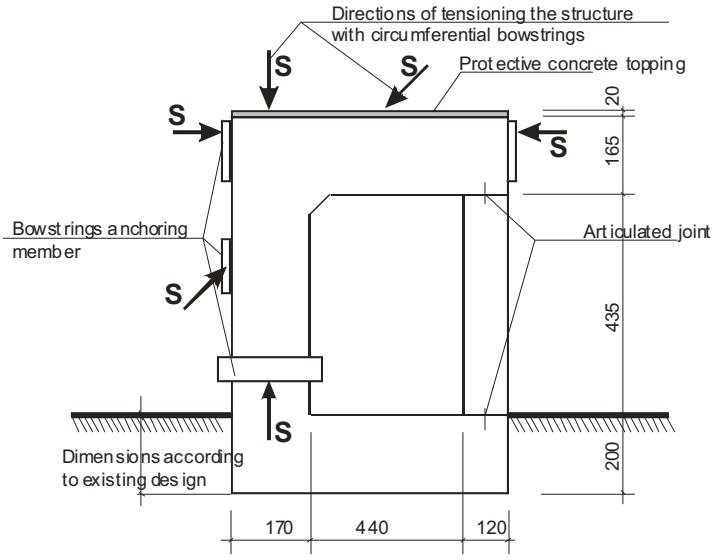

Figure 1. Frame 2. Structural and tensioning scheme

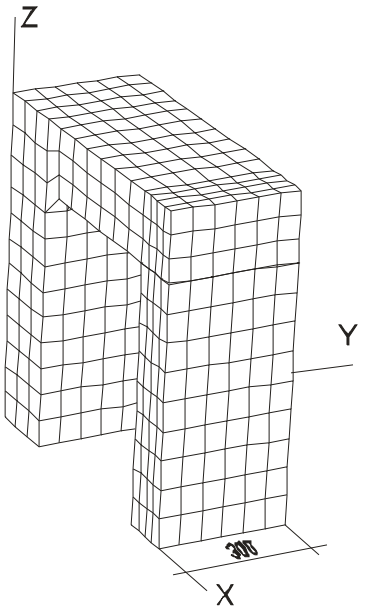

Figure 2. Frame 2. Division into finite elements

3. ANLYTICAL MODELS OF FOUNDATIONS

Program MES DIANA was used for the numerical analysis [4]. Linear physical and geometric relations were assumed for the material and the structure. Isoparametric 3-D finite elements HX24L, described by eight nodes, were used to build the models (Figure 3). In order to obtain more precise results a 3×3×3 Gaussian points integration scheme (triangles in Figure 3) was adopted.

In such finite elements stresses σ_{yy} and strains σ_{zz} are constant in direction x and they can linearly change in directions y and z. Stresses σ_{yy} and σ_{zz} and strains σ_{yy} and σ_{zz} respectively in directions x, y and z behave similarly. A uniformly distributed load or a load linearly variable along each edge can be applied to each wall of the finite element. The latter can also be loaded with temperature which may be different in each of its nodes. The displacements and deformations of the frames are given for the nodes while the stresses are given for the finite element's centre of gravity.

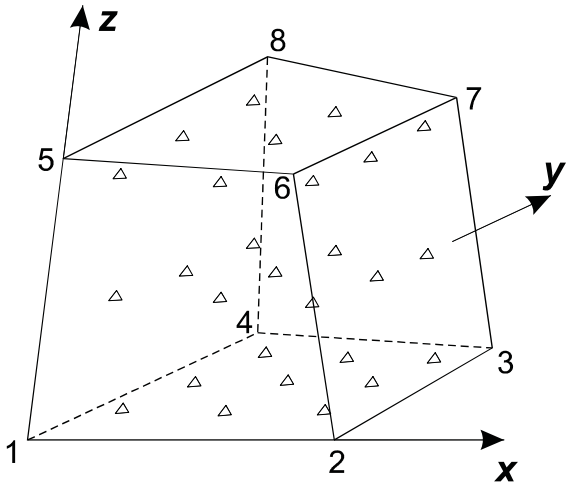

Figure 3. FEM element HX24L

The division of frame 2 model into finite elements is shown in Figure 2. 1022 nodes and 640 brick elements were used to create the model. The articulated joint between the spandrel beam and the rocker column was modelled using short articulated-articulated bars.

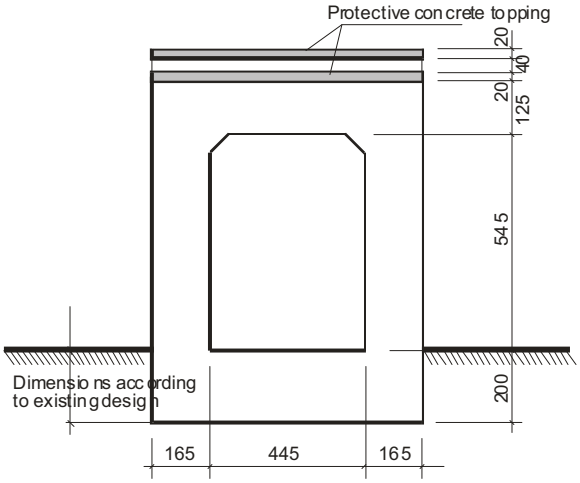

Figure 4. Frame 3. Structural scheme

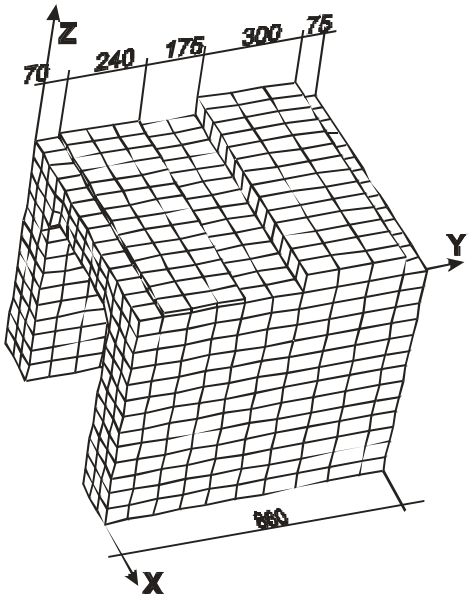

Figure 5. Frame 3. Division into finite elements

The model of frame 3 was created using 1660 nodes and 1104 brick finite elements.

The following load schemes were adopted for frame 2:
- the foundation dead load,
- the characteristic rotary kiln load,
- the design rotary kiln load,
- the frame tensioned with bowstrings,
- loading with a temperature field.

The following load schemes were adopted for frame 3:
- the foundation dead load,
- the characteristic rotary kiln load,
- the design rotary kiln load,
- loading with a temperature field.

The numerical 3-D model calculations were verified for a static flat bar scheme.

4. ANALYSIS OF RESULTS

The check of the deformations of frame 2 confirmed the latter's susceptibility to horizontal loads. The total horizontal displacements of the spandrel beam,

calculated in the elastic phase, exceeded 5 mm. Taking into account material plasticization, deformations about 2.5 cm were yield, i.e. above the permissible values.

The results of the numerical analysis, in the form of σ_{xx} and σ_{yy} graphs for frame 2 are shown in Figure 6 and for frame 3 in Figure 7. In both structures the stresses in the elements lying on the spandrel beam's edge and in its middle (along axis Y) were analyzed. In addition, stresses in the region of the elevated spandrel beam under the motor driving the kiln were taken into account in frame 3. The results are presented for the design service loads, the tension of frame 2 and the temperature increase load.

The total force tensioning the undersurface of the spandrel beam in frame 2 was 3326.4 kN. The load-bearing capacity of the reinforcement with a surface area as in the design was to 2259 kN, which means that it was insufficient to carry the loads. Similarly in frame 3, the total force tensioning the spandrel beam's undersurface was 3345 kN, which means that for the same assumed reinforcement it exceeded the spandrel beam's load-bearing capacity.

An analysis of stresses σ_{xx} in the spandrel beam of frame 2 shows only a slight influence of the temperature load on the degree of strain of the structure. The stresses due to an increase in temperature amount to merely 10% of the service loads, which confirms that lowly over-rigid structures are resistant to this kind of load.

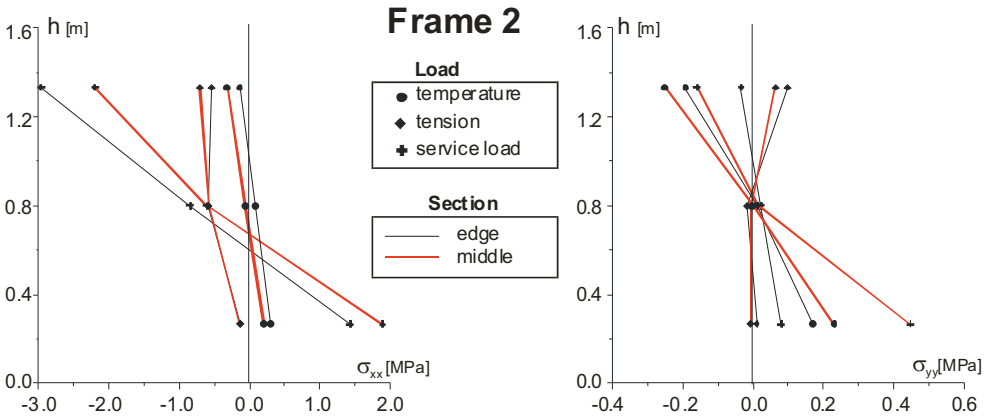

Figure 6. Frame 2. Stresses σ_{xx} and σ_{yy}

The effect of the stresses produced by tensioning was somewhat stronger. But due to the point of application of the steel ropes in the spandrel beam the expected reduction in tensile stress in the spandrel beam's bottom zone was slight (below 10%) while the deflection of the spandrel beam increased. The increase in tensile stress σ_{yy} in the middle of the spandrel beam thickness was significant: considering

that the design tensile strength is 580 kPa it may explain the appearance of cracks propagating perpendicularly to the kiln's axis. This means that the spatial aspect of the behaviour of the spandrel beam should have been taken into account in the design.

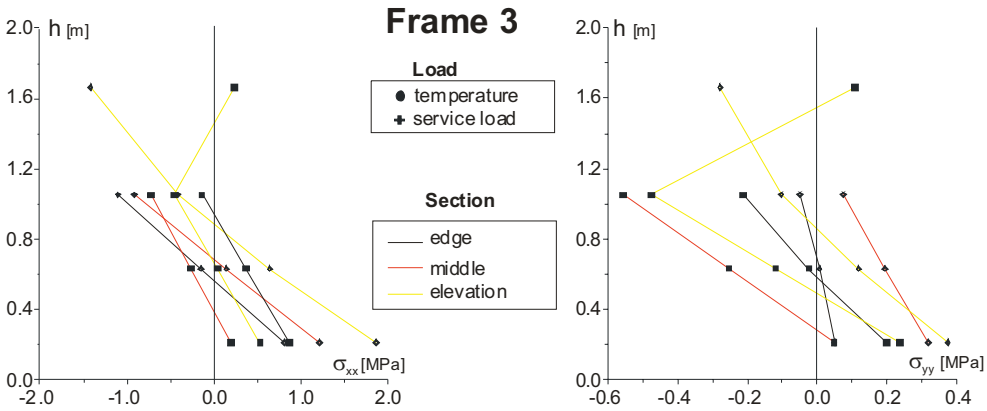

Figure 7. Frame 3. Stresses σ_{xx} and σ_{yy}

In frame 3 the temperature load impact was much greater. Stresses σ_{xx} produced by temperature were nearly as high as the ones due to the design service load whereas stresses σ_{yy} exceeded them significantly. Interesting was the appearance of tensile stresses in the spandrel beam's top zone thickened in order to mount the motor. The stresses did not exceed the concrete's tensile strength but as a result of the long-lasting action of temperature they might cause cracking in and damage to the spandrel beam's top surface.

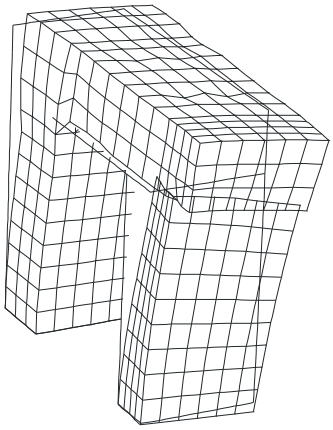

Figure 8. Deformation of frame 2

Similarly as in frame 2, the share of tensile stresses σ_{yy} (acting along the kiln’s axis) produced by the service loads was found to be considerable. The stresses were responsible for the appearance of cracks perpendicular to the rotary kiln’s axis.

Figure 8 shows the deformations of frame 2 under the service load, the tension and the temperature field. The deformations of frame 3 under the service load and the temperature field are shown in Figure 9.

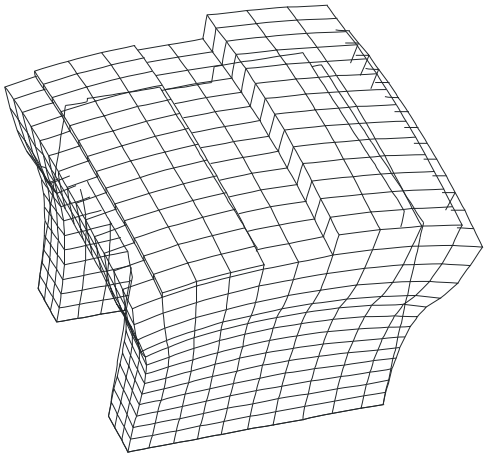

Figure 9. Deformation of frame 3

5. CONCLUSIONS

From the numerical analyses the following conclusions were drawn:

The load-bearing capacity of the spandrel beams in the investigated rotary kiln support frames was insufficient to carry the design loads.

The originally adopted static scheme in the form of a frame with one rocker column was susceptible to horizontal displacements which might increase if disturbances in the operation of the kiln occur or if the kiln components would be nonaxially assembled.

The cracks in the spandrel beam of frame 3, running perpendicularly to the kiln’s axis, were the result of the spandrel beam’s spatial work neglected in the original design.

When designing rotary kiln support frames it should be taken into account the increase in stress, due the thermal field, particularly when the static scheme should be changed for one with two rigid columns.

The 3-D frame model calculations have confirmed the fact that tensile stresses in the column and in the spandrel beam were concentrated closer to their axes and not at their outer surfaces. Therefore additional reinforcement should be provided to carry these stresses.

References

1. Lipiński, J., *Foundations for machines*, Arkady, Warsaw, 1985, (in Polish).
2. Polish Standard PN-84/B-03264 – Concrete, reinforced-concrete and prestressed structures. Structural analysis and design, (in Polish).
3. Kobiak, J., Stachurski, W., *RC structures*, Vol. 1, Arkady, Warsaw, 1984, (in Polish).
4. DIANA, Finite element analysis, Element library, User's manual – release 6.1, TNO Building and Construction Research.
5. Comparison of design loads, POLTEGOR-Projekt Ltd., (in Polish).
6. Design of rotary kiln foundations (in Polish), B.B.P. No. 4 in Gliwice, the Opole Branch, 1950, Extracts, (in Polish).
7. Dmochowski, G., Siwiec, P., Spatial analysis RC frame foundations of rotary cement plant kiln, *Current scientific and research problems in building*, Ed. Warmińsko-Mazurski University, 2000, (in Polish).

"Computational Civil Engineering 2007", International Symposium
Iaşi, România, May 25, 2007

Flood routing using 'Femme'

L. De Doncker[1], P. Troch[1], R. Verhoeven[1],
K. Buis[2], P. Meire[2]
[1]*Hydraulics Laboratory, Ghent University, Ghent, 9000, Belgium*
[2]*Ecosystem Management Research Group, Universityof Antwerp, Wilrijk, 2610, Belgium*

Summary

The environment 'Femme' ('a flexible environment for mathematically modelling the environment') is used to model ecological processes as the transport of nutrients and polluents. The program is user-friendly and based on a Fortran modular open source code and uses a lot of integrated integration tools. For the study of the interaction of ecological processes and flow in the river, a realistic modelling of the surface water flow is necessary. Here, the implementation of a one dimensional hydrodynamic model for surface water flow in 'Femme' is reported.

Because of the lack of hydrodynamic information in the ecological model, the kinematic and parabolic equations are implemented first. They describe accurate the time shift of the wave. The simplification to the parabolic and the kinematic equations allow a faster and easier solution. The parabolic model is known as the convection-diffusion equation and describes the translation and attenuation of the wave in open channels and is valid for short stretches with mild slopes. The kinematic model doesn't take into account the flattening of the wave and corresponds less with the realistic deformation of waves.

First, the context of the research is presented in the introduction. Further, the importance of hydraulic modelling is illustrated. The study area and the modeling environment are further developed. As a conclusion, some calculation results are enclosed.

KEYWORDS: ecosystem modelling, environmental engineering, flood routing, vegetated rivers.

1. INTRODUCTION

This paper is part of the multidisciplinary research project 'A fundamental study on exchange processes in river ecosystems' (University of Antwerp, Vrije Universiteit Brussel, Ghent University, 2004 - 2007). The overall research aim is to study the diverse physical and biological processes in margins and inundation areas of water courses and how their interactions determine the exchange of water, dissolved

compounds and particulate matter. This paper will give an introduction on hydraulic modelling. The first action is exploring the possibilities of surface water modelling, to add in a later phase the vegetational processes. Simplified modelling equations are used.

2. FLOOD ROUTING

2.1 Importance of Hydraulic Modelling

River hydraulics is characterised by changing discharges and water levels due to rain fall. Studies about this topic have although to take into account this non-permanent character of the flow. Time shift and flattening of the peak of the wave can be remarked by studying waves at two different places in rivers as can be seen on Figure 1. The hydrograph of the wave is shown in section I as well as in the more downstream section II.

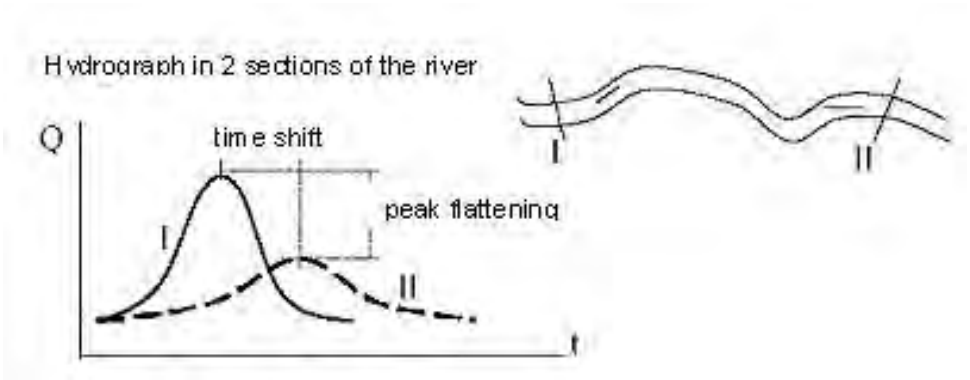

Figure 1: Hydrograph in 2 sections of the river

Description of this phenomenon, i.e. non-permanent flow of surface water is done by the Saint-Venant equations which include the continuity equation (1) and the momentum equation (2):

$$\frac{\partial Q}{\partial x} + B\frac{\partial h}{\partial t} = 0 \tag{1}$$

$$\frac{\partial Q}{\partial t} + \frac{\partial}{\partial x}\left(\frac{Q^2}{A}\right) = gA\left(S_0 - S_f - \partial h/\partial x\right) \tag{2}$$

with Q = discharge [m³/s], B = section width at water surface [m], h = water depth [m], g = gravity [m/s²], A = wetted cross section area [m²], S_0 = tan α = bottom slope [m/m], S_f = energy gradient needed to overcome frictional resistance of channel bed and banks in steady flow = friction slope [m/m].

2.2 Study Area: the river Aa

Focus of the study is the downstream part of the river Aa (Fig. 2), this is the stretch between weir 3 and weir 4, a distance of 1.4 km, near the village of Poederlee. In this area the interaction between groundwater, surface water and vegetation will be studied. Regular measurements of discharge and water level allow to gather data to calibrate the model.

The catchment basin of the river Aa is situated in the region of Antwerp and is hydrographical part of the Nete basin. More than 40 % of the water in the Nete basin is going to the river Aa, which is although an important river. The river Aa flows into in the Kleine Nete near the city of Grobbendonk. The origin of the river Aa is found near the communities of Merksplas and Turnhout and is streaming through Turnhout, Gierle, Gielen, Poederlee and Vorselaar. The river Aa has a total length of 36.8 km and the drainage area is about 23,700 ha.

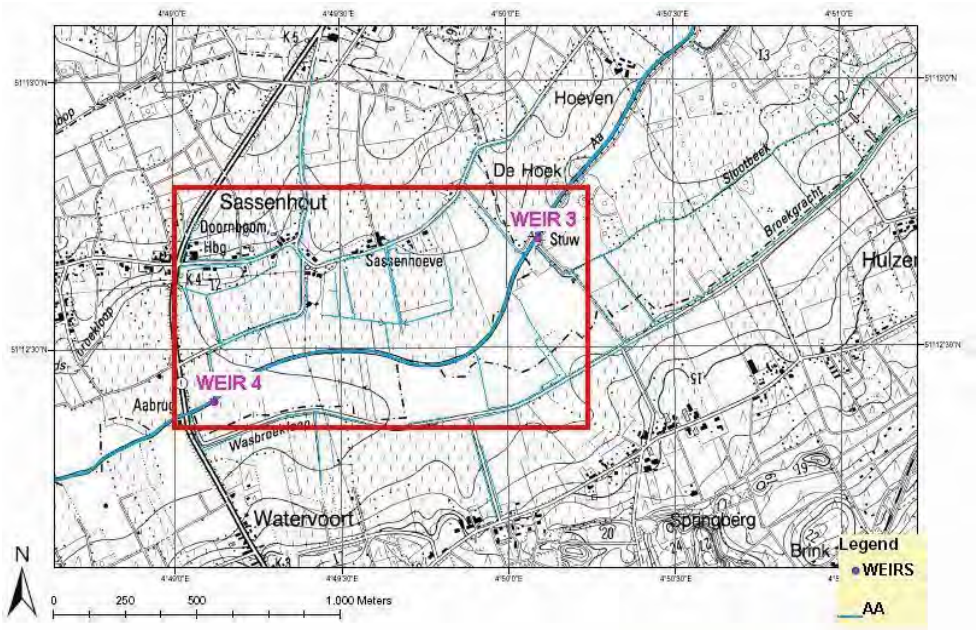

Figure 2: The river Aa

2.3 Simplified Saint-Venant Equations

The Saint-Venant equations can be simplified in some typical cases which can be easily solved. For rivers with a small slope, the acceleration terms are negligible and the equation is known as a parabolic model, which is the convention-diffusion equation. The model describes the attenuation of the wave due to storage and friction.

The maximum discharge will decrease and the minimum discharge will increase in the downstream direction, due to the influence of the diffusion parameter D. So, the wave will become flatter and wider, because the total amount of water has to be the same.

When also the distance between two sections is short, the peak flattening is negligible and the most simplified model is the kinematic model which includes only the friction and the translation of the wave. Peak flattening is not incorporated.

Equations (3) and (4) present respectively the parabolic and kinematic wave model, with D = diffusion parameter, responsible for peak flattening and C = convection parameter, responsible for the translation of the wave. D and C are variables and depend of the values of the discharge and the water level. Therefore, the solution can only be obtained by numerical models.

$$D\frac{\partial^2 Q}{\partial x^2} = C\frac{\partial Q}{\partial x} + \frac{\partial Q}{\partial t} \tag{3}$$

$$C\frac{\partial Q}{\partial x} + \frac{\partial Q}{\partial t} = 0 \tag{4}$$

$$C = -\frac{1}{B}\left(\frac{\frac{\partial S_f}{\partial h}}{\frac{\partial S_f}{\partial Q}}\right) = -\frac{1}{B}\left(\frac{\partial Q}{\partial h}\right) \tag{5}$$

$$D = \frac{1}{B}\left(\frac{1}{\frac{\partial S_f}{\partial Q}}\right) \tag{6}$$

The values of D and C depend of the discharge and the water height and can be found in a numerical way. Values mentioned in (Verhoeven, 2006) are 10^4 to 10^6 m/s for D and C = 1.5 to 1.8V (with V the average velocity). Calculations in this

study resulted in other values as D = 250 m/s and C = 0.29 m/s, which is the translation velocity of the wave and can also be seen on Figure 3. Best values are obtained by fitting the calculation result on measured values or on more detailed simulation results as obtained with the Saint-Venant equations.

In a first phase, the cross sections are simplified to rectangular or trapezoidal sections. Comparison with the effective geometry of the river Aa has shown that the differences are only small (De Doncker et al., 2005).

2.4 The Hydraulic Model 'Femme'

'Femme' or 'a flexible environment for mathematically modelling the environment' is developed by NIOO (Netherlands Institute of Ecology) (Soetaert et al. (2004)). 'Femme' is a modelling environment for the development and application of ecological time dependent processes by use of numerical integration in the time of differential equations. The program is written in Fortran.

'Femme' consists of a wide range of numerical calculations and model manipulations (as integration functions, forcing functions, linking to observed data, calibration possibilities, etc.). These technical possibilities allow the user to focus on the scientific part of the model and detailed research of the model without the confrontation with real program linked problems.

'Femme' is focused on ecosystem modelling, is open source (no black box) and exists of a modular hierarchical structure (implementation of different models next to each other). What was missing up till now was the implementation of a hydrodynamic surface water model to couple ecology and surface water in each timestep.

For the study of the interaction of ecological processes and flow in the river, a realistic modelling of the surface water flow is necessary. Here, the implementation of a one dimensional hydrodynamic model for surface water flow in 'Femme' is reported.

2.5 Implementation of the Flow Equations in 'Femme'

The hydrodynamic model for the transmission of the wave in the river has to be implemented in 'Femme'. Differential equations were converted into algebraic equations using the finite difference scheme. Forward discretisation of the equations in time and central discretisation in space is carried out.

Implementation of the hydrodynamic model in 'Femme' can be done by using the characteristics of this environment. Discretisation in space has to be implemented in the code, the integration routine for timestepping is incorporated in the code.

Further, 'Femme' will be used for the integrated hydrodynamic – ecological modeling. Therefore, it is not advisable to model complex ecological processes with simplified conceptual hydrodynamic models. In this multidisciplinary approach, different research areas have to be integrated to study properly the interaction between surface water and vegetation.

2.6 Calculation Results

2.6.1 Kinematic versus parabolic wave model

The kinematic and the parabolic model are built into the 'Femme' environment. As a first verification of the model, a stretch of a river is modelled. The wave, measured upstream, has a triangular hydrograph Q(t) as indicated in gray dashed line at Figure 3 and Figure 4.

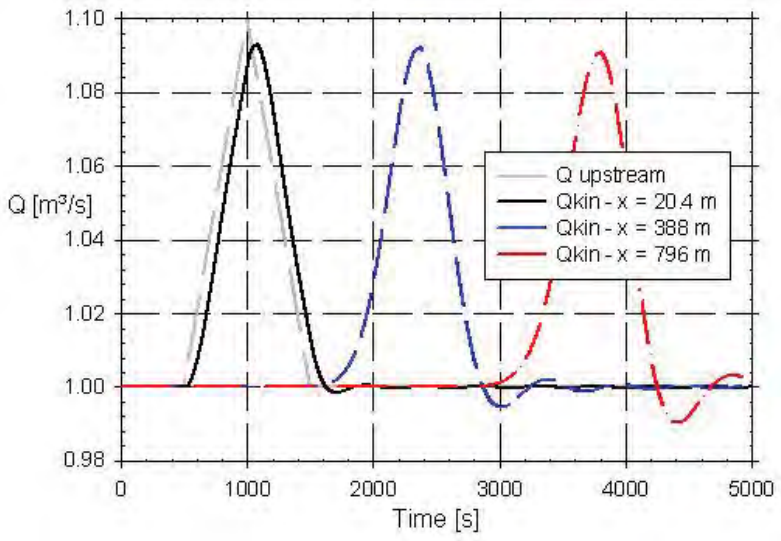

Figure 3: Use of the kinematic wave model: results at different distances

The kinematic as well as the parabolic model calculates the transmission of the wave. The resulting hydrograph at 20.4 m, 388 m and 796 m from the upstream boundary is indicated at Figure 3 and Figure 4. The total length of the channel is 1000 m. The channel is rectangular, has a bottom width of 10 m and a water height of 1 m. The Manning coefficient is 0.05 $m^{-1/3}s$.

In Figure 3, the use of a kinematic model is illustrated. The time shift indicates that the wave moves from upstream to downstream with a constant celerity, without peak flattening. The small decrease of the peak discharge is due to the numerical (non-physical) dispersion as a consequence of the discretisation. Small wiggles at

the base flow are due to the triangular hydrograph, which is not natural and contains discontinuities.

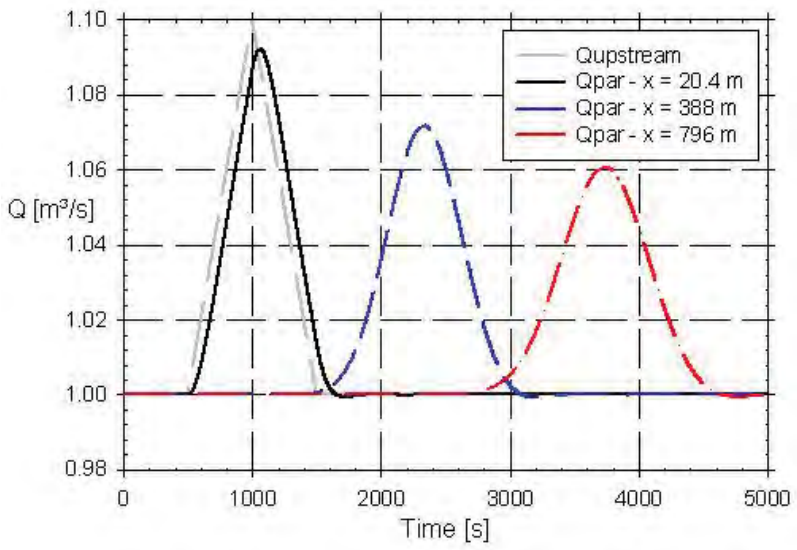

Figure 4: Use of the parabolic wave model: results at different distances

In numerical modeling, a good choice of timestep Δt and cell width Δx is necessary. These values have to be sufficient small to not to miss any effects (e.g. peak discharges) and to be sufficient large to minimize the calculation time. The Courant-Friedrichs-Lewy condition (CFL, Cunge et al.) determines a relation between the time step and the grid size separation to solve the partial differential equations in a convergent way.

For an explicit scheme, it means that the solution will be numerical stable. So, for using the explicit solution scheme of the kinematic and parabolic model, attention have to be paid at this criteria.

This condition can be avoid by using an implicit scheme for solving the Saint-Venant equations (as the Preissmann scheme). Time steps can be taken larger, which is useful for long simulation periods, and the solution will be stable.

The parabolic model, used for the results of Figure 4 contains an extra diffusion term. Next to the time shift, also the peak flattening in the downstream direction can be seen.

2.6.2. Variation of the Manning coefficient

Further, some calculations about the influence of the roughness coefficient n are carried out. Three different values of this friction factor are used: n = 0.05 $m^{-1/3}s$, n = 0.2 $m^{-1/3}s$ and n = 0.5 $m^{-1/3}s$. These are values derived from the research carried out in the river Aa. Winter values were low, due to the low amount of vegetation in the river. In spring and summer, biomass starts to increase and results into higher Manning coefficients.

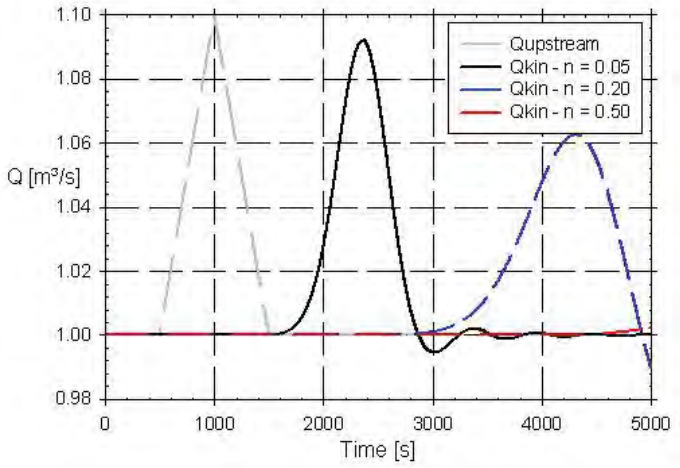

Figure 5: Use of the kinematic wave model: result at the same distance (x = 388 m) for different values of the Manning coefficient n

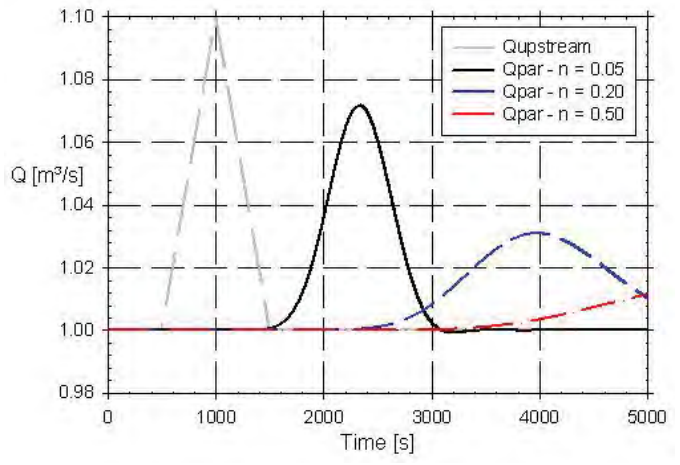

Figure 6: Use of the parabolic wave model: result at the same distance (x = 388 m) for different values of the Manning coefficient n

Differences between winter and summer up to a factor 10 are not rare. As can be seen, the presence of more macrophytes cause obstruction in the channel. For a certain amount of water, it is more difficult for the water to pass and so the discharge will be lower, just as the peak value of the discharge. More vegetation in the river results in a higher friction coefficient of Manning.

2.6.3 Use of the Saint-Venant equations

After having modeled the simplified kinematic and parabolic equations, the proliferation of the triangular hydrograph is also modeled using the Saint-Venant equations. These results can be seen on Figure 7 and Figure 8. Figure 7 shows the results at different sections when the Manning coefficient is set constant (n = 0.05 $m^{-1/3}s$).

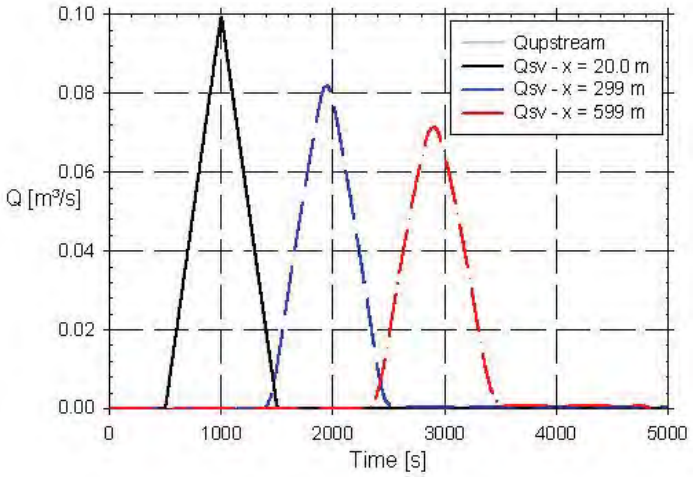

Figure 7: Use of the Saint-Venant equations: result at different distances

At Figure 8, the influence of this friction coefficient in a certain section (x = 299 m) can be seen. The total stretch is 10,000 m and upstream and downstream boundary conditions have to be added, which is different compared to the simplified equations.

The parabolic and kinematic model use the upstream boundary condition and start to calculate one cell after the other. In contrary, the Saint-Venant equations use both boundaries and need well balanced initial conditions. Calculation of the surface water level for permanent steady state flow over the total length of the channel can be a good start and can serve initial conditions. Further more, boundary conditions are important because both of them have influences in the different cells.

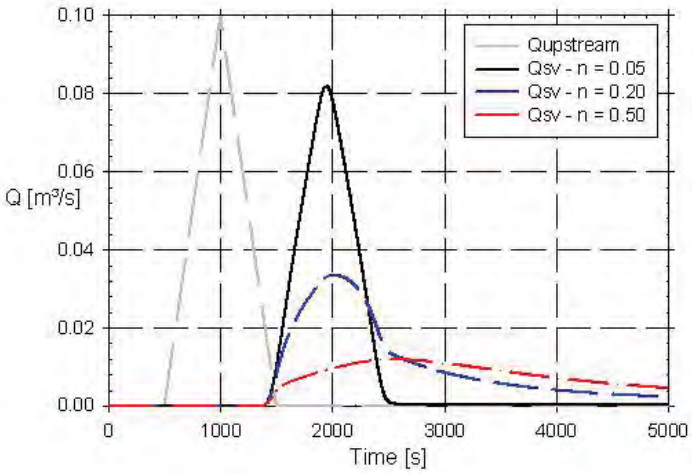

Figure 8: Use of the Saint-Venant equations: result at the same distance (x = 299 m) for different values of the Manning coefficient n

Concerning the morphology of the channel, the slope is important for the water levels in the channel. This bottom slope has an influence on the friction slope S_f (water surface slope). A constant slope of 0 can eliminate that influence.

3. CONCLUSIONS

'Femme' has been used as environment for the description and propagation of waves in rivers. As a study area, the river Aa was selected and its characteristics were implemented in 'Femme'.

By this, three kind of models to simulate the propagation of waves in channels are considered. As can be seen, the one model is more accurate as the other, but accurateness includes also a higher degree of complexity. So depending of the situation and the kind of results that have to be obtained, one model can be chosen.

While studying a variety of ecosystem cases, different wave models (based on the kinematic, parabolic and Saint-venant equations) or even a constant discharge can be used in the hydraulic calculation.

Acknowledgements

This research is funded by the FWO (Fund for Scientific Research) - Flanders (G.0306.04). It is part of the multidisciplinary research project 'A fundamental study on exchange processes in river ecosystems' (University of Antwerp, Vrije

Universiteit Brussel, Ghent University, 2004 - 2007). The overall objective is to study the physical and biological exchange processes in margins and inundation areas of water courses and how their interactions determine the exchange of water, dissolved compounds and particulate matter.

Thanks to Mr. Martin Van Daele and Mr. Stefaan Bliki for their assistance with the discharge measurements.

This research is funded by the FWO (Fund for Scientific Research) - Flanders (G.0306.04).

References

1. Abbott, M. B. et al., *Unsteady Flow in Open Channels,* Vol. 1, Ed. by Mahmood, K. and Yevjevich, V., 1975.
2. Buis, K., Anibas, C., Banasiak, R., De Doncker, L., Desmet, N., Gerard, M., Van Belleghem, S., Batelaan, O., Troch, P., Verhoeven, R. and Meire, P., *A multidisciplinary study on exchange processes in river ecosystems*, W3M, Wetlands: Monitoring, Modelling, Management, 22 – 25 September, Wierzba, Poland, 2005.
3. Cunge, J., Holly, F. and Verwey, A., Practical aspects of computational river hydraulics, Pitman Advanced Publishing Program, London, 1980.
4. Chow, V.T., *Open Channel Hydraulics*, McGraw-Hill, New York 1959.
5. Chow, V.T., Maidment, D. R., Mays, L.W., *Applied Hydrology*, McGraw-Hill, New York 1988.
6. De Doncker, L., Troch, P., Verhoeven, R., *Influence of aquatic weed growth on the flow resistance of the river Aa*, 6th FirW PhD Symposium, 30th November 2005, Ghent University, Belgium.
7. Soetaert, K., de Clippele, V., Herman, P, 'Femme', a flexible environment for numerically modeling the environment, Manual, NIOO-CEME, Yerseke, The Netherlands.
8. Verhoeven, R., Water beheer en waterbeheersing, course for civil engineers, part C: '*Afvoer en berging van water'.*

"Computational Civil Engineering 2007", International Symposium
Iaşi, România, May 25, 2007

Simulation of cooling tower collapse on the basis of non-linear concrete model and FEM analysis

Przemysław Siwiec, Sebastian Toś
Department of Civil Engineering, Wrocław University of Technology, Wrocław, Poland

Summary

In this paper authors attempt to take advantage of a non-linear model of material to create a mathematical model of the cooling tower, and further, taking advantage of the non-linear FEM analysis, they try to recover numerically the course of the collapse. Both for concrete, as well as for steel, an elasto-plastic model of material characterized by specific plasticity criteria has been assumed.

KEYWORDS: cooling tower, non-linear analysis, elasto-plastic material model, FEM analysis

1. INTRODUCTION

The main purpose of design process is to bestow an object a form, shape and guarantee proper technical parameters in order to fulfill its functions and safety of service. As soon as the erecting process begins the object is under influence of destructive factors and interactions tending to ruin it. The purpose of the structure designer is to predict these factors and to counteract properly. Nevertheless crashes do occur. Therefore the new assignment appears: to determine causes and failure sequences. Being in the know with the failure course we are able to determine the safety conditions of a similar already existing structure and to undertake proper improving actions.

In this paper the authors have tried to create a proper numerical model of the reinforced concrete (RC) cooling tower and to investigate the failure course of RC cooling tower in 1987.

2. THE FAILURE SEQUENCE

The failure of over 100 m high RC cooling tower was one of the most spectacular crashes in Poland. On 7th February 1987 at 7 p.m. the RC cooling tower suddenly collapsed. At the level of 38th concreting cycle almost the whole perimeter of its

shell was cut. Only from the north-east side a deep interstice appeared (Fig. 1). At the moment of the failure the RC cooling tower was under regular service. Till that day the object had been exploited uniterruptedly for 23 years and it was considered to be in the best technical state of all six identical RC cooling towers in the battery.

The most characteristic in this failure was the lack of clear cause. On that day it was light windy: 3–5 m/s, so the wind factor could not be the main reason. The unusual influences such as sound waves caused by supersonic airplanes or underground earthquakes were excluded, too. The RC cooling tower collapsed as if under its own weight.

According to the initial investigations [8] — carried out from February to April 1987 — it has been established that at the most of the fracture the concrete was crumbled, cracked and not condensed. At the whole of the fracture perimeter reinforcement bars without any traces of rapture were found. Some of them were strongly crumpled, some cambered downwards only. A few of them were cambered upwards, too.

Fig. 1 RC Cooling tower after the collapse

The examination of the concrete and reinforcement strength of the RC cooling tower confirmed their satisfactory quality. The strength of most of concrete samples reached over 20 MPa.

The initial estimation of collapse causes has revealed concrete corrosion of the operating contact zone leading to loss of the shell stability [8]. However this phenomenon seamed to be too simple and incomplete especially in consideration of the fact of strong winds occurring only a few days before the failure.

A following hypothesis has been proposed: the proximate cause of failure was the improperly performed operating contact zone which in result of variable winds and

corrosion factors led to loss of the whole shell stability. In order to prove this hypothesis the nonlinear FEM analysis on the numerical model of RC cooling tower has been performed, with use of the DIANA system.

3. DESCRIPTION OF THE NUMERICAL MODEL

3.1 Geometry

In order to properly analyze the proposed thesis the numerical model of 100 m high RC cooling tower has been created.

Eight-node shell elements of CQ40 [13] type have been used for creating the numerical model of the bicurvature shell structure. These elements allow to introduce the variable shell thickness in every node so the numerical model has no rapid stiffness changes.

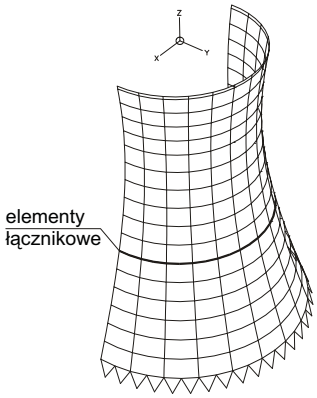

Fig. 2 Numerical model

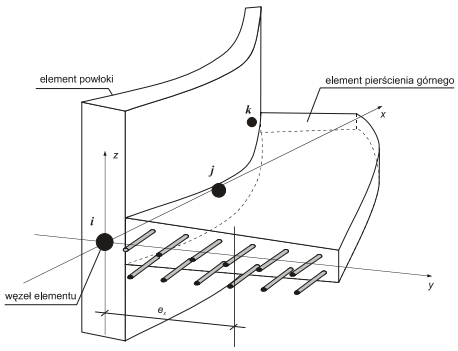

Fig. 3 Elements of upper shelf

The structure has been divided into 17 rings with 12 final elements in every ring (for the half of the structure) — see Fig. 2 [3].

The stiffening ring has been created with the three-node rod elements of CL18B type (Beurnoulli) with 6 degrees of freedom in every node. Their cross-section has been eccentricitaly founded (shifted in relation to) on the net of nodes in order to model the stiffening shelf properly. Due to possibility of unrestricted cross-section shape modeling, the actual trapezoid-shaped shelf has been created — see Fig. 3.

The load carrying poles have been modeled with the rectilinear elements of L13BE type (circle-shaped in cross-section) and they have been connected in a rigid way with the shell elements and with the fundaments.

The DIANA system allows to model the reinforcement as the settled inserts, bound with the mother element and make its stiffness increase. The reinforcement elements have no degrees of freedom of their own so their deformation is determined by the deformation of the mother element. It means that there is no slip phenomenon between the concrete and the reinforcement. Generally it is possible to insert the reinforcement in the mother final element in unrestricted way — regardless of its geometry.

Two kinds of the reinforcement have been used in the numerical model of the RC cooling tower: the linear inserts (rods) settled in rod elements, and the net inserts settled in shell elements. Tab. 1 shows the area of used inserts [8].

All final elements used in the numerical model have been numerical integrable and for each of the groups the modified integral-points-set has been used:

- Poles elements had eight Gauss's integral points at their cross-section surface, evenly distant from the rod center. Three integral zones with 8 points in each one at the rod length have been used (according to the Gauss's rule).
- Upper shelf elements had nine Gauss's integral points at their cross-section surface (3×3) and three integral points groups distributed at the rod length (according to the Gauss's rule).

Tab. 1. The reinforcement area

Element	Area
Load carrying poles	0.34%
Upper shelf	0.28%
Outer horizontal reinforcement	0.25%
Inner horizontal reinforcement	0.25%
Outer vertical reinforcement	0.20%
Inner vertical reinforcement	0.20%

- The reinforcement settled in elements had the integral schemes analogical with their mother elements: three Gauss's points at the length for rods and 3×3 Gauss's integral points for reinforcement nets of shell elements.

In order to investigate the simulation of the failure course, the FEM numerical model has been created in which the connecting elements have been used in order to model the linear damage zone properly [13].

The characteristic feature of these elements is the possibility of physical disconnection into two parts after exceeding the tensile strength. The connecting elements of the N6IF type have defined stiffness against compression/tension and shearing.

Tab. 2. The material parameters

Parameter	
Young's modulus	26·106 kPa
Poisson ratio	0.1667
Density	23 kN/m3
Compression strength	11 500 kPa
sin ϕ	0.5
sin Ψ	0.5
Tensile strength	900 kPa
Damage energy G_f	500 kNm/m2
Weakenig model	Hordijk
Tangential stress ratio β	0.01

In order to create the numerical model properly in accordance with the actual structure, the connecting elements in damage zone (3 to 5 elements long) had the stiffness of the weakened concrete (Hordijk's model - see Tab. 2) and their shearing stiffness has been equal with the reinforcement bar shearing stiffness. The stiffness of the rest of the connecting elements has been defined as equal with the stiffness of the shell elements.

3.2. The material

All final elements had nonlinear characteristics [2] and their parameters have been based partly on published investigations results of the analyzed object and partly on the design project documentation and expert opinions on the cooling tower [7, 8]. There has been taken into consideration the material ductility described by the Drucker-Prager's constitutive model in the compressed zone for the concrete elements.

For the tensile zone the smeared cracks model has been used [14, 15]. The winding effect of the load carrying RC poles has been modeled by increasing the strength parameters of concrete. On the basis of the in situ investigations the concrete strength of f_c=20 MPa has been assumed whereas for the RC poles it has been increased to f_c=25 MPa [8]. The Tab. 2 shows the nonlinear concrete parameters.

Tab. 3 Values of the α parameter

$d_{\max}$ [mm]	α
8	4
16	6
32	10

The most important parameter describing the material in the cracked zone is the damage energy G_f. Its value has been based on the recommendations of the CEB-FIB Model Code (1990), which allowed to estimate the damage energy on the basis of the strength investigations according to the relationship:

$$G_{\mathrm{f}} = \alpha f_{\mathrm{ck}}^{0,7} \tag{1}$$

where f_{ck} is the compression strength, depends on the maximum aggregate size (Tab. 3).

Fig. 4 shows the concrete performance for the biaxial state of stress. Fig. 5 shows the H-M-H criterion for steel.

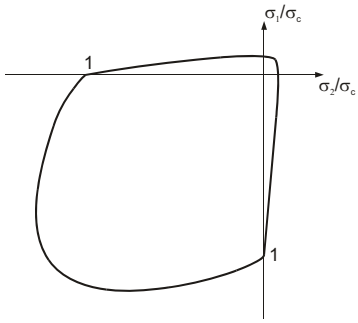

Fig. 4 Biaxial state of stress for concrete

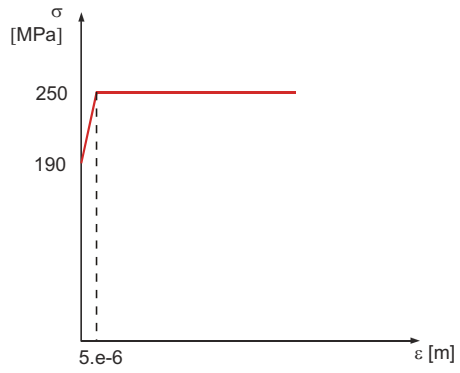

Fig. 5 The steel stiffening model

4. THE LOADS

In the calculation carried out only the deadweight and the wind have been considered [1]. They were the most important factors and most significant for the structure effort. Other loads such as: temperature, hydraulic pressure, unequal insolation effects, unequal foundations subsiding and other exceptional loads have been neglected. As far as the general question is considered taking into account all of these loads will allow to determine the global state of the structure effort.

During the numerical analysis process the structure has been loaded in a few phases:

- First the deadweight was loaded (incrementally) till the nonlinear load coefficient Lf reached the value equal to 1.0.

- Then the wind load was added (incrementally) till the nonlinear load coefficient Lf reached its maximum value.

5. THE TECHNIQUE OF THE NONLINEAR PROBLEM TRACING

In order to solve the nonlinear problem the standard Newton-Raphson's algorithm and the energetic norm of the results convergence control have been used. In nonlinear process the *arc-length* technique based on tracing the selected node displacement has been used in order to control the load growth. At each stage of the load increment the node displacement (degree of freedom) towards the selected direction has been analyzed. Every time the most deformated node - in the previous stage of the analysis - has been taken into account. Calculations have been stopped as soon as the lack of convergence has occurred.

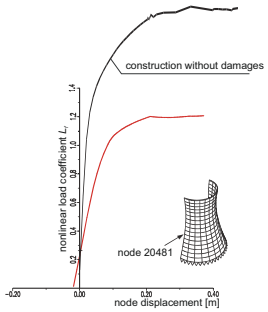

Fig. 6 The structure answer curves

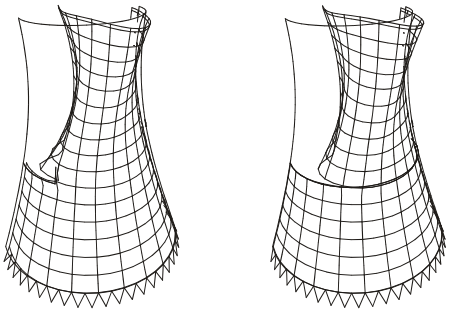

Fig. 7 The deformation development in RC cooling tower under the wind load

The structure performance under the increasing load has been investigated with use of the structure response curve, which described the chosen node displacement as a function of the load increase (defined as the nonlinear load coefficient L_f).

6. THE NUMERICAL SIMULATION OF THE COLLAPSE SEQUENCE

According to the proposed hypothesis it has been assumed that the primary damage area of the operating contact zone reached up to 21 m (three elements of the half-ring). In order to fulfill the symmetry conditions the interstice has been located at the windward side. This is a particular case yet it is sufficient for the essence of the

analyzed matter. The numerical analysis indicates the possibility of the primary shell damage development caused by the wind loads without collapse of the whole structure.

Assuming the variable wind directions, it is probable that the progressive interstice growth up to the whole perimeter would occur. At the next calculation stage the interstice has been assumed as long enough and the cooling tower has been deadweight loaded only. At further stages the size of the totally damaged material in the interstice has been varied. The run of the structure response curve is shown in the Fig. 8 and the deformation development - in the Fig. 9.

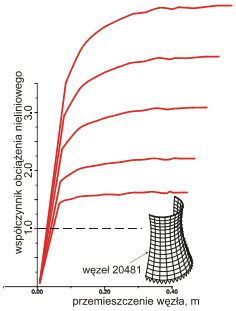

Fig. 8. The structure response curves due to development of initial crack.

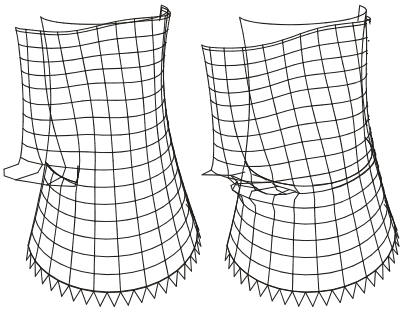

Fig. 9. The deformation development in RC cooling tower under the deadweight

The deformation character confirms the conclusion of locally violent variable displacement character. Displacement occurs within the area of one ring above and one ring below the interstice. What is worth noticing is the deformation form of the upper part of the shell.

At the area close above the interstice the shell goes outwards from its perimeter while the rest of the shell goes towards the inside. According to the above scheme only a small part of the shell should collapse outside the cooling tower and the whole rest of it should collapse towards the inside.

7. THE FAILURE SEQUENCE DETAILS

Phase 1 — improper composition of the concrete mixture, its impurities or not sufficiently careful assembly phase caused the material imperfection which increased during the service of the cooling tower [5, 6]. The negative coincidence was localization of this imperfection in the zone of the highest structure effort — i.e. at of the tower height [3]. At this moment it is impossible to exclude the geometrical imperfection in the analyzed zone, too.

Phase 2 —increasing material degradation process caused by accelerated corrosion of the cracked concrete brings about the interstice or the weakened material zone. Then the variable winds and frost penetration cause enlarging of this zone. It is possible that the weakened zone still holds its geometrical shape in spite of total loss of its strength parameters due to internal cracking. This would explain the fact that the Electric Power Station employers had not noticed the shell defect. Undoubtedly the interstice initiation took place at the operating contact zone.
Phase 3 — when the strong winds cause the increasing of the interstice up to its critical length, further interstice length growth begins which results from the deadweight of the cooling tower only. At first this process was not violent as it was restrained by the reinforcement and could last even for a few days until the moment of a violent collapse. If only the stronger puff of wind occurred during this time, the collapse would undoubtedly have taken place sooner.

The confirmation of the presented above hypothesis of the failure sequence is the occurrence of the most of the concrete debris at the eastern side of the cooling tower. According to the presented model the failure process started exactly above the area where the concrete debris was found outside the cooling tower.

8. CONCLUSION

In this paper the numerical model of the RC cooling tower has been created with consideration of material and geometrical nonlinearity. This model has been investigated on the basis of 100 m high RC cooling towers commonly built in Poland. The presented numerical model enables simulation of the process occurring during regular RC cooling tower exploitation. The numerical model analysis allows the precise determination of the causes and the failure course. Due to possibility of failure results verification — especially the concrete debris localization — the presented numerical model has been proved reliable.

References

1. 1. Siwiec P., Szechinski M.: *Zelbetowa chlodnia kominowa obciazona wiatrem* — Inzynieria i Budownictwo, nr 3, 1997.
2. 2. Siwiec P., Strouven P., Moczko A.: *Study of steel bar corrosion by experimental and analytical simulation* — DIANA Computational Mechanics '94, ed. Kusters M. A., Hendriks A. N., Kluwer Academic Publishers, Dordrecht — 1994.
3. 3. Siwiec P.: *Nieliniowa analiza statyczno-wytrzymalosciowa uszkodzonej, zelbetowej chlodni kominowej* — doctor's thesis, The Institute of the Building Engineering, Wroclaw 2001.
4. 4. Zabiello Z., Hawre L.: *Problemy oceny stanu technicznego chlodni kominowych w kontekscie awarii chlodni nr 6* — The Science-technical Conference: The durability of the RC cooling towers, Czocha — 1989.
5. 5. Persona M.: *Z badan doswiadczalnych chlodni kominowych Elektrowni Turow* — The Science-technical Conference: The durability of the RC cooling towers, Czocha — 1989.

6. 6. Persona M., *Wybrane zagadnienia z badan zelbetowych chlodni kominowych* — Chlodnie Kominowe. Efektywne systemy ochrony i napraw, Sympozjum, Jelenia Gora 1991.
7. 7. Persona M., Szechinski M.: *Remark on failure of a reinforced concrete cooling tower* — IABSE Colloquium, Stuttgart 1991.
8. 8. Persona M., Stus R., Szechinski M.: *Okreslenie przyczyn katastrofy budowlanej chlodni kominowej nr 6 oraz ustalenie stanu technicznego czesci niezawalonej pod katem mozliwości wykorzystania dla ukladu chlodzacego Elektrowni Turow* — Reports of the Institute of the Building Engineering, Wroclaw University of Technology, SPR no. /87.
9. 9. Persona M. i zespol: *Wyniki badań i ocena stanu technicznego konstrukcji plaszcza chlodni kominowej nr 6 w elektrowni Turow* — Reports of the Institute of the Building Engineering Wroclaw University of Technology, SPR nr 43/89.
10. 10. Owczarzy J.: *Katastrofy zelbetowych chlodni kominowych* — The Science-technical Conference: The durability of the RC cooling towers, Czocha — 1989.
11. 11. Niku S. M.: *Finite Element Analysis of Hyperbolic Cooling Towers* — Lecture Notes in Engineering, ed. Brebbia C. A., Orszag S. A., Springer-Verlag 1986.
12. 12. Golczyk M.: *Analiza techniczna przyczyn i skutkow uszkodzen i zniszczen hiperboloidalnych powlok chlodni kominowych* — The Science-technical Conference: The durability of the RC cooling towers, Czocha — 1989.
13. 13. DIANA Finite Element Analysis, *User's Manual*, Release 6.2 — TNO Building and Construction Researche, Delft 1996.
14. 14. Blaauwendraad J.: *Numerical Methods in Structural Mechanics* — Delft University of Techniology — 1993.
15. 15. De Borst R.: Computational Methods in Non-linear Solid Mechanics — Delft University of Technology, series B20, Delft 1993.

"Computational Civil Engineering 2007", International Symposium
Iaşi, România, May 25, 2007

Unsteady axial Poiseuille flow of a Bingham fluid in an annulus

Irene Daprà, Giambattista Scarpi
DISTART, University of Bologna, 40136, Italy

Summary

Several fluids which are of interest in civil engineering, as bentonite, montmorillonite, slurries, behave as Bingham fluids, i.e. fluids which present a yield stress. This paper investigates numerically the start-up, the cessation and some pulsating flows of a Bingham plastic between two coaxial cylinders. The constitutive law presents a discontinuity for zero shear rate which introduces severe difficulties in solving any problem of unsteady motion, both analytically and numerically. A suitable way to avoid the obstacle is to regularize the constitutive equation using a smooth function to approximate the Bingham law. The adopted function depends usually on a parameter: as it tends to infinity the model tends (in distribution theory sense) to the true Bingham law. Several models have been used in literature to regularize the rheological behaviour of a viscoplastic fluid: in this paper a new constitutive equation is proposed, based on the error function (erf). The velocity fields have been calculated using an implicit finite difference method. The numerical results confirm that the time required to reach the final steady state is infinite for start-up, whereas it is finite for stopping. In the pulsating flow the mean velocity of the plug in a period and the mean rate of flow increase owing to the non linearity of the material.

KEYWORDS: Bingham fluid, unsteady flow, Poiseuille flow, flow in annulus.

1. INTRODUCTION

Bingham fluids such as bentonite and montmorillonite are used to solve many engineering problems for example in drilling, in pile works and in rock consolidation. Bentonite is the base material in drilling: it cools the drill and reduces wear, consolidates the excavation, goes back up in the annulus between wall and stick bringing to the surface the debris.

Bingham fluids require the application of a greater shear stress than a critical value, the yield stress, to begin to move. After yielding, the rheological behaviour is that of a Newtonian fluid, while in the core region the material moves as a solid body. Many unsteady flows of Newtonian fluids admit analytical solution in closed form:

the same problems for a Bingham fluid are obviously more difficult to solve because of the non linearity of the constitutive law.

The discontinuity in the constitutive equation at zero shear rate introduces severe difficulties for analytical and even for numerical solutions. To overcome that, Glowinski [1] suggested regularising the constitutive law, substituting the discontinuous function with a continuous one, which, when a given parameter tends to an assigned limit, usually zero or infinity, tends (at least in the sense of distributions theory) to the true Bingham law. Several proposals for regularisation have been made in literature; the most used is that proposed by Papanastasiou [2]. An interesting analysis of advantages and disadvantages of continuous models with exhaustive literature is given by Frigaard and Nouar [3].

Characteristic of a Bingham fluid is the fact that its stopping time is finite, whereas Newtonian fluids and generally any fluid without yield stress need an infinite time to stop. Glowinski [4] and Huilgol et al. [5] give a theoretical upper bound for the stopping time for pipe and plane flow. Chatzimina et al. [6] study numerically the cessation of the Couette and Poiseuille flow of a Bingham fluid using the Papanastasiou model comparing the numerical results with the theoretical predictions. Many authors have written in the past about unsteady flow of Bingham fluids; among these we recall for example Duggin [7] which gives a numerical solution for the start-up flow in a circular pipe; Papanastasiou and Boudouvis [8] solve numerically flow problems in generalised conduits. Hammad [9] studies the pulsatile flow for different waveforms of the pressure gradient. Daprà and Scarpi give an analytical solution to the start-up problem in a circular pipe.

This paper investigates numerically the start-up, the cessation and some pulsating flows of a Bingham plastic between two coaxial cylinders. A new model based on the error function is proposed to regularize the constitutive equation.

2. CONSTITUTIVE EQUATIONS

Being $\mathbf{v}$, $\mathbf{T}$ and $\dot{\boldsymbol{\gamma}}$ the velocity vector, the stress tensor and the rate of strain tensor, the constitutive equation of a Bingham fluid is

$$\begin{cases} \dot{\overline{\boldsymbol{\gamma}}} = 0 & \tau \le \tau_0 \\ \mathbf{T} = \left(\frac{\tau_0}{\dot{\overline{\gamma}}} + \mu \right) \dot{\overline{\boldsymbol{\gamma}}} & \tau \ge \tau_0 \end{cases} \tag{1}$$

where τ_0 is the yield stress and μ is the viscosity of the fluid. To avoid the singularity in the constitutive equation, it is possible to substitute the rheological law (1) with a continuous function. In 1987 Papanastasiou suggested the equation

$$\mathbf{T} = \left[\frac{\tau_0 \left[1 - \exp\left(-m\dot{\bar{\gamma}} \right) \right]}{\dot{\bar{\gamma}}} + \mu \right] \dot{\boldsymbol{\gamma}} \tag{2}$$

The authors propose the following relation which is continuous and infinitely derivable everywhere

$$\mathbf{T} = \left[\frac{\tau_0}{\dot{\bar{\gamma}}} \operatorname{erf}\left(k\dot{\bar{\gamma}} \right) + \mu \right] \dot{\boldsymbol{\gamma}} \tag{3}$$

where, as usual,

$$\operatorname{erf}(x) = \frac{2}{\sqrt{\pi}} \int_0^x e^{-t^2} dt \tag{4}$$

is the error function.

3. AXIAL FLOW IN A CONCENTRIC ANNULUS

3.1. Steady flow

The geometry is shown in Fig. 1. The flow is one-dimensional and the momentum equation is:

$$-\frac{\partial p}{\partial x} + \frac{1}{r}\frac{\partial (r\tau)}{\partial r} = \rho \frac{\partial u}{\partial t} \tag{5}$$

where x is the direction of the motion, r the radial coordinate, p the pressure, τ the shear stress, u the velocity, ρ the fluid density and t the time. Eq. (1) becomes

$$\begin{cases} \dfrac{\partial u}{\partial r} = 0 & \tau \le \tau_0 \\ \tau = \tau_0 \operatorname{sgn}\left(\dfrac{\partial u}{\partial r} \right) + \mu \dfrac{\partial u}{\partial r} & \tau \ge \tau_0 \end{cases} \tag{6}$$

where

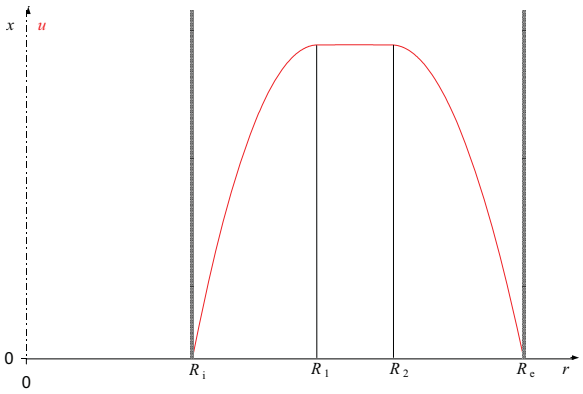

Fig. 1. Flow geometry

$$\operatorname{sgn}\left(\frac{\partial u}{\partial r}\right)=\begin{cases}-1 & \dfrac{\partial u}{\partial r}<0\\ 1 & \dfrac{\partial u}{\partial r}\geq 0\end{cases} \tag{7}$$

Putting $-\dfrac{\partial p}{\partial x}=\bar{P}$, the steady solution for a Bingham fluid is then

$$\begin{cases} u=u_1=\dfrac{1}{\mu}\left(-\dfrac{\bar{P}r^2}{4}+a\ln r-\tau_0 r+b_1\right) & R_i\leq r\leq R_1\\ u=u_2=\dfrac{1}{\mu}\left(-\dfrac{\bar{P}r^2}{4}+a\ln r+\tau_0 r+b_2\right) & R_2\leq r\leq R_e\\ u=u_1\left(R_1\right)=u_2\left(R_2\right) & R_1\leq r\leq R_2 \end{cases} \tag{8}$$

$R_1\leq r\leq R_2$ being the unyielded region, where the material behaves as a solid. The equation

$$a\ln\frac{R_e\left(-\tau_0+\sqrt{\tau_0^2+2a\bar{P}}\right)}{R_i\left(\tau_0+\sqrt{\tau_0^2+2a\bar{P}}\right)}+\tau_0\left(R_e+R_i-\frac{\sqrt{\tau_0^2+2a\bar{P}}}{\bar{P}}\right)-\frac{\bar{P}}{4}\left(R_e^2-R_i^2\right)=0 \tag{9}$$

allows to evaluate a and

$$b_1=\frac{\bar{P}R_i^2}{4}-a\ln R_i+\tau_0 R_i \tag{10}$$

$$b_2 = \frac{\overline{P} R_i^2}{4} - a \ln R_i - \tau_0 R_i \tag{11}$$

$$R_1 = \frac{-\tau_0 + \sqrt{\tau_0^2 + 2a\overline{P}}}{\overline{P}} \tag{12}$$

$$R_2 = \frac{\tau_0 + \sqrt{\tau_0^2 + 2a\overline{P}}}{\overline{P}} \tag{13}$$

the amplitude of the plug is then

$$R_2 - R_1 = \frac{2\tau_0}{\overline{P}} \tag{14}$$

The rate of flow Q, which allows to calculate the mean velocity V, is

$$Q = \int_{R_i}^{R_1} 2\pi r u_1 dr + \pi \left(R_2^2 - R_1^2 \right) u_1 + \int_{R_2}^{R_e} 2\pi r u_2 dr \tag{15}$$

Using the hydraulic radius $R = \dfrac{\pi \left(R_2^2 - R_1^2 \right)}{2\pi \left(R_1 + R_2 \right)} = \dfrac{R_2 - R_1}{2}$ as reference length, eq. (8) and (15) give

$$\begin{aligned} V = \frac{R^2 \overline{P}}{\mu \left(\eta_e^2 - \eta_i^2 \right)} \Bigg\{ & c \left(\eta_2^2 \eta_e^2 \ln \frac{\eta_1 \eta_e}{\eta_2 \eta_i} - \frac{\eta_e^4}{2} + \frac{\eta_2^2 \eta_e^2}{2} + \eta_i^2 \eta_e^2 - \frac{\eta_1^2 \eta_e^2}{2} \right) + \\ & + \frac{\eta_e^4}{8} - \frac{\eta_i^4}{8} + \frac{1}{8} \left(\eta_2^2 - \eta_1^2 \right)^2 - \frac{1}{4} \eta_2^2 \left(\eta_e^2 - \eta_i^2 \right) + \frac{1}{2} \left(\eta_2 - \eta_1 \right) \cdot \\ & \cdot \left(\frac{\eta_1^3}{3} - \frac{\eta_e^3}{3} - \frac{\eta_i^3}{3} - \eta_1 \eta_2^2 - \frac{2}{3} \eta_2^3 + \eta_2 \eta_i \eta_e + \eta_2^2 \eta_e \right) \Bigg\} \end{aligned} \tag{16}$$

where $\eta_e = R_e / R$, $\eta_i = R_i / R$, $\eta_1 = R_1 / R$, $\eta_2 = R_2 / R$ and $c = \dfrac{a}{R_e^2 \overline{P}}$

3.2. Unsteady flow

Introducing the following dimensionless quantities: $\xi = x / R$, $\eta = r / R$, $v = u / V$, $\theta = \tau R / \mu V$, $\theta_0 = \tau_0 R / \mu V = Bn$, $P = \overline{P} R^2 / \mu V$, $K = kV / R$, $T = t\mu / \rho R^2$, eq. (5) becomes:

$$P + \frac{1}{\eta}\frac{\partial(\eta\theta)}{\partial\eta} = \frac{\partial v}{\partial T} \tag{17}$$

The constitutive equation

$$\theta = Bn\,\mathrm{erf}\left(K\frac{\partial v}{\partial\eta}\right) + \frac{\partial v}{\partial\eta} \tag{18}$$

is plotted in Fig. 2.

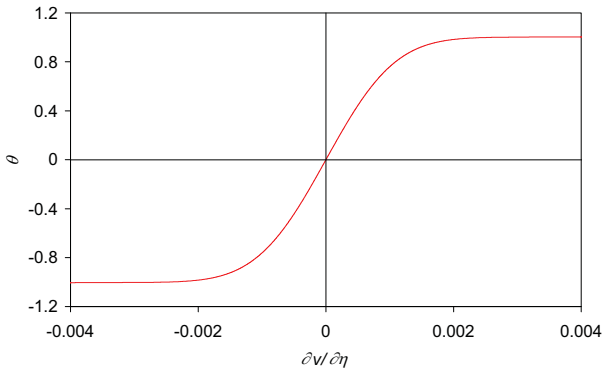

Fig. 2. Regularized constitutive equation

Substituting (1) in (17)

$$P + \left[\frac{2KBn}{\sqrt{\pi}}\exp\left(-\left(K\frac{\partial v}{\partial\eta}\right)^2\right) + 1\right]\frac{\partial^2 v}{\partial\eta^2} + \frac{1}{\eta}\left[\frac{\partial v}{\partial\eta} + Bn\,\mathrm{erf}\left(K\frac{\partial v}{\partial\eta}\right)\right] = \frac{\partial v}{\partial T} \tag{19}$$

For a coaxial pipe of dimensionless internal radius η_i and external radius η_e, the boundary conditions are:

$$v(\eta_i, T) = v(\eta_e, T) = 0 \qquad \forall T \tag{20}$$

Moreover

$$\left.\frac{\partial v}{\partial\eta}\right|_{\eta_1} = \left.\frac{\partial v}{\partial\eta}\right|_{\eta_2} = 0 \qquad v(\eta_1) = v(\eta_2) \tag{21}$$

3.2.1. Start-up flow

A suddenly positive pressure gradient $P = P_0$ is applied to the fluid at rest. P_0 gives rise to a unit non-dimensional mean velocity in steady state and must be greater than $2Bn$ in order for the fluid to move. The initial condition for eq. (19) is

$$v(\eta, T) = 0 \qquad \eta_i \le \eta \le \eta_e \quad T < 0 \tag{22}$$

3.2.2 Cessation of flow

The constant pressure gradient P_0 applied to the fluid in steady flow is suddenly cancelled.

Conditions at $T = 0$ are

$$\begin{cases} v = v_1 = -\dfrac{P_0\eta^2}{4} + A\ln\eta R - \eta Bn + B_1 & \eta_i \le \eta \le \eta_1 \\ v = v_2 = -\dfrac{P_0\eta^2}{4} + A\ln\eta R + \eta Bn + B_2 & \eta_2 \le \eta \le \eta_e \\ v = v_1(\eta_1) = v_2(\eta_2) & \eta_1 \le \eta \le \eta_2 \end{cases} \tag{23}$$

where, referring to eqs. (9)-(11), $A = \dfrac{a}{\mu V}$, $B_1 = \dfrac{b_1}{\mu V}$ and $B_2 = \dfrac{b_2}{\mu V}$

3.2.3 Pulsatile flows

Two different pressure wave are imposed to a fluid at rest

a) rectangular wave

$$P = P_0 \sum_{n=0}^{\infty} \left[\mathrm{H}\left(T - n(T_1 + T_2)\right) - \mathrm{H}\left(T - n(T_1 + T_2) - T_1\right) \right] \tag{24}$$

where $\mathrm{H}(T)$ is the unit step function; in a period $T_0 = T_1 + T_2$ the pressure gradient P is equal to P_0 for the first time interval T_1 and $P = 0$ for the second one T_2.

b) sinusoidal wave superimposed to a constant pressure gradient P_0:

$$P = P_0\left(1 + \varepsilon \sin 2\pi f T\right) \tag{25}$$

where f is the frequency.

4. NUMERICAL RESULTS

The numerical calculations have been carried out for coaxial pipes with $\eta_i = 8$ and $\eta_e = 10$: the annulus width is thus 20% of the radius of the external pipe; the dependence of the unyielded core extension $\eta_2 - \eta_1$ on the Bingham number in steady state is plotted in Fig. 3.

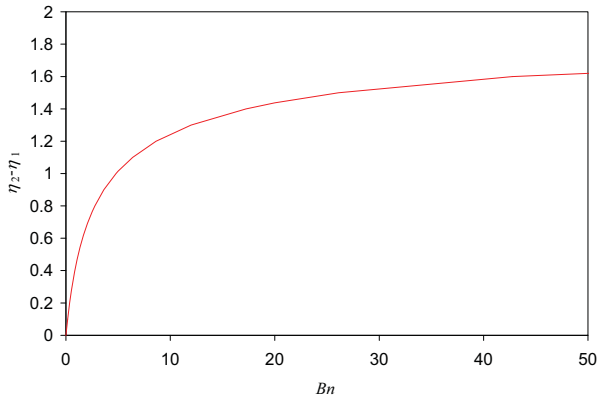

Fig. 3. Solid plug amplitude versus Bingham number

Eq. (19) with boundary conditions (20), (21) and the appropriate initial conditions is solved using an implicit finite difference method. The numerical procedure has been first validated for a Newtonian fluid, for which the analytical results are well known.

Numerical experiments indicated that the maximum value for parameter K in order to obtain valid results can be estimated as $K = 5000\dfrac{\eta_2 - \eta_1}{Bn}$. If K exceeds this value, the numerical procedure can exhibit instabilities. An uniform spatial grid of 1000 points has been adopted, using a time step equal to $4 \cdot 10^{-6}$. Smaller time steps give the same results, whereas greater ones can generate instabilities. The difference between the steady-state velocity profile obtained with the numerical solution and the theoretical one for a true Bingham fluid is less than 1%.

a) Start-up

Fig. 4 illustrates the numerical steady velocity profile for Bingham fluids, with $Bn = 1, 2, 3, 10$ and for a Newtonian one, which can be considered as a Bingham fluid with $Bn = 0$. Fig. 5 shows the development of the plug velocity versus time for the same values of Bn.

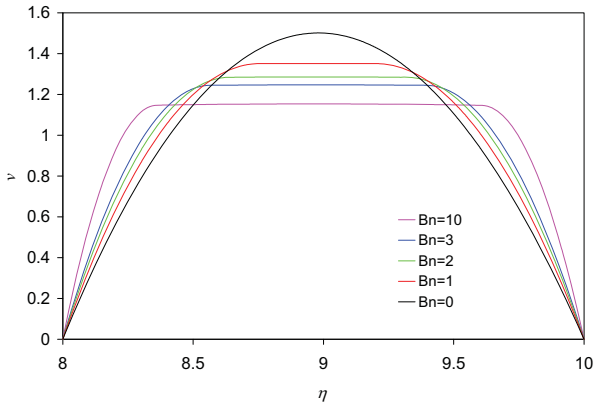

Fig. 4. Steady velocity profiles

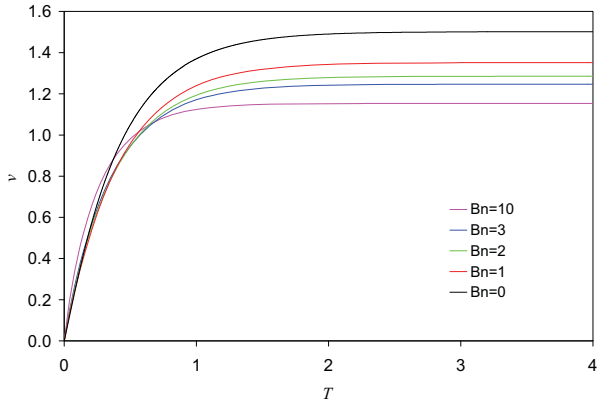

Fig. 5. Start-up: solid plug velocity versus time

b) Cessation of flow

Unlike Newtonian fluids and generally any fluid without yield stress which need an infinite stopping time, Bingham fluids require a finite time T_s to reduce to zero the velocity. Glowinski [5] [6] and Huilgol et al. [7] gave a theoretical upper bound for the stopping time for Poiseuille and plane flow. Fig 6 shows the rate of flow as function of time at different Bingham numbers. As expected, the rate of flow decreases the more rapidly the greater Bn is. Fig 7 shows the time needed to reduce the rate of flow to 10^{-3} and 10^{-5} respectively, as function of Bn: the difference between the two obtained values of time becomes appreciable only if $Bn > 10$. The time required to reduce the rate of flow to 10^{-5} can be considered as the stopping time.

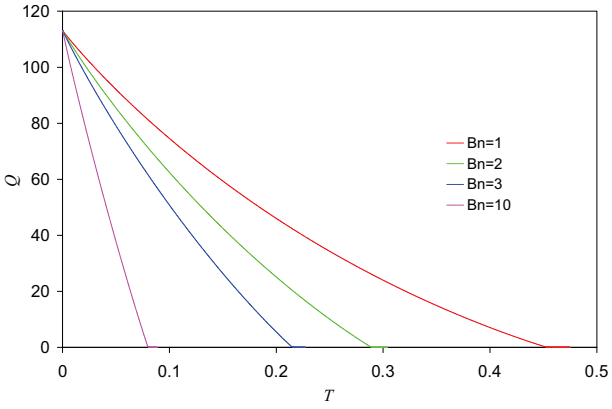

Fig. 6. Cessation of flow: discharge as a function of time

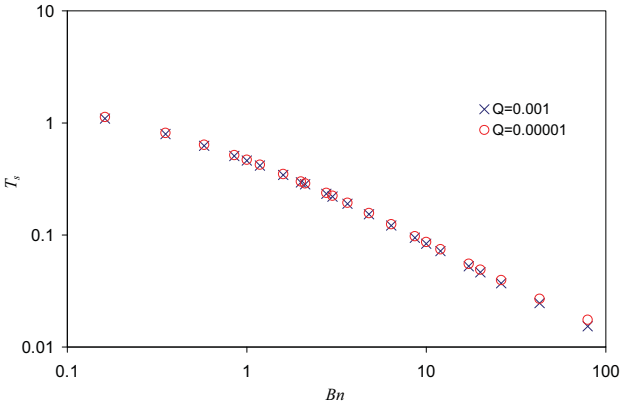

Fig. 7. Cessation of flow: stopping time T_s versus Bingham number

c) Pulsatile flows

For a rectangular wave, Fig 8 illustrates the core velocity versus time for some values of Bn; referring to eq. (24) $T_1 = 2$ and $T_2 = T_1/10$. For $Bn = 10$ the fluid completely stops for a time length about equal to $T_2/2$.

For a sinusoidal wave like eq. (25), putting $Bn = 5$, Figs 9-10 show the time development of plug velocity for some values of ε and frequency $f = 0.05$ and $f = 0.5$ respectively. For $f = 0.05$ and $\varepsilon = 0.5$ the movement stops for a time length of about 15% of the period. Calling v_s, $v_{\max}$, $v_{\min}$ the steady, the maximum and the minimum plug velocity respectively, $v_{\max} - v_s$ is always greater than

$v_s - v_{\min}$, for all values of ε. The quantity $\delta = \left[\left(v_{\max} - v_s\right) - \left(v_s - v_{\min}\right)\right] / v_s$ can be considered as an index of the asymmetry of the velocity with respect to the steady value. Fig. 11 shows δ versus frequency at different ε. Being always $\delta > 0$ it is easy to deduce that the mean rate of flow in a period increases owing to the non linearity of the constitutive equation.

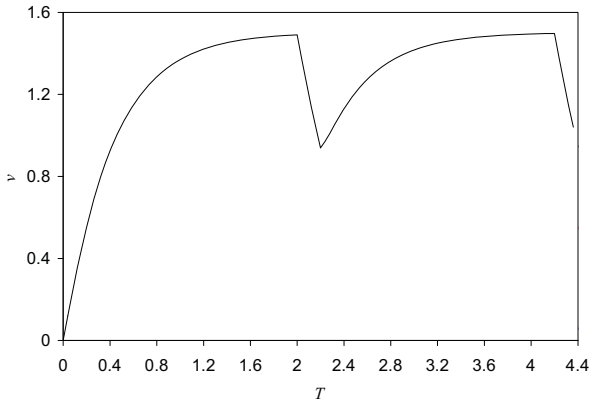

Fig. 8. Rectangular wave: plug velocity versus time

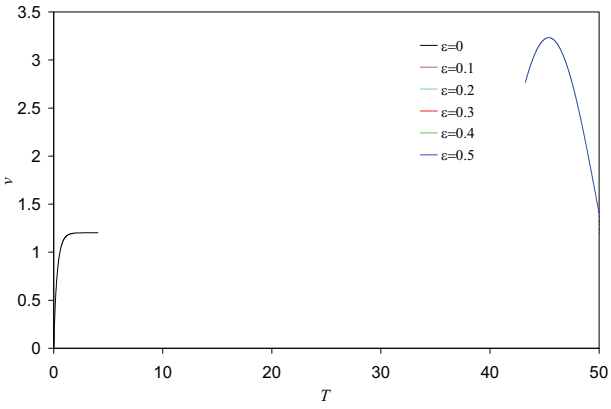

Fig. 9. Sinusoidal wave: plug velocity versus time; $Bn = 5$, $f = 0.05$

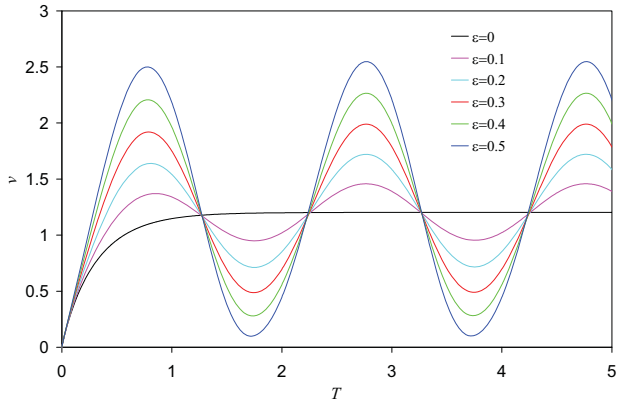

Fig. 10. Sinusoidal wave: plug velocity versus time; $Bn = 5$, $f = 0.5$

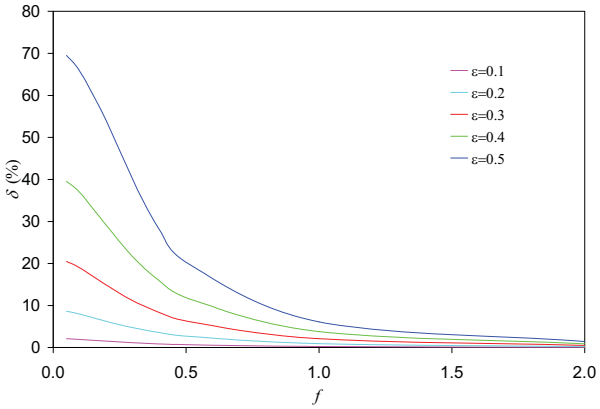

Fig. 11. Sinusoidal wave: δ versus frequency

5. CONCLUSIONS

Unsteady motion of a Bingham fluid in coaxial pipes has been examined numerically. The momentum equation has been written using a regularized constitutive equation proposed by the authors, based on the error function. The solution has been carried out via an implicit finite difference method; numerical experiments indicated that the maximum value for the parameter of the rheological model in order to obtain valid results is $K = 5000\dfrac{\eta_2 - \eta_1}{Bn}$. If K exceeds this value,

the numerical procedure can exhibit instabilities. An uniform spatial grid of 1000 points has been adopted, using a time step equal to $4 \cdot 10^{-6}$. Four different motions have been considered: start-up, cessation and two pulsatile flows. The analysis of start-up flow has been useful to validate the numerical procedure comparing the obtained asymptotic solution to the well known analytical one. In the cessation the rate of flow decreases the more rapidly the greater Bn is: the stopping time which is infinite for Newtonian fluids becomes finite for Bingham fluids and decreases for increasing Bn. In pulsatile flow, applying a rectangular pressure gradient the flow can completely stop for some time if the Bingham number is sufficiently great. The superposition of a sinusoidal wave to the steady pressure gradient gives rise to an increment of the mean discharge in a period, owing to the non linearity of the constitutive equation.

References

1. Glowinski, R., *Numerical methods for nonlinear variational problems*, Springer-Verlag, New York, 1984.
2. Papanastasiou, T.C., Flows of materials with yield*, J. Rheol.* 31 (5), 385-404, 1987.
3. Frigaard, I.A., Nouar, C., On the usage of viscosity regularisation methods for visco-plastic fluid flow computation, *J. Non-Newtonian Fluid Mech.* 127, 1-26, 2005.
4. Glowinski, R., Sur l'écoulement d'un fluide de Bingham dans une conduite cylindrique, *J. de Méc*. 13, 601-621, 1974.
5. Huilgol, R.R., Mena, B., Piau, J.M., Finite stopping time problems and rheometry of Bingham fluids, *J. Non-Newtonian Fluid Mech*. 102, 97-107, 2002.
6. Chatzimina, M., Georgiou, G.C., Argyropaidas, I., Mitsoulis, E., Huilgol, R.R., Cessation of Couette and Poiseuille flows of a Bingham plastic and finite stopping times, *J. Non-Newtonian Fluid Mech.* 129, 117-127, 2005.
7. Duggins, R. K., The commencement of flow of a Bingham plastic fluid, *Chem. Eng. Sci.*, 27, 1991-1996, 1972.
8. Papanastasiou, T.C., Boudouvis A. G.,Flows of viscoplastic materials: models and computation, *Comp. and Struct.,* 64, (1-4), 677-694, 1977.
9. Hammad, K. J., Unsteady pipe flows of a viscoplastic non-Newtonian fluid: effects of pressure gradient waveform, *Proc. ASME FED,* 247,197-204, 1998.
10. Daprà, I., Scarpi, G, Start-up flow of a Bingham fluid in a pipe, *Meccanica,* 40, 49-63, 2005.

"Computational Civil Engineering 2007", International Symposium
Iaşi, România, May 25, 2007

Formation of lime efflorescence on concrete and concrete products

Tomáš Fojtík[1], Jiří Brožovský[2]
[1,2] *Faculty of Civil Engineering, Brno University of Technology, Brno, 602 00, Czech Republic*

Summary

Many specialists from all over the world occupied themselves with the problem of efflorescence formation on concrete and on concrete products. This problem is nearly as old as the concrete itself. The fact that to this very day, the problems of efflorescence formation course and of formed efflorescence elimination is not yet clearly defined up to now, shows how extensive and difficult is this task. This paper concerns the problems of efflorescence formation on concrete and concrete products depending on some conditions to which the concrete is exposed.

KEY WORDS: concrete, concrete product, lime efflorescence, primary, secondary

1. INTRODUCTION

Is the efflorescence on the surface of concrete the demonstration of its degradation? This form of degradation is in contrast with the sulphate corrosion or with other forms of corrosion not dangerous in light of structural properties and the efflorescence has not major effect on the durability of concrete structures. Nevertheless the efflorescence which occurs on the surface of concrete products mostly in the form of white "spots" or layers is an esthetic defect which can significantly influence the quality of concrete soffit products.

The efflorescence consists from inorganic salts or hydroxides which are leached out from concrete (from the cement stone or from the aggregate). The hydrous solution of these salts is transported by the system of capillary tubes in concrete. It evaporates on the surface of the concrete and reacts with atmospheric CO_2 or SO_2 (produced in a high degree by the industrial production). The efflorescence is formed largely in the form of salts (chiefly as sodium, potassium and mainly as calcium sulphates or carbonates). The main component is as a rule $CaCO_3$.

The occurrence of efflorescence is typical on the surface of concrete alternately soaked and dried or exposed to the action of pressure water. Less frequent factors of efflorescence formation on concrete surface are:

- The proportion of individual concrete components and their total concentration in the bearing hydrous solution,

- The relative air humidity in the surrounding atmosphere (φ [%]). It depends on the solubility degree of individual components and on RH whether the given salts crystallize in the pores or on the surface of the material. The crystallization in pores is one of the building materials significant destruction factors [1, 2, 3].

2. LIME EFFLORESCENCE

It is formed by calcium carbonate ($CaCO_3$) which is formed by the action of atmospheric carbon dioxide (CO_2) in humid medium on calcium hydroxide ($Ca[OH]_2$) liberated during maturing (hydration) of concrete [3].

2.1. Primary lime efflorescence

The primary lime efflorescence is formed only for a limited period from the concrete or concrete products production by the reaction of calcium hydroxide (this is the component of both, the hardened concrete and the hardened lime mortar) with the atmospheric CO_2 under moisture, in the surface layers of concrete products.

2.2. Secondary lime efflorescence

The secondary lime efflorescence is formed during the whole service life of concrete by reaction of the calcium hydroxide leached out on the surface of products with the atmospheric carbon dioxide under presence of moisture.

By the effect of atmospheric CO_2 the in water insoluble calcium carbonate is transformed after a longer period in the in water soluble calcium hydrogen carbonate $Ca[HCO_3]_2$.

The secondary efflorescence does not in contrast to the primary efflorescence form only lighter spots on the surface of concrete but it constitutes on the surface crystalline substance, which dusts off as removable dust.

Consequently, after this transformation of the calcium carbonate the lime efflorescence disappears. The time of calcium carbonate conversion into calcium hydrogen carbonate is approximately 1,5 till 3 years (in dependence on internal and outer conditions, first of all on climatic effects) [2, 3].

3. MECHANISMS INFLUENCING FORMATION OF LIME EFFLUESCENCE

The frequency of lime efflorescence formation on concrete depends on many variables. These are first of all the water content (w and φ) and the content of the atmospheric CO_2 [3].

It is necessary to mention that no less than from 75 % the formation of all efflorescence on concrete is caused by the "lack of technological discipline" in the production and the remaining 25 % is the result of the concrete components chemism.

3.1. The main conditions supporting the formation of lime efflorescence on concrete:

- The high w/c ratio,
- Temperature,
- Porosity,
- Improper admixtures,
- Mixing and compacting conditions,
- Additives,
- Water tightness,
- Treatment conditions,
- Capillarity,
- Content of free lime,
- Proportion of cement and aggregate in concrete,
- CO_2 content in the atmosphere,
- Time of products storing,
- Type of construction,
- The storing of products [1,2,3].

4. MEASURES ELIMINATING THE FORMATION OF LIME EFFLORESCENCE IN THE PRODUCTION

4.1. Measures and methods limiting the efflorescence formation used in production

- Elimination or limiting of causes mentioned in chapter 3.1,
- Utilization of additives which contribute to following possible effects:
  - Interruption of capillary tubes and on this way the undesirable mass transfer,

- Increase of water tightness, waterproofing of capillary pores,
- Chemical fixing of lime to insoluble product [3].

4.2. Means and methods removing the already formed efflorescence

As a rule the lime efflorescence can be removed sufficiently mechanically, for instance by sweeping it up. Also special means can be used. The concentrated preparation is diluted with water and after the concrete surface was saturated with water and the superfluous water was removed, the diluted preparation is applied on the surface of the product by means of a brush or sponge. After the efflorescence is dissolved the surface is washed down with water.

If it is not possible to remove the lime efflorescence by one of readily available products, it is possible to apply a special procedure. We can use for instance the 3% solution of hydrochloric acid, phosphoric acid or the solution of some organic acid (for instance acetic acid or oxalic acid etc.) It is necessary to take into account that in the case of lime efflorescence dissolution with acids the shade of concrete products colour and the structure of the surface can change, because the acids attack and disintegrate together with the efflorescence also the cement stone [1, 3].

5. EXPERIMENTAL MEASUREMENTS

5.1. Division of experimental works

Considering the fact, that the formation of efflorescence is influenced by quite a number of factors, the most important effects were selected for testing, namely the general effect of the surroundings and of the concrete composition.

5.1.1. Determination of efflorescence formation conditions

The aim was the laboratory testing of concrete samples of concrete with exactly defined variant composition, exposed to different types of surroundings.

5.1.2. Determination of concrete composition on the formation of the efflorescence

Test pieces with exactly defined proportion of concrete components were prepared in this phase. The test pieces were tested consequently for the dependence of lime efflorescence formation on the type of used concrete, on the method of concrete compacting during the production of these test pieces, on the proportion of cement and aggregate and on the value of w/c ratio.

5.1.3. Determination of efflorescence formation conditions in dependence on the composition of concrete

The aim was to make test pieces with the constant w/c ratio and with variable proportion between cement and aggregate and to expose it to different types of surroundings.

5.2. Methods of testing

5.2.1. Determination of conditions for efflorescence formation

The made concrete prisms were stored in following surroundings:

- Water bath (t = 20 ± 2°C),
- Laboratory surroundings (t = 20 ± 2°C, RH = 40 – 60 %),
- Air tight chamber with 98 % of CO_2 concentration,
- Hot air drier (t = 50°C),

The influence of these surroundings was monitored on the formation of efflorescence. The extent of concrete surface coverage with efflorescence was determined and evaluated by optical microscopy and its mineralogical composition was detected by means of X-ray diffraction analysis.

5.2.2. Determination of the concrete composition influence on the formation of efflorescence

The made test pieces were exposed to surroundings in which the most efflorescence was formed during the preceding phase and the effect of the concrete composition was described on the efflorescence formation at varying:

- Kind of cement (locality),
- Way of concrete compacting,
- Proportion of cement and aggregate,
- Water-cement ratio.

5.2.3. Determination of efflorescence formation conditions in dependence on the concrete composition

The prepared concrete prisms with the cement and aggregate proportion 1:5 or 1:6 were placed into following surroundings:

- Climatic chamber – for the period of 24 hours, temperature 28°C and RH 95 %,
- Normal atmospheric surroundings (outdoor) – for the period of 24 hours,
- Drier – for the period of 6 hours, temperature 60°C.

The effect of climatic conditions on the formation of efflorescence was subsequently monitored on these test pieces and the results were compared with results obtained in the phase I (article 5.2.1.)

5.3. Results of individual phases of work

5.3.1. Determination of efflorescence formation conditions

All efflorescence which arises on the test pieces during this work is so-called primary efflorescence. This is formed only during the limited period from the concrete or concrete products production by the reaction of calcium hydroxide with atmospheric CO_2 in humidity on surface layers of concrete products.

The secondary efflorescence is formed by the effect of atmospheric CO_2 and it is transferred after longer period from the in water insoluble $CaCO_3$ into in water soluble calcium hydrogen carbonate $Ca\,[HCO_3]_2$. This process lasts longer time.

The test pieces made from the cement CEM I 42,5 R from the cement plant Mokrá, and from the aggregate Bratčice with constant proportion of cement and aggregate 1:3 and with the water-cement ratio w = 0.5 with vibration and by manual stamping. The test pieces were exposed for 28 days to individual surroundings and we can state that:

- The formation of efflorescence does not take place in surroundings with fluctuating pressure and relative air humidity with the temperature 50°C and higher,
- In laboratory surroundings at t = 20 ± 2°C, constant atmospheric pressure and in relative air humidity varying from 40 to 60% the efflorescence is admittedly formed but not so quickly as in the water medium with the temperature t = 20 ± 2°C. On the other hand the efflorescence which was already on the surface of the test pieces before they were placed into this surroundings increased moderately their volume,
- In the chamber with constant atmospheric pressure and the temperature t=20±2°C with the content of 98% of CO_2 is the efflorescence formed only in small quantity, but when we have put into the chamber a sample which already contained on the surface efflorescence the efflorescence quantity increased (volumetrically, no the surface area),
- Unambiguously the most favorable conditions for the formation of efflorescence is the aqueous medium with the temperature of t = 20 ± 2°C. In this medium even after 14 days of storing always new efflorescence was formed while in other media the growth of it was stagnating,
- The most important factor influencing the formation of efflorescence is besides the temperature of surroundings the value of the relative humidity (RH) and the rate of air circulation,
- Quick overlapping of the surface with efflorescence takes place after placing the prisms in the chamber with elevated concentration of CO_2 but in a definite moment the formation of new efflorescence stops. The elevated CO_2 concentration in the atmosphere results in the closing of pores on the surface by the formed efflorescence and in the stagnation of its further formation,

- We observed the rapid increase of efflorescence after placing the concrete into water bath at the temperature t = 20 ± 2°C for the period of at least 28 days,
- When we have taken out the samples from the water storing after 28 days, have removed the efflorescence and placed the samples once more into this surroundings, the growth of efflorescence did not start again.

5.3.2. Determination of the concrete composition influence on the formation of efflorescence

- We can state that the intensity of efflorescence formation is not direct proportional to the increasing value of water ratio, i.e. the value of water ratio doesn´t affect the size of efflorescence formation,
- We can further state that with the increasing proportion of cement and aggregate the intensity of efflorescence growth increases,
- The type of cement has an effect on the formation of efflorescence. The intensity of concrete surface coating with efflorescence was in our case with both types of cements nearly identical but in some cases we observed still a higher intensity of efflorescence formation in the case of concrete made from cement CEM I 42.5 R from the cement plant Mokrá. The contributing case can be the higher content of CaO in the cement CEM I 42.5 R Mokrá in comparison with the cement CEM I 42.5 R from the cement plant Hranice,
- The way of compacting in the concrete manufacture can have a significant influence on the formation of efflorescence. The efflorescence during water storage was formed practically on all samples, naturally the concrete compacted by vibro-pressing was much more resistant against the formation of efflorescence in comparison with concrete made only by ramming.

5.3.3. Determination of efflorescence formation conditions in dependence on the concrete composition

The test was carried out in laboratory conditions to precise the hypothesis concerning the efflorescence formation in hot air driers which is connected with the velocity of surface desiccation and with the water vapour diffusion. Two sets of prisms with different ratio of cement and aggregate were placed into the hot air drier, in the damping box and in the laboratory surroundings.

- In the phase I more efflorescence was formed on the concrete surface in the case of the cement : aggregate proportion 1,5 contrary to the proportion 1:6,
- The main effort was of course to describe the processes in the hot air drier during the period of 24 hours since the placing of samples. The rapid desiccation of concrete during the first 8 hours caused intensive formation of efflorescence. Of course the surface of concrete is after 24 hours practically without efflorescence,
- The obtained efflorescence was submitted to X-ray diffraction analysis, which confirmed the similarity of efflorescence concerning the mineralogical

composition. In cements of CEM I 42.5 R type from both the cement plant Mokrá and the cement plant Hranice the prevailing mineral component in efflorecence is calcite.

6. CONCLUSION

We can state following the theoretical analyses and practical realized tests that the less favourable atmospheric conditions under which the formation of efflorescence takes place in a high degree are the temperatures 0 – 5°C in the morning hours of autumn months. The period of fresh concrete products storing has no effect on the quantity of efflorescence, it is rather the measure against their formation which can be easily realized in every manufacturing plant or during the production.

The first condition for the minimization of the lime efflorescence formation is the dosing of optimal batch water quantity for perfect hydration and for achieving of concrete high compactness with small rate of absorption. This can be achieved by the addition of adequate additives and admixtures.

It is further necessary to prevent during the hardening of concrete both its desiccation and the water condensation on its surface owing to the cold surrounding atmosphere. This can be achieved by the use of so-called maturing chambers during the hardening of concrete products.

The type of the used cement with different chemical and mineralogical compositions can affect the formation of possible lime efflorescence.

The tests which we have performed verified the influence of some variables on the possibility of lime efflorescence formation on concrete. It is necessary to remember that the efflorescence formation is influenced by a number of further factors which could not be included into this work.

The further development in this area should be directed towards the deeper understanding of the efflorescence formation reasons under the effect of further outer factors. This research should help to prevent or at least to minimize the formation of efflorescence on concrete and in this way to increase the esthetic value of concrete.

Acknowledgements

The work was supported by the MSM 0021630511 plan: Progressive Building Materials with Utilization of Secondary Raw Materials and their Impact on Structures Durability.

References

1. Matoušek, M., Drochytka, R.: *Atmospheric Corrosion of Concretes*, IKAS Praha, 1998, ISBN 80-902558-0-9.(in Czech)
2. Pytlík, P., Concrete Technology, Brno: Naše vojsko, 1994. ISBN 80-206-0434-0. (in Czech)
3. Kresse, P., Efflorescence-Mechanism of occurrence and possibilities of prevention, Research Centre of the company BAYER AG Krefeld-Uerdingen, published in the Journal: Betonwerk-Fertigteil-Technik (BFT).

"Computational Civil Engineering 2007", International Symposium
Iaşi, România, May 25, 2007

The use of computer means in representation of the ruled surfaces

Monica Gheorghiu and Mirela Chelcea
Descriptive Geometry, Engineering Graphics and Graphics Computer Programs Department, Technical University of Civil Engineering, Bucharest, Romania

Summary

Teaching the Descriptive Geometry by the means of the computer is a recent attempt to make the subjects more understandable and to facilitate the approach of the students to some difficult subjects. This work makes a connection between a 3D representation of some examples of this chapter and there orthogonal projections, the final target of the Descriptive Geometry using the possibility of animation provided by an adequate "software", for example the program "AutoCAD 3D".

KEYWORDS: ruled surfaces, Descriptive Geometry, orthogonal projections, paraboloid, cylindroid, helicoid, hyperboloid.

1. INTRODUCTION

Teaching Descriptive Geometry is, without any doubt, unless a first for the system of university Rumanian education, but a recent attempt to align itself with the last tendencies of education. A particular effort of those who teach is presumed in order to provide such a course of Descriptive Geometry, regarding the adaptation of the means of presenting the matters using an adequate "software", for example the program "AutoCAD 3D".This is why this work is a first step in attempting to build a system of teaching and of evaluation based on the computer.

The subject of this work belongs to the applicable part of this matter and, although it attracts the interest of the student, it is considered as having a high level of difficulty. The presentation in 3D of the ruled surfaces, axonometric, apply the intuition of onlooker and this is why provides a complete sight of the subject however complicate would be.

The successive transformation of that, in images 2D, meaning in orthogonal projections, can easily be done by using the Autocad 3D or other programs which makes possible to use animation 3D. This manner of presenting simultaneously the two methods to visualize can provide a certain easiness to discern the main orthogonal projections in a unit space and can lead to obtain the capacity to

represent in orthogonal projection on any plane of the objects however complicated they are.

The authors also consider that the 3D representation based on the computer of the various types of ruled surfaces, as well as the connection between these views of the examples suggested to be solved and their orthogonal projections could make this subject not only understandable but also more attractive. The elements, which compose certain surfaces, are proposed to be identified in the assembly and to be represented in the usual system of projections.

The following stages were established in the presentation of the subject, in order to fulfil the requests of the problem: the view of the final representation of the defined surface, the 3D representation of it, the turn around of the 3D view, the orthogonal projections due to this proceeding, the 3D and 2D view of the constituent elements and finally, the way to form the surface.

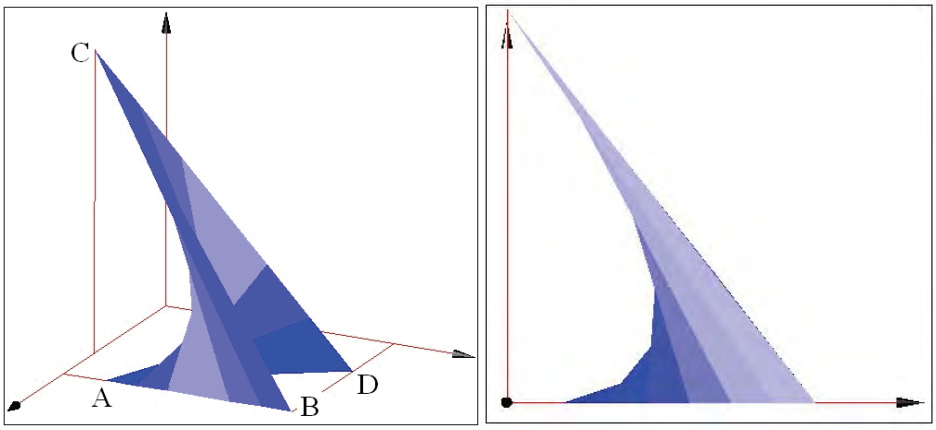

Figure 1. Paraboloid – axonometric representation and projection on the plane [W]

2. EXAMPLES

2.1. Paraboloid

2.1.1. Paraboloid. First example

The figured paraboloid could have the following parameters: first directix – line AB, second directrix – line CD, with A, B and D in [H] and C in [V]. AB is parallel to Oy, BD parallel to Ox (see Figure 1).

2.1.2. Paraboloid. Second example

The application could also require the representation of the symmetrical surface in relation with base plane (see Figure 2).

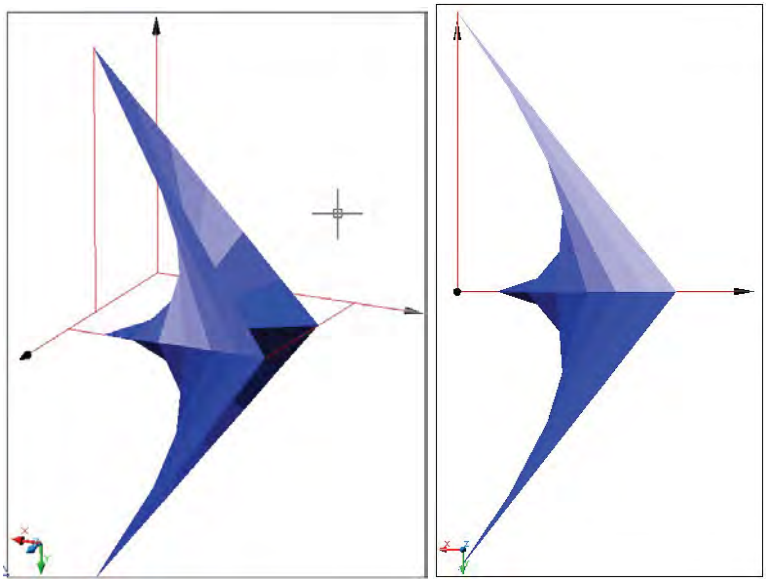

Figure 2. Paraboloid – axonometric representation and projection on the plane [W]

2.2. Conoid

2.2.1. Conoid. First example

This complex problem demands to draw the ruled surface with directrix I a semicircle with the centre the point M and radius 30mm, which belongs to the plane that makes a 60^0 angle to plane [H], and directrix II the segment ST, 20 mm long, on a line perpendicular to [W].

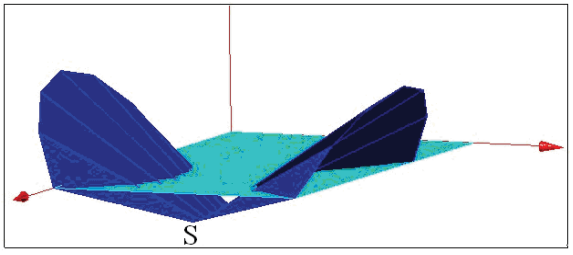

Figure 3. Conoid – axonometric representation

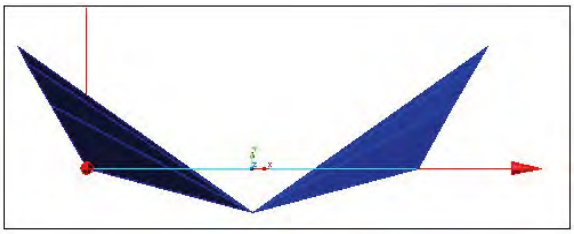

Figure 4. Conoid – projection on the plane [W]

The other request is to represent also the symmetrical surface to the plane that includes points s and T and is parallel to plane [V] and finally to solve the problem of intersection between the rolled surface and plane [H], the requirement could modify as follows: (see Figures 3 and 4).

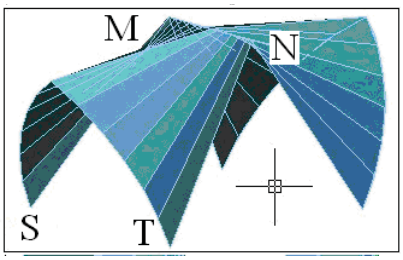

Figure 5. Cylindroid – axonometric representation

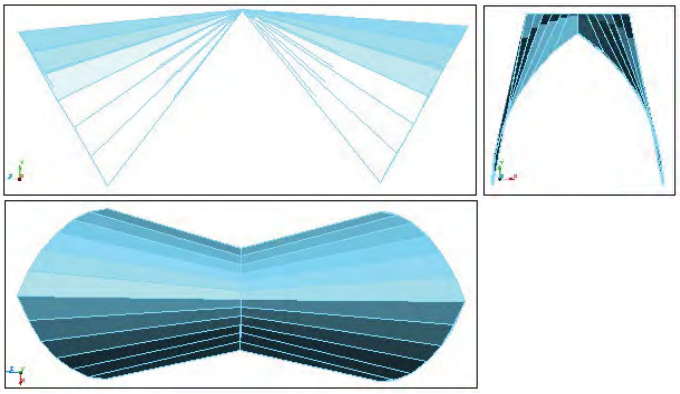

Figure 6. Cylindroid –projection on the plane [V], [W] and [H]

2.2.2. Conoid. Second example

The surface which is suggested to represent is formed by two symmetrical conoids. The first one has the first directrix in a plane inclined at an angle of de 60^0 to the horizontal, composed of 2 circle arcs with a 65 mm radius, passing through points

S and T in [H], positioned between [H] and their point of intersection, above [H] with S and T while directrix II segment MN, which belongs to a line which is perpendicular to [V].
The second conoid is the symmetrical of the first relative to [W] passing through M and N (see Figures 5 and 6).

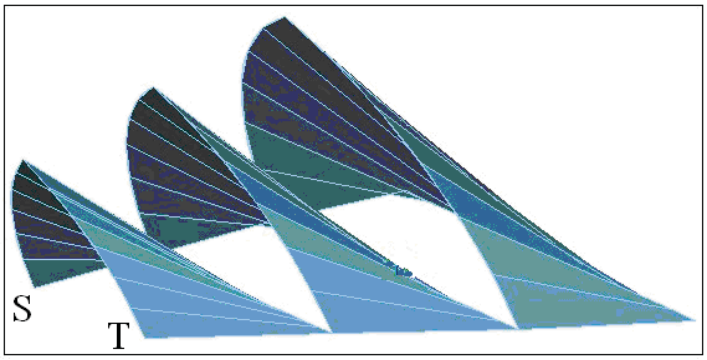

Figure 7. Cylindroid – axonometric representation

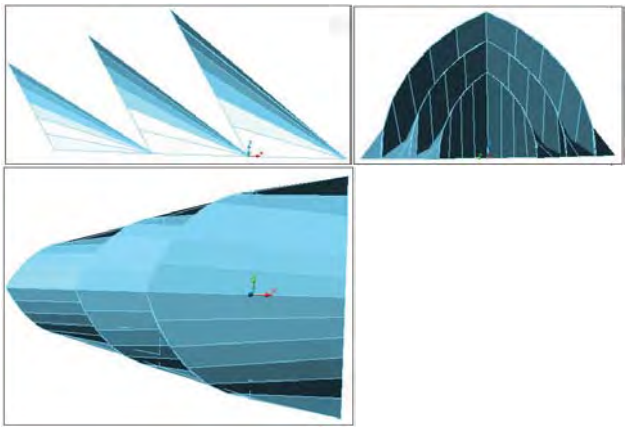

Figure 8. Cylindroid – projection on the plane [V], [W] and [H]

2.2.3. Conoid. Third example

The surface of this exemple is made by three units, from among the first conoid has the first directrix in a plane oriented at an angle of de 60^0 to the horizontal, composed of 2 circle arcs with a 65 mm radius, passing through points S and T in [H], while directrix II segment S1T1 from [H], (see Figure 7).

The second conoid has directrix I in a plane oriented at an angle of de 60^0 to the horizontal, composed of 2 circle arcs with a 80 mm radius, passing through points S1 and T1, positioned between [H] and their point of intersection, above [H] while directrix II segment S2T2 in [H].
The third conoid has directrix I in a plane oriented at an angle of de 60^0 to the horizontal, composed of 2 circle arcs with a 95 mm radius, passing through points S2 and T2, positioned between [H] and their point of intersection, above [H] while directrix II segment S3T3 in [H] (see Figure 8).

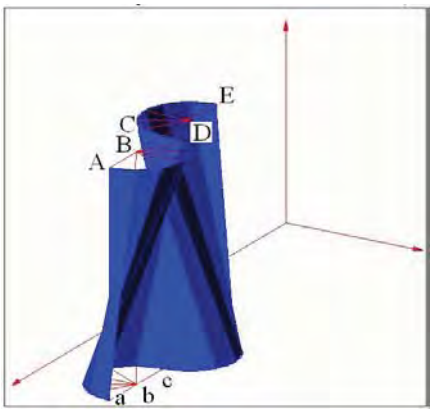

Figure 9. Proposed application. Cylindroid – axonometric representation

2.3 Cylindroid

2.3.1. Cylindroid. First example

The request of this problemis to make an axonometric representation of the cylindroid with directrix I – two semicircles with centers B and D respectively, in a plane parallel to [H], directrix II – two semicircles with centers b and d respectively, in plane [H].

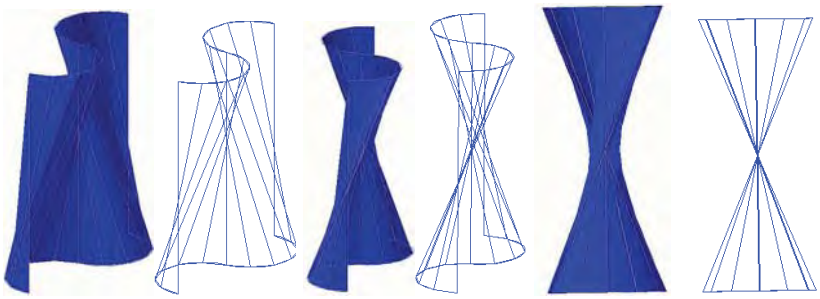

Figure 10. Cylindroid – the rotation of the surface until we see the projection to plane [W]

The semicircles with centers b and D are between plane [V] and a plane parallel to [V] determined by points A, E and a. The semicircles with centers B and d are on the other side of the plane determined by A, E and a, mentioned above (see Figures 9, 10, 11 and 12).

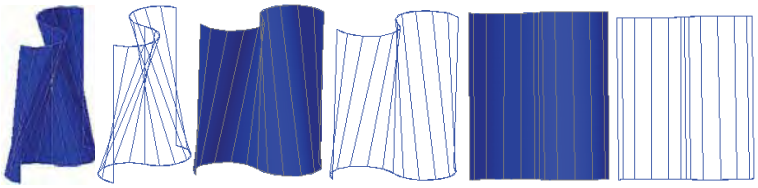

Figure 11. Cylindroid – the rotation of the surface until we see the projection to plane [V]

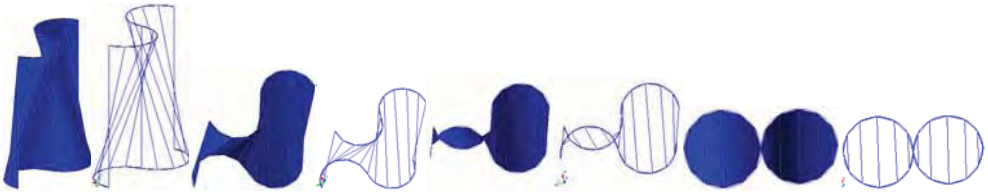

Figure 12. Cylindroid – the rotation of the surface until we see the projection to plane [H]

The problem may be extended by adding the request to repeat the obtained cylindroid surface several times, or by rotating the surface and so changing the data (see Figures 13 and 14).

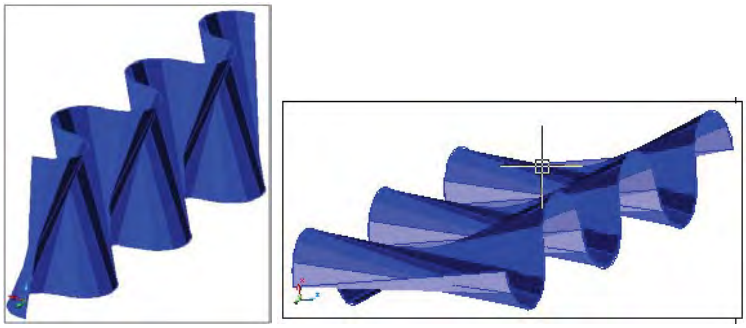

Figure 13. Cylindroid – axonometric representation

2.3.2. Cylindroid. Third example

It is required to draw the ruled surface that has both curves circle arcs with a radius of 30 and 50mm respectively, in a plane that makes a 60^0 angle to plane [H]. Point M is the middle of the segment representing the cord sub-stretched by both

directrixes. It is also required to represent the symmetrical surface to this one relative to the plane that includes point N and is parallel to plane [V] (see Figure 15).

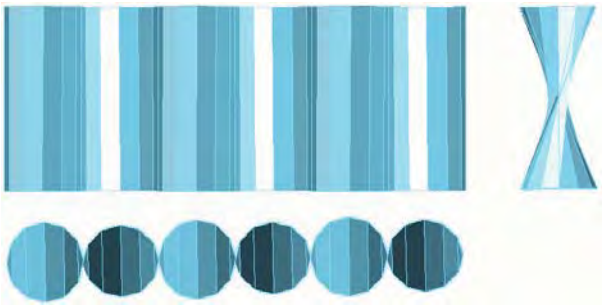

Figure 14. Cylindroid – projection on the plane [V], [W] and [H]

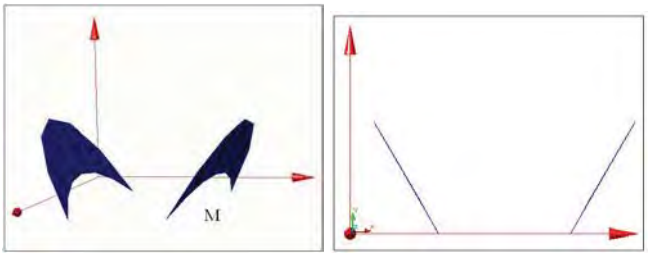

Figure 15. Cylindroid – axonometric representation and projection on the plane [W]

2.3.3. Cylindroid. Fourth example

The problem requires the representation of a ruled surface that has the following parameters: first directrix the segment ST, second directrix a circle arc with a radius of 225mm and the corresponding cord SR. It is also required to represent the surface that is symmetrical to it relative to the parallel plane [V] that includes points S and T (see Figure 16).

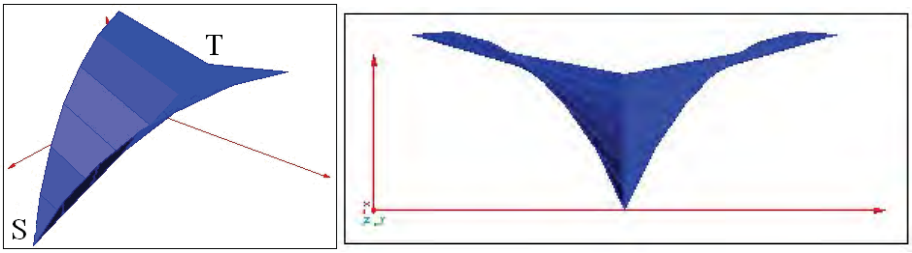

Figure 16. Cylindroid – axonometric representation and projection on the plane [W]

2.3.4. Cylindroid. Fifth example

The surface to be represent is a cylindroid that has directrix I is a circle arc on the semicircle with the radius 45 and the center S, in a plane parallel to [V], above [H], inscribed between its point of intersection with [H] and point R on the semicircle, directrix II is also a circle arc, in a plane perpendicular to [H], that makes with the plane of directrix I an angle of 150, derived from a semicircle with a radius of 70, above [H], that intersects directrix I in point R. Also draw this cylindroid's symmetrical relative to the plane of the first directrix (see Figures 17, 18, 19 and 20).

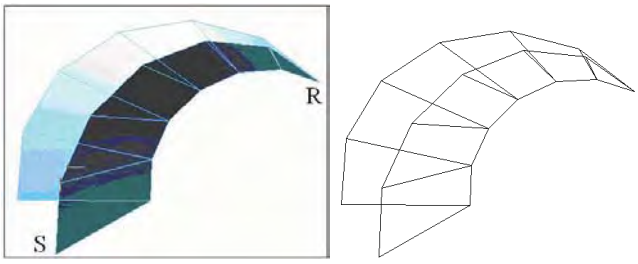

Figure 17. Cylindroid – axonometric representation

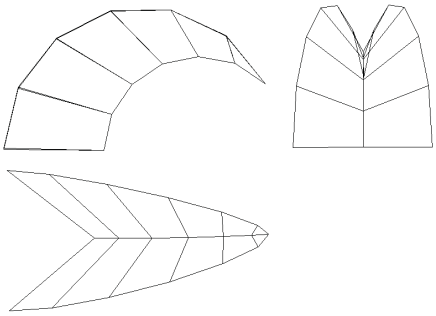

Figure 18. Cylindroid – projection on the plane [V], [W] and [H]

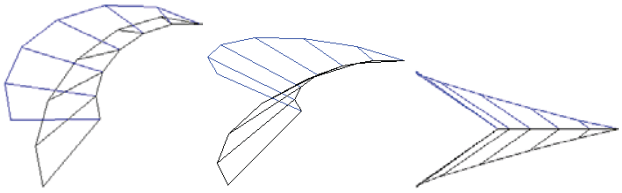

Figure 19. Cylindroid – the rotation of the surface until we see the projection to plane [H]

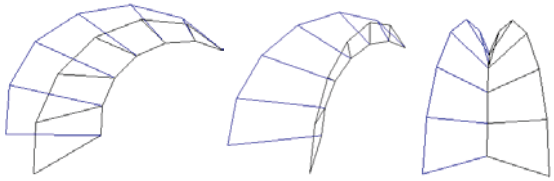

Figure 20. Cylindroid – the rotation of the surface until we see the projection to plane [W]

2.3.5. Cylindroid. Sixth example

The problem demands to represent a ruled surface with directrix I in a plane parallel to [W] determined by points S and T, made up of circle arc derived from a semicircle with a 20mm radius, centre S, with all points more distanced from [H] than from S and the tangents to this circle, symmetrical to the sS segment, starting from point T and T1 respectively, T's symmetrical relative to s. Directrix II has the same shape as directrix I, is parallel to it at a distance of 20 mm, in a plane parallel to [W], at a distance of 90 mm from it. Figure also the ruled surface symmetrical to this one relative to the plane of the second directrix. Figure also the ruled surface which is symmetrical to the one obtained up to now, relative to the plane of the last figured directrix (see Figure 21 and 22).

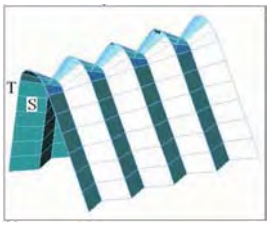

Figure 21. Cylindroid – axonometric representation

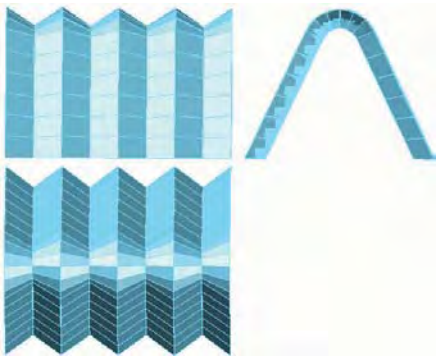

Figure 22. Cylindroid – projection on the plane [V], [W] and [H]

2.4 Helicoidal Surfaces

2.4.1. Helicoidal Surfaces. First example

The problem target is the axonometric representation of the group formed by 4 identical adjoining helicoidal surfaces (see Figures 23 and 24), with directrixes belonging to a cylindrical surface generated thus:

- surface I, directrix I starting from point A and directrix II from B,
- surface II, directrix I starting from point B and directrix II fromC,
- surface III, directrix I starting from point C and directrix II from D,
- surface IV, directrix I starting from point D and directrix II from A.

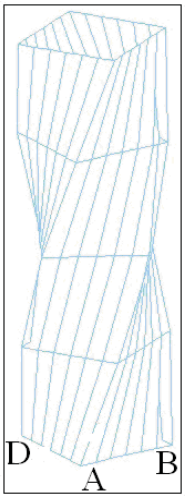

Figure 23. Helicoidal surfaces – axonometric representation and projection on plane [W]

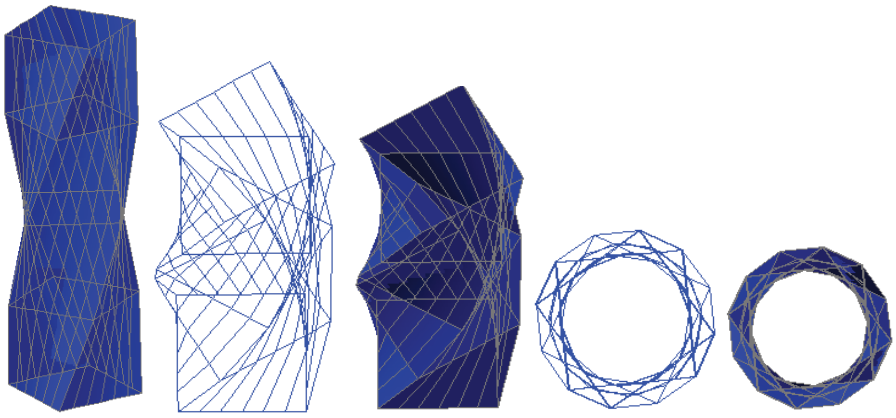

Figure 24. Helicoidal surfaces – axonometric representation and projection on plane [H]

The first rulings of each surface belong to plane [H] and make up a square ABCD with a side of 30 mm. The plane containing the second rulings for each surface is at a distance of 30 mm from [H], while these rulings together make up a square, rotated to the previous one in [H] by 30^0. Each of the next ruling planes is at a distance of 30 mm from the previous one and the square made up by these rulings is rotated by 30^0 to the previous plane.
The last directrixes are in a plane situated at a distance of 120 mm from [H].

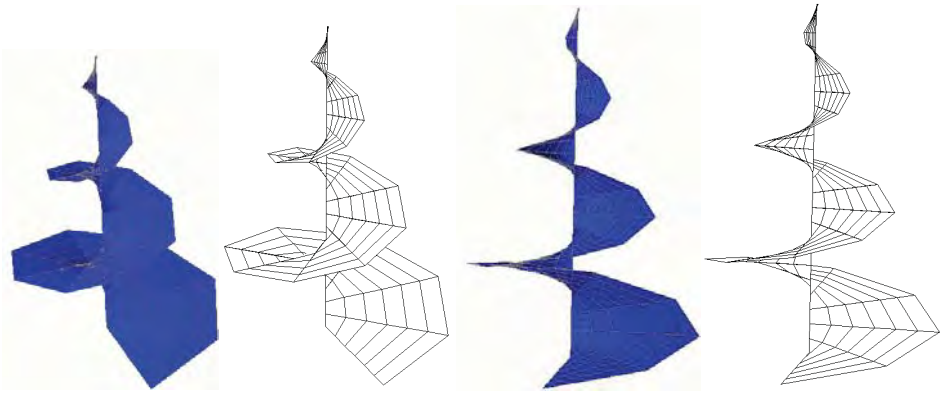

Figure 25. Helicoidal surfaces – axonometric representation and projection on plane [W]

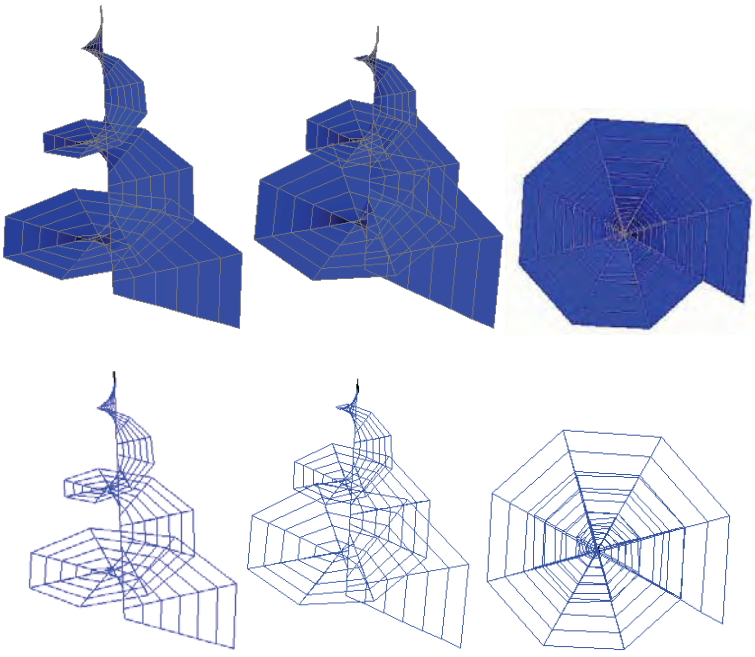

Fig. 26. Helicoidal Surface – rotation of the surface until the projection to plane [H] is seen

2.4.2. Helicoidal Surfaces. Second example

It is demanded to represent the helicoidal surface with a directrix plane in plane [H], which has directrix I a line perpendicular to [H] through the point H(60,60,0) and directrix II a curve belonging to a conoidal surface, with the basis a circle with center H and radius 48 mm. Each ruling is to be in a plane situated at a distance of 5 mm to the previous ruling's plane, rotated by 450, and with a length 2mm less than it (see Figures 25 and 26).

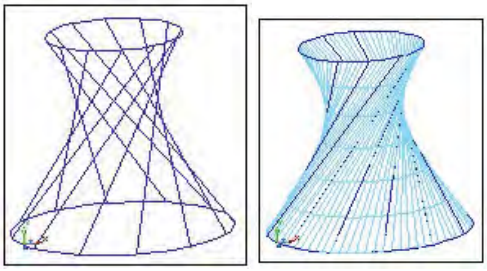

Figure 27. Hyperboloid – axonometric representation

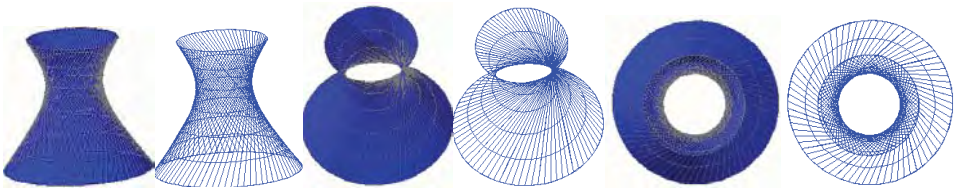

Figure 28. Helicoidal Surface – the rotation of the surface until we see the projection to plane [H]

2.5. Hyperboloid

2.5.1. Hyperboloid. First example

It is required to trace the ruled surface with both basic curves circles, directrix I is the circle with centre S and radius 50 mm in [H], directrix II a circle with radius 30 and centre T in a plane parallel to [H] at a distance of 90 mm from it. The divergence between the horizontal projections of the ends of the segment representing a directrix, is 120^0 for each directrix (see Figure 27 and 28).

2.5.2. Hyperboloid

If the ruled surface described by the above data, but with a divergence of 150^0 is represent (see Figure 29 and 30) some differences will be noticed, the main one would be that the interior diameter is smaller in the second case than in the first.

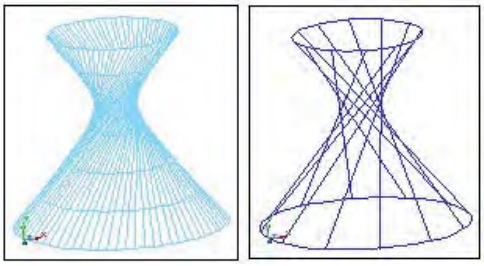

Figure 29. Cylindroid – axonometric representation

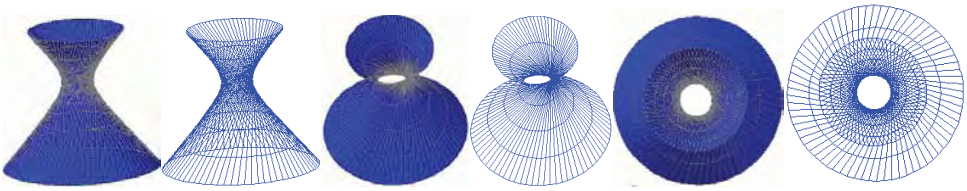

Figure 30. Helicoidal Surface – the rotation of the surface until we see the projection to plane [H].

3. CONCLUSIONS

The new manner of teaching provides not only a maximum efficiency of the study, but, essential more, it radically changes the approach of the students to the geometrical representation. It also makes them involved and responsible in the relationship with their own training to fulfil the university conditions and stimulates simultaneously their creativity.

References

1. Gheorghiu, M., Chelcea, M., *Descriptive Geometry, Problems*, MATRIX ROM Publisher, ISBN 973-755-015-3, Bucharest, 2006. (in Romanian).
2. Gheorghiu, M., Chelcea, M., *Famous buildings as models for ruled surfaces,* The 2nd International Conference on engineering graphics and design – ICEGD - Galați, Romania – 2007.

"Computational Civil Engineering 2007", International Symposium
Iaşi, România, May 25, 2007

Numerical studies on the seismic performance of three structural systems

Horaţiu Mociran, Eugen Panţel
Faculty of Civ. Eng., Technical University, Cluj-Napoca, 400027, Romania

Summary

For many years, the basic intent of the building code seismic provisions has been to provide buildings with an ability to withstand intense ground shaking without collapse, but potentially with some significant structural damage.

The damage to buildings, transportation structures and lifelines wrought by the 1989 Loma Prieta earthquake, the 1994 Northridge earthquake, and the 1999 Hanshin earthquake near Kobe, has forced structural engineers, disaster response agencies and building officials to carefully consider seismic response of the building environment in terms of performance rather than life-safety.

Civil engineering structures normally rely on their ability to dissipate energy to resist dynamic forces such as strong earthquakes. In recent years, to keep the vibration of these structures within the functional and serviceability limits and to reduce structural and architectural damage caused by extreme loads, different passive protective systems have been proposed. Addition of energy dissipation devices (EDDs) is considered one of the viable strategies for enhancing the seismic performance of building structures. For many building structures, EDDs may provide considerable performance improvement or cost saving.

This paper provides a comparison of the performance indices of a three story building with three different structural systems – moment frame, viscously damped frame and a base isolated frame. Fluid viscous damping and base isolation have the same objective of significantly decreasing the response of a structure to earthquake excitation. With both fluid viscous damping and base isolation it is possible to have a structure remain within the elastic region, so there is no permanent deformation from a seismic event. Each of the models were analyzed as linear structures and subjected to time histories for 3 different earthquakes of Vrancea type. The non-dimensional performance indices considered for the models are: Peak Drift ratio, Peak Base Shear and Peak Level Acceleration.

In summary, the viscously damped frame has the best overall relative performance of the three framing schemes. The base isolated frame is better than moment frame.

KEYWORDS: steel frames, passive control, base isolation, viscous damper, time history analysis.

1. INTRODUCTION

Earthquakes represent one of the most damaging disasters. Repairing an area that has experienced an earthquake is an expensive and difficult process. Engineers have introduced different techniques to prevent a large amount of the damage typically caused by earthquakes. The use of passive energy dissipation devices represents a feasible alternative to improve seismic behavior of structures by reducing the structural damage resulting from environmental disturbances [1].

Damping is one of many different methods that have been proposed for allowing a structure to achieve optimal performance when is subjected to an earthquake. The level of damping in a conventional elastic structure is very low, and hence the amount of energy dissipated during transient disturbances is also very low. During strong motions, conventional structures usually deform beyond their elastic limits, and eventually fail or collapse.

The concept of supplemental dampers added to a structure assumes that much of the energy input to the structure will be absorbed by supplemental devices [2]. An ideal damper will be able to reduce both stress and deflection in the structure. Fluid viscous dampers operate on the principle of fluid flow through orifices. A stainless steel piston travels through chambers that are filled with silicone oil. The pressure difference between the two chambers cause silicon oil to flow through an orifice in the piston head and seismic energy is transformed into heat.

Seismic isolation is another alternative for protecting structures from earthquakes. The philosophy behind this method is based on minimizing the earthquake induced forces transferred to the superstructure. During the past 20 years, seismic isolation has emerged as one of the most promising retrofitting strategies for improving the seismic performance of existing buildings. It is also an attractive approach for new construction when conventional design is not suitable or economical [3], [4].

Japan, New Zealand, and a number of European countries pioneered the use of seismic isolation in civil engineering structures. More recently, the United States has begun to implement isolation technology in bridges. In the seismic isolation approach, the superstructure mass is uncoupled from seismic ground motions. This is also referred to as "superstructure" isolation. It uses special types of bearings called "seismic isolation bearings," which are placed below the superstructure and on top of the substructure (foundation). In the event of a strong earthquake, they add flexibility to the structure, by elongating its period and dissipating energy. It could also give rise to large relative displacements across the isolator interface; this can be controlled by incorporating damping elements in the bearing or by adding supplemental dampers.

2. THE STRUCTURE, DAMPERS, BASE ISOLATORS, LOADS

2.1. The structure

Because the majority of buildings in Romania are less than three stories in height, a three story steel frame was selected as a reference frame. The structure was designed as a conventional SMRF (Figure 1) to provide a benchmark for seismic performance comparison with passive control systems. The following design parameters according to P100-1/2006 were used to design SMRF [5]:

- importance class II γ=1,2
- design ground acceleration a_g=0,24cm/sec^2
- T_C=1,6 sec
- behavior factor q=6

All connections between beams and columns are assumed rigid connections.

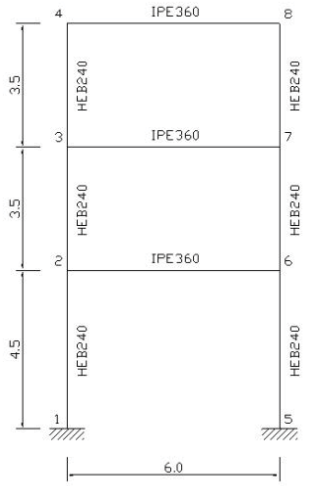

Figure 1. 3 Storey Moment Frame

The structure was then modified by the addition of fluid viscous dampers (Figure 2) or base isolators (Figure 3) to improve the seismic performance, with no attempt made to redesign the main frame elements.

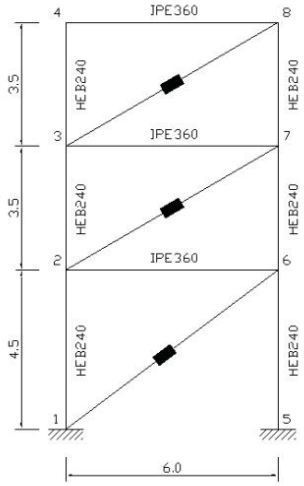

Figure 2. 3 Storey Frame with Linear Viscous Dampers

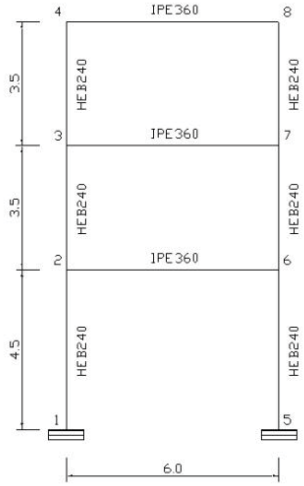

Figure 3. 3 Storey Frame with Base Isolators

2.2. The dampers

The linear viscous dampers (Figure 4) will be installed with a diagonal brace configuration. The inherent damping ratio of the structure is assumed to be 5%, and

the total effective damping ratio of the whole system is designated at 20% of critical.

The damping cofficient used for all dampers is c=245kN-sec/m. In this example, the linear effective stiffness is set to zero so that pure damping behavior is achieved.

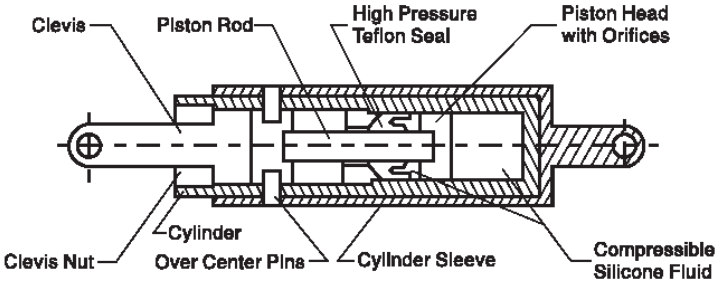

Figure 4. TAYLOR DEVICES Viscous Damper

2.3. The base isolators

The isolators are of elastomeric type (Figure 5) and have been chosen from FIP INDUSTRIALE catalog, according to the vertical reactions requirements [6].

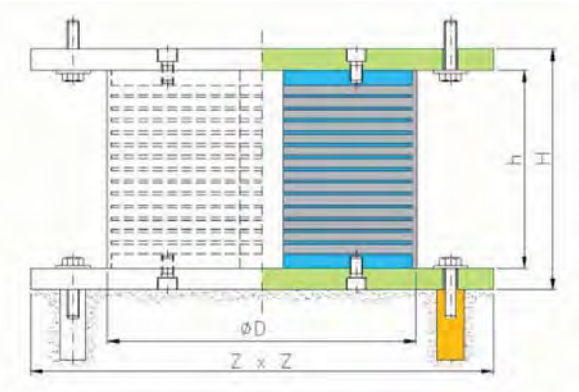

Figure 5. FIP INDUSTRIALE Base Isolator

The selected isolators SI-S 400/78, have the following specifications:

Mechanical properties: Vertical load V=570kN; Horizontal stiffness=0.64kN/mm.

Geometrical characteristics: Diameter D= 400mm; Total height Z=450mm.

2.4. The loads

The seismic performance of these structural systems was studied using linear response-history analysis. Three scaled artificial earthquakes of Vrancea type, that matched on average a P100-1/2006 Provisions response spectrum were used for analysis.

3. NUMERICAL RESULTS

The results of the time history analyses are presented and discussed. Comparisons are made of estimated base shear, interstory drift and floor acceleration.

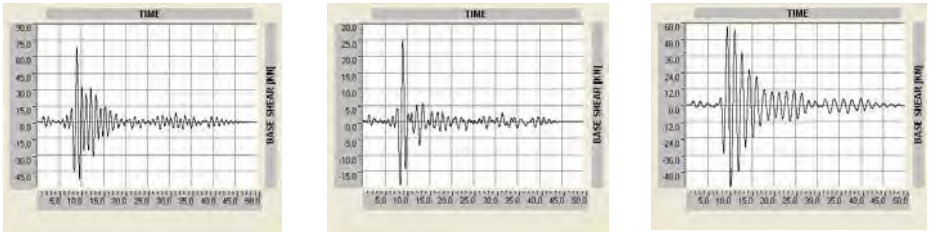

Figure 6. Base Shear for Vrancea type earthquake

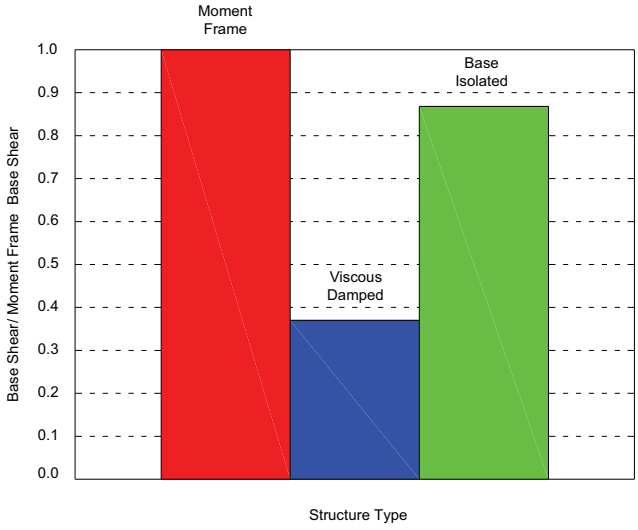

Figure 7. Normalized Maximum Value of Base Shear

3.1. Base shear

Figures 6 and 7 show a comparisons of base shears for the three structural schemes that were studied. Viscous dampers are extremely effective in reducing the base shear of the frame, whereas the addition of base isolators results in a modest reduction in base shear.

3.2. Interstory drift

This is a code design parameter and is something most engineers focus upon during the design process. From a damageability perspective, it is a measure that impacts damage to the framing system, building façade and windows, piping, ductwork and partitions.

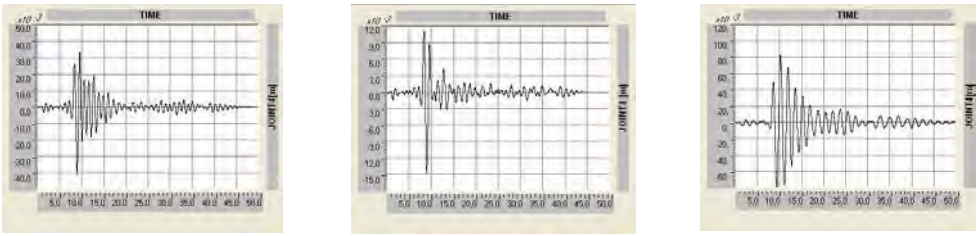

Figure 8 Top floor displacements

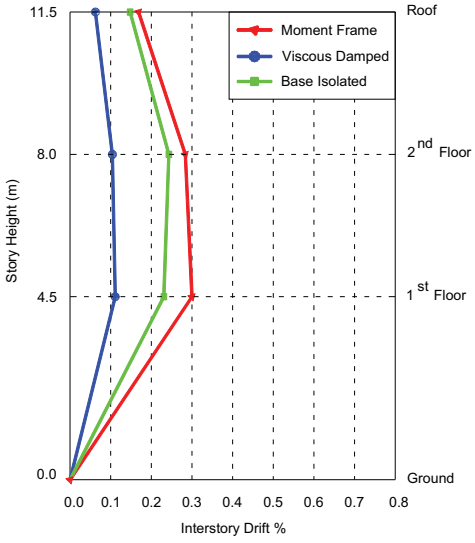

Figure 9 Interstory Drift

Results proved that control methods were successful in reducing the floor displacements of the structure (Figure 8). The viscously damped frame reduced the maximum drift by 63.30%, whereas the base isolated frame reduced the maximum drift by 23.90%. Figure 10 shows a comparison of maximum values of interstory drift for all framing schemes, normalized to the moment frame.

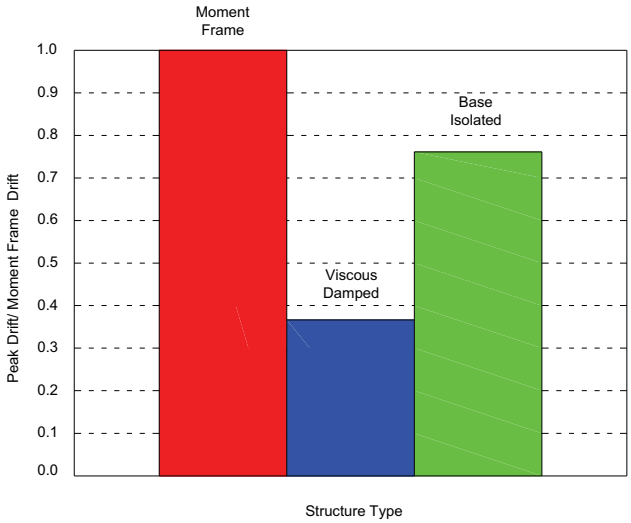

Figure 10 Normalized Maximum Value of Interstory Drifts

3.3. Floor accelerations

This parameter is almost never taking into account in the design process, because it requires a time history analyses to obtain it. From the damageability perspective it is the measure that impacts damage to the ceiling and lights, electrical and mechanical equipment, elevators and the building contents.

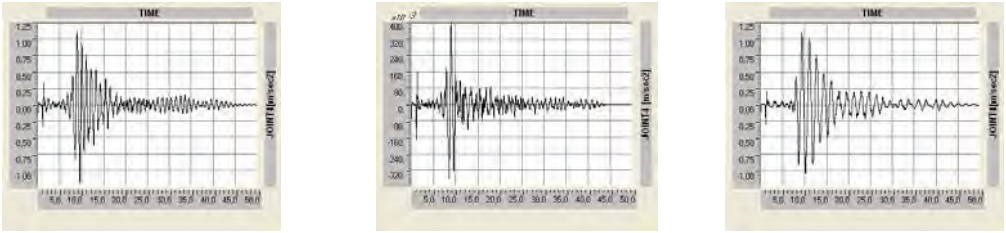

Figure 11 Top floor accelerations

In assessing the acceleration performance, the viscously damped frame has the best performance (Figure 11). The viscously damped frame reduced the maximum floor acceleration by 66.90%, whereas the base isolated frame reduced the maximum floor acceleration by 9.20% (Figure 12).

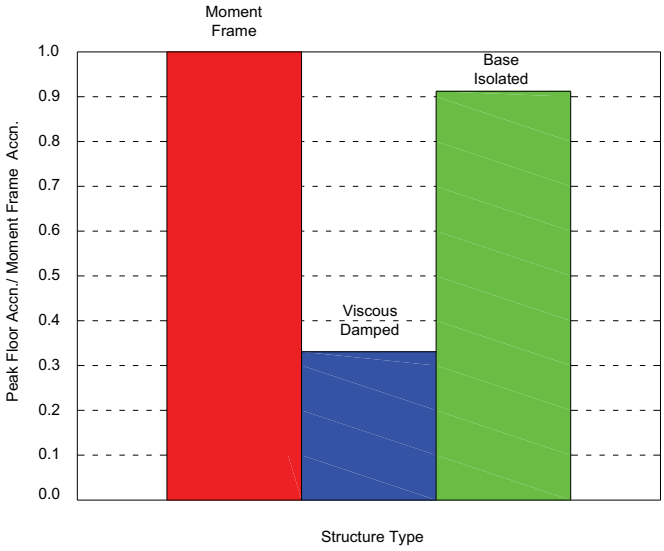

Figure 11 Normalized Peak Floor Accelerations

3.4. Performance indexes

For each control approach considered (i.e. viscous damper and base isolation), the uncontrolled response of the structure was compared with the controlled response [7].

The non-dimensional performance indexes considered in this study are Peak Base Shear (PI_1), Peak Drift ratio (PI_2), Peak Level Acceleration (PI_3).

They are defined as follows: $PI_1 = \frac{F_{b,c}^{\max}}{F_{b,u}^{\max}}$; $PI_2 = \frac{\delta_c^{\max}}{\delta_u^{\max}}$; $PI_3 = \frac{\ddot{x}_c^{\max}}{\ddot{x}_u^{\max}}$; where:

$F_{b,u}^{\max}; F_{b,c}^{\max}$ - the maximum base shear of the uncontrolled/controlled frame;

$\delta_u^{\max}; \delta_c^{\max}$ - the maximum inter storey drift ratio of the uncontrolled/controlled frame;

$\ddot{x}_u^{\max}; \ddot{x}_c^{\max}$ - the maximum absolute floor acceleration of the uncontrolled/controlled frame.

The results presented in Table 1 show that the viscouly damped frame was the most effective in reducing the building's response.

Table 1. Performance index for peak base shear, peak drift and peak acceleration

Cases	Performance Index			% Reduction		
	PI_1	PI_2	PI_3	Base Shear	Story Drift	Acc
Viscous Damped	0.367	0.367	0.331	63.30	63.30	66.90
Base Isolated	0.869	0.761	0.908	13.10	23.90	9.20

4. CONCLUDING REMARKS

The objective of the paper is to evaluate the efficiency of two passive control systems. This paper has presented a comparative study of seismic performance (base shear, interstory drift and floor acceleration) of a three story steel building. The three story moment resisting frame was designed according to P100-1/2006 Provisions and than retrofitted with viscous dampers and base isolators. The structure was subjected to linear time history analyses for different earthquakes of Vrancea type.

The above numerical results presented for the three story one bay frame can not be generalized. The analyses show that the seismic performance of the viscously damped frame significantly exceeds that of the other framing schemes. The three story base isolated frame had better performance than the three moment frame.

These parameters indicate that structural and non-structural damages are significantly reduced in the case of viscously damped frame.

The results emphasis that seismic performances of the building depend upon the structural framing scheme chosen for that building.

References

1. Miyamoto, H.K., Singh, J.P., Performance of Structures with Passive Energy Dissipators, *Earthquake Spectra*, 2002.
2. Haskell, G., Lee, D., Fluid Viscous Damping as an Alternative to Base Isolation, *Technical papers from Taylor Devices*, 2004.
3. Alhan, C., Gavin, H., *Parametric Analysis of Passive Damping in Base Isolation*, 16th ASCE Engineering Mechanics Conference, Seattle, 2003.
4. Alexa, P., Mociran, H., Mathe, A., *Passive control of semirigid steel structures*, Computational Civil Engineering, Iasi, 2005.
5. P100-1/2006, Code for seismic design of residential buildings, agrozootehnichal and industrial structures. (in Romanian).
6. www.fip-group.it
7. Rama Raju, K., et al., Optimum Distribution of Viscous Fluid Dampers in Multi-Storied Buildings, *International Conference on Structural Stability and Dynamics*, Florida, 2005.

"Computational Civil Engineering 2007", International Symposium
Iaşi, România, May 25, 2007

Identification Methods of the Nonlinear Systems Subjected to Seismic Actions

Doina Stefan, Violeta-Elena Chitan
[1]*Structural Mechanics, Technical University "Gh. Asachi" Iasi, 700050, România*

Summary

The need to identify the nonlinear systems subjected to stochastic actions leaded to the development of the classical and/or deterministic methods toward some methods capable to take into account the improved models for structure and excitation.

The identification of the nonlinear systems can be carried out using specific approaches that are based on the reparability hypotheses or on the change of the nonlinear system with an equivalent linear system that has the features closely related to the initial one.

Current nonlinearities that occur in the structural response during a strong earthquake are geometrical and/or physical (nonlinearity of the stiffness and the damping). In order to underline the nonlinearity of the stiffness, in this paper we take advantage of the modeling method for the structural response using a non-stationary linear model and the parameter identification of the equivalent stationary linear model, both for the SDOF and the NDOF systems.

Explaining the nonlinearity of the stiffness can be done in two specific ways: the structure response modeling through the nonstationary linear model and the parameter identification of the equivalent stationary linear model; the real stiffness valuation of the structure during each vibration cycle using the internal force calculus of the structure.

KEYWORDS: nonlinear system, stationary linear model, nonlinearity of the stiffness, structural response.

1. INTRODUCTION

In the context of continuous efforts to improve the knowledge in the field of dynamic-seismic behavior of a building, the direction is toward the study of structural behavior starting from the tests in situ.

This kind of approach gives the means for: structural quality and security level checking in the conditions of real exploitation; validation of the existent analytical

models of behavior, also for the a-priori hypotheses of the structural response prediction; knowledge accumulation, necessary to improve the dimensioning methods and the well argued working out of the new behavior models.

Knowing precisely or often good enough the features of a system implies the discerning use of various theoretical and experimental approaches. The system identification doesn't mean anything else but the convenient processing of some information achieved from the tests, in order to obtain a physical or mathematical model, as sample and easy-to-use as possible.

An identification process consists of: the choice of the model structure; the choice of the criterion to compare the model with the real structure; estimation of the model parameters.

The need to identify the nonlinear systems subjected to stochastic actions leaded to the development of the classical and/or deterministic methods toward some methods capable to take into account the improved models for structure and excitation. For this reason, the non-linear system identification can be carried out using specific approaches that are based on the reparability hypotheses or on the change of the nonlinear system with an equivalent linear system that has the features closely related to the initial one.

Current nonlinearities that occur in the structural response during a strong earthquake are physical and/or geometrical. In the case of physical non-linearity the equations of motion settled in the hypothesis of visco-elstic linear behavior do not remain valid already, and generally, the forces that occur are expressed using non-linear functions, with respect to displacement and velocity, this leading to the non-linear stiffness and non-linear damping.

To underline the non-linear stiffness, two methods are usually carried out: the structural response modeling using a non-stationary linear model and the parameter identification of the equivalent stationary linear model; the estimation of the effective structural stiffness during each cycle of vibration using the computation of internal structural forces.

2. THE EQUIVALENT LINEARIZATION METHOD

Using the fact that linear systems are solved easily, the study of the nonlinear systems can be performed with sufficient accuracy by changing the nonlinear system with an equivalent linear system having the features closely related to the initial one. This technique of linearization for the systems subjected to stochastic actions was proposed for the first time by Booton in 1953.

2.1. SDOF Systems

The simplest mechanical system is the SDOF oscillator, which has the equation of motion as follows:

$$m\ddot{y}(t) + h(y, \dot{y}) = f(t) \tag{1}$$

where:

y, $\dot{y}$, $\ddot{y}$ are denoting the displacement, velocity and acceleration;

$h(y, \dot{y})$ denotes a function that describes the nonlinearity of the oscillator;

f(t) denotes the stochastic action.

The linearization method consists of the change of nonlinear oscillator with an equivalent linear one. Equation (6.6) becomes:

$$m\ddot{\tilde{y}}(t) + c_{eq}\dot{\tilde{y}}(t) + k_{eq}\tilde{y}(t) = f(t) \tag{2}$$

where:

y, $\dot{y}$, $\ddot{y}$ are denoting the displacement, velocity and acceleration of the equivalent linear system;

c_{eq} denotes the viscous damping of the equivalent system;

k_{eq} denotes the stiffness of the equivalent linear system;

(c_{eq} and k_{eq} must be found out).

It is normaly to say that the nonlinear system and the equivalent linear system do not have identically motions, so the solutions $y, \dot{y}, \ddot{y}$ do not verify exactly the equation (2), this becoming:

$$m\ddot{\tilde{y}}(t) + h(\tilde{y}, \dot{\tilde{y}}) = f(t) + \varepsilon(t) \tag{3}$$

where: ε(t) is the error that allows the measurement of the difference between the equations (1) and (2).

$$\varepsilon(t) = h(\tilde{y}, \dot{\tilde{y}}) - c_{eq}\dot{\tilde{y}}(t) - k_{eq}\tilde{y}(t) \tag{4}$$

In order to find out c_{eq} and k_{eq}, the error ε(t) must have the minimum value. This method suggests a minimization process for ε(t), starting from the identity:

$$\frac{\partial E[\varepsilon(t)^2]}{\partial C_{eq}} = \frac{\partial E[\varepsilon(t)^2]}{\partial K_{eq}} = 0 \quad (E[\varepsilon(t)^2] - math.operator) \tag{5}$$

Developing the equation (5) we obtain the system:

$$\begin{aligned} K_{eq} &= \frac{E[h\cdot\tilde{y}]E[\dot{\tilde{y}}^2] - E[h\cdot\dot{\tilde{y}}][\tilde{y}\cdot\dot{\tilde{y}}]}{E[\tilde{y}^2]E[\dot{\tilde{y}}^2] - E[\tilde{y}\cdot\dot{\tilde{y}}]^2} \\ C_{eq} &= \frac{E[h\cdot\dot{\tilde{y}}]E[\tilde{y}^2] - E[h\cdot\tilde{y}][\tilde{y}\cdot\dot{\tilde{y}}]}{E[\tilde{y}^2]E[\dot{\tilde{y}}^2] - E[\tilde{y}\cdot\dot{\tilde{y}}]^2} \end{aligned} \tag{6}$$

where:

h is as a matter of fact $h(y,\dot{y})$;

$E[\tilde{y},h(\tilde{y},\dot{\tilde{y}})]$ and $E[\dot{\tilde{y}},h(\tilde{y},\dot{\tilde{y}})]$ can be expressed as functions of y and $\dot{y}$ and c_{eq} and k_{eq} are functions depending on the terms of the covariance matrix, denoted cov[Y] and having the following format:

$$\text{cov}[Y]=\begin{bmatrix} E[\tilde{y},\dot{\tilde{y}}] & E[\tilde{y},\dot{\tilde{y}}] \\ E[\dot{\tilde{y}},\tilde{y}] & E[\dot{\tilde{y}},\tilde{y}] \end{bmatrix} \tag{7}$$

2.2. NDOF Systems

The nonlinear NDOF system has the following equation of motion:

$$M\ddot{y}(t)+h(y,\dot{y})=f(t) \tag{8}$$

where:

f(t) is a representative gaussian process of the excitation;

W(t) is a stationary gaussian process;

g(t) is a vector with terms as functions that are measurable in time;

y is the displacement vector.

$$f(t)=W(t)\cdot g(t) \tag{9}$$

The equivalent linear system has the form:

$$M\ddot{\tilde{y}}+C_{eq}\dot{\tilde{y}}+K_{eq}\tilde{y}=f(t) \tag{10}$$

where:

C_{eq} is the equivalent damping matrix that depends on the time (because g(t) is not constant);

K_{eq} is the equivalent stiffness matrix.

The vector of errors is defined by the relation:

$$\varepsilon(t)=h(\tilde{y},\dot{\tilde{y}})-C_{eq}(t)\dot{\tilde{y}}-K_{eq}(t)\tilde{y} \tag{11}$$

This vector is computed as a function of variables of the linear system and it is minimized using the least square criterion. The $C_{ij}(t)$ and $K_{ij}(t)$ coefficients from the $C_{eq}(t)$ and $K_{eq}(t)$ matrices are computed from:

$$\begin{aligned} &\frac{\partial E[\,\varepsilon^T(t)\varepsilon(t)\,]}{\partial C_{ij}(t)}=0 \qquad i=1,N \;\;;\;\; j\le i \\ &\frac{\partial E[\,\varepsilon^T(t)\varepsilon(t)\,]}{\partial K_{ij}(t)}=0 \end{aligned} \tag{12}$$

Using equation (11) we can write:

$$E[h(\tilde{y},\dot{\tilde{y}})\tilde{y}^T]-C_{eq}(t)E[\dot{\tilde{y}},\dot{\tilde{y}}^T]-K_{eq}(t)E[\tilde{y},\dot{\tilde{y}}^T]=0$$
$$E[h(\tilde{y},\dot{\tilde{y}})\dot{\tilde{y}}^T]-C_{eq}(t)E[\tilde{y},\tilde{y}^T]-K_{eq}(t)E[\tilde{y},\tilde{y}^T]=0 \quad (13)$$

From above, the $C_{ij}(t)$ and $K_{ij}(t)$ terms can be obtained.

The excitation is a gaussian one, this leading to a gaussian response and allowing to write the $E\left[h(\tilde{y},\dot{\tilde{y}}),\tilde{y}^T\right]$ and $E\left[h(\tilde{y},\dot{\tilde{y}}),\dot{\tilde{y}}^T\right]$ terms as functions of the Y(2n x 2n) covariance matrix terms. The computation of the $E\left[h(\tilde{y},\dot{\tilde{y}}),\tilde{y}^T\right]$ and $E\left[h(\tilde{y},\dot{\tilde{y}}),\dot{\tilde{y}}^T\right]$ terms is easily carried out if we assume the fact that the displacements and velocities are two by two independent.

$$C_{ij}(t)=E\left[\frac{\partial h_i(\tilde{y},\dot{\tilde{y}})}{\partial\tilde{y}}\right] \qquad K_{ij}(t)=E\left[\frac{\partial h_i(\tilde{y},\dot{\tilde{y}})}{\partial\dot{\tilde{y}}}\right] \quad (14)$$

$$Y=\begin{bmatrix} E[\tilde{y}\tilde{y}^T] & E[\tilde{y}\dot{\tilde{y}}^T] \\ E[\dot{\tilde{y}}\tilde{y}^T] & E[\dot{\tilde{y}}\dot{\tilde{y}}^T] \end{bmatrix} \quad (15)$$

The linear system has n(n+1)/2 unknowns, which are the $C_{ij}(t)$ and $K_{ij}(t)$ i=1,n terms and they are computed with respect to the terms of the Y(t) matrix.

3. NONLINEAR SYSTEM IDENTIFICATION. THE MODEL OF THE NONLINEAR OSCILLATOR

It is considered the fact that the measured response at the roof level can be modeled using the nonlinear oscillator, which has the equation of equilibrium as follows:

$$\ddot{y}+f(y,\dot{y})=-p\ddot{y}_{ter} \quad (16)$$

Assuming for the mass and the damping to remain constant, and for the stiffness to be variable, the force f has the expression:

$$f=c_0\dot{y}+k_0(t)y \quad (17)$$

where:

c_o is the damping constant over the unit of mass;

$k_o(t)$ is the structural stiffness over the unit of mass.

The equation (16) can also be written:

$$\ddot{y}+c_0\dot{y}+k_0(t)y=-p\ddot{y}_{ter} \quad (18)$$

In order to compute the response of the assumed model, the non-linear differential equation (17) must be solved for each iteration step of the numerical algorithm for minimization.

The equation of equilibrium in incremental variables is:

$$\Delta\ddot{y} + c_0\Delta\dot{y} + k_0(t)\Delta y = -p\Delta\ddot{y}_{ter} \tag{19}$$

where:

$$\begin{aligned} \Delta\ddot{y} &= \ddot{y}(t+\Delta t) - \ddot{y}(t) \\ \Delta\dot{y} &= \dot{y}(t+\Delta t) - \dot{y}(t) \\ \Delta y &= y(t+\Delta t) - y(t) \\ \Delta\ddot{y}_{ter} &= \ddot{y}_{ter}(t+\Delta t) - \ddot{y}_{ter}(t) \end{aligned} \tag{20}$$

There are many ways to solve the equation (19). The best one is the step-by-step approach. The dynamic equilibrium is stable at the beginning and at the end of each time step Δt, inside in which it is assumed a linear variation of acceleration and the structural features remaining constant during all the range (fig.1).

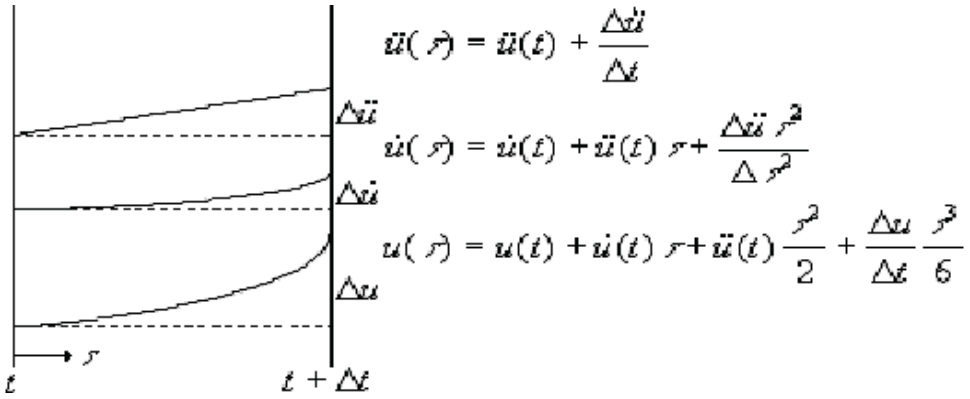

Figure 1. The dynamic equilibrium

The incremental values for velocity and displacement are:

$$\Delta\dot{y}(t) = \ddot{y}(t)\Delta t + \Delta\ddot{y}(t)\frac{\Delta t}{2} \tag{21}$$

$$\Delta y(t) = \dot{y}(t)\Delta t + \ddot{y}(t)\frac{\Delta t^2}{2} + \Delta\ddot{y}(t)\frac{\Delta t}{2} \tag{22}$$

Using the incremental displacement as a basic variable, one can obtain the incremental acceleration from equation (22), which is after substituted in equation (21), this leading to:

$$\Delta\ddot{y}(t) = \frac{6}{\Delta t^2}\Delta y(t) - \frac{6}{\Delta t^2}\Delta\dot{y}(t) - 3\ddot{y}(t) \tag{23}$$

$$\Delta\dot{y}(t) = \frac{3}{\Delta t^2}\Delta y(t) - 3\dot{y}(t) - \frac{\Delta t}{2}\ddot{y}(t) \tag{24}$$

Substituting equations (23) and (24) in equation (19) we obtain:

$$\left[\frac{6}{\Delta t^2}\Delta y(t) - \frac{6}{\Delta t^2}\Delta\dot{y}(t) - 3\ddot{y}(t)\right] + K_0\left[\frac{3}{\Delta t}\Delta y(t) - 3\dot{y}(t) - \frac{\Delta t}{2}\ddot{y}(t)\right] + K_0(t)\cdot\Delta y(t) = -p\ddot{y}_{ter} \tag{25}$$

or:

$$\widetilde{K}(t)\cdot\Delta y(t) = \Delta\widetilde{\ddot{y}}_{ter} \tag{26}$$

where:

$$\widetilde{K}(t) = \frac{6}{\Delta t^2} + \frac{3}{\Delta t}C_0 + K_0 \tag{27}$$

$$\Delta\widetilde{\ddot{y}}_{ter} = -p\Delta\ddot{y}_{ter} + \frac{6}{\Delta t}\dot{y}(t) + 3\ddot{y}(t) + C_0\left[3\dot{y}(t) + \frac{\Delta t}{2}\ddot{y}(t)\right] \tag{28}$$

Therefore, the incremental displacement is computed starting from equation (26) and dividing the effective incremental load by the effective stiffness.

4. CONCLUSIONS

A nonlinear system can be defined as a system that doesn't obey to the superposition principles. This "non-property" occurs to the extremely various systems for which it doesn't exist general solving methods, but only special methods, adapted to each class of problems.

The identification of the nonlinear systems can be carried out using specific approaches that are based on the reparability hypotheses or on the change of the nonlinear system with an equivalent linear system that has the features closely related to the initial one.

Current nonlinearities that occur in the structural response during a strong earthquake are geometrical and/or physical (non-linearity of the stiffness and damping). In this paper we take advantage of the modeling method for the structural response using a non-stationary linear model and the parameter identification of the equivalent stationary linear model, in order to underline the nonlinearity of the stiffness.

References

1. Afra H., P.Argoul, *Identification du comportement sismique des batiments et comparaison avec les donnees reglementaires*, 1990, Annales des Ponts et Chausees, pag.50-65. (in French)
2. Eykhoff P., *Identificarea sistemelor*, 1977, Ed. Tehnica, Bucuresti. (in Romanian, translation from English)
3. Guihot Pascal, *Analyse de la reponse de structures non lineaires sollicitees par des sources d'excitation aleatoire.* These de doctorat de l'Universite de Paris VI, 1999. (in French)
4. Stefan Doina, *Identificarea sistemelor mecanice cu aplica]ii la calificarea seismia a unor cladiri si echipamente din componenta Centralelor Nuclearo-Electrice,* Teza de doctorat, Univ. Tehnica "Gh. Asachi", ian., 1996, Iasi. (in Romanian)

ISBN 978-973-8955-14-1

MANIFESTARI STIINTIFICE